A. Chunikhin M. Zhavoronkov

HIGH VOLTAGE SWITCHGEAR

ANALYSIS AND DESIGN

Mir Publishers Moscow

Aleksandr A. CHUNIKHIN, Cand. Sc. (Eng.), Associate Professor at the Moscow Power Engineering Institute, is a leading authority in the field of high voltage switchgear, with more than 40 years' experience in the design and development of high voltage circuit breakers, current transformers, and special electrical equipment. Was engaged in the development of oil-circuit-breaker interrupters for 6-220 kV, a synchronous circuit breaker for 220 kV, a current transformer for switching transient measurements, and devices to measure residual currents in circuit breakers. Has prepared lecture courses on high voltage switchgear and fundamentals of switchgear. Has published about 100 papers including the textbooks *Electrical Switchgear* and *Fundamentals of Switchgear*, and the monograph *Suspended Isolating Switches.*

Mikhail A. ZHAVORONKOV, Cand. Sc. (Eng.), Associate Professor at the Moscow Power Engineering Institute. His main interests are the design and analysis of high voltage switchgear, special devices for high voltage systems, electrical contacts and their materials. Has experience of international research work and teaching. In 1964-65 he was to the Fontenay-aux-Roses, EdF, laboratory, France, and in 1981-85 he taught electrical engineers at the Higher National Engineering School of Tunis. Has to his credit more than 40 scientific papers, being a co-author of the books *Electrical Erosion of High-Current Contacts and Electrodes* (1978), *High Voltage Switchgear* (1985), and many editions of *Electrotechnical Handbook*.

HIGH VOLTAGE SWITCHGEAR

A.A. Chunikhin and M.A. Zhavoronkov

This book is based on a lecture course on high-voltage switchgear that the authors have taught for many years at the Moscow Power Engineering Institute. The course covers HV power circuit breakers, disconnecting switches, isolators, earthing switches, and related equipment such as current and voltage transformers, reactors, and fusegear.

The authors took pains to collect materials on new switchgear installations scattered over a number of books and papers and present it in a form that is easy for a novice in the field. The study aid surveys many installations and highlights the specific features of particular designs. Analytical and design considerations of HV circuit breakers, current transformers, voltage transformers, and reactors are accompanied by illustrative examples. These excursions into the technicalities and design of upgraded switchgear will be of value for students majoring in switchgear design, engineers preparing for licence examinations, and those electrical engineers who wish to learn more about this equipment and would like to choose it professionally for particular application.

А.А. Чунихин
М.А. Жаворонков

Аппараты высокого напряжения

Москва
Энергоатомиздат

A. Chunikhin M. Zhavoronkov

HIGH VOLTAGE SWITCHGEAR

ANALYSIS AND DESIGN

Mir Publishers Moscow

First published 1989
Revised from the 1985 Russian edition

Translated from the Russian by M. Edelev

На английском языке

Printed in the Union of Soviet Socialist Republics

ISBN 5-03-000078-x

© Энергоатомиздат, 1985
© English translation, Mir Publishers, 1989

CONTENTS

Preface 8

1 Introduction 9

1.1 Switchgear 11
1.2 Application of Protective Systems 13
1.3 Indoor and Outdoor Installations 15
1.4 Switchgear Characteristics and Ratings. Soviet Practice 15
1.5 Requirements of Switchgear Installations 16
References 17

2 Insulation of Switchgear 18

2.1 Rated and Tested Voltage. Coordination Between Inner and Outside Insulation 18
2.2 Insulation Distances in the Air 21
2.3 Insulation Level Design for SF_6 Installations 24
2.4 Insulation Distance in Oil 25
2.5 Bushing Insulation 27
2.6 Solid Insulation Materials and Procedures 30
2.7 Porcelain Insulators. Dielectric and Mechanical Strength Considerations 34
References 37

3 High Voltage A.C. Circuit Breakers. General Requirements 38

3.1 Interrupting Rating 38
3.2 Duty Cycles 39
3.3 Rate of Rise of Recovery Voltage 40
3.4 Circuit Breaker Stability at Let-Through Short-Circuit Currents 41
3.5 Operating Time 41
3.6 Reliability 42
3.7 Circuit Breaker Testing 43
References 50

4 Air and Sulphur-Hexafluoride Circuit Breakers 51

4.1 General Layout 51
4.2 Electric Arc Behaviour in a Longitudinal Flow of Compressed Air 54
4.3 Thermodynamic Clogging of the Blast Nozzle. Nozzle Section vs. Breaking Current Relation 57
4.4 Recovery of Dielectric Strength in Axial Blast Interrupters 64
4.5 Aiding Arc Extinction with Shunt Resistors and Capacitors 71
4.6 Gas Dynamics of Air Circuit Breakers 79
4.7 Analysis and Selection of Interrupting Chamber Parameters 85
4.8 Control System Components 91
4.9 Air Circuit Breaker Design 100
4.10 Insulating and Interrupting Properties of SF_6 111
4.11 SF_6 Circuit Breaker Analysis 117
4.12 Construction of SF_6 Circuit Breakers 122

4.13 Trends in the Development of Oilless Circuit Breakers 124
4.14 Illustrative Analysis of Air-Blast Interrupter 126
References 135

5 Oil Circuit Breakers 137

5.1 Layout of Bulk and Low-Oil Breakers 137
5.2 Construction and Operation of Interrupters 146
5.3 Extinction-Chamber Pressure Analysis 149
5.4 Auto-Reclosing Duty and Frequent Make-Break Operations 154
5.5 Operating Mechanisms 156
5.6 Driving and Tripping Mechanisms 164
5.7 Steps in Breaker Design 168

6 Magnetic Air-Break Circuit Breakers 169

6.1 General 169
6.2 Current-Voltage Behaviour of the Arc Cooled in the Arc Chute 171
6.3 Interruption of a Strongly Inductive Circuit 172
6.4 Heating of the Chute Walls 174
6.5 Arc Speed in the Chute 176
6.6 Residual Conductivity of Magnetic Breakers 179
6.7 Arc Chute Construction 179
6.8 Magnetic Air-Break Circuit-Breaker Design Procedure 182

7 Vacuum Circuit-Breakers 183

7.1 General 183
7.2 Status and Trends in Continuous Current and Interrupting Ratings 185
7.3 Mechanical and Thermal Withstand Capabilities. Erosion of Contacts in Vacuum Circuit Breakers 189
7.4 Electric Strength 191
7.5 Construction and Layout 193
7.6 Conclusion 197
References 197

8 Isolating, Earthing, and Load Switches 198

8.1 General Requirements 198
8.2 Constructions of Discriminators 200
8.3 Isolators and Earthing Switches 207
8.4 Load Switches 208
References 211

9 High-Voltage Fusegear 212

9.1 Protective Characteristics 212
9.2 Construction of Fusegear 216
9.3 Parameter Selection and Design 219
References 219

10 Current Transformers 220

10.1 General 220

10.2 Error Compensation 228
10.3 Operating Modes 230
10.4 Types of Construction 241
10.5 Coreless Current Transformers 245
10.6 Optoelectronic Current Transformers 247
10.7 Instrument Transformers for D. C. Transmission Systems 250
10.8 Choice of Current Transformers 254
10.9 Calculation of an Electromagnetic C. T. Illustrative Example 254
References 264

11 Voltage Transformers 266

11.1 General 266
11.2 Phasor Diagram and Errors 268
11.3 Error Compensation 271
11.4 Construction of Voltage Transformers 273
11.5 Components of Electromagnetic V.T.s 278
11.6 Capacitor-Divider V.T.s 281
11.7 Constant-Voltage Transformers 284
11.8 Optoelectronic Voltage Transformers 286
11.9 Calculation of a Magnetic V.T. Illustrative Example 288
References 299

12 Reactors 300

12.1 General 300
12.2 Constructions of Reactors 303
12,3 Calculation of Reactor Inductance 305
12.4 Thermal Design 308
12.5 Mechanical Rating 311
12.6 Insulation 325
12.7 Taps and Contacts 325
12.8 Duplex Reactors 326
12.9 Calculation of a Reactor. Illustrative Example 329
References 335

13 Surge Arresters 336

13.1 Application and Characteristics 336
13.2 Tube-Type Arresters 336
13.3 Valve-Type Surge Arresters 337
13.4 Overvoltage Limiters 346

14 Modular Switchgear Installations 348

14.1 General 348
14.2 Modular Installations for 10 kV 348
14.3 SF_6-Insulated Substations 352
14.4 Constructional Designs of SF_6-Substation Modules 357

Index 360

PREFACE

This book is based on a lecture course on high-voltage switchgear that the authors have taught for many years at the Moscow Power Engineering Institute. This course covers high-voltage power circuit breakers, isolators, earthing switches, sectionalisers, and related equipment such as current and voltage transformers, reactors, and fusegear.

While preparing our lecture course we recognised that materials on the relevant concepts and new switchgear installations are scattered over a large number of books and papers. Moreover they are often presented in a form that is hard to grasp by a novice in the field of switchgear. Therefore we took pains to overview the available publications with the aim to write a study aid for students majoring in switchgear design, which would facilitate the perception of this nontrivial subject.

The theoretical insights of the text are accompanied by illustrative examples of analysis and design considerations carried out for circuit breakers, current transformers, voltage transformers and reactors. These elaborate excursions into the philosophy and technicalities of upgraded switchgear will be of value for those who wish to learn more about this equipment and those who would like to have a reference handbook for student examination works or for professional engineer licence examination studies.

A. Chunikhin
M. Zhavoronkov

1
INTRODUCTION

In modern power engineering there is a characteristic trend toward growing power outputs of new thermal, nuclear and water generating stations. Growth of generated power needs higher line voltages in view of long distances from generator to user. Quite appropriately the designers of high voltage switchgear have to increase the voltage and current ratings and interrupting capacity of circuit breakers and other equipment that serve to distribute power and protect plants and lines from faults due to overvoltage and overcurrents (Fig. 1.1).

By way of example voltage ratings of 735-750 kV are now in wide use and switchgear sets rated for 1150 kV are being phased in. Figure 1.2 illustrates the trend exhibited by current ratings which reach 8-12 kA in high voltage busducts rated above 110 kV and about 4-5 kA in line tappings. In generator busducts at 16-27 kV current ratings can be as high as 7-50 kA depending on the generating capacity. Rated current values are especially large in the generators of nuclear power stations.

The most critical duty of high voltage switchgear is on short circuit. Figure 1.3 demonstrates the growth of short-circuit current, I_{sc}, on 123-420 kV power systems. In the 1980s the interrupting current rating reached 63 kA, with the prospective values of 80-kA short-circuit current in 420-kV systems.

In 16-27 kV generator busducts short circuit currents can be as high as 180 kA. The short circuit current passing in the generating system through the transformers from a fault on the high voltage side can reach values of 380 kA and higher, and the instantaneous current can be as high as 1000 kA. A survey of circuit breakers on rotating generating machinery may be found in the book by Bronstein [1.1].

A notable development of late is d.c. power transmission systems. This mode of power transmission offers large technical and economical advantages for long-line systems. The principal diagram of such a system is shown in Fig. 1.4. The generated a.c. power is converted by thyristors into a high voltage d.c. power to be transmitted. The DC/AC converter at the end of the line reconverts the transmitted power into an a.c. waveform to convey it further to the plant. The d.c. transmission systems proved to be especially efficient for transmission lines in excess of 500-800 kilometers. Several d.c. transmission lines at 1500 kV are operational in the Soviet Union.

Rapid growth of rated system voltage, short-circuit currents and rated currents imposes severe requirements on the respective switchgear. Sulphur hexafluoride (SF_6) insulated circuit breakers are a promising solution for 110 kV and higher system voltages, whereas vacuum circuit breakers will be predominantly developed for circuits under 110 kV. The associated high voltage equipment, such as current and

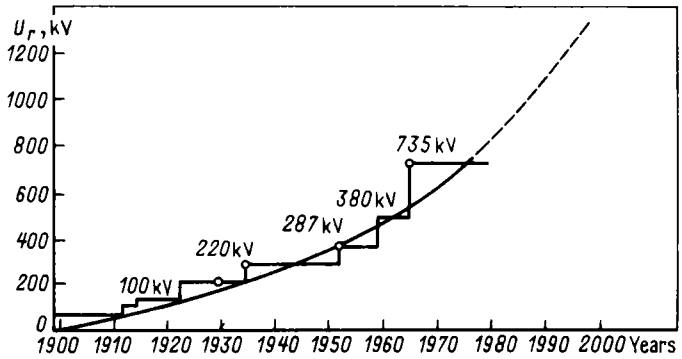

Fig. 1.1. Growth of switchgear voltage ratings over the years

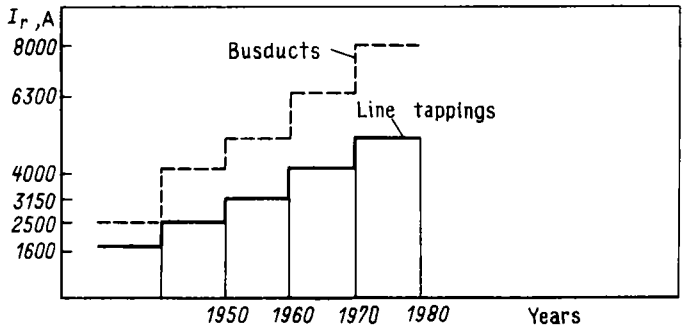

Fig. 1.2. Growth of switchgear current ratings over recent decades

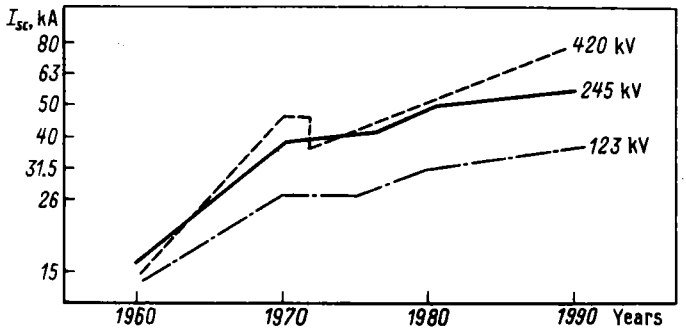

Fig. 1.3. Variation of short-circuit currents over recent decades

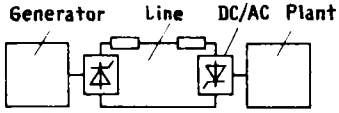

Fig. 1.4. Schematic diagram of a d.c. power transmission system

voltage transformers, isolators, arresters, and such, are also being refined. Higher short-circuit currents call for shorter total break times which implies lower current-transformer errors in sensing switching transients.

An important trend of modern power engineering is associated with the growing power of certain installations. This necessitates high voltage (110-220 kV) power supply directly to the plant. Outdoor switchyards rated for this voltage occupy large areas and therefore are prohibitively expensive in urban conditions. A way out is to develop high voltage SF_6 switchgear installations whose space requirements are only a few percent of that for the ordinary equipment. Sulphur hexafluoride insulated units enable one to fit the substation into a small room thereby protecting the high voltage equipment from the adverse environmental impacts.

1.1 Switchgear

The term switchgear is used to describe not only circuit breakers, but also auxiliary equipment such as current transformers, voltage transformers, isolating switches, operating mechanisms and some other devices. In the Soviet literature on the subject this equipment is commonly treated under a few separate headings as follows.

Switches, isolators and fusegear

The *high-voltage circuit breaker* is the central item of this equipment. It serves to make and break rated currents, interrupt short-circuit currents, and open and close on magnetizing currents of power transformers, and charging currents of lines and cables. The crucial component of this unit is an arc extincting device, called interrupter, that suppresses the arc struck in breaking the high voltage circuit.

The *disconnecting switch* is to make and break high voltage circuits under no-load conditions. Disconnecting switches are provided to isolate a circuit for maintenance on particular items of plant (transformers, generators, etc.) or to rewire the isolated circuit. The characteristic feature of this device is a visible break of the contacts when the switch is open. No arc-extinction device is installed in this switch. The isolated equipment should be connected to earth, therefore isolating switches are often provided with earthing buswork.

The *high-voltage fuse* disconnects the protected circuit at short circuit or on overload by melting the fusible element and by subsequent extinction of the arc in an arc-control device.

The *load switch* serves to make and break rated currents of the plant. Short circuit and overload discrimination is relegated to the series-connected high-voltage

fuse. The switch is provided with an arc-control device which is able to handle rated currents, magnetizing currents of transformers, and line charging currents.

Isolators and short-circuiting switches. Increased ratings of power consuming plants necessitate that 35-220 kV power be fed directly to factories and urban areas. Circuit breakers for this voltage range are bulky and costly devices. To alleviate the problem, simplified switching circuits have been developed where high-voltage switches have been replaced by compact, simple and cheap units of isolating switches and short-circuiting switches.

The high-speed isolating switch serves to isolate a dead high-voltage circuit in a short time span. This device is essentially a disconnecting switch that can be opened by a high-speed drive within 0.1 s.

The short-circuiting switch, as the name implies, is used to establish a short circuit in the high-voltage circuit. Physically it looks like the earthing buswork of the disconnecting switch. The short circuiting switch is closed and opened by a high speed drive. The operating time, from the arrival of the control signal to a contact closure is within 0.1 s. Consistent operation of the isolating and short-circuiting switches is controlled by an automatic circuit.

Current and voltage limiting devices

The *current-limiting reactor* is an inductor that limits short circuit currents and aids in maintaining the necessary voltage on the busbars of the distributing circuit. Reactors allow for low-rating switches and improve the reliability of the system. Other types of reactors are also applicable in high-voltage systems for shunting, line charging, arc extinction, and the like.

Lightning arresters are applied to achieve effective transient overvoltage protection due to breaker operation and atmospheric overvoltage. This equipment reduces requirements imposed on the basic insulation level (BIL) of the system, thus reducing the size and cost of the equipment.

Measuring equipment

This group is constituted by high-voltage current and voltage transformers. These are instrument transformers used to insulate measuring and control devices, in the secondary circuit, from the primary-circuit operating voltages. The transformers allow the rated currents and voltages of high-voltage circuits to be reduced to proper values of current and voltage (1 and 5 A and 100 V, respectively) for the measurement and control circuits.

Complete distribution sets

Complete distribution sets is a somewhat synthetic name for the essential equipment of substation lineups, such as circuit breakers, disconnectors, current and voltage transformers, reactors, etc., packaged in one cubicle to effect power distribution and fault protection. Such a set is ordinarily manufactured at Power Machinery Works and shipped to substation site ready for installation. The constituent units are manufactured on a modular-design basis so that an appropriate high-voltage distribution set can be assembled on site into one of the typical circuits. This ap-

proach reduces the installation period and labor involved in the assembly of the substation, cuts active material requirements, and improves reliability of the installation.

1.2 Application of Protective Systems

High-voltage plants as a rule use three-phase supply voltage. Schematic representation of a 3-phase supply system evolves rather complicated. To simplify the graphical presentation the three-phase system is usually replaced by the associated single-phase or linear scheme as shown in Fig. 1.5. The circuit shown represents power station machinery and a segment of distribution system for 10, 110, and 220 kV.

The 10-kV generators of the power station feed a system of doubled busducts, labelled I and II. Duplication allows maintenance of a bus without de-energizing of the following equipment, improves operational reliability of the system and allows for switching of certain equipment, depending on the mode of the installation, from one bus system to another. The 10-kV busducts are connected through a sectionalised bus reactor *R1*.

Making and breaking of rated load currents and short-circuit currents is effected by the breakers *B1* through *B4*. Assume that a fault has occurred on the left-hand section of the 10-kV buses. It entails opening of the circuit breaker *B1* on the left generator, the breaker *B1* on the bus reactor, and the breaker *B2* on the 10-kV side of the left-hand transformer group, thus interrupting the short-circuit current flowing to the fault from the 10/110/220 transformer group.

To switch the load from the system of busduct I to busduct II one is to close the bus breaker *BB1* to equalize the potentials of the buses I and II. Then follows closing the disconnecting switches of the bus II system and opening the disconnectors of the bus I system. While these operations are taking place, the disconnectors are shunted for safety by the circuit breaker *BB1* that opens after the disconnecting switches of bus I. This arrangement considerably reduces the number of circuit switches in the system.

The generator *G1* can be removed from the system for maintenance by opening its switch *B1* and disconnecting switch *DS1*. Afterwards the left-hand section of busducts is fed by the generator *G2* via the sectionalised reactor *R1*. For better safety of the personnel maintaining the isolated generator the lower (on the scheme) contacts of the isolator are earthed by a conductor capable of passing short circuit currents at this point of the circuit.

Disconnecting switches de-energize any equipment scheduled for maintenance or for inspection. Before the disconnector is operated the circuit must be de-energized by the respective circuit breaker.

The voltage profile in the 10-kV bus is measured with the aid of the voltage transformer *VT1* connected to the bus via a fuse *F1*. Commonly the current in the voltage-transformer primary is 10-20 mA. In the case of a breakdown of the transformer insulation, short circuit currents can reach 100 kA and higher values. In order to protect the busbars from a through fault in the event of transformer breakdown, a current limiting fuse is incorporated in the circuit.

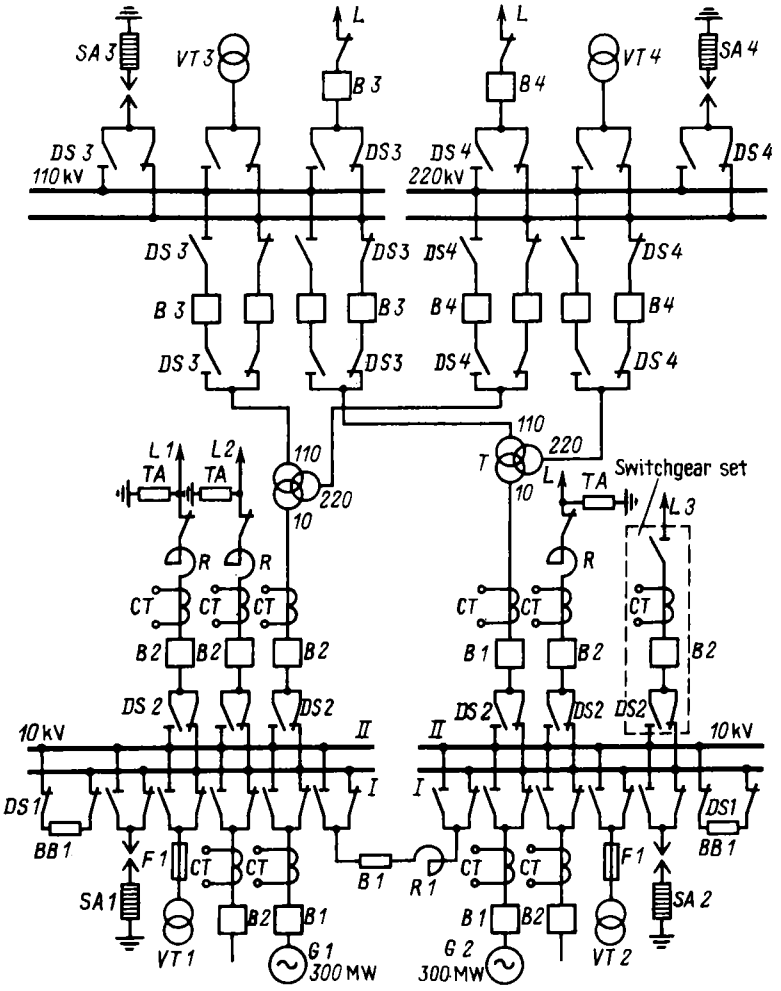

Fig. 1.5. Single phase circuit of a high voltage power distribution system

Current transformers, *CT*, placed in the high-voltage circuit in series with the load, supply low voltage for the measurement circuits and protective relays. Reactors, labelled *R* in the schematic diagram, are incorporated to limit short circuit current in the lines *L1*, *L2*, and *L*. On short circuit, these inductive reactors maintain the busbar voltage near the rated voltage.

Overvoltage protection of high voltage circuits is effected by lightning arresters of the switch (*SA*) and tube (*TA*) type. Application of switchgear and other protective equipment will be discussed in more detail in Chapter 14.

1.3 Indoor and Outdoor Installations

Depending on the conditions in which they will be operated switchgear installations are designed and manufactured for outdoor and indoor service. In the former case the power distributing facilities are exposed to snow, rain, ice, and loads of the connected overhead lines, especially when these are covered with ice or subjected to strong wind loads. Outdoor installations should be operable in the temperature range from $+40°$ to $-40\,°C$.

Indoor installations avoid the effects of rain, snow, ice, and wind, but they often have to operate in high humidity conditions, such that the condensation of moisture on insulating surfaces may be a trouble. Tolerable temperature variations are from $-25°$ to $+40\,°C$. The dielectric strength of switchgear insulation depends on the parameters of environmental air. The normal operating parameters are deemed to be the standard temperature (20 °C) and pressure (STP) at an absolute humidity of 11 g/m^3. At all rated voltages (except 750 kV) switchgear installations should be operable at an elevation of up to 1000 m above see level. Ultimate elevations are half as high for the 750 kV ratings.

1.4 Switchgear Characteristics and Ratings. Soviet Practice

Rated system voltage is the key parameter of all switchgear installations. This is the nominal system voltage of the three-phase system in which the unit is to operate. High voltage switchgear comprises the units designed for rated voltages of 3 kV (elsewhere 1 kV) and higher. Rated voltages of a.c. switchgear are listed in Chapter 2.

To compensate for the voltage drop in the feeders and windings the voltage at the generator busbars is maintained somewhat above the rated level. Accordingly, switchgear is characterized by the *rated maximum voltage*, $U_{r,max}$, at which the unit remains operable for time spans however long. This voltage exceeds the system voltage rating by 5 to 20%.

Switchgear insulation designed to withstand rated voltages is also subjected to overvoltages due to lightnings and breaker operation transients. Therefore in breaker's tests the insulation is subjected to test voltage levels of power frequency and to impulse voltage levels. Both inner and outer insulation of the unit under test must withstand the standard test ratings.

Rated continuous current is an important characteristic for those installations that pass load currents in normal operation. The relevant Soviet standard stipulates rated current levels as follows: 200, 400, 630, 800, 1000, 1250, 1600, 2000, 2500, 3150, 4000, 5000, 6300, 8000, 10 000, 12 500, 16 000, 20 000, 25 000, and 31 500 A. These current ratings heat the current-carrying elements up to 80-120 °C depending on the current carrying materials and insulation used.

On a short circuit the current through the switchgear may be 10-20 times the rated value. The live elements of the unit are subjected to high thermal and mechanical loads. The appropriate thermal withstand capability of an installation may be given either in terms of the maximum tolerable current I_t (called short-time current

rating or 'thermal rating' on manufacturers' lists) during a specified time period (normally 1 to 5 seconds) or on a per-unit basis in terms of the ratio of this current to the rated continuous current, $n_t = I_t/I_r$. It is worth noting that the admissible temperature under the circumstances varies between 200 and 300 °C depending on the circuit materials and insulation.

The ability to withstand severe mechanical forces of electromagnetic origin, called 'mechanical rating', is expressible in terms of the impulse current that the unit can withstand without deleterious effects preventing its further use. This current may be specified in the form of the peak momentary current rating in kA proportional to the short circuit value $I_{pk} = k_{mw}\sqrt{2}I_{sc}$, or in the form of the ratio of this current to rated circuit $n_{mw} = I_{pk}/I_r\sqrt{2}$.

Units with detachable contacts may be also characterized by their stability at let-through short-circuit currents. It is specified by the currents of mechanical and thermal ratings that the unit can withstand without damage at rated pressing forces in the breaking contacts (completely closed position).

1.5 Requirements of Switchgear Installations

1. *Reliability.* Fault currents can reach values as high as 300 kA. Therefore the fault should be discriminated in as short a time as possible to limit its effects on the neighbouring equipment. Powers absorbed by the plant in this period can be tremendous. For example, with a short circuit current of 80 kA the power dissipated in a 750 kV equipment is $\sqrt{3} \times 80 \times 10^3 \times 750 \times 10^3 = 103\,800$ MVA. If the circuit breaker fails to discriminate the fault in time, it may spread and cause considerable mutilative effects that may result in a prolonged blackout. Large factories and transportation may be de-energized and emergency situations may occur in other industrial and social fields. High voltage switchgear passes high powers and failures in this equipment incur heavy losses.

Reliability analysis for high voltage switchgear is a formidable task as the transient processes involved are rather hard to describe mathematically and avoid sufficiently complete modelling. On the physical side, the reliability is contingent on the materials used and the technological procedures involved in the switchgear manufacture.

2. *Maintenance interval.* Removal of a switchgear from the circuit for maintenance and overhaul entails technological complications and may be a cause of costly faults. Improvements in the switchgear design and technology have enlarged the maintenance interval from the recent period of one year to three years, and vacuum circuit breakers with a maintenance interval of 25 years have been developed.

3. *Ability to withstand high thermal, mechanical, and electrical overloads* should be painfully observed in the design, manufacture, and operation of high voltage switchgear because faults due to overload may incur heavy losses.

4. *Resistance to environmental impacts.* Outdoor installations should be prepared to resist the effects of high humidity, rain, snow, ice, contamination of the external insulation, high windloads, and shocks due to earthquakes.

5. *Suitability for mass production, transportation handling, and convenient*

operation. The mass and size of the equipment should be kept as low as practicable.

In addition each type of switchgear has its own particular requirements. The total break time is an important consideration, because for a 500-kV circuit breaker a reduction of break time by a mere 0.02 s allows the system to pass 250 MW of additional power. Another requirement is concerned with the reduction of relaying errors of the current transformers in protective circuits.

REFERENCES

1.1 A. M. Bronshtein: *Kommutatsionnye apparaty dlya glavnykh tsepey generatorov* (Switchgear for generator busducts). Informelektro, Moscow 1982.

1.2 V. V. Afanasyev: *Sostoyaniye vysokovoltnoy apparatury v SSSR i za rubezhom za period 1970-1975* (High-voltage switchgear of 1970-1975 in the USSR and abroad. Status and perspectives). Informelektro, Moscow, 1977.

2
Insulation of Switchgear

2.1 Rated and Tested Voltage. Coordination Between Inner and Outside Insulation

Reliable operation of switchgear at many hundred kilovolts depends among other things on the correctly designed insulation. In Soviet design establishments it is developed in compliance with the rated voltage or 'voltage class' as it is referred to in the respective documentation. The rated voltage values established in the USSR for a.c. equipment in the range from 3 to 750 kV are listed in Table 2.1. The distribution switchgear for 1150 kV power lines is being developed.

The switchgear insulation commonly comprises an outside insulation where ambient air is the insulating medium, and an inner insulation where the insulating medium is some gaseous, liquid, or solid dielectric, or vacuum. The concept of inner insulation is extended to sealed insulating facilities immersed in a gaseous fluid, say in compressed air, special gas, or vacuum.

Figures 2.1 and 2.2 illustrate the insulating structures of a low-oil content circuit breaker and a current transformer. Breakdown of both inner and outer insulation can occur through the gap between current carrying elements, or between live elements and earthed components, or in the form of flashover over the surface connecting these elements. With reference to these figures, breakdown can occur through gaps labelled l_1 between the primary and secondary of the current transformer and between the open contacts of the breaker. The paths of flashover are labelled l_1', l_2', and l_3'.

Following a breakdown or flashover and the fast discrimination of the fault area from the live parts, the dielectric strength of the outside insulation can recover to the pre-fault level, whereas that of the broken inner insulation (especially solid) cannot. Accordingly the insulation is designed so that overvoltage might cause a breakdown of outer rather than of inner insulation.

Over many years of service (several decades) the insulating structure of a switchgear installation must withstand the maximum operating voltage and the multiple action of instantaneous (within a few milliseconds) overvoltage due to lightnings and switching transients. Therefore the electrical characteristics of switchgear structure should be matched with the insulation level.

The reliable operation of porcelain and glass insulators exposed to maximum operating voltage is ensured at the design stage by the appropriate choice of a parameter called *insulation (creepage) distance*. This is the least distance over the surface of the insulator between the live parts of different potential (excluding the segments of cementitious and like materials). The creepage distance of a composite insulator is taken as the sum of the distances of the series-connected insulating components. The creepage distance of outer insulation is summarised in Table 2.2.

Table 2.1. Rated and Service Voltage of Switchgear (kV, r.m.s.)

Voltage class	Maximum rated voltage	Nominal voltage	Maximum admissible system voltage
3	3.6	3.0	3.5
		3.15	3.5
		3.3	3.6
6	7.2	6.0	6.9
		6.6	7.2
10	12.0	10.0	11.5
		11.0	12.0
15	17.5	13.8	15.2
		15.0	17.5
		15.75	17.5
20	24.0	18.0	19.8
		20.0	23.0
		22.0	24.0
24	26.5	24.0	26.5
27	30.0	27.0	30.0
35	40.5	35.0	40.5
110	126.0	110.0	126.0
150	172.0	150.0	172.0
220	252.0	220.0	252.0
330	363.0	330.0	363.0
500	525.0	500.0	525.0
750	787.0	750.0	787.0

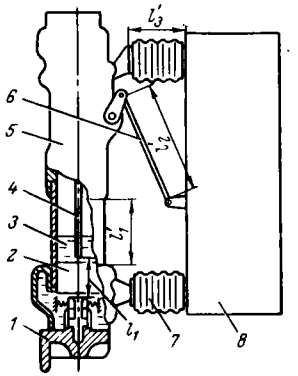

Fig. 2.1. Paths of flashover in a low-oil content circuit breaker. (1) Stationary contact assembly; (2) arc-extinction chamber; (3) oil; (4) movable contact; (5) interrupter; (6) insulated link of operating mechanism; (7) support insulator; (8) frame

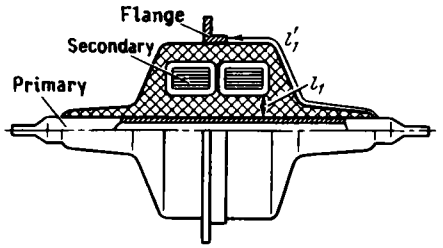

Fig. 2.2. Structural arrangement of a single-turn current transformer

Depending on the value of creepage distance of outer insulation the Soviet-made switchgear is categorised into (A) normal duty, (B) heavy duty, and (C) extremely heavy duty. The values of test voltage correspond to voltage classes of particular switchgear. Both impulse and normal frequency voltage profiles are used for insulation tests. By its action, test voltage of power frequency is taken to be equivalent to multiple internal overvoltages, and an impulse voltage of a specified profile (magnitude, front rise, pulse length) is taken to be equivalent to atmospheric overvoltage.

The standard lightning-simulating voltage waveforms are shaped as a full cycle with a front rise time of 1.2 μs and pulse width of 50 μs (denoted as 1.2/50) and as a complete cycle chopped at a pre-arcing time of 2-3 μs. A complete evaluation of the dielectric strength of switchgear insulation is achieved by testing with switching transient waveforms shaped as aperiodic profiles of 250/2500 μs and as harmonic profiles.

Table 2.2. Creepage Distance for Outside Insulation

Voltage class	Service voltage (kV r.m.s.)	Insulation distance (cm) for duty categories A	B	C
	In insulated-neutral systems			
3	3.6	6	9	12.5
6	7.2	12	18	25.0
10	12.0	20	30	42.0
15	17.5	30	45	62.0
20	24.0	40	62	84.0
35	40.5	70	105	140.0
	In solidly-earthed neutral systems			
110	126	190	280	390
150	172	260	390	535
220	252	380	570	790
330	363	540	800	1120
500	525	800	1180	—
750	787	1180	—	—

Lightning simulating pulses are applied three times in inner insulation tests and fifteen times in gas-insulated switchgear tests. The inner insulation is tested by applying a test voltage during one minute, while the inner and outer insulation between the contacts of gas-insulated circuit breakers is tested by a three-fold application of gradually increased test voltage.

It is beyond doubt that the dielectric strength of insulation must be such that the test voltage causes no damage to the tested equipment. The appropriate insulation level is achieved by choosing marginal factors at the design and development stage of the insulation structure. The r.m.s. value of breakdown voltage in the air, U_{bd}, is assumed to be by 5-10% higher than the test voltage of dry outer insulation, $U_{t,dry}$, for a stated voltage class of power frequency (50 Hz),

$$U_{bd} = (1.05 \text{ to } 1.1)U_{t,dry}$$

For insulators tested separately for breakdown by a gradually increased voltage of power frequency, the breakdown voltage of inner insulation should exceed $U_{t,dry}$ at least 1.2 times where liquid or paper-oil insulation is used, and at least 1.6 times for other insulators.

2.2 Insulation Distances in the Air

Switchgear must have appropriate insulation between live and earthed parts, between live parts of neighbouring poles, and between separated contacts of the same pole. Auxiliary equipment, such as reactors and voltage transformers, must be appropriately isolated between turns and layers.

Designers provide a device with appropriate insulation by selecting the spacing between the live parts under study so that the unit can withstand voltage tests specified by the relevant standard. This selection is facilitated by the experimental curves of spacing versus breakdown voltage of power frequency or pulse-shape, obtained for various shapes of arcing electrodes (point-point, and point to surface) to reflect the nonuniformity of the electric field. Test pulses are applied in various polarity and waveform. Some curves are fitted by empirical expressions so that arc spacing under certain conditions can be obtained analytically.

For test voltage of power frequency, insulation spacings may be derived from available curves, such as the one presented in Fig. 2.3 [2.1, 2.2]. The plots at (*b*) demonstrate that the dielectric strength of large spacings appreciably depends on the field nonuniformity — an important fact that should not be overlooked in the design.

Insulation distances in the air likely to be subjected to lightning overvoltage hazards may be determined from experimental curves plotted with test impulse voltage applied in different polarity to various arc spacings in the air at atmospheric pressure. Figure 2.4*a*, *b* shows the curves derived with full-profile impulse voltage. For large insulation spacings between pin and plane, the plots derived with voltage pulses of different polarity that cause discharge with a probability at least 0.5 are shown in the diagram at (*c*). For point-point spacing geometry, the values of breakdown voltage lie between these curves, and the polarity of test pulses is of less

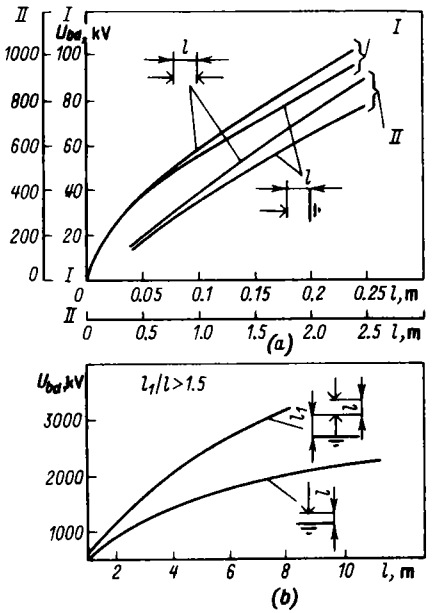

Fig. 2.3. R.m.s. (*a*) and peak (*b*) values of a.c. breakdown voltage for air spacing at 50 Hz

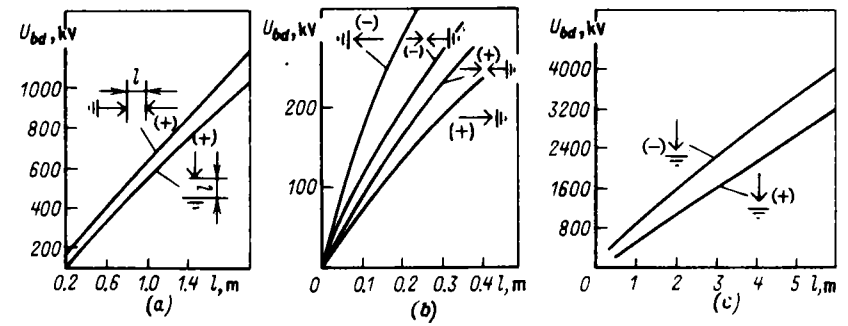

Fig. 2.4. Impulse 0.5-probability breakdown voltage in air for different arc spacings, *l*, electrode geometry (indicated) and polarity of 1.5-μs rise time and 40-μs wide pulses

significance. Designers assume that the value of breakdown voltage is by 5-10% higher than the rated impulse level established by the relevant standard.

Switchgear installations designed to operate at 330 kV and higher voltage levels are subjected to switching-transient pulse tests to derive appropriate air spacings. Voltage levels in these tests are higher than in service voltage tests, while the insulation levels of air spacings are close in both tests. The final spacing is dimensioned

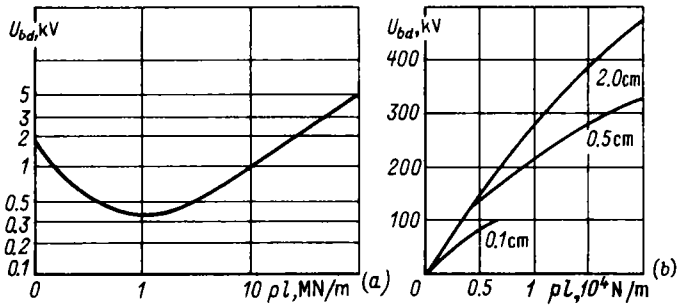

Fig. 2.5. Experimental pressure-spacing dependence of the dielectric strength of air in a uniform field of a.c. voltage (*a*) at low values of *pl* (Paschen's curve) and (*b*) at large values of *pl*

as the largest distance resulted from the tests with service voltage, and lightning and switching transient pulses.

The dielectric strength of a gas spacing is a function of gas pressure. The breakdown voltage increases substantially at high pressures (compressed air or SF_6) and at very low pressures (vacuum) and this phenomenon is harnessed in continuously-pressurized-air, SF_6, and in vacuum circuit breakers. This pressure-spacing dependence of the dielectric strength, known as Paschen's law, is plotted in Fig. 2.5*a*. The law had been first derived as an experimental curve and then explained theoretically on the basis of self-sustained discharge in a uniform electric field. The curve has a minimum (Paschen's minimum) and the rise of strength on its left-hand segment is associated with low pressure on approach to vacuum rather than with smaller arc spacings.

At high pressures, experimental pressure-spacing curves deviate from the classical Paschen's law describing the self-sustained discharge in a uniform electrical field. Experimental curves for various spacings are presented in Fig. 2.5*b*. The deviations are caused by the factors disturbing the field uniformity in the spacing and facilitating a self-sustained discharge. The measures counteracting these factors include purification of the compressed air from particulate matter, raise of air pressure, and improvement of surface finish of the parts that are not affected by the arc.

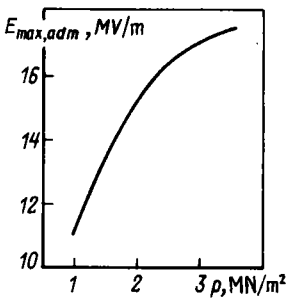

Fig. 2.6. Pressure dependence of the maximum admissible strength of the electric field between pressure-tight air breaker's contacts

Figure 2.6 shows the maximum admissible strength of electric field as a function of air pressure; this plot may be used to design arc spacings for air circuit breakers in the open position.

The discharge in air over the surface of solid dielectric will be further discussed for most popular types of switchgear insulation — molded and porcelain.

2.3 Insulation Level Design for SF_6 Installations

Sulphur hexafluoride (SF_6) gas has been finding ever wider use as an excellent arc-quenching and insulating medium for circuit breakers. Above a pressure of 2.28×10^5 Pa sulphur hexafluoride can be present in all three phases, gaseous, liquid, and solid, depending on temperature. Present day circuit breakers utilize gaseous SF_6, however, some patents describe liquid SF_6 designs.

The dielectric strength of SF_6 gas, like any other gas, is a function of pressure, field inhomogeneity, and material and surface texture of the electrodes. It exhibits a higher sensitivity to local inhomogeneities of the electric field than air does, therefore using this gas as an insulating medium major attention is paid to the factors influencing the uniformity of the electric field.

In the absence of generalized data on insulation spacings in SF_6 gas, one may derive the spacings from the curves of Fig. 2.7 [2.3] showing the breakdown voltage in SF_6 gas as a function of pressure, electrode surface texture, and voltage frequency. These curves have been obtained for a rather uniform electric field provided by the electrode geometry and the walls of the porcelain insulating bottle.

In designing creepage distances over a dielectric one should observe that this material can markedly disturb the homogeneity of the field between the electrodes. Surface charges can be accumulated on the dielectric owing to, say, adsorption of water. The adsorbed water contains free ions of opposite polarities that move in

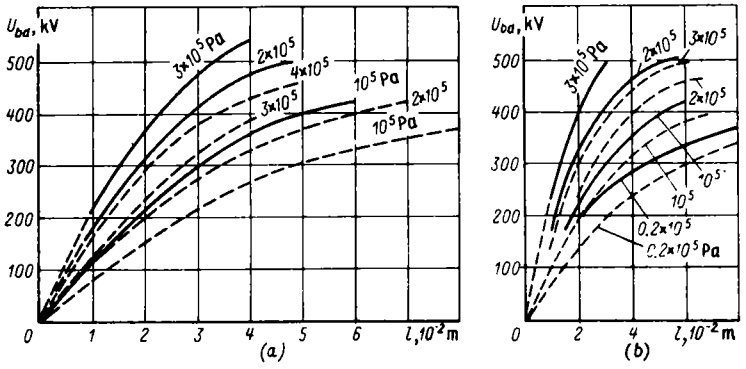

Fig. 2.7. Dependence of breakdown voltage in SF_6 on arc spacing for smooth (solid curves) and fused (dashed curves) electrodes 80 mm in diameter and a 160-mm dia. porcelain insulator (*a*) at a.c. voltage (50 Hz) and (*b*) at impulse voltage

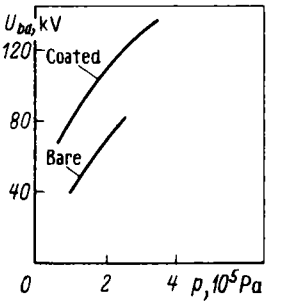

Fig. 2.8. Pressure dependence of a.c. breakdown voltage over the surface of coated and bare 30-mm dia specimens of glass-based laminate insulator for a 40-mm electrode spacing

the electric field and form bulk charges. The resultant field becomes weaker at the mid-spacing, thus depressing the breakdown voltage U_{bd}. Where the contact of electrodes with the dielectric is poor or electrode spacing is very small, the electric field is no longer uniform and U_{bd} may fall to almost half the expected value. The breakdown is preceded by a corona that appears at a substantially lower voltage than the breakdown value.

The highest breakdown voltage can be achieved by making the dielectric piece of the same diameter as the electrode [2.3]. The dependence of breakdown voltage U_{bd} in kV on SF_6 pressure p in N/m^2 and the height of a dielectric sample between the electrodes 0.01 m $< h <$ 0.05 m is described by the empirical formula

$$U_{bd} = 40 + 1.67 \times 10^{-2} ph$$

In insulators of fabric-based laminate, glass-based laminate, or glass reinforced plastics, the electric field directed along the fibres or laminae of the material facilitates the development of discharge. Fluoroplast coating of such dielectrics markedly increases breakdown voltage. This effect is illustrated in Fig. 2.8; the presented curves may be used to estimate U_{bd} and its gradients under unfavourable conditions of absent coating and nonuniform electric field produced by an electrode protruding beyond the dielectric. Under the circumstances the U_{bd} gradient over the surface of glass-based laminate amounts to 1-2 MV/m depending on pressure, whereas under the most favourable conditions it increases up to 4-6 MV/m.

It is instructive to note that with impulse waveforms the breakdown will occur at higher voltage than with power frequency waveforms because of a different time profile of bulk charge formation on the surface of dielectric.

2.4 Insulation Distance in Oil

The dielectric strength of technical grade oil depends on the concentration of impurities and type of the particulate matter because oil-born particles cause local inhomogeneities of the electric field and form particulate chains facilitating the development of discharge. The products of oil contamination by burning arc, by arc interaction with the walls of arc-suppression chamber, and dissolved gases also lower its dielectric strength.

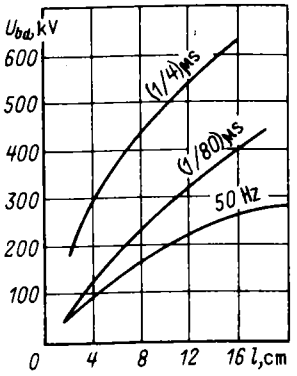

Fig. 2.9. Dielectric strength of transformer oil as a function of arc spacing and voltage waveform (50 Hz a.c. and two pulse forms of 1-μs rise time and 4- and 80-μs width)

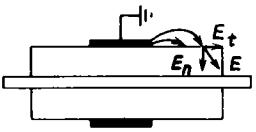

Fig. 2.10. Simulation of a strongly nonuniform electric field

Water is the most frequent contaminant of switchgear oil. Above the maximum solvability at a given temperature water forms emulsions. Coalescence of tiny water droplets into thin water strings at some voltage applied across the spacing causes distortion of electric field uniformity and decreases the insulation level.

Figure 2.9 shows arc spacing in oil as a function of applied voltage and waveform for the point-point contact geometry.

When oil breaks down along a solid insulator, one ought to observe that, similar to discharge in gases, the effect of solid insulation is defined by the position of its surface relative to the field force lines and by the field configuration. In weakly nonuniform fields, the oil-insulator interface parallel to force lines influences U_{bd} only and the breakdown occurs approximately along a force line. For arc spacings under 20 cm breakdown voltage can be reduced by at most 10-15% with power frequency voltage (50 Hz) and by a smaller value with impulse waveforms.

For strongly nonuniform fields having appreciable component normal to the surface of solid isolator (E_n in Fig. 2.10), the arc development pattern is qualitatively the same as in gases. As the voltage increases a corona appears at the sharp edge of the electrode (initial partial discharges), then creeping discharges occur that, when developed over the entire length, cause discharge over the surface of the dielectric. In normal condition of the surface (dry, clean) the creeping discharge voltage, U_c, is mainly controlled by the thickness, d, and relative permittivity ε_r of the solid insulation. For widely accepted solid insulation materials (ε_r = 4.0-4.5) of thickness d (m), empirical formulae have been developed for r.m.s. value of U_c (kV) and length l_c (m) of creeping discharge in oil when subjected to power frequency voltage

$$U_c = 310 d^{0.45}$$
$$l_c = (U_{bd} - U_c)/1280$$

For coaxial cylinder electrodes of radii r_{out} and r_{in} the equivalent thickness of dielectric can be calculated as

$$d_{eq} = r_{out} \ln (r_{out}/r_{in})$$

At $l_c = l$ flashover occurs, therefore $U_{bd} = U_c + 1280\, l$. This expression holds true for $l > 0.05$ m.

2.5 Bushing Insulation

Because of nonuniformity of the electric field the dielectric strength of large spacings in oil is relatively low. This value is usually increased by using coatings and solid insulation of the electrodes, more often than not by layers of craft paper, and by providing barriers of solid dielectrics. This type of insulation is furnished on dead-tank oil circuit breakers where the walls of the tank are insulated by layers of solid dielectric. It is also installed in some low-oil volume circuit breakers, in oil current and voltage transformers, and in bushings for breakers and transformers.

Craft paper insulation is used in the type of bushing shown in Fig. 2.11*a*. The assembly consists of the central current carrying pipe, insulation core that is the basic piece of the internal insulation structure, top porcelain weather casings, a metal flange keeping the top and bottom parts of the bushing together and used to fix the bushing to a breaker or transformer, and a current transformer inside the bushing, a bottom porcelain immersed in oil, and the oil expansion chamber necessary to compensate for the temperature variations of the oil.

The insulation core can be of the oil-barrier type, i.e. consisting of layers of oil and barriers of solid insulation, of the oil-impregnated paper type where the paper is wrapped on the current-carrying part, and of solid insulation type where the insulating barrier is made of varnished paper baked upon shaping to the form. Additional electrodes are installed on the barriers and between the layers to control the electric field.

In the bushing with oil-barrier insulation, the principal insulation is provided by transformer oil separated into layers as its dielectric strength is the highest of all components making up this insulation. Owing to good circulation of oil this type of bushing offers reliable performance and good electric characteristics. Thermal breakdown is practically impossible in this structure. The bushing can be cleaned by replacing contaminated oil. Among the disadvantages of this construction one finds large size and weight.

Bushings with solid insulation offer light weight and small size. The bottom part of the bushing has no porcelain casing and is immersed directly in oil. The disadvantages of these bushings are the need for paper and resins having high dielectric strength. The tolerable level of electric field strength for solid insulation is somewhat lower than for paper-oil insulation. Accordingly, hard insulation bushings are furnished on oil circuit breakers rated up to 35 kV.

Paper-oil-insulated condenser bushings shown in Fig. 2.11*b* have received wide acceptance in oil circuit breakers for 110 kV and higher ratings.

In all aforementioned constructions of insulation core, consecutive layers of insulation are essentially series-connected cylindrical condensers that share the applied voltage in inverse proportion to layer capacitance. Assuming U is the voltage applied across the insulator and n is the number of condensers connected in series gives for the voltage across the ith layer

$$U_i = U/C_i \sum_{i=1}^{n} (1/C_i)$$

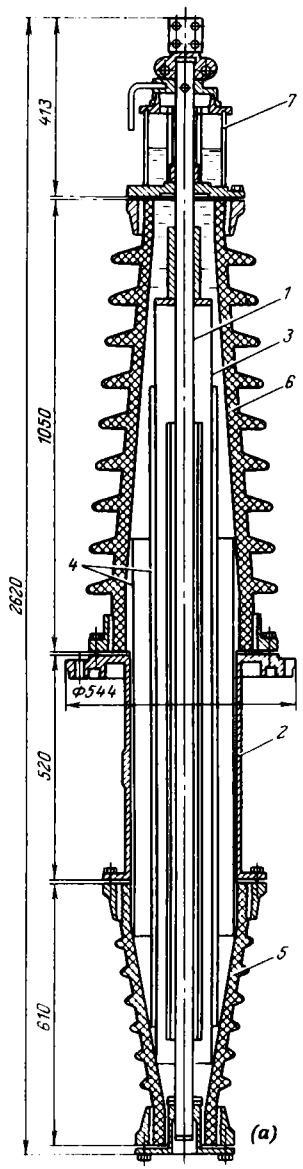

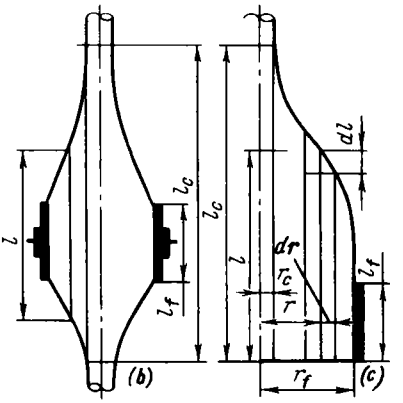

Fig. 2.11. Oil-barrier bushing for 110-kV oil circuit breakers. (*a*) Sectional view: (1) current carrying tube, (2) flange, (3) barrier, (4) additional electrodes, (5) bottom porcelain, (6) top porcelain, (7) transparent glass expansion chamber; (*b*) condenser insulation profile; (*c*) calculation geometry

The capacitance of the cylindrical condenser is defined as

$$C = 2\pi\varepsilon_0\varepsilon_r l_i / \ln (r_i/r_{i-1})$$

where r_{i-1} and r_i are the internal and external radii of the elementary condenser, l_i is the condenser height taken equal to the length of sheeting material (m), $\varepsilon_0 = 8.85 \times 10^{-12}$ F/m is the dielectric constant, and ε_r is the relative permittivity of the medium. Clearly the smaller the capacitance of a layer in the multilayered insulator the higher will be the voltage apportioned to this layer.

A version of the paper-oil bushing, known as *condenser bushing*, has the electrodes of metal foil alternating with sheets of paper in the insulating structure so that the resultant capacitors are about equal. The applied voltage is then equally divided among the partial condensers. The layers of foil are made stepped off to give the desired dielectric gradient: each next partial condenser away from the axis is lower than its preceding counterpart. The profile is illustrated schematically in Fig. 2.11*c*.

The voltage applied to a layer produces a field with radial and axial components. In an incorrectly designed bushing, the radial component can cause breakdown of the insulating layer, and the axial component can cause discharge over the surface of the step between two adjacent condensers.

This type of condenser insulation is widely used in current transformers. The suggested approach to condenser bushing insulation may be carried over to current transformer insulation. Some guidelines on admissible electric field strength in these structures are given below [2.1, 2.2].

It is assumed that the design voltage is 1.1-1.15 the test voltage that the paper-oil insulation tolerates in dry state. The highest admissible electric field strength in the radial direction of the impregnated insulating-paper core structure is taken to be 9-10 MV/m at the design voltage and 3.5-4 MV/m at the service voltage. The admissible field strength in the axial direction is taken to be 8-10 MV/m at the design voltage and 2.5-3.5 MV/m at the service voltage. For solid insulation bushings, the highest admissible field strength at service voltage is 2 MV/m.

The schematic of this calculation is presented in Fig. 2.11*c*. The potential difference across the elementary condenser is

$$dU = -E_r dr = E_a dl$$

where E_r is the radial field strength, E_a the axial field strength, dr the radial thickness of elementary condenser insulation, and dl the length of insulation step.

Capacitors of constant radial component E_r are not used since this may lead to large E_a. In addition, the admissible value of E_a is much less than E_r. Therefore the used insulation has constant axial component E_a where

$$E_a = -E_r dr/dl$$

This condition leads to the dependence between the length of a capacitor l and radius r, namely,

$$l^2 = l_c^2 - (l_c^2 - l_f^2)(\ln r - \ln r_c)/(\ln r_f - \ln r_c)$$

where the subscripts c and f refer to the elements connected with the current carry-

ing bar and flange. The axial field strength

$$E_a = U/(l_c - l_f)$$

The radial field strength in the general form is defined as

$$E_{r,i} = U/\left[r_i\varepsilon_{r,i}\left(\frac{\ln(r_2/r_1)}{\varepsilon_{r,1}} + \ldots + \frac{\ln(r_n/r_{n-1})}{\varepsilon_{r,n}}\right)\right]$$

where $E_{r,i}$ is the field strength in the ith layer, U is the voltage between the electrodes, $\varepsilon_{r,i}$ is the relative permittivity of layer i, and r_i is the radius of the ith concentric cylinder generating concentric layers.

For condenser insulation this expression takes the form

$$E_{r,i} = U/r_i[\ln(r_2/r_1) + \ldots + \ln(r_n/r_{n-1})]$$

Observing the dependence between r and l yields the expression for the radial field strength

$$E_r = U(l_c + l_f)/2rl \ln(r_f/r_c)$$

This formula suggests that the highest values of field strength are achievable where the product rl is at a minimum, that is in the outer layers, whereas in mid-layers the insulation is subjected to lower field intensities.

There exists a ratio of $r_f/r_c = 3.6$ that minimizes the maximum radial field strength, but in order to attain the least volume of insulation this ratio is taken equal to 4.1. Now, the radius of the sheet connected with the flange can be determined as

$$r_f = 1.8U_{des}/E_{r,max}$$

where $U_{des} = (1.1\text{-}1.15)U_{dry}$.

Care should be taken to see that no creeping discharge occurs along the surface of bushing insulation and to prevent ionization phenomena inside the bushing. For paper-oil insulation, the creeping discharge voltage $U_{cr,i} = 396\sqrt{r_i \ln(r_i/r_{i-1})}$ must exceed the voltage applied to this particular layer U_i.

2.6 Solid Insulation Materials and Procedures

Solid insulating materials for high-voltage switchgear include
high-polymer organic dielectrics: rigid PVC, fluoroplastic, acrylic plastics;
insulation grade craft paper, cardboard and fibre;
laminated insulation plastics: paper-, fabric-, or glass-cloth based laminate;
cast and impregnating compounds: bituminous and epoxy-polyesters;
electroceramics: porcelain, steatite, cordierite.

These materials are used to make insulation enclosures, arc-extinction chambers, panels, barriers, and links. The manufactured components should exhibit high electrical and mechanical strength, remain operable in a wide range of temperatures, withstand impacts of chemicals, high temperature, electric arc and some other specific conditions. Principal physical characteristics of these materials are summarized in Table 2.3.

Table 2.3. Physical Characteristics of Solid Dielectrics

Material	Density, kg/m^3	Ultimate strength, MN/m^2			Plastic yield temp, °C	Thermal conductivity, W/m K	Resistivity, Ω m	Rel. permittivity, at 50 Hz	Loss tangent at 50 Hz	Electric strength, MV/mm
		tension	compression	bending						
Rigid PVC	1350-1400	40-60	90-150	150-180	65-75	0.18	10^{10}-10^{11}	3.2-4.0	0.01-0.05	15-30
Fluoroplastic	2100-2180	30-40	80-150	60-80	70-75	0.06-0.08	10^{14}-10^{16}	2.8-3.0	0.01-0.015	13-20
Acrylic plastic	1180-1200	45-55	70-85	60-65	50-80	0.17	10^{11}-10^{12}	3.5-3.9	0.02-0.06	20-40
Fibreboard	1100-1200	7-8	25	9-11	—	1.1-1.4	10^{10}	—	—	3.5-7.5
Synthetic-resin bonded laminate	1280-1450	60-80	130	80-100	150	0.17	10^{8}-10^{11}	6-8	0.04-0.18	12-38
Fabric-based laminate	1300-1450	35-90	130-150	70-140	135-150	0.15-0.17	10^{7}-10^{10}	5-7	0.06-0.19	3-16
Glass-cloth-based laminate	1600-1800	70-200	250-360	95-240	185	0.18	10^{8}-10^{12}	6-8	0.02-0.05	10-22
Impregnated hardwood	1300-1400	140-260	155-185	180-280	140-180	0.16	10^{8}-10^{10}	7-8	0.06-0.3	5-9
Bakelite	1050-1100	—	40-50	80-95	—	0.12-0.25	10^{8}-10^{10}	—	0.02-0.03	8-16
Impregnating epoxy compound	1220	55	—	120	65	—	—	—	—	18
Thermo-setting casting epoxy compounds	—	70	—	—	—	—	10^{14}	4-5	0.012	20
Porcelain	2200-2300	30-54	100-250	60-100	—	1-1.5	7×10^{11}-4×10^{12}	6-7.2	0.015-0.03	28-38
Steatite	3000	60-70	—	170-190	—	—	10^{13}-10^{14}	6.5-7	0.001-0.003	40-42
Kordierite	2800	—	—	70-88	—	—	10^{9}-10^{11}	5-6	—	4.5-6

Rigid PVC is a synthetic material based on polyvinylchloride. It is a thermoplastic material and shows good weldability and liability to mechanical treatment. On the other hand, it is resistant to chemically aggressive media, active solvents, and oils. It is resistant to fire, the decomposition temperature lies in the range 150-160 °C. When exposed to electric arc, it evolves gases that aid in arc extinction.

Fluoroplastic may be allowed to operate at higher temperatures — it remains stable in the range from −180 °C to 190 °C, is inflammable and resistant to chemicals.

Acrylic plastic is resistant to mineral oil, petrol, and alkalis. It softens at 80-120 °C, decomposes at 250-300 °C, and generates gases when subjected to electric arc.

Fibre is produced by pressing together sheets of paper impregnated by zinc chloride. It is suitable for all kinds of mechanical treatment and pressing and lends itself to form after softening in hot water. Tendency to gas generation is also evident.

Laminated insulation plastics are prepared on the base of special sorts of impregnation paper, cotton and glass fabrics, and delta-wood. Binders are bakelite or organo-silicon resins that are cured by hot pressing into nonmelting and unsolvable state.

The working temperature intervals are from −45 °C to 90 °C for delta-wood, −60° to 105 °C for paper and cotton fabric materials, −60° to 155 °C for bakelite-bound glass-fabric materials, and −60° to 180 °C for organo-silicon-bound glass-fabric materials.

Electroceramic materials are obtained by burning clay with additions of quartz, and feldspar (electric-grade porcelain), or talcum and barium carbonate or calcium carbonate (steatite), or talcum and synthetic corundum (kordierite). Electric ceramics exhibit high resistance to atmospheric impacts and hydrophobic properties. Kordierite absorbs water in noticeable quantities, but exhibits high arc puncture.

Epoxy-resin compounds used for case insulation of circuit breakers, cable features, and bushings may be broadly classed into impregnating and casting materials. Impregnating compounds as the name implies are used to impregnate transformers with the aim of improving the electrical and mechanical strength of the interlayer and turn insulation and enhancement of heat removal by eliminating air inclusions, reducing water absorption, and rendering the structure more uniform and solid.

An impregnation procedure presupposes, of course, some preliminary operations of drying, including vacuum drying, vacuum treatment of resin, the final impregnation being carried out under a moderate or high vacuum. The time taken to perform the compounding process and the use of vacuum impose a number of requirements on the compound composition, namely, it should take more time to gelate at the impregnation temperature as compared with the cast compounds and exhibit a low vapour density of hardening substance to maintain the desired vacuum during the impregnation process.

The principal requirements to impregnating compound are high dielectric characteristics, low viscosity at process temperature, high impregnating ability, absence of solvents in the compound, good adhesion to wire and cast compound, because frequently impregnation is followed by casting of another compound to form a solid insulating structure.

Casting compound should fill a form freely, exhibit low viscosity in casting. The components of compound should be consistent and compatible in mixing. The polymerization temperature should be within 120-150 °C. Compound should possess only a low shrinking. The linear expansion coefficient should be as close as possible to those for the materials in contact. High and stable dielectric characteristics, mechanical strength, low water absorption, high temperature resistance and chemical resistance are also required.

The aforementioned list of requirements to impregnating and casting compounds favoured the choice of materials based on epoxy-dian resins that harden after pouring of or impregnation by hardeners (anhydrides of dicarbonic acids). Filling materials in cast compounds are silicates, carbonates, oxides, and hydroxides of metals, and sulphates. The most popular filling material is finely ground quartz sand.

The dielectric strength of cast insulation is viewed in two aspects, namely, as the strength under short period of high-voltage impact and the strength in continuous service. The mechanism of breakdown at transient voltage phenomena includes two stages, the initial stage when the dielectric suffers a partial destruction due to incomplete breakdown in areas of the maximally inhomogeneous electric field (sharp edges, thin wires, etc.) and the final stage due to thermal and mechanical destruction.

Thermal destruction occurs as a result of high pre-arcing current or as a result of temperature rise associated with partial breakdown or discharges. Temperature difference gives rise to thermoelastic stresses that cause mechanical destruction of insulation.

The dielectric resistance of cast insulation subjected to short-time currents reduces appreciably with the growth of insulation thickness and volume of compound, but increases with the content of filling material. Its temperature dependence is rather weak up to 120 °C but shows a sharp fall above this point.

When subjected to continuous overvoltage, the breakdown mechanism of cast insulation is controlled by the accumulation of mechanical and electrical micro- and macro-fractures and development of defects under the action of partial discharges.

Ageing processes begin in local areas of highest electric field strength arising between the electrodes of small curvature radii, where pores, gas inclusions, clusters of filler, fissures, etc. are involved. These processes are accompanied by the formation of tree-like traces that proliferate over the areas of weakened structure.

Thus, the dielectric strength of epoxy resin insulation is controlled by the engineering features and by the technology of insulation making. Under the circumstances, the admissible values of electric field strength recommended for design of insulating structures are far lower than the tolerable maximum levels of 15-20 MV/m achievable in uniform electric fields.

The thickness of main insulation, that must be at least 4 mm from mechanical strength considerations, should be determined on the basis of the heavy and moderate duty strength of electric field in the epoxy-resin insulation. The maximum strength must not exceed 8 MV/m, and the mean strength should be 2.4 MV/m for

transformer windings heated up to 105 °C and 1.8 MV/m for those heated up to 130 °C.

In analytical investigations of flashover the maximum field strength on the surface at rated voltage should be taken up to 0.11 MV/m. The average field strength over the surface should be at most 0.05 MV/m. These values are also substantially below the field strength of experimental flashover for nonuniform fields observed at 1.4-1.5 MV/m.

2.7 Porcelain Insulators. Dielectric and Mechanical Strength Considerations

Porcelain is widely accepted for manufacturing a variety of high-voltage switchgear insulating features such as supporting and enveloping insulators, weather casings, rods, and links. The dielectric strength of porcelain is rather high, but its mechanical strength, especially tensile and bending strength, is rather low (see Table 2.3). Besides the dielectric strength, therefore, adequate consideration should be given to the mechanical strength of porcelain insulating parts in view of unfavourable mechanical loads that may be met in service.

For standard specimens of porcelain subjected to system test voltage (50 Hz) at 20 °C, the dielectric strength lies between 28 and 35 MV/m. It decreases markedly for greater thickness of porcelain and for higher temperatures, the effect being especially pronounced above 125-130 °C. Figure 2.12 demonstrates how the porcelain's dielectric strength varies with thickness for two grades of porcelain.

For a.c. insulators of annular cross section the minimum dielectric strength (MV/m) may be estimated by the empirical formula

$$E_{\mathrm{bd,min}} = 6.5 + 0.195/\sqrt{d}$$

where d is the insulator thickness in m. The impulse insulation level is about twice this value.

The voltage of breakdown over the surface of a porcelain insulator depends on the specific surface capacitance that is a function of the geometry of electrodes, layout of electrodes with respect to the surface, electrode spacing, and the shape and dimensions of the edges. The time period and profile of the applied voltage

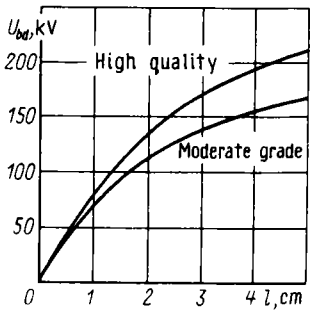

Fig. 2.12. Dielectric strength of porcelain insulators as a function of wall thickness for two grades of porcelain

as well as surface status (surface defects, water and contaminations tend to reduce flashover voltage) also affect the level of breakdown. This long list of factors influencing the process of surface discharge forces the designers to turn to empirical formulae derived for specific types of isolators. By way of example, for insulating rods widely used in switchgear, given the flashover distance l_{dry} in metres for a dry surface one may determine the insulation level in kV by the expression $U_{dry} = 24 + 378\, l_{dry}$. For rainy weather the insulation level of these insulators may be estimated with the formula $U_{rain} = 296\, l_{dry}$. The test impulse voltage (kV) may be estimated with the expression $U_p = 670\, l_{dry}$ related to the positive polarity pulse which causes lower values of breakdown voltage than the negative pulse.

For air and transformer oil, the levels of breakdown voltage for various electrode geometries may be estimated by the empirical expression $U_{bd} = kl^{\beta}$ with the values for k and β from Table 2.4.

The flashover distances calculated for Soviet-made outdoor insulators must be consistent with the values recommended by the relevant Soviet Standard (see Table 2.2).

Like any other insulating structure of solid dielectric, porcelain isolators are subjected in service to compression, tension, bending, twisting and combinations of these loads. The mechanical strength of supporting insulators is usually analysed for the case of a bending moment, bending and twisting moments or longitudinal

Table 2.4. Coefficients k and β

Electrodes in dielectric medium	f*	Arc spacing, m	k	β
a. Medium: *ambient air*				
(1) sphere to 1-m dia.	50 Hz	0.05-0.5	1350	0.85
earthed sphere	−p	0.05-0.5	1900	0.85
(2) rod to earthed rod	50 Hz	0.02-0.2	260	0.70
	50 Hz	0.2-2.5	390	0.97
	+p	0.02-0.2	400	0.62
	−p	0.2-2.5	640	0.85
(3) rod to earthed plane	50 Hz	0.2-2.5	350	0.9
	+p	0.2-2.5	540	0.92
b. Medium: *transformer oil*				
(1) rod to earthed rod	50 Hz	0.01-0.1	760	0.74
	50 Hz	0.1-0.5	660	0.68
	+p	0.01-0.1	1910	0.80
	+p	0.1-0.5	1390	0.64
(2) rod to earthed plane	50 Hz	0.01-0.1	760	0.86
	50 Hz	0.1-1.0	500	0.65
	+p	0.02-0.08	3300	1.1
	+p	0.08-1.2	1070	0.64

* The symbols +p and −p indicate positive and negative polarity pulses of 1.2 μs rise time and 50 μs pulse width.

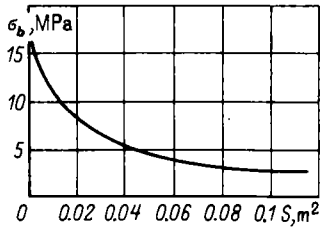

Fig. 2.13. Bending strength versus cross section of porcelain insulators

forces applied to the insulator and causing shear stresses where the porcelain is attached to the flanges. For concentric insulators, bending stresses are more typical.

A strength analysis consists in the evaluation of bending, shear or crushing stresses and comparing the calculated values with the admissible levels for the given material. It is instructive to note that the mechanical strength of brittle materials like porcelain depends on the load profile, the values for dynamic loading being only fractions of the static loading figures. An increase of porcelain thickness above certain values gives no significant enhancement of structural strength as can be seen from Fig. 2.13.

The supporting insulators for indoor service may be subdivided in accordance with their construction into four groups, namely, with external fixture of the top cap and bottom flange, with the internal fixture of the cap and flange, with the internal fixture of the cap and external fixture of the flange, and with mechanical fixture of the cap and flange inside the porcelain.

In insulators of the first group, the cap and flange are connected with the porcelain body by means of a portland cement-sand bond, the seam thickness being at least 2 mm. The isolator is a paraboloid of revolution on the outside, therefore any section of the body offers equal resistance to bending. The porcelain body has annular cross-section and a spherical top.

In insulators with the internal fixture of the cap and flange, the cast iron inserts are cemented in recesses by portland cement-sand bond. Bending stresses are taken up mainly by the porcelain element between the recesses that experiences mainly compressive forces.

Resistance to bending improves considerably (from 5-10 to 24-29 MN/m^2) in insulators with the combined fixture of the elements.

In insulators with mechanical fixture of elements, the inserts are prevented from longitudinal motion by means of coil springs nested in annular recesses in the porcelain body.

For insulators with the external fixture of elements, the mechanical analysis consists in evaluation of stresses arising in bending the porcelain body, σ_b, and crushing stresses, σ_c, in the cement bond arising under bending moment M_b, or in evaluation of shear stress τ_{sh} under the action of tensile forces applied to the insulator.

The bending stress is determined as

$$\sigma_b = M_b / W$$

where W is the moment of resistance in the section under study, m^3, which takes

the form

$$W = \pi D^3/32 \approx 0.1D^3$$

for circular cross-sections, and

$$W \approx 0.1(D^4 - d^4)/D$$

for annular cross-sections.

The crushing stress of the cementitious bond can be obtained as

$$\sigma_c = 3M_b'/h^2D$$

where M_b' is the bending moment about the upper edge of the bond (N m), h is the height of the bond (m), and D is the bond diameter (m). Admissible compression stresses for portland cement-sand bonds lie in the range 40-60 MPa.

The shear stress may be found by the formula

$$\tau_{sh} = F/\pi Dh$$

where F is the tensile stress (N). The ultimate shear stress for portland cement-sand bonds amounts to 7 MPa.

REFERENCES

2.1 *Elektrotekhnicheskii spravochnik* (Electrotechnical handbook). Vols. 1-2, 7th ed. Energoizdat, Moscow 1985-86.

2.2 M. I. Sysoyev and V. V. Yakovlev: Elektrotekhnika No. 3, 59-61 (1970).

2.3 D. V. Razevig (ed.): *Tekhnika vysokikh napryazhenii* (High voltage switchgear). Energiya, Moscow 1976.

2.4 A. I. Poltev: *Konstruktsiya i raschet elegasovykh apparatov vysokogo napryazheniya* (SF_6-insulated HV switchgear. Analysis and design). Energiya, Leningrad 1979.

3

HIGH VOLTAGE A.C. CIRCUIT BREAKERS. GENERAL REQUIREMENTS

3.1 Interrupting Rating

The interrupting ability of a circuit breaker is stipulated as the periodic component of the short-circuit current (r.m.s.) that exists at the instant the breaker contacts open. The opening stroke should be effected under the following conditions:

(1) at the stipulated content of aperiodic component;

(2) with the duty cycles as indicated by the standard for high voltage switchgear tests (Section 3.2);

(3) at the maximum rated system voltage; and

(4) under the conditions of voltage recovery as stipulated by the standard (Section 3.3).

The oscilloscopic trace of short-circuit current observed in interrupting the circuit is indicated in Fig. 3.1. The interrupting current is determined at the instant the breaker contacts open. From the oscilloscope screen, the periodic component of breaking current can be measured as

$$I_{b,p} = AA' \, m_i/2\sqrt{2}$$

and the aperiodic component as

$$I_{b,a} = OB' \, m_i$$

where m_i is the current scaling factor (A/mm), AA' is the vertical spacing between the enveloping curves $C'A'$ and CA, and OB' is the ordinate of the mid-point locus of the two envelopes.

The content of aperiodic component in breaking current is described by its ratio to the rated braking current $\beta = I_{b,a}/I_{b,r}\sqrt{2}$ and the admissible value can be deter-

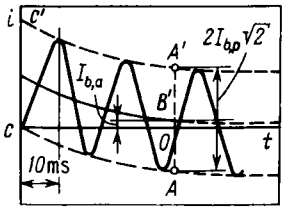

Fig. 3.1. Oscillogram of a short-circuit current

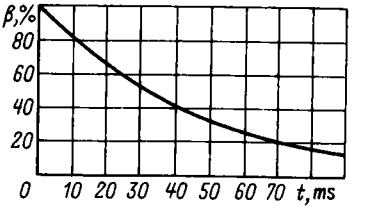

Fig. 3.2. Standardised percentage of the aperiodic component

mined from the curve in Fig. 3.2 where β is plotted with respect to the total break time equal to the breaker operating time plus 0.01 s for protective gear tripping. The time constant of this curve is taken equal to 0.05 s.

Another useful rating is the *interrupting capacity* $P_b = \sqrt{3}\, I_{b,r}\, U_{r,max}$. As a rule the power released in the burning arc $U_a \times 3I_{b,r} \ll P_b$. When the arc is extinguished and the process of voltage recovery is under way, the breaker appears at high voltage while the current through the breaker is practically zero so that the breaking power P_b is never released in the breaker proper. The interrupting capacity is essentially the total power, mainly reactive, that the rotating machinery connected to the system at the time of short circuit can pass through the breaker. The higher the power of this machinery, the greater the current $I_{b,r}$ and the greater must be the interrupting capacity of the breaker.

A circuit breaker must interrupt rated currents many times without periodic checks, the number of shots increasing with rated current from 6 interruptions at heavy currents to 16 at small currents.

3.2 Duty Cycles

Most faults in networks are due to transient phenomena. By way of example assume that a lightning overvoltage has caused flashover of outer insulation and following the current impulse the flashover path carries continuous system current. If the fault circuit is disconnected to allow the dielectric strength of the insulation to be restored with the aid of wind or air thermal motion currents, then the subsequent reclosing restores the normal operation of the system.

Fault statistics indicates that lightning or other transitory faults amount to 80% of the total number of faults. Therefore, reclosing devices considerably improve system reliability and efficiency. Situations should not be overlooked, however, when the fault remains after circuit breaking. The circuit breaker, therefore, must be provided with a capability of repeated clearing of a short-circuit fault.

The duty cycles of an automatic recloser are stipulated by the respective standard. The Soviet standard recommends that the duty cycles of opening (O) and closing (C) the circuit after a zero-current dead time t_d be as follows when operated at rated current

$$\text{(1) O} - t_d - \text{CO} - 180\ \text{s} - \text{CO}$$

or for ratings below 220 kV with a 20-s pause

$$\text{(1a) O} - t_d - \text{CO} - 20\ \text{s} - \text{CO}$$

The zero-current delay t_d extends from the instant of arc extinguishing after the first interruption to the instant a current appears after the following reclosure. The delay (reclaim) time t_d depends on the type of breaker and varies in the range from 0.3 to 1.2 s. For a fast reclosure device this time period equals 0.3 s.

Circuit breakers not intended for reclosing operations should be tested with the sequence

$$\text{(2) O} - 180\ \text{s} - \text{CO} - 180\ \text{s} - \text{CO}$$

3.3 Rate of Rise of Recovery Voltage

The rate of rise of the recovery voltage in switching transients is also standardized. In describing the transient voltage behaviour the voltage curve is replaced by tangents to this curve as illustrated in Fig. 3.3. The tangent *OB* is drawn from the origin, and the tangent *BC* touching the first peak is drawn parallel to the time axis.

At the circuit breaker installation, the rate of rise of the recovery voltage curve should be within the stipulated *OBC* envelope and have only one crossing point in common with the lag line. It is worth noting that to test marginal behaviour of the breaker the test recovery voltage is made to run somewhat above the curve given by the standard. For special applications, the recovery voltage curve may be adjusted in agreement with the customer's requirements. For ratings up to and equal to 35 kV, the rate of rise of the recovery voltage is given by two parameters, namely, the system peak value U_s and the rise time to this value t_3. The peak value is defined by the equation

$$U_s = k_p k_a \sqrt{2/3}\, U_r$$

where k_a is the amplitude coefficient and k_p is a coefficient accounting for increased voltage U_s that occurs in the 3-phase system pole disconnected first. For ratings up to 35 kV, $k_p = 1.5$, and for ratings of 110 kV and above, $k_p = 1.3$.

The variation of k_a and t_3 with the fractional breaking current is as follows

	$I_{b,r}$	$0.6I_{b,r}$	$0.3I_{b,r}$
t_3	t_3	$(3/7)t_3$	$(3/14)t_3$
k_a	1.4	1.5	1.5

The rise-time variation of the system recovery voltage with voltage rating at the same breaking current is given by the table below

U_r, kV	6	10	15	20	35
t_3, μs	35	51	60	75	90

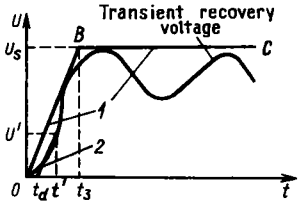

Fig. 3.3. Transient recovery voltage is standardised by specifying (1) enveloping tangent lines, and (2) delay line

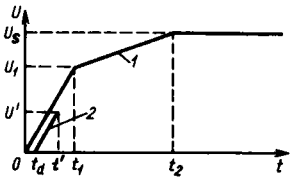

Fig. 3.4. Four-parameter envelope of transient recovery voltage (1) and delay line (2)

It will be noted, however, that as breaking current decreases so does t_3. The point is that high short circuit currents occur as a result of feeding the fault location through long lines of wave resistance about 450 ohms. These lines damp the rate of voltage recovery. Small currents ($0.3I_{b,r}$) arise after the transformer and the transient recovery voltage is formed by the parameters of this transformer. As a result, the rate of rise of the recovery voltage increases 6-7 fold.

The lag line in Fig. 3.3 is parallel to *OB* and its parameters are given as $t_d = 0.15t_3$ and $U' = U_s/3$. On the breaker terminals there is always some stray capacitance in the form of busbar capacitance, measurement gear capacitance, etc. This capacitance aids in depressing the rate of rise of the recovery voltage on the early segment of the transient curve.

For ratings of 110 kV and above the stipulated characteristics of transient recovery voltage are determined (Fig. 3.4) by four parameters U_1, t_1, and U_s, t_2 [3.1].

3.4 Circuit Breaker Stability at Let-Through Short-Circuit Currents

A closed circuit breaker must withstand let-through short-circuit currents for stated time periods. Circuit breakers rated for up to 220 kV should withstand heating by the thermal withstand current $I_{tw} \geqslant I_{b,r}$ for 1 to 3 seconds, and designs rated for 330 kV and above should carry this 'short-time current' for one or two seconds. The short-time peak current of *mechanical withstand capability* is specified as $I_{pk} = 1.8\sqrt{2}\, I_{b,r}$.

The *rated making current* is a short-circuit current on which the circuit breaker can close without damage preventing its further use. For the r.m.s. value of this current $I_{m,r}$ taken over one cycle after the short circuit incipience, and peak value $I_{m,max}$ the following inequalities must hold

$$I_{m,r} \geqslant I_{b,r} \text{ and } I_{m,r,max} \geqslant 1.8\sqrt{2}\, I_{b,r}$$

In testing with this current rating, the closing operation should be effected at 85-105% rated pressure in the pneumatic drive and 85-110% rated release-coil voltage of the electromagnetic driving mechanism.

The breaker current-carrying circuit and contacts should also be tested for mechanical stability with the current $I_{m,r,max}$.

3.5 Operating Time

The *total break time* t_b of a circuit breaker is counted from the instant the control signal is given to the tripping coil to the instant of arc extinction in all the three poles. In breakers for heavy interrupting ratings of 80-100 kA with two-step breaking aided by shunting resistors, the total break time results as the sum of main-contact opening time and arcing (arc extinction) time.

For ratings up to 330 kV where fast interruption of short circuit faults is essential, the total break time t_b should not exceed 40 ms; for 110-220 kV ratings, t_b = 40-80 ms; and for installations under 20 kV, t_b = 100-200 ms.

The *total make time t* is measured from the instant a signal is ussued to the switching electromagnet to the instant the high-voltage circuit is closed in all three phases. In circuit breakers with shunting resistors, the time of closing the resistor circuit and the make time of the main contacts may be stipulated.

3.6 Reliability

The circuit breaker is the most complicated and significant unit of a switchgear set and its reliability determines the reliability of the entire power distribution system.

Failures that prevent further use of a circuit breaker include situations when the unit fails to function on arrival of control signals for closing (C) or opening (O), flashover of breaker insulation, damage of current-carrying circuit disabling current passage, and malfunctions in the arc extinction device.

Some standards also stipulate types of deficiencies that do not interfere with the normal operation of the circuit breaker and can be eliminated during periodic maintenance.

Reliability assessment does not take into account failures and deficiencies that result from incorrect utilization of the breaker.

Quantitatively the reliability of a circuit breaker may be expressed in terms of the probability of fail-free operation or, more frequently, in terms of failure rate, i.e. the number of failures per unit time. Reliability assessment of breakers is commonly achieved by gathering statistical data on the performance of one type of breaker. Analysis of breaker statistics indicates that 70% of failures is due to damage of driving mechanisms, 10% is accounted for breakdown of insulation, and 20% is caused by other factors [3.2]. Accordingly, the major attention in breaker design, manufacturing, testing, and operation should be drawn to the performance of the driving mechanism.

In the Soviet Union mechanical reliability tests are carried out according to Soviet Standard GOST 687-78 [3.1]. Circuit breakers in ratings of up to 35 kV with interrupting capability of 12.5-80 kA should withstand 2000 C-O mechanical operations without current in the circuit. Circuit breakers with higher interrupting ability or for voltage of 110 kV and above should withstand 1000 C-O mechanical operations.

Life tests are run with 2000-4000 shots per test series. A strictly limited number of failures is allowed after 1000 or 2000 shots. Manufacturers outside the Soviet Union warrant 5000 to 10 000 C-O operations between maintenance intervals, that is, the period after which main contacts of other parts subject to wear and tear would have to be replaced.

An analysis of failure rate of 6000 identically rated air circuit breakers for ten years has established that the mean annual failure rate for these units does not exceed 0.01, i.e. only one in hundred breakers may fail after a year of service [3.2].

Present day developments tend to reduce this figure by a factor of 0.2. Figure 3.5 shows percent failure rate n for Brown Boveri type DLF air-blast circuit breakers manufactured for a number of years. As the design and technology have been im-

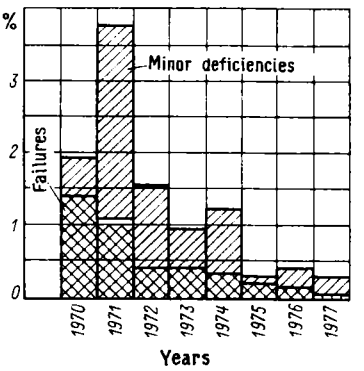

Fig. 3.5. Percent failure rate (crosshatched) of air circuit breakers in the seventies

proved over the years, the failure rate is seen to fall down to a level of 0.0003 for the 1977 make.

It should be noted that gathering testing statistics for circuit breakers in the way it is commonly done for relays, contactors and other gear is rather hard to do owing to insignificant number of breakers manufactured (tens to hundreds) especially for 110 kV and higher ratings. Reliability assessment of novel designs or breakers with different parameters is extremely difficult. If a new make uses elements of existing structures, then reliability assessment may involve available failure rates for these elements [3.2].

In new developments, the key assemblies and elements are subjected to reliability tests. Limited number of tested assemblies is compensated for by ample tests. Life tests of the operating mechanism are carried out with a new unit ready for use. The number of mechanical operations reaches 10 000 and mechanical tests are alternated with heating tests, cooling tests, and other environmental impacts adapting the test conditions to those of actual operation.

3.7 Circuit Breaker Testing

In the Soviet Union, circuit breakers must be tested in agreement with standard GOST 687-78. A high voltage circuit breaker is tested for its mechanical operation, dielectric strength of insulation, thermal stability under rated current heating, short-time stability at short-circuit current, interrupting capability, stability to the action of environmental factors, and mechanical reliability.

Of the long testing programme we consider only testing of interrupting capability because this rating is the major functional characteristic of a circuit breaker. These tests are important also because they involve special and at times unique equipment.

As mentioned above, circuit breakers interrupt considerable currents. Assuming that the breaker under test is rated for interrupting ability of 63 kA at a rated voltage of 750 kV implies that a power source for this test should generate

$$P = \sqrt{3}\, U_r I_{b,r}$$
$$= \sqrt{3} \times 750 \times 10^3 \times 63 \times 10^3 = 81\ 742\ \text{MVA}$$

Powers of this range can be generated only where a few generating systems are united into a single-grid. Rated breaking currents of generator circuit breakers may reach 200 kA and above. The testing of modern circuit breakers is a complicated engineering challenge.

Appropriate power levels for breaking capacity tests can be obtained from (1) power systems, (2) special generating units, (3) oscillatory circuit of A. Gorev, and (4) synthetic test circuits.

Power systems are rarely used for switchgear testing because interrupting duty cycle means severe stresses for system's equipment and may result in breaking of power transformers, burning of nondetachable contacts, and impairing reliability of power supply.

Testing with purposely designed generators is a more convenient means for the development of breadboards of arc extinguishing devices and circuit breakers. A simplified layout of switchgear test station is shown in Fig. 3.6. The plant is a synchronous generator designed with (1) low transient reactance (2-4%), (2) high thermal and mechanical ratings of the windings, and (3) large inertia torque of the rotor.

The low transient reactance of the stator allows for heavy short-circuit currents. By way of example, a TI-100 Soviet made generator provides 100 MW of rated power at U_r = 13.8 kV and I_r = 5780 A. In testing, this generator can give up to 118 kA of short-time current. The equivalent three-phase power attains 2500 MVA. Heavy currents in the stator give rise to considerable mechanical stresses in the front parts of generator windings. Heavy currents in generator circuits are rated operating mode for this equipment — generators can operate for decades without maintenance or repair withstanding up to 15 short circuit tests a day. Therefore

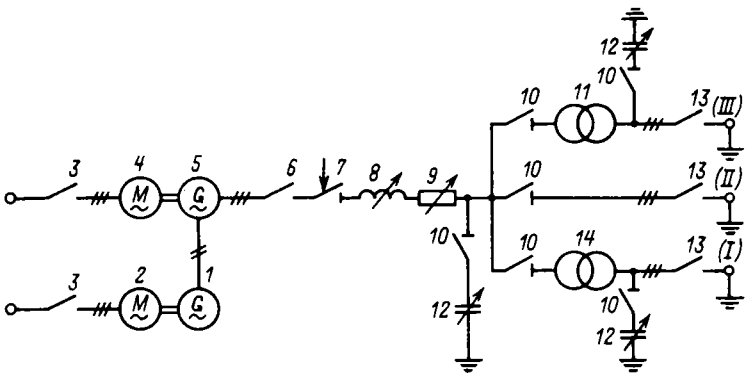

Fig. 3.6. Schematic diagram of a generator-based test station: (1) exciter, (2) exciter drive motor, (3) drive motor switch, (4) drive motor, (5) surge generator, (6) master switch, (7) main closing switch, (8) adjustable reactor, (9) variable resistor, (10) make switch, (11) step-up transformer, (12) capacitor bank, (13) test breaker, (14) step-down transformer

high requirements are imposed on the winding in respect of its thermal and mechanical ratings.

The rotor of the generator is accelerated at no load up to 3000 rpm by a 1000-kW motor. Owing to 50 tons of rotor mass it accumulates a tremendous kinetic energy of $J\omega^2/2 = 300$ MJ, where J is the rotor moment of inertia and ω the angular velocity. The acceleration lasts about 6 minutes.

Under test load conditions the rotor is decelerated as a result of active losses in the winding, busbars, and the power, $3U_aI_{b,r}$ released in the arc (3-phase tests). Lower speeds of the rotor mean a decrease in generator frequency. In order to limit this phenomenon the rotor is provided with a flywheel and the short-circuit conditions (at peak current) last no longer than 0.1 s.

To attain maximum short-circuit currents the exciter provides the rotor with 8000 kW of power. Additional power preventing significant speed drop is supplied by the flywheel on the exciter shaft. The motor-exciter system moment of momentum equals 800 kN m^2.

With reference to Fig. 3.6, an O cycle test involves closing of the test breaker 13(11), make switch (10) and master switch (6). The automatic sequence control unit performs switching of the components in the following order. The main closing switch (7) closes the circuit after which the test breaker (13) should operate and break the circuit. This is followed by tripping the master switch (6). The main closing switch can close the circuit at any point on the current wave. The master breaker is provided for breaking the circuit when the test breaker fails. If the test breaker has operated normally and has broken the circuit, the master switch disconnects the de-energized circuit.

The parameters of the short-circuit current are adjusted by the variable inductor and resistor circuit (8, 9). Capacitors (12) are needed to control the rate of rise of the recovery voltage.

The transformer (11) is used for high-voltage testing and the transformer (14) for low-voltage testing. These transformers are designed with low reactance at short circuit and with high thermal and mechanical ratings.

The High-Voltage Switchgear Testing Station (NIC VVA) in Moscow is equipped with two TI-100 generators and is capable of testing circuit breakers with interrupting capacity of 5000 MVA.

An oscillatory circuit suggested by A. A. Gorev of the Soviet Union for switchgear testing is shown in Fig. 3.7*a*. A large battery of capacitors C of several thousand microfarads is precharged by the transformer through the rectifier up to a voltage of 50 kV. The test breaker, *TB*, is closed first and then the master switch, *MS*, enabling the current

$$I = UC\sqrt{LC} = U/\sqrt{L/C}$$

The circuit parameters L and C are adjusted so that the circuit frequency be 50 Hz. The necessary short-circuit current is ensured by the potential of the capacitor and the LC circuit. The breaking conditions are practically the same as in the circuit with the test generator (see Fig. 3.6). Gorev's circuit is considerably cheaper and simpler in maintenance, but it is not tailored for all types of testing (complicated duty cycle sequences, three-phase testing).

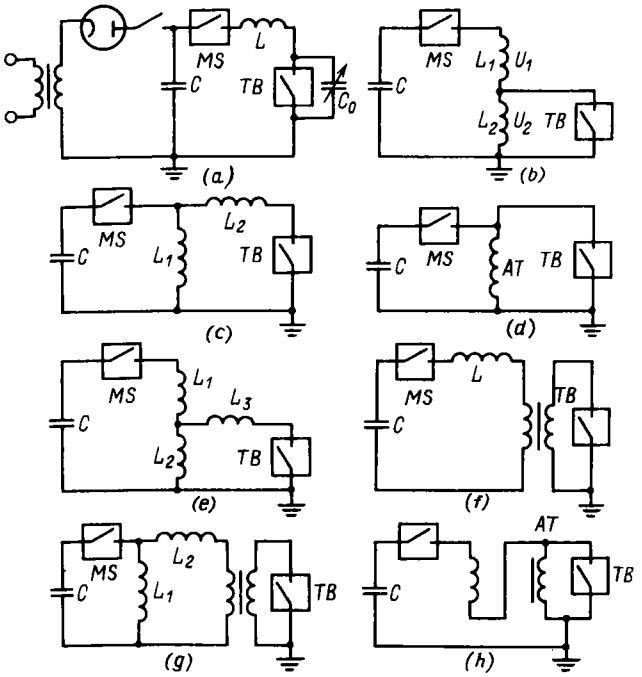

Fig. 3.7. Basic oscillatory circuits

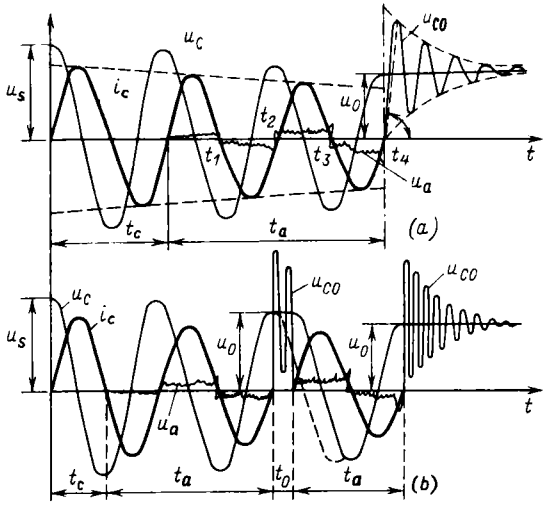

Fig. 3.8. Oscillograms of typical break tests in an oscillating circuit

Figure 3.8*a* shows oscillograms of a typical break test in an oscillating circuit. The curve u_C represents the voltage across the capacitor, i_c the current flowing through the breaker contacts, and u_a is the voltage across the arc. Both i_c and u_C are seen to fall in amplitude with time owing to losses in the circuit. After a time t_c the contacts of the breaker part and an arc is struck. At the instants of current zero, t_1, t_2, and t_3, the arc is cancelled but then restrikes again. At a time t_4 of current zero the arc is extinguished. The recovery voltage is plotted as the curve u_{C0}. The voltage recovery process relies on the capacitor voltage u_0. Figure 3.8*b* illustrates the process of interrupting in the presence of arc restriking that occurs in the time interval $t = t_c + t_a + t_0$.

The circuits shown in Fig. 3.7*b-h* allow for variation of the voltage across the test breaker in a wide range with the same voltage at the capacitor battery. The energy for testing, $P = CU^2/2$, is accumulated in the capacitor, therefore to attain a largest test current the capacitor should be charged to the maximum voltage. Power transformers and autotransformers are inserted in the circuit with the view to control the recovery voltage at the breaker and to completely utilize the energy stored in the capacitor. For example, in the circuit of Fig. 3.7*f*, the circuit inductance is constituted by the inductance L of the reactor and the short-circuit inductance $L_t = X_t/\omega$ of the transformer. Some arrangements include no reactors if $f = 1/2\pi\sqrt{L_t C}$.

Because of the ohmic resistance of the reactor, buswork, and the arc, the current abates in magnitude. Therefore the testing interval should be as short as possible, normally within 20 to 30 ms.

An obvious disadvantage of Gorev's circuit is a rapid fall of test current amplitude because of active losses. Accordingly, it would be wise to use this arrangement for high-speed breakers testing. The range of breakers tested in this circuit may be expanded by testing each interrupter individually. For example a VNV-750 circuit breaker in which the voltage is uniformly distributed over the breaks may be tested at 63 kA and a voltage of 125 kV per break.

It should be noted that the power ratings of circuit breakers keep increasing while the capabilities of testing stations lag this process because of considerable capital costs and development time needed.

A way of substantial expansion of test station capabilities has been found in so-called synthetic tests which allow for high testing powers at moderate additional costs. Synthetic testing circuits are so called because they use a low-voltage high-current source to provide the current to be interrupted and a low-current high-voltage source to provide the recovery voltage.

To illustrate the operating principle of a synthetic circuit we refer to Fig. 3.9 illustrating the process of arc burning and extinguishing in high voltage circuits. During the half-cycle A when the burning arc is fed by the power supply, the instantaneous power consumption is $u_a i$. In modern air and SF_6 circuit breakers the voltage across the arc amounts to 2-3% of rated system voltage. In this half-cycle therefore, the arc can be supported by a surge generator of 12 kV rated voltage or by a low-voltage high-current oscillatory circuit.

After the current zero the process of voltage recovery begins (region B). The recovery voltage U_{rec} is close to the rated value and the high-frequency current ac-

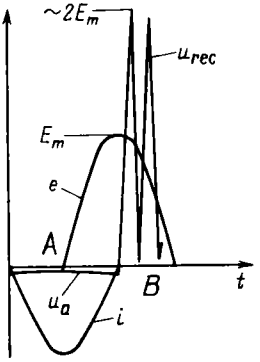

Fig. 3.9. Two phases of arc control: *i*, short circuit current, and *e*, source e.m.f.

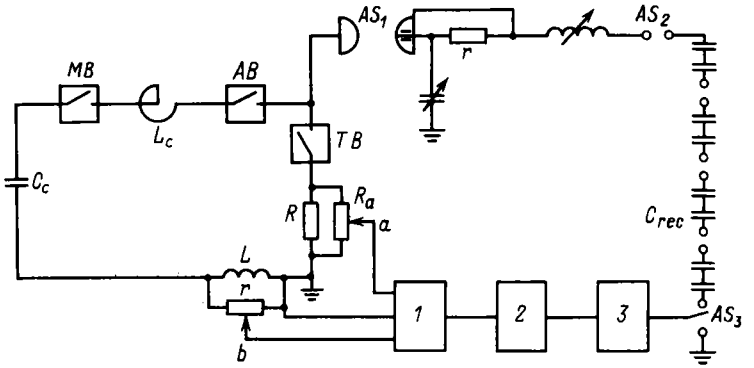

Fig. 3.10. Block diagram of Chernyshev's synthetic test station based on an oscillating circuit: (1) current-zero relay, (2) interlock circuit, (3) firing circuit and time relay

companying the recovery is rather small. Therefore, the second phase of the process can be fed by a low-power high voltage source. As a rule an impulse waveform generator is used for this purpose.

The critical point of this type of testing is concerned with the synchronization of the instant at which the recovery voltage should be applied. Fedchenko [3.3] discusses the contribution of Soviet researchers into the development of synthetic tests.

Figure 3.10 shows the block diagram of a synthetic test circuit developed by N. M. Chernyshev. The large current is provided by a Gorev's circuit including a master circuit breaker, *MB*, auxiliary breaker, *AB*, and test breaker, *TB*. The recovery voltage is formed on the high voltage side by variable inductor and capacitor connected to the impulse voltage circuit.

At a current zero the arc in the auxiliary breaker *AB* designed for operation at 100-200 kV is extinguished and thereby disconnects the test breaker from the

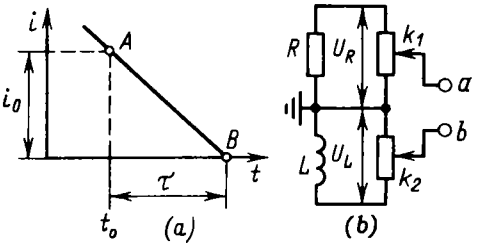

Fig. 3.11. Illustrating the Chernyshev synchronisation circuit

Gorev circuit. The synchronization is effected with the aid of the *RL*-shunting circuit.

To illustrate the point consider the waveform of current at the end of the half-cycle. For a sufficiently small time interval τ this waveform may be rather accurately approximated by a straight line AB in Fig. 3.11*a*, then

$$i_0/\tau = -\mathrm{d}i/\mathrm{d}t|_{t=t_0} \tag{3.1}$$

or

$$i_0 + \tau \mathrm{d}i/\mathrm{d}t|_{t=t_0} \tag{3.2}$$

The last equation holds true from t_0 to the instant of current zero. The voltage from the R and L parts of the shunt is sensed via the dividing resistors R_d and r with dividing factors k_1 and k_2 (Fig. 3.10) so that the voltage between points a and b is

$$U_{ab} = k_1 iR + k_2 L\mathrm{d}i/\mathrm{d}t$$

At the instant t_0, $U_{ab} = 0$ and

$$k_1 iR + k_2 L\mathrm{d}i/\mathrm{d}t = i + k_2 L\mathrm{d}i/k_1 R\mathrm{d}t = 0 \tag{3.3}$$

whence by comparing with Eq. (3.2) we have

$$k_2 L/k_1 R = \tau \tag{3.4}$$

Thus the instant when Eq. (3.3) holds true is determined by the potentiometric ratios k_1 and k_2 (Fig. 3.11*b*). By changing these ratios one can shift the instant of $U_{ab} = 0$. The voltage U_{ab} is applied at the zero relay which sends a signal for the impulse generating circuit to start the discharge at t_0 when $U_{ab} = 0$. Because Eq. (3.3) holds at each current zero some interlocking device is needed to pass zero relay signal only if the arc has been burning in the preceding half-cycle.

Consider the sequence of operation of this circuit with reference to Fig. 3.10. The capacitors of the oscillatory circuit C_c and the recovery voltage capacitor C_{rec} are charged from individual power supplies. The auxiliary switch AB and the test breaker TB are closed. As often as not the auxiliary breaker is just an adjacent pole of a 3-phase circuit breaker. When the master circuit breaker MB closes the circuit, the auxiliary and test breakers pass the current of oscillatory circuit, i_c in Fig. 3.8*a*. At each zero crossing of the current the zero relay (1) yields a signal

to the interlocking circuit (2) which prevents the firing circuit (3) from triggering the impulse generator so long as there is no arc within the test breaker. The sequence control block (not shown) sends a command to the test breaker and auxiliary breaker to break. When the arc appears in the test breaker the interlock allows for the impulse generator firing. At a current zero the arc in the auxiliary breaker is extinguished because the arc control device of this pole is designed for 50-100 kV whereas the oscillatory circuit voltage is about 10 kV.

Once the auxiliary breaker has disconnected the oscillatory circuit from the test breaker, the current in this circuit approaches zero and within a time τ from the current zero (Fig. 3.11*a*) circuit (1) yields a command to the elements (2) and (3) to fire the arc spacings of the impulse generator. All the arc spacings broken down connect the series capacitors for discharge. The breakdown of the arc spacing AS_1 starts the discharge of the capacitor C_{rec} into the variable inductor. Because the capacitance of the variable capacitor is far below C_{rec} all the voltage of C_{rec} is impressed on the test breaker. The waveform of the transient recovery voltage can be altered by adjusting the variable capacitor and inductor. The circuit produces recovery voltage 10 μs before current zero accurate to within $\pm$ 1 μs.

The Chernyshev synchronization circuit allows variation of the instant of the recovery voltage application in a rather wide range and with a high accuracy. The synthetic test station developed in the Soviet Union on the basis of this circuit enables testing of a breaker pole at a voltage up to 400 kV and breaking current of 100 kA.

REFERENCES

3.1 GOST 687-78. *A. C. circuit breakers for 1000 V and higher.*

3.2 A. M. Bronshtein, G. S. Puzyriiskii, and K. I. Seryakov: *Gasovye kommutatsionnye apparaty i KRU vysokogo napryazheniya* (Gas-insulated HV switchgear and modular substations). VINITI, Moscow 1979.

3.3 I. K. Fedchenko: *Tekhnika vysokikh napryazhenii* (High-voltage switchgear). Vysshaya shkola, Kiev 1969.

4

AIR AND SULPHUR-HEXAFLUORIDE CIRCUIT BREAKERS

4.1 General Layout

In air circuit breakers the arc is extinguished in interrupting chambers which are essentially compartments where arc is cooled by air flow blown at high velocity with respect to the arc column.

Feasible designs of interrupters with longitudinal air blast are presented in Fig. 4.1. In all of these devices air blasting from a high pressure compartment at a pressure $p_{comp} = 1.0\text{-}4.0\ MN/m^2$ is directed along the axis of the arc. These extinction chamber designs have received wide acceptance in modern air-blast circuit breakers.

There are also designs where air blasting is at right angles to the arc axis as indicated in Fig. 4.2. This cross-blast type of interrupter is used at system voltages up to 20 kV and is capable of interrupting s.c. currents up to 120 kA. These designs are disadvantageous because of large size and rapid wear of the organic insulating materials used in their structure. A more detailed analysis of modern arc control devices will be given in Sect. 4.9.

Figure 4.3 shows the layout of 110-kV air circuit breakers. The diagram at (*a*) illustrates a breaker with its series outdoor isolating switch in the open position.

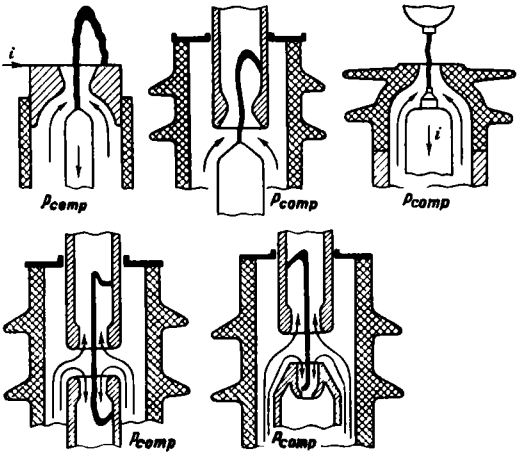

Fig. 4.1. Axial-blast extinction chambers

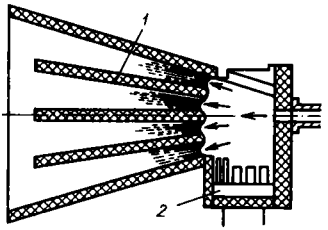

Fig. 4.2. Cross-blast interrupting chamber: (1) baffles of fibrous material, (2) fixed contact

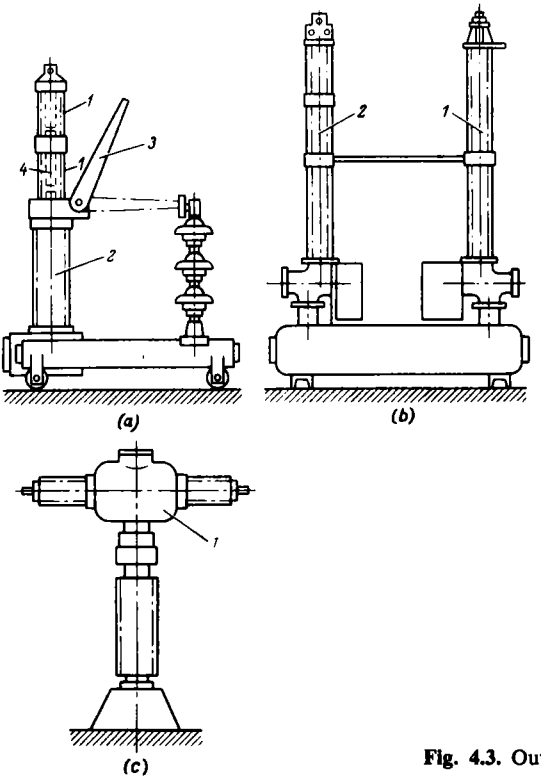

Fig. 4.3. Outline of 110-kV circuit breakers

The compressed air tank, called air receiver, is at the breaker's base. Two interrupter chambers (1) and the mechanism of isolator knife (3) are earth insulated by a hollow porcelain insulating pole (2) which houses the main air duct feeding the interrupters and an auxiliary air duct driving the isolator mechanism.

For an efficient extinction of the arc, the contacts (4) should part at an optimal distance. This distance, however, is insufficient to withstand the action of the reco-

very voltage at atmospheric pressure. Therefore, once the circuit has been interrupted, the contacts of the isolator separate and the blade (3) opens to give a sufficient surface clearance to maintain the necessary dielectric strength. The contacts (4) of the interrupter then close again. The breaker is closed by the isolator knife. This arrangement with a series isolating switch is employed in circuit breakers for 10-20 kV.

Unreliable operation of outdoor isolators (under adverse conditions of rain, snow, and ice) forced designers to depart from this version for the system with the isolator sealed in a gas medium (Fig. 4.3*b*). The contacts of isolator (1) are inside a porcelain compartment protecting them from environmental effects. In circuit interruption, the contacts of the main interrupters (2) part first and the arc is extinguished, then the contacts of the series isolator (1) are forced to open. The open isolator is filled with compressed air. This layout allows the main interrupters to be shunted by a low-ohmic resistor and the isolator arc with the shunt current can be easily quenched in the isolator interrupting chamber. A disadvantage of this design is due to the loss of time for air filling in the interrupters. The entire unit is rather unwieldy because it essentially consists of two breakers, one for heavy current and the other for small current, connected in series. In addition, this design is not suitable for enhancement of voltage rating as this would need a greater number of series breaks. The associated requirements for air duct diameters and clearance between the main interrupter and isolator would also increase. Owing to these setbacks such units are no longer popular with switchgear manufacturers and system engineers.

A more popular alternative in enhancing the voltage rating in various ranges of system voltage is the modular principle of breaker design. For example, having developed a 110-kV module for a given rated current and interrupting capability, one can obtain a 220-kV switchgear lineup by connecting two 110-kV modules and providing the respective enhancement of the support insulation.

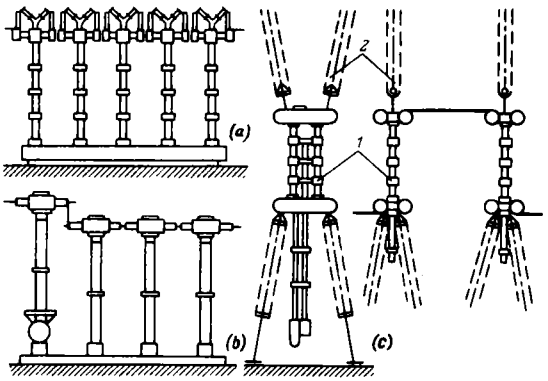

Fig. 4.4. Layout of circuit breakers rated above 110 kV

Figure 4.3*c* shows a VVB-type (continuously pressurised) air-breaker module. The interrupter of the module is within a steel tank (1) filled with compressed air. The 110-kV breaker has two breaks per pole. A 220-kV unit has two such series-connected modules with enhanced insulation of each module.

Extremely high-voltage circuit breakers have a large number of such modules connected in series — a feasible layout is sketched in Fig. 4.4*a*. Where overall system dimensions are critical, the number of series-connected modules is cut down by increasing the rating of each module. For example, a Soviet-made VNV-type module has two breaks and a rated voltage of 250 kV. For a 1150 kV system, four of five modules of this type are connected in series.

Figure 4.4*b* shows in switchgear lineup consisting of a few modules, the first of which having an integrated current transformer that aids in reducing the substation area.

The support insulation of extremely-high voltage circuit breakers is very heavy and bulky because it must withstand maximum rated voltage of the system and heavy mechanical loads. Lighter circuit breaker structures have been lately achieved on the lines of suspension designs (Fig. 4.4*c*) where high pressure air reservoirs and interrupters (1) are suspended from strings of cheap and plain disc insulators (2). The control signals in these designs are transmitted through compressed-air pipes, insulated for rated voltage, or through optical communication links (Chapter 11).

4.2 Electric Arc Behaviour in a Longitudinal Flow of Compressed Air

In air circuit breakers the voltage across the arc can reach many hundred volts. Therefore, analysis of the physical processes in the arc may neglect voltage drops at the cathode and anode. The process of arc extinction is governed by the arc column [4.2]. This section will discuss the column of an electric arc subjected to the action of an air puff. Kukekov [4.1] has carried out a fundamental study into the processes of arc control in high voltage circuit breakers.

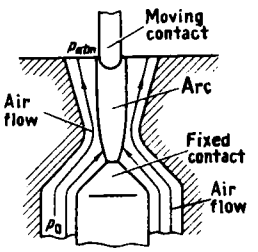

Fig. 4.5. Axial-blast interrupting chamber

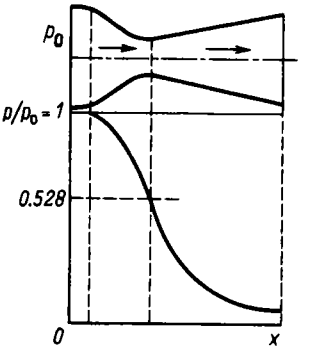

Fig. 4.6. Variation of pressure in an axial-blast interrupter at the critical flow regime

The schematic diagram of an interrupting chamber with longitudinal flow of air is shown in Fig. 4.5. The air flow (1) streaming in low pressure area connected with atmosphere acts on the arc (2) that has been formed between the moving contact (4) and the stationary contact (3). Since the pressure in the compartment p_0 is much higher than the atmospheric pressure p_{atm}, the air flows at a high velocity reaching critical values, w_{cr} (Sect. 4.6). Axial pressure variations along the nozzle are represented in Fig. 4.6. The highest pressure gradient arises in the narrow cross-section (throat) of the nozzle.

The flow temperature sharply varies across the flow. Accordingly, the flow may be thought of as consisting of a cold air flow at T_{cold} about 0.3×10^3 K and a hot plasma flow at T_h about 15×10^3 K. With reference to Fig. 4.7 consider velocity of gas flow at nozzle segment *ab*. The velocity of gas flow [4.3] is given as

$$w = \sqrt{kRT}$$

where k is the polytropic exponent, R is the gas constant, and T is the absolute temperature of the gas. Assuming $k_h = 5/3$, $k_{cold} = 7/5$ and $R_h = R_{cold}$ we obtain for the velocity ratio

$$w_h/w_{cold} = \sqrt{k_h R_h T_h / k_{cold} R_{cold} T_{cold}} \approx 7.7$$

the hot plasma velocity being about 2540 m/s, and cold gas velocity about 330 m/s. The large velocity gradient at the boundary between the two flows gives rise to a great deal of eddies, thus providing conditions for intense heat transfer and mass transport from the arc. Unfortunately, the complicated processes of this boundary layer have not received appropriate investigation. It has been established only that air blasting removes 12 times as much heat from unit length of arc as still air can abstract, the respective ratio of heat abstraction per unit volume (1 cm^3) of plasma amounting to 10^4.

The heat transferred from unit length of arc to the air flow may be divided into the heat transported by convection and radiation, A_c, and the heat transported by hot plasma, A_w, given as [4.1]

$$A_c = Pk(T)T^m \quad \text{and} \quad A_w = Sw_h h(T)\gamma_h$$

where $P = \pi d_a$ is the arc section perimeter, cm; $k(T)$ is the effective heat transfer coefficient [W / cm^2 K^m] depending on temperature; $S = \pi d_a^2/4$ is the arc cross section, cm^2; $h(T)$ is the specific enthalpy, J / kg; and γ_h is the plasma density,

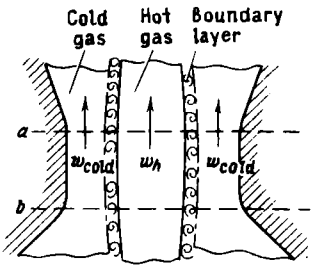

Fig. 4.7. Cold air and hot plasma flows in an axial-blast interrupting chamber

kg/m^3. The specific energy abstracted from unit length of arc is therefore

$$A_a = Pk(T)T^m + Sw_h h(T)\gamma_h \tag{4.1}$$

The arc diameter d_a is a function of current shown in Fig. 4.8 [4.1]. The higher the arc current, the larger its diameter. The diameter also depends on the pressure differential $\Delta p = p_0 - p_{atm}$, more specifically it varies in inverse proportion with Δp. At $\Delta p = 0.6$ MPa the current density $j = 40$ kA / cm^2.

For larger arc diameters, the heat abstracted by the transport of plasma (second term in Eq. (4.1)) increases strongly. The proportion of either of these heat transfer mechanisms depends on the ratio $P/S = 4/d_a$. Accordingly, at heavy currents, heat from the arc is transferred mainly by moving plasma (volumetric cooling), whereas at small currents, including where current is close to zero, heat is abstracted predominantly by convection and radiation.

For high currents, the power released per unit length of arc is given as

$$P_a = I_a E = \pi r_a^2 h(T)\,\gamma_h\, w_h(T) = r_a^2 f_2(T) \tag{4.2}$$

and

$$I_a = \pi r_a^2\, \sigma(T)\, E = r_a^2 f_1(T) E \tag{4.3}$$

where r_a is the cross-sectional radius of the arc, m; σ is the conductivity, S/m, and E is the voltage gradient across the arc spacing, V/m. In terms of the functions defined in Eqs. (4.2) and (4.3),

$$E = \sqrt{f_P(T) / f_1(T)} = f(T)$$

Investigations at high currents, when the transport of plasma is the predominant mechanism of heat transfer, have demonstrated that E depends on current only insignificantly and is mainly controlled by the temperature regime.

In the range of low currents, when arc cooldown is defined mainly by the term A_c, the voltage gradient E is contingent on current and falls off as the current grows. This dependence may be estimated by the expression

$$E \approx 1400 / I^{0.25} \tag{4.4}$$

The same conclusions have been drawn on the basis of experimental evidence, namely, at small currents the voltage across the arc spacing falls off as the current grows, whereas at heavy currents the voltage across the arc remains practically constant while the current increases considerably.

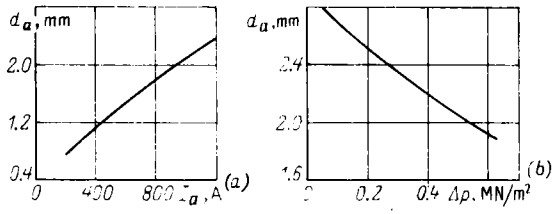

Fig. 4.8. Arc-column diameter as a function of arc current I_a and pressure differential Δp

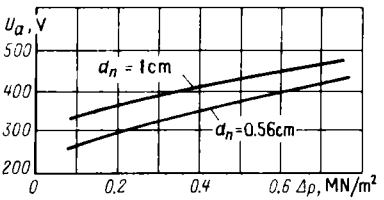

Fig. 4.9. Arc voltage as a function of pressure differential and nozzle diameter, d_n, at $\hat{I}$ = 1200 A

The voltage gradient E also depends on the pressure difference Δp and on the diameter of the narrowest section (throat) of the nozzle d_n. Figure 4.9 shows arc voltage-pressure difference data borrowed from the book of Kukekov [4.1]. The arc voltage and consequently E are seen to increase with Δp and d_n. Kukekov [4.1] suggests for the average gradient E_{av} the following dependence on Δp and relative d_n (in cm / cm)

$$E_{av} = U_a / l_a \approx 30\ [4.6(1 - 0.25 d_n / d_0) + 3.3\ \Delta p^{0.5}]$$

where d_0 is the column diameter equal to 1 cm.

4.3 Thermodynamic Clogging of the Blast Nozzle. Nozzle Section vs. Breaking Current Relation

When breaker's contacts separate in the absense of arc the air flows at the critical velocity $w_{cr} = (kRT_2)^{1/2}$ = 330 m / s since the pressure p_0 is well above the critical level (see Sect. 4.6). A burning arc rapidly warms the air in the nozzle and raises the pressure. As a result of this heating the flow velocity diminishes, the deceleration of the flow being stronger for higher currents. At a certain current the flow virtually stops and a thermodynamic clogging of the nozzle occurs. Experimental situations have been reported when the air reversed the direction of flow — towards the reservoir. Obviously, a thermodynamic clogging does not aid in arc extinction as there is no desired heat abstraction from the arc.

Experimental evidence suggests that for efficient arc extinction the velocity of air blast should not fall below 7-10 m / s at peak current values. Therefore, the prime objective of an interrupter design is to select the pressure p_0 in the compartment and the nozzle section $S = \pi d_n^2 / 4$ such that would not allow the air-flow velocity to fall below 7-10 m / s at peak interrupting capability. Below we discuss the design procedure developed by Kukekov [4.1] under the following assumptions: (1) the air flow is quasi-stationary, i.e., the air parameters in the chamber are constant; (2) the heat released by the arc is distributed uniformly over the length of arc in the nozzle; and (3) the air flow is frictionless.

The idea of an interrupter chamber is sketched in Fig. 4.10*a* and the associated design geometry is given in the adjacent diagram at (*b*). The basic equations that will be useful in design are discussed below.

The energy balance equation

$$dQ = c_p\, dT + w\, dw \tag{4.5}$$

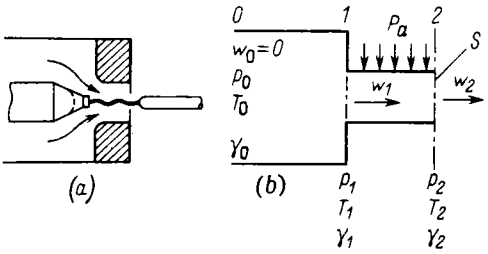

Fig. 4.10. To calculate the flow parameters in an axial-blast interrupting chamber

where $Q = P_a / G$ is the heat released into unit mass of gas per unit time, W / kg; G is the mass of gas, kg; c_p is the heat capacity at constant pressure, J / K kg; T is the absolute temperature of the gas; and w is the gas velocity, m / s.

The first term on the right hand side is the heat expended for gas temperature rise and the second term is the heat increasing the gas flow velocity.

The equation of state for unit mass of gas

$$pv = RT \tag{4.6}$$

where p is the pressure, N / m^2; $v = 1 / \gamma$, m^3 / kg; $\gamma = G / V$ is the density of gas, kg / m^3; $R = 287$ J / kg K is the gas constant.

With reference to Fig. 4.10*b*, the continuity equation for cross sections S_1 and S_2 will be

$$w_1 \gamma_1 S_1 = w_2 \gamma_2 S_2 \tag{4.7}$$

Also, according to gas dynamics laws,

$$-v \, dp = w \, dw \tag{4.8}$$

The parameters at section labelled 0 in Fig. 4.10*b* are known, while those at sections *1* and *2* are to be evaluated. This is a hard task because there are only four equations in eight unknowns (w_1, p_1, T_1, γ_1, w_2, p_2, T_2, γ_2). A number of additional constraints may be invoked, for example, the fact that the pressure p_2 at the nozzle exit is well above the atmospheric, therefore the air velocity w_2 reaches the critical value (see Sect. 4.6)

$$w_2 = w_{cr} \tag{4.9}$$

Kukekov [4.1] used this and some other constraints and managed to express the velocity w_1 at the nozzle entrance section as a function of pressure p_0 in the compartment, nozzle cross section S, and arc power $P_a = U_a I_a$. This function is shown graphically in Fig. 4.11 as $w_1 = f(P_a / p_0 S)$. The analytical details of the derivation of this function may be found in the book of Kukekov [4.1].

The presented dependence is a way to select an appropriate nozzle cross section S for given P_a and p_0. In modern circuit breakers, p_0 ranges from 1 to 5 MN / m^2. Lower values relate to low voltage ratings of 10-20 kV, while higher values to high and extremely-high voltage ratings ($\geqslant$ 110 kV).

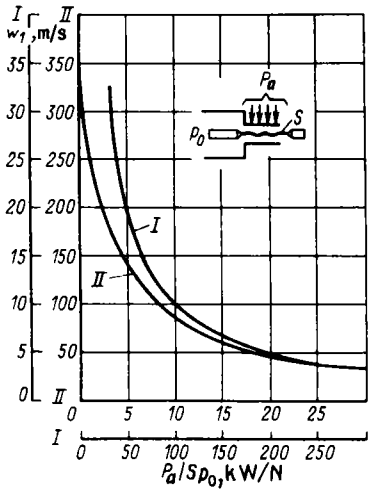

Fig. 4.11. Air flow velocity at the inlet of a nozzle with arc

In calculations of the power $P_a = U_a I_a$, I_a is taken to be the peak rated breaking current

$$I_a = \hat{I} = \sqrt{2}\, I_{b,r}$$

The voltage across the arc $U_a = E_{a,av} l_a$, where the length of arc is taken conditionally as the distance between the stationary contact and the exit section of the nozzle.

Arc control devices with bilateral blast may be approximately treated as consisting of two ordinary blast nozzles connected in series. Accordingly, the power per nozzle is half the power released in the arc. The analytical length l_a of the arc is the distance from the mid-point of the arc spacing to the exit section of the nozzle.

The average voltage gradient $E_{a,av}$ may be taken equal to 150 V / cm. Figure 4.11 shows two curves, one valid for air blast velocities up to 35 m / s, the other valid for velocities up to 330 m / s. The respective simplified analytical equations for $w_1 \leqslant 70$ m / s are as follows [4.1]

$$w_1 = 86 \times 10^6\, \Delta p S / P_a$$

where the pressure differential may be approximated as $\Delta p = p_0 - p_2 \approx p_0$; whereas in the range 70 m / s $< w_1 <$ 333 m/s

$$w_1 = 333 - 110 \sqrt[3]{10^{-5}\, P_a / \Delta p S}$$

For a normal frequency supply, $P_a = U_a \hat{I} \sin \omega t$ and the velocity equations become

$$w_1 = 860 \times 10^5\, \Delta p S / U_a \hat{I} \sin \omega t \qquad (4.10)$$

for $w_1 \leqslant 70$ m / s, and

$$w_1 = 333 - 110 \sqrt[3]{10^{-5}\, U_a \hat{I} \sin \omega t / \Delta p S} \qquad (4.11)$$

for $70 < w_1 < 333$ m / s.

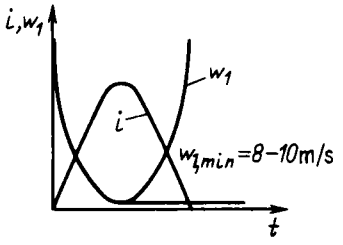

Fig. 4.12. Variation of air velocity over a current half-cycle

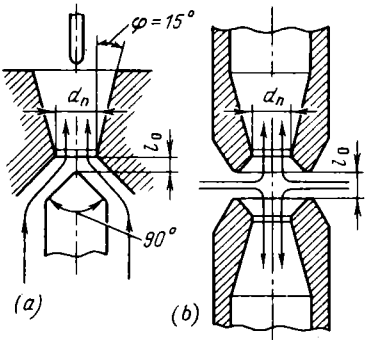

Fig. 4.13. Axial-blast arc-extinction systems: (*a*) unilateral flow, (*b*) bilateral flow

The velocity of air flow w_1 is a minimum at $\omega t = \pi / 2$. As the interrupting current decreases, w_1 increases and attains the critical flow values of 333 m / s at $\omega t = \pi$. An approximate variation of w_1 is indicated in Fig. 4.12. It is worth noting that while the current falls from $\hat{I}$ to zero for a relatively short time interval of 5 ms, w_1 should increase from about 8 to 333 m / s. The extinction process can be influenced by the inertia of the air that must be accelerated during this time span. Actually current chopping can occur near a current zero and, consequently, one may expect high accelerations of the air flow. Calculations indicate that the acceleration period of the air flow is very short, amounting to several microseconds. A current chopping near a current zero may be taken into account by means of an increment of frequency. If the current varies by the law $k_f \omega \hat{I} t$, then

$$w_1 = 333 - 110 \sqrt[3]{10^{-5} k_f \omega U_a \hat{I} t / \Delta p S}$$

where $k_f > 1$ allows for a steeper fall of the current.

Stabilization of the arc in the nozzle is a significant factor for arc extinction. At moderate deceleration the blast keeps the arc coaxially within the nozzle, thus providing optimal conditions for heat transfer, mass transport, and efficient quenching. These conditions are observed at $w_1 \geqslant w_{1,\min} = 8\text{-}10$ m / s. At $w_1 < w_{1,\min}$ the arc loses its stability and starts rotating at the nozzle inlet. The ionized gases occupy most of the arc spacing and extinction can no longer be effected notwithstanding the optimal geometry.

Arc column stabilization and thermodynamic clogging depend on geometrical factors as follows:

(a) the nozzle geometry and the nozzle inlet profile formed by the walls of the confuser and the contact tip;

(b) the relative length of the arc spacing.

Two axial-blast arc-control devices are shown in Fig. 4.13. The best performance has been achieved with conical nozzle (diffuser) at $\varphi = 15°$. The inlet portion of the

nozzle is shaped so that optimal conditions will be ensured for arc stabilization by air blasting and efficient elimination of the plasma column at the end of the quenching half-cycle. On the other hand, the electric field between the contacts, governed by the shape of these contacts, should be well below the electric strength level of the cold air filling the arc spacing after the plasma has been blown out.

The two aforementioned conditions are incompatible. Uniform air blast needs sharp shape of the moving contact. This geometry eliminates dead zones not affected by the air blast (see Fig. 4.10*a*). However, the resultant electric field becomes strongly inhomogeneous, consequently, the dielectric strength of the cold arc spacing will be low. Rounding the contact tip (dashed line in Fig. 4.10*a*) results in a more uniform electric field, but penalizes the streamlining properties of the air flow.

Good performance has been achieved with an asymmetric axial blast system [4.7]. The moving contact has a vent into the atmosphere with the hole area occupying 20-30% of the nozzle section. This configuration increases interrupting capability of the device by 25%. The opening in the contact eliminates the dead zone at the end of the contact. This type of interrupting chamber is installed in the Soviet-made type VVBK (modified continuously pressurized circuit breaker) (Sect. 4.9).

The distance between the contacts is an essential parameter of the arc quenching process. Longer air spacings mean higher energy release in the arc and increasing deceleration of the air flow. As a result, hot, rather than cold, air arrives at the break of the residual arc column at the end of the quenching half-cycle, the dielectric strength of the arc spacing falls off and the arc fails to extinguish itself.

Small arc spacing limits the access of blast air to the nozzle. The injected air cannot provide the desired influence on the arc. There exists an optimal arc spacing having highest effect on the arc. From the standpoint of air consumption for bilateral blast devices, the optimal arc spacing, l_a, is conditioned as

$$\pi\, d_n l_a = 2\pi\, d_n^2 / 4 \text{ or } l_a = d_n / 2$$

where $\pi\, d_n l_a$ is the surface of the cylinder of air flow between the contacts and $2\pi\, d_n^2 / 4$ is the area of two exit sections of the nozzles. It is worth noting that the derived relation of the optimal arc spacing being half the nozzle diameter is close to the experimental proportion. Figure 4.14 presents breaking current as a function of contact spacing l_c for unilateral blast devices. A similar profile has been observed with bilateral blast systems.

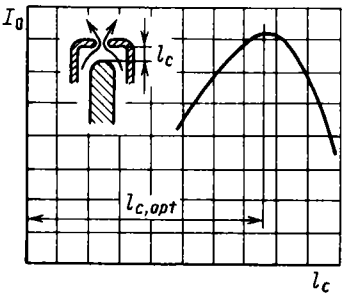

Fig. 4.14. Interrupting current versus contact spacing

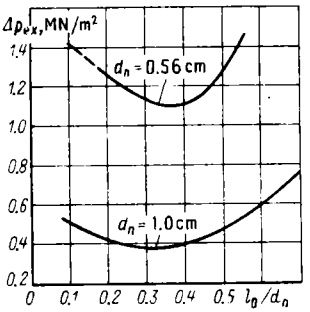

Fig. 4.15. Dependence of the pressure differential required to extinguish the arc within one half-cycle on the relative contact spacing

The air blast moves the quenched arc that can extend much longer than the optimal contact spacing $l_{c,opt}$. To limit the length of arc special limiting electrodes are installed in the interrupting chamber between which the arc is burning after its base points have begun moving around the nozzle interior (see, e.g., Fig. 4.47 item 41).

The pressure differential vs. relative contact spacing relations [4.1] shown in Fig. 4.15 are noteworthy. The pressure differential plotted in the vertical axis represents the value necessary for arc extinction in one-half cycle, the horizontal axis shows the ratio of arc spacing to nozzle diameter, l_0 / d_n. For a given nozzle diameter there exists an optimal spacing $l_{0,opt}$ at which the arc can be quenched at the least pressure differential (for notation see Fig. 4.13). For unilateral blast chambers, $l_0 = (0.3\text{-}0.4)\, d_n$. It is instructive to note that as the nozzle diameter decreases from 1 to 0.56 cm, Δp_{ex} increases from 0.38 to 1.1 MN / m^2, while the product ΔpS remains constant.

Experiments have proved that the optimum spacing $l_{0,opt}$ corresponds to the path of travel of cold air particles from the contact tip to the front face of the

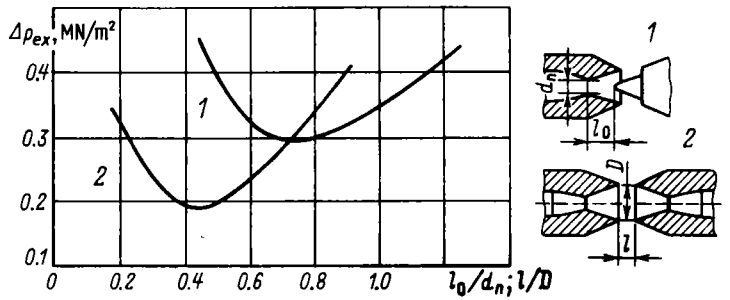

Fig. 4.16. Comparison of nozzle performance for (1) unilateral-blast and (2) bilateral blast designs

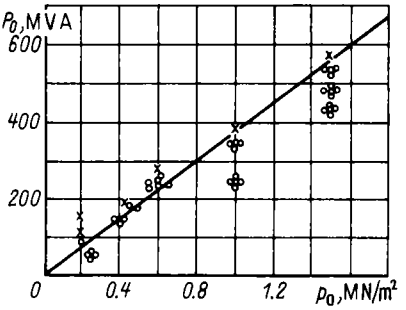

Fig. 4.17. Interrupting power versus pressures: (○) interrupted, (×) non-interrupted current

nozzle in one-half cycle. Therefore, to determine this distance one needs to know the velocity of air flow, being a function of time and position in the nozzle.

It is instructive to compare unilateral and bilateral blast designs of interrupting chambers. Unilateral blast versions have been successful in providing a better field of air flow having no stagnation zones. Among the disadvantages of this nozzle one finds evaporation of electrode metal into the arc zone. This impairs the arc quenching process because the ionization potential of metal vapour is well below that of the gas (mainly nitrogen).

Bilateral blast blows metal vapour away from the arc spacing thus aiding in arc extinction. However, in this nozzle, the air blast is at first at right angles to the arc and then turns through 90 °. At the turning point there occurs a dead zone where the effect of air on the arc is weakened. At this location the arc diameter is larger than elsewhere. Figure 4.16 shows the experimental plot of the minimum extinction pressure differential $\Delta\, p_{ex}$ necessary to extinguish the arc during one-half cycle versus relative arc spacing [4.1]. The plots for versions (1) and (2) indicate that the unilateral blast (1) requires about 1.6 times higher pressure, but half as much air in a puff than does the bilateral blast version (2). The exit velocity $w_1 = w_{1,cr} = 333$ m / s is the same in both versions, but the bilateral blast version has two nozzles. The interrupting current of unilateral blast designs may be assumed equal to about 0.8 the value of the bilateral blast design. Concluding the comparison we note that the minimum ratio $l_{0,opt} / d_n$ may be taken equal to 0.33 for unilateral blast versions and 0.5 for bilateral blast versions.

Consider now the dependence of interrupting capacity or ability on pressure p_0 and nozzle diameter of the interrupting compartment. For a given value of w_1 the ratio $P_a / p_0 S = E_{av} l_a \hat{I} / p_0 S$ is a constant. At higher pressures the peak breaking current $\hat{I}$ also increases. Therefore, breaking current and interrupting capacity are proportional to gas pressure (Fig. 4.17). The electric strength of the arc gap also increases with pressure allowing for greater voltage ratings and higher rate of rise of the recovery voltage.

It should be noted that an increase of pressure calls for improved structural strength of the breaker components. It also means complications for the valves of

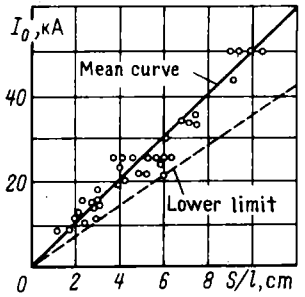

Fig. 4.18. Breaking current as a function of the ratio of nozzle cross-sectional area S to contact spacing l_c

the control system and heavier breaker designs. In modern power circuit breakers p_0 is at most 5 MN / m^2.

Interrupting current is also proportional to the nozzle cross section S. The respective experimental dependence is plotted in Fig. 4.18 by two curves representing the lower limit and mean value. It is conceivable that higher S leads to greater air consumption and air tank dimensions.

4.4 Recovery of Dielectric Strength in Axial Blast Interrupters

General

Extinguishing the arc restores the electric strength of the arc spacing. Two types of breakdown, thermal and electrical, will be discussed. Thermal breakdown is characterized by a rather high density of ionized species (in excess of 3×10^{10} cm^{-3}) at current zero. The conductivity of arc spacing is then rather high, that is, the residual resistance r is low. With a recovery voltage at the contacts, the arc spacing passes a residual current $I_{res} = u_{rec} / r$ that heats the plasma and increases thermal ionization. If the heat abstracted by the air flow is less than the heat released by the residual current, then the thermal ionization develops and finally causes breakdown of the arc spacing (positive energy balance). When the energy balance is negative, the cooldown of the arc space aids in increasing the residual resistance to a level sufficient for circuit interruption. A specific feature of thermal breakdown is its relatively slow development (plasma heating) in time.

In Fig. 4.19, the curves joined by label (1) illustrate the recovery of electric strength for various currents in the case of thermal breakdown. The higher the current, the lower runs the curve of discharge voltage characterizing the dielectric strength.

Electrical discharge is characterized by relatively low density of charged species (below 2×10^{10} cm^{-3}) in the arc spacing at current zero. Recovery voltage tends to break down this air gap. The restrike occurs as a result of an avalanche ionization if the dielectric strength of the arc spacing is lower than the peak recovery voltage. Restriking can also occur at low residual conductivity. In the circumstances a glow discharge occurs which then grows into an arc discharge.

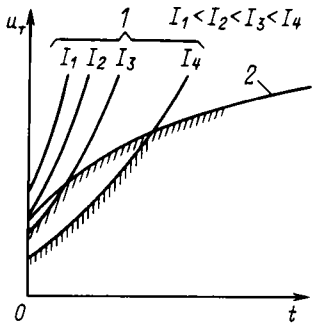

Fig. 4.19. Dielectric strength recovery of an arc gap after a current zero

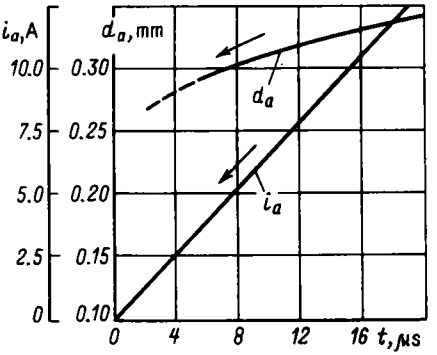

Fig. 4.20. Arc diameter on approach to current zero. Δp = 0.35 MN/m^2, d_n = 1.0 cm, $\hat{I}$ = 1200 A

The recovery of the dielectric strength of the contact space after electric breakdown is approximately illustrated by curve (2). Which type of discharge occurs is governed by the initial parameters of the residual arc column and by the blast parameters.

The process of dielectric strength recovery depends on the variation of arc diameter. Figure 4.20 illustrates how the arc current and diameter vary as the current in the breakboard interrupter approaches zero. It is interesting to note that the arc diameter varies only weakly as the current falls and the arc column collapses in about 4 μs.

Figure 4.21 illustrates the variation of arc resistance as the current approaches zero. It will be noted that the resistance remains almost invariable beyond the 4 μs interval and depends on pressure only insignificantly. It experiences a sharp ascent within the last 2 μs from the current zero.

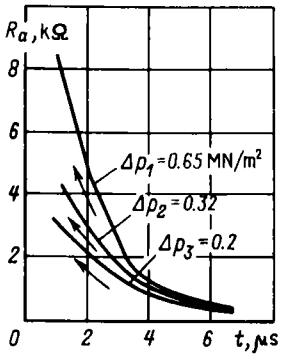

Fig. 4.21. Arc resistance on approach to current zero under unilateral air blast

The rate of fall of the current at a current zero is also of significance in arc extinction. This rate depends on the peak current of a shunting capacitor or resistor and on the action of the cooling air blast. Experimental evidence indicates that the rate of fall is steeper the higher the pressure differential [4.1].

A very important parameter of the arc column is its thermal time constant. As the capacitor, rather than the arc, carries a greater proportion of the circuit current, the amount of energy dissipated in the arc decreases and the arc is cooled down. The lower the time constant, the faster will be the cooldown, temperature drop and dielectric strength recovery. In the general case the thermal balance of unit length of the arc can be given as

$$\gamma \mathrm{d}(hS) / \mathrm{d}t = E^2 \sigma S - \alpha_{\mathrm{contr}} hS \gamma - kS \tag{4.12}$$

where h is the specific enthalpy, J / kg; S is the cross section of the arc column, m^2; E is the voltage gradient across the arc, V / m; σ is the plasma conductivity, S / m; α_{contr} is the coefficient of arc column contraction due to the heat abstraction by the air blast, s^{-1}; k is the volumetric power transfer coefficient, W / m^3; and γ is the density of plasma, kg / m^3.

At and about current zero the delivery of energy to the arc column ceases, $E = 0$, and Eq. (4.12) becomes

$$\gamma \, \mathrm{d}(hS) / \mathrm{d}t + \alpha_{\mathrm{contr}} hS \gamma + kS = 0$$

This equation is hard to solve because, h, S, σ and k are complicated functions of temperature, location in the arc, and some other factors. The problem will be solvable if we assume that these quantities are constant in a short time interval. Then

$$hS = (hS)_{\mathrm{initial}} \, e^{-t/\tau_0} \tag{4.13}$$

where

$$\tau_0 = \gamma h / (\alpha_{\mathrm{contr}} h \gamma + k) \tag{4.14}$$

is the thermal time constant of the arc.

Recovery of Dielectric Strength in Axial Blast Chambers

The type of discharge of the contact space depends on many a factor including the conditions of voltage recovery. At heavy current and high rate of voltage recovery (close short circuit fault) a thermal breakdown is more probable. It is instructive to note that restriking due to electric breakdown is rather frequent in air-blast circuit breakers. Therefore, we consider a simpler case of arc extinction in the framework of the recovery rate theory that compares the rate at which the contact space recovers its dielectric strength with the rate at which the voltage across the contacts rises.

Our consideration will be based on the analytical method developed by Kukekov [4.1] for the recovery of dielectric strength by the arc space after an electric breakdown in an axial blast interrupter. Following a current zero the air flow begins cooling the arc column, the cooling being more intense where the velocity is higher.

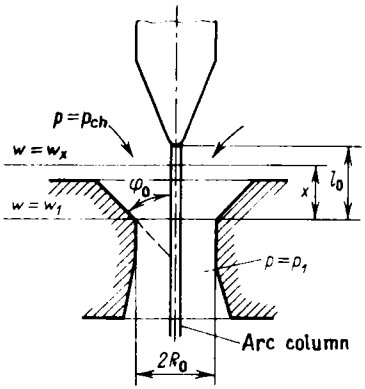

Fig. 4.22. Interrupter geometry to assist dielectric strength calculations

Kukekov suggests that under the circumstances the dielectric strength should be characterized by the breakdown voltage of the arc column area cooled to 293 K. The dielectric strength increases as this area approaches the nozzle outlet. Therefore, the factor that controls the process of recovery is the temperature of various points of the contact spacing. In the general case, the temperature is a function of time and coordinate within the chamber. The associated geometry is sketched in Fig. 4.22.

When no heat is put into the arc its temperature decays exponentially

$$T(x, t) = T_0 e^{-t/\tau(x, t)} \tag{4.15}$$

where T_0 is the initial temperature of the arc column, K; $\tau(x, t)$ is the thermal time constant, s; x is the coordinate along the arc in the nozzle, cm; and t is the time elapsed from the current zero, s. Because of nonstationary air velocity along the arc, the arc cooling and, consequently, thermal time constant τ are functions of coordinate x and time t.

According to the general definition of the thermal time constant (normalized per unit length)

$$\tau(x, t) = c_p \pi d_a^2 / 4k(x)\, \pi d_a = c_p d_a / 4k(x) \tag{4.16}$$

where c_p is the specific heat of the residual column, J / cm^3 K; d_a is the arc diameter at section x and time instant t, cm; and $k(x)$ is the generalized heat transfer coefficient, W / cm^2 K.

The velocity of air is greatest and τ is smallest in the narrowest cross section of the nozzle. In wider sections of the nozzle, air flows slower and τ increases. With reference to Fig. 4.22, at $t = 0$ and $x = 0$ [4.1]

$$\tau_0 = 0.163 \times 10^{-6} c_p p_{av} I_0^{0.25} T_0 \exp(-0.87 p_{av}) \tag{4.17}$$

where $c_p \approx 50 \times 10^4$ J / cm^3 K; p_{av} is the average pressure, MN / m^2; T_0 is the initial temperature of the arc identical throughout the column and equal to about 12×10^3 K; and I_0 is the chopping current, A. The chopping current may be estimated by

the expression

$$I_0 \approx \hat{I}\omega\Delta t = \omega\hat{I}/6f_0 \tag{4.18}$$

where f_0 is the transient recovery voltage frequency, s^{-1}; $\hat{I}$ is the peak breaking current, A; and Δt is the time [s] to the current zero at which current chopping occurs.

As will be recalled, at small currents heat is abstracted mainly by convection, the heat transfer coefficient being proportional to the flow velocity raised to a power of 0.8. Then for points with coordinates x and 0 we have

$$k(x) = k_1 (w_x / w_1)^{0.8} = k_1[f(x)]^{0.8}$$

where k_1 is the heat transfer coefficient at $x = 0$.

At the initial time instant ($t = 0$) the time constant function varies along the axis as

$$\tau(x, 0) = \tau_0 / [f(x)]^{0.8} \tag{4.19}$$

while the expression suggested [4.1] for its time-space variation is

$$\tau(x, t) = \tau(x, 0) \exp [-w_{1,h} f(x) t / 4] \tag{4.20}$$

where $w_{1,h}$ is the velocity of hot air. The velocity of hot air can be expressed through the velocity of cold air $w_{1,c}$ with the aid of findings of Sect. 4.2, taking $T_{1,h} = 6000$ K and $T_{1,c} = 1000$ K, viz.,

$$w_{1,h} = w_{1,c}\sqrt{R_h T_{1,h} / R_c T_{1,c}} \approx 2.5\ w_1 \tag{4.21}$$

Now,

$$\tau(x, t) = \tau(x, 0) \exp [-2.5\ w_1 f(x) t / 4] \tag{4.22}$$

Figure 4.23 shows the plots of functions $f(x)$ and $\tau(x, 0)$. As x increases the velocity w_c falls because of expanding orifice of the nozzle. Accordingly, $\tau(x, 0)$ increases and the intensity of cooling decreases.

For a given value of x one may compute the variation of $\tau(x, t)$ in time by means of Eq. (4.22). Calculation for nozzle geometry of Fig. 4.22 is displayed in Fig. 4.24 for $\hat{I} = 45$ kA and $f_0 = 1$ kHz. Greater x's are seen to be accompanied by increased τ and worse cooling of the arc column.

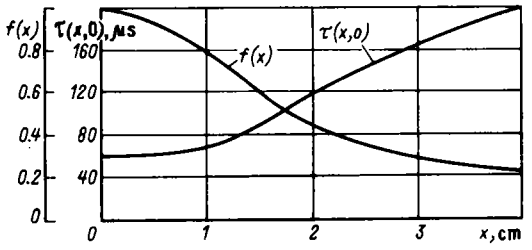

Fig. 4.23. To calculate the arc time constant: $\tau(x, 0) = \tau_0 \times [f(x)]^{-0.8}$ with $\tau_0 = 60\ \mu s$

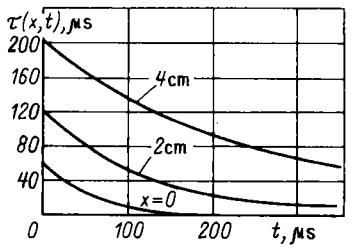

Fig. 4.24. Time constant behaviour with time (τ_0 = 60 μs)

Equations (4.15) and (4.22) can be used to construct a family of curves as those shown in Fig. 4.25. At $t = 0$, according to Eq. (4.15) the temperature is the same $T(x, 0) = T_0$ over the nozzle and equals 12 000 K (straight line *a*). Then one can choose $t = 20$ μs and by virtue of Eq. (4.22) find τ for various points of the nozzle (similar to Fig. 4.23). The temperature $T(x, 20 \times 10^{-6})$ is computed by Eq. (4.15) and traces out the penultimate top curve in Fig. 4.25. Application of this procedure results in curves for other time instants.

When the arc temperature drops below 4000 K, the conductivity of the column decreases and the dielectric strength of such segments of the arc column varies inversely as the temperature. For simplified calculations we may safely assume that the dielectric strength is recovered at the segments of cool air only (T = 293 K). At $x = 0$ the arc temperature is the lowest. Therefore, from time zero to 40 μs the column temperature is above 3000 K and the dielectric strength of the gap is zero. The cold dielectric strength of the gap is recovered after 60 μs. In 80 μs the cold air space is 0.7 cm high, in the next 20 μs it grows to 1.6 cm (t = 100 μs), and in t = 200 μs the cold air occupies practically the whole contact spacing. The dielectric strength of the spacing increases with the length of the cold column.

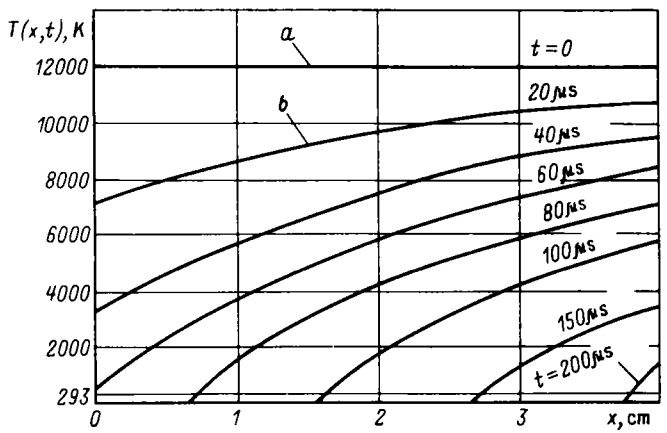

Fig. 4.25. Temperature variation in arc column after a current zero (τ_0 = 60 μs)

The dielectric strength of the gap may be estimated either with the aid of the experimental curves [4.1] or by empiric formulas. For aligned electrodes of 32 mm diameter (rounded), dielectric strength, in kilovolts, may be determined as

$$U_{calc} = 119\,(pl)^{0.45} \tag{4.23}$$

where p is the average air pressure, MPa; and l is the length of arc spacing, cm.

It is important to note that eddies and dead zones at low pressure present in the flow make the breakdown voltage lower than that of stationary air. Therefore it would be wise to introduce some safety margin

$$U_{bd} = (0.8\text{-}0.65)\,U_{calc}$$

Along the arc column the pressure in the nozzle does not remain constant, too. Experimental evidence [4.1] suggests that the average pressure p_{av} is 0.8 the pressure in the chamber at $w_0 = 0$.

After the cool air has occupied the entire nozzle, the electric field strength equalizes and the dielectric strength of the gap rises sharply. This phenomenon may be explained as follows. When cold air occupies only part of the gap, the field is formed by a contact and a sharp electrode of the hot gas. When the cool air sweeps the hot gas out of the spacing, the field is formed by the breaker contacts and must be rather uniform. The curve U_T of dielectric strength recovery in Fig. 4.26 has been constructed with the aid of the analytical procedure outlined above (t_1 is the time of incipient recovery of cold dielectric strength, and t_2 is the instant of the whole nozzle being filled with cold air). The voltage recovery curve u_{rec} at this figure has been plotted with $t = 0$ corresponding to the instant of current chopping in the arc. The time of the recovery voltage crossing zero can be calculated by the empirical formula $\Delta t_1 = 1 / 6 f_0$.

If the cold dielectric strength $u_{calc} = 1.25\,u_{rec,\,max}$, then circuit interruption will be effected in this half-cycle. One important point deserves emphasizing. In the outlined analytical procedure the recovering dielectric strength is deemed zero during time t_1. Actually this is not the case. By the instant of the next current zero the voltage across the arc has grown and attained the extinction peak value that may be taken as the initial dielectric strength of the gap. This strength will remain invariable until additional dielectric strength builds up due to the cooling of arc

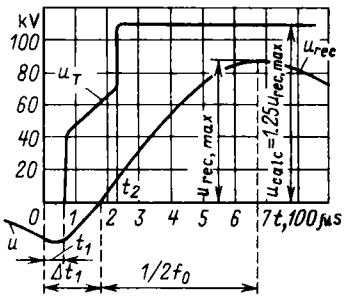

Fig. 4.26. Analytical curves of recovery voltage and recovering dielectric strength

column as was computed above. This initial dielectric strength, characterized by the breakdown voltage, may be deemed approximately equal to $u_{bd} = E l_a$.

The most severe duty of a circuit breaker is to interrupt a short circuit accompanied by a thermal breakdown. A large number of analytical expressions are available that tend to relate gas-dynamic and thermal processes in the arc with the processes in the circuit to be interrupted. Difficulties encountered in deriving these expressions are invariably connected with the definition of some physical quantities and accounting for the features of the interrupting chamber design. Certain processes in the arc are studied insufficiently. Therefore much research is being done on the development of a mathematical model of the electric arc whose parameters will be determined from experiments with heavy currents including currents above interrupting capacity [4.4].

Oscillograms of breaker tests record current, voltage across the contacts, and residual current behaviour. These data form a basis of model parameters.

4.5 Aiding Arc Extinction with Shunt Resistors and Capacitors

In Sect. 4.2 we have learned that at a given gas pressure in the interrupting chamber higher interrupting capabilities need wider sections of the nozzle as these would increase the amount of effluent air. Because the breaker has to perform multiple interrupting duty cycle, higher interrupting capacity would call for a larger air tank, heavier breaker structure, and larger size.

One more point is worthwhile. An air circuit breaker has a low initial dielectric strength of the contact spacing. At high rate of rise of the recovery voltage (close short circuit) this gap breaks down. Therefore air circuit breakers are very sensitive to the rate of rise of the recovery voltage. Figure 4.27 demonstrates that breaking current, I_b, falls rapidly as this rate (or frequency of recovery voltage transient) increases. In order to shorten the time t_1 (Fig. 4.26) the pressure in the interrupter chamber p_0 should be increased and nozzle opening expanded, which inevitably means heavier breaker structure and higher unit costs. As a way out the low-

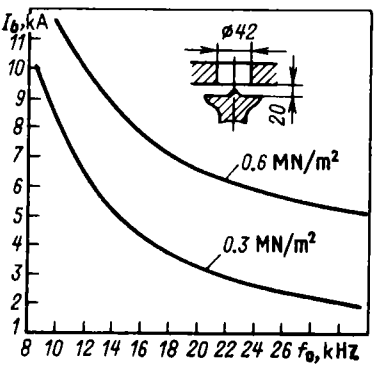

Fig. 4.27. Interrupting current versus recovery voltage frequency

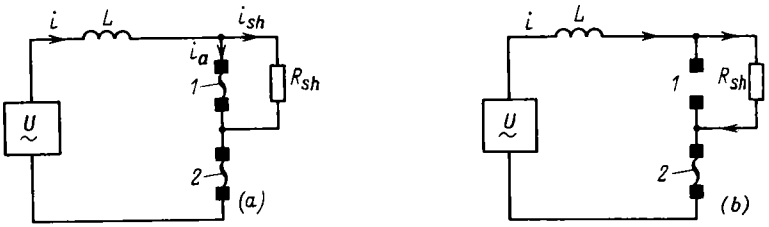

Fig. 4.28. To calculate arc extinction aided by a low-value resistor

resistance interruption method is used. It makes use of shunt resistors placed in parallel with the arc contacts to damp transient overvoltages.

Consider the operating principles of shunt resistors with reference to a two-break switch represented schematically in Fig. 4.28. The first break is shunted by a resistor R_{sh}. Assume that break (1) is to open first and an arc forms in the contact spacing. The circuit current is divided into the arc and shunt so that

$$i = i_{sh} + i_a \text{ and } i_{sh} R_{sh} = u_{sh} = u_a$$

When the current is high, the arc resistance is low, the voltage drop across the arc is low and the shunt current i_{sh} is small. As the current approaches a current zero the arc voltage increases as stated in Eq. (4.4), namely,

$$u_a = A l_a / i_a^{0.25} = 1400\ l_a / i_a^{0.25}$$

The shunt current rises proportionally. Figure 4.29 presents current-voltage characteristics of the arc, $u_a = f(i_a)$, and the shunt $u_{sh} = f(i_{sh}) = R_{sh} i_{sh}$. Summing up these curves we obtain the resultant curve $u_a = f(i)$. With the voltage U_1 across the arc the circuit current is $I_1 = I_{a1} + I_{sh1}$. When the current falls down to I_0, the arc is no longer able to maintain itself, and the entire circuit current has to flow through the shunt. The arc would continue if the circuit current could increase with the arc voltage u_a (curve *ab*), but owing to the circuit being inductive

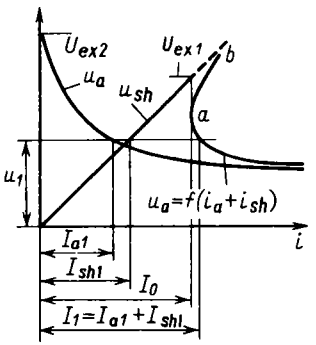

Fig. 4.29. Current-voltage characteristics of the arc and shunt resistor

$L\mathrm{d}i/\mathrm{d}t < 0$, that is, the current will decrease. Therefore at $i = I_0$ the arc extinguishes itself and there is no tendency of restriking. Thus the current is chopped prior to the oncoming current zero. From Fig. 4.29 it can be seen also that the shunt resistor reduces the peak extinction voltage U_{ex1} from the level of a shuntless break U_{ex2}.

The time t_0 of the arc current chopping may be determined as follows:

$$i_0 = i_{a0} + i_{sh0} = \hat{I} \sin \omega t_0 \tag{4.24}$$

For a constant l_a,

$$u_a = A l_a / i_a^{0.25} = A_1 / i_a^{0.25} \tag{4.25}$$

The arc current is chopped when $\mathrm{d}i / \mathrm{d}u_a = 0$, i.e.,

$$\frac{\mathrm{d}(i_a + i_{sh})}{\mathrm{d}u_a} = \frac{\mathrm{d}}{\mathrm{d}u_a}(A_1^4 / u_a^4 + u_a / r_{sh}) = 0 \tag{4.26}$$

This equation yields the voltage U_{a0} across the arc contacts at the inflection point a (Fig. 4.29) in terms of r_{sh}. In view of Eqs. (4.24) and (4.25)

$$I_0 = \hat{I} \sin \omega t_0 = U_{a0} / r_{sh} + A_1^4 / U_{a0}^4 = f(r_{sh})$$

Given r_{sh} one may determine the instant of current chopping t_0.

In order to facilitate extinction of the arc the process of voltage recovery is converted from periodic to aperiodic by choosing

$$R_{sh} < 0.5\sqrt{L / C} = X f_0 / 2f \tag{4.27}$$

where L and C are the circuit parameters controlling the voltage recovery process, $f_0 = 1 / 2\pi\sqrt{LC}$, and X is the inductive reactance of the short circuit.

With allowance for the time of current chopping t_0 it is recommended [4.1] to take

$$R_{sh} \approx 0.2\sqrt{L / C} = X f_0 / 5f \tag{4.28}$$

If the interrupting current is known as a function of rate of recovery voltage, then this dependence can be used to determine the tolerable rate of recovery voltage, measured in V / μs, for a desired interrupting capability. Then R_{sh} can be found from the equation

$$\mathrm{d}U / \mathrm{d}t_{tol} = 0.636\, U_0\, R_{sh}\, 10^{-6} / L \tag{4.29}$$

where U_0 is the normal-frequency recovery voltage, and L is the short circuit inductance, H.

After the arc in break (1) has been extinguished, break (2) is opened and there forms an arc whose current is limited by R_{sh} (Fig. 4.28). The peak value of this current is defined as

$$\hat{I}_1 = 0.87\sqrt{2}\, U_{r,max} / \sqrt{R_{sh}^2 + X^2} \tag{4.30}$$

where $U_{r,max}$ is the rated maximum voltage of the circuit-breaker system. The phase

angle between the short-circuit current and the system e.m.f is

$$\varphi = \arctan (X / R_{sh}) \tag{4.31}$$

The reduction of arc current due to the incorporation of R_{sh} and the rise of a substantial phase angle reducing the recovery voltage ease the operating conditions of the second break. As a rule, the first break has to endure a much more severe duty cycle.

The value of the shunt resistor is a function of breaker's voltage rating, being in the range of units and fractions of an ohm at low voltage ratings (10-20 kV) and in the range of hundreds of ohms at 220 kV and above.

It should be noted that breaks (1) and (2) can be opened simultaneously. In this case, the arc in break (1) is the first to extinguish (Fig. 4.28*a*) and the arc in break (2) is the next. At present the widely used type of breaker is built around the scheme of Fig. 4.44*b*. The contact system of the second break in this breaker is designed for a lighter duty with account for the current limited by the shunting resistor.

Because shunting resistors markedly ease the extinction of arc in break (1) and in break (2), the level of minimum admissible air blast velocity may be lowered down to $w_{1,\min} = 4\text{-}5$ m / s. The design of the nozzle for break (1) should be carried out with the interrupting capability whereas the design for nozzle (2) may be based on the current limited by the shunting resistor.

The properties required of shunting resistor are as follows.

(1) The resistor should be of small inductive reactance. If inductive reactance is present in break (1), the recovery voltage will experience sharp rise proportional to this inductive reactance.

(2) After the circuit current is diverted into the resistor this has to carry a considerable current that heats it rapidly. Therefore a thermal analysis of the resistor should be performed. Since this current flows for a very short period, about 10-20 ms, the heating occurs adiabatically. The thermal time constant of the resistor is rather high, and it has not enough time to cool under no-current condition. Therefore, in the analysis the time of current flowing through the resistor should be taken equal to the total time of the test duty cycle, namely

$$\int_0^{t_{dc}} I^2 R_{sh} \, dt = cG\Theta \tag{4.32}$$

where I is the current through the resistor, A; R_{sh} is the resistance of the shunt, Ω; t_{dc} is the total time of current passage through the resistor in the given duty cycle with an allowance of 0.01 s per breaking, s; c is the specific heat capacity, J / kg K; G is the resistor weight, kg; and Θ is the maximum admissible temperature, °C.

The shunt resistors are made of heat resistant alloys of high resistivity, like Ni-Cr alloys, which results in resistors of $\Theta \approx 1000$ °C having reasonable size and weight. Recognizing the small temperature coefficient of resistance for materials of this group, the heating increment of R_{sh} may be neglected in a preliminary analysis.

(3) Following the diversion of circuit current into the interrupting resistor, the voltage across this resistor rises to

$$U_{sh} = \sqrt{2}\, U_{r,\,max}\,(1.3\text{-}1.5)\, R_{sh} / \sqrt{3}\sqrt{R_{sh}^2 + X^2}$$

The insulation of this resistance must withstand this voltage with account of the maximum admissible temperature in the order of 1000 °C.

It is worth noting that circuit breakers rated 500 kV and above used to connect power systems via long lines may have to fulfill breaking duties when the systems are out of phase. In this case the recovery voltage may reach (2.5-3) $U_r \times \sqrt{2}/3$. Accordingly, the thermal analysis of the resistors should be carried out for this heavy duty. A detailed discussion of resistor analysis can be found in the book by Afanasyev and Vishnevsky [4.7].

In making high voltage lines switchgear experiences overvoltages that are caused by transient processes in the connected systems and equipment. Overvoltage protection requires that the circuit breaker and the equipment be appropriately insulated. This problem may be especially acute at extremely high voltage ratings where the margins of electric strength have to be reduced. To reduce overvoltage transients, on making long lines the circuit is made in two steps. The contacts (2) (see Fig. 4.28) are closed first and resistor damping overvoltages are brought into the circuit. Then, after a short time delay of about 6 ms, the contacts (1) are closed. Analysis of resistors damping switching overvoltages that arise in making and breaking long lines can be found in Ref. [4.7].

At times three-step circuit making is used to limit switching overvoltage to 1.7 voltage rating. A composite 1500-Ω resistor is connected, then its 1200 Ω part is shunted leaving 300 Ω in the circuit, and finally the 300 Ω resistor is shunted. This system is employed in circuit breakers manufactured by Westinghouse Electric Corporation.

Modern circuit breakers for rated voltage of 220 kV and above have several series breaks per pole. For example, the Soviet-made 750 kV VNV-series circuit breaker (shown in Fig. 4.40) has six breaks. Different stray capacitances of the current carrying elements to earth produce unequal voltage distribution over the contacts. Let us look at the distribution of voltage in a two-break circuit breaker in an earth short-circuit fault. In Fig. 4.30 schematizing this case, C represents the capacitances between the separated contacts and C_1 the capacitance to earth of the connector between the breaks. Break (2) carries the current $i = i_1 + i_2$ and because the capacitances of the breaks are identical, the voltage drop across break (2) is higher

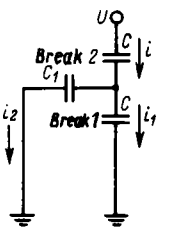

Fig. 4.30. Equivalent circuit of a circuit breaker with two breaks per pole

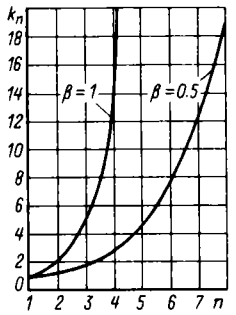

Fig. 4.31. Nonuniformity of voltage distribution over the breaks versus number of breaks for two coefficients

than across break (1). The relative voltage drops across the first break and second break are as follows:

$$\begin{aligned} U_1 / U &= i / \omega (C + C_1) U \\ &= U \omega C (C + C_1) / (2C + C_1) U (C + C_1) \omega \\ &= C / (2C + C_1) \end{aligned}$$

$$\begin{aligned} U_2 / U &= i / \omega CU \\ &= U \omega C (C + C_1) / (2C + C_1) \omega CU \\ &= (C + C_1) / (2C + C_1) \end{aligned}$$

If $C_1 = C$, then the voltage across break (2) will be twice that across break (1), thus $U_1 / U = 1 / 3$ and $U_2 / U = 2 / 3$.

Still greater nonuniformity of voltage distribution is typical of multiple-break circuit breakers. In an n-break circuit breaker, the voltage across break m is given as [4.3]

$$U_m = U \sinh (\beta m) / \sinh (\beta n) \tag{4.33}$$

where $\beta = \sqrt{C_1 / C}$.

A useful means in assessing the voltage distribution across multiple-break switchgear is the absolute degree of nonuniformity defined as the ratio of the most loaded break to the least loaded break

$$k_n = (U - U_{n-1}) / U_1 = (e^{\beta (n-1)} + 1) / e^{\beta (n-1)} (e^{\beta} + 1) \tag{4.34}$$

Figure 4.31 shows k_n as a function of n for various β. At $\beta = 1$ and four breaks per pole the voltage across the fourth break is 14 times the voltage across the first. The relative degree of nonuniformity defined for the system voltage U distributed over n breaks as

$$p_n = n U_n / U$$

may be used to characterize the break overload with regards of a uniform distribution of the system voltage with

$$p_n = n \left[e^{2 \beta n} - 1 - e^{\beta} (e^{2\beta (n-1)} - 1) \right] / e^{2\beta n} - 1$$

Circuit breakers with horizontal arrangement of interrupters have received wide acceptance at present (see Fig. 4.4). These layouts have typically large values of β and markedly nonuniform distribution of voltage across the breaks. For VNV 750-kV circuit breaker, C = 55 pF, and C_1 = 40-70 pF. Experimental evidence indicates that the first break (from earth) receives 0.01 U and the sixth break receives 0.65 U.

The system voltage drop across the breaks is equalised with the aid of shunting capacitors and equalising resistors. If a capacitor C is shunted by a capacitance $C_{sh} \gg C$, then $\beta = \sqrt{C_1 / (C + C_{sh})}$ decreases appreciably thus aiding in voltage equalisation among the breaks. Normally C_{sh} is of the order of 1500-2000 pF. Small size high-voltage capacitors with ceramic insulation have been developed for this purpose and superceded metallic and ceramic resistors that parallelled the break. If $R_{sh} \ll 1 / \omega_0 C_1$, where ω_0 is the highest frequency of the recovery voltage, a satisfactory voltage distribution can be attained.

Present switchgear systems rarely use equalising resistors because these are difficult to produce (metal resistors are 100-200-k Ω units and should have low inductive reactance) and need an isolating switch to break the resistor current. In addition, the equalising action of the resistor diminishes with the growth of frequency. Therefore, the appropriate resistance is determined [4.3] with allowance for these phenomena as

$$R_{sh} \leqslant 1 / 20 \omega_0 C_1$$

where ω_0 is the highest angular frequency of the transient recovery voltage.

Once C_{sh} or R_{sh} has been selected, the equivalent circuit is analysed and the nonuniformity coefficient p_n is determined that should not exceed 1.05 to 1.15. This coefficient should be taken into account while the axial dielectric strength of the breaker pole is determined.

Shunt resistors are also used to ease disconnection of unloaded lines. The resistance of these interrupting resistors is lower than that of their equalising counterparts. Circuit breaking is effected in two steps: the first break (Fig. 4.28*b*), shunted by a resistor, opens first, then the second break interrupts the current of the resistor. The value of this resistor may be selected with the aid of the curves shown in Figs. 4.32 and 4.33 borrowed from the book of Tseirov [4.3]. The abscissa shows the product of shunt resistance R_{sh} by the line capacity C_l, and the ordinate gives the ratio of the peak voltage $\hat{U}_1$ in 0.01 s after arc extinction to the peak voltage on the power supply side, $\hat{U}$, and half this ratio $\hat{U}_1 / 2\hat{U}$. Figure 4.33 will be used to determine the overvoltages setting up across auxiliary interrupting breaks; here, $\hat{U}_2 / \hat{U}$ is the ratio of peak voltages across the break and on the supply side, and $\hat{U}_2 / 2\hat{U}$ represents half this ratio.

The shunt resistor is a complicated piece of electrical gear. Inductance of the unit is reduced by a bifilar winding of round or ribbon-shaped wire put on a ceramic resistor core. The resistor is heavy and its technology is involved and costly. One of the recent additions in the field is concerned with shunting resistors of electrotechnical concrete [4.7], called 'betel' in the Soviet literature. The desired resistivity is adjusted by adding conductive admixtures, such as graphite, to the

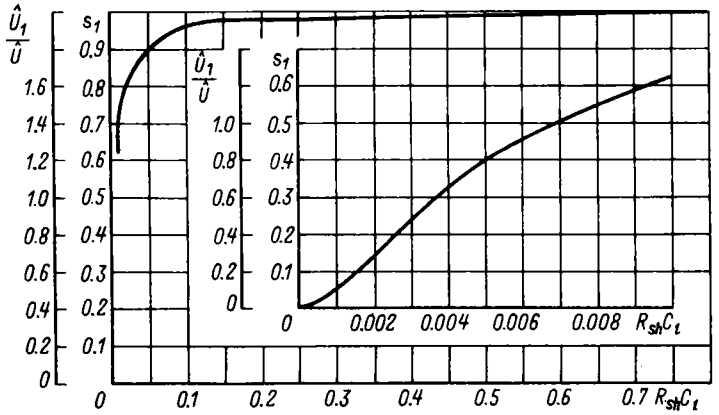

Fig.4.32. Relative voltage across the breaker as a function of the product $R_{sh}C_l$ upon opening of the first break

concrete mix. This material exhibits a nonlinear current-voltage behaviour

$$U = R_0 I^{\alpha}$$

where U is the applied voltage, kV; I the current in kA, R_0 the initial resistance in ohms (at 110-220 V), and α the nonlinearity exponent equal to 0.8-0.95. A sectional view of such a resistor is shown in Fig. 4.34. The active core (2) is assembled of 'betel' concrete discs encapsulated within the porcelain insulator (3) with caps (5) and (6). The contact pressure of the discs is ensured by the spring (4). A membrane valve (1) is provided to prevent destruction of the hollow insulator in case of internal flashover. Resistors of this type are of low inductance (below 40 μH

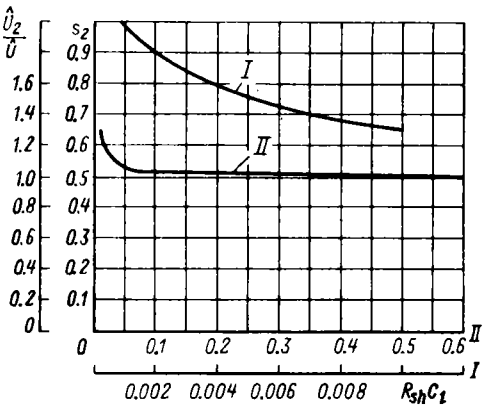

Fig. 4.33. Relative voltage across the breaker as a function of $R_{sh}C_l$ upon opening the auxiliary break

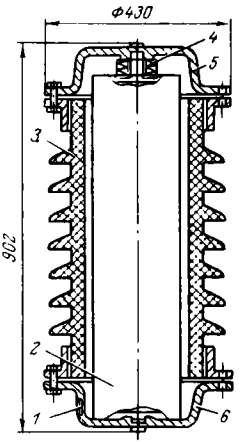

Fig. 4.34. Shunt resistor of electrotechnical-grade concrete. All dimensions are in mm

at $R_0 = 200\ \Omega$), whereas for the sake of comparison metallic resistors of the same resistance have an inductive reactance of the order of 1200 μH. Concrete resistors are attractive propositions for the industry because of cheap material, high reliability, and simple design.

4.6 Gas Dynamics of Air Circuit Breakers

Whenever an air-blast circuit breaker is called upon to open or close a circuit, the control system opens the respective blast valves and the compressed air stored in the air reservoir is fed to separate the contacts and extinguish the arc. For the breaker to operate reliably and within the specified break or make time limits the breaker design must ensure a certain law of pressure and air blast variation in the various pertinent components of the breaker.

Two regimes of gas outflow are characteristically different and dependent on the relative backpressure of the medium in which the gas is injected. At small pressure difference the velocity of air flow depends on backpressure. This flow regime is referred to as a subcritical (subsonic) flow. If the pressure difference is rather high, then the flow velocity becomes independent of backpressure and is governed solely by the parameters of the emitted gas. This regime is referred to as a supercritical (supersonic) flow. For most of gas dynamics processes the problem under consideration may be simplified by assuming that (i) the outflow of gas occurs adiabatically (without heat supply and dissipation), (ii) the outflow is steady state, and (iii) the flow is frictionless. Which of the flow regimes takes place is decided by the critical ratio of pressures

$$(p_b / p_{rvr})_{cr} = \left(\frac{2}{k+1}\right)^{k/(k-1)} \tag{4.35}$$

where p_b is the backpressure, p_{rvr} gas pressure in the reservoir, and k the adiabatic

exponent. Accordingly, a subcritical flow forms for $p_b / p_{rvr} > (p_b / p_{rvr})_{cr}$, whereas a supercritical flow takes place for $p_b / p_{rvr} < (p_b / p_{rvr})_{cr}$.

In the subcritical flow, the medium pressure and density in the nozzle exit section are p_b and γ_b, that is, equal to the parameters of the medium where the gas is flowing. In the supercritical flow, the parameters of the section medium are the pressure, density and temperature of the critical regime, which depend only on the reservoir gas parameters, namely,

$$p_{cr} = \left(\frac{2}{k+1}\right)^{k/(k-1)} p_{rvr}$$

$$\gamma_{cr} = \left(\frac{2}{k+1}\right)^{1/(k-1)} \gamma_{rvr} \tag{4.36}$$

$$T_{cr} = 2T_{rvr} / (k+1)$$

The flow velocity in the subcritical regime is given by the equation

$$v_{sub} = \sqrt{\frac{2k}{k-1} \frac{p_{rvr}}{\gamma_{rvr}} \left[1 - \left(\frac{p_b}{p_{rvr}}\right)^{(k-1)/k}\right]} \tag{4.37}$$

valid for $p_b / p_{rvr} > (p_b / p_{rvr})_{cr}$.

At $p_b / p_{rvr} = (p_b / p_{rvr})_{cr}$ the critical flow velocity is set up at the nozzle exit section

$$v_{cr} = \sqrt{2kp_{rvr} / (k+1)\gamma_{rvr}} = \sqrt{2kRT_{rvr} / (k+1)} \tag{4.38}$$

where R is the gas constant equal to 287 J / kg K.

The mass flow rate of gas passing section S per second is

$$G = S\gamma v \tag{4.39}$$

where γ is the gas density in the section, and v is the flow velocity. For the subcritical regime,

$$G = S\gamma_{sub} v_{sub} \mu$$

where μ is a coefficient allowing for the efficient section of the outflowing jet being smaller than the orifice because of jet contraction. This contraction occurs owing to sharp edges of the exit section and its shape. The coefficient varies from 0.4-0.5 for sections with sharp edges to 0.8-0.9 for round profile and the edges machined to high surface finish. Manufacturers tend to raise μ in order to gain higher flow rates.

Because the outflow process is adiabatic and $p / \gamma^k = \text{const}$, we may write

$$\gamma_b = \gamma_{rvr} (p_b / p_{rvr})^{1/k} \tag{4.40}$$

For the subcritical regime we have

$$G_{sub} = \mu S \gamma_{rvr} (p_b / p_{rvr})^{1/k} v_{sub}$$

$$= \mu S \sqrt{\frac{2k}{k-1} p_{rvr} \gamma_{rvr} \left[\left(\frac{p_b}{p_{rvr}} \right)^{2/k} - \left(\frac{p_b}{p_{rvr}} \right)^{(k+1)/k} \right]}$$

$$= \mu S \Psi_{sub} \sqrt{p_{rvr} \gamma_{rvr}} \tag{4.41}$$

where

$$\Psi_{sub} = \sqrt{\frac{2k}{k-1} \left[\left(\frac{p_b}{p_{rvr}} \right)^{2/k} - \left(\frac{p_b}{p_{rvr}} \right)^{(k+1)/k} \right]} \tag{4.42}$$

Similarly for the supercritical regime we have

$$G_{cr} = \mu S \gamma_{cr} v_{cr}$$

$$= \mu S \left(\frac{2}{k+1} \right)^{1/(k-1)} \sqrt{\frac{2k}{k+1} p_{rvr} \gamma_{rvr}}$$

$$= \mu S \Psi_{sup} \sqrt{p_{rvr} \gamma_{rvr}}$$

$$= 0.687 \mu S \sqrt{p_{rvr} \gamma_{rvr}} \tag{4.43}$$

Here, G is the mass flow rate, kg / s; S is the area of the orifice, m^2; $k = 1.4$ is the adiabatic exponent for two-atomic gases and air; p_{rvr} is the pressure in the reservoir, N / m^2; and γ_{rvr} is the density of air in the reservoir, kg / m^3.

In view of Eqs. (4.36) and (4.38) for air we have $p_{cr} = 0.527 p_{rvr}$, $\gamma_{cr} = 0.636 \gamma_{rvr}$, $T_{cr} = 0.833 T_{rvr}$ and $v_{cr} = 18.2 T_{rvr}^{1/2}$. Since the velocity of sound in a medium at temperature T is $a = (kRT)^{1/2}$ [4.7], the critical flow velocity $v_{cr} = 0.914a$. Hence, the critical velocity of outflow approaches the velocity of sound in a medium at temperature T.

Consider some typical problems of gas dynamics with reference to air circuit breakers.

(i) *Discharge of the air from a limited capacity vessel.* The mass flow rate of air in time dt is

$$G\mathrm{d}t = -V\mathrm{d}\gamma_{rvr} \tag{4.44}$$

Air leaving the reservoir causes the pressure and density in the vessel to decline. This depression is indicated by the minus sign on the right-hand side of the equation.

Assume that we need to determine the time interval after which the pressure p_0 falls to p_i. For exhaust in the atmosphere, $p_b = p_{atm}$ and

$$p_{rvr} > p_{cr} = p_{atm} [(k+1)/2]^{k/(k-1)} \tag{4.45}$$

and the exhaust proceeds in the supercritical flow regime. Recall that for air $k = 1.4$.

Expressing p_i and γ_i in terms of the initial parameters

$$p_i = p_0 (\gamma_i / \gamma_0)^k \tag{4.46}$$

introducing relative pressure

$$\varepsilon = p_i / p_0 \tag{4.47}$$

and observing Eqs. (4.43-47) we get

$$\mathrm{d}t = \frac{V}{\mu S \Psi_{\mathrm{sup}} k} \sqrt{\gamma_0 / p_0}\ \varepsilon^{(1 - 3k) / 2k}\, \mathrm{d}\varepsilon \tag{4.48}$$

Solving this equation, we obtain for the supercritical flow regime

$$t_{\mathrm{sup}} = \frac{2V}{\mu S \Psi_{\mathrm{sup}} (k - 1)} \sqrt{\frac{\gamma_0}{p_0}} (\varepsilon^{(1 - k) / 2k} - 1)$$

$$= \frac{2V}{\mu S \Psi_{\mathrm{sup}} (k - 1)} \sqrt{\frac{1}{RT_0}} (\varepsilon^{(1 - k) / 2k} - 1) \tag{4.49}$$

The value $\varepsilon = \varepsilon_{\mathrm{cr}} = \varepsilon_{\mathrm{atm}} [(k + 1) / 2]^{k / (k - 1)} = 0.527$ terminates the regime of supercritical flow ($\varepsilon_{\mathrm{atm}} = p_{\mathrm{atm}} / p_0$ is the relative atmospheric pressure). This occurs at the time instant

$$t_{\mathrm{cr}} = \frac{2V}{\mu S \Psi_{\mathrm{sup}} (k - 1)} \sqrt{\frac{\gamma_0}{p_0}} (\varepsilon_{\mathrm{cr}}^{(1 - k) / 2k} - 1)$$

$$= \frac{2V}{\mu S \Psi_{\mathrm{sup}} (k - 1)} \sqrt{\frac{1}{RT_0}} (\varepsilon^{(1 - k) / 2k} - 1) \tag{4.50}$$

After t_{cr} the flow becomes subcritical. Analytical expressions for this flow regime result by incorporating in Eq. (4.44) the expression for G calculated by Eq. (4.41). The full subcritical flow time ($\varepsilon = \varepsilon_{\mathrm{atm}}$) results as [4.3]

$$t_{\mathrm{sub,\,full}} = 0.309 \frac{V}{\mu S \varepsilon_{\mathrm{atm}}^{1/7}} \sqrt{\frac{1}{RT_0}} \tag{4.51}$$

and the total time is $t_{\mathrm{total}} = t_{\mathrm{cr}} + t_{\mathrm{sub,\,full}}$.

In the case when the air volume in the reservoir and the nozzle section $f(t)$ vary with time, the mass flow equation will be written as

$$G\,\mathrm{d}t = \mu v \gamma f(t)\ \mathrm{d}t = -\mathrm{d}(V \gamma_{\mathrm{rvr}}) = -V\mathrm{d}\,\gamma_{\mathrm{rvr}} - \gamma_{\mathrm{rvr}}\,\mathrm{d}V \tag{4.52}$$

or

$$f(t)\,\mathrm{d}t = (\varepsilon^{(1 - k) / 2k}\mathrm{d}V + \frac{1}{k} V\varepsilon^{(1 - 3k) / k}\mathrm{d}\varepsilon) /$$

$$/ \mu \Psi \sqrt{RT_0} \tag{4.53}$$

In order to determine $\varepsilon(t)$ the functions $f(t)$ and $V(t)$ must be given.

(ii) *Filling a limited capacity vessel from unlimited volume.* This problem is different from the previous one in that the air dumped into the vessel compresses the gas there. The rise of pressure in the vessel is accompanied by a rise of gas temperature. The equation of gas flow is now written as

$$G\,dt = d(V\gamma - V\gamma_{atm}) \tag{4.54}$$

where γ_{atm} is the initial density of air in the vessel assumed to be equal to the density of air at atmospheric pressure.

In view of γ_{atm} = const, from Eq. (4.54) we have

$$\mu S \Psi \sqrt{p_0 \gamma_0}\,dt = V\,d\gamma \tag{4.55}$$

where γ_0 is the density of air in unlimited volume.

For the supercritical flow regime, the solution of Eq. (4.55) has the form

$$t_{sup} = V(\gamma - \gamma_{atm}) / \mu S \Psi_{sup} \sqrt{p_0 \gamma_0} \tag{4.56}$$

or in view of the dependence between γ and ε [4.3] we get

$$t_{sup} = V(\varepsilon - \varepsilon_{atm}) / \mu S \Psi_{sup} \sqrt{RT_0} \tag{4.57}$$

where T_0 is the air temperature in unlimited volume.

Above $\varepsilon_{cr} = 0.527$ the flow becomes subcritical and the respective analytical expression will be

$$\mu S \Psi_{sub} \sqrt{p_0 \gamma_0}\,dt = V\,d\gamma \tag{4.58}$$

Solving this equation [4.3] yields

$$t_{sub} = \frac{2V}{\mu S \sqrt{2k(k-1)RT_0}} \left(\sqrt{1 - \varepsilon_{cr}^{(k-1)/k}} - \sqrt{1 - \varepsilon^{(k-1)/k}}\right) \tag{4.59}$$

The temperature of the gas may be determined from an energy balance analysis

$$h_0\,dG = d(hG) - (G/\gamma)\,dp \tag{4.60}$$

where h_0 is the air enthalpy in the source volume, $h_0\,dG$ is the heat introduced with the feed air, $d(hG)$ is the variation of air enthalpy in the vessel, and $(G/\gamma)\,dp$ is the compression work of the gas filling the vessel.

Solving Eq. (4.60) yields [4.3] gas temperature and density

$$\gamma = \gamma_{atm}(k-1)/(k - T/T_0) \tag{4.61}$$

At $\gamma = \gamma_0$ the air temperature will be

$$T_{fin} = \frac{k}{1 + (k-1)\gamma_{atm}/\gamma_0} T_0 \tag{4.62}$$

(iii) *Simultaneous inflow of air in a vessel V_2 and exhaust of air from this vessel through an orifice S_2* (Fig. 4.35*a*). This situation takes place after contact separation in an interrupting chamber. For variation of air density in vessel V_2 we have

$$d\gamma/dt = (G_1 - G_2)/V_2 \tag{4.63}$$

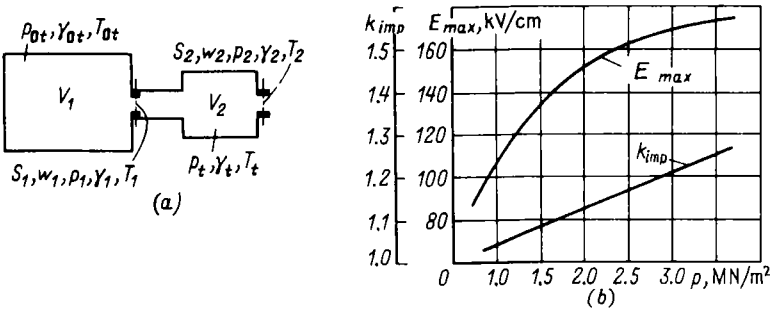

Fig. 4.35. (*a*) Schematic diagram to calculate the pressure in the interrupter chamber (space V_2) after uncovering port S_2. (*b*) Dielectric strength of compressed air as a function of pressure

where G_1 is the flow rate through the orifice S_1 and G_2 the flow rate through the orifice S_2.

At the moment of full contact separation, the pressure set up in V_2 (interrupter chamber) is $p_t \geqslant 0.53\, p_{0t}$. Thus, air flows in the chamber through the orifice S_1 in the subcritical regime and G_1 is defined by virtue of Eq. (4.42)

$$G_1 = \mu_1 S_1 \gamma_1 v_1 \tag{4.64}$$

The exhaust occurs in the supercritical flow regime and

$$G_2 = \mu_2 S_2 \gamma_{cr} v_{cr} \tag{4.65}$$

Substituting Eqs. (4.64-65) in Eq. (4.63) and rearranging yields [4.1]

$$t = \frac{V_2}{kS_1 v_{cr}} \int_{\varepsilon_{in}}^{\varepsilon_t} \frac{1}{\varepsilon_t} \left[\varphi(\varepsilon) \left(1 - \frac{V_2}{V_1} \varepsilon^{1/k} \right) - 0.57 \frac{S_2}{S_1} \varepsilon^{1/k} \right]^{-1} \mathrm{d}\, \varepsilon_t \tag{4.66}$$

where $\varepsilon_t = p_t / p_{0t}$; $\varepsilon_{in} = p_{t,in} / p_{0,in}$ is the relative pressure at the moment the nozzles set open, $t = 0$; and

$$\varphi(\varepsilon) = \sqrt{2 (1 - \varepsilon^{(k-1)/k}) / (k-1)}$$

In a real circuit breaker, $p_{0t} = p_{0,in} = \text{const}$, so that the pressure in the chamber

$$p_t = p_{0,in}\, \varepsilon_t \tag{4.67}$$

The integral in (4.66) is determined graphically for a given ε_t. In a steady state, the pressure in V_2 is at the critical level $p_{2,cr}$, and the exhaust velocity is $v_{2,cr}$.

Some other problems of pertinent gas dynamics and examples of analytical investigations can be found in the books by Kukekov [4.1], Tseirov [4.3], and Afanasyev and Vishnevsky [4.7].

(iv) *Filling and emptying the pipes.* The process of filling a pipe by air or of

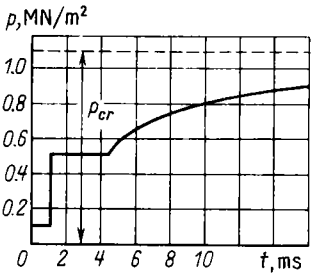

Fig. 4.36. Time variation of pressure at the tube outlet

discharging the compressed air from a pipe takes a certain time span. In designs rated for 750-1150 kV, the length of pipes selected for reasons of appropriate insulation reaches 8-10 m and the process of transition flow in the piping takes considerable time.

Figure 4.36 illustrates the variation of pressure at the outlet of a 8.5-m long pipe connected with an air reservoir at $p_0 = 2.1$ MN / m^2. In 16 ms the outlet pressure is seen to be far from steady state. Under the circumstances the breaker would not operate at a desired speed. Therefore upgraded fast-speed circuit breakers have their interrupters placed in compressed air reservoirs and the blast valve is controlled by means of long glass-reinforced plastic links. The resultant break time is then as low as 40 ms.

4.7 Analysis and Selection of Interrupting Chamber Parameters

The point of departure in a nozzle analysis is the arc spacing, l_a. We assume that this distance equals the contact spacing l_c in arc extinction. For rough estimations this contact spacing may be calculated with a formula from Sect. 3.3. as

$$l_c = \frac{k_a k_p \sqrt{2}\, U_{r,\max}}{\sqrt{3}\, n E_{air}} k_s k_{nu} \tag{4.68}$$

where $U_{r,\max}$ is the rated maximum voltage, $k_s = 1.2$ is a safety factor; $k_{nu} = 1.1$ allows for nonuniform distribution of voltage over the breaks; k_a is the amplitude coefficient; k_p is the coefficient for the pole opened first; n is the number of breaks per pole; and E_{air} is the dielectric strength of air flowing through the interrupting chamber, kV / m.

The number of breaks may be selected considering that for an air tank pressure of 2 MN / m^2 the voltage rating per break is about 55 kV, and for 4 MN / m^2 the rating is about 125 kV. Therefore a two-break module will be rated for 110 and 250 kV at these pressures.

The dielectric strength of an air gap depends on the shape of the electrodes, pressure, and blast velocity. The dielectric strength of moving air is 0.67-0.80 the strength of stationary air at the same pressure. One may approximately let that for a moving air $E_{max} = 34$-45 kV / m at interrupter pressures of 0.9-1 MN / m^2.

Accordingly, the distance between the arcing contacts may be selected from the curves of breakdown voltage versus electrode spacing for the electrode geometry close to the actual interrupter contacts immersed in rapidly flowing air.

It is recommended to calculate the nozzle diameter on the lines of the procedure outlined in Sect. 4.3. For bilateral blast designs, the arc power per break is $P_a / 2$. An order-of-magnitude estimation can be achieved with Tseirov's formula [4.3] derived for a symmetric bilateral-blast nozzle

$$d_n = 2.77 \times 10^{-2} \sqrt{I_{b,r}}$$

where $I_{b,r}$ is the rated breaking current, A; and d_n is the nozzle diameter, cm.

For unilateral-blast designs, interrupting current can be estimated by the Labouret empiric formula allowing for the contact spacing

$$I = 5000 S_n / l_c$$

where I is the current being interrupted, A; S_n is the nozzle section area, cm^2; and l_c is the contact spacing, cm.

An optimal contact spacing from a standpoint of arc extinction may be taken as $0.35 d_n$ for unilateral-blast designs, and $0.45 d_n$ for bilateral-blast versions (Sect. 4.3). This value of l_c should be compared with the value of l_c derived by Eq. (4.68). The calculation is repeated if necessary with an optimal l_c value.

The distance between pole contacts should be checked with the test voltage at normal frequency and with the impulse voltage level as

$$l_c = U_{test} k_{nu} k_{coord} / E_{adm} \eta n k_{imp} \tag{4.69}$$

where k_{coord} is a coefficient allowing for the coordination (ratio) of the test voltage for the insulation to that for the inner insulation (since the outer insulation is subjected to atmospheric impacts $k_{coord} \approx 2.4$ for 750-kV voltage rating; E_{adm} is the largest admissible field strength for a given pressure (Fig. 4.35*b*), k_{imp} is an impulse coefficient which depends on pressure and is used in the calculation of l_c for the impulse test voltage; and $\eta = E_{av} / E_{max}$ allows for the nonuniform distribution of the electric field, found to be about 0.65 [2.4].

Circuit breakers with two-step contact separation, first for an optimal distance, then, after extinction is over, for a wider spacing, should be tested with Eq. (4.69) for open contact state.

Once the nozzle diameter d_n and contact spacing l_c have been evaluated, the dielectric strength recovery between the contacts is calculated and compared with the recovery curve specified by the respective standard [3.1].

Contacts and Current-carrying Circuit

Increasing current ratings and interrupting currents motivated predominant use of finger contact systems over other designs. The current passing through one finger contact is

$$I_f = I_r k_{nu} / n$$

where I_r is the rated continuous current, A; k_{nu}, normally equal to 1.3, allows for

the nonuniform distribution of current over the finger contacts, and n is the number of fingers.

High-rating designs have $n = 20$ to 40. The pressing (mechanical) force per contact finger is given [4.1] as

$$F_c = (I_r \times 1.3 / n)^2 \times A\pi H / 16\lambda^2 [\arccos (T_0 / T_c)]^{-2} \tag{4.70}$$

where $A = 2.42 \times 10^{-8}$ V^2 / K^2; H is the Vickers hardness number; λ is the thermal conductivity, W / m K; T_c is the temperature at the point of contact, K; T_0 is the temperature of the contact body, K, computed by the Newton formula, for which the recommended difference is $T_c - T_0 \leqslant 5$ to 10 K.

The selected pressing force F_c should be verified by the current of mechanical rating. The necessary force of the spring can be estimated by the formula derived by G. V. Butkevich, viz.,

$$F_c \geqslant \frac{1}{k^2} (k_{mw} \sqrt{2}\, I_{b,r} \times 1.3 / n)^2 \tag{4.71}$$

where k is an empirical coefficient selected in the handbook [2.1] and $k_{mw} = 1.8$ is the mechanical withstand coefficient.

This pressing force should be also verified for the temperature at the contact point. The actual force of contact which determines the bearing pad area may be represented as

$$F_{act} = F_{sp} + F_{ed} - F_{rep} \tag{4.72}$$

where F_{sp} is the pressing due to spring action, F_{ed} is the electrodynamic pressing of contacts due to the attraction of the particular finger to other fingers, and F_{rep} is the repulsive force due to contraction of the streamlines. This equation can be rewritten as

$$F_{act} = S_0 H_{max} = F_{sp} + F_{ed} - 10^{-7} i_f^2 \ln (S / S_0) \tag{4.73}$$

where S_0 is the bearing area, i_f instantaneous current through the finger contact, S the contact cross section, and H_{max} the Vickers hardness number at a maximum admissible temperature which may be taken at 1073 K (see Fig. 4.63). Solving this equation one can determine the bearing pad area S_0.

The temperature at the point of contact can be found with Kukekov's formula [4.1]

$$T_c = T_0 / \cos (2.65\, i_f \sqrt{H_{max}} \times 10^{-4} / 4\lambda \sqrt{F_{act}}) \tag{4.74}$$

where T_0 is the temperature of the contact body taken to be 573 K at short circuit.

The force F_{act} is determined from Eq. (4.73) after S_0 has been found. If T_c determined by Eq. (4.74) differs from the adopted level of 1073 K, then S_0 should be recomputed with Eq. (4.73) incorporating the value of H_{max} for the derived value of T_c.

In modern circuit breakers, the current carrying element is made of a pipe surrounded by the concentric layers of air, glass epoxy cylinder and porcelain insulator. At rated current this element is in a heated condition. Figure 4.37*a* is a cross section of the extinction chamber of a VNV-type circuit breaker (see Fig. 4.47). The heat abstraction conditions are poorest in the mid-section of this pipe.

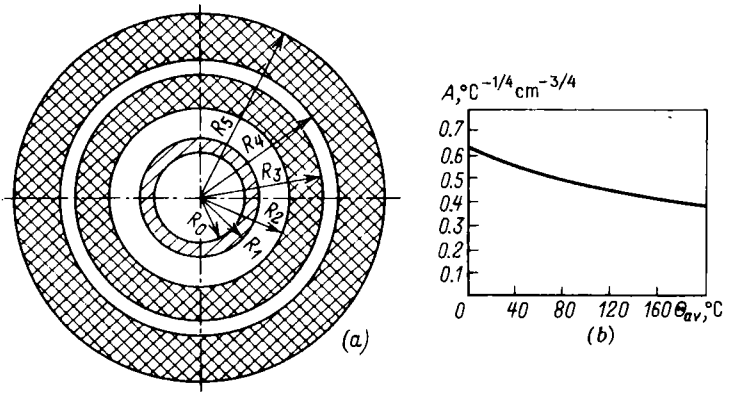

Fig. 4.37. (*a*) Cross section of a VNV-type interrupter. (*b*) Coefficient A for average layer temperature θ_{av} in Eq. (4.79)

The inner diameter of this pipe is taken to be 3 to 8 d_n to facilitate the removal of arc-burning products. The external diameter of the pipe is evaluated after the cross section of the pipe has been found. The heat flux is assumed to flow in radial directions only. To simplify consideration, a 1-cm length of pipe is analysed. In steady state all heat energy released by the pipe streams in the radial direction through the concentric envelopes and is dissipated by the outer surface of the porcelain insulator to the surroundings:

$$I_r^2 \varrho_0 (1 + \alpha\Theta_{max}) / S = (\Theta_{max} - \Theta_p)/R_{th} = k_p S_1 (\Theta_p - \Theta_0) \tag{4.75}$$

where S is the section of the pipe, α is the temperature coefficient of resistance, Θ_{max} is the temperature of the pipe, Θ_p is the temperature of the porcelain surface, Θ_0 is the ambient temperature, S_1 is the cooled insulator area per unit length, k_p is the heat transfer coefficient per unit surface of porcelain insulator, and R_{th} is the total thermal resistance of the pipe from inside to the surface of porcelain insulator. This equation may be rearranged to the form

$$S = I_r^2 \varrho (R_{th} k_p S_1 + 1)/k_p S_1 (\Theta_{max} - \Theta_0) \tag{4.76}$$

where $\varrho = \varrho_0 (1 + \alpha\Theta_{max})$ and is taken for a maximum admissible temperature of 110°C.

The total thermal resistance is given as

$$R_{th} = \frac{1}{2\pi} \sum_{i=1}^{n} \frac{\ln (r_{i+1} / r_i)}{\lambda_i} \tag{4.77}$$

In evaluating the thermal resistance of the layer of compressed air one has to observe appreciable convection in addition to heat conductance. Therefore Eq.

(4.77) may be used upon incorporation of the equivalent thermal conductivity of air [4.1] as

$$\lambda_{\text{air, eq}} = \lambda_{\text{air}}\, \varepsilon_{\text{conv}} \tag{4.78}$$

$$\varepsilon_{\text{conv}} = A \sqrt[4]{\Delta\, \Theta\, \delta^3} \tag{4.79}$$

where δ is the thickness of the air layer, m; $\Delta\,\Theta$ is the expected temperature difference, K; A is the coefficient found in the curve of Fig. 4.37*b* for the mean temperature of the layer

$$\Theta_{\text{av}} = (\Theta_i + \Theta_{i+1}) / 2 = \Theta_i + \Delta\,\Theta / 2$$

With reference to the structure of Fig. 4.37 we have

$$R_{\text{th}} = \frac{1}{2\pi} \left[\frac{\ln (R_2 / R_1)}{\lambda_{\text{air, eq1}}} + \frac{\ln (R_3 / R_2)}{\lambda_{\text{ep}}} + \frac{\ln (R_4 / R_3)}{\lambda_{\text{air, eq2}}} + \frac{\ln (R_5 / R_4)}{\lambda_{\text{p}}} \right] \tag{4.80}$$

where $\lambda_{\text{air, eq1}}$ and $\lambda_{\text{air, eq2}}$ are equivalent thermal conductivities for cylindrical air spacings, λ_{ep} is the thermal conductivity of the epoxy cylinder, and λ_{p} is the thermal conductivity of porcelain insulator. A more elaborate computational procedure for $\varepsilon_{\text{conv}}$ is given in Sect. 4.14.

Contact Operating Mechanism

The analytical schematic diagram of the drive mechanism is shown in Fig. 4.38. The moving contact (1) is pressed to the stationary contact (2) by a spring (3). The moving contact piston (4) is free to move in the cylinder (5). When compressed air is allowed in the chamber the air pressure p_{ch} in the chamber increases from ambient p_{atm} to the takeoff level p_{to}. Accordingly, the contact will be set in motion when $F_{\text{open}} = F_{\text{closed}}$,

$$F_{\text{open}} = p_{\text{ch}} (S_1 - S_2) = F_{\text{closed}} = F_{\text{sp}} + p_{\text{atm}} (S_1 - S_2) \tag{4.81}$$

$$p_{\text{to}} = F_{\text{sp}} / (S_1 - S_2) + p_{\text{atm}} \tag{4.82}$$

The pressing force of spring F_{sp} is determined from analysis of the contact system, and the section of the nozzle S_2 is found by analysis of thermodynamic deceleration. Therefore, the take-off pressure is related to section S_1. The takeoff pressure is of significance for both arc extinction and contact wear. It is normal for such extinction chambers that $p_{\text{to}} = 0.3\text{-}0.4$ MN / m^2.

The time of contact separation is determined from the equation of motion

$$m \frac{\mathrm{d}^2 l}{\mathrm{d}\, t^2} = (S_1 - S_2)\, (p_{\text{ch}} - p_{\text{to}}) \tag{4.83}$$

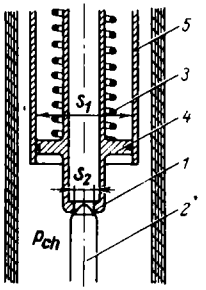

Fig. 4.38. Closing mechanism of an air-blast interrupter

where m is the mass of the moving contact, l the contact travel, and p_{ch} the pressure in the extinction chamber.

It is worth noting that pressure in the chamber p_{ch} varies in time in a rather complicated manner and depends on the parameters of air pipe, nozzles, tank pressure, and the like. Good performance has been obtained [4.3] at p_{ch} = const. In this case

$$l = \frac{p_{ch} - p_{to}}{2m} (S_1 - S_2) t^2 \tag{4.84}$$

The contact moves with an acceleration. In circuit breakers with this mechanism, the total travel time is under 15 ms. The chamber pressure can be taken equal to 0.6-0.7 MN / m^2 [4.3].

In order to avoid shocks mutilative for the porcelain insulator the moving contact should be decelerated at the end of opening stroke, otherwise shock forces in the order of 10^4 newtons might occur. A usual solution is rubber shock mounts. The deceleration process is described by the equation

$$(S_1 - S_2)(p_{ch} - p_{to}) - \eta l = m \frac{dV}{dt} \tag{4.85}$$

where V is the speed of contact, m / s; η is the rigidity of the rubber shock mount, N / m; and l is the contact travel in deceleration. The braking law of motion may be described as [4.3]

$$l = V_{in} \sqrt{m / \eta} \sin (\sqrt{\eta / m}\, t) + (S_1 - S_2)(p_{ch} - p_{to})[1 - \cos (\sqrt{\eta / m}\, t)] / \eta \tag{4.86}$$

This equation yields the total time of contact travel and the maximum deceleration force.

In modern circuit breakers, arc control chambers are put in compressed-air tanks in order to achieve more efficient arc control and diminish contact wear. As soon as the contacts part, the nozzle finds itself at the critical pressure (1.0-2.0 MN / m^2) ensuring high interrupting capacity, high dielectric strength of the arc spacing, and small wear of the contacts.

Some designs employ two-step contact separation procedure: the contacts first

separate at an optimal distance from the standpoint of arc control, then the moving contact is withdrawn further to give a sufficient contact clearance to withstand test voltage levels. To increase the dielectric strength of the contact spacing, the exhaust valves of the chamber are closed, the extinction chamber is sealed and the arc spacing appears filled with stationary high-pressure air of high dielectric strength.

4.8 Control System Components

Make-break operations in circuit breakers are initiated by control system valves. How fast a circuit breaker will close or open the circuit largely depends on the operating time of the control valves. On interrupting a circuit the blast (dump) valve has to release 3-5 m^3 of air in a time of a few hundreds of a second, therefore the orifice of the valve must have a diameter of 100 mm or larger and a rather bulky structure. Referring to Fig. 4.39*a*, let us calculate the force necessary to drop the disc (1) and port compressed air in the pipe S_1:

$$F_{open} \approx \pi d_1^2 (p_0 - p_{atm}) / 4 \approx S_1 p_0$$

Given $d_1 = 120$ mm and $p_0 = 2$ MN / m^2, we have

$$F_{open} = 3.14 \times 0.12^2 \times 2.0 \times 10^6 / 4 = 22\ 608 \text{ N}$$

If the designer decided to use a d.c. tripping coil for this purpose, then it would be a heavy large-size structure with a current requirement of 200 A at 220 V. Above all, however, it is its operating time, and this electromagnet would not operate faster than 1 s, which is inadmissible. The speed for the blast valve must be within 10-20 ms. Therefore, a pneumatic control system is used in which a tripping electromagnet develops about 300-400 N of force at a desired speed of action.

Differential Valve

In the differential valve shown in Fig. 4.39*a*, the sealing disc (1) seals the air pipe of cross section S_1. The valve is inside a compressed air tank (3). The disc is linked with the drive piston (4) equipped with a piston ring (5). The valve is controlled by opening and closing the port S_3. When the port is closed, the forces applied to the piston are in equilibrium, so that the pressure under the piston is $p = p_0$ (air is passing through the port S_4). The disc is sealed by the force $F = (p_0 - p_{atm}) S_1$ and the force of spring F_{sp}. Once the port S_3 is opened the pressure under the piston (4) drops rapidly (S_4 is small compared with S_3) and after a certain time the force of valve opening

$$F_{open} = p_0 S_2 + p_{atm} S_1 \tag{4.87}$$

exceeds the closing force

$$F_{closed} = p S_2 + F_{sp0} + p_0 S_1 \tag{4.88}$$

and sets the valve in motion. The nomenclature of the penultimate and last equations is as follows: p_0 is the initial pressure in the tank, S_2 is the cross section of the piston, p_{atm} is atmospheric pressure, p is the pressure under the piston, and F_{sp0} is the initial force of spring (2).

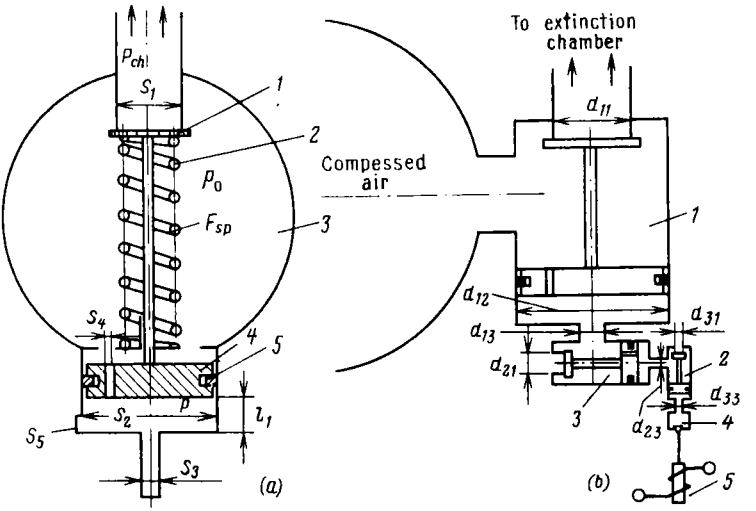

Fig. 4.39. Differential valve: (*a*) schematic diagram, (*b*) control circuit

Letting $F_{\text{open}} = F_{\text{closed}}$ yields

$$\varepsilon_{\text{to}} = p_{\text{to}} / p_0 = 1 - \frac{S_1}{S_2}\left(1 - \frac{p_{\text{atm}}}{p_0}\right) - \frac{F_{\text{sp0}}}{p_0 S_2} \tag{4.89}$$

Observing that p_{atm} / p_0 and $F_{\text{sp0}} / p_0 S_2$ are very small, we get

$$\varepsilon_{\text{to}} \approx 1 - S_1 / S_2 \tag{4.90}$$

For the sake of obtaining faster t_{to} it is desirable to have $\varepsilon_{\text{to}} \to 1$.

The section S_1 is constituted by the total cross-sectional area of extinction chamber nozzles $S_1 > nS$, where n is the number of nozzles.

The total time of the valve uncovering the port is

$$t_{\text{open}} = t_{\text{pn}} + t_{\text{m}}$$

where t_{pn} is the time interval from the instant of pneumatic uncovering of S_3 to the instant of pressure rising to $\varepsilon = \varepsilon_{\text{to}}$, and t_{m} is the time interval of valve motion.

To shorten t_{pn} one has to enlarge S_2, but this entails heavier pistons with slower motion. Analysis indicates that it would be wise to choose $S_2 \leqslant 4S_1$ [4.3]. An analytical expression for t_{pn} can be derived by considering the depressurising of the volume $V = S_2 l_1$. The inflow of fresh air through port S_4 may be neglected. The flow of air through port S_3 is supercritical. By virtue of Eq. (4.49) we have

$$t_{\text{pn}} = 5.48 \times 10^{-3} V(\varepsilon_{\text{to}}^{-1/7} - 1) / \mu d_3^2 \sqrt{T_0} \tag{4.91}$$

where T_0 is the air temperature in volume V [cm^3], K; and d_3 is the port diameter, cm.

While the piston S_2 is moving, pressure p keeps falling and the volume beneath the piston is diminishing. The time t_m can be derived by simultaneously solving two equations, the equation of motion and the equation reflecting the variation of pressure under the piston. This problem is complicated by the fact that the volume varies and the rate of this variation depends on the velocity of the piston. The problem, however, may be solved with an accuracy sufficient for practical applications by making an assumption as follows. The outflow of air proceeds much faster than piston motion, therefore the volume of outflow may be deemed constant [4.3] and equal to

$$V_{av} = (V_{in} + V_{fin}) / 2 = (S_2 l_1 + V_{fin}) / 2 \tag{4.92}$$

where V_{in} and V_{fin} are the initial and final volumes defined by the position of the piston and a stray space.

The equation of motion

$$m \frac{d^2 l}{d t^2} = F_{open} - F_{closed}$$

$$= p_0 S_2 + p_{atm} S_1 - p S_2 - F_{sp} - p_0 S_1 \tag{4.93}$$

where the force of the spring is assumed invariable ($F_{sp} = F_{sp0}$) and the pressure on the disc (1) from above is p_{atm}. The relative pressure $\varepsilon = p / p_0$ is related with time by the equation

$$t = 213.4 V (\varepsilon^{-1/7} - \varepsilon_{to}^{-1/7}) / \mu S_3 \tag{4.94}$$

where V and S_3 are in cm^3 and cm^2, respectively.

Solving Eqs. (4.93) and (4.94) together, we get

$$l = 50 N t_m^2 - N_1 (39.5 t_m / N_3 + \varepsilon_{to}^{-1/7})^{-5}$$

$$- 198 N_2 N_3 \varepsilon_{to}^{6/7} t_m + N_1 \varepsilon_{to}^{5/7} \tag{4.95}$$

where

$$N = \frac{7.7}{m} \left[p_0 d_2^2 \times 10^{-5} - d_1^2 (p_0 - 10^5) \times 10^{-5} - 0.127 F_{sp0} \right]$$

$$N_1 = N_2 N_3^2$$

$$N_2 = p_0 d_2^2 / 60.8 \times 10^5 m \tag{4.96}$$

$$N_3 = 1.27 \times 10^{-4} V / \mu d_3^2$$

and d_1, d_2, and d_3 are the diameters of disc (1), piston (4), and valve S_3 (Fig. 4.39*a*).

In order to close the valve, the port S_3 must be covered. Then the port S_4 and the cavity S_5 feed compressed air in the lower space. It is important to note that the valve S_3 is closed very rapidly to reduce air consumption from the tank so that at the incipient valve closure the pressure beneath the piston is rather high. Accordingly, the air flow into the lower space is subcritical. The takeoff pressure is defined

by the equation

$$p_{\text{to, closed}} = p_{0,\text{fin}} - F_{\text{sp}} / S_2 \tag{4.97}$$

where $p_{0,\text{fin}}$ is the pressure in the tank by the instant S_3 is covered; F_{sp} is the force of spring when the valve is completely uncovered, $F_{\text{sp}} = F_{\text{sp},0} + \beta l_1$, where β is the spring coefficient.

In the flow process analysis one may assume that the tank volume is far larger than the space to be filled and the temperature of the gas is constant (isothermic process) [4.3]. The last assumption is fairly justified because the filling space is small and good conditions are provided for heat dissipation to the cylinder walls and the piston.

The time of pressure rise can be calculated as [4.3]

$$t_{\text{pn}} = \frac{2V_{\text{stray}}}{\mu (S_4 + S_5)} \sqrt{\frac{k}{2(k-1)} \frac{\gamma_{0,\text{fin}}}{p_{0,\text{fin}}} (1 - \varepsilon_{\text{res}}^{(k-1)/k})} \tag{4.98}$$

where V_{stray} is the stray space (to be filled), $\gamma_{0,\text{fin}}$ and $p_{0,\text{fin}}$ are the parameters of the air in the tank while covering S_3, and

$$\varepsilon_{\text{res}} = p_{\text{res}} / p_{0,\text{fin}}$$

The time of mechanical motion, t_{m}, can be found by solving the equation of motion and the equation of air flow into the sub-piston space simultaneously,

$$m \frac{\mathrm{d}^2 l}{\mathrm{d}t^2} = F_{\text{closed}} - F_{\text{open}}$$

At small pressure differentials, the equation of flow rate may be given as [4.3]

$$G\mathrm{d}t = \mu S_4 \sqrt{p_{0,\text{fin}} \gamma_{0,\text{fin}} 2(1-\varepsilon)}\ \mathrm{d}t = \mathrm{d}V\gamma \tag{4.99}$$

The sub-piston space is filled in an isothermic process under a low pressure differential. In addition, this air is filling a variable space whose volume depends on pressure beneath the piston. Exact solution of this problem is rather involved, but the problem can be simplified by assuming that $\mathrm{d}\varepsilon / \mathrm{d}t$ is very small and $\varepsilon \approx 1$ [4.3]. Then

$$l \approx \frac{1}{2a} \left(\sqrt{a F_{\text{sp}} / m}\, t - 1.4 \right) \tag{4.100}$$

where $a = \gamma_{0,\text{fin}} S_2^3 / 2m\mu^2 S_4^2$, and F_{sp} is the force exerted by the spring while the valve is open.

Given the stroke of the valve l, we may find the time t_{m}. It is worth noting that while the valve is covering the port, the bottom surface of the disc (1) experiences higher pressure than the top surface, therefore the actual closing time t_{m} is smaller than the theoretical figure.

In selecting the parameters of the differential valve (Fig. 4.39*a*) the designer is recommended to observe the following.

The travel of valve l_1 is selected subject to the inequality

$$\pi d_1 l_1 \geqslant \pi d_1^2 / 4$$

The diameters are proportioned in the ranges as follows:

$$d_2 = (1.7\text{-}2)\, d_1, \quad d_3 = (0.14\text{-}0.25)\, d_2, \quad d_4 = (0.14\text{-}0.26)\, d_3$$

$$\text{and} \quad S_5 = (0.005\text{-}0.007)\, d_2^2$$

When the piston (4) descends in valve opening, the pressure under the piston may rise if it moves too fast. This phenomenon can impede reliable operation of the valve. This will not occur if the descent proceeds so that $\mathrm{d}\varepsilon / \mathrm{d}t < 0$. The larger the port S_3 the more likely that this condition will be met. To verify whether or not this section is suitable one may invoke the following constraint from Ref. [4.3]

$$S_2\, \mathrm{d}l / \mathrm{d}t \leqslant 0.687\, \mu\, S_3 \sqrt{RT_0}\ \varepsilon_{\mathrm{to}}^{(k\,-\,1)\,/\,2k} \tag{4.101}$$

where $\varepsilon_{\mathrm{to}}$ is the relative pressure at valve takeoff. If this condition is met, then $\mathrm{d}\varepsilon / \mathrm{d}t < 0$, otherwise $\mathrm{d}\varepsilon / \mathrm{d}t > 0$ and S_3 should be increased.

In order to reduce the force requirement of the electromagnet a system of series valves illustrated in Fig. 4.39*b* is employed. When the electromagnet (5) operates and opens the servo valve (4) the air is exhausted in the atmosphere through the port of diameter d_{33} and opens the servo valve (2). Release of air through ports d_{31} and d_{23} opens the servo valve (3). This series of servo-valves causes the main blast valve (1) to open.

The diameter of the starting servo valve (4) is determined as

$$d_{\mathrm{st}} = d_{11} / 3 \times 2^{n\,-\,1} \tag{4.102}$$

where n is the number of valves in the system. It is assumed that $d_{11} / d_{13} = 3$ and $d_{21} / d_{23} = d_{31} / d_{33} = 2$. For $n = 3$, this yields $d_{\mathrm{st}} = 0.083\, d_{11}$. The servo-valve system reduces the tripping force required of the electromagnet in the proportion 1 / 145 of the force opening the blast valve (1).

It is instructive to note that the main blast-valve opens in a time of 10-15 ms. The auxiliary servo-valves operate in a few milliseconds. The complete operating time of the pneumatic system amounts to 20 ms. A Soviet-developed tripping unit, called the induction-dynamic starting element, reduces the operating time from 10-15 ms (electromagnet) to 1-2 ms.

Direct-Action Valve

A direct-action valve is shown schematically in Fig. 4.40*a*. The blast valve (3) placed within the air tank (1) is held in a closed position by the load of the spring (6) and pressure differential $(p_0 - p_{\mathrm{atm}})\, \pi d_1^2 / 4$ so that compressed air from the tank cannot be released in the air pipe (2). On either side of the piston (5) there is air at atmospheric pressure. When the starting valve (4) opens and releases compressed air to the cylinder on the left of the piston, this moves against the action of the spring and pressure differential and opens the blast valve. The time of valve opening is

$$t_{\mathrm{open}} = t_{\mathrm{pn}} + t_{\mathrm{m}}$$

The instant of takeoff is achieved when the balance is striken

$$pS_2 + p_{\mathrm{atm}}\, S_1 = p_0\, S_1 + F_{\mathrm{sp}} + p_{\mathrm{atm}}\, S_2 \tag{4.103}$$

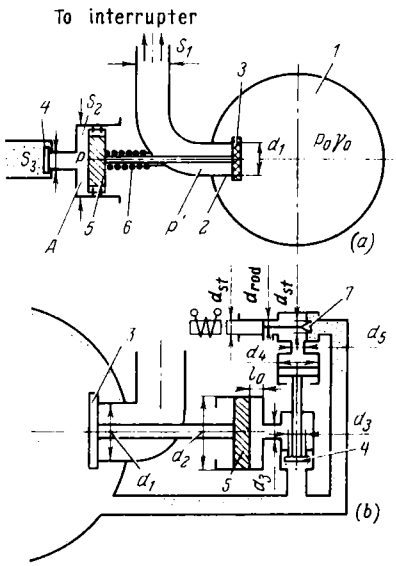

Fig. 4.40. (*a*) Schematic diagram of a direct action valve. (*b*) Control circuit built around direct action valves

The relative pressure of takeoff

$$\varepsilon_{to} = \frac{p_{atm}}{p_0} + \frac{S_1}{S_2}\left(1 - \frac{p_{atm}}{p_0}\right) + \frac{F_{sp}}{p_0 S_2} \tag{4.104}$$

Analysis of pressure-rise time t_{pn} should take into account that the process of air flow in the cylinder space can occur in both the supercritical, t_{sup}, and subcritical, t_{sub}, flow modes,

$$t_{sup} = \frac{V_{stray}}{0.687\, k\, \mu\, S_3}\sqrt{\gamma_0 / p_0}\ (\varepsilon - \varepsilon_{atm}) \tag{4.105}$$

where V_{stray} is the volume of the space that has to be filled prior to the piston (and the valve) will be set in motion.

For the subcritical flow pattern,

$$t_{sub} = \frac{2V_{stray}}{0.6\, S_3 \sqrt{2k\,(k-1)}}\sqrt{\gamma_0/p_0}$$
$$\times \left(\sqrt{1 - \varepsilon_{cr}^{(k-1)/k}} - \sqrt{1 - \varepsilon_{to}^{(k-1)/k}}\right) \tag{4.106}$$

where $\varepsilon_{cr} = 0.527$ is the relative critical pressure. Accordingly, when $\varepsilon < 0.527$ use is made of Eq. (4.105), and when $\varepsilon > 0.527$ of Eq. (4.106). The total time of pressure buildup is the sum

$$t_{pn} = t_{sup} + t_{sub} \tag{4.107}$$

The mechanical motion time is evaluated by solving, as before, two simultaneous equations, of motion and of flow rate,

$$m \frac{\mathrm{d}^2 l}{\mathrm{d}t^2} = F_{\text{open}} - F_{\text{closed}} \tag{4.108}$$

$$\mu S_3 \Psi \sqrt{p_0 \gamma_0}\, \mathrm{d}t = \mathrm{d}(V\gamma) = V\mathrm{d}\gamma + \gamma \mathrm{d}V \tag{4.109}$$

where $V = V_{\text{stray}} + S_2 l$.

Simultaneous solution of Eqs. (4.108-109) can be obtained by numerical methods only. However, if $S_2 l \ll V_{\text{stray}}$, then variation of this volume may be neglected and analytical solution of these equations can be attained:

$$l = \frac{0.687 k \mu S_2 S_3}{6Vm} \sqrt{p_0^3 / \gamma_0}\; t_{\text{m}}^3 \tag{4.110}$$

yielding t_{m} for a given l.

Theoretical analyses and experiments indicate that the direct action valve needs half as much time to open as the differential piston valve. This speed, however, is achieved at the expense of a rather complicated control system (Fig. 4.40*b*). Accordingly, in power circuit breakers, main blast valves are made of the direct action type, and auxiliary blast valves of the differential type.

The valve is closed by connecting the cylinder cavity of the piston (5) with the atmosphere. The pressure applied to the piston falls and at $p = p_{\text{to}}$ it starts moving

$$p_{\text{to}} S_2 = F_{\text{sp}} + p_{\text{atm}} S_2$$
$$\varepsilon_{\text{to}} = p_{\text{to}} / p_{0,\text{fin}} = F_{\text{sp}} / S_2 p_{0,\text{fin}} + p_{\text{atm}} / p_{0,\text{fin}} \tag{4.111}$$

If the takeoff occurs at the relative supercritical pressure $p_{\text{to}} / p_{\text{atm}} \geqslant 1.89$, then

$$t_{\text{sup}} = \frac{2V_1}{(k-1)\, 0.687 \mu S_3} \sqrt{\gamma_{0,\text{fin}} / p_{0,\text{fin}}} \left(\varepsilon_{\text{to}}^{(1-k)/2k} - 1\right) \tag{4.112}$$

where $V_1 = V_{\text{stray}} + S_2 l_1$ and l_1 is the full travel of the valve.

If $p_{\text{to}} \leqslant 1.89 p_{\text{atm}}$, then

$$t_{\text{sub}} = 5.7 \times 10^{-3} V_1 / \mu d_3^2 \sqrt{T_0} + 1.55 \times 10^{-3} V_1 A / \mu d_3^2\, \varepsilon_{\text{atm}}^{1/7} \sqrt{T_0} \tag{4.113}$$

where $\varepsilon_{\text{atm}} = p_{\text{atm}} / p_{0,\text{fin}}$, $A = 0.67 / p_{0,\text{fin}} + 0.165 (p_{\text{atm}} / p_{0,\text{fin}})^8 - 0.355$.

In motion time analysis, one may assume that the valve closes under the action of the spring alone, because pressure is the same on either side of the piston (5) and disc (3). Then,

$$m \frac{\mathrm{d}^2 l}{\mathrm{d}t^2} = F_{\text{sp}} = p_{\text{to}} S_2 - p_{\text{atm}} S_2 \approx S_2 p_{0,\text{fin}} \varepsilon_{\text{to}} \tag{4.114}$$

and on integration

$$t_{\text{m}} = \sqrt{2m l / \varepsilon_{\text{to}} S_2 p_{0,\text{fin}}} \tag{4.115}$$

The proportions recommended [4.8] for port diameters (for nomenclature, see Fig. 4.40*b*) are as follows: $d_2 = (1.7\text{-}2)\, d_1$, $d_3 = (0.3\text{-}0.35)\, d_1$, $d_5 = (0.3\text{-}0.35)\, d_3$, and the diameter of the starting valve (7) $d_{st} = (d_5^2 - d_{rod}^2)^{1/2}$, where d_{rod} is the rod diameter, and $l_0 = 2$ to 4 mm.

Compressed Air Tank

The volume of the compressed air tank is mainly controlled by the process of current interruption since for an arc extinction the tank has to release large amounts of air (up to a dozen of cubic metres).

The air flow through the nozzle is supercritical. Air release depressurizes the tank. In view of Eq. (4.49) we have

$$V_{tank} = \frac{nt\,\mu\Sigma\, S_n\,(k - 1)\,0.687}{2\sqrt{\gamma_0 / p_0}\left[(p_{0,\min} / p_0)^{(1-k)/2k} - 1\right]} \tag{4.116}$$

where n is the number of break operations supported by the tank without repumping, t is the operating time of the blast valve, μ is the nozzle flow coefficient, ΣS_n is the total cross-sectional area of the nozzles fed by this tank, $k = 1.4$ is the adiabatic exponent for air, γ_0 is the initial density of air in the tank, p_0 is the rated air pressure in the tank, and $p_{0,\min}$ is the lowest pressure in the tank that is still able to support a reliable extinction.

For circuit breakers where an air blast starts as soon as the contacts part, the time t should be taken as the time interval from the instant the contacts part to the instant of the exhaust valves being closed (for example, in VNV-type circuit breakers).

In Soviet-made circuit breakers, $p_0 / p_{0,\min} \leqslant 1.25$. Modern power circuit breakers operate at a tank pressure of 2-4 MN / m^2. Therefore, high strength requirements are imposed on the tank structure [4.8]. Air tanks are made of various grades of steel or glass-epoxy cylinders. The wall thickness of a cylindrical air receiver may be estimated as

$$S_{cyl} = pD_{int} / (2\varphi\sigma_r - p) + (0.05 \text{ to } 0.1) \tag{4.117}$$

where p is the pressure (gauge) in the reservoir, MN / m^2; σ_r is the rated admissible stress, MN / m^2; D_{int} is the internal diameter of the reservoir, cm; and φ is the strength coefficient of the weld ranging between 0.7 and 0.95 depending on technology [4.8].

The thickness of the plane round bottom

$$s_{bot} = 0.93\,(s - 0.1)\sqrt{\frac{0.19p}{k\,\sigma_r}\left(\frac{D}{s - 0.1}\right)^2 - 1} + 0.1 \tag{4.118}$$

where s is the wall thickness of the cylinder, cm; p is the pressure (gauge), MN / m^2, and k is the structural factor taken between 0.5 and 0.85 depending on the weld design.

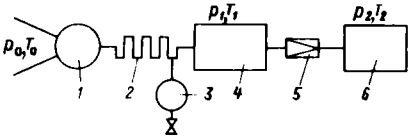

Fig. 4.41. Schematic of a thermodynamic drying system

For external diameters exceeding 50 cm, the bottoms of the air receiver are made spherical. Analysis and design of such reservoirs may be found in Ref. [4.8].

The VNV-type circuit breaker has an air receiver made of glass-epoxy tubes set within hollow porcelain insulators protecting the tubes from weather impacts. The tubes do not load the porcelain insulators with compressed air pressure. To release the support insulators of the pressure, VVB-type (continuously pressurised) and VNV-type circuit breakers feed compressed air in the upper reservoirs through small-diameter air pipes made of epoxy-glass plastic or steatite.

In conclusion we touch briefly on quality requirements of compressed air. Atmospheric air used by the air supply unit of a circuit breaker contains dust and moist. If dust filters were not provided, the dust would clog the valves, disturb their sealing capabilities, and cause air leakage. Dust settled on the internal surface of insulators reduces the surface breakdown voltage and facilitates flashover conditions. The internal electric strength of a circuit breaker is strongly contingent on the concentration of particulate matter, the effect of dust being stronger the higher the air pressure. At a pressure of 2 MN / m^2, purification of the air from particulate matter enhances the dielectric strength by 70% [2.2].

Moisture of air is especially hazardous for circuit breaker use. At lower temperatures the moisture tends to condensate in the form of droplets. This water has mutilative effect on valve performance, causes corrosion of the drive mechanism and can cause failure of the breaker. At freezing temperatures snow and ice can clog air pipes and valves. Water condensed on insulator surface impairs the dielectric strength of these insulators. Therefore, drying purge with compressed air is provided for breaker cavities, and water adsorbing facilities are fit in the air supply units.

Thermodynamic drying and water adsorbents have received wide acceptance. The block diagram of a thermodynamic drying unit is shown in Fig. 4.41. The compressor (1) feeds air at 4 MN / m^2 to the coiled cooler (2) where condensed water is trapped in the water receiver (3) to be drained. Water is also condensed in the first air storage (4) from which air is fed at a pressure halved by the air reducing valve (5) to the air reservoir (6). On entering the reservoir the moisture content of the expanding air diminishes in the proportion p_2 / p_1. This method, however, is disadvantageous in the need for a high-pressure compressor.

Water may be also absorbed by passing compressed air through porous water absorbing material. Silica gel is widely used for this purpose because of effective adsorbing properties. As a rule, both methods of air dewatering, thermodynamic drying and adsorption, are employed in combination.

4.9 Air Circuit Breaker Design

Generator Circuit-Breakers

Soviet power plants are equipped with Soviet-made air circuit breakers of the VV-20 type with the performance characteristics as follows.

Rated voltage	20 kV
Rated current	12 and 20 kA
Interrupting capacity	up to 160 kA
Short-time (withstand) current rating	410 kA
Rated total break time, from the tripping command to arc extinction, within	140 ms
Break time of resistor-limited breaking current, within	170 ms
Rated air pressure	2.0 MN / m^2
Pressure drop per interrupting cycle	0.5 MN / m^2

The electric and pneumatic circuit diagram of this generator breaker is shown in Fig. 4.42*a*. At the base of each pole there is an air tank (4). Hollow epoxy insulators support two main arc extinction chambers *EC1* and *EC2*. The auxiliary air extinction chamber *EC3* is located near the interrupting head of *EC2*.

The high-voltage circuit of the breaker is shown in the diagram at (*b*). When the circuit is closed, the contacts (1-3) are closed as well as the contacts of the line isolator (5) and of the isolating switch (6). About 80% of the rated current passes from *A* to *B* through the line isolator (5).

In breaking the circuit, compressed air is first fed into the driving mechanism of the line isolator (5), it trips and the entire current is directed to the interrupting heads. Simultaneously the air is directed to the arc extinction chambers *EC1-EC3*. The contacts (1) and (2), shunted by low-value resistors (7) and (8) of 0.8 Ω each, separate. On approaching a current zero the arc current is directed in the shunt resistor and an aperiodic process of voltage recovery begins. Small value of the resistor and two breaks per pole used ensure that the arc current as high as 160 kA is extinguished in one or two half-periods. Then compressed air is allowed to the driving mechanism of the movable contact (3) in the interrupter *EC3*. The 11-kA arc of the resistor (7) is extinguished at the first current zero because of light conditions of arc extinction (Sect. 4.5).

On interrupting a small (5-10 kA) inductive current, the circuit resistance $\omega L > 2R_{sh}$ ($R_{sh} = R_1 + R_2$), the phase angle between the circuit e.m.f. and the shunt current is close to 90 ° and the interrupter *EC3* is unable to extinguish the arc. The transient recovery voltage across the contacts of *EC3* breaks down the arc gap (10) and brings into the circuit the 30-Ω resistor (9). Now the circuit carries an active current controlled by this resistor (9) ($\omega L \ll 30\ \Omega$). An air blast extinguishes the arc with a current of about 500 A in the arc gap (10).

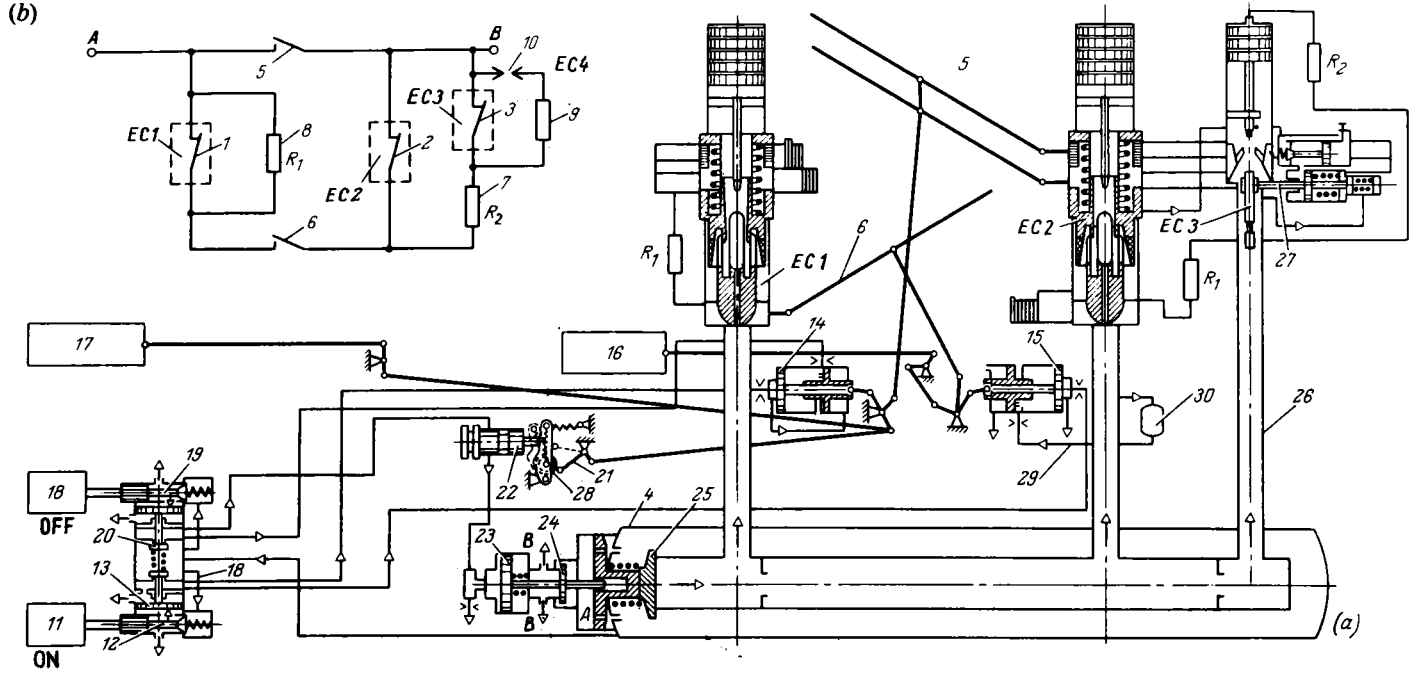

Fig. 4.42. Pneumatic diagram (*a*) and electric scheme (*b*) of the type VV-20 air circuit breaker

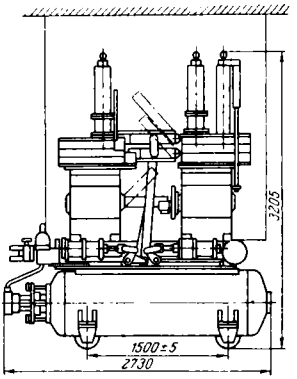

Fig. 4.43. Outline of the VV-20 air circuit breaker (all dimensions in mm)

Once the arc in the arc gap (10) has been extinguished, the control circuit signals a command to open the isolating switch (6) which breaks the dead circuit and the status of its contact is visible from outside. The general layout of this type of circuit breaker is shown in Fig. 4.43.

Let us consider the operation of the breaker mechanism with reference to Fig. 4.42.

Making. When the electromagnet (11) is energized, it opens the valve (12) and compressed air is admitted to the valve (13) which ports the air to the pistons (14) and (15) of the driving mechanism. The make switch (6) and then the isolating switch (5) are closed. The signalling and interlock contacts (16) and (17) switch over to signal that the making operation is completed.

An electric-contact pressure gauge monitors pressure in the air tank and blocks the circuits of the electromagnets (11) and (18) if the pressure falls below the tolerable level

Breaking. When a tripping signal energizes the electromagnet (18), it opens valves (19) and (20). Admission of compressed air to the piston (14) shifts it to the left and opens the isolator (5). A link (21) opens a valve (22) for a short time and ports compressed air to the plate of a valve (23). A valve (24) opens and space *A* is connected to the atmosphere through port *B*. The main blast valve (25) operates as a differential pressure valve and allows admission of compressed air to the extinction chambers *EC1-EC3*. The operational principle of the extinction chambers has been discussed in Sect. 4.7.

These extinction chambers are equipped with unidirectional (axial) blast nozzles. The interrupting head of *EC3* is fed by compressed air through a thin pipe (26), therefore its contacts (27) separate only after the arc in *EC1* and *EC2* has extinguished itself. It should be noted that the valve (22) closes after the level (21) has left a roll (28). This limits the consumption of air per one interruption that reaches 13 m^3 (reduced to atmospheric pressure).

Simultaneously with the admission of air in the interrupter, air is ported to the piston (15) through a pipe (29) and space (30) thus resulting in opening of the make switch (6).

VVB-type Continuously Pressurised Air Circuit-Breakers

This design, called VVB, has been developed in the Soviet Union for voltage classes of 35 kV and higher. The outline of a circuit breaker for 110 kV, continuous current of 2000 A and symmetric interrupting rating up to 31.5 kA is shown in Fig. 4.44*a*. It operates with a total break time of 60 ms, total make time of 200 ms, and at a rated pressure of 2.0 MN / m^2. This type of breaker is developed for voltage classes up to 1150 kV, interrupting capacity up to 40 kA, and continuous current of 4000 A [4.7].

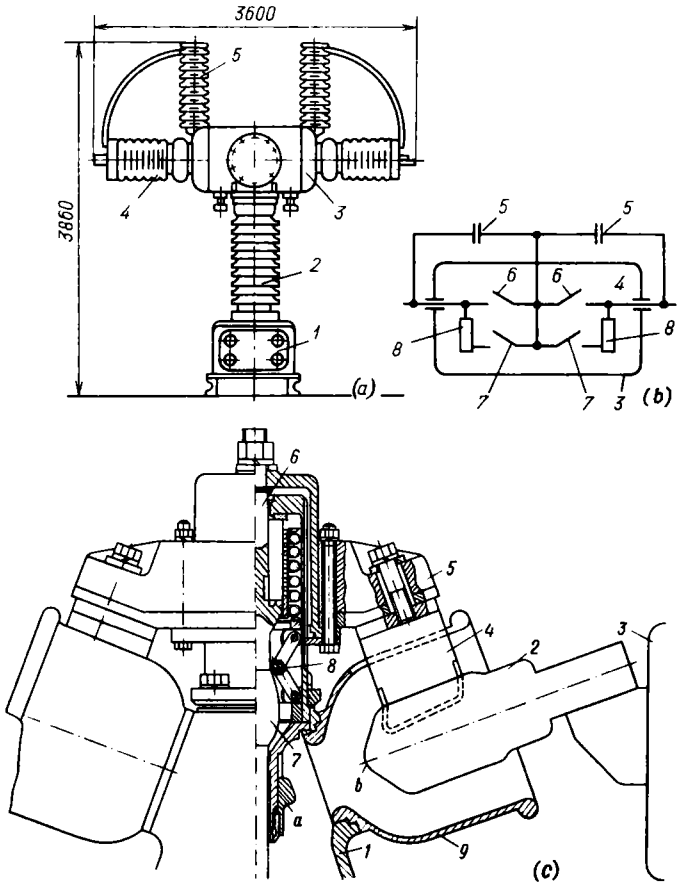

Fig. 4.44. Outline of the type VVB-110 continuously pressurised air circuit breaker and functional details of the interrupting head

Let us consider the layout and operation of a 110-kV circuit breaker of this type. The base of the unit (1) houses a control box and an auxiliary reservoir of compressed air. A support insulator (2) provides a base for the main steel air tank (3) housing two breaks of the pole. The bushings of the breaker are made as thoroughfare epoxy insulators protected from outside by porcelain weather casings (4). Uniform distribution of voltage over the breaks is achieved by capacitors (5).

The electrical scheme of the high voltage circuit is shown in Fig. 4.44*b*. Contacts (6) are the main contacts carrying continuous rated current and short circuit currents. These contacts are paralleled by auxiliary breaks (7) and shunting resistors (8). On interrupting a circuit, the contacts (6) part first and the arc formed between them is rapidly extinguished owing to an intense air blast and the low-value (100 Ω) shunt resistance that converts the oscillatory voltage recovery process into an aperiodic transient process. In 30-35 ms after the main contacts have been separated the contacts (7) are opened and the arcing current controlled by the value of the resistors (8) is interrupted. The arc is extinguished at the first current zero because the interrupted circuit has no reactive components. This two-stage extinction process renders breaker operation practically independent of the voltage recovery conditions for a particular circuit.

Figure 4.44*c* shows the functional details of the main contact system and an interrupting head. The current-carrying part of the bushing (3) is connected to a stationary contact (2) of the finger type (five pairs of contact fingers). A knife type moving contact (4) enters between the fingers of the stationary contact (2). The contacts (4) are fixed on a cross head (5) connected with a vertical driving rod.

Each break has an interrupting head for unidirectional (axial) blast formed by a nozzle (9). The nozzles are vented to the atmosphere through a pipe (1) uncovered when the arc is extinguished.

The breaker is designed as a live-tank apparatus. The main air tank is at high potential. The arc extinction device is inside the tank. This arrangement was devised by a Soviet engineer F.F. Baburšky as far back as 1944. It is devoid of a long air pipe for interrupting heads which aids in cutting down the break time. Since the interrupters are housed within the air reservoir, the process of arc extinction is rather efficient.

On interruption the driving rod (6) ascends, the contacts (2) and (4) open and an arc is formed between them. An air blast flowing through the nozzle (9) in the pipe (1) rapidly blows the arc out to points *a* and *b* where it is subjected to intense cooling by an axial blast. After the arc has been extinguished, the pipe (1) is covered by a valve and the arc spacing recovers its high electric strength since the air pressure is equal to the pressure in the tank. The driving rod (6) is locked in the 'off' position by a step (7) on the rod and by a roll mechanism (8) (the step is above the mechanism as indicated in Fig. 4.44*c*).

Let us turn now to the control system of the breaker diagrammed in Fig. 4.45. The breaker is shown in the 'off' position. The system makes use of differential-piston type valves discussed in Sect. 4.8. Stippling represents compressed air filling the components of the system. The air pipe (2) ports compressed air from the lower air reservoir to the upper air tank.

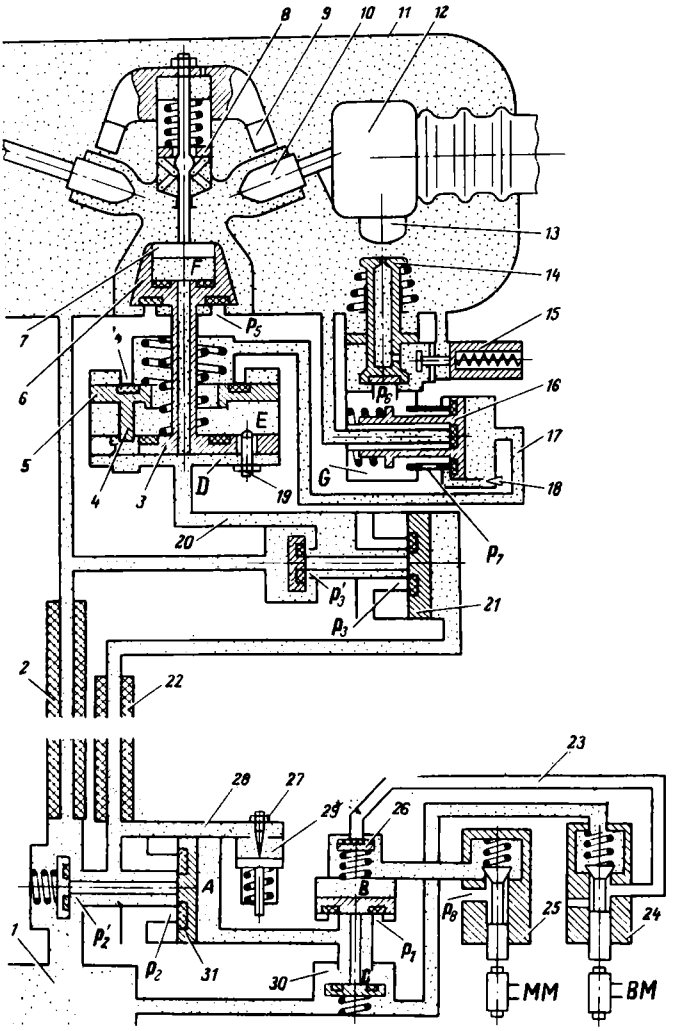

Fig. 4.45. Pneumatic diagram of the VVB-110 circuit breaker

Making. When the making electromagnet *MM* is energised it opens the valve (25) and vents space *B* of a valve (30) to the atmosphere through a port P_8. The valve (30) opens to connect space *A* of a valve (31) to the atmosphere through a port P_1. This valve uncovers a pipe (22) and connects it to the atmosphere through a port P_2. The valve also covers a port P_2'. Note that the lower plate of the valve (30) seals space *C*.

Connection of the pipe (22) to the atmosphere allows a valve (21) to open. This valve covers a port P_3' and uncovers a port P_3. A pipe (20) vents spaces *D*, *E*, and *F* of a blast valve (3) to the atmosphere. A piston (7) pressurised from the upper side descends into the space *F* and pulls the cross head down to close the main contacts (9) and (10).

As compressed air leaves the space *E* through air flow constrictors (19) and (4), the pressure in this space falls and a spring loaded plate (5) descends until it touches a piston (3). A port P_4 is uncovered and a pipe (17) is connected to the atmosphere.

A piston (16) has a tube stem loaded by a spring. Initially a space *G* is connected to the atmosphere through a port P_7. An auxiliary moving contact (14) covers a port P_6 by its bottom end and finds itself under the action of a downward force. When a pipe (17) is connected to the atmosphere, a piston (16) is moved to the right by a spring action. The plate of this piston seals the space *G* for atmospheric air and it is filled by compressed air from a tank (11). The underside of the contact (14) is loaded by compressed air.

When the pneumatic forces on either side of the contact balance each other, it ascends until it contacts the stationary contact (13). A shunting resistor (12) connected to the stationary contact is connected by its other lead to the contact (10). Therefore the main break is shunted by a low-value resistor.

A pneumatic interlock unit (15) prevents the contacts (13) and (14) from closing the circuit when the pressure in the tank falls below the admissible level. Should this happen, the spring moves the movable pin to the left until its left end enters the recess in the movable contact and locks this contact.

As the pressure in a pipe (28) falls, a spring loaded piston (29) ascends and opens the contact of the electromagnet control circuit thus deenergizing the magnet *MM*. The operating time of the auxiliary contacts is adjusted by an air flow restrictor (27). The spring resets the valve (25) thereby completing the make cycle.

Breaking. The break electromagnet *BM* is energised and opens a valve (24). A pipe (23) ports compressed air to a check valve which also opens. The compressed air fills space *B* and the valve (30) closes to assume the position indicated in Fig. 4.45. The port P_1 is covered. The compressed air flows in space *A* through space *C* and a valve (31) is closed. Admission of compressed air from the tank (1) to the piston of a valve (21) closes this valve. The port P_3 is covered and port P_3' uncovered. Compressed air flows by the pipe (20) to the piston (3) of the blast valve, uplifts this piston, plates (5) and (6), a piston (7) and the movable contact (9). The main contacts (9) and (10) separate and an arc forms, but a bit earlier a port P_5 is uncovered and compressed air exhausted from the reservoir (11) into the atmosphere cools the arc.

Within a time determined by an air-flow constrictor (19), the pressure in spaces *D* and *E* is equalised, and the spring-loaded piston (3) descends and closes the blast valve (6) (port P_5), thus terminating the blast. The movable contacts (9) are kept in the top position by an interlock (8).

While the space *E* is being filled by compressed air, the air pressure transmitted by the pipe (17) closes a piston (16) and the space *G* is connected to the atmosphere by a port P_7. The pressure loading the underside of the contact (14) falls and it moves away from the contact (13). A low-current arc that is fired is soon extin-

guished. The moment of separation of the contacts (13) and (14) with respect to the main contacts is adjusted by an air-flow restrictor (18), the time difference normally amounting to 35 ms.

After the valve (31) has been closed, compressed air is ported by the pipe (28) to the driving mechanism (29) of control circuit contacts. The contacts of the breaking electromagnet *BM* are disconnected, the valve (24) is closed and the air from the pipe (23) is exhausted in the atmosphere. The compressed air in the space *B* forces the check valve (26) to close, thus preventing the air from leaving this space.

This insight into the operation of the pneumatic control system indicates that considerable time is spent for close-open cycles of the series-connected valves. Therefore, there is a trend to replace pneumatic components of the system with fast-acting mechanical elements, as, for instance, in the upgraded continuously-pressurised air circuit-breaker VVBK. It should be noted that the continuously pressurised group of VVB air-blast circuit breakers has been consistently improved to reach voltage ratings of 1150 kV (12 breaks per pole), interrupting capability of up to 50 kA, break time of 40 ms at an air pressure of 4 MN / m^2.

VNV-Type Air Circuit Breakers

This type of air-blast circuit-breaker has been developed for voltages ranging from 110 to 1150 kV, continuous currents up to 4000 A, interrupting ratings up to 63 kA, with a break time of under 40 ms and make time of under 100 ms at a rated pressure of 4 MN / m^2 [4.6]. A photograph of this circuit breaker is shown in Fig. 4.46.

The VNV type of circuit breaker has a modular design. The generic module with two breaks per pole is designed for 250 kV. The functional diagram of one pole of a 500-kV circuit breaker is presented in Fig. 4.47. A compressed air reservoir (1) is at the base of the module. Compressed air is ported by an air pipe to the upper tank formed by a metal cylinder (9) and a glass-reinforced epoxy cylinder (11). The interrupting head is placed within the continuously pressurised upper tank.

Control of the contact system and valves is effected by light insulated links. This design enables the break time to be reduced down to 40 ms (half the break time of the VVB circuit breaker).

Figure 4.47 shows the breaker in the closed position. The main contact assembly comprises finger-type contacts (19) and a movable contact (18). The fingers of an arc interrupting contact (20) slide along the inner surface of the contact (18). These fingers (20) are placed in the slots of the stationary contact nozzle. In the position indicated in the figure, the contact (18) rests in a saddle (25) thereby connecting the inner space of the contact (18) to the atmosphere (through an open exhaust valve (24)), while the outer surface of the contact (18) and the fingers (19) remain in compressed air.

A nozzle (17) is made movable. The initial distance between the contact (20) and the nozzle (17) is optimal for the given throat of the nozzle. After the arc has been extinguished the movable nozzle (17) is forced to travel by the pressure inside the interrupting chamber until it seats at a saddle (26) and seals the chamber.

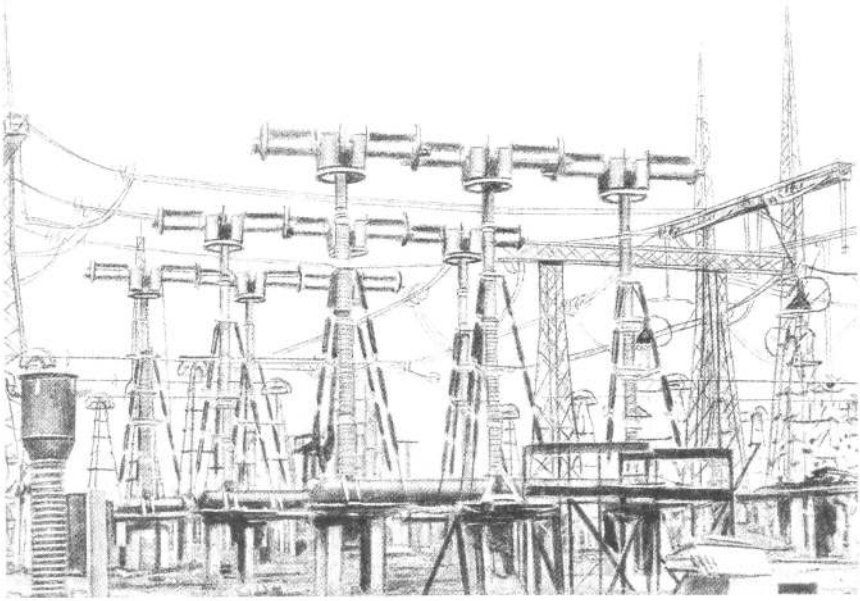

Fig. 4.46. Outlook of a VNV-type circuit breaker rated 750 kV

A high electric strength of the contact spacing is achieved with the aid of screens that equalise the electric field between the contacts.

Breaking. When a trip electromagnet (3) is energised, it opens a valve (6) and admits compressed air to a piston (7) actuating a link (8). This effort is transmitted by the linkage (5), (4) and (2) to insulating ties (13) and forces them to descend. This movement is transmitted by links (37) and (15) to a horizontal pulling rod (36) linked with the contact (18). The links (15) and (37) are tied with the pulling rod (13) by a pipe (14).

The contact (18) is first separated from the finger contacts (19) then from the finger contacts (20). An arc struck between the last finger contacts and the inner surface of the contact (18) is rapidly moved by an air flow exhausted in the atmosphere through the nozzle of the stationary contact and the movable nozzle (17). Extinction of the arc is effected by a bilateral blast.

The rod (31) is tied with the pulling link (13). When the link (13) descends, the rod (31) actuates the lever (30) which opens a valve (34) and allows the compressed air beneath the piston to flow in the atmosphere by a coil (29). A piston (35) releases levers (27) and (28) and allows the valve (24) to close. This valve is controlled by links (22) and (23) and a rocker (21). The moving nozzle simultaneously moves to the right along with the limiting electrode (41) until the nozzle sits down on the

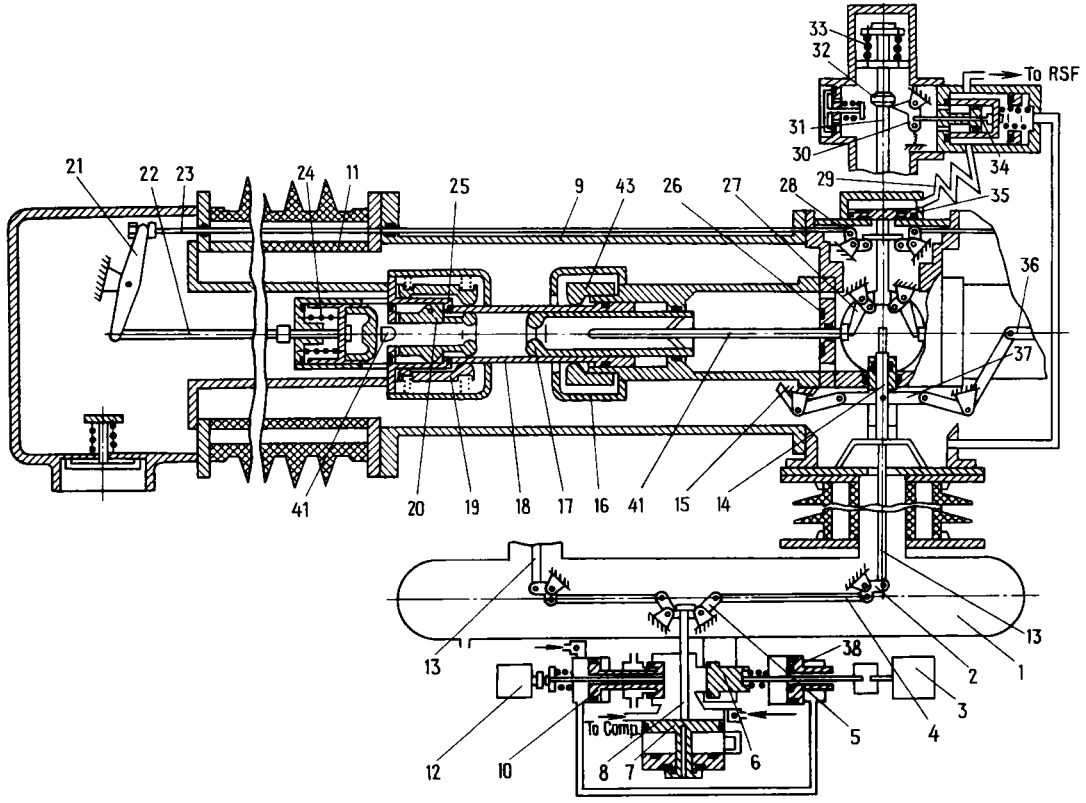

Fig. 4.47. Pneumomechanic diagram of a VNV-500 breaker pole. RSF — resistor switching facility; Comp — compressor

seat (26), thus sealing the inner compartment of the extinction chamber off the atmosphere.

For interrupting ratings up to 40 kA, the breaker has no resistors in the arc control circuit. For interrupting capacity of 63 kA or heavy duty of recovery transient, the breaker is equipped with a low-value resistor and an auxiliary interrupting head to break resistor current. The resistor is placed along with the contacts in a container located aside of the main interrupting chamber. The auxiliary interrupter receives control from a valve (34).

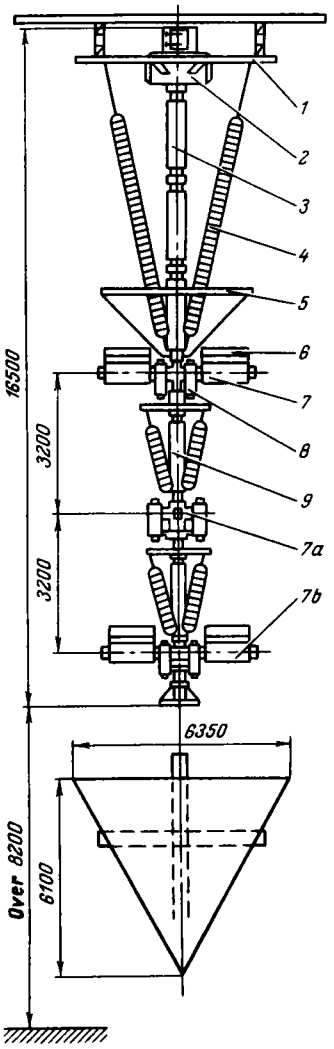

Fig. 4.48. Suspended version of the type VNV-750 circuit breaker (all dimensions in mm)

Making. A making electromagnet (12) opens a valve (10) and vents a cavity above a piston (7) to the atmosphere. Compressed air is simultaneously admitted to a piston (38) which seals the reservoir off the piston (7).

A charged spring (33) forces the stem (32) to descend and close the valve (34). Compressed air is allowed to a piston (35) which descends and actuates the linkage (28) and (27). The valve (24) opens and the movable nozzle (17) sets in a position as indicated in the figure. On moving to the left the nozzle leaves the seat (26) and the inner space of the contact (18) and nozzle (17) is ported to the atmosphere. Once the valve (34) has been closed, compressed air flows to the container of the auxiliary interrupter and it brings the resistor in the circuit. As the rod (13) ascends, the movable contact (18) sets in the 'on' position and simultaneously the piston (7) swings in the position indicated in the figure. After the air has left the space over the piston (7), valves (10) and (6) are closed and a piston (38) is returned to the initial position by the action of respective springs.

In a circuit breaker developed and operated at 1150 kV, on making a circuit the auxiliary contacts are closed first and bring into the circuit a resistor whose resistance per pole is about equal to the wave resistance of the closed line. Then, within a time interval of about 10 ms the contact (18) closes the circuit shunting the resistor.

Where weight and size of circuit breakers are critical, smaller installations can be achieved with suspended designs. Figure 4.48 illustrates the layout of a suspended version. The frame (1) is fixed to the portal. The frame holds a compressed air tank (2). Modules (7), (7a), and (7b) designed for 250 kV each are suspended from the frame by strings of insulators (4). Compressed air is fed in the interrupting chamber by air pipes (3) and (9). A screening ring (5) is provided to equalise the distribution of voltage over the suspended insulators. Voltage equalisation over the breaks is ensured by capacitors (6). The breaker also comprises containers with resistors and auxiliary breaks (8). A preliminary analysis indicates that the suspended version of circuit breaker for 750 V reduces weight of the unit by 25 %.

4.10 Insulating and Interrupting Properties of SF_6

Improvement of interrupting capacity and voltage rating may be achieved not only by upgraded designs of the breaker structure but also by the use of new arc extinction media possessing high dielectric strength and extinction capabilities. Investigations with freons, carbon tetrachloride, and sulphur hexafluoride (SF_6) have indicated that the latter gas, called electrotechnical gas, or elegas for short, in Soviet literature, suits switchgear applications best because of high dielectric strength and good arc extinction properties. This gas is an electro-negative gas as its molecules have an affinity for free electrons. This property converts an SF_6 molecule upon capturing an electron into a heavy negative ion with a slow response to the accelerating effect on an electric field. Therefore, SF_6 exhibits a high dielectric strength. Its dielectric strength is several times that of air at the same pressure and at a pressure of only 0.23 MN / m^2 is equal to that of transformer oil (Fig. 4.49). This property also facilitates the recombination of charges in the arc.

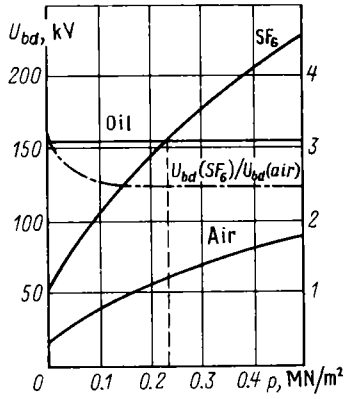

Fig. 4.49. Comparison of breakdown voltage in SF_6, air, and transformer oil. The chain-line curve shows $U_{bd}(SF_6)/U_{bd}$ (air) as a function of pressure

The high dielectric strength of SF_6 enables the designer to shorten insulation distances and reduce gas pressure, which means considerable advantage in dimensions and weight of switchgear and distribution substations.

In a uniform electric field the breakdown voltage for an arc spacing of l cm long in SF_6 at a pressure p may be described [2.4] as

$$U_{bd} = 8.9 \times 10^{-4} pl \tag{4.119}$$

The high electric strength of SF_6 will be used most efficiently in uniform electric fields. Nonuniform fields may give rise to a corona discharge leading to decomposition of SF_6 into SF_4 and SF_2 which have adverse effect on many constructional materials of the interrupting chamber. Therefore, the metal screens used to equalise electric fields are made with smooth surface. Dirt, dust, and especially metal particles deposited on the screen surface create local inhomogeneities of the field and impair the dielectric strength of an SF_6 insulating atmosphere. Poltev [2.4] discusses problems pertinent to SF_6 insulation analysis at sufficient length. The physical properties of SF_6 are compared with those of other gases in Table 4.1.

Although the specific heat of SF_6 is far smaller than that of air, the specific heat capacity per unit volume, i.e. the energy required to raise the temperature of 1 cubic centimetre of SF_6 per one degree Celcius, is almost four times that of air. This explains why SF_6 possesses a higher cooling ability than air. Under natural convection, heat transfer in SF_6 is 1.9 times that of air. Therefore continuous-current rating may be increased by 15-25 % and the cross section of current-carrying parts of the switchgear can be cut down.

SF_6 is a chemically inert gas up to 800 °C, therefore the admissible temperature of copper contacts may be increased from 75 °C (for air) to 90 °C. This means an additional increase in current rating. SF_6 is nonflammable and therefore is widely used in power transformers, high-voltage cables, and sealed distribution switchgear. A disadvantage of SF_6 is that it turns from gaseous into liquid state at relatively high temperatures.

Table 4.1

	SF_6	Air	H_2	N_2
Density, mg/cm^3	6.7	1.29	0.089	1.25
Specific weight/air	5.19	1.0	0.069	0.96
Molecular weight	146	28.9	2.0	28
Boiling temperature, °C	−63.8	−194.0	−252.8	−195.8
Dielectric strength/air	2.3	—	—	1.0
Specific heat capacity at 70 °C, J/g K	0.73	1.00	1.42	1.03
Heat capacity per unit volume, mJ/cm^3 K	4.89	1.29	0.026	1.28
Velocity of sound at 30°C, m/s	138.5	330	1200	330

Figure 4.50 shows the binary constitution diagram of SF_6. At 0 °C the gas turns into liquid at a pressure of 1.25 MN / m^2 (density, 105 g / dm^3) whereas at −40 °C it becomes liquid at a pressure of about 0.4 MN / m^2 (density, 30 g / dm^3). Accord-

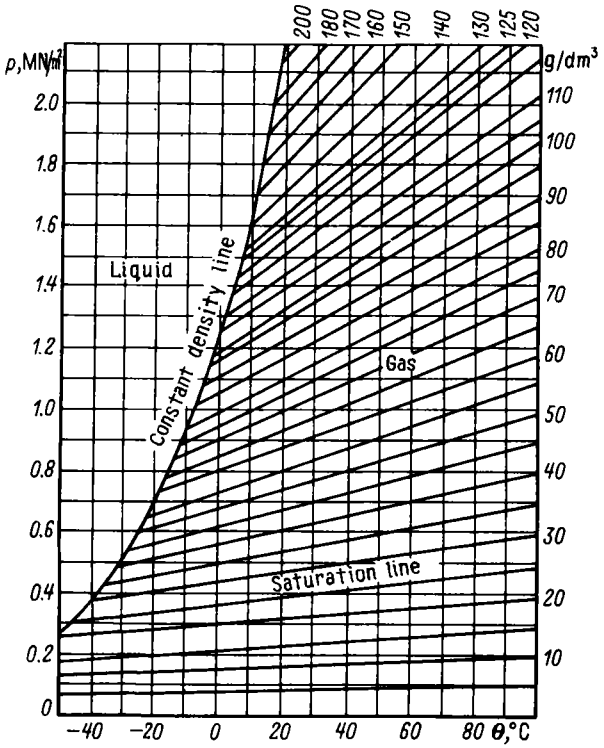

Fig. 4.50. SF_6 constitution diagram

ingly, if the breaker is to operate at temperatures close to -40 °C the pressure of the SF_6 gas should not exceed 0.4 MN / m^2 (density, under 30 g / dm^3). At higher pressures, the gas will liquefy at higher temperatures.

Most SF_6 circuit breakers are built around two principles of arc extinction. In the first method the arc is cooled by SF_6 gas flowing from the high pressure reservoir (about 2 MN / m^2) to the low pressure reservoir (0.3 MN / m^2), that is the cooling principle is essentially the same as in the air-blast circuit breaker. To prevent SF_6 gas liquefaction at freezing temperatures (-40 °C) the high-pressure reservoir must be heated up to 12°C. If liquefaction occurs, the density of the remaining gas phase reduces and its arc extinction property deteriorates. Gas heating is achieved by an automatic system that markedly complicated the switchgear structure.

In the second method, the circuit breaker is filled with SF_6 gas at a pressure of 0.3-0.4 MN / m^2, ensuring a high dielectric strength of the gas and enabling breaker operation at temperatures down to -40 °C. The necessary pressure differential is created by a special compressing device mechanically connected with the movable contact of the breaker. This device is actuated by a burning arc generating a pressure differential of 0.6-0.8 MN / m^2. Features to ensure a critical flow velocity and effective arc extinction are provided. These piston-type circuit breakers are called 'autopneumatic' or 'autocompression' breakers in the Soviet literature on the subject.

Pure SF_6 gas is nonflammable and withstands heating up to 800 °C. Below this temperature SF_6 is an inert gas. Arcing produces a number of corrosive and toxic compounds in SF_6 gas. These products are absorbed by inbuilt sorption filters made of activated Al_2O_3 or as molecular sieves that absorb both gaseous products of decomposition and moisture and keep the impurities below safety level. It should be noted that powder products of SF_6 gas decomposition that settle out on insulating surfaces of the breaker and auxiliary equipment do not practically influence the electric strength of the insulation.

For SF_6 circuit breakers to operate reliably the moisture content in the gas should not exceed 100 parts per million by volume. This condition can be met by a special drying of SF_6 gas before putting the breaker into operation and by taking special measures to keep moisture content under admissible level during a maintenance period [3.2].

Like air-blast circuit breakers SF_6 gas circuit breakers use intense flow of gas to cool and extinguish the arc. Under equal conditions the arc extinction ability of SF_6 gas is 4.5-5 times that of air blast [4.1]. This superiority is explained mainly by the composition of plasma and the temperature profile of the specific heat, thermal conductivity, and electric conductivity [3.2]. Decomposition of SF_6 produces molecules of SF_2 and SF_4 and atomic fluorine and sulphur.

Figure 4.51 shows the temperature profiles of the specific heat and thermal conductivity of air and SF_6 plasma. A striking feature in the plot for SF_6 gas is a sharp rise of specific heat at 2000 K associated with dissociation of SF_6 molecules. The dissociation process terminates at 4000 K. Accordingly, in the temperature range 2000-3000 K the thermal conductivity of SF_6 plasma is almost by two orders of magnitude greater than that of air. The presence of atomic sulphur of low ionisation potential (10.4 eV) in the dissociation plasma leads to a situation when the

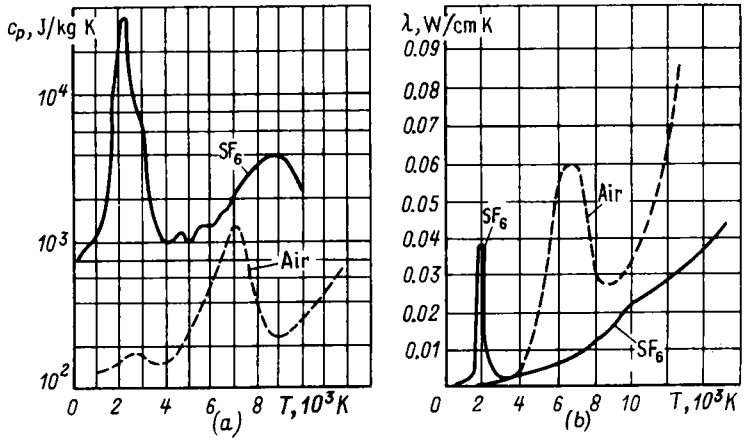

Fig. 4.51. Temperature profiles of (*a*) specific heat capacity and (*b*) thermal conductivity of SF_6 and air

concentration of electrons even at 3000 K is sufficient to sustain the arc. At higher temperatures the thermal conductivity of plasma first falls off to that of air, then rises again. Air dissociation begins only at 7000 K. The above processes in SF_6 are responsible for the voltage across and resistance of an arc steadily burning in SF_6 gas being by 20-30 % less than the parameters of its air counterpart.

The resistance of an arc cooled by SF_6 gas is lower than the resistance of arc in air during the entire half-period. The diameters of a 100-A arc are about 1 mm in both cases. The temperature of a 40-A arc column is 12 600 K in SF_6 and 10 850 K in air. The arc time constant has been found equal to about 1 μs. Thus, good interrupting characteristics of SF_6 gas cannot be explained by the small time constant in the middle of a current half-period.

A depression of arc temperature from 12 000 to 8000 K has low effect on the resistance of the arc and the dielectric strength of the arc gap. When the temperature falls below 7000 K, the concentration of electrons in plasma sharply decreases (under 10^{15} cm^{-3}) and the conductivity of the gap falls considerably. At 6000 K the electron concentration becomes equal to 10^{13} cm^{-3}, the degree of sulphur ionisation falls sharply and the mechanism of electron capture by atomic fluorine and molecules of SF_6, SF_4, and SF_2 intensifies.

The stability of arc in SF_6 gas is retained down to rather small values of current and, respectively, relatively low temperatures. Therefore, SF_6 gas circuit breakers are free from current chopping that brings about large transient overvoltages in air-blast circuit breakers.

When the arc temperature falls below the level of complete dissociation of SF_6 gas (4000 K), the recombination process begins, atomic sulphur combines with fluorine and the amount of free sulphur and the electron density fall sharply. This temperature range exhibits a high plasma thermal conductivity which aids in cooling

the arc column and recovery of the dielectric strength of the arc spacing. The capture of electrons by SF_6 molecules and atomic fluorine also plays a significant part.

The high arc interrupting characteristics of SF_6 gas are explained by the behaviour of the gas at current zero. The physico-chemical properties of SF_6 gas favour the retention of arc column over the entire half-period including near current zero. The arc extinguishes itself in the last instant of current zero.

In air, the arc having the same radius over the entire half-period increases in diameter at the end of the half-period owing to turbulence of the gas flow. The arc current can be chopped even prior to current zero. The time constant of the arc proportional to the square of arc radius increases in the air-blast interrupting chamber whereas it remains constant in the SF_6 interrupter. After a current zero the residual arc column remains under intense cooling effect of SF_6 gas and the dielectric strength of the break is rapidly recovering. Growing specific heat of plasma at 2000 K aids in intense cooling of the arc.

In the air-blast interrupting chamber, the dielectric strength of the arc gap is higher at current zero, but beyond the current zero the rate of dielectric strength recovery is slower because of the higher time constant.

Figure 4.52 shows the dielectric strength recovery profiles for interrupting chambers with air (4) and SF_6 gas (3). The initial dielectric strength of the air-blast interrupter is higher than that of its SF_6 counterpart, but the rate of dielectric strength recovery in the SF_6 interrupter is considerably higher. It has been found experimentally that SF_6 circuit breakers are very sensitive to close short-circuits at 0.9 of the rated current. The sensitivity is explained by a very high frequency of the recovery voltage (1). The breakdown occurs at point *a*.

Air circuit breakers are especially sensitive to close short-circuits at 0.75 of the rated current, $I_{0,r}$. The amplitude of the high-frequency component in this case is higher and the frequency is lower (curve 2) than would be in the SF_6 circuit breaker. Breakdown occurs at point *b*.

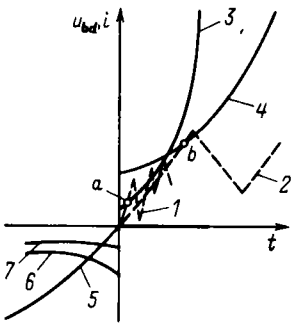

Fig. 4.52. Comparison of dielectric strength recovery in SF_6 and air interrupters: (1) and (2) recovery voltage in clearing a close and long-line short circuit fault; (3) and (4) recovery electric strength in SF_6 and air interrupters; (5) arc current; (6) and (7) arc voltage in air and SF_6 interrupters

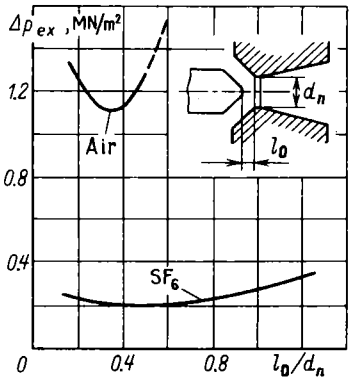

Fig. 4.53. Dependence of one-half-cycle-extinction pressure differential on relative contact spacing ($\hat{I}$ = 1200 A, d_n = 0.56 cm)

Owing to the peculiarities of arc interruption in SF_6 gas, the effect of thermodynamic clogging is far less significant. Figure 4.53 gives pressure differential as a function of contact spacing for a unidirectional blast interrupter. The plot is slanter than the one of air-blast circuit breaker, therefore the SF_6 unit may have a greater spacing between the arc contacts and can tolerate higher recovery voltage levels at this break. SF_6 interrupting chambers have been developed which clear 40-kA current at 240 kV across the break.

Piston-type SF_6 circuit breakers are incapable of recovering dielectric strength to high values. This setback can be eliminated by the use of higher SF_6 gas pressures, higher compression ratios, and other design features, all of which, however, are very costly. The interrupting capacity of SF_6 units can be increased by admixtures of helium to the gas which raise interrupting capacity considerably at the same partial pressures. By way of example, at the rate of rise of the recovery voltage of 2000 V / μs the interrupting current is 14.5 kA in the SF_6 interrupter and 22 kA in the SF_6 / He unit.

4.11 SF_6 Circuit Breaker Analysis

Effective interruption of power arcs in SF_6 gas can be achieved by cooling the arc with a flow of SF_6 gas. Blasting can be obtained by allowing the gas to flow from the high pressure reservoir to the low-pressure reservoir (dual pressure unit). The interrupting chamber of such a breaker is similar to that of the air circuit breaker [2.4, 4.1]. Dual pressure versions are complicated in design and require an automatic compressor to pump the gas from the low-pressure compartment into the higher pressure reservoir. Heating of the gas in the high pressure reservoir is another requirement. All these requirements penalize the reliability of the breaker. At the present time such breakers are used on the circuits that require break times under 40 ms and have break currents as high as 60-80 kA.

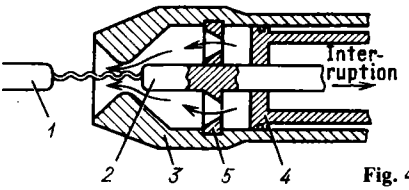

Fig. 4.54. Layout of a piston-type (puffer) interrupter

Figure 4.54 shows a piston-type (putter) SF_6 interrupting head. The movable contact (2) carries a baffle (5) fit into a nozzle (3) made of fluoroplast, an arc-resistant insulating material. A piston (4) is fixed with respect to the stationary contact (1). In the breaking operation the movable contact (2) and the parts it carries move to the right. An arc stricken between the contacts (1) and (2) is quenched by a puff of SF_6 gas compressed between the piston (4) and the baffle (5) from the insulation pressure 0.3-0.4 MN / m^2 to the quenching level 0.8-1.0 MN / m^2. The arc is extinguished in a matter of 20-30 ms.

Piston type interrupters obtain excess pressure by means of a driving mechanism retracting the movable contact. In view of considerable power required for gas compression and contact acceleration in the breaking operation a pneumatic driving mechanism is preferred. Because a pressure differential necessary for the arc extinction appears in this unit only after the contacts have been set in motion, the puffer interrupter cannot extinguish the arc within 10 ms.

A low level of insulating pressure (0.3-0.4 MN / m^2) in the closed interrupter enables normal operation of this system without gas warming at freezing ambient temperatures down to -40 °C. At present these units have received wide acceptance in numerous switchgear installations.

In an electromagnetic type SF_6-insulated circuit breaker, the gas remains at rest in make-break operations. The arc occurring after the contacts break apart is acted upon by a magnetic field. The electromagnetic force arising in this interaction moves the arc at a high speed with respect to the stationary SF_6 gas. In low-current load switches, the magnetic field is provided by permanent magnets, whereas in high-interrupting capacity breakers this field is created by a special winding passed over by short circuit current. Electromagnetic-blast SF_6 insulated circuit breakers are considered by Poltev [2.4]. In view of breaking current limitations these circuit breakers have received acceptance mainly as load switches.

Let us consider the selection of the principal parameters of a piston-type SF_6 circuit breaker. The procedure of Prof. Kukekov developed for air-blast circuit breakers (Sect. 4.3) will be used to determine the nozzle diameter. Accordingly, the nozzle inlet velocity w_1 (m / s) is given as

$$w_1 = 620 \times \Delta pS \times 10^5 / U_a \hat{I} \sin \omega t \text{ for } 0 < w_1 \leqslant 30$$
$$= 140 - 40 \sqrt{\frac{U_a \hat{I} \sin \omega t}{\Delta pS}} \times 10^{-5} \text{ for } 30 < w_1 < 140 \qquad (4.120)$$

where Δp is the pressure differential, MN / m^2; U_a is the voltage across the arc, V; $\hat{I}$ is the peak interrupting current, kA; and S is the nozzle throat area, m^2.

According to Kukekov's recommendations [4.1], the velocity of SF_6 gas puff should not fall below 6-7.5 m / s. The average voltage gradient across the arc is E_{av} = 115-150 V / cm.

The arc voltage is $U_a = E_{av} l_a$. The optimal distance between the contacts (see Fig. 4.53) is governed by the ratio $l_0 / d_n = 0.5$. Assuming that the effect to thermodynamic clogging is negligible, l_0 may be increased against the optimal distance. The resultant distance l_0 must be verified by the test voltage. Once l_0 has been determined, a refining calculation of d_n should be carried out with $l_a = l_0$.

For effective arc quenching, the pressure differential Δp produced by the compression in the piston chamber should be sufficiently high to ensure the supercritical flow of gas. The parameters of the piston assembly are mainly determined experimentally and from design experience. When this assembly is dimensioned, the pressure in the piston chamber, velocity of gas outflow and pneumatic drive requirements must be determined.

It is worth noting that an electric arc heats the gas in the interrupter and raises gas pressure. Experimental evidence suggests that arc extinction becomes more effective at higher breaking currents. However, inclusion of the arc effects into an analytical procedure renders it rather unwieldy. Therefore, preliminary estimations do not consider arc effects.

Because the arc extinction process is very fast, it is assumed that SF_6 gas parameters are changing adiabatically.

Interrupter dimension analysis needs piston velocity v and nozzle throat section S as functions of piston stroke l. Such dependences (Fig. 4.55) may be derived from theoretical considerations on the base of available experience. The calculation is carried out as follows.

(1) Determine the initial parameters of SF_6 gas, namely, volume $V_0 = S l_0$, density γ_0, and mass $M_0 = V_0 \gamma_0$, using the given piston area S and the cylinder length l_0.

(2) Assume a piston stroke Δl (15-20 mm) and determine density γ_1 and pressure under the piston p_1 as

$$V_1 = V_0 - \Delta l S, \quad \gamma_1 = M_0 / V_1, \quad p_1 = p_0 (\gamma_1 / \gamma_0)^k$$

where k is the process exponent (experimentally, k = 1.086). Denoting the insulating medium pressure by p_j and pressure at the piston underside by p_i we have for the critical flow

$$(p_j / p_i)_{cr} = \left(\frac{2}{k+1}\right)^{k/(k-1)} = 0.591$$

If p_j / p_i exceeds this level, the gas flow is subcritical. This flow regime is normally present at the initial stage of the opening operation.

(3) Determine the amount of outflowing gas $\Delta M = G \Delta t$. The mass flow rate in the subcritical flow regime

$$G = \mu S \sqrt{2 \frac{k}{k-1} p_i \gamma_i \left[(p_j / p_i)^{2/k} - (p_j / p_i)^{(k+1)/k}\right]}$$
$$= \mu S \Psi_{sub} \sqrt{p_i \gamma_i}$$

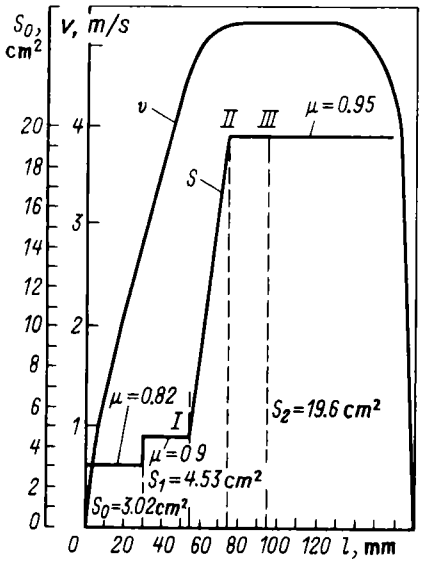

Fig. 4.55. Piston speed v and gas outlet port area S as functions of contact travel. Stages in contact travel: (I) contact starts leaving the nozzle, (II) critical flow incipience, (III) contact leaves the nozzle

where μ is the flow coefficient, S is the area of gas flow openings, and the subscript i refers to the gas under the piston. Obviously,

$$\Psi_{sub} = \sqrt{2 \frac{k}{k-1} \left[(p_j / p_i)^{2/k} - (p_j / p_i)^{(k+1)/k} \right]}$$

where $p_i = (p_0 + p_1) / 2$ and $\gamma_i = (\gamma_0 + \gamma_1) / 2$.

The time of outflow can be found if the average velocity of flow $v_{1,av}$ over a trial stroke Δl is known as $\Delta t_1 = \Delta l / v_{1,av}$, where $v_{1,av} = v_1 / 2$.

(4) By a time instant Δt_1

$$M_1 = M_0 - G \Delta t_1$$

Having the results for the trial travel Δl, give a new increment to the piston stroke and repeat the calculations.

When p_j / p_i falls below 0.591 the flow regime becomes critical with

$$\Psi_{sup} = [2 / (k+1)]^{1/(k-1)} \sqrt{2 k p_i \gamma_i / (k+1)}$$

This calculation yields pressure and mass flow rate G as functions of piston travel (Fig. 4.56). Cooling SF_6 gas will have sufficient arc quenching capability if the design provides the conditions for the critical flow regime.

When the dependence of pressure on piston travel is available, one can readily

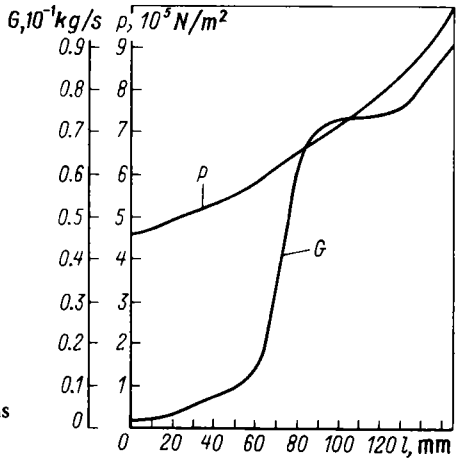

Fig. 4.56. Pressure and flow rate as functions of piston travel

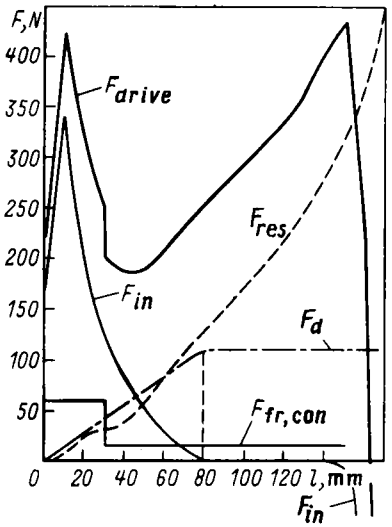

Fig. 4.57. Variation of forces acting on the driving mechanism with contact travel

find the resistance to piston stroke to dimension the drive power capability. In the breaking operation the pneumatic driving mechanism has to deliver the total force

$$F_{\text{drive}} = n F_{\text{res}} + F_{\text{in}} + F_{\text{fr}} + n F_{\text{fr,con}} + F_{\text{d}}$$

to overcome the resistance to the motion of an interrupting head piston F_{res} which is multiplied by n interrupters per drive, the forces of inertia F_{in}, the friction force in the mechanism F_{fr}, the force of friction in the opening contacts, and to work against the damping force F_{d} needed for smooth deceleration of the mechanism at the end of stroke: normally after the piston of the pneumatic drive has travelled

one half of the stroke the compartment of the pneumatic cylinder connected to the atmosphere is closed by a valve and the air trapped in this area decelerates the piston travel. Development of the aforementioned forces with contact separation spacing is shown in Fig. 4.57.

The analysis has been performed on the assumption that SF_6 is a perfect gas. However, the actual behaviour of SF_6 gas in the interrupter is described by the equation $p = \gamma RT$ only approximately. Computational errors may run into several ten percent. Therefore this equation receives a correction coefficient $\varkappa$ depending on gas density

$$p = \gamma RT\varkappa \tag{4.121}$$

A computational procedure for piston-type SF_6 interrupters based on this equation has been developed by Pozdnyakov [4.10].

4.12 Construction of SF_6 Circuit Breakers

For SF_6 insulated 110 and 220 kV switching substations Soviet manufacturers have developed, manufactured and tested circuit breakers for 2000-A rated continuous-current, 40-kA interrupting capacity, 65-ms break time, 80-ms make time, 0.7-MN / m^2 rated SF_6 gas pressure, and 2.0 MN / m^2 rated drive pressure.

The 110-kV circuit breaker has one interrupter shown schematically in Fig. 4.58. The device is placed in a reservoir filled with SF_6 gas at an insulating pressure of 0.7 MN / m^2 at 20 °C.

An arcing contact (3) is made in the form of a hollow receptacle. This contact is joined into a single assembly with a main contact (2) and a cylinder (1). In the closing operation this assembly moves to the right, the arcing contact (4) enters the cluster contact (3) and the female contact (5) slides over the main contact (2). The contact (3) is connected to the stem (7). A fluoroplast nozzle (6) also travels to the right and engages the pipe contact (4). SF_6 gas is admitted to area *A* and forced from area *B*.

On opening the cylinder (1) and the main contact (2) travel to the left. The piston (10) remains stationary. The main contacts (2) and (5) separate first followed by the arcing contacts (3) and (4). When the contacts (3) and (4) move apart an arc strikes and finds itself cooled by a flow of SF_6 gas. A compressed SF_6 gas forms

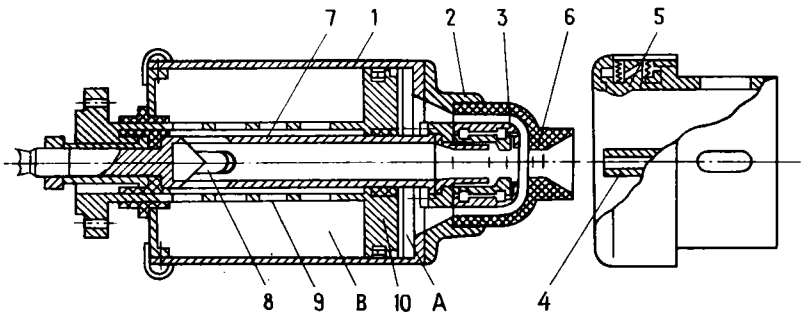

Fig. 4.58. Interrupting chamber of an SF_6 circuit breaker

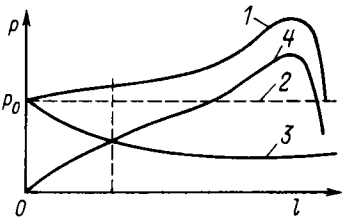

Fig. 4.59. Variation of pressure differential in the interrupter of Fig. 4.58 with piston travel

in area *A* and rarefied gas in area *B*, as a result a gas flow occurs from *A* to *B* through ports (8) and (9) as supported by the pressure differential $p_A - (-p_B) = p_A + p_B$. Pressure profiles in the interrupter areas as functions of contact separation are shown in Fig. 4.59. The dashed line (2) is the initial pressure level in the tank, p_0. Curves (1) and (3) are pressure levels in the *A* and *B* areas, respectively; curve (4) is the pressure difference between these areas. Increasing the pressure differential one can achieve the critical flow condition for short arc spacing and interrupt the circuit at small travel distance of the movable contact within 10 ms, given that interrupted currents are within the medium range and the rate of rise of voltage recovery is slow. When the interrupted current is 0.9 interrupted capacity and the voltage recovery conditions are rather heavy (short circuit fault is close to the substation busbars) the interruption process is more complicated and arc extinction takes place when the contact (4) leaves the nozzle (6). Additional blast for the arc in the nozzle (6) provides reliable interruption of currents up to 36 kA at a voltage recovery rate of 8.4 kV / μs.

The interrupter design using rarefaction of SF_6 gas in area *B* was devised by Soviet engineers and has resulted in the development of highly competitive equipment.

Figure 4.60 shows the functional details of the SF_6 circuit breaker for SF_6 insulated 220-kV substations. The stationary contact (7) is attached to the breaker enclosure by means of a moulded insulator (8). The breaker comprises two interrupters

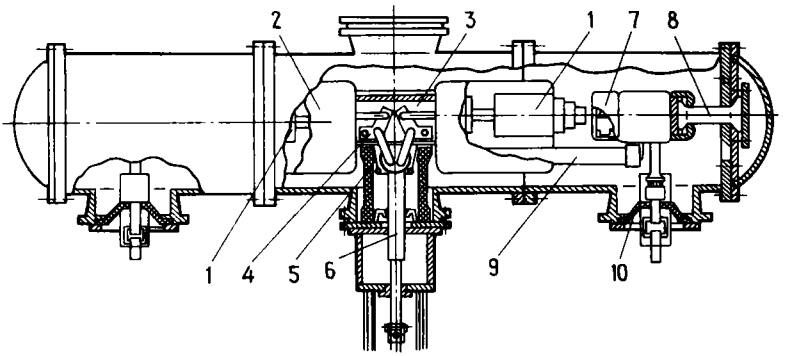

Fig. 4.60. Outline and functional details of an SF_6 circuit breaker pole for SF_6 insulated switchgear for 220 kV

connected in series by means of the body (3). The ceramic capacitors (9) take care of uniform distribution of voltage over the interrupters. The moving contact (1) is actuated by the insulator rod (6) through the linkage (4). The movable contact (1) and the capacitor (9) are shielded by a screen (2). The cylinder (5) insulates the contact (1) from the breaker enclosure.

Make-brake operations are effected by a pneumatic driving mechanism. The breaker is filled with SF_6 gas at a pressure of 0.55 MN / m^2. The stationary contacts (7) are brought out by SF_6-to-SF_6 bushings. The insulating wall (10) of the bushing seals the interior gas in the breaker including when the unit is removed from the substation set.

This type of circuit breaker has demonstrated high performance under heavy duty conditions. It is capable of 20 interruptings of maximum short circuit current up to 40 kA without maintenance. The gas leakage rate is within 1 % a year. The life expectancy to overhaul of this circuit breaker is 10 years [4.5].

4.13 Trends in the Development of Oilless Circuit Breakers

Nominal system voltage, U_{nom}. The highest voltage rating in common use in the Soviet Union is 750 kV. The necessary switchgear for this rating is ready available in this country. It is expected that 200-300 GW power grids will be connected by 500-1500 kV tie lines. Therefore, switchgear designed for 1500 kV and even for 2000 kV should be expected [3.2]. Development of SF_6 insulated switchgear for 1150 kV is underway in this country.

Rated continuous current, I_r. Most systems with rated voltage of 110 kV never experience currents higher than 4000 A. The development of systems for 750-1200 kV would require switchgear installations with 12 kA continuous current. Current ratings at a generator voltage of up to 20 kV are expected to grow up to 40-50 kA so that circuit breakers have to be developed for these ratings.

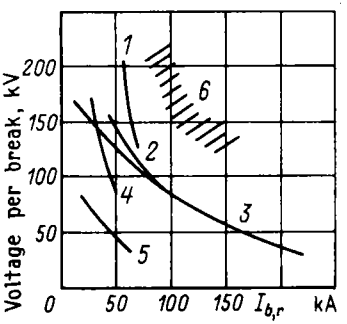

Fig. 4.61. Application areas of various types of circuit breaker: (1) SF_6 dual-pressure system, (2) SF_6 piston-type version, (3) air circuit breakers, (4) low-oil content circuit breakers, (5) vacuum circuit breakers, (6) prospective enhancement in the coming decade

Interrupting capability, $I_{b,r}$. In 110-750 kV circuit breakers the highest breaking current, $I_{b,r}$, attains 63 kA. In the years to come this level will be hardly exceeded in most points of the 110-750 kV power grid, although current ratings up to 130 kA are expected [3.2] in some locations of the 750-1200 kV power grid. At the generator voltage (10 % generator reactance) short circuit currents up to 500 kA are probable.

Figure 4.61 illustrates the feasible application ranges for various types of circuit breaker. For example, with rated breaking currents of 20-200 kA air circuit breakers with 170-30 kV voltage per break are common use. The range of vacuum circuit breakers encloses 20-70 kA short circuit current at 80-30 kV per break, respectively.

Rate of rise of the recovery voltage. Growing power ratings and short circuit current values entail an increase in rate of rise of the recovery voltage across the breaker contacts. At 110-750 kV system voltage and corresponding rated breaking current (Soviet standard GOST 687-78), the rate of recovery voltage reaches 1.2-2.7 kV / μs. In 500 kV systems, the rate of rise of the transient recovery voltage is expected to grow up to 5-10 kV / μs. It is worth noting that at a breaking current of 0.3 interrupting capability, the rate of recovery voltage increases considerably and attains values as high as 8-10 kV / μs.

Break time. In the best circuit breakers available at present, the break time does not exceed 40 ms. A pressing problem for 750-1200 kV transmission lines is increase of the power transmitted by these systems. The power can be increased by reducing the break time of the circuit breakers used on these systems. Break times of the order of 20 ms will be required for 750-1200 kV ratings [3.2].

Switching transient overvoltage. For circuit breakers designed to operate at 750-1200 kV, it is essential that the test voltage levels of the switchgear and related equipment should be lowered since it would be technically difficult and economically unfeasible to provide the insulation with safety margins as high as that for 10-20 kV ratings. Accordingly, switching transient overvoltages should be limited by the breaker operating on this circuit. The level of these overvoltages is of decisive importance in setting up the test voltage level. The admissible per unit values should reduce with the growth of rated voltage. By way of illustration, in the Soviet Union, this level is 2.5 p.u. at 500 kV and 1.8 p.u. at 1150 kV. Lower per-unit values at high rated voltage have a favourable effect on the switchgear weight, size, and cost.

Especially high overvoltage (up to 4 p.u.) sets up in closing a long unloaded line. This problem receives much attention in the development of extra-high voltage switchgear. A most efficient way of damping this overvoltage consists in placing a multiple-step resistor into the circuit prior to the closing operation or a synchronous closure when the potential difference across the breaker contacts is small [3.2].

Reliability. The average annual failure rate of modern circuit breakers is estimated at one in a hundred. The designers current task is to reduce this figure to 1 in 500 [3.2]. An interesting discussion of circuit breaker designs and trends may be found in the book edited by Fleurshaim [4.9].

4.14 Illustrative Analysis of Air-Blast Interrupter

Given: $U_{nom} = 750$ kV, $I_r = 4000$ A, $I_{b,r} = 63$ kA, $t_b = 0.04$ s, air pressure in the reservoir is 4 MN / m^2.

Determine: basic parameters of the interrupter.

Analytical procedure

The analysis will be based on a 250-kV module of a type VNV air-blast circuit breaker. The module comprises two interrupters connected in series with 125 kV per break.

(1) *Blast nozzle diameter* d_n. The interrupter has a bidirectional blast design. To reduce main contact wear and achieve efficient cooling of the arc, this is blown out from the contacts within a few milliseconds and continues on the arcing electrodes (see item (41) in Fig. 4.47). These electrodes are spaced at $l_e = 16$ cm. Determine the arc power per one nozzle

$$P_a = U_a I_{b,r} \sqrt{2} / 2 = E_{av} l_e I_{b,r} \sqrt{2} / 2$$

Recalling the average voltage gradient $E_{av} = 150$ V / cm (see Sect. 4.3), we get

$$P_a = (150 \times 16 \times 63\ 000 \sqrt{2}) / 2 = 106\ 596 \text{ kW}$$

In view of the large breaking current we take the minimum velocity at $w_1 = 8$ m / s. Referring to Fig. 4.11 we get

$$P_a / Sp_0 = 12.5 \text{ kW / N}$$

$$S = 106\ 596 / (12.5 \times 10^{-4} \times 4.0 \times 10^6) = 21.3 \text{ cm}^2$$

so that $d_n = (4S / \pi)^{1/2} = 5.2$ cm, and we take $d_n = 5$ cm.

(2) *Optimal contact spacing.* In Sect. 4.3 we found that for a bidirectional blast design $l_{c,opt} = d_n / 2 = 2.5$ cm.

(a) Evaluate the electric strength recovered in the process of transient voltage recovery. The voltage recovering across the break opened first is

$$U_p = \frac{U_{r,max} \sqrt{2}}{\sqrt{3}\, n} k_{nu} k_p k_a$$

For $n = 6$, $k_{nu} = 1.1$, $k_p = 1.3$, $k_a = 1.5$ (see Sect. 3.3), and $U_{r,max} = 787$ kV, we obtain $U_{bd,max} = 229.3$ kV.

To estimate the dielectric strength of the chosen arc spacing we resort to Eq. (4.23)

$$U_{bd,max} = 119\ (pl)^{0.45} = 119\,(4.0 \times 2.5)^{0.45} = 336 \text{ kV}$$

Moving air reduces the breakdown voltage by a factor of 0.7-0.8, hence, $U_{bd,max} = 336 / 1.4 = 240$ kV. We see that the recovering voltage value is under the calculated breakdown voltage, consequently the selected electrode spacing is adequate from a dielectric strength standpoint.

Actually the arc spacing will have a breakdown voltage higher than 240 kV because the outside diameter of the contact with allowance for pipe thickness is about 60 mm. The distance between contacts l_c for this type of circuit breaker may be

selected with reference to Eq. (4.69) and Fig. 4.35*b*, namely $E_{max} = 175 / 1.5$ kV / cm (the denominator 1.5 allows for air motion)

$$l_c = U_{bd,max} / E_{max} = 229.3 \times 10^3 \times 1.5 / 175 \times 10^3 = 2.35 \text{ cm}$$

Since this distance is well below the selected optimal contact spacing, the original choice is correct.

(b) Compare the dielectric strength of the interrupter against the test voltage. In the open unit, voltage is applied across the cages of the movable and fixed contacts. The Soviet standard GOST 1516-76 stipulates the normal-frequency (50 Hz) test-voltage 1770 kV and peak impulse voltage 2600 kV.

The distance between the cages may be determined by Eq. (4.69)

$$l_{cage} = U_{test} k_{nu} k_{coord} / E_{max} \eta k_{imp} n$$

where $\eta = 0.65$, $k_{nu} = 1.1\text{-}1.15$, $n = 6$, $k_{imp} = 1.3$ (see Fig. 4.35*b*), $k_{coord} = 0.9$ (see Sect. 4.7), and $E_{max} = 175$ kV / cm.

For the power frequency voltage

$$l_{cage} = 1770 \times 10^3 \times 1.15 \times 0.9 / (175 \times 10^3 \times 0.65 \times 6 \times 1.3) = 2.1 \text{ cm}$$

and for the impulse voltage

$$l_{cage} = 2600 \times 10^3 \times 1.15 \times 0.9 / (175 \times 10^3 \times 0.65 \times 6 \times 1.3) = 3.0 \text{ cm}$$

Allowing some margin, we choose a safe spacing of 4.0 cm.

(3) *Thermal analysis of the current carrying pipe* (item (42) in Fig. 4.47). The inner diameter of the pipe is selected by a factor of 3-8 larger than the nozzle diameter to facilitate residual-arc-plasma evacuation; accordingly, $D_{in} = 3 \times 50 = 150$ mm. To simplify the analysis we assume that the heat flows in radial direction only. The pipe section is determined by Eq. (4.76) with $\Theta_{max} = 110$ °C, $\Theta_0 = 40$ °C, $\varrho = \varrho_0 (1 + \alpha \Theta_{max})$, and $k_p = 12$ W / m^2 K.

The thermal resistivity R_{th} is calculated by Eq. (4.80) with

$$\lambda_p = 125 \times 10^{-2} \text{ W / m}^2 \text{ K}, \quad \lambda_{cp} = 17 \times 10^{-2} \text{ W / m K, and}$$

$$\lambda_{air} = 0.0259 \text{ W / m K}$$

The cylinder radii (see Fig. 4.37) are as follows: $R_1 = 0.075$ m, $R_2 = 0.14$ m, $R_3 = 0.16$ m, $R_4 = 0.18$ m, and $R_5 = 0.23$ m. Assume first that the current carrying tube is thin and $R_0 = R_1$. To evaluate $\lambda_{air,eq}$ we calculate the product of the Grashof number Gr by the Prandtl number Pr for the first air gap. The Grashof number [4.11] is determined as

$$\text{Gr} = 9.81 (R_2 - R_1)^3 \beta (\Theta_1 - \Theta_2) / \nu^2$$

where β is the voluminous expansion coefficient of gas equal to 3.67×10^{-3} m^3 / K; $\Theta_1 - \Theta_2$ is the temperature difference of the layers; $\nu = \mu / \varrho$ kinematic viscosity, m / s^2; μ is the viscosity, Pa s; and ϱ is the gas density, kg / m^3.

An approximate temperature difference is selected $\Theta_1 - \Theta_2$. This approximation is compared with the actual temperature difference determined after the computation $\Theta_1 - \Theta_2 = (P / 2\pi \lambda_{air,eq}) \times \ln (R_2 / R_1)$. If these values differ significantly,

then a new computation is attempted with another approximation for $\Theta_1 - \Theta_2$. We set this difference at 30 °C.

The density of air at normal temperature and pressure is $\varrho = 1.2$ kg / m^3; at 4 MN / m^2 $\varrho = 1.2 \times 40 = 48$ kg / m^3. The dynamic viscosity of air is $\mu = 18.1 \times 10^{-6}$ Pa s; the kinematic viscosity is

$$\nu = 18.1 \times 10^{-6} / 48 = 0.377 \times 10^{-6} \text{ m s}^{-2}$$

The Grashof number

$$\begin{aligned} \text{Gr} &= 9.81\,(0.14 - 0.075)^3 \times 3.67 \times 10^{-3} \times 30 / (0.377)^2 \times (10^{-6})^2 \\ &= 2.0867 \times 10^9 \end{aligned}$$

The Prandtl number

$$\text{Pr} = \mu\, c_p / \lambda_{\text{air}}$$

where c_p is the specific heat capacity of air at constant pressure in the selected temperature range equal to 1005 J / kg K,

$$\text{Pr} = 18.1 \times 10^{-6} \times 1005 / 2.59 \times 10^{-2} = 0.702$$

The product Gr · Pr is then

$$\text{Gr} \cdot \text{Pr} = 2.0807 \times 0.702 \times 10^9 = 1.46 \times 10^9$$

At this value of the Gr · Pr product cooling by convection is significant. Convection can be taken into account by incorporating $\lambda_{\text{air, eq1}} = \varepsilon_{\text{conv}} \lambda_{\text{air}}$ in the analysis in place of λ_{air}, where $\varepsilon_{\text{conv}}$ allows for convection and can be calculated for Gr · Pr $> 10^3$ by the equation

$$\varepsilon_{\text{conv}} = 0.18\,(\text{Gr} \cdot \text{Pr})^{0.25} = 0.18 \sqrt[4]{1.46 \times 10^9} = 35$$

so that

$$\begin{aligned} \lambda_{\text{air, eq1}} &= 2.59 \times 10^{-2} \times 35 = 0.906 \text{ W / m K} \\ &= 0.906 \cdot 10^{-2} \text{ W / cm K} \end{aligned}$$

Assuming the temperature difference at the second air gap being 20 °C, we get

$$\begin{aligned} \text{Gr} &= (0.18 - 0.16)^3 \times 9.81 \times 10^{-3} \times 20 \times 3.67 / (0.377)^2\,(10^{-6})^2 \\ &= 0.04 \times 10^9 \\ \text{Gr} \cdot \text{Pr} &= 0.04 \times 10^9 \times 0.702 = 0.0288 \times 10^9 = 2.88 \times 10^7 \\ \varepsilon_{\text{conv}} &= 0.18\,(2.88 \times 10^7)^{1/4} = 0.18 \times 73.2 = 13.18 \\ \lambda_{\text{air, eq2}} &= 2.59 \times 10^{-2} \times 13.18 = 0.3413 \text{ W / m K} \\ &= 0.3413 \times 10^{-2} \text{ W / cm K} \end{aligned}$$

The thermal resistivity

$$R_{\text{th}} = \frac{1}{2\pi} \left[\frac{\ln (R_2 / R_1)}{\lambda_{\text{air, eq1}}} + \frac{\ln (R_3 / R_2)}{\lambda_{\text{epoxy}}} + \frac{\ln (R_4 / R_3)}{\lambda_{\text{air, eq2}}} + \frac{\ln (R_5 / R_4)}{\lambda_{\text{p}}} \right]$$

$$= \frac{1}{6.18}\left[\frac{\ln(14/7.5)}{0.906\times10^{-2}} + \frac{\ln(16/14)}{17\times10^{-4}} + \frac{\ln(18/16)}{0.341\times10^{-2}} + \frac{\ln(23/18)}{12.5\times10^{-3}}\right] = 31.9\ °C/cm\ W$$

The cross-sectional area of the tube by Eq. (4.76)

$$S = [(4\times10^3)^2\,2.33\times10^{-6}(31.9\times1.2\times10^{-3}\times145+1)] \div [1.2\times10^{-3}\times145(110-40)] = 20\ cm^2$$

From Fig. 4.37 $S = \pi(R_1^2 - R_0^2)$ whence $R_0^2 = R_1^2 - S/\pi$ and we get $R_0 = 7.06$ cm. Now the temperature difference at the first layer

$$\Theta_1 - \Theta_2 = P \swarrow \ln(R_2/R_1)/2\pi\lambda_{air,\,eql}$$
$$= (4\times10^3)^2[2.33\times10^{-6}\,0.624/20\times2\times3.14\times0.906\times10^{-2}]$$
$$= 20.44\ °C$$

This value of temperature difference is below the originally assumed approximation (30 °C). Therefore, another approximation at a lower value, say 25 °C, is needed for the final analysis. One is to determine the thermal resistivity R_{th} and keeping the value of S to find the actual temperature difference across the first layer. Compare the derived value with the set 25 °C.

It should be noted that this analysis takes into account heat transfer by convection and conduction only. Radiative heat transfer may be neglected in view of low temperature differences ($\Theta_1 - \Theta_2 < 50$ °C).

(4) *Contact system analysis.* The movable contact of the interrupter module is a hollow copper tube (item *18* in Fig. 4.47). Each break has three fixed socket contacts: a current collecting contact in the form of a let-through socket (43), the main cluster contact (19) and arcing contact (20). The cross-sectional view of the main contact is presented in Fig. 4.62 ($d_{mid} = 13.2$ cm). We assume that in the closed position the main contact carries the whole current. The socket has 24 fingers. The contact engagement force per finger at rated current is found with Eq. (4.70). For this calculation we assume that $I_f = 4000\times1.3/24$; $T_0 = 75 + 273 = 348$ K, $T_m - T_0 = 5$ K, $T_m = 353$ K; $H = 37\,000$ N/cm^2 at $T_m = 353$ K (see Fig. 4.63). Substituting these values into Eq. (4.70) yields

$$F_c = (4000\times1.3/24)^2[2.42\times10^{-8}\times3.14\times37\,000/16(3.9)^2(0.17)^2]$$
$$= 18.65\ N$$

The pressing force of contacts is determined by Eq. (4.71) which expresses the condition of the contacts being not welded together at short circuit current. For a copper contact, $k = 1900\ A/N^{1/2}$.

$$I_{s.f} = 1.8\sqrt{2}\times63\times10^3\times1.3/24$$
$$F_c = (1900)^{-2}(1.8\sqrt{2}\times63\times10^3\times1.3/24)^2 \approx 21\ N$$

The temperature of the contact point at short circuit current is checked by Eq. (4.74). Since the temperature of the contact point T_m is not known, neither are

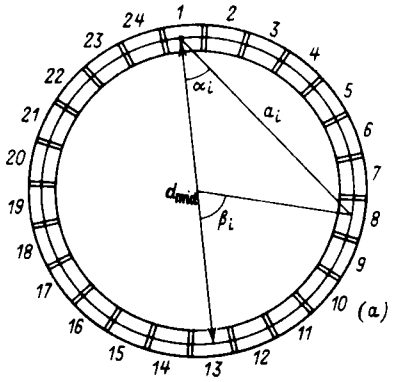

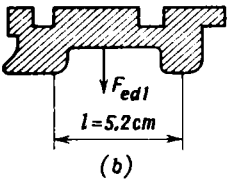

Fig. 4.62. (*a*) Cross section of a cluster contact of a VNV type circuit breaker. (*b*) Cross section of a finger contact

H_{max} and F_p. To determine these quantities we resort to Eq. (4.73). In order to solve this equation for S_0 we determine first the pressing force contribution due to electrodynamic forces F_{ed}. Referring to Fig. 4.62, the force applied to one finger can be written as

$$F_{ed1} = 2 \sum_{i=2}^{12} F_{1/i} \cos \alpha_i + F_{1/13}$$

where

$$F_{1/l} = 10^{-7} I_{s,f}^2 2 (l / a_{1i}) \left[\sqrt{1 + (a_{1i} / l)^2} - a_{1i} / l \right]$$

is the interaction force between the 1st and *i*th fingers, $a_{1i} = d_{mid} \cos \alpha_i$, $d_{mid} = 13.2$ cm, and $l = 5.2$ cm.

The force F_{ed1} is applied to the midpoint of the finger, therefore the contact force $F_{ed} = F_{ed1} / 2 = 27$ N.

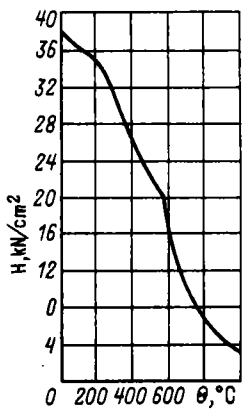

Fig. 4.63. Temperature dependence of the Vickers hardness number

To resolve Eq. (4.73) we choose the temperature T_m at about 1000 K and find H_{max} from Fig. 4.63 as 10 000 N / cm^2. Now S_0 is 4.8 × 10^{-4} cm^2.

The next step is to determine the calculated value of T_m by Eq. (4.74)

$$T_{m,\,calc} = (273 + 250) / \cos (2620 \sqrt{2.4 \times 10^{-8} \times 3.14 \times 10\ 000} / (4 \times 3.9 \sqrt{48})$$
$$= 670 \text{ K}$$

It is desirable that the margin between $T_{m,\,calc}$ and T_m should not exceed 20 %. In the evaluation of $T_{m,\,calc}$ with Eq. (4.74), I_f is the peak short-time current through the finger in the case when the contact time constant τ_c is well below half-period of the current (10 ms); according to Kukekov [4.1]

$$\tau_c = c \gamma \pi F_p / 24 \lambda H_{max}$$

where c is the specific heat capacity, J / kg K; λ is the thermal conductivity of the contact material, W / m K. In the event of τ_c being comparable with 10 ms, the calculation uses the effective value of current in the finger.

The time constant of the contact [4.1]

$$\tau_c = 0.386 \times 8.9 \times 3.14 \times 48 / 3.9 \times 24 \times 10\ 000 = 5 \text{ ms}$$

Since this value is close to 10 ms, the choice of r.m.s. current through the finger in the calculation is quite appropriate.

Because the resultant $T_{m,\,calc}$ is below the maximum admissible temperature of the contact point for copper (1346 K), the pressing contact force has been selected correctly. It should be noted that the calculation of $T_{m,calc}$ did not include the repulsive force F_{rep}. With allowance for this force the temperature will rise somewhat but remain safe below the admissible level.

(5) *Break time.* The illustrative evaluation of break time and make time will be carried out for the type VNV breaker mechanism rated for 750 kV. All the mechanical parameters involved are borrowed from the manufacturer's list.

From a mechanical point of view the break time consists of a takeoff time t_{to} and a moving time t_m so that

$$t_b = t_{to} + t_m$$

In the type VNV air-blast circuit breaker, the pneumatic pressure driving the piston provides the moving force (Fig. 4.64*a*). Before the takeoff occurs the motion is opposed by the forces of friction (in the main contacts $F_{fr,\,mc}$, in sliding contacts $E_{fr,\,sc}$, in arcing contacts $F_{fr,\,ac}$, and in sealing elements $F_{fr,\,se}$) and the force of contact-closing springs which are charged in the opening operation. Let us estimate each of these forces

$$F_{fr,\,mc} = F_c n \mu$$

where n is the number of finger contacts, and $\mu = 0.2$ is the friction factor. Also, $F_{fr,\,mc} = F_{fr,\,sc}$ since these contacts are essentially of the same design.

For the arcing contacts, the normal force per contact is F_a = 140 N, μ = 0.2, so that for n = 4 we get

$$F_{fr,\,ac} = F_a n \mu = 140 \times 4 \times 0.2 = 110 \text{ N}$$

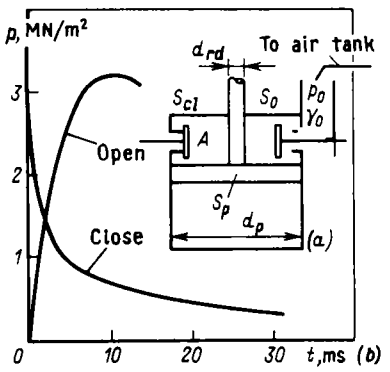

Fig. 4.64. Time variation of pressure above the piston of a VNV-type circuit breaker in make-break operations

The friction force in the sealing device if $F_{fr,se} = 120$ N.

This type of circuit breaker has six breaks per pole, hence the total friction force is

$$\Sigma F_{fr} = 6\,(101 + 140 + 110 + 120) = 2600 \text{ N}$$

Each module of the pole has a closing spring with initial and final force $F_{in} = 2000$ N and $F_{fin} = 6550$ N, deformation $\Delta x = 50$ mm, so that the spring coefficient $k = (6550 - 2000) / 50 = 91$ N / mm. The total motion-opposing force is now

$$F_{opp} = \Sigma F_{fr} + 3 F_{in} = 8604 \text{ N}$$

The diagram of the driving mechanism is sketched in Fig. 4.64*a*. The parameters of the mechanism are as follows: the volume of space $A = 0.000343$ m^3, piston diameter $d_p = 160$ mm, stem diameter $d_{rd} = 24$ mm, inlet valve diameter 24 mm, exhaust valve diameter 41 mm. The dynamically equivalent mass of the moving parts in three modules brought to the piston is $m = 8.55$ kg. The piston travel is 50 mm. The initial conditions are as follows: $p_{atm} = 10^5$ N / m^2, $\gamma_{atm} = 1.2$ kg / m^3, the tank pressure $p_0 = 4.0$ MN / m^2, $\gamma_0 = \gamma_{atm}\,(p_0 / p_{atm}) = 48$ kg / m^3.

The cross section of the inlet (opening) valve is $S_o = \mu\pi\, d_0^2 / 4 = 0.5 \times 3.14 \times \times 24^2 \times 10^{-6} / 4 = 226 \times 10^{-6}$ m^2 (μ allows for jet constriction). The effective area of the piston

$$S_p = \pi\,(d_p^2 - d_{rd}^2)\,/\,4 = 0.0204 \text{ m}^2$$

When the valve S_o is opened, it admits compressed air in area A, and as soon as the pneumatic force applied to the piston becomes equal to the opposing force F_{opp}, the contacts are set in motion. The takeoff pressure

$$p'_{to} = F_{opp} / S_p = 8604 / 0.0204 = 421\ 600 \text{ N / m}^2$$

The full takeoff pressure

$$p_{to} = p'_{to} + p_{atm} = 521\ 600 \text{ N / m}^2$$

Assuming the gas flow process proceeds adiabatically, the density of air at this instant can be defined as

$$\gamma_{to} = \gamma_{atm}\,(p_{to} / p_{atm})^{1/k} = 1.2\,(521\ 570 / 105)^{1/1.4}$$
$$= 3.95\ \text{kg} / \text{m}^3$$

Because the pressure differential is high ($4\ \text{MN} / \text{m}^2 \gg 0.1\ \text{MN} / \text{m}^2$) we find the mass flow rate for the critical flow regime as [4.1]

$$G_{cr} = 0.57\, S_o\, c_{cr}\, \gamma_0$$
$$= 0.57 \times 226 \times 10^{-6} \times 330 \times 48 = 2.05\ \text{kg} / \text{s}$$

The time elapsed in filling space A up to takeoff

$$t_{to} = (\gamma_{to}\, V_A - \gamma_A\, V_A) / G_{cr}$$
$$= 0.000343\,(3.89 - 1.7) / 2.05 = 0.45\ \text{ms}$$

The time in motion t_m can be found by solving the differential equation

$$m\mathrm{d}^2x / \mathrm{d}t^2 = F_m - F_{opp}$$

where $m = 8.55$ kg is the total mass of moving parts driven by the piston, F_m is the force of motion provided by compressed air, and F_{opp} is the motion opposing force due to friction of the sliding contacts and the three springs of the modules.

The cylinder space is filled while the volume is varying (because the piston is travelling), therefore to find piston speed which is a function of the pressure in this cylinder the equation of motion has to be solved by numerical methods [4.1] as follows. At $t = 0$ both $\mathrm{d}x / \mathrm{d}t = 0$ and $\mathrm{d}^2x / \mathrm{d}t^2 = 0$. The values of p_{to} and γ_{to} are known and the initial volume V_A is filled in the supercritical flow regime. For a given first time interval Δt_1 and the initial volume $V_0 = V_A$ we obtain the finite value of air density γ_{t1} in the cylinder by the equation

$$\gamma_{t1} = (G_t\, \Delta t_1 + \gamma_{to}\, V_0) / V_0 = G_t\, \Delta t_1 / V_0 + \gamma_{to}$$

Here, $G_t\, \Delta t_1$ is the amount of air entering the cylinder in Δt_1.

Let $\Delta t_1 = 3 \times 10^{-3}$ s, then

$$\gamma_{t1} = (2.04 \times 3 \times 10^{-3} - 3.95 \times 343 \times 10^{-6}) / 343 \times 10^{-6}$$
$$= 21.8\ \text{kg} / \text{m}^3$$

In the subsequent computation we assume that in each interval Δt_i the quantities γ_{ti}, p_{ti}, and G_{ti} are constant and equal to mean values over this interval so that

$$\gamma_{t1,m} = (\gamma_{t1} + \gamma_{to}) / 2 = (21.8 + 3.95) / 2 = 12.9\ \text{kg} / \text{m}^3$$

The pressure in space A will be found by a formula derived by Kukekov [4.1]

$$p_{tn} = \frac{B_n\, C_n}{kB_n - D_n}\left\{1 - \exp\left[-(kB_n - D_n)\,\Delta t_n\right]\right\} - p_{t\,(n-1)}\left[-(kB_n - D_n)\,\Delta t_n\right]$$

where $k = 1.4$, $B_n = G_{tn} / (G_{tn}\, \Delta t_n + \gamma_{0t}\, V_0)$, $C_n = k\, \gamma_{tn}\, p_0 / \gamma_0$, and $D_n = kG_{tn} / \gamma_{tn}\, V_{tn}$. The quantities B_n, C_n, and D_n are invariable over Δt.

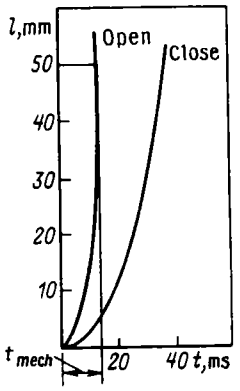

Fig. 4.65. VNV breaker contact travel in make-break operations

For the subcritical flow regime, the flow rate is computed as

$$G_{tn} = \varphi(\beta) S_0 c_{cr} \gamma_0$$

where $\beta = p_t / p_0$ and $\varphi(\beta)$ is borrowed from Ref. [4.1].

The calculation yields $p_1 = 3.04$ MN / m^2,

$$p_{1,m} = (p_{to} + p_1) / 2 = (0.53 + 3.04) / 2 = 1.785 \text{ MN / m}^2$$

For $\beta = p_{t1} / p_0 = 3.04 / 4 = 0.76$ Ref. [4.1] gives $\varphi(\beta) = 0.61$.

The acceleration

$$a_1 = \left[p_{1,m} S - (F_{sp} + \Sigma F_{fr})\right] / m = 317 \text{ m / s}^2$$

The speed increment $\Delta v_1 = a_1 \Delta t_1 = 0.95$ m / s, that is at the end of interval Δt_1 the piston has a velocity of $v_1 = 0.951$ m / s. The piston travel at this instant (for 3 ms) is $x_1 = v_1 \Delta t_1 = 2.9$ mm.

Let $\Delta t_2 = 5$ ms. Similar calculation yields for volume increment $\Delta V_1 = x_1 S_p = 2.9 \times 10^{-3} \times 0.02 = 58 \times 10^{-6}$ m^3. The new volume will be

$$V_1 = V_0 + \Delta V_1 = (343 + 58)\, 10^{-6} = 401 \times 10^{-6} \text{ m}^3$$

$$G_{t2} = S c_{cr} \varphi(\beta) \gamma_{t1,m}$$

$$= 226 \times 10^{-6} \times 330 \times 0.61 \times 12.9 = 0.59 \text{ kg / s}$$

$$\gamma_{t2} = (G_{t2} \Delta t_2 + \gamma_{t1} V_1) / V_1$$

where γ_{t1} is taken to the end of interval Δt_1.

The subsequent computations are similar to the procedure outlined for $\Delta t = \Delta t_1$. The full travel of the piston is $x = 50$ mm.

The results of the computation are plotted in the form of a pressure time variation over the piston and piston travel shown in Figs. 4.64*b* and 4.65. The time of stroke $t_m = 13.5$ ms is sufficiently small to keep the break time (including the extinction time) within a two-period interval (40 ms).

(6) *Make time.* Once the contact closing valve has been opened the air leaves space A and the pressure in this space falls down. At the closing stroke incipience the spring force is equal to the forces of friction and downward force applied to the piston, viz.,

$$p'_{to} S_p + \Sigma F_{fr} = F_{sp,o}$$

where $F_{sp,o}$ is the force of compressed spring in the open position of the breaker.

$$p_{to} = p'_{to} + p_{atm} = (F_{fr,o} - \Sigma F_{fr}) / S_p + p_{atm} = 0.99 \text{ MN} / \text{m}^2$$

Because the cylinder is vented in the atmosphere and $p_{to} > 0.2$ MN / m^2, the exhaust will be a supercritical flow regime. The initial pressure $p_0 = 4.0$ MN / m^2, air density $\gamma_0 = 48$ kg / m^3, cylinder volume $V_A = 1360 \times 10^{-6}$ m^3. The time of takeoff at $p_{to} = 0.99$ MN / m^2 is determined by Eq. (4.49)

$$t_{to} = \frac{2 V_A}{\mu S_{make} \times 0.687 (k - 1)} \sqrt{\frac{\gamma_0}{p_0}} \left[\left(\frac{p_{to}}{p_0} \right)^{(1 - k) / 2k} - 1 \right]$$
$$= 0.012 \text{ s}$$

the density of air at takeoff

$$\gamma_{to} = \gamma (p_{to} / p_0)^{1 / k} = 48 (9.9 / 40)^{1 / 1.4} = 17.7 \text{ kg} / \text{m}^3$$

During the time periods of takeoff and piston motion the pressure of air above the piston exceeds 0.2 MN / m^2, therefore the air is exhausted in a supercritical flow regime. It should be noted, however, that owing to falling air density the mass flow rate of air also decreases

$$G_n = 0.57 S_{make} c_{cr} \gamma_n$$

The density of air decreases with pressure as

$$\gamma_n = (\gamma_{n-1} V_{n-1} - G_n \Delta t_n) / V_n$$
$$p_n = p_{n-1} (\gamma_n / \gamma_{n-1})^{1 / k}$$

The equation of motion in the closing operation

$$dv / dt = a = (F_{sp} - p_n S_0 - \Sigma F_{fr}) / m$$

where variation of F_{sp} and friction forces ΣF_{fr} should be taken into consideration.

The velocity at the n-th time interval is $v_n = a \Delta t_n + v_{n-1}$, the mean velocity over this interval is $(v_n + v_{n-1}) / 2$. The calculation data are plotted in Figs. 4.64*b* and 4.65.

REFERENCES

4.1 G. A. Kukekov: *Vyklyuchateli peremennogo toka vysokogo napryazheniya* (A.C. high voltage circuit breakers). Energiya, Moscow 1972.

4.2 I. S. Tayev: *Elektricheskiye apparaty, obshchaya teoriya* (Fundamentals of switchgear). Energiya, Moscow 1977.

4.3 E. M. Tseirov: *Vozdushnye vyklyuchateli vysokogo napryazheniya* (Air-insulated high-voltage circuit breakers). Gosenergoizdat, Moscow 1957.
4.4 A. V. Avdonin, A. L. Buinov, V. G. Egorov *et al.*: Elektrotekhnika No. 1, 30-33 (1979).
4.5 V. P. Kuritsyn, A. M. Bronshtein, K. A. Pozdnyakov *et al.*: *Elektrotekhnika* No. 2, 19-22 (1980).
4.6 A. L. Biryukov, A. L. Buinov, C. S. Puzyriiskii *et al.*: *Elektrotekhnika* No. 7, 11-14 (1975).
4.7 V. V. Afanasyev and Yu. I. Vishnevskii: *Vozdushnye vyklyuchateli* (Air circuit breakers). Energoizdat, Leningrad 1981.
4.8 V. V. Afanasyev, N. M. Adonyev, and L.N. Karpenko: *Elektricheskie apparaty vysokogo napryazheniya* (High voltage switchgear). Energiya, Leningrad 1977.
4.9 C. H. Fleurscheim (ed.) *Power Circuit Breaker Theory and Design.* Stevenage Peregrimus 1975.
4.10 K. A. Pozdnyakov: *Elektrotekhnicheskaya promyshlennost.* AVN. No.5, 13-17 (1978).
4.11 A. M. Zalesskii and G. A. Kukekov: *Teplovye raschety elektricheskikh apparatov* (Thermal analysis of electric apparatus). Energiya, Leningrad 1967.

5
OIL CIRCUIT BREAKERS

5.1 Layout of Bulk and Low-Oil Breakers

Oil circuit breakers were among the first switchgear installations for high-voltage systems. They came to be used in the late 19th century and remain in wide use despite the considerable advance in the development of other kinds of circuit breaker.

The oil-type circuit breakers can be roughly divided into two large groups: (i) the bulk-oil construction where the oil serves both for arc extinction and as a main insulation, and (ii) the low-oil-content (or minimum oil) construction in which the oil is used for arc extinction alone.

Bulk-oil circuit breakers are favourable for 35, 110, and 220 kV voltage ratings, although they are also in use in the medium-voltage range.

The research and development of the early 70's has markedly reduced the metal and oil requirement of bulk-oil breakers because of the smaller oil tanks. The interrupting capacity has been also considerably enhanced owing to the improved arc extinction devices.

Low-oil-content circuit breakers are predominantly used at 10 kV and this status seems to remain for another extended period of time. This will be especially true if their continuous rated current is increased up to 4 kA and the interrupting capacity up to 40-50 kA.

Low-oil-volume circuit breakers for outdoor application rated for 35, 110, and 220 kV are capable of interrupting smaller currents than bulk-oil breakers, but because of lower cost, material demand, and fire hazard the low-oil version may markedly displace the bulk-oil design and become competitive with air circuit breakers.

The layout of one pole of a modern bulk-oil circuit breaker is shown in Fig. 5.1. The main structural element of each pole is a steel tank (2), cylindrical or ellipsoidal in form, carrying at its cap bushings (5), an operating mechanism (3), a safety valve, the cores and the secondary windings of bushing current transformers (4), and oil-filling pipes.

Each oil tank has manholes for access to the contacting device (1) of an oil heater (10) energized at low temperatures to prevent excessive rise of oil viscosity.

The operating mechanism is connected with an insulating rod (6) which lifts the cross head.

The lower ends of each bushing carry arc interrupters (8) each of which has a shunt resistor (7) to facilitate interruption of inductive currents and equalise voltage distribution. The interior of the tank is insulated by sheets of electric-grade cardboard (9).

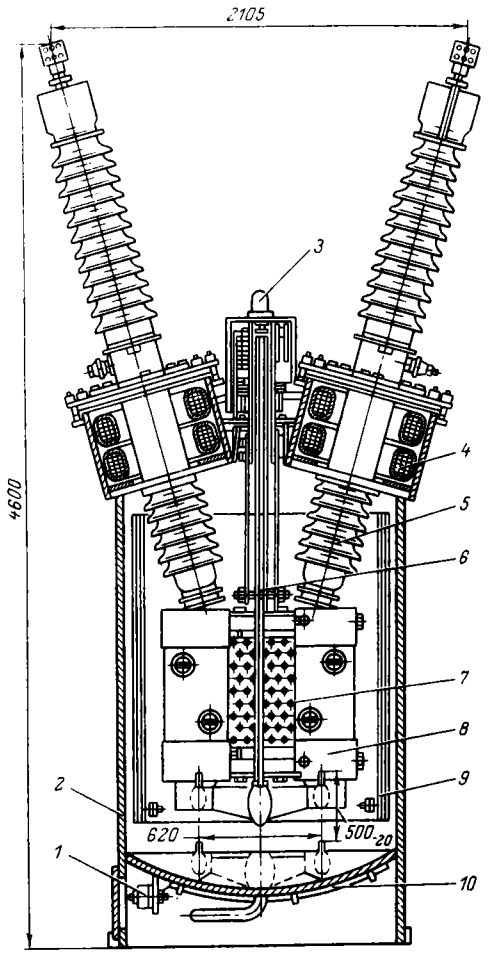

Fig. 5.1. One pole of a U-110-2000-40 circuit breaker

The circuit breaker is controlled by an electromagnetic or pneumatic operating mechanism, fixed at one of the poles. In 110-kV breakers, shown in Fig. 5.2, the mechanisms of all three poles are ordinarily interlinked by a tie and connected to the driving mechanism (1). The 220-kV oil circuit breakers have each pole equipped with an individual operating mechanism.

In the low-oil-content circuit breaker shown in Fig. 5.3, the insulation is mainly achieved by solid dielectrics. The enclosure of these circuit breakers is made of less strong materials and has a smaller size than the casing of bulk-oil breakers. Therefore, low-oil-content circuit breakers cannot withstand severe mechanical stresses involved in the interruption of heavy short-circuit currents. The interrupting capacity of the low-oil-volume design is limited by its poor mechanical strength and the absence

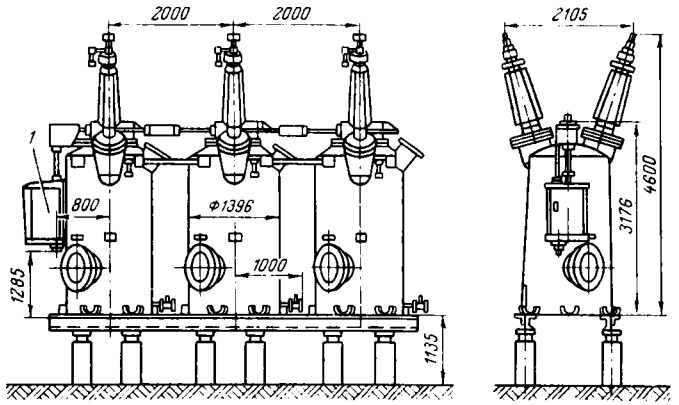

Fig. 5.2. U-110-2000-40 circuit breaker. All dimensions are in mm

of small-size interrupting chambers that would reliably extinguish arc over the entire range of short circuit currents.

Present day low-oil-content circuit breakers are manufactured in two versions. One version has the interrupter installed in the lower part of the pole for downward motion of the moving contact in the closing operation. In the other version the movable contact ascends in closing and the interrupter is located in the top portion of the pole. This design is preferable for enhancement of rupturing capacity.

Figure 5.3 shows the outline of a type VMPE-10 low-oil-content circuit breaker with an electromagnetic driving mechanism. The breaker is built in the first design type for suspended installation. It is rated for 10 kV nominal system voltage, a rated continuous current of 630 to 1600 A depending on the cross section of the current

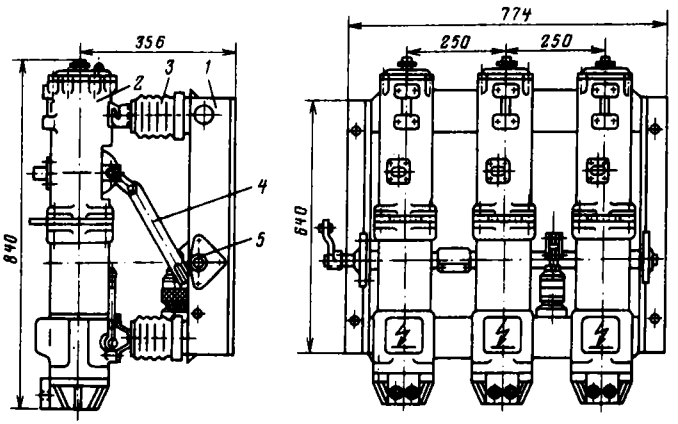

Fig. 5.3. Type VMPE-10 low-oil-content circuit breaker

carrying parts and contacts, interrupting capacity of 20 and 31.5 kA, total break time of 120 ms, and arcing time at rated breaking current being within 20 ms. The frame (1) and support insulators (3) carry the poles (2) that are linked by the insulating rods (4) to the shaft (5) common for all three poles and installed in the breaker frame.

The breaker is closed by energizing the integral coil via a contactor. The electromagnetic drive works against the action of release springs and a buffer spring at the end of the stroke to rotate the shaft and through the actuating rods cause the contacts within the poles to close. The electromagnetic driving mechanism also interlocks the charged release and buffer springs in the closed contact position.

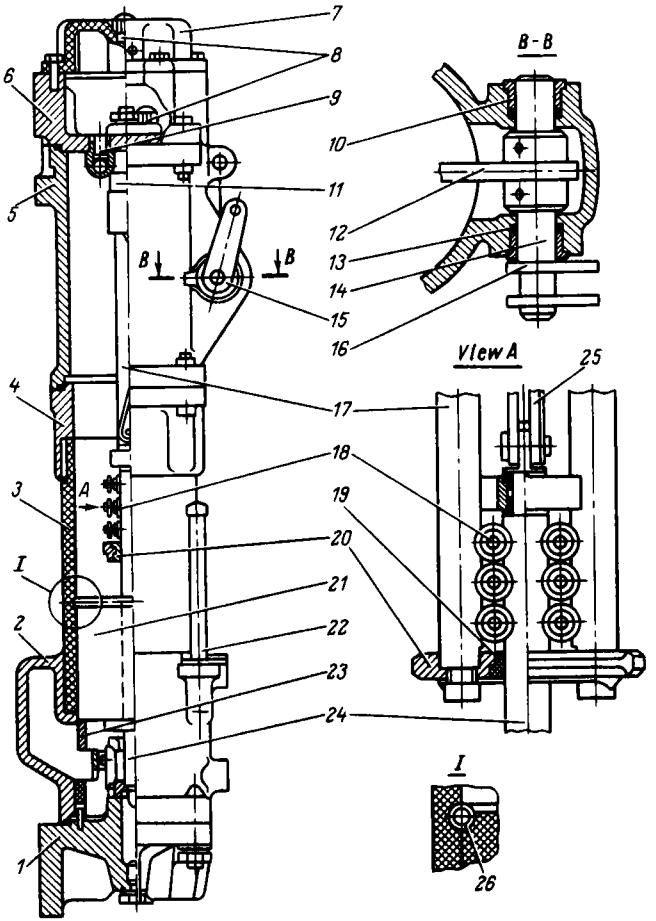

Fig. 5.4. One pole of a VMPE-10 circuit breaker

In the opening operation the interlock is removed and the release springs and the buffer spring, operating over a short distance, force the movable contacts to travel. At the end of the opening stroke the moving parts are decelerated by an oil buffer which is provided to eliminate vibrations of the movable contacts.

The poles are partitioned by insulating walls saving space between the poles. The frame of the breaker is earthed. The metal cover closing the frame from the side of the driving mechanism has two windows to monitor the level of oil in the poles and to see the intricator of the breaker's on and off positions.

The breaker pole, shown in Fig. 5.4, consists of an insulating cylinder (3) with metal flanges (2) and (4) screwed on two ends. The bottom flange is covered by a cover (1) carrying a movable contact of cluster (plug-in) type. The upper flange carries the casing (5) and the head of the pole (6). The casing houses the driving mechanism of the lift rod. The mechanism consists of two levers, external (16) and internal (12), fixed on the common shaft (14). The external lever is linked by an insulating tie with the shaft of the breaker, and two shackles (25) connect the internal lever with the movable contact (24). The shaft (14) is supported in plain bearings (10) with sealings (13) that prevent escaping gas and oil in breaking operations. The insulated rod is fixed to the lever (16) of the mechanism (15).

The pole head has four ports passing gas and oil in breaking operations and a check valve (9). The head is sealed by an insulating cover (7) with a plug (8) of the oil filling port and two pressure relief vents.

The pole head carries two guiding rods (17) joined below by a plank (20) carrying a sleeve (19) which guides the moving contact. Interrupting shocks are absorbed by buffers (11) installed on each rod. Between the guiding rods and the movable contact there are copper current collecting rolls (18) with pressing springs. The number of rolls varies from 4 to 10 depending on the rated current and interrupting capacity. The moving contact diameter is 22 mm for current ratings of 630 A and 1000 A and 24 mm for 1600 A.

The stationary cluster-type contact (Fig. 5.5) is installed in the cover (1). The bars (5) are fastened to the base through flexible links (8). Their upper butt ends have brazed-on arc-resistant cermet caps. Each bar has an outside recess (6) to receive an insulation insert cup of the spring (7) which bears against the ring (4). The bars rest on the supporting ring (3). The interlock (2) secures the cylinder and the interrupting chamber. The cluster-type contact rated for 630 and 1000 A has five bars and the contact for 1600 A has six bars.

Referring to Fig. 5.4, the arc extinction chamber (21), installed on the cylinder (23), is manufactured in two principal makes, namely, with cross-blast of oil for 20 kA interrupting rating, and with counter-cross blast of oil for 31.5 kA interrupting rating. The upper part of the chamber rests on the spring (26). The oil level can be monitored with a glass tube (22) with two oil level marks confining the range of admissible oil level variation.

The column type VK-10 low-oil-content circuit breakers have been developed for the same ratings as the VMPE-10 breaker, except the break time which has been shortened by 20 ms. The breaker for rated continuous currents of 630 and 1000 A and 31.5 kA interrupting capacity is shown in Fig. 5.6 and the functional details of its pole are illustrated in Fig. 5.7. The three poles of the breaker are supported

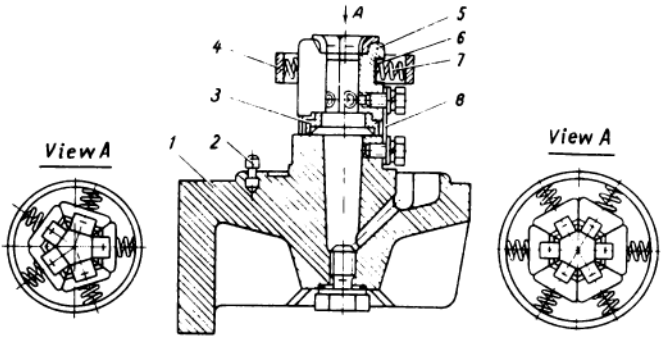

Fig. 5.5. Fixed cluster-type contact

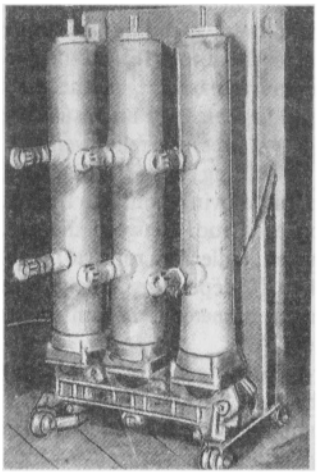

Fig. 5.6. VK-10 circuit breaker

by a cast base which houses the levers of the operating mechanism connected with the integrated spring-powered drive.

A pole of the breaker is formed by an insulating cylinder (1) which comprises the current carrying parts connected with the upper fixed cluster-type contact inclosed within the cylinder (2) and the holder (3) connected to the guiding rods (4). Current collection from the moving contact (5) is effected by the roll contactor (6). The movable contact is connected to the driving mechanism by an insulating rod (7). The holder (3) carries the cylinder (8) and this supports the interrupting chamber (9). The oil levels (10) can be seen at the pole tops.

The post-type circuit breakers considerably reduce metal requirements of the switchgear and are easily adaptable in voltage distribution systems.

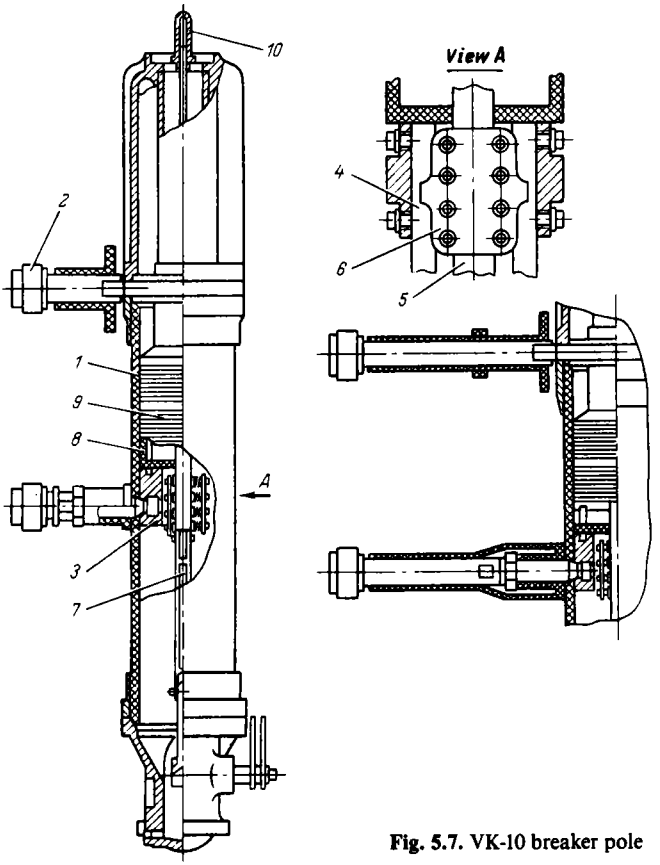

Fig. 5.7. VK-10 breaker pole

The type VMT low-oil-content circuit breakers are manufactured in the three-pole modification for 110 kV and in the single-pole modification for 220 kV, as shown in Fig. 5.8.

The 110-kV design is equipped with a single-break interrupter having 'counter-cross-blast' facilities. The air cavity of the interrupter is filled with compressed gas. High make-break operating speeds are provided by virtue of the lowered weight of the movable parts. This unit uses a cable operating mechanism instead of heavy insulating rods commonly employed in outdoor circuit breakers of this rating. The high potential parts are actuated via high-strength glass-reinforced plastic rods 12-mm in diameter loaded by tensile stresses only.

The 220-kV design employs two series-connected 110-kV interrupters. Circuit breakers of this type are controlled by strong spring-powered driving mechanisms.

Low-oil-volume circuit breakers can be exploited as generator breakers. By way of example, Fig. 5.9 depicts the VGM-20-90/11 200 minimum-oil generator circuit

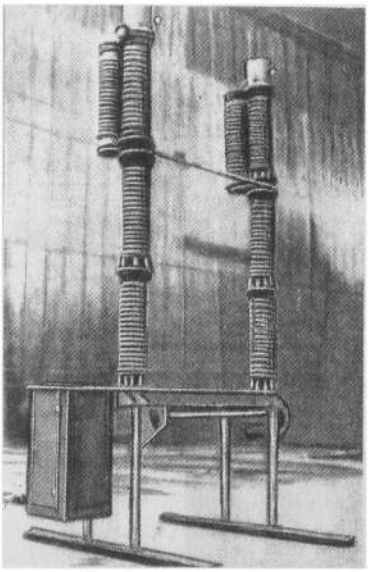

Fig. 5.8. Low-oil-content circuit breaker for 220 kV

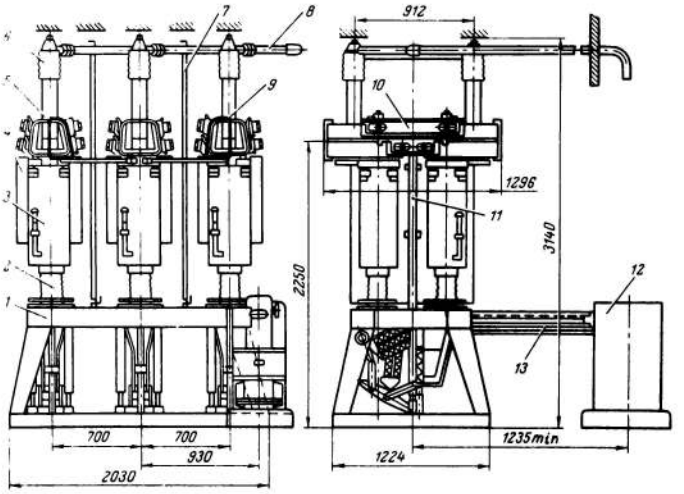

Fig. 5.9. Type VGM-20-90/11200 low-oil-content generator circuit breaker

breaker for 20-kV rated voltage, 90 kA interrupting capacity, and 11 200 A rated continuous current. The three poles of the breaker are supported by a common base structure (1) which houses the operating mechanism connected with the drive (12) by a rod (13). Each pole comprises two earth-insulated tanks (3) supported

by insulators (2). The covers of the tanks carry the assembly of the stationary contacts. The magnetic core (9) equalises the distribution of current over the current carrying parts. The movable contacts are on cross pieces (10) linked to the operating mechanism by means of insulating rods (11). The covers of the tanks carry the thrust pipe (5), oil-separators (6), and a gas relief vent (8).

To prevent the spacing between the tanks of each pole from breakdown, the insulating spacer walls (4) are provided. The insulating panels (7) insulate the poles from one another.

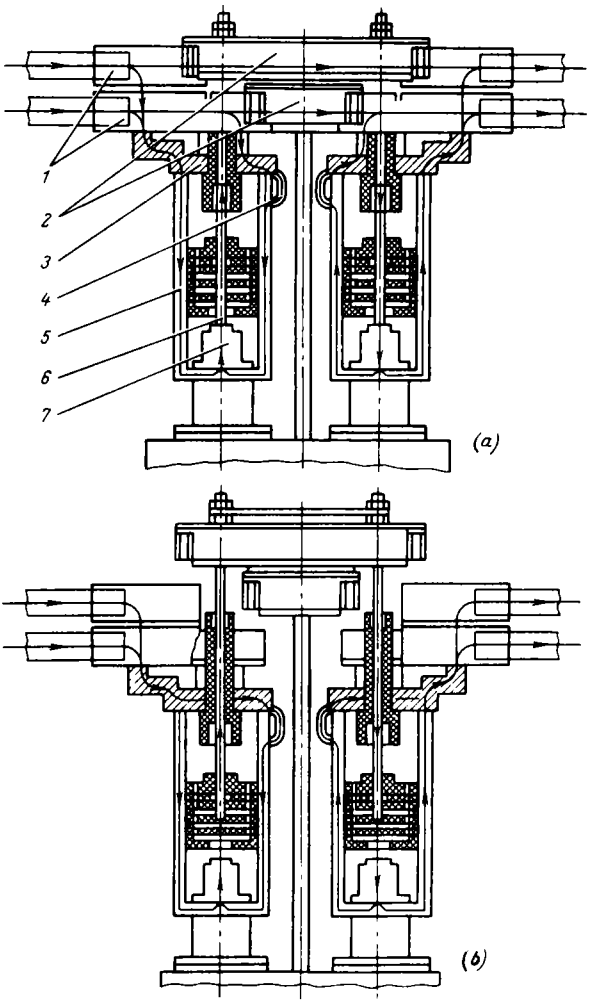

Fig. 5.10. Current-carrying parts of the type VGM-20-90/11200 low-oil-content generator circuit breaker

Each pole of the breaker has two current circuits, the one of the main contacts, and the auxiliary circuit of the arcing contacts illustrated in Fig. 5.10. The main circuit includes the contacts of the first and second tanks (1) and knives (2). The arc extinction circuit is formed by the lid (3), copper brackets (4) connecting the lid with the tank, the tank wall (5), the stationary arcing contact (7) and the stem of the arcing contact (6) of the first tank, the knife (2) and the same elements of the second tank.

In the closed position both circuits are connected in parallel, the major portion of current passing through the main circuit having a considerably lower resistance than the arcing-contact circuit.

In the opening operation, the main contacts separate first and the current is diverted into the arcing circuit whose contacts will part later on in the oil. The arising electric arcs are extinguished in counter-cross-blast interrupting chambers. The hot gases formed by the burning arc are routed to oil separators where oil is condensed on porcelain spheres and is recirculated in tanks while the gas free from oil is cooled on the spheres and vented into the atmosphere through relief pipes.

5.2 Construction and Operation of Interrupters

Modern oil circuit breakers use the puffer blast principle for arc extinction. The arc that forms after the contacts have parted decomposes oil and produces gases that contain up to 60% of hydrogen and markedly raise the pressure in the interrupting chamber. The advance of the moving contact creates the conditions for the outflow of the gas through the blast slits provided for this purpose. The flow of gas and oil cools the arc column and aids in efficient extinction.

Depending on the direction of the flow with respect to the arc there exist arc control devices where the flow is directed along the arc, at right angles to the arc or at some angle to the arc from one side or symmetrically from opposite sides as if in counterflow. Frequently arc control devices make use of a few types of blast, the flow intensity being proportional to the magnitude of interrupting current.

The arc control chamber of a VMP-10 minimum-oil circuit breaker, shown in Fig. 5.11, exploits the cross-jet principle for arc extinction. It is assembled as a package of insulating baffles tied with studs. The chamber is provided with three lateral-flow blast-slits (2) placed one above another and connected with the top space by two vertical channels (3). The top part of the chamber has two oil pockets (4). The bottom baffle has an interchangeable ring (1) that can be replaced if badly burnt.

The operation of this chamber is illustrated in Fig. 5.12. In the closed position (Fig. 5.12*a*), the moving contact pin (1) enters the fixed plug-in contact (2). In the opening stroke, the contact pin ascends leaving behind an arc that decomposes oil and forms a gas bubble (Fig. 5.12*b*). The pressure of gases that form inside the chamber and cannot escape out of it is partly lowered by an air dashpot (3) that has been produced in the pocket while filling the breaker with oil. It is worth noting that such a dashpot is not necessarily an element of the oil circuit breaker. As the

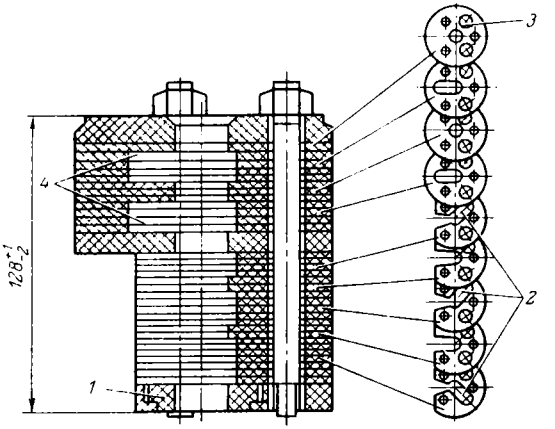

Fig. 5.11. Cross-jet interrupting chamber

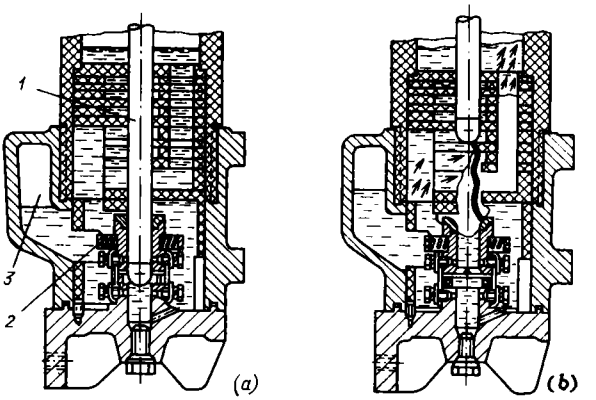

Fig. 5.12. Arc extinction in a cross-blast extinction chamber

contact pin opens the lower and subsequent blast slits a forced flow of oil through the slits and vertical channel begins followed by gas blasting.

In interrupting small currents the pressure in the extinction chamber is not very high, the arc extends considerably and the extinction occurs as the arc is forced into the pockets at the top of the chamber. Because of small volume the pressure in these pockets is well above that in the bottom part of the chamber.

The counter-cross-jet arc control device (Fig. 5.13), also called a turbulator, consists of a package of insulating plates tied by four studs. The chamber has a central bore for the movable contact pin. In the bottom part of the chamber, the insulating partitions form two opposing-flow slits (1) having common vertical channels (2)

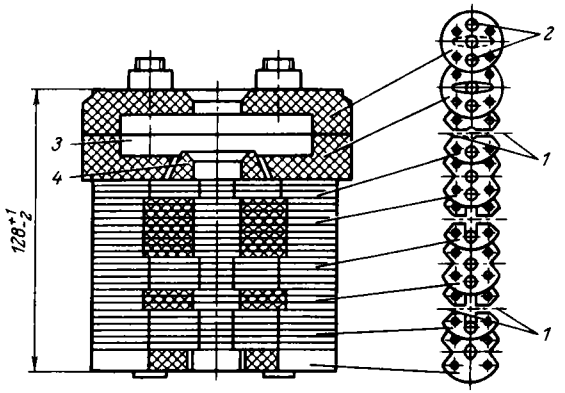

Fig. 5.13. Counter-cross-jet interrupting chamber

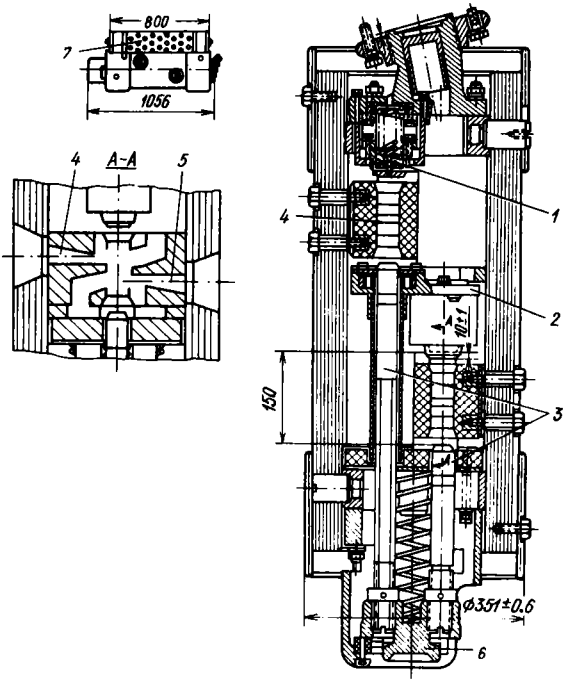

Fig. 5.14. Cross-jet arc control device of the type U-110-2000-40 circuit breaker

connecting them with the space at the top of the chamber. The gas flow from the slits flows round the arc and on making a turn through 90° leaves into the channels (2).

The baffles form an oil pocket (3) in the upper part of the chamber. The insulating cone split-sleeve (4) in the top part of the chamber prevents excessive acceleration of the moving contact by means of friction increasing at high pressure inside the chamber.

Figure 5.14 shows the interrupting chamber employed in bulk-oil circuit breakers of the U-type. The chamber has two breaks connected in series that form in opening the stationary contacts (1) and (2) and the movable contacts (3). When the moving contact is set in motion, the blast slits (4) open and an intensive blow of exhaust gases begins around the arc. The second blast slit (5) is located farther along the travel of the contact pin and it is turned through 180° with respect to the first slit. Arc extinction is facilitated by introducing the shunt resistors (7) with a resistance of 750 Ω for circuit breakers operating at 110 kV and 2650 Ω for circuit breakers at 220 kV. The interruption of the resistor current occurs in a free arc spacing between the contact of the movable cross head and the outer contact (6) of the chamber.

To improve extinction of capacitive currents some bulk-oil and low-oil-content circuit-breakers make wide use of various forced-blast facilities such as piston accessories and hollow contacts. Some designs exploit the compressed-air space over the oil surface to accelerate the flow of fresh oil into the contact spacing.

5.3 Extinction-Chamber Pressure Analysis

For effective extinction of the arc in the interrupting chamber, it must be under a certain pressure (0.6-1.0 MN/m^2) near a current zero. However, excessive gas generation in arc extinction may blow the interrupter pot. Therefore, analysis of the gas generation processes in the interrupting chamber is an important stage of oil circuit breaker design.

When the contacts of the oil circuit breaker part, the burning arc produces oil vapour and decomposes oil into a number of gases such as H_2, C_2H_4, and the like. Each kilojoule of energy produces 70 cu. cm of gas reduced to the STP conditions (293 K and 0.1 MN/m^2). The released gas is actually at a high temperature (the average temperature of the gas bubble is about 800 K) and under a high pressure of up to 6 MN/m^2.

Calculation of pressure inside the oil circuit breaker interrupter pot is rather complicated. In this text we present an approximate calculation of the pressure, to be more specific, we assume that the oil flows out of the interrupting chamber in a stationary regime, i.e., obeying Bernoulli's law. The calculation is based on the equation of state

$$pV = mRT_g$$

where p is the gas pressure, V is the gas volume, m is the mass, R is the universal gas constant, and T_g is the absolute temperature of the gas.

To improve the operation of the interrupting chamber it is equipped with an

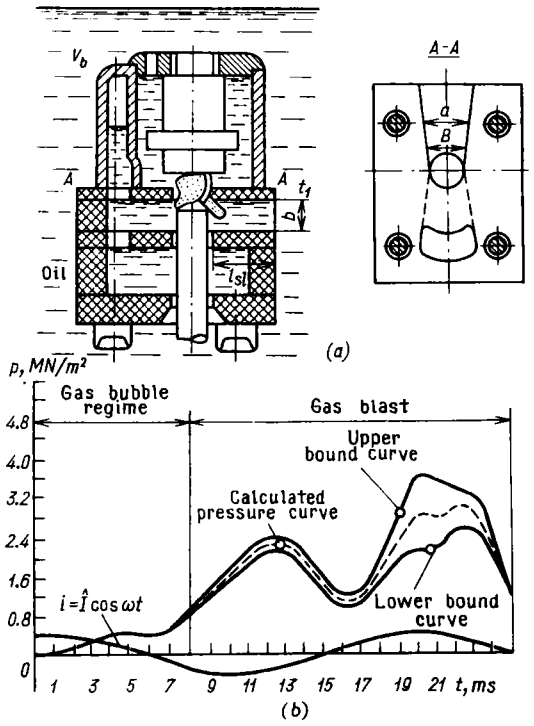

Fig. 5.15. (*a*) Sketch of an arc control device. (*b*) Approximate pressure histories inside the interrupting chamber for the arc extinction process

air dashpot of volume V_b (Fig. 5.15*a*), which cuts off pressure surges and aids in obtaining the required pressure near current zero. In what follows we wish to discuss two modes of gas extinction, the gas bubble regime and the gas blast regime.

Gas bubble regime. The gas formed in the chamber, after the contacts have parted, occupies the volume evacuated by the moving contact and the oil outflowing through the clearance spaces and the volume provided by the compression of the air buffer. This stage is typical of the operation of most interrupting chambers prior to opening of the blast slit. The gas equation for this regime is as follows:

$$p(V_{oil} + V_c + V_{b,i}) = m_{air} R T_{air} + p_{atm} K \int_0^t P \, dt = p_{atm} V_{b,i} + p_{atm} V_g^0$$

$$p = (V_{b,i} + V_g^0) p_{atm} / (V_{oil} + V_c + V_{b,i})$$

$$V_{oil} = \int_0^t \sum_{k=1}^{n} \mu_k S_k \sqrt{2p/\varrho} \, dt$$

where V_{oil} = volume of oil leaving the chamber, m^3
V_c = volume of space evacuated by the moving contact, m^3
$V_{b,i}$ = initial volume of the air dashpot at p_{atm} and 293 K, m^3
m_{air} = mass of air in the air dashpot, kg
$K = 250 \times 10^{-6}\ m^3/kJ$ = volume of gas produced by 1 kJ of energy at $T = 800$ K and p_{atm}
V_g^0 = volume of gas produced by the arc at $T = 800$ K and $p = p_{atm}$
μ_k = effusion coefficient of port k
S_k = section of port k, m^2
R = 500-1200 J/kg K, gas constant for gas-vapour mix
ϱ = density of oil, kg/m^3
p = pressure at time t, N/m^2
P = power of the arc at time t, kW
n = number of ports for oil outflow
p_{atm} = atmospheric pressure, N/m^2

From the equation of state we get

$$p = p_{atm} V_{b,i} + p_{atm} K \int_0^t P\,dt$$

$$\times \left[V_{b,i}^{3/2} + \frac{3}{2} \sum_{k=1}^{n} \mu_k S_k \sqrt{\frac{2}{\varrho}} \int_0^t \left(p_{atm} K \int_0^t P\,dt + p_{atm} V_{b,i} \right)^{1/2} dt \right]^{-2/3}$$

A number of idealizations have been made in deriving the equation as follows.

1. The process inside the chamber is isothermic ($T = 800$ K).
2. The volume V_c is neglected because $V_c \ll V_{oil}$.
3. The velocity of oil is computed by Bernoulli's equation with no account taken of the transition process. The velocity of oil outflow is

$$v_{oil} = \sqrt{2/\varrho}\, p^{1/2}$$

4. Observing that $p \gg p_{atm}$, we neglect the atmospheric pressure.

The arc energy is calculated by the formula

$$A_a = \int_0^t u_a i\,dt = \int_0^t E l_a i\,dt = \int_0^t E v_{av} t i\,dt$$

where u_a is the arc-over voltage, V; l_a is the arc length, m; E is the voltage gradient over the arc, V/m; v_{av} is the average speed of contacts in the gas bubble regime, m/s; t is current time, s; and i is the momentary magnitude of arc current, A.

Assuming that the arcing time up to the first quenching attempt is partitioned in m intervals of 1 ms each, we obtain that the arc energy released by the end of the last interval is

$$A_a = \int_0^t P\,dt = \int_0^t u_a i\,dt \approx \Delta t \sum_{i=1}^{m} u_{a,i} i_i$$

After the first current zero a similar calculation is carried out in the following half-period.

For the quenching regime under consideration we may safely assume E = 6-8 kV/m.

The computation is performed by numerical integration or on a computer.

Once the moving contact has opened the slit, a flow of oil occurs. The amount of outflowing oil, or the time of flow, may be found with the formula

$$V_{sl} = \int_{t_I}^{t} \mu_{sl} S_{sl} \sqrt{2p/\varrho}\, dt$$

The function $p(t)$ of pressure variation with time must be known from the pressure analysis. For approximate calculations one may take $p = p_{av}$ over a short time interval.

As soon as $V_{sl} = abl_{sl}$ (see Fig. 5.15*a*) the oil flow through the slit ceases and the regime of gas blast begins.

Gas blast regime. The gas formed in the interrupting chamber leaves it in part through the blast slit and partly flows to fill the volume evacuated by the moving contact and by the oil outflowing through the available gaps.

Because the pressure in the chamber is well above atmospheric, the velocity of gas flow in the blast slit reaches the critical value, $v_{g,cr}$.

For this regime we assume E = 20-30 kV/m.

The equation of state for the gas blast regime is as follows:

$$p(V' + V_{oil} + V_c) = m_{air} R T_{air} + p_{atm} K \int_0^t P\, dt - \left(\frac{2}{k+1}\right)^{1/(k-1)} v_{g,cr} \int_{t_{II}}^{t} v_c (t - t_I) B p\, dt$$

where $V' = V_{b,i} + V_{oil,II} + V_{c,II}$ is the volume occupied by the gas by the instant t_{II}, $V_{oil,II}$ is the volume emptied by the oil by the instant t_{II}, $V_{c,II}$ is the volume of space evacuated by the contact by the instant t_{II}, $v_{g,cr}$ = 318 m/s is the critical velocity of gas outflow, k = 1.4 is the adiabatic index, m_{air} is the mass of air in the air dashpot, B is the minimum width of the slit, m (see Fig. 5.15*a*), v_c is the average velocity of contact during the gas blast regime, and t_I is the instant of slit opening.

Written in the differential form the equation of state is

$$\frac{dp}{dt}\left[V' + \sqrt{\frac{2}{\varrho}} \int_{t_{II}}^{t} \sum_{k=1}^{n} \mu_k S_k p^{1/2}\, dt + S_c v_c (t - t_{II})\right] + p^{3/2} \sqrt{\frac{2}{\varrho}} \sum_{k=1}^{n} \mu_k S_k + p S_c v_c = p_{atm} K P - v_{g,cr} B V_c (t - t_I) p [2/(k+1)]^{1/(k-1)}$$

where S_c is the cross section of the moving contact, t_I is the time of slit opening, and μ_k are the oil effusion coefficients of the ports.

The equation is nonlinear because of terms containing $p^{1/2}$. These terms determine the space that is left to the gas by the outflowing oil.

The equation is solved by the method of S. A. Chaplygin. The initial equation is approximated by two linear equations, where $p^{1/2}$ is assumed constant. The desired solution is between the solutions of these linear equations. Indeed, by letting $p^{1/2} = p_{\min}^{1/2} = \text{const}$ we obtain a linear equation for the least discharge of oil yielding the upper boundary curve for pressure. Likewise by letting $p^{1/2} = p_{\max}^{1/2} = \text{const}$ we take an overestimated oil discharge and the resultant linear equation yields the lower boundary curve of pressure. The solution of the original equation lies between these curves.

The boundary values of $p_{\min}^{1/2}$ and $p_{\max}^{1/2}$ may be taken as accurately as desired to draw the curves closer to each other with the desired accuracy. For $p^{1/2} = \text{const}$, the equation takes the form

$$\frac{dp}{dt} + p(a'_{1,2} + bt_1 + bt)/(V'_{1,2} + a'_{1,2}t) = p_{atm}KP/(v'_{1,2} + a'_{1,2}t)$$

Denoting by the subscripts 1 and 2 the pressure curves obtained with overestimated and underestimated $p^{1/2}$, respectively, we have for the solution of this equation

$$p_{1,2}(t) = \left(\frac{V'}{V'_{1,2} + a'_{1,2}t}\right)^{n_{1,2}} \exp\left[-m_{1,2}(t - t_{II})\right]$$
$$\times \int_{t_{II}}^{t} \frac{p_{atm}KP}{V'_{1,2} + a'_{1,2}t} \left(\frac{V'_{1,2} + a'_{1,2}t}{V'}\right)^{n_{1,2}}$$
$$\times \exp\left[-m_{1,2}(t - t_{II})\right] dt + p_{II}\left(\frac{V'}{V'_{1,2} + a'_{1,2}t}\right)^{n_{1,2}} \exp\left[-m_{1,2}(t - t_{II})\right]$$

where

$$a'_{1,2} = 4.7 \times 10^{-2} \sum_{k=1}^{n} \mu_k S_k p_{1,2}^{1/2} + S_c v_c$$

$$V'_{1,2} = V' - a'_{1,2}t_{II}$$

t_I is the time instant of the incipient slit opening, t_{II} is the instant of gas blasting incipience, V' is the volume filled by gas at $t = t_{II}$, p_{II} is the pressure by the instant t_{II},

$$n_{1,2} = 1 + b(t_{II} - t_I)/a'_{1,2} - V'b/a'_{1,2}$$

$$m_{1,2} = b/a'_{1,2}$$

$$b = v_c B v_{g,cr}\left(\frac{2}{k+1}\right)^{1/(k-1)} = 200\, B v_c$$

For the lower boundary curve $p_1(t)$, the constants a'_1, V'_1, n_1, and m_1 are calculated at $p = p_{\max} = \text{const}$. Correspondingly, for the curve $p_2(t)$, the constants a'_2, V'_2, n_2, and m_2 are those found at $p = p_{\min} = \text{const}$.

Usually, $p_{\min} = 0.2\ \text{MN/m}^2$. This is the maximum pressure obtained in the first regime. The actual pressure is found as the mean value between the boundary values obtained. When the blast slit is uncovered completely, then

$$p_{1,2}(t) = \left(\frac{V''}{V''_{1,2} + a''_{1,2}t}\right)^{q_{1,2}} \int_{t_{\text{III}}}^{t} \frac{KP}{V''_{1,2} + a''_{1,2}t} \times \left(\frac{V''_{1,2} + a''_{1,2}t}{V''}\right)^{a_{1,2}} \mathrm{d}t + p_{\text{III}} \frac{V''}{V''_{1,2} + a''_{1,2}t}$$

$$V'' = V_{\text{b,i}} + V_{\text{oil,III}} + V_{\text{c,III}}$$

where V'' is the volume [m^3] occupied by gas by the instant t_{III} of full uncovering of the slit, $V_{\text{oil,III}}$ and $V_{\text{c,III}}$ are the volumes of oil outflown and that left by the contact by the instant t_{III},

$$a''_{1,2} = 4.7 \times 10^{-2} \sum_{k=1}^{n} \mu_k S_k p_{1,2}^{1/2} + S_c v_c$$

$$V''_{1,2} = V'' + a''_{1,2} t_{\text{III}}$$

$$q_{1,2} = 1 + \left(\frac{2}{k+1}\right)^{1/(k-1)} v_{\text{g,cr}} S_{\text{sl}} / a''_{1,2}$$

p_{III} is pressure by the time t_{III}. The approximate variation of pressure for the interrupting chamber shown in Fig. 5.15*a* is presented in Fig. 5.15*b*.

The experimental evidence collected with interrupting chambers indicates that at current zero the pressure in effectively quenching chambers is within 0.6-1 MN/m^2. If the theoretical pressure plots suggest that at probable points of extinction the pressure in the chamber is insufficient, the parameters of the exit slits and air dashpot should be redesigned to obtain the necessary pressure at current zero.

The mechanical strength of the chambers is calculated by the maximum pressure derived in an analysis of the interrupter with the safety factor 1.5. If no pressure data are available, one may take the internal (gauge) pressure at 6 MN/m^2.

5.4 Auto-Reclosing Duty and Frequent Make-Break Operations

Auto-reclosing duty imposes special requirements on the construction of the oil-circuit-breaker interrupter. To be more specific, the interrupting chamber must exhaust its arc burning product, mainly hot gases, and receive fresh cold oil under the no-current condition. If this requirement cannot be met because of the design of the chamber, then the amount of oil inside the chamber must be made sufficient for the reliable operation of the breaker in auto-reclosing duty cycles. Under these circumstances, analysis of the amount of oil outflowing from the interrupting chamber while interrupting the rated breaking current becomes of significance. The analysis is performed in parallel with the estimation of pressure inside the interrupter.

In a correctly designed interrupting chamber, the amount of oil outflowing from the device during the breaking operation must be markedly smaller than the amount of oil left in the chamber.

Experimental studies have indicated that auto-reclosing duty cycles and frequent make-break operations of the oil circuit breaker may entail alterations of interrupting properties, breakdown conditions for the spacing between the approaching contacts in the making operation, and the dielectric strength of the inner insulation. Excessive wear of the chamber walls and contacts should be also expected.

A deterioration of quenching performance which manifests itself in longer arcing times occurs in frequent interruptions of both load currents and short circuit currents. The main cause of this phenomenon is due to the impaired insulating characteristics of the oil which accumulates particulate decomposition products (soot) and particles of metals removed from the contacts.

It should be noted, however, that notwithstanding an appreciable reduction of the dielectric strength of oil (down to one third or one fourth of the basic insulation level) the arc control device provides the specified interrupting capacity and the interrupter with a sufficient amount of oil in the interrupting chamber is capable of 100 interruptions of load current and dozens interruptions of rated breaking currents.

After multiple interruptions of short-circuit currents the dielectric strength of the inner insulation of an interrupting chamber with a considerable amount of oil can remain at a sufficiently high level. By way of illustration, an interrupting chamber with 16 litres of oil withstood continuous voltage tests and the respective switching overvoltage level after 70 break operations at 11 kA, whereas a 3-litre interrupting chamber failed to withstand continuous voltage tests after 30 interruptions at 5 kA.

The deterioration of the insulating properties of oil has a pronounced effect on the processes of contact spacing breakdown in making operations. The construction of a breaker and its operating mechanism should ensure reliable closing onto a short circuit. On making the circuit, the breakdown occurs prior to contact closing and there forms an arc that causes decomposition of oil and production of gases opposing the closing movement of the contact. In addition, electrodynamic forces working against the closing contact occur in the closing contacts.

The arcing time depends on the arc space broken down, which in turn is a function of applied voltage, insulating properties of the medium, filling the arc space, and speed of approach of the contacts. Whereas for pure oil at 30 kV the maximum contact spacing broken down was found to be 8 mm, after multiple breaking operations and also in tests with repeated auto-reclosure cycles this length was found to decrease substantially in low-oil-content circuit breakers. The latter duty cycles experienced considerable pressure surges (4-6 MN/m^2) and to overcome the opposing forces of the pressure some additional work was required of the driving mechanism.

In order to reduce arcing times in breaking operations and the associated erosion of contacts, oil decomposition and pressure rise, at the moment of closure the speed of moving contacts of modern minimum-oil circuit breakers should be in the range from 4 m/s for 10 kV ratings up to 10 m/s for 110 kV ratings.

An increased concentration of soot in oil after multiple switching operations leads to the deterioration of both insulating and interrupting properties of the circuit breaker. Longer arcing times in making and breaking operations enhances wear of the insulating parts of the interrupting chamber and accelerates the erosion of contacts. Therefore, for low-oil-content circuit breakers, frequent change of oil is recommended. For example, in the 10-kV type VMPE-10 low-oil-content circuit breaker, oil should be replaced after ten interruptions of 20-kA current or six interruptions of breaking currents as high as 31.5 kA.

The erosion of contacts accelerated under frequent switching operations belongs to the factors governing the intervals between periodic checks of the breaker exposed to frequent switching duty-cycles. For low-oil-content circuit breakers, erosion of contacts has been rather well studied. Erosion of contacts in mg of removed substance can be estimated as a function of current, kA r.m.s., and arcing time, ms, by the formula due to W. Pucher

$$M = kI^a t$$

where k and a are constant coefficients; for contacts of copper, $a = 1.58$ and $k = 2.15$; for copper-tungsten contacts (70% of W by weight), $a = 1.81$ and $k = 0.274$.

Accurate estimations of erosion for copper-tungsten alloy (70 wt. % of W) contacts may be obtained with the formula due to I. L. Shleifman

$$M = 1.35kI^{1.7}t$$

where $k = 0.38$ for the bars of the stationary contact, $k = 0.46$ for the tip of the moving contact pin, and the coefficient 1.35 takes into account possible deviations of the erosion data from the average values.

These formulae are helpful in determining the tolerable number of breaking operations at a given current and a given arcing time if the dimensions of arc-resistant tips are also given. The maximum number of switching operations is determined for the total wear of the tips.

5.5 Operating Mechanisms

The elements of the breakers joined into a linkage providing the necessary variation of movable-contact position are collectively called the operating mechanism. The constituting elements are ties, levers, hinges, shafts, and the like. Consider an operating mechanism typical of suspended low-oil-content circuit breakers. Figure 5.16 shows a sectional view of one pole of such a breaker (type VMP-35) operating at 35 kV. The frame (1) supports the support insulators (2) carrying the casing of the breaker, the top portion of which (3) houses the elements of the mechanism of the movable contact (4) and current collecting facilities. The movable contact (4) and the stationary contact (7) are placed in an insulating cylinder (5) containing the arc-control device (6).

The frame (1) also carries the breaker shaft (8) with a few levers rigidly attached to it: a lever (9) for connection to the driving mechanism, two levers for connection

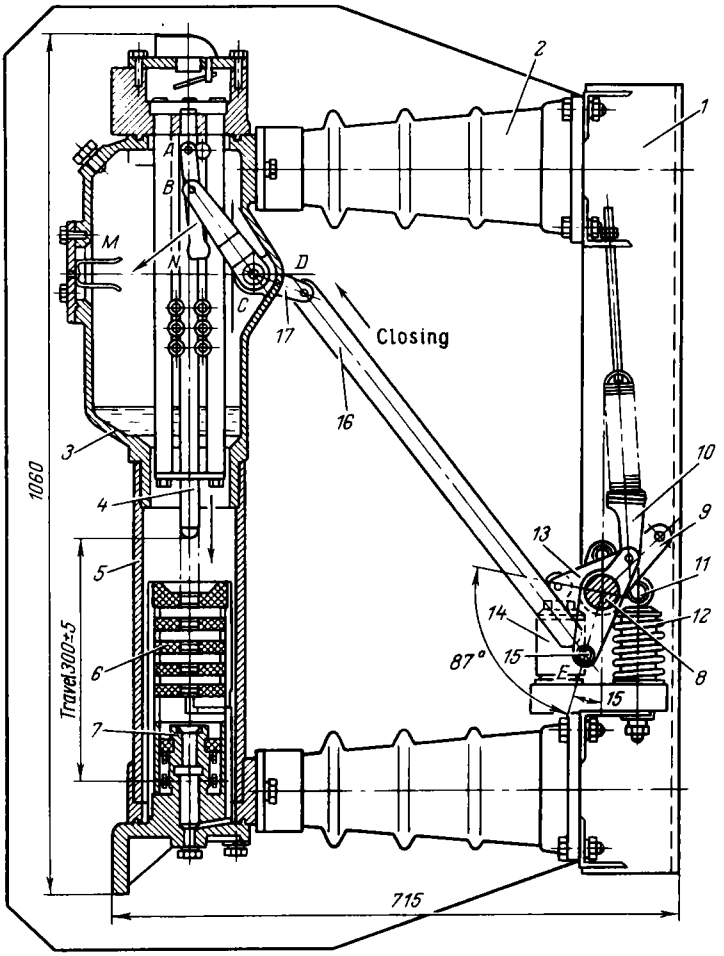

Fig. 5.16. Vertical section through a pole of a 35-kV low-oil-content circuit breaker

of the tripping springs (10), two links (11) of two spring buffers (12), a lever (13) of the oil buffer (14) and a lever (15) linked by a hinge with the insulating rod (16).

In the making operation, the drive rotates the shaft clockwise and extends the tripping springs (10). At the end of the closing stroke the moving parts are decelerated by the spring buffers and the entire mechanism is interlocked by a tripping mechanism installed in the drive. Rotation of the breaker shaft causes the insulating rod (16) to move, lever (17) to rotate, and the rectilinear motion mechanism in the breaker enclosure moves the movable contact (4).

Figure 5.17 shows a kinematic diagram of the operating mechanism of the break-

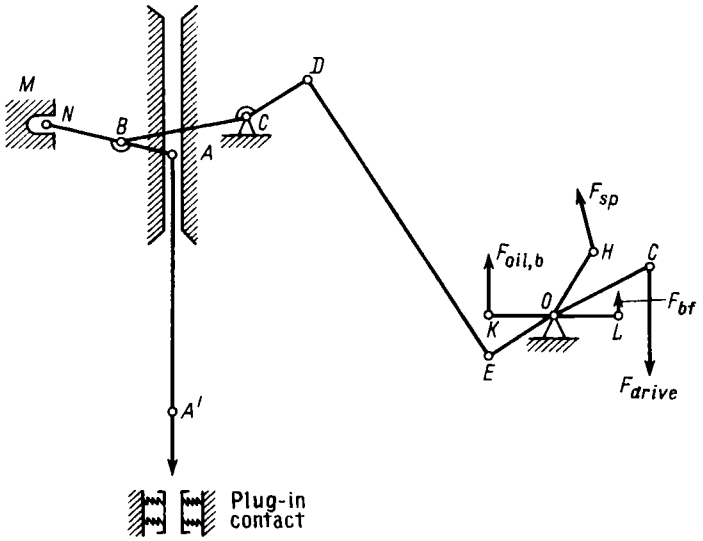

Fig. 5.17. Kinematic diagram of the operating mechanism (intermediate position of the moving contact) of the circuit breaker from Fig. 5.16.

er in Fig. 5.16. Rotation of the lever *BC* is transformed into translational motion of the contact *AA'* by the mechanism *ABCD*. The link *ABN* and the fork *M* perform a more accurate transformation of the rotational motion of the lever *CB* into translational motion of the contact *AA'*.

The breaker interrupts the circuit after the tripping mechanism has automatically operated by a signal from the relay protective circuit, breaker control circuit, or manual release knob. The motion of the movable contacts interrupting the circuit is provided by the energy stored in the charged release springs, operating over the entire travel of the movable contacts, and by the energy of the buffer springs contributing at the initial stretch of the parting contacts. At the end of the breaking contact travel, the kinetic energy of the moving parts is given to the oil buffer.

The driving mechanism and the release and buffer springs must provide the specified contact travel velocities in the make-brake operations. A high making speed decreases arcing times, erosion of contacts, and the likelihood of contact welding. The breaking speed of a circuit breaker is set up in accordance with the dynamics of the pressure build up inside the interrupting chamber and so that it will be consistent with the gas blasting. In addition, high make-break speeds reduce the operating times of the breaker and cut down the dead intervals in power supply for breakers operating in the auto-reclosing mode. The reclaim time is of the order of 0.3-0.5 s for modern low-oil-content circuit breakers and of the order of 0.8-1.2 s for modern bulk-oil circuit breakers.

Thus the operating mechanism of a circuit breaker should be designed as to provide the specified speeds of the moving contacts within the given break and

make times. Friction forces which cause wear and increase the power demand of the driving mechanism should be reduced to a minimum.

In a dynamical analysis of both make and break operations two problems may be solved: (i) determine the velocity by the given forces of the drive or release and buffer springs and also the operating time in making and breaking operations; (ii) determine the force requirements of the driving facilities and tripping devices by the given profile of velocity as a function of the contact travel. Both problems are solvable on the basis of the Lagrange equation which, in its simplest form, is written as

$$\frac{\mathrm{d}}{\mathrm{d}h}\frac{M_{\mathrm{rd}}v^2}{2} = F_{\mathrm{m}} - F_{\mathrm{opp}}$$

where M_{rd} is the total mass reduced to the contact or shaft of the breaker, kg; v is the velocity of the contact or breaker shaft, m/s; F_{m} is the moving force, N; and F_{opp} is the opposing force, N.

Let us consider the analysis of tripping and buffer spring by a given breaking velocity. Such an analysis is carried out with the kinematic diagram of the respective operating mechanism. Figure 5.17 also indicates the forces acting on the levers rigidly tied to one another and rotating about the hinge labelled 0. Here, F_{drive} denotes the force applied by the drive, F_{bf} the force of the buffer spring, F_{sp} the force of the release spring, and $F_{\mathrm{oil,b}}$ the force of the oil buffer. All these forces enter the calculation of the release spring.

To calculate masses reduced about a point one needs first to determine the actual masses of the elements and links of the linkage. Then these masses are replaced by a convenient system of point values concentrated at certain node points and constituting a dynamically equivalent system. Three rules are in use in the evaluation of such a dynamically equivalent system.

1. In translation of a link its equivalent mass equals its actual mass placed at the centre of mass of the link.

2. The equivalent mass of a link in rotation equals the mass moment of inertia of the link divided by the squared distance of the node point from the axis of rotation.

3. For a link having a composite motion, the equivalent system masses are placed in three points, say A, B, and C. The coordinates of these points are determined from the following system of equations

$$\begin{aligned} m_A + m_B + m_C &= m \\ m_A x_A + m_B x_B + m_C x_C &= 0 \\ m_A x_A^2 + m_B x_B^2 + m_C x_C^2 &= J \end{aligned}$$

where m is the actual mass of the link, kg; m_A, m_B, and m_C are the equivalent system masses at points A, B, and C; and J is the moment of inertia of the link about the centre of mass, kg m^2.

In evaluating the moment of enertia of a link, its shape may be simplified and broken down into simple geometric forms of known moments of inertia.

For light links having a complicated motion with insignificant displacements,

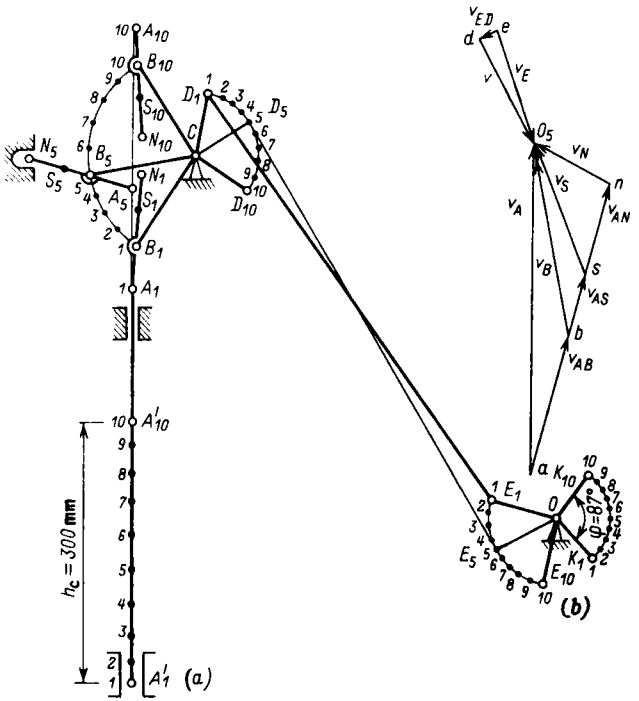

Fig. 5.18. Illustrating the construction of velocity polygons for the operating mechanism of a low-oil-content circuit breaker: (*a*) kinematic diagram and (*b*) velocity polygons

the actual mass of the link may be represented by half-value point masses placed at two nodal points connected by a rigid massless rod.

The arithmetic sum of the equivalent masses at a point forms a node mass. To reduce a node mass to point A from point B, use is made of the formula

$$M_A = m_B(v_B/v_A)^2$$

where v_A and v_B are the velocities at the respective node points.

The reduced mass is determined by contructing the kinematic diagram of the operating mechanism reflecting a few phases of its motion (ten phases in Fig. 5.18*a*) with the construction of velocity polygons, as illustrated for phase *5* in Fig. 5.18*b*.

The moving contact has a straight upward motion, $A_1' - A_{10}'$. The velocity of the contact is denoted by $\mathbf{v}_A$ (arbitrary magnitude). Assuming the velocity of a point B_1 with respect to point A_1 be $\mathbf{v}_{A_1B_1}$, we obtain for the velocity of B_1 at phase *1*

$$\mathbf{v}_{B_1} = \mathbf{v}_{A_1} + \mathbf{v}_{A_1B_1}$$

Consider now the evaluation of velocities at phase *5*. Since point B revolves about centre C, we draw from centre O_5 (see Fig. 5.18*b*) a straight line O_5b perpen-

dicular to the radius CB_5 in Fig. 5.18*a*. This line gives the direction of the velocity of point B_5. The velocity $\mathbf{v}_{AB}$ is perpendicular to link A_5B_5, therefore to construct the velocity triangle we draw a straight line perpendicular to A_5B_5 from point *a*. This line intersects the direction of $\mathbf{v}_B$ at point *b*. The segment *ab* gives the magnitude of $\mathbf{v}_{AB}$, and segment O_5b gives the magnitude of $\mathbf{v}_B$.

Similar constructions are performed to determine the velocities of points *N* and *S*. The relative velocity $\mathbf{v}_{AS}$ is proportional to the length of *AS*, namely,

$$\mathbf{v}_{AB}/\mathbf{v}_{AS} = A_5B_5/A_5S_5 = ab/aS$$

The direction of $\mathbf{v}_{AS}$ coincides with that of $\mathbf{v}_{AB}$. To determine the velocity we lay out a line *as* so that

$$as = ab\ A_5S_5/A_5B_5$$

The velocity $\mathbf{v}_s$ is then found by connecting pole O_5 with *s*. A point *n* and the velocities $\mathbf{v}_{NA}$ and $\mathbf{v}_N$ can be evaluated in a similar manner.

The velocity $\mathbf{v}_D$ is perpendicular to the radius D_5C and the magnitude of this velocity is determined as

$$v_D = v_BD_5C/B_5C$$

The velocity $\mathbf{v}_E$ is perpendicular to the radius E_5O, and

$$\mathbf{v}_E = \mathbf{v}_D + \mathbf{v}_{ED}$$

From point *d* a straight line is drawn perpendicular to D_5E_5. This line intersects the ray from point O_5 in the direction of $\mathbf{v}_E$ at point *e* giving the magnitude of $\mathbf{v}_E$ and $\mathbf{v}_{ED}$.

For all other phases of the mechanism, the construction of velocity polygons can be done in a similar manner. The velocity polygons form a basis for evaluation of velocities for any node point and the velocity of any centre of mass.

An actual velocity profile as a function of movable contact travel can be given as illustrated in Fig. 5.19 by the velocity at the instant of contact separation, v_{sep}, and the maximum value of velocity. At the end of an interrupting stroke, the contact velocity rapidly vanishes owing to the counter-action of the oil buffer.

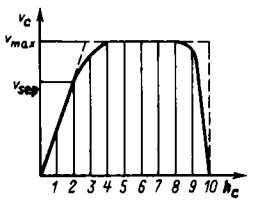

Fig. 5.19. Idealised velocity graph for a contact separation

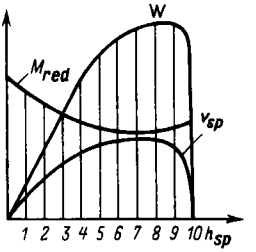

Fig. 5.20. Reduced mass, velocity, and work of inertia forces as functions of a position where the force of the release spring is applied

The velocity polygons for ten phases of the operating mechanism and the given interrupting speed form a basis of analysis of the bahaviour of the reduced mass about the point of fixture of the release spring with the travel of the spring, which is determined from the kinematic diagram of the mechanism. The function $v_{sp} = f(h_{sp})$ can be derived from the velocity polygon with the curve for contact travel $v_c = f(h_c)$, Fig. 5.18.

For each phase of the mechanism, the work of inertia forces, $W = M_{rd}v_{sp}^2/2$, is determined, Fig. 5.20. Applying the graphic differentiation to the plot $T = f(h_{sp})$ one can construct the dependence of the intertia force F_{inert} on the travel of the point of mass reduction, Fig. 5.21. If the forces opposing the motion or breaking forces are reduced about this point and added up, then the resultant function will yield the behaviour of the moving force with respect to the mass reduction point, Fig. 5.22. Reduction is effected with the relation $F_1l_1 = F_2l_2$ expressing the energy conservation law, where F_1 and F_2 are the forces at the point of reduction and at the node point, respectively, and l_1 and l_2 are the arms of these forces determined from the kinematic diagram of the operating mechanism (Fig. 5.18).

The forces opposing the motion of the contact in a breaking operation can be the forces of friction arising in the operating mechanism and in the plug-in contacts, the viscous friction of the moving contact about the oil, the breaking forces of the oil buffer, and weight the contribution of which depends on the position of the operating mechanism about the moving contact.

The pressure of gases emerging in arc burning aids the process of interruption and acts in opposition to the making process.

The electrodynamic forces compressing the bars of the plug-in contact oppose both making and breaking operations. In butt contacts, the electrodynamic repulsive forces interfere with making and facilitate breaking operations.

The forces of friction in the operating mechanism may be taken into account by assuming the efficiency of the mechanism at 0.75-0.80. The force of friction of the movable contact in cluster plug-in contacts may be found by the formula

$$F_{fr.c} = mnF_c\mu$$

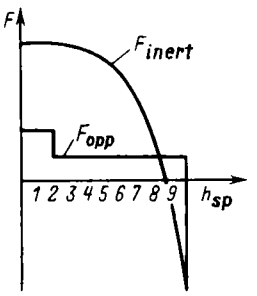

Fig. 5.21. Inertia forces and opposing forces as functions of the spring-force-application point

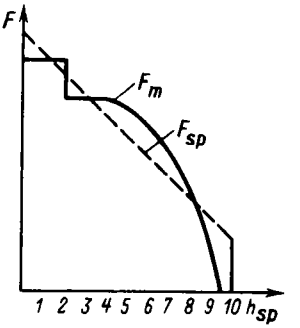

Fig. 5.22. Dependence of the moving forces on the location of spring-force application

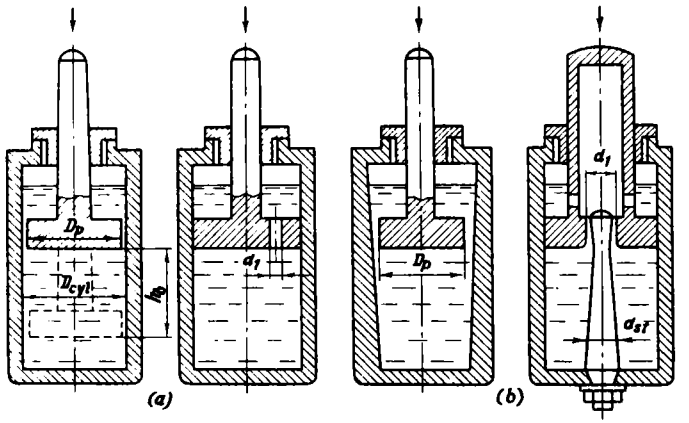

Fig. 5.23. Oil-buffer designs with (*a*) constant section and (*b*) variable section of the oil-passing slit

where m is the number of cluster contacts per breaker, n is the number of bars in the receptacle, F_c is the force exerted by a bar on the moving contact stem, and μ is the coefficient of friction in oil assumed to be 0.15-0.20. The force exerted by a contact bar on the moving contact stem is governed by the mechanical force of the contact spring and the resultant electrodynamic force at short circuit current.

Having constructed the dependence of the moving force F_m on the point of spring force application (point of reduction), Fig. 5.22, we are able to develop the force characteristic of the spring assuming that the amount of work done by F_m and F_{sp} is the same. We arrive at a curve $v_c = f(h_c)$ somewhat different but close to the given dependence. In the actual breaker, the work of the moving forces F_m is done by a few release springs and one or several buffer springs over a short travel — an important circumstance in analysis of these springs.

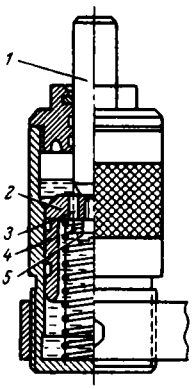

Fig. 5.24. Oil buffer of a minimum-oil circuit breaker

Deceleration of the moving parts at the end of a breaking stroke is usually effected by oil buffers of two main designs: with a slit of a constant section, and with a variable slit. Designs with a constant slit section (Fig. 5.23*a*) have to cope with a rather strong initial shock received by the piston rod. The piston travel compresses oil through a peripheral ring gap or a port in the piston.

Smooth deceleration is achieved in buffers with variable gap between the piston and a conic cylinder (Fig. 5.23*b*) or a conic pin and the piston.

In the oil buffer with a constant slit formed by a number of through holes (3) in the piston head (2) (Fig. 5.24), the effect of slit-width variation is produced by some features of the design. The screw (5) on the piston axis has a washer (4) free to move about the stem of the screw. The washer can partially cover the ports (3) in the piston thus reducing the slit section for oil when the piston is forced downward by the rod (17). In an upward motion of the piston, forced by the spring, oil is allowed to flow through totally uncovered ports (3) into the piston rock, thus rapidly resetting the piston into the stand-by position for the next breaking operation. Analysis of this design can be found in Ref. [4.8].

5.6 Driving and Tripping Mechanisms

Oil circuit breakers of new installations are controlled by d.c. electromagnetic drives, pneumatic drives, and spring-actuated driving mechanisms, integrated into the breaker system or installed as a separate unit.

The electromagnetic driving mechanism shown in Fig. 5.25 is built around a shell-type electromagnet with an armature (1) and a coil (2). When the coil is ener-

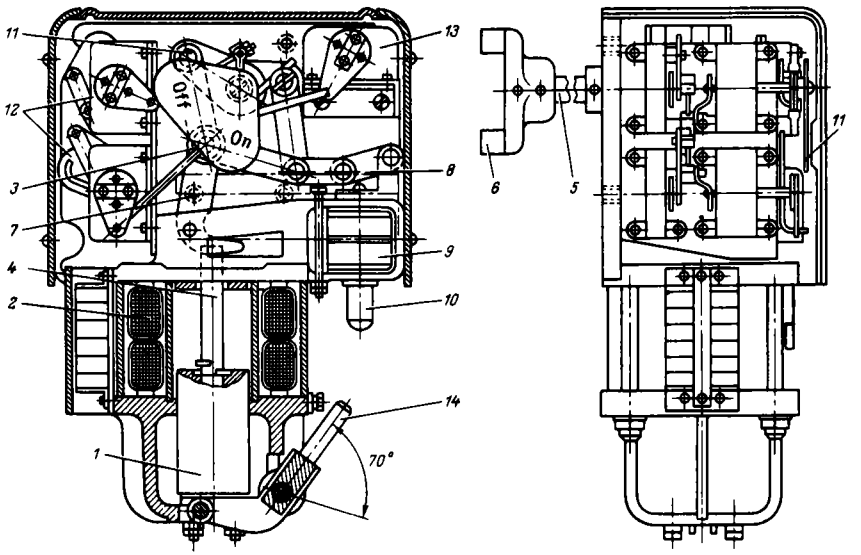

Fig. 5.25. Electromagnetic driving mechanism (type PE-11)

gized, the pushing rod (4) actuates the roll (3) connected by a linkage system with the driving shaft (5) coupled through a coupling (6) and a system of links with the breaker shaft.

The closed position of the breaker is locked by the L-shaped lever (7) receiving the roll axis. The force of the release and buffer springs is transmitted from the breaker shaft to the linkage (8) forced beyond the dead point. To open the breaker, the tripping coil (9) is energized by the breaker control system and the armature (10) releases the mechanism from the stable position. The roll axis comes off the lever (7) and the drive shaft turns freely.

The breaker status is indicated by a flag (11) visible from outside through a window in the drive enclosure. The block-contacts (12) and (13) are connected with the drive shaft to monitor the sequence of operations of the control and indication

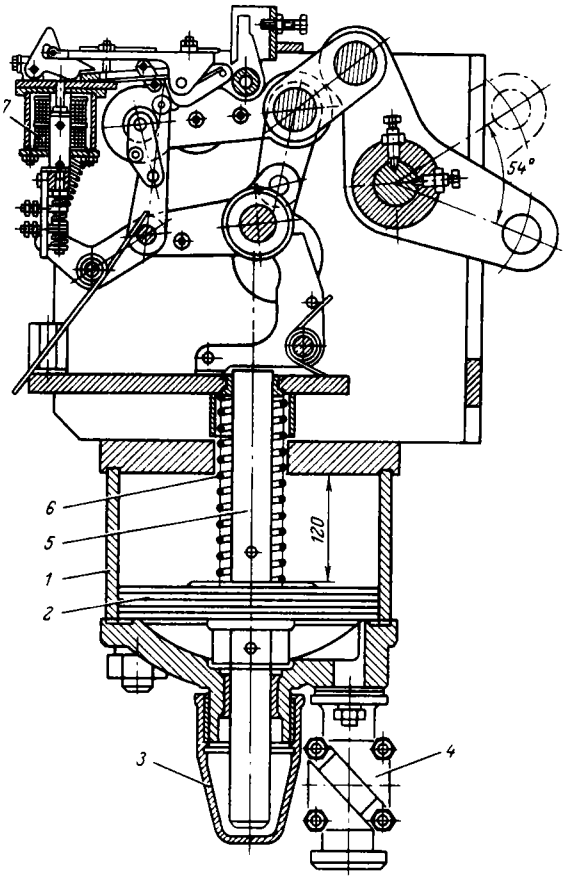

Fig. 5.26. Pneumatic driving mechanism

circuit of the breaker. Manual control of the breaker, used in adjustment operations, is effected by the lever (14).

The advantages of this design are constructional simplicity, high reliability, and consistency of the force characteristics to the profile of the opposing forces. The disadvantages accrue from a need for high-capacity batteries as a power source, a high demand of copper for coils and connecting wiring, and due to a considerable operating time associated with the electromagnetic processes in the drive. A numerical analysis of the coil for such a driving mechanism is outlined in Ref. [2.1].

The pheumatic driving mechanism shown in Fig. 5.26 has roughly the same layout and the operating mechanism as the electromagnetic counterpart discussed

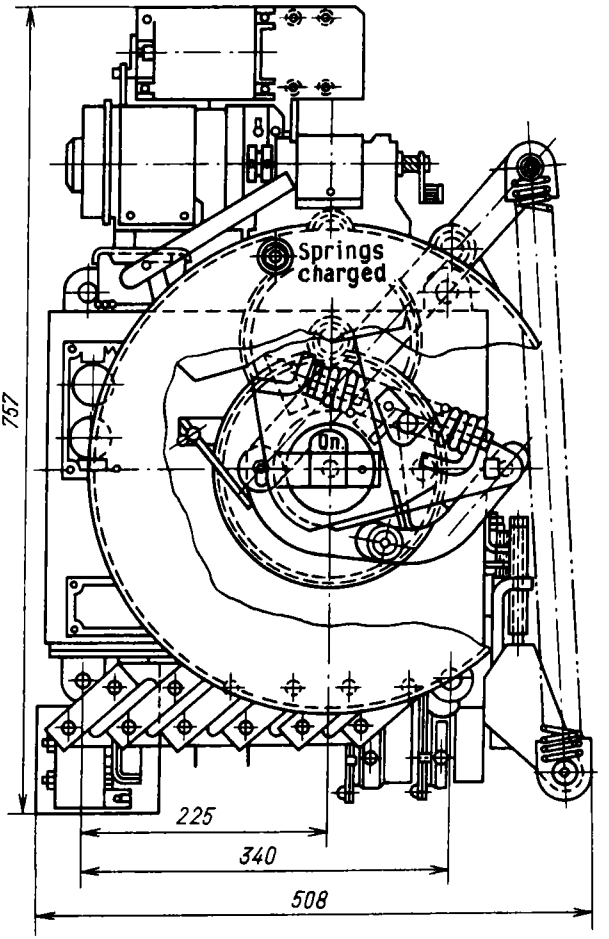

Fig. 5.27. Spring-actuated driving mechanism (type PP-67)

above, but the electromagnet is replaced by a pneumatic cylinder (1) with a piston (2). The driving mechanism can be rapidly reset for reclosure thanks to the ports for air exhaust provided in the bottom enclosure (3) and in the valve assembly (4), so that the depressurized piston with the rod (5) is rapidly removed by the spring (6) in the original position.

This breaker is tripped by a common coil (7). The installation includes a compressed-air reservoir whose pressure is varied in the range 1-2 MN/m^2 depending on the power required of the driving mechanism.

The pneumatic driving mechanism is advantageous in its small making time (under 0.3 s), a steep pulling-force characteristic that can be readily varied by altering the section of the air-feed port, and invariability of the mechanical characteristics in frequent make-break operations. The drive, however, requires special measures, such as air cleaning and drying, at freezing temperatures.

The spring-actuated driving mechanism shown in Fig. 5.27 receives the energy required for closing operations from strong springs (1) which are charged through a reducer by a low-power motor (2) or manually. Because the tractive characteristics of the springs fall at the end of the travel, the spring-actuated drives make use of an inertial mass (3) which is accelerated at the early stage of the travel and aids in keeping the speed of travel at the end of the stroke by its kinetic energy. Modern spring drives can operate in the auto-reclosing mode providing make times in the range 0.2-0.35 s.

An element that is invariably present in all driving installations is a tripping mechanism or interlocking mechanism that locks the breaker in the closed position.

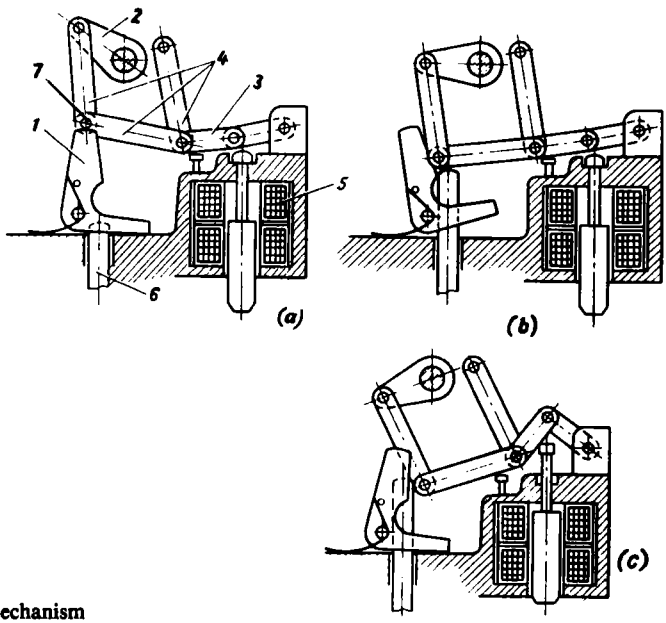

Fig. 5.28. Tripping mechanism

The sequence of operations for such a mechanism is illustrated in Fig. 5.28. The diagram at (*a*) shows the position corresponding the closed breaker when the axis of the roll (7) is retained by the L-shaped lever (1), and the force transmitted from the breaker to the driving shaft lever (2) is taken up by the linkage (3) and (4) forced beyond the dead point.

The diagram at (*b*) shows the tripping mechanism at the incipient making operation initiated by the pusher rod (6). The diagram at (*c*) illustrates the mechanism in closing on to a short circuit when the moving contacts of the breaker are not locked by the interlock and following the closure reverse for opening operation because the tripping coil (5) has removed the linkage (3) and (4) beyond the dead point and the roll (7) runs off the pushing rod (6) prior to touching the stop (1).

5.7 Steps in Breaker Design

The package of specified characteristics includes a rated voltage, rated continuous current, interrupting capability, and mechanical characteristics. The recommended sequential steps of a breaker analysis would be as follows.

1. Select a similar design.
2. Determine the cross-section of the current-carrying parts and the pressing force of the contacts for continuous duty at rated current.
3. Determine the sections of the current-carrying parts and contact mechanical forces at short-circuit current. The contact pressing forces are evaluated with allowance for the electrodynamic forces at contacting surfaces such that no welding of the contacts could occur.
4. Compare the findings of items 2 and 3 and choose the larger values.
5. Calculate the breaker insulating level.
6. Determine the mechanical strength rating of the breaker.
7. Find the necessary pressure in the arc-control device.
8. Use the specified breaking speed to determine the operating mechanism and design the release and buffer springs.
9. Based on the static work of contact closure select from available options or calculate the driving mechanism subject to attaining the given making speed.
10. Estimate contact erosion and the check and maintenance interval required.

6
MAGNETIC AIR-BREAK CIRCUIT BREAKERS

6.1 General

Both oil and air-blast circuit breakers considered in earlier chapters are not free from disadvantages. Bulk-oil circuit breakers, for example, are heavy and large units requiring frequent oil cleaning and care of fire and explosion hazard. Low-oil-content circuit breakers need much less oil than bulk-oil breakers for their operation but frequent operations rapidly deteriorate oil with soot particles therefore the number of switching operations is limited for these units. For all its advantages of frequent switching operations the air-blast circuit breaker needs a source of compressed air.

Magnetic air-break circuit breakers use atmospheric air and high resistance interruption. The arc is lengthened and forced, by magnetic action, into an arc chute where it is presented to a large cooling surface. Then the arc is cooled down and extinguished being no longer able to support itself. The magnetic circuit breaker does not need oil or compressed air for its operation and is capable of a large number of make-break operations without maintenance. These units are common in a voltage range of 6 to 20 kV on circuits where frequent switching operations are anticipated.

Figure 6.1 sketches the contact and arc extinction systems of a 6-kV type VEM-6 magnetic circuit breaker. The support insulators (2) mounted on the steel frame (1) carry the arc chute (3) and the magnetic blowout coil (4) with poles (6). The movable contact (5) is rotated on a support insulator (10) by an insulating rod. The breaker is equipped with the main contact system (7) and the auxiliary contact system (8) for arc extinction. The arcing contacts (8) part first and an electric arc forms between them. Electrodynamic action of the current carrying circuit and convective heat fluxes lift the arc into the position indicated by the continuous solid line *AFG*. The segment *AF* of the arc is shunted by the arc-extinction coil (4). Because the coil resistance is small the arc *AF* is extinguished and the coil appears to be placed in the circuit in series. Now the arc is between the horn (9) and the movable contact horn (8) in the position indicated by the dashed line *B*. The magnetic field produced by the blowout coil (4) and the poles (6) forces the arc farther upwards into the insulated plate-type ceramic chute (3). The arc becomes wavy and extends considerably.

The arc column diameter d_a is much larger than the slit width δ. As a result the arc forced into the chute is flattened and a good thermal contact with the plates (11) of the chute is ensured. The high thermal conductivity of the ceramic plate aids in effective cooling of the arc and in rise of electric strength E. The voltage

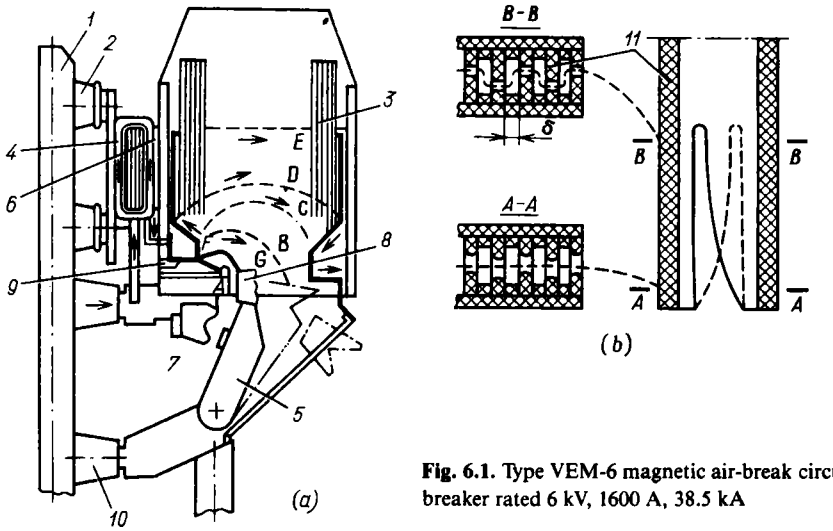

Fig. 6.1. Type VEM-6 magnetic air-break circuit breaker rated 6 kV, 1600 A, 38.5 kA

drop across the arc is

$$U_a = El_a$$

therefore the longer the arc and the higher the field gradient E the greater should be the voltage U_a supporting the arc, so a point will be reached where this is not true any longer.

The principal difference between the operating conditions of a magnetic air circuit breaker and an air-blast circuit breaker is that the former has the arc-over voltage comparable with that of the voltage source and so the current curve profile is sharply distorted (because of the nonlinear arc current-voltage behaviour) and the current is diminished substantially. Since the active resistance of the arc is comparable with the reactance of the high voltage circuit, the phase angle between the system current and e.m.f. decreases. All these conditions favour an effective extinction of the arc.

In an air-blast circuit breaker, the power released in the arc is proportional to its length

$$P_a = U_a I_{sc} \approx El_a \; U/X \propto l_a$$

where X is the circuit inductive reactance.

In order to diminish the likelihood of thermodynamic clogging the length of arc should be limited (see Sect. 4.3). In this type of circuit breaker the arc voltage U_a is not very high and amounts to only a few per cent of the breaker's rating (r.m.s.). Therefore in the interrupting process the short circuit current (r.m.s.) cleared by the air-blast circuit breaker remains invariable and in quadrature with the source e.m.f. If we neglect the reactance X and assume that the arc resistance R_a is constant for a given arc length, then for the magnetic air-break circuit breaker we have

$$P_a \approx U^2/R_a \propto l_a^{-1}$$

that is the power in the arc is inversely proportional to its length and will be decreased for longer arc lengths.

In the magnetic circuit breaker, arc extinction occurs as a result of the increasing arc resistance and depressed recovery voltage which decrease the arc current. At the current zero the voltage across the arc becomes higher than the system can sustain.

6.2 Current-Voltage Behaviour of the Arc Cooled in the Arc Chute

The current-voltage behaviour of the arc cooled in the arc chute of a magnetic air-break circuit breaker has a decisive effect on the arc extinction process. We consider this current-voltage characteristic on the lines of Ref. [4.1].

The heat flux density dissipated by the arc chute walls [W/cm^2] is

$$q_1 = \alpha (T - T_0) \tag{6.1}$$

where α is the generalized heat transfer coefficient, W/cm^2 K; and $T - T_0$ is the wall superheat created by the arc, K.

For the energy balance of the arc we may assume that the plasma layer is thin, therefore the temperature variation over the arc cross-section is negligible. Then,

$$\gamma c_p \frac{dT}{dt} = E^2\sigma - 2\alpha(T - T_0)/\delta \tag{6.2}$$

where c_p is the specific heat capacity, J/g K and γ the density of plasma, g/cm^3; E is the voltage gradient, V/cm; σ is the conductivity, S/cm; δ is the width of the chute channel, cm; and $T - T_0$ is the temperature difference at the wall, K.

The first term on the right-hand side is the heat released in one cu.cm of plasma, the second term is the heat transported to the chute walls. The left-hand side is the power expended in plasma temperature rise.

The conductivity of plasma in a narrow temperature interval may be deemed proportional to the superheat $T - T_0$, namely,

$$\sigma = \beta(T - T_0) = I/E$$

whence

$$T - T_0 = I/\beta E \tag{6.3}$$

where β is a proportionality factor.

Substituting (6.3) into (6.2) yields the equation of the arc current-voltage characteristic

$$\tau\left(\frac{1}{I}\frac{dI}{dt} - \frac{1}{E}\frac{dE}{dt}\right) = E^2\beta\delta/2\alpha - 1 \tag{6.4}$$

where $\tau = \gamma c_p \delta/2\alpha$ is the thermal time constant of the arc characterizing the thermal inertia of the arc. If τ is small, the arc temperature follows closely the variations of current, and the static and dynamic current-voltage characteristics almost coincide. This time constant is a function of slit size δ and varies between 25 and 100 μs in magnetic air circuit breakers.

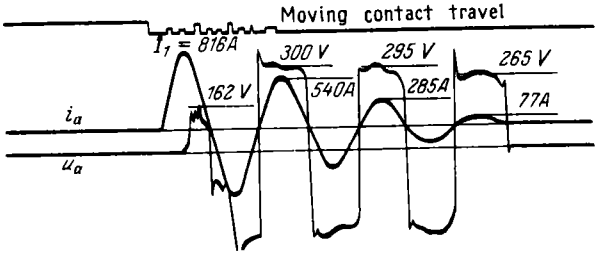

Fig. 6.2. Oscillograms of circuit breaking by a magnetic air-circuit breaker

For design purposes the static current-voltage characteristic may be used as derivable from Eq. (6.4) by letting its left-hand side equal to zero, viz.,

$$E = \sqrt{2\alpha/\beta}/\sqrt{\delta} = A/\sqrt{\delta} \tag{6.5}$$

The coefficient A increases with the growth of the heat transfer coefficient α and decrease of β. The calculation of E by Eq. (6.5) agrees well with experimental evidence [4.1], so that one can safely let for the static current-voltage curve $E = 19/\sqrt{\delta}$, where δ is in cm. This means that $U_a = El_a$ is also constant for l_a = const. At a sinusoidal current the voltage across the arc remains invariable. This means that at the early half-period when the current is low the arc resistance is high. As the current increases the arc resistance decreases. By the end of the half-period the arc resistance increases again. At any current $U_a = I_a R_a = El_a$ = const.

The oscillograms shown in Fig. 6.2 illustrate the arc current i_a and voltage u_a for moving contact travel. At the breaking incipience the arc-over voltage is low because the arc has not had enough time to enter the narrow slits of the arc chute. When the arc finds itself in the slits of the chute the arc voltage variation over a half-period becomes very small. The voltage also varies slowly from one half-period to the next despite the significant drop of current magnitude found experimentally with the Gorev circuit. The calculations of E by Eq. (6.5) agree well with that derived from experimental data.

6.3 Interruption of a Strongly Inductive Circuit

The equivalent circuit is shown in Fig. 6.3. The consideration will be carried out under two simplifying assumptions.

(i) The entire arc has entered into the chute (l_a = const and δ = const). The arc resistance is high and the circuit current is decreasing.

(ii) The voltage recovery process is aperiodic in nature since it is damped by rather high conductivities of the arc column and the heated ceramics. For the circuit of Fig. 6.3 we can write

$$\hat{U} \sin(\omega t + \varphi) = L\, di/dt + U_a \tag{6.6}$$

where $U_a = 19l_a/\sqrt{\delta}$, and φ is the phase angle between the voltage and current.

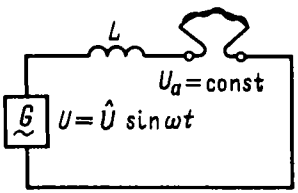

Fig. 6.3. Equivalent circuit to calculate the chute current in a magnetic air circuit breaker

Consider the quasi-stable process with the arc resistance placed into the circuit. The voltage across the arc resistance is constant. The solution of Eq. (6.6) for current has the form

$$i_a = \hat{I}\left[-\cos(\omega t + \varphi) + \frac{U_a}{\hat{U}}\left(\frac{\pi}{2} - \omega t\right)\right] \tag{6.7}$$

The current has two components

$$-\hat{I}\cos(\omega t + \varphi) \quad \text{and} \quad \hat{I}\frac{U_a}{\hat{U}}\left(\frac{\pi}{2} - \omega t\right) \quad \text{with} \quad \hat{I} = \hat{U}/\omega L$$

which, summed up, give the current i_a in the circuit (Fig. 6.4).

Figure 6.4 indicates that the current magnitude decreases from $\hat{I}$ to $\hat{I}_a$ and the phase angle decreases from 90° to φ. As the arc-over voltage U_a increases, both $\hat{I}_a$ and φ decrease. The decreasing angle entails a decrease in the power-frequency recovery voltage

$$U_{rec} = \hat{U}\sin\varphi$$

If $U_a < U_{rec}$, i.e., the voltage applied to the arc gap exceeds that required for the arc to exist, then restriking occurs after the current zero. The conditions for arc extinction are not satisfied. If $U_a > U_{rec}$, then the voltage applied to the arc is insufficient to sustain it and the arc extinguishes itself. The boundary condition obviously is

$$U_a = U_{a0} = U_{rec} = \hat{U}\sin\varphi_0 \tag{6.8}$$

where φ_0 is the angle corresponding to arc extinction.

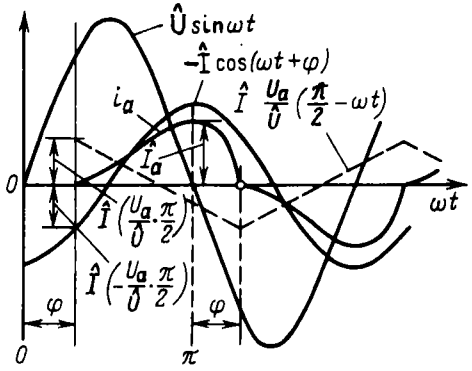

Fig. 6.4. Variation of arc current in the arc chute of a magnetic air circuit breaker

At current zero $t = 0$ and Eq. (6.7) becomes

$$0 = \hat{I}\left[-\cos\varphi_0 + \frac{U_{a0}}{\hat{U}}\left(\frac{\pi}{2}\right)\right] = \hat{I}\left(-\cos\varphi_0 + \frac{\pi}{2}\sin\varphi_0\right)$$

$$\tan\varphi_0 = 2/\pi \quad \text{and} \quad \varphi_0 = 32.5°$$

The condition for arc extinction can now be written as

$$U_{a0} = 19l_a/\sqrt{\delta} \geqslant \hat{U}\sin 32.5° = 0.537\hat{U} \tag{6.9}$$

The Soviet standard GOST 687-78 stipulates $\hat{U} = 1.5\sqrt{2}U_{r,max}/\sqrt{3}$.

For a selected value of δ Eq. (6.9) immediately yields the length of arc l_a. With allowance for simplifications assumed in deriving Eq. (6.9) this length should be increased by 20%

$$l_{a,calc} = 1.2l_a = 1.2\frac{\sqrt{\delta}}{19}0.537\frac{1.5\sqrt{2}}{\sqrt{3}}U_{r,max} = 41.5 \times 10^{-3}U_{r,max}\sqrt{\delta} \tag{6.10}$$

where $U_{r,max}$ is measured in volts and δ in centimetres.

The amplitude of arc current $\hat{I}_a$ can be obtained from Eq. (6.7) if the time instant is found when $di/dt = 0$. Approximately we may assume that the current maximizes at $\omega t = \pi - \varphi_0$, then

$$\hat{I}_a = \hat{I}[1 + 0.537(\pi/2 - \pi + \varphi_0)] = 0.463\hat{I}$$

It is worth noting that when the breaking current has a large and weakly decaying aperiodic component, the recovery voltage approaches zero, i.e. zero current approaches zero source voltage. A shift of current zero caused by the arc voltage leads to a situation when the recovery voltage approaches the peak value of the source e.m.f. Thus the aperiodic component of current appreciable impairs the breaker operation.

6.4 Heating of the Chute Walls

The arc plasma contacting the walls of the arc chute heats them to a high temperature. For the breaker to operate normally this temperature must not exceed the tolerable level for this grade of ceramics. It is quite obvious that the maximum temperature depends on both the power of the heat source (arc) and the time the arc resides at this point of the ceramic chute. If b is the height of the flattened arc and v its velocity, the residence (contact) time is $t_0 = b/v$. The ceramic temperature is lower the higher the velocity v and the shorter the time t_0. However, higher arc propagation velocity necessitates higher chute chambers, because the arc must remain within the chute during the quenching time. Accordingly the arc speed is selected such that at the rated breaking current the temperature of chute ceramic remains below the tolerable level. For the cordierite ceramics used in the Soviet Union, the ultimate temperature is 2000 °C.

In addition to the requirements of high arc resistance and thermal conductivity, the chute ceramics should not release gases under the action of a power electric arc. The evolved gases would increase pressure in the chute and decelerate or stop

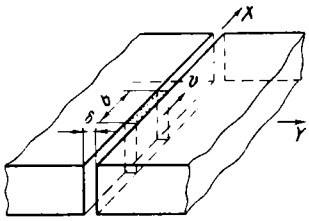

Fig. 6.5. Construction to evaluate wall heating in the arc chute

altogether the arc propagation. This obviously may lead to the breakdown of ceramic walls. Also the chute material should exhibit a sufficient mechanical strength.

The evaluation of ceramic temperature is carried out under an assumption that the entire arc heat is transferred in the direction to the walls only. The relevant geometry is sketched in Fig. 6.5. The arc is represented as a flat heat source of power density P, W/cm^2. The released heat is transported along the wall in the direction Y by conduction only. The arc travels in the direction X. The wall temperature was found [4.1] to be described by the expression

$$T(Y, t) = \frac{2P}{\lambda}\left(\frac{at}{\pi}\right)^{1/2} \exp\left(-\frac{Y^2}{4at}\right) - \frac{Y}{2}\left[1 - \Psi\left(\frac{Y}{2\sqrt{at}}\right)\right] \tag{6.11}$$

where λ is the thermal conductivity of the wall material, W/cm °C; $a = \lambda/c\gamma$ is the thermal diffusivity, cm^2/s; $c\gamma$ is the specific heat capacity of unit volume, J/cm^3 °C; and $\Psi(Y/2\sqrt{at})$ is a tabulated function.

The temperature maximizes at $Y = 0$

$$T_{\max} = 2\hat{P}\sqrt{t_0}/\sqrt{\pi c\lambda\gamma} \tag{6.12}$$

where $\hat{P}$ is the power density at peak current

$$\hat{P} = E\hat{I}_a/2vt_0$$

Therefore, the maximum temperature

$$T_{\max} = E\hat{I}_a/v\sqrt{\pi c\lambda\gamma t_0} \tag{6.13}$$

In terms of the peak current density $\hat{J}_a = \hat{I}_a/\delta b$ the time t_0 becomes

$$t_0 = b/v = \hat{I}_a/\hat{J}_a\delta v \tag{6.14}$$

In order that the wall temperature not exceed the tolerable level a certain speed should be imparted to the arc. Assuming $E = 19/\sqrt{\delta}$ and $\hat{I}_a = 0.463\hat{I}$, we obtain for the minimum speed

$$v_{\min} \approx 170\hat{I}\hat{J}_a/\pi c\lambda\gamma T_{\max} \tag{6.15}$$

For interruption of heavy rated currents the current density may be assumed equal to $J_a = 5000$ A/cm^2, then

$$v_{\min} \approx 0.85 \times 10^6\hat{I}/T_{\max}^2\pi c\lambda\gamma \tag{6.16}$$

6.5 Arc Speed in the Chute

The arc formed between the contacts of the magnetic circuit breaker undergoes the action of a magnetic field created by the magnetic system. A simple arc chute is shown in Fig. 6.6. Distinction is drawn between two stages of arc travel. The first stage immediately after the contact separation finds the arc travelling in air without contact with the ceramic walls (1) confined by the insulated plates (2). During the second stage the arc propagates in a narrow slit δ.

For the first stage, the arc speed can be calculated by the expression [4.1]

$$v = 185 i_a^{1/3} B^{2/3} / c_0 \gamma^{2/3} \tag{6.17}$$

where B is the induction at the arc location, T; γ is the gas density, kg/m^3; and c_0 is a generalized coefficient allowing for the forces opposing the motion. In estimations $c_0 = 2.4$ for $0 < B < 0.1$ T; and at normal pressure $\gamma = 1.1$ kg/m^3. Then

$$v = 73 i_a^{1/3} B^{2/3} \tag{6.18}$$

The magnetic system of the arc chute consists of a blowout coil (5), a core (4) and pole pieces (3). The poles embrace the arc zone completely or partially.

At the arc location the induction can be calculated as

$$B_\delta = \mu_0 H_\delta = \mu_0 iwk/\delta_p \tag{6.19}$$

where $\mu_0 = 4\pi \times 10^{-7}$ H/m; iw is the magnetomotive force of the coil, A-turns; δ_p is the pole distance, m; and k is a coefficient allowing for the drop of the m.m.f. in the core.

By virtue of Eqs. (6.19) and (6.18) we have

$$v = \frac{2.16 \times 10^{-2}}{c_0 \gamma^{2/3}} \left(\frac{kw}{\delta_p}\right)^{2/3} i = 8.5 \times 10^{-3} (kw/\delta_p)^{2/3} i = Ai \tag{6.20}$$

with $A = 8.5 \times 10^{-3} (kw/\delta_p)^{2/3}$.

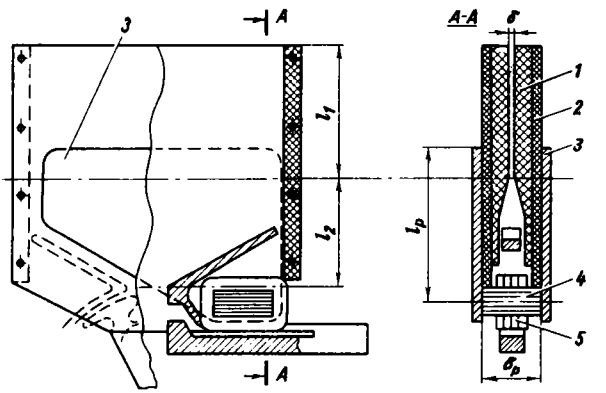

Fig. 6.6. Simple arc chute design

The distance travelled by the arc under magnetic action can then be found as

$$x = \int_0^t v\,dt = A\int_0^t \hat{I}_a \sin \omega t\,dt = A\hat{I}_a(1 - \cos \omega t)/\omega \tag{6.21}$$

The arc current $\hat{I}_a$ may be taken equal to the interrupting capacity $\hat{I}$ since at this stage the arc is not in the slit and its resistance is low.

After the arc has travelled a distance l_2 it enters the chute δ (see Fig. 6.1*b*) and its resistance increases sharply — the second stage of arc travel. The width of the chute is selected on the basis of two considerations, firstly, the slit should be narrow enough $\delta < d_a$, but not narrower than $0.1\delta_{min}$

$$0.1\delta_{min} < \delta < d_a \tag{6.22}$$

where the arc column diameter d_a can be estimated as

$$d_a = \sqrt{4\hat{I}_a/\hat{J}_a\pi}$$

The width δ_{min} is the doubled thickness of the turbulent layer of arc 2Δ. In agreement with Ref. [4.1] it can be determined by the approximate equation

$$\delta_{min} = 2\Delta = 1.1(v/\nu)^{-1/9}(\hat{I}_a/\hat{J}_a)^{1/2} \tag{6.23}$$

where ν is the kinematic viscosity of gas, cm^2/s.

Propagating through a narrow slit the arc has to overcome the aerodynamic resistance of the air (piston effect). The narrow chute prevents the arc from forming loops. The aerodynamic resistance decreases and the velocity of arc propagation in the chute increases. When inequality (6.22) is satisfied, the arc speed becomes higher than in free air.

The least width of the chute is also governed by technological considerations. Very small δ may lead to appreciable constrictions of the chute which can retard the arc motion and lead to breakdown temperatures for the ceramic plates. Therefore, δ is never smaller than 2 mm.

Kukekov [4.1] describes the arc velocity in a narrow chute under the conditions (6.22) by the equation

$$v \approx 370\sqrt{\delta i_a B}$$

In the chute the arc is formed into a wavy stripe, therefore the angle α between the magnetic flux density B and arc current i_a (Fig. 6.7) should be taken into account, viz.,

$$v = 370\sqrt{\delta i_a B \sin \alpha} \tag{6.24}$$

Substituting for the induction its expression in terms of the circuit current, we get

$$v = 370\sqrt{k\mu_0 w\delta(i_a/\delta_p) \sin \alpha} \tag{6.25}$$

In modern circuit breakers the velocity of arc reaches 100 m/s.

When arc extinction occurs beyond the zone of the system pole pieces, the fall of magnetic induction for travelling arc should be taken into account. The magnetic field beyond the poles can be represented as shown in Fig. 6.8 [4.1]. At small x

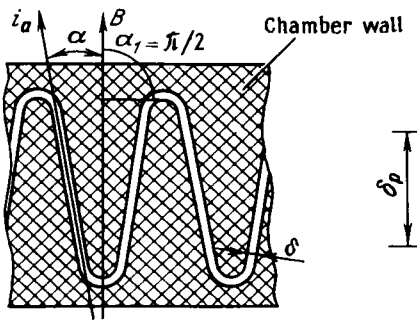

Fig. 6.7. Construction to calculate the arc speed in a narrow arc chute

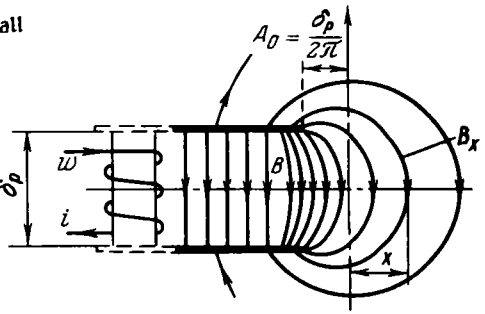

Fig. 6.8. Magnetic flux density in an arc chute

values, $x \leqslant 0.5\delta_p$, the magnetic flux density may be defined as

$$B_x = B_\delta = k\mu_0 iw/\delta_p \tag{6.26}$$

where B_δ is the magnetic induction between the poles, and δ_p is the distance between the pole plates.

For $0.5\delta_p < x < \delta_p$ the magnetic flux density is defined as

$$B_x = B_\delta/\sqrt{2}\sqrt{1 + 2\pi x/\delta_p} \tag{6.27}$$

For considerable distance x, exceeding δ_p, the magnetic flux density is given by

$$B_x = B_\delta/(2\pi x/\delta_p) \tag{6.28}$$

The saturation of the core steel, that occurs at high currents, should be allowed for in the calculation of the magnetic circuit parameters. The magnetic flux density B_x should be determined by the magnetic field pattern especially valuable for the space areas distant from the pole plates.

The total time of arcing is composed of a time t_1 from the instant of contact separation to the total immersion of the arc into the narrow chute, and a time t_2 of arc motion in the chute. The time t_1 is determined by Eq. (6.21) because the distance from the contacts to the chute is known. Referring to Fig. 6.6, we have

$$t_1 = \frac{1}{\omega} \arccos \left[1 - \frac{\omega l_2}{8.5 \times 10^{-3} (kw/\delta_p)^{2/3} \hat{I}} \right] \tag{6.29}$$

where l_2 is the travel of the unconfined arc.

The time $t_2 = 0.01$ s for the pole interrupted first. In the two remaining poles the arc is extinguished at the next current zero. To be on the safe side one may take $t_2 = 0.02$ s. If the magnetic induction is known for various locations of the arc path, the velocity at these locations can be found by Eq. (5.24). With this velocity and the total time span of the second stage of arc motion t_2 one can determine the height of the chute l_1 (depth of the narrow slit) and the total height of the extinction chamber $l_1 + l_2$.

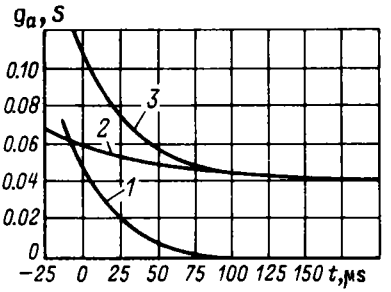

Fig. 6.9. Variation of residual conductivity in an arc chute following a current zero

6.6 Residual Conductivity of Magnetic Breakers

After current zero two types of electric conductivity can be found in the extinction chamber between the contacts of the magnetic circuit breaker: (i) through the residual gas plasma like in other types of circuit breaker, and (ii) due to the hot walls of the chamber. Figure 6.9 presents the time behaviour of residual conductivity for a magnetic air-break circuit breaker [4.1]. Curve *1* shows the conductivity of the residual plasma of the arc column decaying with a time constant $\tau \approx 35\text{-}38\ \mu s$ and vanishing by $t = 100\ \mu s$. Curve *2* is due to the hot trace of the arc on the walls of the chute. This component falls off with a higher time constant of 200 μs. The total conductivity is given by curve *3*, governing the residual current.

Restriking can occur either as a result of thermal breakdown of the gas spacing or as a result of flashover over the heated ceramic surface. Narrower chute can be recommended to reduce the gas spacing time constant τ. A reduction of hot wall conductivity is presented with large difficulties, especially at high breaking currents. The interruption process is facilitated by the fact that the recovery voltage is relatively low because of a small phase angle. In addition the residual conductivity damps the recovery voltage process.

The behaviour of the residual conductivity of the contact spacing limits to a considerable measure the rated voltage of magnetic circuit breakers, especially at high breaking currents.

6.7 Arc Chute Construction

A simple arc chute design is shown in Fig. 6.6. The main element of the chute is a narrow slit. The electric arc forms between the horn of the movable contact and the horn of the stationary contact, tracing an arc path in the form of a circular arc. To facilitate the entrance of the arc into the chute, the latter is flared near the contact system. For high voltage ratings, say 10 kV, and $\delta = 2$ mm, the calculated length of arc $l_{a,calc} = 1.84$ m, that is, the length of an extincted arc approaches 2 m, implying large size of the circuit breaker and an unwieldy design. Accordingly, these designs are never used for voltages higher than 3 kV and are preferred in applications with low breaking currents.

In the arc chute shown in Fig. 6.6, the blowout coil is placed in the circuit permanently. Therefore, it is wound by a wire designed to pass the continuous rated cur-

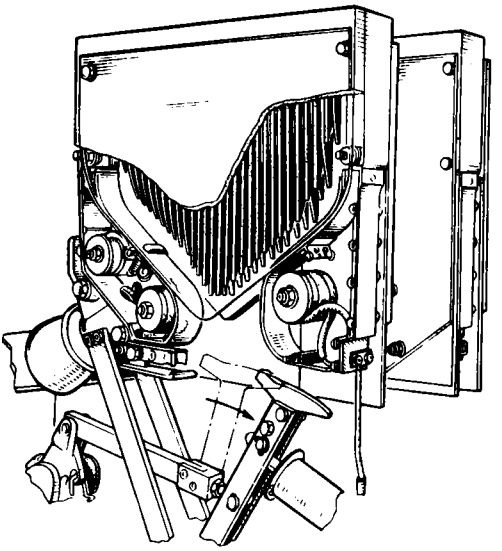

Fig. 6.10. Insulated-plate arc-chute magnetic air circuit-breaker

rent. The magnetic circuit is built up of stampings to depress eddy current losses and hysteretic losses causing additional heating of the contact system.

Figure 6.10 shows an insulated-plate arc-chute design used in magnetic air-break circuit breakers for voltage ratings up to 17.5 kV, interrupting capacities up to 500 MVA at an interrupting current of 16.5 kA. The chute is a ceramic base-plate with variable-height fins made of insulating splitter plates. The fins of one side enter the gaps between the fins of the other. As the arc is driven deeper into the chute it becomes a wavy shape and extends in length. The gradual reduction of chute width δ ensures a uniform arc invasion of the chute.

It is worth noting that various segments of the arc undergo action of various forces. This is attributed to the fact that in the mid-portion the arc current is acted upon by the magnetic induction $B_\delta \sin \alpha$ with $\alpha < \pi/2$, and where the arc experiences a turn and $\alpha_1 = \pi/2$ it is subjected to the action of magnetic induction B_δ (see Fig. 6.7). Nonuniform propagation velocity also aids in extension of the arc length.

Immediately above the arc chute there is a divided flame-quenching exhaust compartment. It is divided by copper plate dividers insulated one from another and porting the ionized gas for outlet. The gas is cooled and the zone of exhaust of ionized gases dangerous for live switchgear components is reduced. The divided exhaust chamber also operates as a muffler decreasing the sound load during a circuit breaking.

In this type of magnetic air circuit breaker, rated for high continuous current (2500 A), the blowout coil is placed in the arc circuit in the process of circuit break-

ing only (see Fig. 6.1). As a rule two or three independent magnetic systems are employed.

In low-current interruption (from several amperes up to a few dozen amperes), the initial electrodynamic force acting on the arc is weak and unable to drive the arc into the position where the blowout coils of the magnetic system would be brought into the play. Therefore, the movable contact is connected with pneumatic 'puffer' piston which blows air onto the arc when the contact travels clockwise and shifts the arc upwards.

It is important to note that near a current zero the magnetic induction in the arc chute is also small and the magnetic blow-out action is inefficient at the moment. To enhance the breaker performance the magnetic system is provided with a turn closed on itself. The magnetic flux lags the current in the coil, consequently, at current zero the magnetic induction is nonzero, thus aiding arc blowout and extinction.

The technology of ceramic plate manufacturing for arc chutes (Fig. 6.10) is extremely involved as the chute width δ is rather small and dimension tolerances are very narrow. The arc-chute design shown in Fig. 6.1*b* has received wide acceptance in the Soviet Union. The chute is assembled of ceramic plates (11) having a converging gap displaced from the plate axis. In the assembled chute the gaps of adjacent plates are staggered. Blown upwards the arc enters the gaps and becomes a wavy shape. The manufacturing technology is fairly simple and well suited for producing profiles to close tolerances. The 6-kV type VEM-6 magnetic airbreak circuit breaker equipped with this chute operates at a continuous current rating of 1600 A and is capable to interrupt 38.5 kA short-circuit current. The construction allows 10 000 make-break operations at rated current within a maintenance interval and warrants 75 000 operations before an overhaul. The Rovno Works of high-voltage switchgear has developed magnetic air circuit breakers for about the same ratings but having considerably reduced weight and size.

An original construction has been presented to the market by a French company Merlen Geren. The outline and functional details of this design are presented in Fig. 6.11. When the contacts (1) part, the 'puffer' piston (7) and magnetic action drive the arc upwards onto the arc runners (2). The magnetic blowout system (3) and (4) forces the arc farther upwards until it touches intermediate contacts (5). These contacts have a form facilitating the circular arc formation between the insulating splitter plates. The arc grows in radius aided by the action of electrodynamic forces operable in the arc circuit. The plane of the arc loop coincides with the plane of the plates. The number of arcs formed equals the number of insulating plate sections. This design known as the Solenarc forms an arc resembling a solenoid.

Individual turns of the arc are attracted by one another (coil compressed in length) with a good contact between the arc and ceramic plates. The contact (6) connects the breaker terminal with the outward plate of the arc chute. When the arc is extinguished the contact (6) is retracted from the chute chamber. This breaker has 250 MVA interrupting capacity at 24 kV voltage rating. A distinctive feature of this design is its small size.

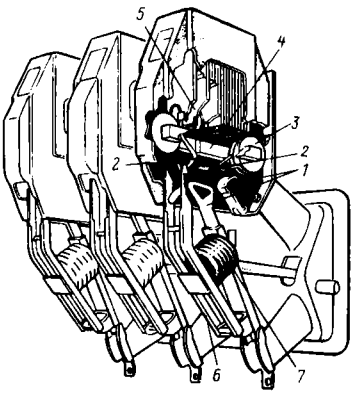

Fig. 6.11. Type Solenarc magnetic air circuit breaker

It is worth noting that the idea of arc extinction in a chute forming an arc solenoid was devised by B. P. Petrov of the Soviet Union who came up with this device in the 1930s suggesting it being used for traction switchgear.

6.8 Magnetic Air-Break Circuit-Breaker Design Procedure

1. Determine the chute width δ by virtue of the inequality (6.22) subject to the technological limitation $\delta \geqslant 2$ mm. The calculation is performed for the rated breaking current.

2. Calculate the length of the arc by Eq. (6.10) and allow some safety margin.

3. Select the shape of the wavy chute from constructive considerations and determine angle α.

4. Determine the overall width of the chute chamber and the air spacing of the magnetic blowout system.

5. Calculate the minimum arc speed in the extinction zone by Eq. (6.16). Allow a safety factor of 1.1.

6. Use Eqs. (6.26-28) to calculate by the known calculated arc speed the peak value of magnetic induction $\hat{B}$ in the arc spacing and determine the number of turns in the magnetic blowout coil.

7. Calculate the travel of arc by the time $t = 0.01$ s and evaluate the height of the arc chute l_1 with some safety margin as the actual quenching time is assumed equal to $t_2 = 0.02$ s.

8. Choose the height of the arc expansion zone, l_2. Find convenient locations for the main contacts,arcing contacts, arcing horns, and provide for a smooth conversion from the wide to narrow section of the chute.

9. By virtue of Eq. (6.29) determine the time t_1 of arc travel in the preliminary arc extension zone.

10. Be sure that the total extinction time $t_0 = t_1 + t_2$ does not exceed 0.03 s.

7
VACUUM CIRCUIT-BREAKERS

7.1 General

In vacuum circuit breakers arc extinction occurs in vacuum. The outstanding extinction properties of this medium have led to the development of circuit breakers for voltages in the range 6-35 kV. These breakers are practically displacing air-blast, oil, and magnetic air-break switches.

The advantages of vacuum circuit breakers are as follows:

(i) there is no need for replacement or replenishment of the arc quenching medium, no need for pumps or oil systems;

(ii) high wear resistance in switching rated and short-circuit currents;

(iii) maintenance and operational costs are minimized (almost half as much as in the existing breakers) with 25 years of life-time;

(iv) rapid recovery of electric strength at 10-50 kV/μs;

(v) absence of fire and explosion hazards;

(vi) reliable operation in the situation when a short-circuit current occurs in low-current interruption (interrupters of oil circuit breakers are usually blown in this case);

(vii) a wide range of operating ambient temperatures, from -70 °C to 200 °C.

(viii) enhanced shock and vibration strength;

(ix) arbitrary orientation of the vacuum pot;

(x) silent and environment-pleasing operation, convenient maintenance due to small energy released in the arc and the absence of external effects in clearing short-circuit faults;

(xi) no emission into the surroundings;

(xii) small weight, overall dimensions and dynamic loads on the supporting structure;

(xiii) high speed;

(xiv) suitability for mass production technology.

The disadvantages of vacuum circuit breakers include:

(i) difficulties encountered in the development and manufacture associated with the need for special contact materials, sophistication of vacuum production technologies, and tendencies of contact materials to welding in vacuum conditions;

(ii) large capital costs involved in mass production.

The mass-produced vacuum circuit breaker is only 5-15% more expensive than the oil breaker and cheaper than the magnetic air breaker. Cost-efficient operation is another attractive feature aiding in widespread application of vacuum circuit breakers (half of all the circuit breakers in Japan are vacuum units).

The sectional view of a vacuum circuit breaker is shown in Fig. 7.1. The cylindri-

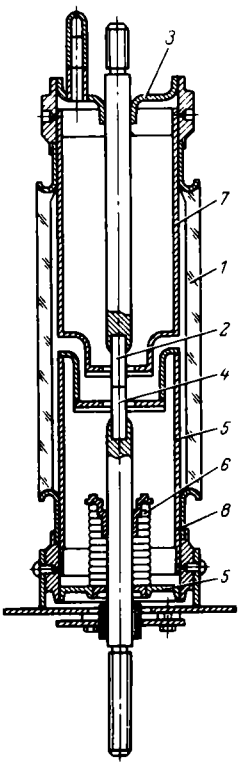

Fig. 7.1. Type KVD-5 vacuum interrupting bottle rated 10 kV, 250 A, and 1 kA interrupting ability

cal vessel (1) made of porcelain or vitrified glass contains a stationary contact (2) fixed in a metal flange (3) sealed into the cylindrical pot (1). The movable contact (4) is connected to a flange (5) by a bellows (6) of stainless steel. The bellows is a rather strong structure allowing the contact a travel up to 20 mm.

In modern circuit breakers the air is evacuated from the vacuum pot to a pressure of $1.33(10^{-4}\text{-}10^{-6})$ N/m^2 (10^{-6}-10^{-8} mm Hg). The mechanical pressure of the movable contact against the fixed contact is provided by atmospheric pressure. For large current ratings an additional contact spring is provided.

When contacts part, high breaking current forms a short liquid metal bridge of electrode material. This bridge is rapidly heated to a high temperature because of a high current density and sharp rise of resistivity of the melted material. This heating leads to evaporation of the bridge and formation of an arc that is burning in the medium of electrode metal vapour. This is a typical vacuum arc. This arc is characterized by a low arc-over voltage being only 20-40 V. It is only at heavy currents (10-100 kA) that the voltage increases to 50-200 V.

The arc is extinguished at current zero. Because of a high difference of particle density in the quenched arc and the surrounding vacuum, the velocities of diffusing

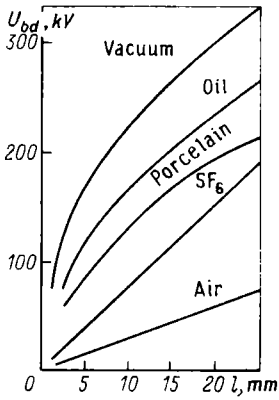

Fig. 7.2. Relation of the breakdown voltage to the contact spacing for various media

charges are extremely high. The dielectric strength of vacuum is recovered within 10 μs after the current zero. In a uniform field this strength reaches values as high as 10^5 V/mm. Figure 7.2 compares breakdown voltage as a function of contact spacing for various media.

Because of the high rate of rise of the dielectric strength of the contact spacing, the vacuum interrupter is insensitive to high rates of recovery voltage and can operate under most severe voltage recovery conditions.

Returning to Fig. 7.1, the buffles (7) and (8) serve to protect the walls of the insulating enclosure from the adverse effect of electrode vapour. In the absence of these buffles the metal vapour sedimented on the internal surface of the cylinder (1) would lead to flashover of the insulation between the contacts (2) and (4). The baffles also aid in equalising the electric field between the contacts, thus improving the reliability of breaker operation.

7.2 Status and Trends in Continuous Current and Interrupting Ratings

Rated continuous current. For high operating speeds, vacuum circuit breakers widely use the butt-contact system. It allows for short contact travel (10-20 mm) and small operating times. The simple construction of the contact is amenable to technologies with well degassed current-carrying parts of the breaker — an important point in providing high vacuum with stable properties.

The butt contact is known of having a high resistance and, consequently, of incurring large heat losses at rated currents of 2000-4000 A. Since the contact rods are immersed in vacuum, the transport of heat occurs mainly by conduction along the contact rod and by external terminals of the breaker and the contacting buswork. Some portion of the heat released in the contact and in the contact body is conveyed by radiation.

Large power released in a butt contact owes its scale in part to the fact that the material of contacts is commonly tungsten or cerment material based on tung-

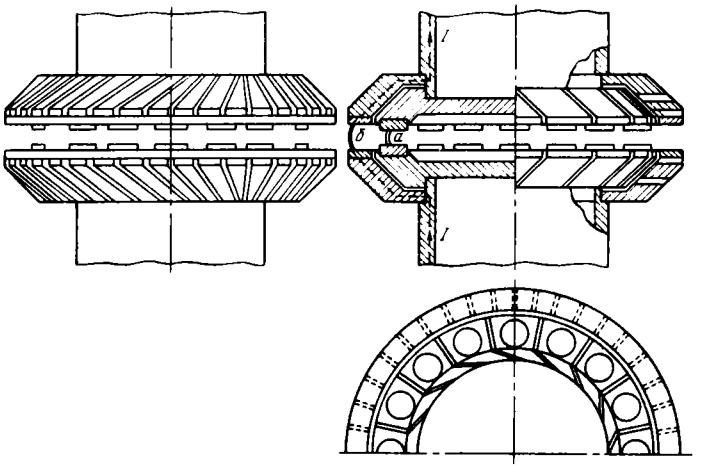

Fig. 7.3. Multipoint butt contact of a vacuum interrupter

sten to ensure high mechanical rating of the contact system and to handle high breaking currents. Owing to the physical properties of these materials, the resistance of the transient contact is rather high. The external terminal is made of silvered copper allowing temperatures as high as 105 °C. If the ambient temperature is 40 °C, then the power conveyed to the external terminal must be dissipated at a temperature difference of 65 °C. With the butt-contact design, the temperature can be kept within the stated limits at rated currents of 600-700 A. The heat losses sharply increase for higher currents implying that the contact rod of large cross section is required. To decrease the temperature of the external terminal, the connection is effected by a few copper buses with developed surface. With 8 × 100-mm^2 copper buses current ratings of up to 2000 A can be achieved.

In new installations vacuum breakers operate at 84 kV. To serve systems of 110-220 kV, several vacuum interrupters are connected in series. A 220-kV circuit breaker can be obtained by connecting four 84-kV interrupters in series. The connecting elements should dissipate heat transported from the contact rods of both adjacent interrupters, that is, at a contact temperature of 105 °C the interconnections have to dissipate twice as much heat in the surroundings. This is one of the major problems of a multiple-break vacuum circuit breaker. One way of reducing the transition resistance of the butt contact is by means of the multipoint butt contact shown in Fig. 7.3.

Interrupting capacity. In the vacuum interrupter the arc burns in an atmosphere of contact-metal vapour. Vozdvizhensky and Kozlov [7.2] and Lukatskaya *et al.* [7.3] have supposed that the breaker may fail to interrupt a circuit because the electrodes are heated to a certain critical temperature T_{cr} at which the metal vapour pressure in the contact spacing is as high as 1 N/m^2 (10^{-2} mm Hg). The dielectric strength

recovering at this pressure is fairly low and the spacing is broken down by the recovery voltage.

The contact heating temperature can be described by the expression [7.1]

$$T = \frac{k_1 k_2}{\sqrt{\pi c \lambda \gamma}} \int_0^t \frac{u_a i_a}{S\sqrt{t-\tau}} \, d\tau + T_0 \tag{7.1}$$

where k_1 is the fraction of heat power dissipated in one of the electrodes; k_2 is the arc concentration coefficient being the ratio of the maximum heat flux density to the mean value over the area occupied by the arc; S is the electrode area occupied by the arc; t is the time elapsed from the instant the arc has occurred; τ is the current time from the arc incipience; c is the heat capacity; γ is the density of electrode material; and λ is the thermal conductivity. The energy $u_a i_a d\tau$ released by the arc in time $d\tau$ causes a rise of temperature proportional to $1/\sqrt{t-\tau}$.

Analysis of Eq. (7.1) suggests that electrode material should exhibit a high value of the quantity $T_{cr}\sqrt{\lambda c \gamma}$. For some materials this criterion is quoted in Table 7.1 along with heat flux densities q_{10} and q_1 which are capable of heating the anode, more loaded of the two electrodes, to the temperature T_{cr} in 10 ms and 1 ms, respectively. The tabulated data indicate that admissible heat load is much higher for arcing times of 1 ms (q_1) than for 10 ms (q_{10}). The rated breaking current may be increased substantially provided that interruption is synchronous.

Given an ultimate heat flux q_{10} and the arc-over voltage u_a, one can readily obtain the admissible current density. For copper operating in the range 1-10 kA, the voltage drop across the arc is 20-40 V. At 1 kA the arc power is 20 kW, $q_{10} = 41$ kW/cm^2, arc cross section $S_a = P_a/q_{10} \approx 0.5$ cm^2, and the admissible current density is 2 kA/cm^2. At higher currents (10-100 kA), the voltage drop across the arc increases up to 50-100 V and the admissible current density amounts to (0.5-2) $\times$ 10^3 kA/cm^2. Clearly, the contact cross section 100 cm^2 will be sufficient for handling interrupting currents as high as 100 kA.

Table 7.1 also suggests that the more suitable material for contacts is tungsten as having the highest value of $T_{cr}\sqrt{\lambda c \gamma}$. In addition tungsten contacts are stable against welding. This property explains why the early vacuum circuit breakers used tungsten capable of handling highest interrupting currents. Later designs have revealed a number of disadvantages for tungsten contacts. On interrupting circuits with high wave resistance $\sqrt{L/C}$ these breakers revealed considerable overvoltages

Table 7.1. Thermophysical Characteristics of Vacuum Interrupter Electrode Materials

Material	T_{cr}, °C	$T_{cr}\sqrt{\lambda c \gamma}$	q_{10}, kW/cm^2	q_1, kW/cm^2
Copper	1280	4600	41	130
Iron	1470	2360	21	66
Tungsten	3300	6450	57	180

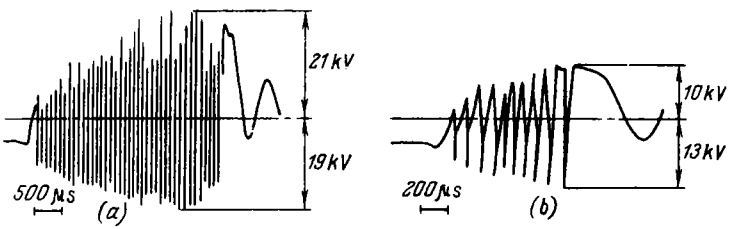

Fig. 7.4. Overvoltage (*a*) damped by placing a shunt varistor in the circuit (*b*)

which often led to breakdown of the insulation in the discriminated equipment. This phenomenon is explained by the low density of tungsten vapour at low currents in the vacuum arc. The arc is unstable and current chopping occurs before current zero. The load appears at the voltage $u = i_{ch}\sqrt{L/C}$, i_{ch} being the chopping current. Copper contacts also exhibit current chopping, but the currents are well below that for tungsten. To reduce chopping currents for tungsten contacts, the contact material received additions of antimony in proportion of 4-5%. The chopping current has reduced down to 4 A. However, this method of overvoltage damping is used in vacuum contactors only, for in high-current circuit breakers the antimony combines with the copper of contacts during the interruption process and increases the transition resistance and the heating of the contacts by rated current.

Power circuit breakers use copper contacts. To damp overvoltages occurring in interrupting loads of high $\sqrt{L/C}$ the use is made of either shunting circuits or nonlinear limiting resistors (varistors) [7.2]. The chopping current should be under 4-5 A. The resistors are placed between the phase and earth. Performance of a nonlinear resistor of varistor type is illustrated in Fig. 7.4.

Higher interrupting currents can be handled if the heat flux from the arc is distributed uniformly over the contact area. To achieve this purpose the arc is acted upon by a magnetic field. In the absence of these measures, the arc concentrates within a small spot of 1-3 cm diameter and interrupting ability falls to 5-10 kA even for large contact diameters.

Interrupting capacity can be enhanced by placing a few interrupting chambers in parallel. The current-voltage relation of arc increases with the current and this can be distributed between, say, three parallel interrupting chambers with a nonuniformity within 10%. *Toshiba* of Japan claims that for a contact diameter of 200 mm the interrupting capacity increases to 120-60 kA at 10-30 kV. For a contact of 140-mm diameter the interrupting capacity reaches 70 kA at 10-45 kV and 25-35 kA at 50-70 kV. This approach, therefore, is useful in improving the interrupting capability of vacuum circuit breakers.

Vacuum circuit breakers can be used to advantage on d.c. circuits. For currents as high as 1000 A at 10 kV, interruption is effected by separating contacts in vacuum. For higher currents a capacitor converts d.c. into a.c. waveform to interrupt this current at the first current zero [4.1]. Two interrupting chambers connected in series interrupted a current of 5 kA at 60 kV using a 3-μF capacitor.

7.3 Mechanical and Thermal Withstand Capabilities. Erosion of Contacts in Vacuum Circuit Breakers

Butt contacts are known to possess inadequate mechanical withstand capability. This problem has been separately studied for vacuum circuit breakers. At high currents two causes of contact repulsion are operative: the forces due to convergence of current lines in the contacts and the forces that appear as the result of explosion of the contact bridge.

Heavy currents heat the contact bridge to high temperatures and vaporise the material. This vapour produces a pressure forcing the contacts apart. The force repelling a contact on bridge explosion is proportional to the first power of the current. The movable contact, therefore, finds itself under the action of the resultant force due to these two effects.

For butt-type tungsten contacts, the minimum current of repulsion and the pressing force are related by the empirical equation [7.3]

$$F = 0.95I^2 \tag{7.2}$$

The force F is combined of a force due to atmospheric pressure on the bellows and a force produced by an additional contact spring (at heavy currents). Equation (7.2) suggests that at a breaking current of 40 kA the minimum pressing force should be 1520 N — a rather high value. The driving mechanism should develop this force in the opening operation.

A great deal of designs have been devised to obtain the necessary mechanical rating of contacts. The main idea hinges around a multipoint contact. The current passing through a contact point is then sharply reduced implying a proportional reduction in the mechanical pressing force. Ten contact points per contact reduce the mechanical force at one point almost 100-fold. The total pressing force reduces to one tenth of its value.

By way of illustration, one of such contact systems is shown in Fig. 7.3. This is the so-called 'chrysanthemum' system. Essentially, this is a multipoint butt cluster contact containing a large number of individual butt contacts. In the closed state current flows through both contacts *a* and contacts *b*. On interrupting, contacts *b* part first followed by contacts *a*.

The current-carrying parts of the contact form a circuit creating a magnetic field directed tangentially to the circle. This field produces a radial electromagnetic force forcing the arc to run from contact *a* to contact *b*. Fast travel of the arc reduces contact temperature and aids in increasing the interrupting ability of the breaker and reducing wear of its contacts. For a single butt contact, the wear (in mm) after 10^4 switching operations with a current I (in kA) can be estimated by the empirical formula

$$\Delta l = 0.9I^{2.3}$$

The respective lifetime number of operations of the breaker can be estimated as

$$N = 1.1 \times 10^4 \Delta l_{\text{adm}} I^{-2.3}$$

where Δl_{adm} is the admissible wear of contacts, mm.

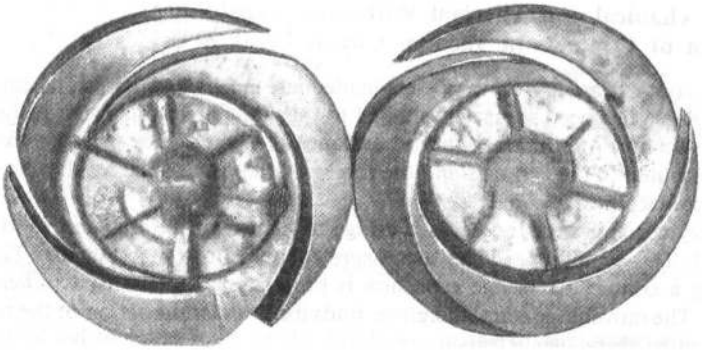

Fig. 7.5. Contact system of the interrupter from Fig. 7.8 after tests

Figure 7.5 pictures the widely used contact system, installed in particular in the type KDB-10-1600-20 vacuum circuit breaker, shown in Fig. 7.8. In the closed position contact occurs over the six ridges of the butt cluster. The diameter of the ridges exceeds that of the current carrying rods. In opening, the arc comes under the action of the magnetic field produced by the currents flowing in the zone of contact. The radial force moves the arc along a spiral path. Rapid movement of the arc over the contact surface prevents nonuniform erosion. This contact system warrants interruption of currents up to 25 kA. The multipoint cluster contact shown in Fig. 7.3 is rated for a continuous current of 1250 A and rated breaking current of 10 kA.

The interrupting capacity depends on the speed of arc travel over the electrodes and the last is governed substantially by the magnetic field acting on the arc. To study the magnetic action designers use live breadboards where the arc is represented by a jumper of circular cross section. The magnetic flux density is measured by a probe in the form of a coil whose e.m.f. is proportional to the flux density as its location. The studies have revealed that magnetic action of the arc helps reduce the size of melted spots on the contacts, cuts down arcing times, and improves the interrupting capacity.

Studies carried out in Japan [7.5] have indicated that in circuit breakers for high breaking currents (100 kA and higher), a magnetic field parallel to the arc is of decisive importance. This field spins the arc electrons producing a so-called diffuse form of arc with the cathode spots uniformly distributed over the contact surface. It appears as if many arcs are striken parallel to each other. The arc-over voltage is then sharply damped, down to 20 V, even at 100-200 kA. This approach paves the way for circuit breaker designs for very high short circuit currents (above 200 kA) since the arc-over voltage is independent of the current and the arc energy is moderate.

Figure 7.6 shows the schematic diagram of the contact system of a 13.8-kV vacuum circuit breaker for 3000 A continuous current and 100 kA interrupting capability. The current flows from the stem (1) in the radial direction and then through the arc-conductor (2) (currents i_1-i_4) producing an axial magnetic field represented

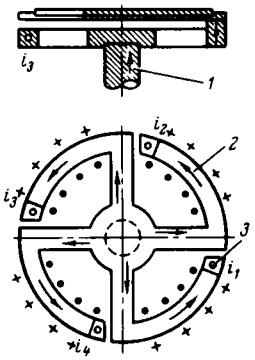

Fig. 7.6. Contact system of a vacuum interrupting chamber with a longitudinal magnetic field

by crosses and dots. The arc-shaped conductors terminate with butt contacts (3) passing the current from the lower into upper contact. The contact system, therefore, has the total of four contact points. The total mechanical force for the entire system attains 12 000 N. Compared with an air-blast circuit breaker for this rating, the vacuum unit has lower weight (by 47%) and occupies lesser volume (by 46%). Accordingly, the volume of the switchgear cubicle for a distributing substation reduces by 42% and the area it occupied by 70%. The vacuum circuit breaker warrants 20 000 C-O duty cycles at rated current whereas the life of the air-blast breaker contacts is only 500 operations.

7.4 Electric Strength

The early vacuum circuit breakers enclosed nothing but the contacts inside the vacuum pot. The vapour of metal electrodes deposited on the internal surface of the pot after each interruption and thus assisted flashover of the insulation. To cope with the problem the device received metal baffles. Figure 7.1 shows one of the early Soviet vacuum interrupters of the type KDV-5 rated for 10 kV which was equipped with baffles. These barriers provided reliable protection of the enclosure from the metal vapour but the voltage distribution inside the chamber was insufficiently uniform and occasional breakdowns occurred inside the pot after the interruption had been over [7.4]. This phenomenon has motivated research and development efforts aimed at enhancement of electric field homogeneity in the interrupter.

As the contacts of the vacuum interrupter separate the dielectric strength of the contact spacing first increases with the distance then the rate of rise falls off because of the field inhomogeneity. Therefore, the rise of electric strength in the interrupter is achieved by attaining a more uniform electric field rather than by farther spreading of the electrodes. Designs with a more homogeneous electric field have allowed the rated system voltage for these units to be increased up to 35 kV.

Figure 7.7*a* shows an interrupter with three baffles, one insulated and the two other connected with the contacts. The equivalent circuit in the diagram at (*b*) as-

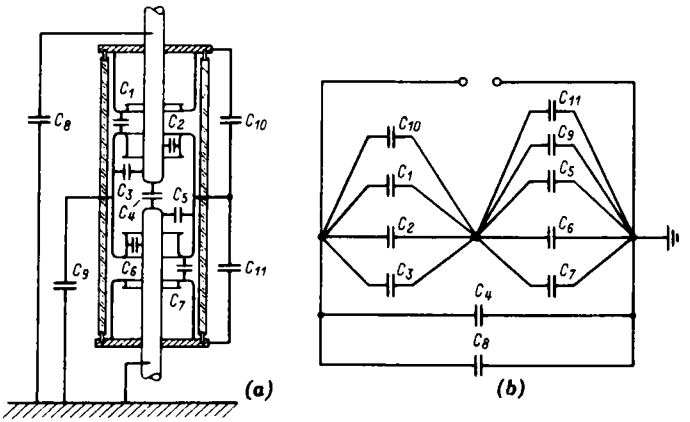

Fig. 7.7. Interrupting chamber with three baffles: (*a*) distribution of capacitance inside the chamber and (*b*) equivalent circuit

sists in the evaluation of voltage distribution in this system. Use of baffles allows for shorter length of the pot and warrants a dielectric strength conforming with the standards. Experimental prototypes for 50 kV have been developed.

Because of the intrinsically high dielectric strength vacuum circuit breakers are widely used to interrupt capacitive loads and charging-line currents. However, interruption of small line currents may be accompanied by restriking. These breakdowns are caused by minute sharp points formed on the electrode surface where they contact with each other. In a contact shock of closing caused by strong mechanical closing force, the pure surfaces of the contacts are apt to bonding. In contact separation this bonding is broken leaving behind sharp microridges creating a high strength of electric field that leads to breakdown. On interruption of heavy currents these sharp stings are melted off and the electric strength rises sharply. Elimination of restriking on interrupting charging-line currents is a formidable problem that would be solved by a material not liable to microstings formation in low-amperage interruptions.

Installations for system voltage of 110 kV and higher employ several vacuum interrupters connected in series. Capacitive dividers take care of uniform distribution of voltage among the interrupters. Because of high vacuum in the chamber the spread of arc proceeds very fast (in less than 10 μs) resulting in response currents well below 1 A on interrupting 10-kA currents. The self-capacitance of a 50-kV vacuum interrupter is about 20-40 pF. A numerical analysis has indicated that the capacitance of the divider shunting the interrupter does not exceed 200 pF. This divider provides the desired equalisation of voltage distribution both in the steady state and in the voltage recovery process during a short circuit fault clearing.

In the USSR the development of a vacuum circuit breaker for 110 kV, 1600 A and 20 kA interrupting current will be based on a layout with four interrupting chambers. This number of interrupters has been adopted to handle line-charging

currents associated with low rates of recovery of electric strength. All other duties reveal considerable margin of electric strength. The breaker evolves in about the same size as an air-blast or SF_6 unit. There is a trend to reduce the number of breaks by means of enhancing the rated voltage for each break.

General Electric Company has reported the development of a 242-kV circuit breaker with five vacuum interrupters per pole rated for 40-kA interrupting capability. The layout of this unit is similar to that of the continuously pressurized SF_6 breaker. Japanese engineers have constructed and phased in a vacuum circuit breaker for 160 kV, 40 kA interrupting current and only two breaks per pole.

7.5 Construction and Layout

An intense vacuum-circuit-breaker development project is under way in the Soviet Union. Vacuum interrupters for 10 kV, 400-3200 A continuous current and 4-31.5 kA interrupting capability have been successfully tested. Figure 7.8 shows the type KDV-10-1600-20 interrupting chamber. The flanges (6) are connected with the vacuum-strong ribbed ceramic cylinder (10). The contact stem (4) carries fixed contacts (1, 2) in the form of six-point butt cluster-contact. The movable contact (1, 2) is fixed to the rod (5) sealed by the bellows (7) allowing for its vertical movement. The pieces (1) and (2) of the contacts are connected with a gap (3). The current-carrying flexible cable connects the external feeder to the rod (5) and a rigid bus connects the line to the flange (6). The baffles (8) and (9) are installed to provide for a more uniform electric field and to protect the cylinder (10) from deposition of metallic vapour. The baffle (8) is fixed to the insulator by means of a ring (11). The technical data of this interrupter are outlined below.

Nominal system voltage	10 kV
Rated current	1600 A
Resistance of current carrying circuit at 1600 N	16 $\mu\Omega$
Rated content of aperiodic component	0.35
Arcing time	20 ms max
Rated making current	
peak	51 kA
initial value of periodic component	20 kA
Short time current (thermal rating), for 4 s	20 kA
Average chopping current	10 A max
Number of shots with fault current	
$I_{b,r}$ = 1.6 kA	100
$I_{b,r}$ = 20 kA	25
Number of mechanical operations	20 000
Movable contact travel	12 mm
Admissible wear of contacts	4 mm
Movable contact speed	
on breaking	1.7-2.3 m/s
on making	0.6-0.9 m/s
Reclaim time (no-current condition)	0.3 s min
Number of service years	25
The interrupter may be used in auto-reclose duty cycles	

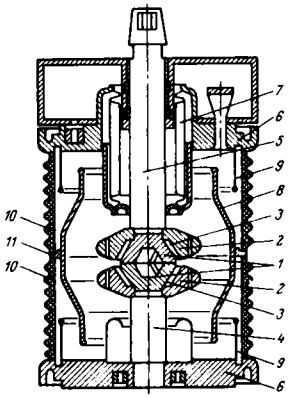

Fig. 7.8. Vacuum interrupting bottle rated 10 kV, 630-1600 A, 20 kA

Experimental models of 35-kV vacuum interrupters for 1600-A continuous current and 20-kA interrupting rating have been tested in the Soviet Union. A 10-kV circuit breaker built on the basis of the type KVD-10-630/1600-20 arc chute is shown

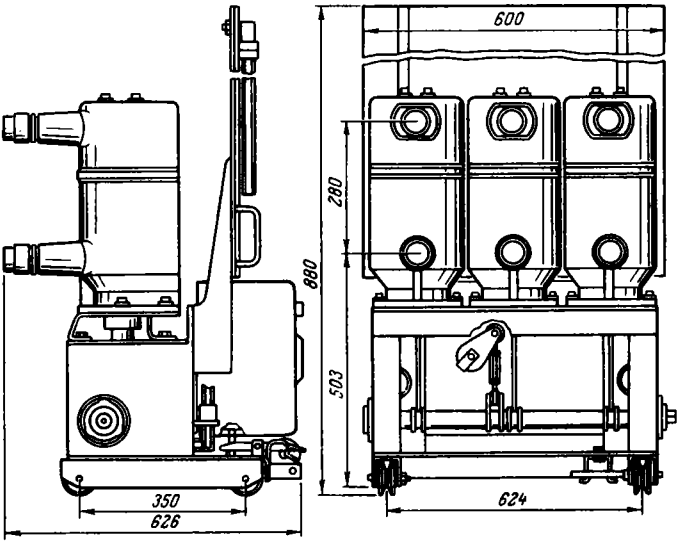

Fig. 7.9. Type VEI vacuum circuit breaker for U_{nom} = 10 kV, I_r = 1600 A, and $I_{b,r}$ = 20 kA

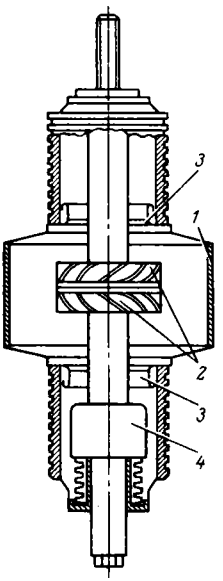

Fig. 7.10. Silmens vacuum interrupter bottle for U_{nom} rated up to 24 kV, I_r up to 2500 A, and $I_{b,r}$ up to 25 kA

in Fig. 7.9. Standard connections make the unit easily adaptable in switchgear cubicles and distribution systems.

Figure 7.10 shows the Siemens 12-kV vacuum interrupter for 1250 A normal current and 25 kA interrupting capability. A modification of this device can operate at 2500 A and up to 24 kV interrupting short circuit currents of 16 kA. The remarkable feature of this design is the absence of a continuous insulating enclosure. The extinction chamber (1) is a metallic cylinder so the metal vapour deposited on its wall cannot impair the insulating properties of the interrupter any longer. The contacts are provided with spiral groovers that reduce wear and improve the interrupting performance. The electric field inside the interrupter is equalised by two barriers (3) connected with the extinction chamber and two baffles (4) connected with the flanges of the interrupter. The circuit breaker built around this interrupter is represented in Fig. 7.11. Two support insulators carry the interrupting chamber with the aid of two holders (1) and (7). Connection is effected by the cables (2) and (6). The lead (6) is connected with the movable contact (4) by a flexible tie. The fixed contact (3) is connected with the lead (2). The interrupter is mounted on the frame with the aid of porcelain insulators (5). The movable contact is actuated by the linkage (8) and (9). The contact spring (10) provides an additional mechanical contact force. The operating mechanism is controlled by a latch (11). Operation is effected by a motor drive. The breaker is operable in the voltage range 7.2-24 kV, at a rated current of 630-2500 A and interrupting current of 8-25 kA. The rate of rise of the dielectric strength of the interrupter is 50 kV/μs. The arcing time is not more than 11 ms. The manufacturers warrant 20 000 C-O operations with the rated current and 100 shots at the fault current. A compact option is provided for smaller interrupting capacities.

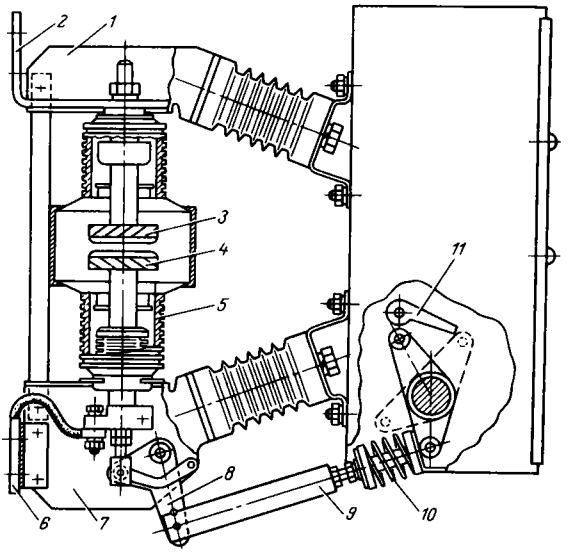

Fig. 7.11. Siemens vacuum circuit breaker incorporating the interrupter shown in Fig. 7.10

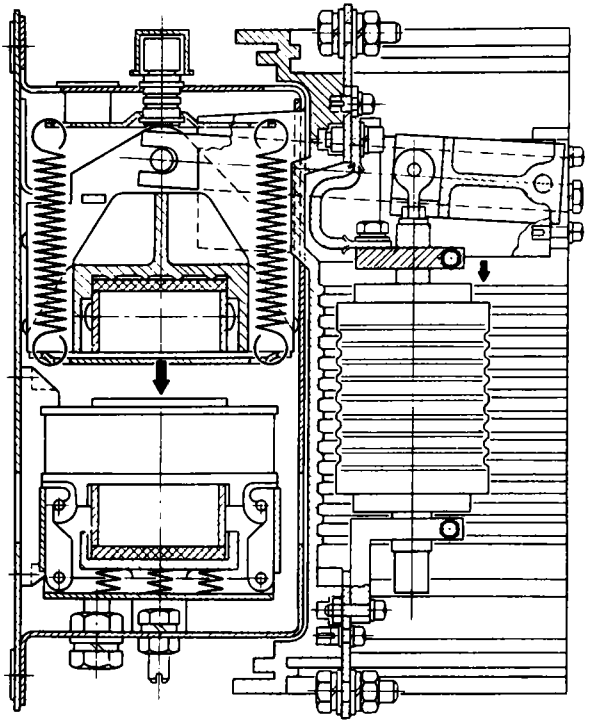

Fig. 7.12. Siemens small-size vacuum circuit breaker for 3.3-6.6 kV

Figure 7.12 shows a vacuum circuit breaker for 3.3-6.6 kV and 400 A rated current. The general guidelines applying with respect to its maintenance intervals are 5×10^6 mechanical operations and 10^6 C-O cycles.

7.6 Conclusion

Vacuum circuit breakers offer an extremely high reliability and wear resistance. The vacuum high-voltage contactors are capable to withstand 2×10^6 switchings in electrical and up to 10^7 operations in mechanical tests. Power circuit breakers withstand 10^6 switching operations at 400 A continuous current. The breaker warrants 50 C-O duty cycles at the rated interrupting current.

A small mass of the movable contact and slow breaking speed appreciably relax the requirements imposed on the operating mechanism. The most likely causes of failure in these units are due to faults in the mechanism or some other parts outside the interrupter. Therefore, in designing a vacuum circuit breaker considerable attention should be paid to the reliability problems of the mechanism.

It is instructive to note that beyond their normal duty vacuum circuit breakers can be used as current limiting switches which disconnect fault current when this rises above a set level prior to a natural current zero. Also these units may be applied as controlled lightning arresters for rapid switching of various gear and overvoltage damping. It is important to note that the control voltage of such an arrester amounts to 1% of contact voltage and the breaking current reaches dozens of kiloamperes.

Vacuum arresters offer the following advantages:

(1) variation of the rated voltage in a wide range by adjusting the vacuum;

(2) small wear of contacts, long service life;

(3) high rate of recovery of the dielectric strength enabling high-frequency-circuit applications;

(4) small weight and size.

In view of the high electric strength of the vacuum, firing of the contact gap is effected by a special device.

Development is under way for high-voltage switchgear with semiconductor devices. A more advanced version is a hybrid system with the current-carrying contact being shunted by thyristors. However, the relatively low voltage and current characteristics of thyristors constrain their use in such circuit breakers.

REFERENCES

7.1 V. A. Vozdvizhenskii: *Elektrichestvo* No. 1, 83-85 (1977).

7.2 V.A. Vozdvizhenskii and V. B. Kozlov: *Elektrichestvo* No. 6, 57-63 (1973).

7.3 I. A. Lukatskaya, S. I. Voskresenskii, and N. N. Ketsaris: *Elektrichestvo* No. 6, 64-68 (1973).

7.4 A. A. Chunikhin and B. Karekar: *Elektrichestvo* No. 7, 60-64 (1969).

7.5 I. N. Ulissova: *Vakuumnye kommutatsionnye apparaty za rubezhom* (Vacuum switchgear. Foreign technology review). Informelektro, Moscow 1983.

8
ISOLATING, EARTHING, AND LOAD SWITCHES

8.1 General Requirements

An isolating switch is used for making and breaking electric circuits under the conditions where its contacts do not experience a long open arc-discharge. The separation of isolator contacts is visible from outside. The isolating (disconnecting) switch is not equipped with an interrupter. The arc is extinguished as a result of its lengthening by the movable contact, thermal-flow action, or electromagnetic force action whereby the arc attains a critical length which is a function of the interrupted current and system voltage. Figure 8.1 illustrates the maximum reach of the arc at the isolator ends related to current at various voltage ratings. Relatively small currents are seen to produce arc reaches such that can cause the spread of the arc over the neighbouring phases and earthed parts giving rise to interphase short-circuit or earthing. Quite appropriately, therefore, the isolating switches are used to isolate dead segments of the circuit where the current has been interrupted by a circuit breaker. Also, under normal conditions, they switch a distribution system from one line tapping to another without having to interrupt the current, and switch very low magnetising currents of transformers and charging-cable currents [8.1].

On dead circuits, isolating switches are commonly used to provide safety conditions for maintenance or inspection of the switchgear. To prepare a segment of a distribution system, say a circuit breaker as in Fig. 8.2, for maintenance, it must be disconnected from the live segments of the system by disconnecting switches

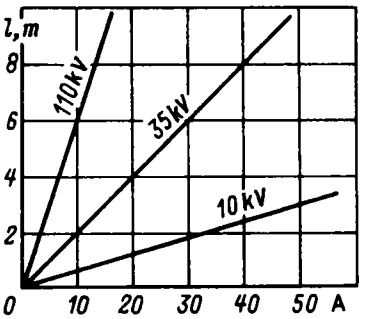

Fig. 8.1. Maximum reach of arc at the isolator contacts as a function of current and voltage

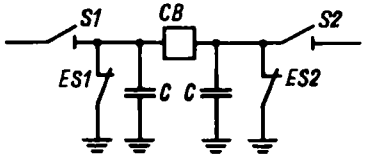

Fig. 8.2. Schematic of circuit isolation for circuit-breaker maintenance

S1 and *S2* after tripping the circuit breaker *CB*. The disconnecting switches interrupt a very small capacitive current due to the system voltage and the capacitance of the breaker and other equipment.

Once the disconnecting switches have been opened, the circuit breaker must be earthed by transportable earthing switches or additional earthing blades *ES1* and *ES2* integrated in the disconnecting switch.

In the open position of a disconnecting switch there is a visible air gap between the live parts and dead parts of the circuit.

In order to connect the system from one branch to another (Fig. 8.3) the disconnecting switch (1) is closed with the closed disconnector (2) allowing the current to pass through both branches, then the disconnector (2) opens diverting the current in the branch of disconnector (1). These switching operations do not normally lead to arc discharge at the contacts of disconnector (2) because of small voltage drops across the contact gap.

The principal requirements imposed on disconnecting switches are as follows:

(1) visible contact separation;

(2) thermal and mechanical ratings precluding the repulsion and welding of contacts and warranting the integrity and serviceability of disconnector parts at through fault currents;

(3) reliable insulation under continuous system voltage and under overvoltage in adverse atmospheric conditions;

(4) reliable make-break operations and latching of the movable contact under adverse operating conditions (for outdoor applications these include icing, strong wind, etc.);

(5) interlock of the disconnector with the circuit breaker preventing the disconnector operation at load.

Short-circuiting (earthing) switches and isolating switches are placed on the high-voltage side of less critical substations where circuit breakers are provided on

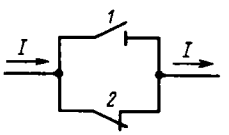

Fig. 8.3. Switching from one branch to another

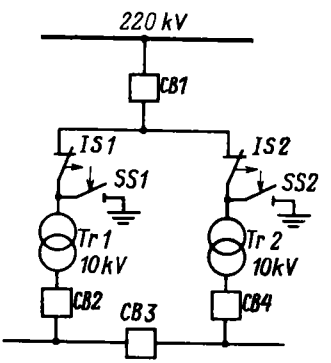

Fig. 8.4. Substation system with a circuit breaker on the feeder side and isolating and short-circuiting switches in the branches

the low-voltage side because of capital cost and space economy considerations. In case of a substation fault with a fault current insufficient to trip the relaying equipment protecting the feeder side, a short-circuiting switch, say *SS1* in Fig. 8.4, earthes the line and increases the short circuit current thus causing a reliable tripping of the protective relaying system and the discrimination of the fault by the circuit breaker *CB1* at the high voltage side. This interruption is followed by opening the circuit breaker *CB2* and isolating the switch *LS1*. Then the breaker *CB1* recloses and owing to the closed circuit breaker *CB3* the feed is restored for the equipment on the 10-kV buses of the first transformer group *Tr1*.

Short-circuiting and isolating switches must be high-speed devices to reduce the time of fault to a minimum. In addition a correct sequence of operations should be observed, so that the tripping of the isolating switch occurs only after the current in the short-circuiting switch has ceased, otherwise a situation can arise when fault current has to be cleared by the isolating switch.

8.2 Constructions of Discriminators

Classification of Soviet-made disconnecting switches by constructional and some other features may be found in Ref. [8.1]. According to the motion of the movable contact (blade) this classification discriminates between the switches with (1) the blade rotating in the vertical plane, (2) the blade rotating in the horizontal plane, (3) the blade rotating along with the support insulator in the vertical plane, (4) the support insulator and the movable contact fixed on it reciprocating (on rolls) relative to the stationary contact, (5) the rectilinear movement of the blade in the vertical plane along or across the axes of support insulators, (6) the blade folding in the vertical plane, (7) the blade and the support insulators holding it travelling in the vertical plane.

Other features of classification may be the type of installation, number of poles, method of control, and provision or absence of earthing blades.

Disconnecting switches for outdoor installation should reliably operate under any atmospheric conditions, including icing and severe wind loads. The thickness of admissible ice cover may reach 20 mm, and wind velocity up to 15 m/s. In the absence of icing the admissible wind velocities are as high as 40 m/s.

Electrodynamic forces arising in current-carrying parts and contacts can cause considerable mechanical loads on insulators under short-circuit conditions. The insulators of outdoor isolating switches can be loaded by wind and cable tension. The switches for such installations should possess a certain margin of mechanical strength, the safety factor should be at least 1.5 for 35-kV switches for outdoor installation and indoor switches, and at least 2.5 for insulators of outdoor isolating switches for 35 kV and higher. The safety margin is taken as the ratio of the ultimate static load for the insulator to the largest sum of loads (assuming they are applied simultaneously) due to electrodynamic forces, drive, cable tension, and wind.

The mechanical endurance of an isolating switch in general is defined by the number of operations it can withstand without damage preventing its further use. For voltage ratings up to 35 kV and rated currents up to 6300 A, the number of mechanical operations should be at least 2000, and for higher ratings at least 1000.

Earthing blades can be attached to the switch structure at one side or on either side. The blades earth the cables and buses connected to the isolating switch.

Earthing blades and other parts of the earthing circuit of a disconnecting switch should withstand the maximum let-through current and thermal withstand rating specified for the main-contact system of the disconnector. Admissible structural defects include welding of contacts and other malfunctions which do not break the earthing circuit and do not interfere with opening of the circuit by the earthing-blade drive. The cross section of flexible copper connectors between the blade shaft and the disconnector frame should be at least 50 mm^2.

The movable parts of the main and earthing contact systems should be interlocked (mechanically, as a rule) so that on making the main contact system no closing of the earthing contact system would be possible and vice versa.

Type RVO single-pole indoor disconnecting switches (Fig. 8.5) comprises a base (1), support insulators (2), and a current buswork. The base in the form of a channel carries small insulators and disconnector fixtures.

The current buswork is formed by two identical fixed contacts (3) and (4) and the movable blade (5) connecting them. In the closed position the blade is latched by a special latch precluding a spontaneous opening of the blade under the action of gravity and electrodynamic forces. The latch has an eye (6) which receives a finger of the operating rod in making and breaking of the switch. The blade rotates through 75° and is withheld in the open position by the weight and contact friction. In order to use this action appropriately this type of disconnecting switch is installed vertically so that the blade axis of rotation is at the bottom.

Type RV three-pole disconnecting switches for indoor use (Fig. 8.6) comprise three current terminals (1) mounted on the same frame (2) with a common shaft and driving rod. Each pole has two support insulators (4) and a porcelain lever (5) connected to the common shaft. Blades (6) are actuated by the lever (3).

Isolating switches with earthing blades have one or two shafts connected to the

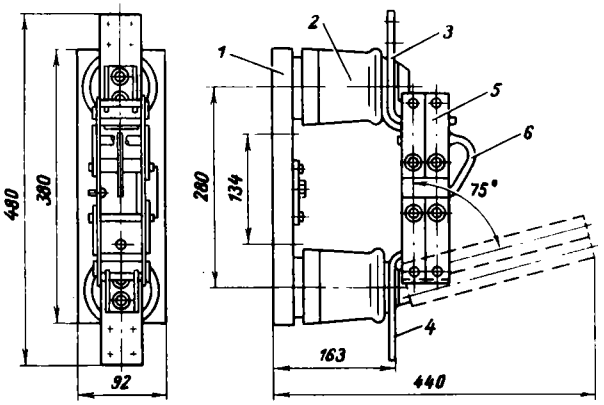

Fig. 8.5. Type RVO-10/1000 single-pole disconnecting switch for indoor application

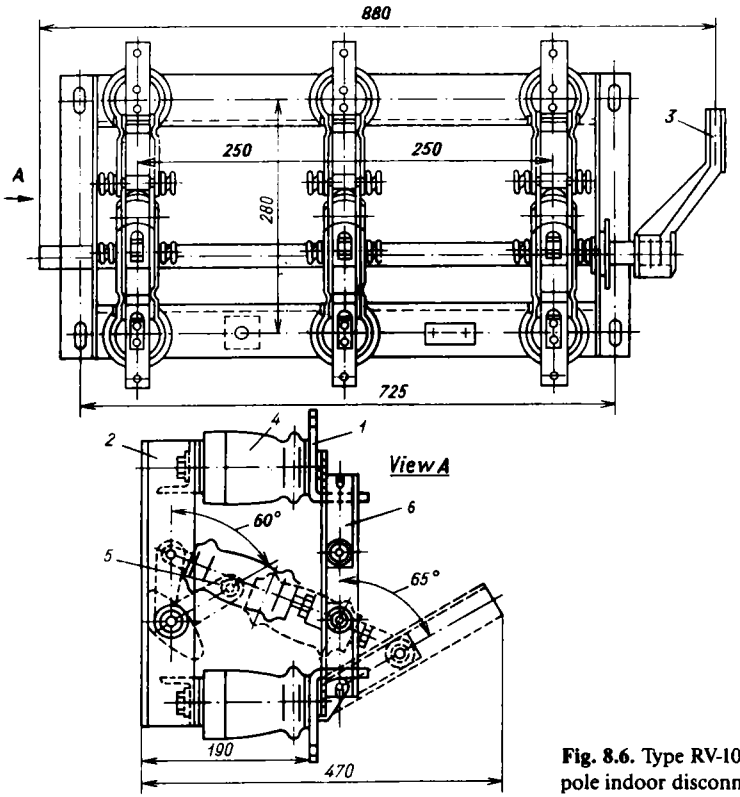

Fig. 8.6. Type RV-10/1000 three-pole indoor disconnector

frame. Earthing blades close additional earthing contacts fixed beneath the main stationary contacts. This type of disconnectors is also manufactured with through insulators in place of support insulators for the same ratings.

Disconnectors for rated currents in excess of 1000 A are commonly made as pole modules assembled in a two-pole or three-pole installation. Type RVR isolating switches are designed for rated currents up to 8000 A. Stationary contacts of such a disconnector consist of two channel-shaped parts and the contact blades are copper box sections placed pairwise in a two-layer arrangement as shown in Fig. 8.7.

The 12 500 A rating is served by type RVP disconnecting switches with translational movement of the contact blades. These units offer small torque at the shaft owing to a cam system connected with the movable blade. This system acts to remove the contact pressure before the blade starts moving in opening and applies this pressure after the blade terminates motion in making (Fig. 8.8).

Isolators for outdoor installation (type RND) close or disconnect a pole by giving rotational motion to either one or both insulators (connected by ties) carrying contact blades. Isolators of this type (Fig. 8.9) are assembled on site of one driving

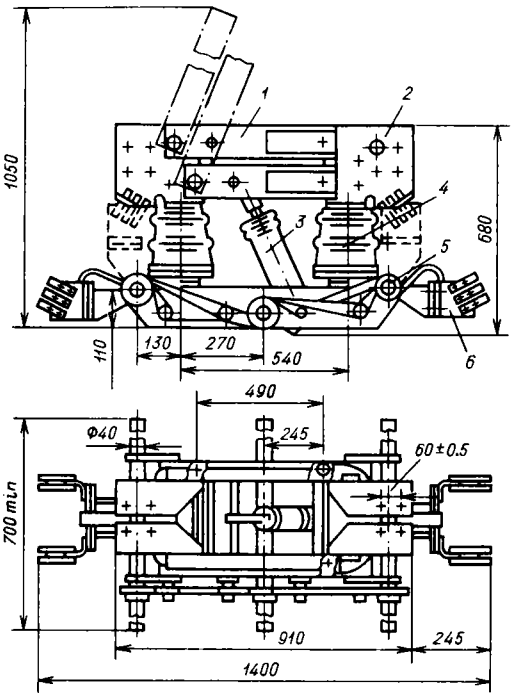

Fig. 8.7. Type RVR indoor disconnecting switch: (1) movable contact blades, (2) stationary contact, (3) porcelain rod, (4) base insulator, (5) frame, (6) earthing blades

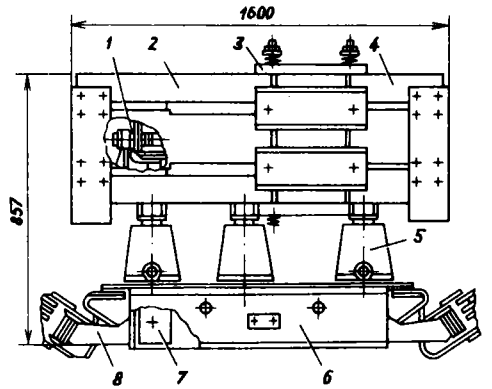

Fig. 8.8. Type RVPZ-20/12500 indoor disconnecting switch: (1) reductors, (2) and (4) stationary contacts, (3) movable contact blades, (5) base insulators, (6) frame, (7) hinge, (8) earthing blades

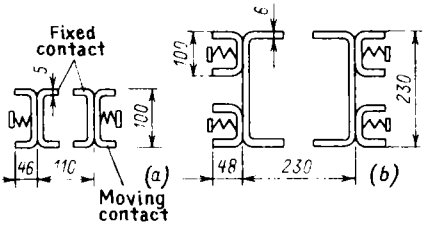

Fig. 8.11. Basic dimensions (in mm) of the contact system for type RVR and RVK disconnectors: (*a*) for 3200 A, (*b*) for 6300 A

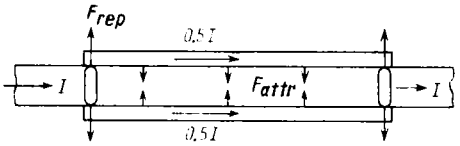

Fig. 8.12. Electrodynamic forces in the current-carrying circuit

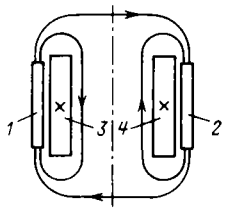

Fig. 8.13. Electromagnetic lock

heated in the contacts flows by pipes, embedded in contacts and other cooled parts, to a radiator placed above the isolator. The heated liquid extends and ascends in the radiator by the ascending pipe and after cooling descends by the descending pipe in the isolator.

Research is under way to replace silver with other contact materials, specifically, composite materials in the form of fabric impregnated by liquid metal filler.

The mechanical withstand capability of contacts with load current can be achieved by employing current carrying systems where the electrodynamic forces of attraction, F_{attr}, arising in the circuit are exploited to compensate completely, or partly, the electrodynamic repulsive forces at the point of contact (Fig. 8.12). This effect is amplified with the use of so-called magnetic locks the idea of which is illustrated in Fig. 8.13. The magnetic lock constitutes ferromagnetic elements (1) and (2) placed near current-carrying parts (3) and (4). Short circuit currents magnetise these elements and cause them to attract each other creating additional mechanical force in the contacts.

Ferromagnetic parts incur heat losses due to reversal of magnetisation and eddy currents rendering magnetic locks not always desirable. These locks, however, may be used to advantage in contact systems of earthing blades designed for left-through current duty and where continuous currents are not anticipated.

In isolating switches with lever-actuated drive mechanism, the mechanism is driven beyond the dead point in the closed position, therefore, the electrodynamic forces arising in short circuit cannot produce a spontaneous tripping and separation of the blade.

8.3 Isolators and Earthing Switches

Short circuiting switches are three-pole or single-pole switchgear with an earthing blade rotating in the vertical plane. The earthing switch in Fig. 8.14 comprises a base, insulating column, stationary contact with a terminal for line connection and an earthing blade of ribbed aluminium pipe with a removable contact plate at the end.

The base (4) supports on bearings a shaft (6), two adjustable closing springs connected with the base and levers of the switch shaft, and a hydraulic buffer for deceleration of the movable parts in the closing operation.

In its normal open position the blade (3) is removed from the stationary contact to the left for a sufficient insulation distance and the closing springs are charged. This position of the blade is locked by the drive. When the closing signal arrives

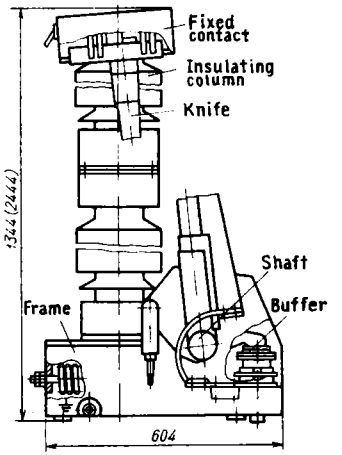

Fig. 8.14. Type KZ-110U short-circuiting switch

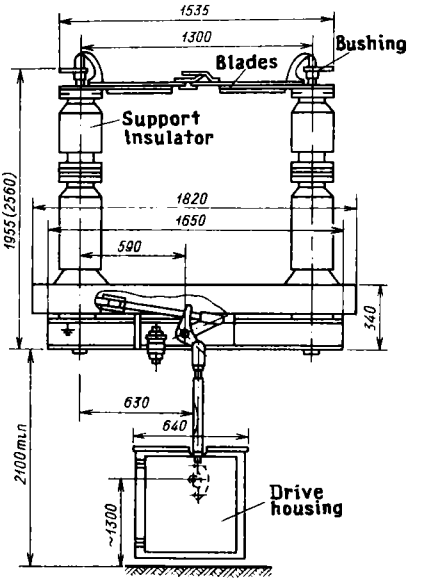

Fig. 8.15. Type OD-110U/1000 isolator

at the drive, it releaves the blade (3) which is forced by the springs into the stationary contact (1) causing a short circuit.

Isolators of the type shown in Fig. 8.15 are single-pole switches with two rotating support insulators (1) whose upper flanges carry contact blades and contact terminals (4). Blades (2) rotate in the horizontal plane through 90°. Three poles for 35 and 110 kV are assembled into one installation and controlled by one drive (3). Each 150-kV and 220-kV pole is controlled by an individual drive. The isolator is opened by springs charged in the closing operation. Hydraulic buffers with variable section of the oil-passage are provided for smooth deceleration of the movable parts. The base and contacts are protected by enclosures from rain and icing.

The make time of the isolator depends on the rating and under unfavourable operating conditions amounts to 0.2-0.35 s, and the break time equals 0.5 s.

The next step in the structural improvement of isolators and short-circuiting switches can be the use of devices with a shortened travel of contacts, for example SF_6 or vacuum units, and consequently, having higher speeds and better protection from environmental impacts.

8.4 Load Switches

Modern distribution switchgear are quite costly installations because of expensive components, that is a circuit breaker proper and the elements of relaying protective system such as current transformers, relays, and battery facilities. In systems with small rated currents, however, the circuit breaker with protective relaying may be displaced by a load switch and a fuse system. The load switch is normally designed for interruption of load current or a somewhat higher rated current. It does not interrupt short circuit currents, but in versions equipped with all types of drives except manual its making current capability should not be inferior to the respective mechanical rating at let-through short circuit currents. In an event of a short circuit, the short circuit current is interrupted by a high-voltage fuse placed in series with the switch.

Until recently the main type of equipment in this range of current has been the puffer-type load switch (Fig. 8.16) harnessing the principle of arc extinction by a blast of gases formed in arc interaction with the walls of the extinction chamber made of some gas-generating material such as acrylic plastic or rigid PVC. The switch comprises a system of main contacts and an arcing contact travelling into the duct of the arc extinction chamber. In circuit interruption, the main contacts part first followed by the arcing contacts. An intensive blast of gas through the narrow duct of the extinction chamber facilitates extinction of arc currents in the range 200-400 A.

In the open position a visible break of contacts renders this device with the properties of isolator in addition to its breaking facility.

The admissible number of make-break operations is defined by the wear of inserts and arcing contacts. In 10-kV systems such a load switch is capable of 75 interruptions of 200-A current, and only 3 interruptions of 400-A current.

The moderate reliability of the puffer type load switches, low number of rated-current interruptions tolerable, and limited making and mechanical ratings at let-

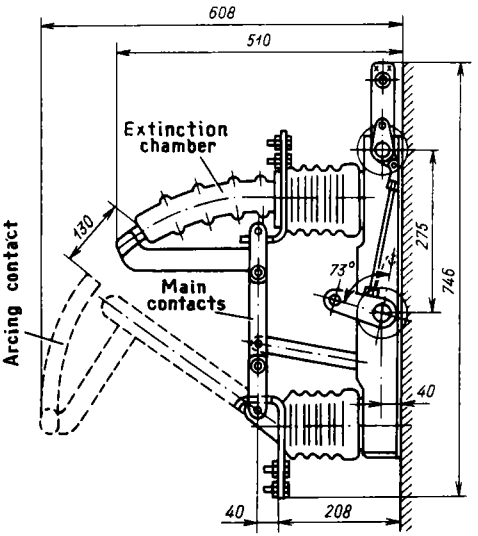

Fig. 8.16. Type VN-11 puffer load switch

through short-circuit currents have motivated development programmes aimed at new types of this equipment.

One of the recent designs is a magnetic air load switch (Fig. 8.17*a*) designed for interruption of currents of 630 and 400 A at 6 and 10 kV.

The maximum breaking currents exceed the nominal rating by about 1.5 times. Thus the maximum let-through current is 51-kA crest with 20-kA periodic component in terms of r.m.s. The switches are manually-charged spring-actuated devices with remote control facility.

Three poles of the switch are mounted on a steel frame (1). Porcelain insulators (2) carry the main stationary contact (3) and the blade of the main movable contact seen beneath the extinction chamber (5). The arc chute of this chamber (Fig. 8.17*b*) is formed by two insulating walls (6) with two flat slabs (7) of arc resistant cordierite ceramic in between. The slabs are separated by a thin fibre toothed gasket (8) providing separations in the arc chute. The copper electrode (11) is connected to the stationary arcing contact (9) fixed at the back wall (10) of the chamber. The magnetic blowout system is a U-shaped electromagnet with a coil (12) placed in the central cylindrical piece of the core (13). The core passes through the chute walls and pole pieces (14) of sheet steel embracing the chute from both sides. The coil is connected between the main stationary contact (3) and an arcing contact (9) insulated from each other.

The movable contacts (4) are made as blades. The blade shaft (15) also carries light movable arcing contacts (16) with accelerating springs (17). The movable contacts are actuated from the common shaft (18) through insulating rods (19). The switch is equipped with earthing contacts (20).

In circuit interruption the main contacts part first and the current passes

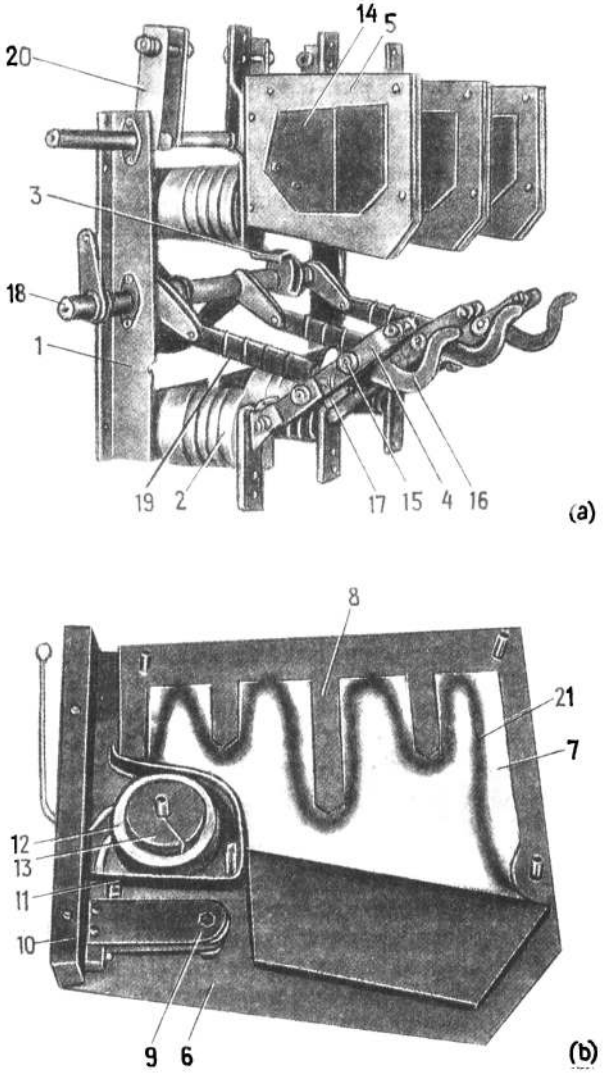

Fig. 8.17. Magnetic air load switch

through the arcing contacts and the blowout coil. At a certain distance between the main contacts, the movable arcing contact is pulled out of the stationary contact at a high speed. The arc formed in the arc chute is extended by magnetic action in view of separating elements, the arc resistance increases and attains a critical

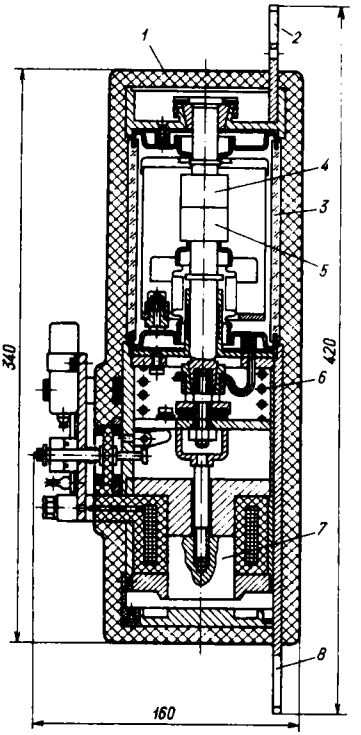

Fig. 8.18. Type VNVL-10/400 vacuum load switch

value. The arc extinguishes itself at a current zero. The arcing time in such a type of switch is not more than 20 ms for currents in excess of 50 A. The contact wear is insignificant in such a switch, for in an opening operation the arc base moves over the arc runner (11) and the arcing contact (16). The arc path (21) is clearly seen in Fig. 8.16*b*. In the open state the switch has a clearly visible contact separation. High mechanical and electrical endurance and small size make this switch an attractive proposition in the role of a load switch.

Figure 8.18 shows the type VNVL-10/400 vacuum-bottle switch in a molded case for 10 kV and rated current of 400 A. The molded case (1) encloses current carrying buses (2) and (8) and a vacuum interrupting unit (3) with solid butt contacts (4) and (5). Breaking occurs by the action of interrupting spring (6) that is charged by an electromagnet (7) during the closing operation.

REFERENCES

8.1 V. V. Afanasyev and E. N. Yakunin: *Razyediniteli* (Isolators) Energiya, Leningrad 1979.

8.2 V. A. Yevtushenko and A. A. Chunikhin: *Podvesnye razyediniteli* (Suspended disconnecting switches). Energoatomizdat, Moscow 1984.

9
HIGH-VOLTAGE FUSEGEAR

9.1 Protective Characteristics

The high-voltage fuses are far less common than their low voltage counterparts, being mainly used for protection of power transformers, overhead and cable lines, capacitors, electric motors, and voltage transformers.

Soviet protection practice categorises H.V. fuses by the construction features and performance characteristics. Distinction is made between fuses that limit current during the interruption process and those which do not. By the method of arc extinction H.V. fuses are divided into those exploiting the contact with a fine-grained heat-dissipating material that fills the fuse container and those quenching the arc with the aid of a jet of vapour originating from the arc action and, possibly, also from a volatile solid that vapourises under the heat of arc (expulsion principle fuse).

High-voltage fuses for use on distribution systems have two distinct classes defined with the concepts of one-hour fusing current and rated breaking current (interrupting rating or rupturing capacity). The 1-h fusing current, as the name implies, melts the fusible element in one hour. The interrupting rating of a fuse is the highest r.m.s. symmetric alternating current (at the arc-striking, current cutoff instant) that the fuse can interrupt at full rated voltage of the protected circuit.

(i) Class 1 comprising the full range or general purpose fuses which interrupt currents ranging from 1-h fusing current up to the rupturing capacity.

(ii) Class 2 comprising the backup current-limiting fuses. These are devices which have a definite minimum interrupting rating (exceeding 1-h rating) and require other protective devices in electrical series (switch-fuse units) to protect them from currents below their minimum interrupting rating.

The current-limiting fuses cover the range of system voltage from 3 to 35 kV, and the non-current-limiting operate at 6-220 kV. The respective ranges of rated currents are 2-1000 A and 2-200 A, and the ranges of rupturing capacity are 2.5-63 kA and 1.6-20 kA. For some fuses manufacturers also give the rated currents of constructional elements such as base, fuse-refill holder, and container.

The performance of a fuse is described by the time-current characteristic (Fig. 9.1) which shows the minimum time to melt as a function of r.m.s. current level. As a rule manufacturers plot the characteristics for one type of fuse covering the entire range of ampere ratings with curves for different fusible inserts so that the user can readily identify the suitable fuse for a particular circuit. From Fig. 9.1 it can be seen that the fuse provides a reliable protection at high overloads whereas at low currents its protective functions are much weaker. The upper sections of the plots indicate that with small variations in overload, say from two to three continuous current ratings, the time to melt the fusible insert can be varied in a wide

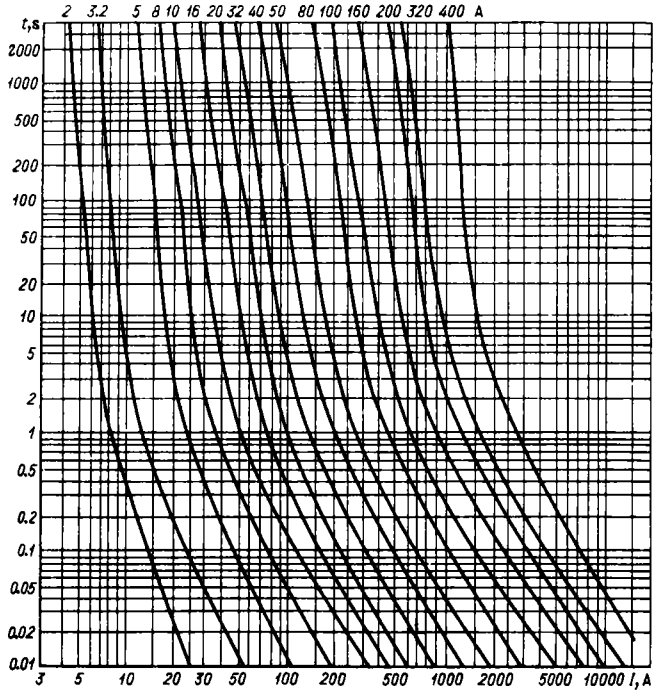

Fig. 9.1. Minimum melt time-current characteristics of type PK1-PK4, PKE1 fuses

range from one hour to 10 seconds. Some instability of this characteristic in the range of small overloads is admissible. For example, one-hour fusing current should be within 1.3-2 continuous current ratings.

Another valuable characteristic is the maximum arcing time. Figure 9.2 shows the arcing time of type PK and PKE fuses as a function of the periodic component of prospective current (r.m.s.) at arc incipience, i.e. cutoff current, in terms of rated current I_r. For overloads in excess of 100 p.u. values, arcing times should be within 10 ms for fuses filled with quartz sand (see Fig. 9.6) and 50-80 ms for expulsion fuses (see Fig. 9.7). The total time of fuse operation (clearing time) is measured as the melting (pre-arcing) time plus arcing time.

The ability of a fuse to withstand overloads at let-through currents and multiple pulses of such currents can be determined from the time-current characteristic of maximum overloads which is constructed on the base of the minimum melting time-current characteristic in the time interval 0.01-90 s with a factor k determined by preliminary tests (Fig. 9.3).

The fuse should interrupt all the range of currents at the maximum system voltage, that is, from one-hour fusing current for Class-1 general-purpose fuses, or from minimum interrupting current for Class-2 backup fuses, up to rated interrupt-

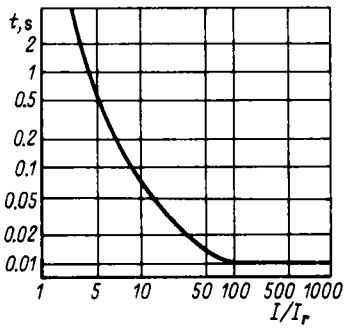

Fig. 9.2. Maximum arcing time versus overload for type PK1-PK4, PKE1-PKE3 fuses

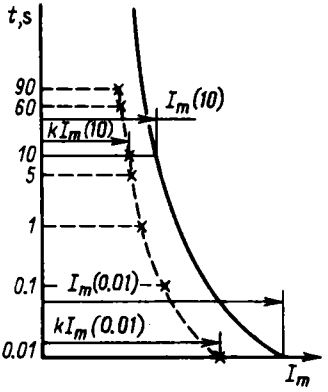

Fig. 9.3. Construction of a time-current characteristic of maximum allowable overload (*dashed line*) by the minimum melting time-current characteristic (*solid line*). $I_m(10)$ and $I_m(0.01)$ are fusing currents of 10-s and 0.01-s times to melt respectively

ing current. This should be true for any point of the short-circuit current waveform with respect to voltage zero. At prospective rated interruption current, the transient recovery voltage induced by the fuse should not exceed the specified voltage-time curve. The slope of this boundary curve defines the rate of rise of the recovery voltage. Table 9.1 summarises the key points of this curve for current-limiting and non-current-limiting fuses.

The effect of current limitation by a fuse owes its existence to the high resistance of the fuse arc. High current melts and vaporises the thin wire of the fusible element practically over the entire length in a matter of microseconds. High pressure generated in the arc channel assists the subsequent deionization processes causing the arc resistance to rise sharply thus limiting current and cutting it off to zero — until a natural current-zero crossing. The e.m.f. of self-induction induced at the current cutoff overlaps the system voltage and brings about switching overvoltages. Special

Table 9.1. Maximum Admissible Rate of Rise of the Recovery Voltage, kV/μs, for Normal Fuse Operation

Fuse type	Rated voltage, kV								
	3	6	10	15	20	35	110	150	220
Current limiting	0.31	0.35	0.41	0.50	0.55	0.70	—	—	—
Non-current-limiting	0.16	0.18	0.21	0.25	0.28	0.35	0.52	0.56	0.62

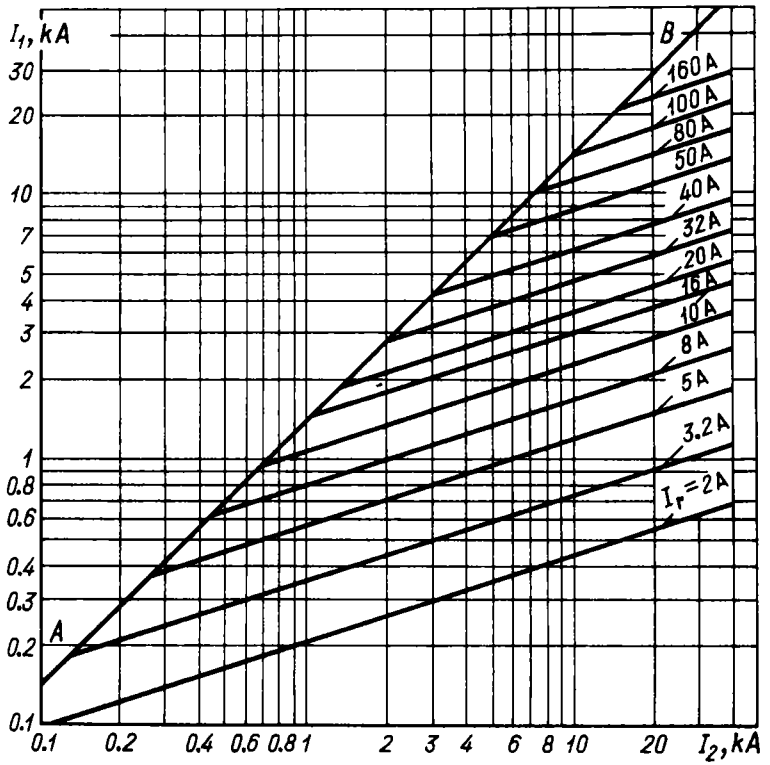

Fig. 9.4. Relation between the cutoff value and prospective values of current for a typical range of medium-rupturing-capacity type PK1-PK4, PKE1-PKE3 fuses. *AB* represents the boundary of the current-limiting effect

features of design are used to limit overvoltages across the fuse to within the following admissible bounds

System voltage, kV	3	6	10	20	35
Max. admissible overvoltage, peak kV	12	23	38	75	126

The current limiting characteristics of fusegear are expressed as the dependence of the momentary peak current on the r.m.s. prospective symmetric current, Fig. 9.4. The prospective short-circuit current is the one flowing until the fusible element starts melting. The characteristics are plotted for various fuse ampere ratings. The current limitation effect occurs beginning with certain values of interrupted current depending on the fusible insert rating. In terms of the fuse rating this effect should be effective at p.u. values of prospective symmetric current at most 40.

9.2 Construction of Fusegear

The quartz-filled fuse for 3-35 kV, shown in Fig. 9.5*a*, consists of two support insulators (3) which carry contacts (2) and the cartridge (1) inserted in the contact ferrules. The cartridge, shown in Fig. 9.5*b*, is a porcelain tube (5) with the contact ferrules (8) attached to it on either end. Depending on rated current the fusible insert (6) consists of one or a few silvered copper conductors.

Fusible elements of variable cross section are employed for switching overvoltage limitation. To interrupt overload currents tin spheres are soldered over thin sections of the fusible element. These attachments reduce the melting point of the element from 1080 °C for copper to a temperature somewhat above the melting temperature of tin (230 °C) owing to the dissolution of copper in the tin. After the copper wire has melted under a tin sphere an arc forms which melts the wire over the entire length.

Quartz sand (7) filling the porcelain envelope (5) is charged through an opening which is then covered by a cap (9) brazed over the ferrule (8). The bottom cap

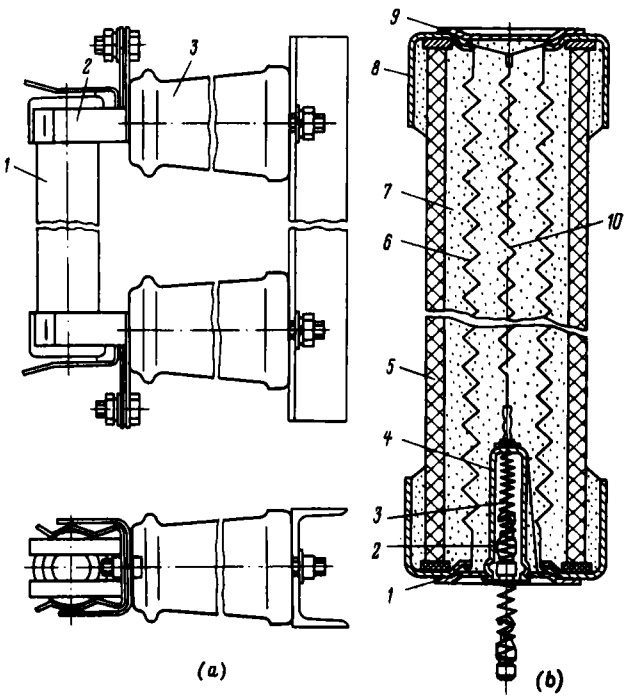

Fig. 9.5. (*a*) Outline of a quartz-filled fuse. (*b*) Sectional view of the fuse refill showing construction details

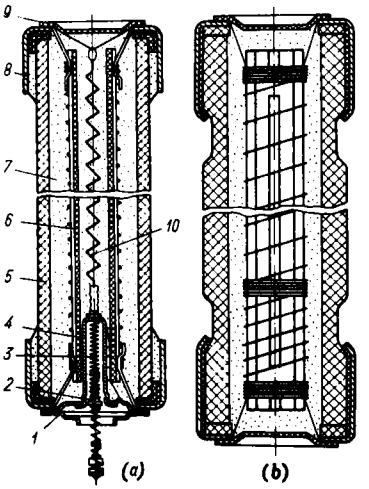

Fig. 9.6. Sectional views of fuse refills (*a*) with a ceramic core former, and (*b*) for voltage transformer protection. (1, 9) Discs, (2) operation indicator, (3, 4) indicator spring and body, (5) insulating container, (6) ceramic former, (7) sand, (8) contact ferrule, (10) indicator fusible insert

(1) holds an indicator (2) to show that the fuse has operated. The fusible element keeps the spring (3) compressed in the holder (4). When the main fusible elements (6) blow, the fusible insert (10) also burns away, thus releasing the spring which pushes the indicator outside. In fuses subjected to vibrations and shocks and also in fuses for small rated current (up to 8 A) and rated voltages of 20 and 35 kV, the fusible element is wound on a ribbed ceramic former (Fig. 9.6*a*). This construction increases the length of fusible insert and enhances the current limiting effect. However, at small overloads the heating current may cause a conducting channel to appear on the former surface and lead to thermal failure of the fuse.

Soviet type PKTN fuses have been developed for voltage transformer protection. The container of this fuse, shown in Fig. 9.6*b*, is not equipped with an operation indicator. The fusible element is a constantan wire of three different sections wound on a ceramic former. The low current rating of such fusible inserts allows for very thin wire with a considerable current-limiting effect. As a result, this type of fuse offers unlimiting rupturing capacity and clears short-circuit faults in a matter of 0.1-1 ms.

Quartz sand used to fill the fuse body has a high heat absorbing capacity under normal conditions. The intense heat abstraction from the fusible element enables thinner insert wires to be used. The sand is also an effective vehicle of heat abstraction from the arc. However, water inside the fuse can impair the arc quenching properties of the quartz sand. Therefore, adequate attention should be paid to the fuse sealing technology.

Quartz-filled fuses for system voltage in excess of 35 kV have not been developed

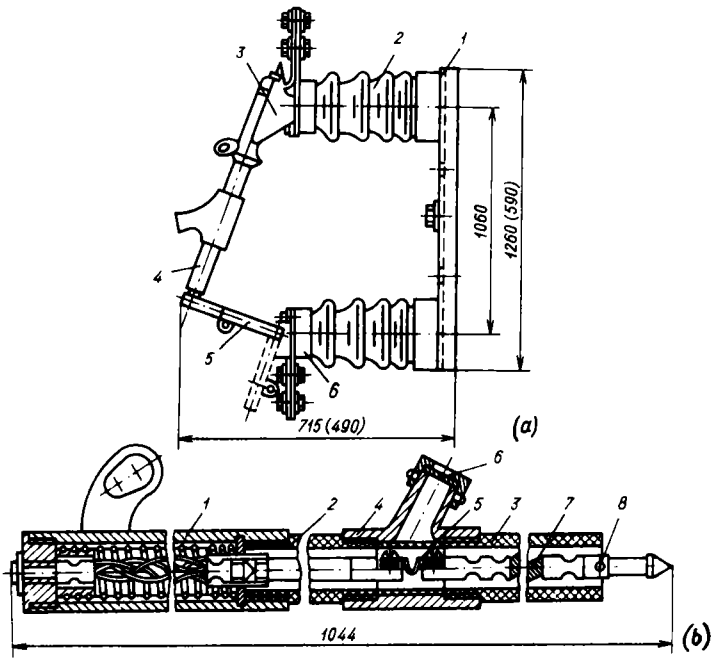

Fig. 9.7. (*a*) Outline of type PSN-35 expulsion-fuse cutout (dimensions in mm). (*b*) Sectional view of the fuse cartridge showing construction details

because of high size requirements due to the need for arc extinction at high rates of voltage recovery.

At 35 kV and higher outdoor protection needs are satisfied by expulsion fuses. This type of fuse also covers the 10-kV rating. Figure 9.7*a* shows an open-type cutout consisting of a base (1) carrying base insulators (2) with the upper (3) and lower (6) contact heads that connect the fuse to the circuit. The lower head (6) carries a contact blade (5) linked to the fuse ferrule (4) and held in the closed position by a spring.

Figure 9.7*b* shows the longitudinal section through the fuse cartridge (1). The cartridge is constituted by tubes (2) and (3) of rigid PVC connected by a steel body (4) with a safety valve (6). The flexible cable (7) with a striker pin (8) is kept within the body by the spring of the contact blade. It is tensioned by the left-hand spring and locked with the aid of the fuse link (5). When the fuse link blows, the contact blade tripped by the striker pin is released and being forced by the spring moves to the open position pulling the flexible cable behind. The cable motion is accelerated by the gases generated by the decomposition of the PVC tube with the arc action. The arc elongates as the cable moves away and is extinguished by the gas flow from the tube opening. After the arc has been quenched, the blade and the bottom contact

ferrule find themselves separated by an arc spacing sufficient to maintain the desirable level of insulation for the discriminated circuit.

Arcing times in such type of fusegear are essentially dependent on the magnitude of interrupted current, rising from 40 ms at high currents of 3-5 kA (for the expulsion type fuse) to 300 ms at hundreds of amperes. The fuse link is made of a Ni-Cr-alloy wire and copper wires or ribbons in number and section determined by current rating.

9.3 Parameter Selection and Design

The fuse designer has to solve a number of coupled problems aimed at securing reliable operation at all feasible duties. The fusible element is selected such that the fuse could pass rated current without ageing effects. The fusible element should melt within a specified time under the specified overloads and should not at switching transients which occur, for example, in switching power and voltage transformers and in starting electric motors when inrush currents reach 8-10 current ratings. Arcing times at short circuit currents should be small enough with no way for considerable overvoltages. The selectivity of discrimination should be also ensured.

Notwithstanding numerous research efforts [9.1] no practically suitable design procedures have been resulted for fusible link section, length, constructional parameters and relevant arc control devices. The continuous heating of a fusible element of variable cross section with allowance for the M-effect (addition of a fusible metal on the base element metal) is a most formidable problem. Under the circumstances the research and development data verified by successive testing and performance histories may come in handy.

By way of example, for a copper wire in quartz-sand-filled containers it has been established that the reliable-arc-extinction length should not be less than $l = 0.16 + 0.07U_r$ metres, where the rated fuse voltage U_r is in kV. The minimum melting current for such wire may be estimated by the expression $I_{min} = 78d^{1.2}$, where d is the wire diameter in mm selected between 0.1 and 1.5 mm.

Given a fault current density J [A/mm^2] in the fusible element when the process of heating is almost adiabatic, the time to melt may be calculated as $t_m = (A_1 + A_2)/J^2$, where A_1 is the energy expended to raise the fusible insert to melting temperature and A_2 is the energy expended for the melting proper. For copper element, $A_1 + A_2 = 91\,600\ \mathrm{A^2\,s\,mm^{-4}}$. This formula gives somewhat overestimated times to melt as it fails to take into account that the element breaks at the neckings before it is melted over the entire length.

Fusegear for protection of equipment, overhead and cable lines should be selected in manufacturers lists by the given principal parameters and characteristics, such as time-current characteristics of melting, interrupting, and admissible overloads.

REFERENCES

9.1 K. K. Namitokov, R. S. Khmelnitskii, and K. N. Anikeyeva: *Plavkiye predokhraniteli* (Fusegear). Energiya, Moscow 1979.

10
CURRENT TRANSFORMERS

10.1 General

Current transformers are used to insulate measuring and control devices connected in the secondary circuit from the operating voltages of the primary circuit. The normal secondary ratings for these devices are 5 A and 1 A. Current transformers transform the primary current to values suitable for standard ratings for instruments, meters, relays, and control devices. The electromagnetic current transformers (c.t.) are more commom of all available types [10.1, 10.13, 10.14]. This type of transformer comprises a magnetic circuit carrying primary and secondary windings.

Connection of the current transformer is illustrated in Fig. 10.1. The primary current is independent of whether the secondary circuit is open or short circuited. It is governed by the primary load impedance Z_1 which is several orders of magnitude higher than the input impedance of the transformer referred to the primary side at any value of impedance Z_2. No fuse is placed in the secondary circuit of the transformer because a disconnection of this circuit is a fault duty for the current transformer (see Sect. 10.3).

Equivalent circuit. Analysis of current transformer operation will be neater if we replace the scheme of Fig. 10.2*a* showing the magnetically coupled windings with the equivalent circuit of Fig. 10.2*b* in which these windings are connected electrically. The equivalent circuit parameters can be derived with the turn ratio w_2 / w_1 [10.1]. It is usual to refer the c.t. parameters to the secondary side. The secondary inductive reactance of the equivalent circuit is

$$x_{2s} = x_2 = x_{22} - x_{21}\, w_2 / w_1$$
$$= \omega (L_{22} - L_{21}\, w_2 / w_1)$$

where L_{22} is the secondary inductance and L_{21} is the mutual inductance.

The inductance L_{22} can be determined by impressing a voltage U_2 across the secondary terminals with the primary being open circuited. The impedance of the secondary winding with the open-circuited primary is

$$Z_{22} = U_2 / I_2$$

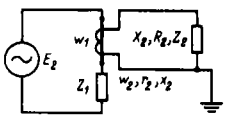

Fig. 10.1. Connection diagram of a current transformer

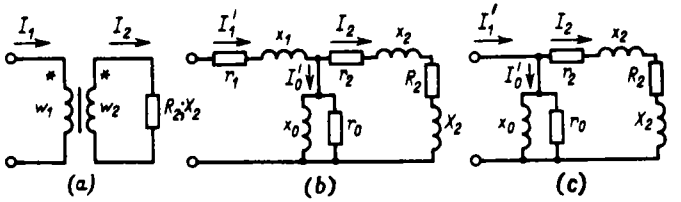

Fig. 10.2. Equivalent circuit of a current transformer

The inductance of the secondary winding is

$$L_{22} = x_{22} / \omega = \sqrt{Z_{22}^2 - r_2^2} / \omega$$

The values of U_2, I_2, and r_2 are readily measured. The mutual inductance L_{21} can be inferred from the e.m.f. E_2 measured across the terminals of the open secondary while having a current passing through the primary when

$$L_{21} = \Psi_{12} / \hat{I}_1 = w_2 \Phi_m / \hat{I}_1 = E_2 / 4.44 f \hat{I}_1$$

It is worth noting that $x_{2s} = \omega L_{2s}$ is a calculated value in the equivalent circuit. For some c.t. parameters $L_{22} < L_{21} w_2 / w_1$ and the inductive reactance x_{2s} is negative. This by no means implies that the secondary winding does have a negative reactance. The latter exists in the equivalent circuit only. The equivalent circuit is just a convenient tool of c.t. analysis in the steady state and transition modes of operation.

Because the existing primary current is governed by the primary impedance Z_1 and is independent of the c.t. parameters, for many applications the primary parameters in the equivalent circuit may be neglected. This leads to the equivalent circuit of Fig. 10.2*c* where x_0 is the inductive reactance of the core, r_0 is the resistance of the magnetising branch defined by the ohmic losses in the core, r_2 is the secondary resistance, and R_2 and X_2 are the resistance and inductive reactance of the load.

Phasor diagram. The phasor diagram of the current transformer is represented in Fig. 10.3. The secondary current I_2 is in phase with the secondary m.m.f. $I_2 w_2$. The secondary current passing through the load $Z_2 = R_2 + jX_2$ causes the voltage drop U_2. Another voltage drop in the secondary is due to its reactance $r_2 + jx_2$. The sum of these drops equals to the e.m.f. E_2. By convention the positive directions of the primary and secondary currents are those shown in Fig. 10.2*a*, that is, when the primary current flows into the marked terminal of the primary winding, the positive I_2 flows out of the marker into the load. This implies that both windings are wound in the same sense.

By Ampere's circuital law (phasors)

$$I_1 w_1 - I_2 w_2 = I_0 w_1 \tag{10.1}$$

where I_0 is the magnetising current referred to the primary side.

For the ideal current transformer, $I_0 = 0$, then

$$I_1 w_1 = I_2 w_2$$

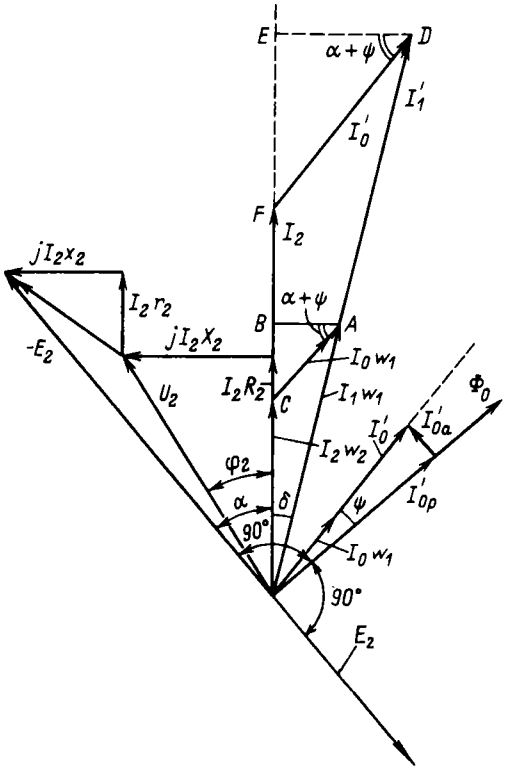

Fig. 10.3. Phasor diagram of a current transformer

Referring the current to the secondary side yields

$$I_1' = I_1 w_1 / w_2 = I_2$$

Therefore I_1' and I_2 must have the same phase in the phasor diagram of the ideal current transformer. The actual current transformer has a phase-angle error δ measured as the angle of lead (positive) of the current I_2 leaving the marked secondary terminal over the current entering the marked primary terminal I_1'. The e.m.f. E_2 induced by the flux Φ_0 lags behind this flux by 90° for the above direction of currents. To provide for the flux Φ_0, i. e. to keep the e.m.f. E_2 at the rated level, the primary winding has to supply an m.m.f. $I_{0r} w_1$ to compensate for core losses (to overcome "active" magnetic resistance) and an e.m.f. $I_{0a} w_1$ to act against the reactive countervoltage, i.e. against the reactive magnetic resistance.

The resultant e.m.f. producing the flux Φ_0 is $I_0 w_1$. In view of Eq. (10.1) and with account of $I_1' = I_2$, we may write

$$I_1' = I_0 + I_2$$

where $I_0' = I_0 w_1 / w_2$ and $I_1' = I_1 w_1 / w_2$ are the magnetising and primary currents referred to the secondary winding.

In the ideal current transformer $I_0' = 0$ and $I_1 / I_2 = w_2 / w_1$ or $I_2 = I_1 w_1 / w_2$, that is the secondary current is proportional to the primary current and there is no phase-angle or ratio error.

Denoting the rated currents of the current transformer by $I_{1,r}$ and $I_{2,r}$ and the inverse (name plate or rated) turn ratio $w_2 / w_1 = I_{1,r} / I_{2,r}$ by k_r, we get

$$I_1 = k_r I_2$$

$$I_1' = I_1 / k_r$$

Now, the per unit ratio error is [10.1]

$$\begin{aligned} \Delta I &= k_r (I_2 - I_1) / I_1 = (I_2 - I_1') / I_1' \\ &= -(I_1 w_1 - I_2 w_2) / I_1 w_1 \end{aligned} \tag{10.2}$$

When $I_0' = 0$, $I_1 w_1 - I_2 w_2 = 0$ and there is no error. Observing that the angle δ is small, the difference $I_1 w_1 - I_2 w_2$ may be approximately represented by the projection of the phasor $I_0 w_1$ upon the vertical axis, i. e. BC in Fig. 10.3. Thus, the current error is proportional to the segment BC. The errors, therefore, can be evaluated with reference to the triangle ABC [10.1]. The per cent ratio error is

$$\Delta I_{\%} = -I_0 w_1 \sin(\alpha + \psi) \times 100 / I_1 w_1 \tag{10.3}$$

The phase-angle error (minutes) is found as

$$\tan \delta \approx \delta = 3440 I_0 w_1 \cos(\alpha + \psi) / I_1 w_1 \tag{10.4}$$

where α is the angle which the secondary e.m.f. E_2 makes with the current I_2, and ψ is the angle of losses in the core equal to arctan I_{0a} / I_{0r}, I_{0a} and I_{0r} being the active and reactive components of the magnetising current.

In addition to the ratio and phase-angle error the relevant Soviet state standard contains the total error characterising the relative value of the magnetising current

$$\varepsilon_{\%} = \frac{100}{I_1} \left[\frac{1}{T} \int_0^T (k_r i_2 - i_1)^2 \, dt \right]^{1/2}$$

where T is the current period.

It is apparent that the ratio and phase-angle errors are smaller the less the magnetising current. For a magnetic circuit of length l and field strength H the magnetising current will be given as

$$Hl = I_0 w_1 \tag{10.5}$$

The secondary e.m.f. is induced by the flux Φ_0

$$E_2 = 4.44 f w_2 \Phi_0$$

Accordingly, the higher is the required e.m.f. E_2 the higher must be the flux Φ_0, which means higher H and m.m.f. $I_0 w_1$. To keep the ratio error as small as possible the secondary impedance should be small as this means lower e.m.f. requirement

$$E_2 = I_2 \sqrt{(R_2 + r_2)^2 + (X_2 + x_2)^2} = I_2 z_{02}$$

Therefore the current transformer operation is essentially a short circuit operating mode, both the secondary impedance and load being small.

Ratio error as a function of primary current. In electric plant operation the primary current varies in a wide range — from about 5% of $I_{1,r}$ to short circuit values. Let us consider the current transformer operation at rated current values. For the sake of simplification we let $\sin(\alpha + \psi) = 1$ in Eq. (10.3). Then,

$$\Delta I = I_0 w_1 / I_1 w_1 \tag{10.6}$$

Since $I_1 w_1 \approx I_2 w_2$,

$$\Delta I = I_0 w_1 / I_2 w_2 \tag{10.7}$$

where

$$I_2 = E_2 / z_{02} = 4.44 f w_2 B_m S_{\text{core}} / z_{02} \tag{10.8}$$

Here, B_m is the maximum magnetic inducation in the steel core of cross section S_{core}.

Substituting (10.5) and (10.8) in (10.7) yields

$$\Delta I = H l z_{02} / 4.44 f w_2^2 B_m S_{\text{core}} \tag{10.9}$$

or in view of $B_m / H = \mu$

$$\Delta I = l z_{02} / 4.44 f w_2^2 \mu S_{\text{core}} \tag{10.10}$$

When the primary current varies all the parameters remain constant except for permeability μ.

If $I_1 w_1 \approx I_2 w_2$, then

$$I_1 w_1 = I_2 w_2 = E_2 w_2 / z_{02} = 4.44 f w_2^2 S_{\text{core}} B_m / z_{02} \tag{10.11}$$

i. e. the magnetic induction increases linearly with the primary current.

The permeability as a function of B_m is plotted in Fig. 10.4, along with the curve $B_m(H)$. As the primary current grows the permeability of the core increases and the current error falls off. At B_{opt} the error is a minimum. Then μ falls due to the core saturation and ΔI increases. The angle β_{opt} corresponds to the point $B = B_{\text{opt}}$ where the permeability is largest and the ratio error is least.

It is important that the current transformer produce no large errors at the rated current and on short circuit. In view of the magnetic induction of saturation being in the range of 2 T, for uncompensated current transformers the rated magnetic induction is selected within 0.06-0.1 T. In the absence of compensation the ratio error is always negative and has a U-profile along the primary current coordinate. The phase error has a similar profile but with a positive sign.

In order that a current transformer should comply with a certain accuracy class, its error should be within the stipulated limits. For the Soviet accuracy class 0.5, the error curves (labelled by (2) in Fig. 10.5) should be within the area confined by the shadowed broken lines so long as the load varies from 0.25 $Z_{2,r}$ to $Z_{2,r}$ and $\cos \varphi_2 = 0.8$. According to the relevant Soviet standard, the accuracy class of a current transformer is defined by its percent ratio error at the primary current (1-1.2) $I_{1,r}$ [2.1].

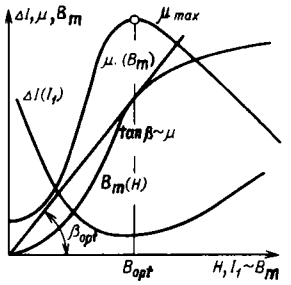

Fig. 10.4. Current ratio error as a function the primary current

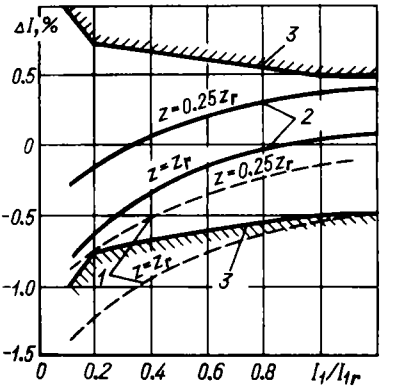

Fig. 10.5. Ratio error compensation by unwinding the secondary

In the actual range of magnetic induction (up to 0.1 T) the magnetising curve may be well approximated by the expression

$$H = 0.82\, B_m^{0.6} \tag{10.12}$$

Denoting the per unit value of the primary, and consequently, the secondary m.m.f. by n leads to the expression for ratio error in the form

$$\Delta I = \frac{Hl}{nI_{1,r}\, w_1} = \frac{l}{nI_1\, w_1}\, 0.82\, B_m^{0.6} \tag{10.13}$$

Let us express magnetic induction through $I_{2,r}$

$$\begin{aligned} B_m &= nI_{2,r}\, z_{02} / 4.44 f w_2 S = nI_{2,r}^2\, z_{02} / 4.44 f I_{2,r}\, w_2 S \\ &= nI_{2,r}^2\, z_{02} / 4.44 f I_{1,r}\, w_1 S \end{aligned} \tag{10.14}$$

and substitute this expression for B_m in (10.13), then

$$\Delta I = \frac{0.82 l}{nI_{1,r}\, w_1} \left(\frac{nI_{2,r}^2\, z_{02}}{4.44 f I_{1,r}\, w_1 S} \right)^{0.6} = \frac{0.82 l\, I_{2,r}^{1.2}\, z_{02}^{0.6}}{(4.44f)^{0.6}\, n^{0.4}\, (I_{1,r}\, w_1)^{1.6}\, S^{0.6}} \tag{10.15}$$

This expression clearly indicates that the current error increases sharply as the rated primary m.m.f. $I_{1,r} w_1$ decreases.

The bar-type c.t. in which the primary winding is a current carrying bar or bus is the most popular design. However, high accuracy c.t.s. (class 1, 0.5, etc.) require that the rated primary ampere-turns be above a certain value to ensure small ratio error. For modern magnetic materials and designs, the accuracy class 0.5 needs a minimum current of 600-900 A in the bar-type transformer. If a primary current below 600 A is anticipated, the primary winding should be of a multi-turn type.

Effect of burden impedance. The secondary burden impedance Z_2 can vary de-

pending on the protective relaying system or the resistance of the connected measuring devices. Increasing Z_2 leads to greater values of z_{02}. In agreement with Eq. (10.15) the ratio error increases proportional to $z_{02}^{0.6}$. It should be noted, however, that when the burden impedance is varied within the limits of the rated $Z_{2,r}$, the magnitude of the secondary current will vary only insignificantly because I_1 is independent of z_{02}.

If z_{02}, say, halves, so do E_2 and B_m. The field strength H and m.m.f. $I_0 w_1$ decrease accordingly and lead to a smaller ratio error $\Delta I = I_0 w_1 / I_1 w_1$. In agreement with Eq. (10.1) the secondary current will increase as the magnetising and core loss ampere-turns $I_0 w_1$ decrease. However, this rise of the secondary current is of low significance.

In order to achieve more accurate performance of a c.t. its secondary resistance r_2 and reactance x_2 should be reduced.

Effect of constructional parameters. Equation (10.15) suggests the ratio error increase with the length of the magnetic circuit l. Therefore, designers seek to reduce this linkage length.

Increasing the cross section S of the core decreases the ratio error in proportion to $1/S^{0.6}$. A greater length of a turn wound on this core means a greater wire resistance and some increase of the ratio error. Therefore, a thicker core is not necessarily a rational solution.

Usage of higher permeability materials for the core will reduce the ratio error, other conditions being equal.

Inductive reactance of the secondary winding x_2 in the equivalent circuit. To reduce the impedance z_{02}, the inductive reactance of the secondary winding x_2 in the equivalent circuit must be kept as low as possible. The reactance x_2 is greatest in c.t.s with the primary and secondary windings placed on distinct core legs (see Fig. 10.9). This reactance reduces sharply in c.t. types with concentrically arranged windings (Fig. 10.6).

In a bar-type c.t. with toroidal gap-less core and uniformly wound secondary winding, the reactance $x_2 = 0$. Some transformer types have a portion of core left bare (Fig. 10.7) for the sake of fixture. The reactance x_2 may be calculated by the empirical formula

$$x_2 = (6.7\text{-}8)\, x_1\, w_2^2 \times 10^{-6} \log (360 / \alpha)$$

where x_1 is the reduced length of leakage flux path depending on the size of the core and winding, and α is the angular segment covered by the winding.

It is instructive to note that even at $\alpha = 360°$, x_2 can be an appreciable negative value if the radius of the winding is large. This relates usually to transformer types with large name-plate ratio — 5000 / 5, 10 000 / 5, etc. — having a large number of secondary turns [10.8, 10.9].

Multi-turn c.t.s are frequently built with concentric windings (see, e.g., Fig. 10.14). The leakage flux for this arrangement is schematised in Fig. 10.8. The respective reactance x_2 can be determined by Rogovsky's formula. For the case of identical winding heights $h_1 = h_2 = h$ (see, e.g., Fig. 10.6),

$$x_2 = \omega 2\pi\, x_2\, w_2^2 \frac{l}{h} \left(\frac{\Delta}{2} + \frac{\Delta_2}{3} \right) 10^{-9}$$

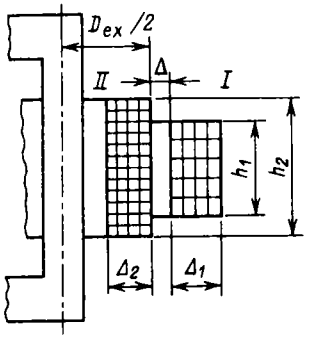

Fig. 10.6. Construction to determine the inductance of the secondary for concentric coils

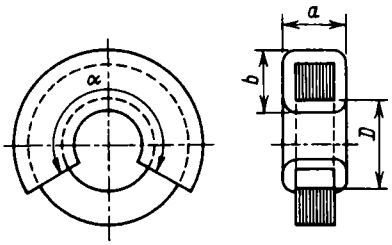

Fig. 10.7. Schematic diagram to determine the secondary inductance in the equivalent cirucit of toroidal cores

D, mm	x_1
≤150	a
150-400	$a + b$
400	$a + 2b$

where $\omega = 314\ s^{-1}$; $x_2 = 1 - (\Delta + \Delta_1 + \Delta_2) / \pi h$ is the Rogovsky coefficient; $l = \pi (D_{2ex} + \delta / 4)$ is the average length of circle receiving the leakage flux of the secondary winding, cm; D_{2ex} is the external diameter of the secondary winding, cm; Δ is the distance between the windings, cm; and Δ_2 is the thickness of the secondary winding.

For constructions with $h_1 \neq h_2$, the coefficient x_2 should be selected in Table 10.1.

Table 10.1. Correction Factor x_2 for $h_1 \neq h_2$

$100(h_2 - h_1)/h_2$	Δ_2, cm	Δ, cm	h_2, cm	x_2
17	1.2	1.5	12.8	1.27
17	1.2	1.7	12.8	1.24
19	1.2	2.4	12.6	1.15
22	1.3	3.7	16.0	1.05
25	1.6	5.6	10.2	0.9

Bachurin [10.1] discusses the calculation of x_2 for other c.t. design versions.

Experimental evalution of x_2. If the windings are on distinct core legs, an appropriate technique will be that of an auxiliary winding, w_2' in Fig. 10.9. The secondary winding is short circuited and its e.m.f. is expended on the compensation of ohmic and inductive voltage drops

$$E_2^2 = (I_2 r_2)^2 + (I_2 x_2)^2$$

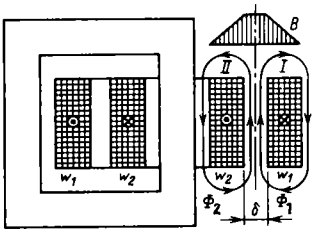

Fig. 10.8. Leakage fluxes in a current transformer with concentric windings

The e.m.f. E_2 is evaluated with the aid of the auxiliary winding

$$E_2 = E_2' w_2 / w_2'$$

where E_2' is the e.m.f. of the auxiliary winding.

The resistance r_2 is measured by a bridge, the current by an ampermeter, so that finally

$$x_2 = \sqrt{E_2^2 - (I_2 r_2)^2} \; / I_2$$

A more versatile technique, suitable for any type of c.t. is by evaluating x_2 using the c.t. errors. Short circuiting the secondary winding yields $\tan \alpha = x_2 / r_2$. Since r_2 is known, one may obtain x_2 by calculating α. From Eqs. (10.3) and (10.4)

$$\Delta I_{\%} / \delta = 100 \tan (\alpha + \psi) / 3440 \qquad (10.16)$$

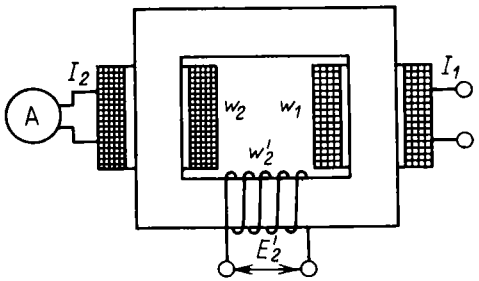

Fig. 10.9. Schematic diagram to derive the inductive reactance of the secondary winding

whence

$$\alpha = \arctan (34.4 \, \Delta I_{\%} / \delta) - \psi$$

For a given primary current the values of $\Delta I_{\%}$ and δ are determined by an error-measurement bridge. The angle ψ is found from the curve $\psi (i_0 w_{pk})$ for the given operating mode of the current transformer.

10.2 Error Compensation

Turn compensation. The simplest way of compensating for a ratio error is by reducing the number of turns. If $w_2 = w_{2,r}$, the ratio error is always negative and can be determined by Eq. (10.3). Reducing the number of turns in the secondary winding below $w_{2,r}$, we introduce an artificial positive ratio error that will partly compensate for the negative error because thereby we reduce the transformer ratio

and the resultant secondary current $I_2 = I_{1,r}\, w_1 / w_2$ can even grow above $I_{2,r}$. Thus, a positive ratio error will result.

With account for the turn correction a new per cent ratio error may be determined as

$$\Delta I_{\%} = -\left[\frac{I_0\, w_1}{I_1\, w_1} \sin(\alpha + \psi) - \frac{w_2 - w_{2,r}}{w_{2,r}}\right] 100 \qquad (10.17)$$

Here the last term in brackets represents the turn compensation.

Once the number of secondary turns has been reduced, the ratio error curve shifts parallel to itself into the range of smaller errors (see Fig. 10.5) and can even assume positive values at large currents. If the secondary burden is small (0.25 of $Z_{2,r}$), the resultant ratio error can even go beyond the limits stipulated for the given accuracy class.

Referring to Fig. 10.5, the dashed curves (labelled (1)) relate to uncompensated c.t., and curves (2) to the same c.t. after unwinding a number of secondary turns.

The largest compensation is necessary in the region of small primary currents. This approach, however, results in a positive ratio error extending beyond the class limits at low burdens in the region of rated currents. Therefore, the turn compensation does not always produce a desirable effect which is an obvious drawback of the method.

It is quite obvious that this change in ampere-turns does not affect the phase-angle error. This error can be reduced by introducing a short-circuited turn which causes an increase of ohmic losses and a greater loss angle ψ (see Fig. 10.3). This compensation is appropriate where there is a ratio error margin.

Miscellaneous error compensation techniques. Bachurin [10.1] discusses a number of other error-compensating solutions. A method suggested by G. N. Petrov and S. S. Okun is in wide use. It consists in an increase of core permeability with the aid of leakage fluxes. The idea of this method is represented schematically in Fig. 10.10.

The secondary winding (terminals T_1 and T_2) is made of two about equal parts (1) of w_2' turns and (2) of w_2'' turns in aiding connection. The primary winding (3) of w_1 turns is placed on the right core limb. In the core window there is a magnetic shunt (4). In neglection of the magnetising current

$$I_1 w_1 - I_2 w_2' - I_2 w_2'' = 0$$

The distribution of the secondary winding over the two core limbs produces increased leakage fluxes. The shunt (4) increases these fluxes considerably. The left-limb ampere-turns $I_2\, w_2'$ produce a leakage flux Φ_2 that completes its path through the shunt. The ampere-turns in the right core limb are $I_1\, w_1 - I_2\, w_2''$. This is essentially the excess of the primary m.m.f. This m.m.f. produces a leakage flux Φ_1 that also passes through the shunt (4). By choosing an appropriate magnetic resistance of the shunt one is able to shift the operating point in the region of high μ even at low primary current, thus reducing the reluctance of the core. As a result the magnetomotive force necessary to induce the mutual flux Φ_0 falls off sharply thereby reducing both the ratio and phase-angle errors. At currents close to the rated

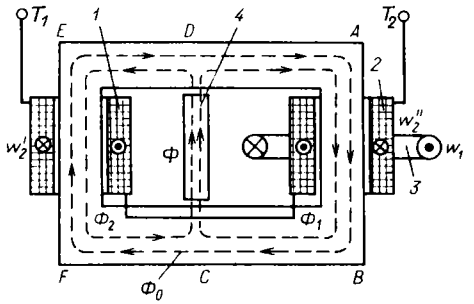

Fig. 10.10. Current transformer having a magnetic shunt compensation

values and higher the shunt saturates and this way of compensation is no longer operable.

In addition to the rise of the core permeability, the reduction of the secondary inductive reactance as a result of the "double leakage" [10.1] also contributes to improved accuracy of c.t. performance.

Closing this section it is worth noting that high-quality magnetic materials of high permeability and low ohmic losses would enable the designer to develop c.t.s having small ratio and phase-angle errors without having to resort to compensation techniques.

10.3 Operating Modes

Operation under short circuit conditions. On short circuit the primary current increases several ten times. Current transformers for relaying service must be able to carry very large currents, i. e., possess the necessary thermal and mechanical short time stability as well as supply the secondary current with a ratio error not disturbing the normal operation of the protective system.

At primary currents several ten times normal value the core steel is driven to saturation and the ratio error rises sharply. Experience collected with c.t.s operating at heavy primary currents indicates that if the total error attains 5-10%, a further rise of primary current will entail so rapid growth of ratio error that a normal operation of the relaying service will not be possible any longer. Therefore, the maximum admissible primary current rating of a c.t. for relaying service should exceed the anticipated short circuit value.

The maximum admissible primary current values are frequently expressed as per unit factors of rated value, at which the total error attains 5% and 10%; these factors are denoted by K_5 and K_{10}, respectively. These per unit values are taken at rated burden and power factor. The respective classes of accuracy for Soviet c.t.s are denoted by 5P and 10P. The computational procedure for these per unit factors outlined in Ref. [10.3] is as follows.

1. Construct the analytical characteristic $E_2 = f(I_0)$. Assume the magnetic flux density B_m = 0.3-1.9 T. Refer to the magnetisation curves to determine H_0; $I_{01} = H_0 l / w_1$;

$$E_2 = 4.44 f w_2 B_m S$$

2. For the given load Z_2 and $\cos \varphi_2 = 0.8$ determine the impedance of the secondary circuit as

$$z_{02} = \sqrt{(r_2 + 0.8\, Z_2)^2 + (x_2 + 0.6\, Z_2)^2}$$

3. Plot the curve $I_{01} = f(I_1)$. Assume various values of primary current I_1 and determine the respective secondary current $I_2 = I_1 / k_r$ (without ratio error correction) and the secondary e.m.f. $E_2 = I_2 z_{02}$. With this value of E_2 determine I_{01} from the function $E_2 = f(I_{01})$. Repeat this evaluation of I_{01} for a number of I_1 values.

4. Carry out the computation of item 3 for a number of Z_2 values including $Z_{2,r}$.

5. Construct the functions of items 3 and 4 in one coordinate system (curves *1-3* in Fig. 10.35).

6. Because for K_{10} the magnetising current referred to the primary side is $I_{01} = 0.1\, I_1$, draw the straight line representing this function. This line intercepts curves *1-3* at points defining I_1 at which the total error is 10%. The respective per unit value is then found as $K_{10} = I_1 / I_{1,r}$. The K_5 factor is determined in a similar manner.

Deep saturation of the core results in a heavily distorted curve for I_2. The calculation of the secondary current and ratio error estimation for such an operating mode can be found in Ref. [10.3].

A typical plot of per unit primary current versus secondary load is represented in Fig. 10.11. It can be seen that lower burdens allow for greater overload in the primary circuit.

The transformers for differential protective systems are selected such that their maximum per unit primary current be the same. This secures low imbalance current of relaying systems, equal to the difference of the c.t. secondary currents, taken at the same primary current.

A short circuit fault in the primary circuit saturates the c.t. core and results in heavily distorted curve of the secondary current. The maximum per unit value of secondary current may be estimated with the expression

$$n_{max} = B_s / B_{m,r} + (2\text{-}3)$$

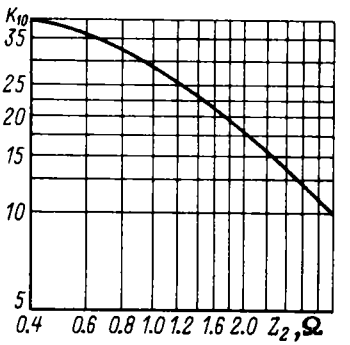

Fig. 10.11. Maximum primary overload (per unit value) versus load in the secondary

where B_s is the saturated magnetic induction (about 2 T for electrotechnical steel), and $B_{m,r}$ is the amplitude of the magnetic flux density at the rated primary current.

On short circuit the current transformer with multi-turn primary winding is subjected to overvoltage hazard. The inductive reactance of such a winding is comparable with the resistance of the rest short-circuited system and may store an appreciable proportion of the source voltage so that interturn insulation breakdown may result.

Operation of a ferromagnetic c.t. on short circuit current with an aperiodic component. A short circuit fault in a 3-phase system inevitably gives rise to an aperiodic component. The magnitude and sign of this component vary in a wide range under arbitrary laws. Let us consider a more severe situation of the component being positive and a maximum. For simplification we drop the primes at referred currents i_0 and

$$i_1 = -\hat{I}_1 \cos \omega t + \hat{I}_1 e^{-t/\tau_1} \tag{10.18}$$

where $\hat{I}_1$ is the amplitude of the primary current referred to the secondary side, and $\tau_1 = L_1 / R_1$ is the time constant of the short circuited network.

The transformation ratio analysis for this current will be carried out under the following assumptions:

(1) the core permeability is invariable;

(2) the secondary inductive reactance x_2 in the equivalent circuit is zero;

(3) the core steel does not incur any eddy current losses; and

(4) the burden is purely ohmic.

The respective equivalent circuit is shown in Fig. 10.12. Here L_0 is the magnetising inductance and R_2 is the total resistance of the secondary circuit. Because the c.t. under discussion is a linear device (L_0 = const), the transient process may be treated separately for the aperiodic and periodic components of the current. A profound treatment of c.t. operation in transient modes is outlined in Ref. [10.4]. Some findings of this treatment will be incorporated in the procedure displayed below.

Consider the transfer of the aperiodic component of primary current into the secondary circuit. It is apparent that

$$i_{2a} = i_{1a} - i_{0a} \tag{10.19}$$

where i_{0a} is the aperiodic component of the magnetising current. It can be represent-

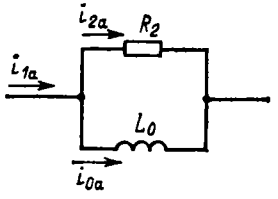

Fig. 10.12. Equivalent circuit for analysis of c.t. transient performance

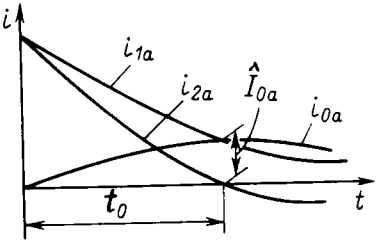

Fig. 10.13. Aperiodic components of current in the c.t. transient mode

ed as [10.2]

$$i_{0a} = \hat{I}_1 \frac{\tau_1}{\tau' - \tau_1} \left(e^{-t/\tau'} - e^{-t/\tau_1} \right) \tag{10.20}$$

where $\tau' = L_0 / R_2$ is a c.t. time constant. Graphically i_{0a} is presented in Fig. 10.13.

The instant when the magnetising current is a maximum is defined by the equation

$$t_0 = - \frac{\tau' \tau_1}{\tau' - \tau_1} \ln (\tau_1 / \tau') \tag{10.21}$$

The aperiodic component of secondary current, i_{2a}, results by combining currents i_{1a} and $-i_{0a}$. It can be demonstrated that at the instant t_0 when i_{0a} is a maximum the secondary current i_{2a} crosses zero and changes its sign. Variation of the aperiodic component $i_{0a} / \hat{I}_1$ at different values of time constant τ' is shown in Fig. 10.14*a*. At $\tau' = 0$ the aperiodic component follows in step with the primary current i_{1a}, while the secondary current i_{2a} is zero. As τ' increases i_{0a} decreases.

Figure 10.14*b* demonstrates $i_{2a} / \hat{I}_1$ as a function of τ'. Reduction in τ' incurs a sharp distortion of the secondary current. Distortions in the transfer of aperiodic

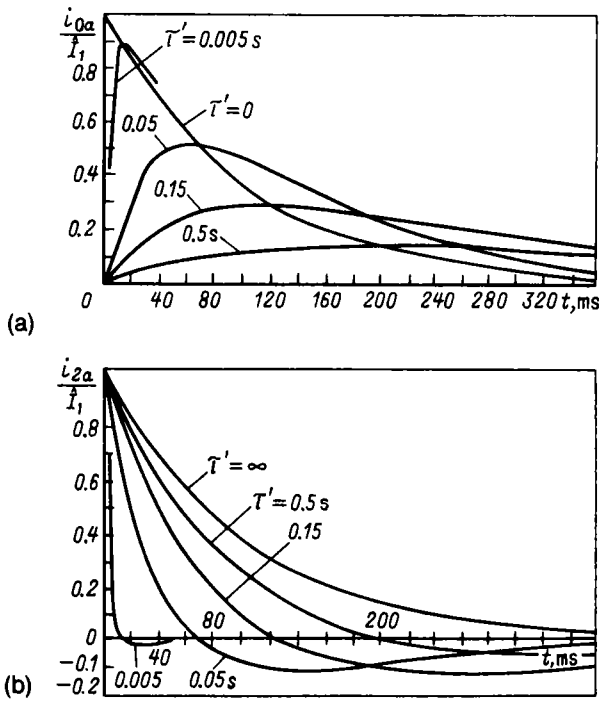

Fig. 10.14. Aperiodic component of secondary current and magnetising current at $\tau_1 = 0.1$ s and $\tau_2 = L_2/R_2 = 0$

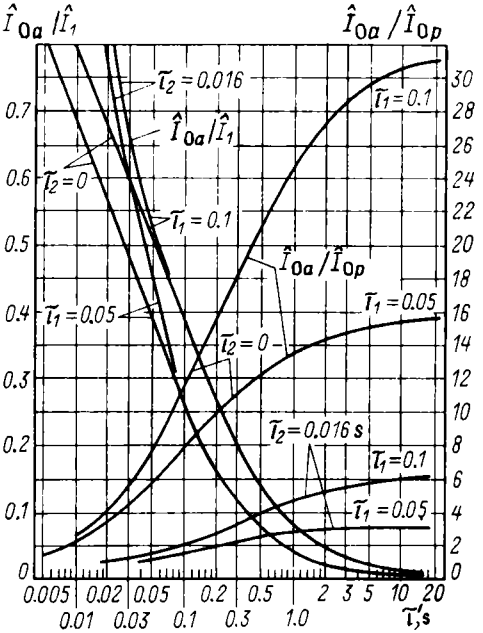

Fig. 10.15. Dependence of $\hat{I}_{0a}/\hat{I}_1$ and $\hat{I}_{0a}/\hat{I}_{0p}$ upon time constants τ', τ_1, and τ_2

component lead to the curve crossing below the t axis, thus causing errors in the transfer of current zero instants.

Let us consider how the amplitudes of aperiodic $\hat{I}_{0a}$ and periodic $\hat{I}_{0p}$ components of magnetising current depend on diverse factors depicted in Fig. 10.15. The relevant computations have been carried out with account of the burden inductance L_{2L}. The time constant of the burden is $\tau_2 = L_{2L} / R_{2L}$. For $\tau' = 0.1$ s, $\tau_1 = 0.1$ s, and $\tau_2 = 0$ the amplitude ratio $\hat{I}_{0a} / \hat{I}_1 = 0.38$, that is the weight of the aperiodic component amounts to 38% of the primary current amplitude. The ratio $\hat{I}_{0a} / \hat{I}_{0p} = 12$ implies that the aperiodic component of magnetising current is 12 times its periodic counterpart.

Because L_0 = const, B_p and B_a are proportional to the respective currents. If a rated induction selected for the linear c.t. (at $I_1 = I_{1,r}$) equals 0.08 T, then at a current ten times the rated primary value, B_m will be 0.8 T. The amplitude of aperiodic magnetic flux density $B_{m,a}$ is proportional to $\hat{I}_{0a}$ and equal to $0.8 \times 12 = 9.6$ T. At this level of magnetic induction an actual c.t. will produce a secondary current of entirely different wave profile than the primary current. A severe distortion will be also observed in the transfer of the periodic component (Fig. 10.16) [10.3].

The ratio of aperiodic to periodic current component $\hat{I}_{0a} / \hat{I}_{0p}$ increases for greater τ' and attains a value of 31 at $\tau_1 = 0.1$ s, $\tau' = 20$ s, and $\tau_2 = 0$. This rise of magnetising current drives the core into deep saturation and causes inadmissible ratio errors. It is important to stress that for the linear c.t. under evaluation

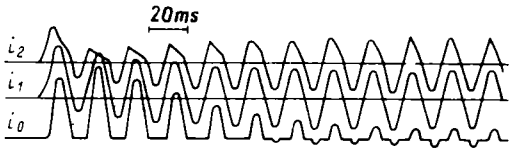

Fig. 10.16. Actual transient secondary current waveform on a short circuit

(μ = const) each m.m.f. component produces a proportional magnetic induction

$$B_{m,\,p} = \hat{I}_{0p}\, w_2\, \mu / l$$

$$B_{m,\,a} = \hat{I}_{0a}\, w_2\, \mu / l$$

where μ is the core permeability and l is the core linkage length. The resultant magnetic flux density is then $B_m = B_{m,\,p} + B_{m,\,a}$, or in per unit fractions with respect to $B_{m,\,p}$

$$k = (B_{m,\,p} + B_{m,\,a}) / B_{m,p} = 1 + \hat{I}_{0a} / \hat{I}_{0p}$$

For large time constant τ' and $\tau_1 = 0.1$ s,

$$k = 1 + \omega \tau_1 = 32$$

It is worth noting one more specific feature of c.t. operation on short circuit. In the presence of an aperiodic component in the primary current the core saturates. After the short circuit fault has been cleared the core retains some magnetic induction B_{rem} that can be stored for a rather long time. In currently used transformer steels $B_{rem} \geqslant 1.0$ T and if a new short circuit occurs, the magnetic flux density starts to grow from this remanence level rather than zero, provided that the aperiodic component of the magnetic induction has the same polarity. This causes fast saturation of the core and inadmissible high errors.

To improve the c.t. performance in transient modes the magnetic circuit is manufactured with nonmagnetic gaps [10.2, 10.5]. The nonmagnetic gap is advantageous primarily in reducing the remanence B_{rem}. This improves the stability of c.t. operation, and reduces saturation hazard.

Estimation of B_{rem} can be done with the expression

$$H_c\, l = \Phi\, R_\mu = B_{rem}\, S\, k_s\, l_{gap} / \mu_0\, S \tag{10.22}$$

whence

$$B_{rem} = H_c\, l \mu_0 / k_s\, l_{gap} \tag{10.23}$$

where H_c is the coercive force, A / m; R_μ is the magnetic resistance, H^{-1}; k_s is the solid core proportion factor; $\mu_0 = 4\pi \times 10^{-7}$ H / m; S is the cross section of the core, m^2; and l_{gap} is the total gap length, m.

The incorporation of a nonmagnetic gap, however, increases the magnetic resistance of the magnetic circuit and, consequently, results in higher errors.

Let us look at the basic relations for a c.t. with nonmagnetic gap. For a linear c.t. and at large τ', Fig. 10.15 suggests that the periodic components of magnetic flux density and magnetising current be neglected as compared with their aperiodic counterparts, so that the magnetic status of the c.t. be governed by the aperiodic magnetising current. For current transformers controlling operation of a syn-

chronised circuit breaker the burden is purely ohmic [10.4]. The leakage loss of the secondary winding in the equivalent circuit may be neglected (magnetic flux leakage in the nonmagnetic gaps may be neglected and the thickness of the secondary winding is small compared with the core diameter [10.5]). In the presence of aperiodic component in the primary current special attention is paid to keeping the phase-angle error as small as possible. For normal operation the core material should not be saturated. The maximum ratio error is defined as

$$\Delta I = I_{0a} / \hat{I}_1$$

The phase shift between the current zero of the primary and secondary currents, δ, is largest when i_{0a} attains the value $\hat{I}_{0a}$, moreover, by Ref. [10.4]

$$\sin \delta \approx \hat{I}_{0a} / \hat{I}_1$$

Following Sirota [10.2], we may write

$$\Delta I = \frac{\tau_1}{\tau' - \tau_1} \left(e^{-t_0/\tau'} - e^{-t_0/\tau_1} \right) \tag{10.24}$$

$$t_0 = -\frac{\tau' \tau_1}{\tau' - \tau_1} \ln \frac{\tau_1}{\tau'} \tag{10.25}$$

For a given τ_1 the ratio error ΔI is controlled by solely τ'. By virtue of Eqs. (10.24-25) for c.t.s with unsaturated core τ' has been found in the form

$$\begin{aligned} \tau' &= \mu_0 S w_2^2 / l_{gap} (R_L + r_2) \\ &= \mu_0 k_s a^2 w_2^2 / l_{gap} \left(R_L + \varrho \frac{4 K_w a}{q_2} w_2 \right) \end{aligned} \tag{10.26}$$

where $\mu_0 = 4\pi \times 10^{-7}$ H / m; r_2 is the resistance of the secondary winding, Ω; a is the side of core section square (made to this shape to reduce r_2), m; R_L is the load resistance, Ω; ϱ is the resistivity, Ω m; q_2 is the cross section of the secondary wire, m^2; K_w is a coefficient allowing for increasing length of an average turn due to the winding thickness and the insulation between the secondary and the core; and w_2 is the number of turns in the secondary.

The gap size l_{gap} is controlled by two conditions.

1. The magnetic flux density must not saturate the core, i. e.

$$B_{m,a} \leqslant B_s$$

For a rather wide gap such that $l_{gap} / l_{steel} \geqslant 0.01$ the magnetic resistance of core steel may be neglected. Then the magnetic flux density can be found by the equation

$$\begin{aligned} B_{m,a} &= \hat{I}_{0a} w_2 / S R_\mu \; k_s = \hat{I}_{0a} w_2 / S \frac{l_{gap}}{\mu_0 S} k_s \\ &= \Delta I \hat{I}_1 w_2 \mu_0 / l_{gap} k_s \end{aligned} \tag{10.27}$$

where

$$l_{gap} = \Delta I \hat{I}_1 w_2 \mu_0 / B_{m,a} k_s \tag{10.28}$$

In order that the nonlinear distortions may be kept small the operating mode should be such that $B_{m,a} \leqslant 1.3$ T in quality steels.

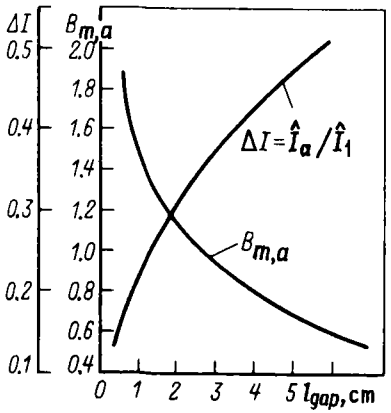

Fig. 10.17. Magnetic flux density $B_{m,a}$ and ratio error ΔI as functions of gap width l_{gap}

Figure 10.17 shows the functions $B_{m,a}(l_{gap})$ and $\Delta I(l_{gap})$ computed for one type of current transformer. It is instructive to note that for a selected value of l_{gap} the ratio error can be reduced to a required level by increasing the cross section of core steel S (this increases the time constant τ').

After the gap length l_{gap} has been determined, Eq. (10.26) yields the core section side a by known w_2, R_L, and q_2. Experimentally found current densities in the secondary of such c.t.s were only 5-6 A / mm^2 at the ultimate short circuit current. Under the circumstances the crros section of wire q_2 can be determined by the current density J as $q_2 = I_{2max} / J$.

2. The maximum remanence, determined by Eq. (10.23), must be $B_{rem} \leqslant 0.1$ T.

An example of synchronisation-service-c.t. design may be found in Ref. [10.4]. This development has been awarded a bronze medal in the USSR Exhibition of Economic Achievements [10.6].

This development has opened the way for use of c.t.s with nonmagnetic gaps in measurements of high currents during switchgear tests. The technical data of the developed c.t. are as follows: I_1, up to 120 kA; $\tau_1 = 0.1$ s; measurement time within 0.1 s; purely ohmic burden $R_L \doteq 1\ \Omega$; ratio error $i_{0a} / \hat{I}_1 = 0.01$; and rated voltage, 12 kV. An extensive report of this work is given in Refs. [10.5] and [10.8].

At the Institute of Electrodynamics of the Ukrainian Academy of Sciences, the research groups headed by I. M. Sirota and B. S. Stogniya are being involved in the development of c.t.s with nonmagnetic gap for all voltage classes to be used in relaying service. The time constant τ' of these units will be small to depress the aperiodiç component of magnetic flux density. This type of c.t. transfers correctly the periodic component of short circuit current only.

Concluding this topic we note that in accordance with Recommendations of the International Electrotechnical Commission (IEC) current transformers dedicated for relaying protection service are divided into three classes, TPX, TPY, and TPZ.

The class TPX covers c.t.s with annual gap-free core capable of accurate reproduction of the a.c. and d.c. components of short circuit current in the secondary winding. The duty cycle should be such that the core material has had not enough time to saturate.

The class TPY covers similar c.t. designs as TPX except that these c.t.s include a nonmagnetic gap in the core to reduce remanence.

The class TPZ includes c.t.s used in circuits where the reproduction of the d.c. primary component is of no interest. These units are advantageous in very low remanence and a small time constant τ'.

At rated primary current the error and phase angle errors should not exceed, respectively $\pm 0.5\%$ and $\pm 30'$ for TPX, $\pm 1\%$ and $\pm 60'$ for TPY, and $\pm 1\%$ and $\pm 200'$ for TPZ. At short circuit primary current the ratio and phase-angle error should not exceed, respectively, 5% and 3.0 ° for TPX, 7.5% and 4.5 ° for TPY, and 10% for TPZ.

Ferromagnetic c.t. operation in reclosing duty. Let us consider the most severe reclosing duty cycle when the first and second short-circuit current bursts produce the maximum aperiodic component and core magnetisation proceeds in the same sense. We assume the time constant τ' is invariable (linear c.t.). Then the aperiodic component of magnetising current varies as stated in Eq. (10.20).

Assume that the first s.c. fault is cleared in a time t_0 after the short circuit has occurred. In this case i_{0a} attains its amplitude value $\hat{I}_{0a}$. This current circulates in the magnetising and secondary circuit decaying by the law

$$i_{0a} = \hat{I}_{0a} \exp(-t/\tau') \tag{10.29}$$

In order that i_{2a} be reproduced with only a small error the time constant should be $\tau' = 5\text{-}10$ s [10.2]. The shortest no-current condition in reclosing lasts 0.25 s. Therefore, at $\tau' = 5$ s after a pause $t = 0.25$ s the current i_{0a} is to fall down to

$$i_{0a} = \hat{I}_{0a} \exp(-0.25/5) = 0.95\,\hat{I}_{0a}$$

If the second s.c. fault occurs with the same polarity of the aperiodic component, then the aperiodic magnetising current flowing through the magnetising branch is

$$i_{0a} = 0.95\,\hat{I}_{0a}\, e^{-t_{II}/\tau'} + \hat{I}_{1p} \frac{\tau_1}{\tau' - \tau_1} \left(e^{-t_{II}/\tau'} - e^{-t_{II}/\tau_1} \right)$$

where t_{II} is the duration of the second s.c. fault.

In a linear c.t. the aperiodic component of magnetic flux density has two components

$$\begin{aligned} B_a &= B_{a1} + B_{a2} \\ &= B_{a,0}\, e^{-t_{II}/\tau'} + \hat{I}_{1p} \frac{\tau_1}{\tau' - \tau_1} \left(e^{-t_{II}/\tau'} - e^{-t_{II}/\tau_1} \right) \frac{w_2}{R_\mu} \end{aligned} \tag{10.30}$$

Observing the fact that t_{II}/τ' is small, the curve B_{a2} is shifted upwards by a value close to the initial flux density $B_{a,0}$ (at $t = 0.25$ s). Hence, on the second short circuit B_a grows from a considerable background rather than zero and may rapidly reach saturation level. The incorporation of a nonmagnetic gap in the core reduces τ' and facilitates the reclosing duty of the c.t.

Figure 10.18 shows oscillograms of a high-speed recloser recorded at low burden of the c.t. At the first short circuit burst the secondary current exhibits small distortions because the magnetic flux density has not reached the saturation level. The

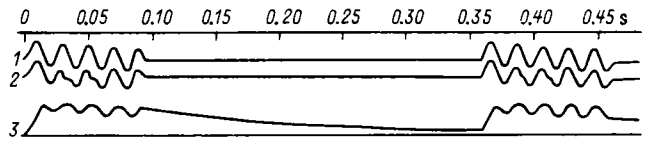

Fig. 10.18. Transient performance of a gap-free current transformer: (1) primary current ten times rated value, (2) secondary current, (3) magnetic flux density

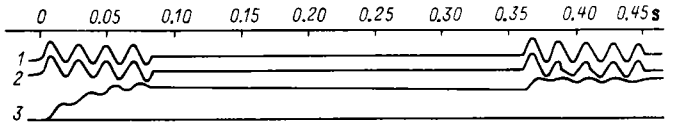

Fig. 10.19. Transient performance of a c.t. with nonmagnetic gap

reclosing follows in about 0.3 s. By this time instant the magnetic induction has decreased only insignificantly because of large τ'. Therefore, the reclosing results in a rapid saturation of the core and distortion of the secondary current waveform.

Figure 10.19 shows the oscillograms of the same reclosing process for functions of a c.t. with about the same parameters but also incorporating a nonmagnetic gap in the core. The reduced τ' facilitates a considerable reduction of the remanence. Thus, the incorporation of a nonmagnetic gap makes the fast reclosing duty easier and enables the reduction of the core section.

Operation with an open-circuited secondary. In the normal operating mode the magnetising ampere-turns $I_0 w_1$ account for a few per cent to fractions of per cent of the primary ampere-turns $I_1 w_1$. The maximum magnetic flux density in the core amounts to 0.06-0.1 T. When the secondary is open circuited, the demagnetising secondary m.m.f. ceases. Because primary current remains the same the primary m.m.f. will now perform the magnetising role. This leads to an increase of the m.m.f. by a hundred times and the appearance of a high e.m.f. at the secondary terminals.

Operation of a current transformer with open-circuited secondary is illustrated in Fig. 10.20. The primary current i_1 is here the magnetising current i_0. Each momentary value of i_1 is associated with its own magnetic flux density B and flux Φ (Fig. 10.20*b*). The flux variation with time is illustrated in the diagram at (*c*). The instantaneous e.m.f. at the secondary terminals is $e_{20} = -w_2 \, \mathrm{d}\Phi / \mathrm{d}t$. The diagram at (*d*) represents the history of this voltage.

In view of the formidable analysis, Bachurin [10.1] divided a simplified approach based on experimental curves of specific e.m.f. (per one turn of the secondary winding on 1 cm^2-section core) recorded as a function of $I_{1,r} w_1 / l$ (Fig. 10.21). Accordingly, the full e.m.f. is

$$\hat{e}_{20} = E_{sp} w_2 S$$

The higher the primary rated ampere-turns $I_{1,r} w_1$, the higher the peak e.m.f.

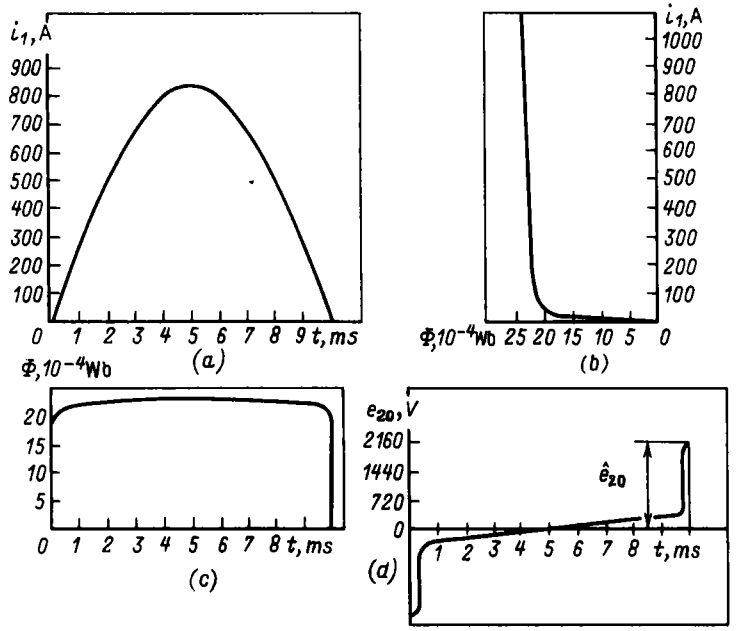

Fig. 10.20. Current transformer performance at open secondary: (*a*) primary current i_1, (*b*) magnetising curve, (*c*) time variation of magnetic flux, (*d*) e_{20} as a function of time

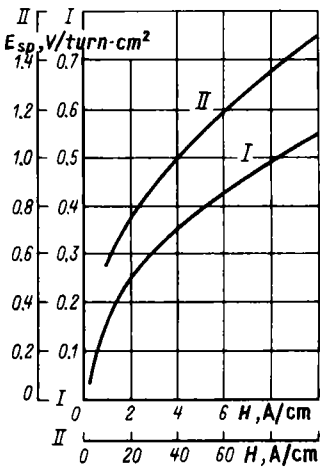

Fig. 10.21. Specific e.m.f. versus magnetic field strength

$\hat{e}_{20}$ that can attain a value of dozen kilovolts in some cases. This voltage is dangerous both for the transformer windings and for maintaining personnel.

When the core reaches saturation its eddy losses increase sharply and it can found itself heated up to inadmissibly high temperature which may result in a winding insulation failure.

The open-circuited secondary winding means an emergency operating mode for a current transformer. Therefore, all instrument transformers and relaying-service c.t. secondary windings should be short circuited before disconnecting the burden.

10.4 Types of Construction

Depending on the number of turns in the primary winding c.t.s are divided into 'single turn' of bar-type, whose primary is a single straight conductor of the bar type, and 'multi-turn' or wound-primary type.

The primary winding of a bar-type transformer may be a bar or busbar cluster. An example of such a transformer is the type TPOL-10 moulded-insulation c.t. represented schematically in Fig. 10.22. This unit is used as a through insulator in carrying a circuit from one room into another. Moulded epoxy insulation simplifies the c.t. construction drastically. The bar primary, magnetic circuits and a fixture ring are placed in a special form filled with a compound consisting of liquid epoxy resin, quartz sand powder, and curing agent. After polymerisation the insulating mass hardens and acquires high dielectric and mechanical properties.

On short circuit the primary bar is heated and expands in radial dimension. In order to prevent the epoxy mould from cracking the bar is enveloped by glass and peforated bands. The resulting envelope provides a sort of buffer insulation making up for thermal stresses caused by heated bar expansion.

The core made in a shape of torus is manufactured of stripe wound on a cylinder form. The secondary winding is wound atop the core. The toroidal shape of the magnetic circuit allows for complete utilization of the properties of the grain-oriented core steel.

If the secondary winding is uniformly distributed over the core, the inductive reactance of the winding in the equivalent circuit equals zero, thus contributing to high performance of the transformer.

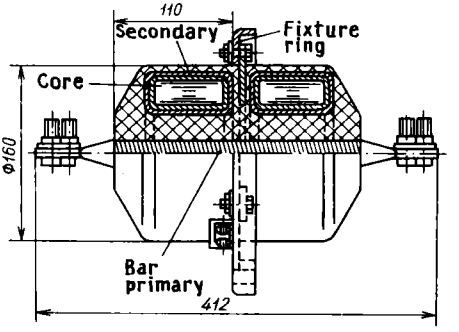

Fig. 10.22. Bar-type TPOL-10 c.t. for 10 kV

This construction allows a few different-parameter cores to be installed on one primary bar. Another advantage of the construction is its high mechanical short-time rating because its primary is acted upon by solely the forces of the adjacent buses and neighbouring phases.

A three-phase short circuit fault gives rise to mechanical forces between the primaries of the neighbouring phases. In addition forces are transferred to the bar end and act on the feeding bus fixed with one of its ends to the nearest support insulator, the other end being connected to the c.t. primary bar. The mechanical rating is assigned by the c.t. manufacturer and usually relates to a certain distance between the phases and a definite length of the buses connecting the support insulator with the current transformer.

Among the disadvantages of this construction one may find large ratio errors at small rated primary current due to $w_1 = 1$. Therefore bar-type c.t.s are used at currents of 400 A and higher. Window-type c.t.s are employed at primary current above 2000 A. The primary of this construction is a package of buses of a switchgear, which is passed through the window of c.t. core. The manufacturer does not normally indicate mechanical short-time ratings for such c.t.s because this current is here controlled by the mechanical strength of the bushes and their fixture.

The bushing type c.t. is a special window type designed to fit over apparatus bushing, the conductor through the bushing being used as the primary winding. Such apparatus may be circuit breakers, power transformers, through insulators, to name just a few. The arrangement of such c.t.s in a circuit breaker is illustrated in Fig. 5.1. Bushing-type transformers are very efficient economically. As a rule these transformers operate under severe environmental conditions where extensive moisture may be a problem. Therefore bushing transformers are impregnated by tarnish after the windings have been made and fixed.

A through insulator as a rule carries a few magnetic circuits and the respective secondaries can be connected in series or in parallel. Series connection of the secondaries does not change the ratio as it doubles the number of primary and secondary turns. The secondary current remains the same whereas the e.m.f. E_2 doubles enabling the secondary output to be increased two times. This is a very important fact for bushing-type transformers because they are distant from relays and measuring devices and have to be connected with them by long cables of high resistance.

At primary currents up to 100 A the secondary windings are connected in parallel so as to obtain a load current close to the standard value 5 A even at small primary currents. In addition the secondaries are provided with taps allowing ratio control in a narrow range. If the normal current flowing through the bar primary is lower than the rated primary current of the c.t., then the secondary current can be raised by reducing the number of turns in the secondary.

At small primary currents (up to 400 A) a high accuracy class for a c.t. may be achieved with the aid of multi-turn primary. Wound-primary type c.t.s are advantageous in that the ampere-turns $I_{1,r} w_1$ necessary for the given accuracy class can be obtained by increasing the number of turns in the primary.

Figure 10.23 shows a wound-primary type c.t. with moulded insulation. The rectangular laminated core (1) carries a coil-type secondary (2). The primary (3) is made of a copper bus with a necessary number of turns. The ends of the primary

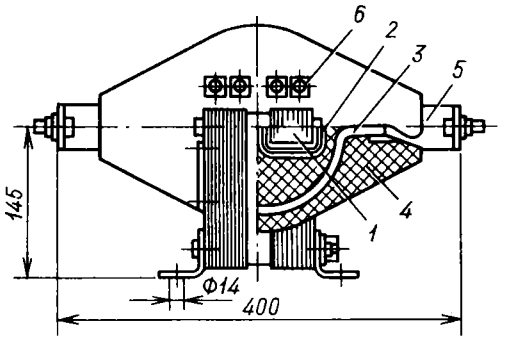

Fig. 10.23. Wound-type c.t. for 10 kV

have brazed terminals (5). All the c.t. parts are enveloped into an epoxy moulded casing (4). The secondary taps are connected to terminals (6).

A short circuit current gives rise to mechanical forces between the turns of the primary defining the mechanical short time rating of the unit. In addition the primary can experience an appreciable voltage drop because of its relatively high magnetic induction.

In 35-kV installations for outdoor service oil-insulated c.t.s are common. The 8-type design with interleaved windings shown in Fig. 10.24 is most popular in the Soviet Union. The toroidal core (1) with secondary windings (2) is passed through the window formed by the primary winding (4). The primary is wound by a soft multiwire conductor usually with several parallel branches (two branches in Fig. 10.24). Changing from parallel to series connection halves the rated current. The primary is insulated from the secondary by cable insulating paper (5). Cable paper

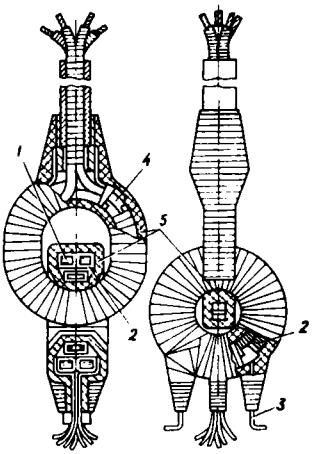

Fig. 10.24. Core with windings of a c.t. having paper-oil insulation

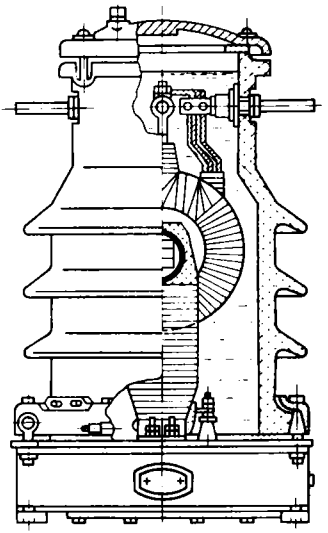

Fig. 10.25. Type TFN 35-kV current transformer for outdoor application

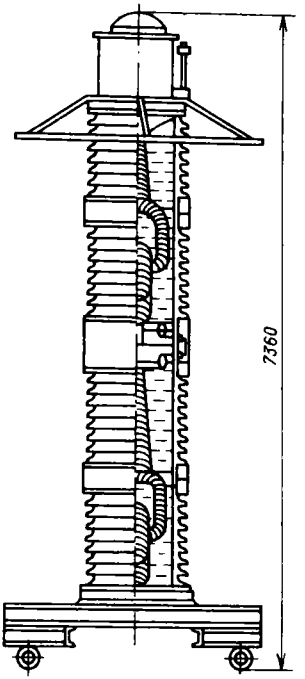

Fig. 10.26. Cascade c.t. for 500 kV

band of 0.12-mm thickness is wound with half-width overlap over both the primary and secondary windings. The insulated core with windings is fixed to the transformer base by foots (3). A porcelain protective casing is also secured to the same base.

After vacuum drying the inner cavity is filled with transformer oil. It impregnates the cable paper and fills all voids. Such c.t.s are manufactured for 220 kV. The sectional view of a c.t. for a voltage rating of 35 kV and higher is given in Fig. 10.25.

The cost of current transformer increases at about the square of rated voltage primarily due to the cost of insulation. Therefore in systems operating at voltages above 220 kV the cascade scheme is employed. A two-stage cascade connected c.t. for 500 kV is shown in Fig. 10.26. The secondary winding of the first stage feeds the primary of the second. Each stage filled with oil arrives at the assembly site in a separate package. This transformer costs about half as much as a similar single-stage unit. Further reduction of size and weight can be achieved with the use of capacitor paper-oil insulation. There is a setback connected with an increased ratio error due to increased winding resistance [10.1].

10.5 Coreless Current Transformers

Current transformers with air core (more accurately, with a core of nonmagnetic material) have been found useful in transient performance testing of electric switchgear. A c.t. of this type with an integrating amplifier is sketched in Fig. 10.27*a*. The primary (1) made of a round or rectangular bus passes through a core of electric-grade card-board (2) carrying a w_2-turn secondary (3) connected to an *RC*-circuit feeding a d.c. amplifier (4) and an oscilloscope (5).

The load resistance $R - j / \omega C$ is rather high, therefore the c.t. operates practically in a short-circuit mode. The e.m.f. across the secondary winding is

$$e_2 = -w_2 \, \mathrm{d}\Phi / \mathrm{d}t = -w_2 k \mathrm{d}i_1 / \mathrm{d}t = -w_2 k \mathrm{d}i_1 / \mathrm{d}t \tag{10.31}$$

Resistor R is selected such that $R \gg 1 / \omega C$ at power frequency ω. Then the voltage across the capacitor is

$$U_C = \frac{1}{C} \int_0^t \frac{e_2}{R} \, \mathrm{d}t = -\frac{1}{RC} \int_0^t k w_2 \frac{\mathrm{d}\, i_1}{\mathrm{d}t} \, \mathrm{d}t = (k w_2 / RC) \, i_1 \tag{10.32}$$

where RC is a time constant that controls the error of integration [10.10]. The greater the time constant the smaller the error. However, greater time constants tend to reduce the output U_C, imposing higher requirement on the amplifier. A d.c. amplifier is used because it is to transmit the aperiodic component of short circuit current.

The theoretical analysis of transients in the air-core c.t. and the development of a measurement setup have been done by V. D. Lyashenko at the All-Union Power Institute, Moscow. Current transformers of this type are employed in test stations both in the USSR and abroad.

The equivalent circuit of the coreless c.t. installation is shown in Fig. 10.27*b*. The differential equation describing the output signal u_C is

$$LC \frac{\mathrm{d}^2 u_C}{\mathrm{d}t^2} + RC \frac{\mathrm{d}u_C}{\mathrm{d}t} + u_C = M \frac{\mathrm{d}i_1}{\mathrm{d}t} \tag{10.33}$$

Since the resistance in the secondary winding is large, the current i_2 is small and can be neglected as compared with i_1. The air-core c.t. is a linear transformer, therefore the transformation of periodic and aperiodic components may be treated in separate. We assume that the symmetric component of the current varies as

$$i_1 = \hat{I} \sin(\omega t + \psi) \tag{10.34}$$

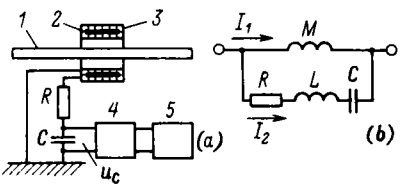

Fig. 10.27. Coreless c.t. installation

Eliminating i_1 between (10.33) and (10.34), denoting $2L / R = \tau_L$ and $RC = \tau_C$, and rearranging yields

$$u_C = \frac{M}{\tau_C} \hat{I} \cos\varphi \left\{ \sin(\omega t + \psi - \varphi) - \frac{1}{k_1 - k_2} \left[-k_2 \sin(\psi - \varphi) + \omega \cos(\psi - \varphi) \exp(k_1 t) + k_1 \sin(\psi - \varphi) - \omega \cos(\psi - \varphi) - \omega \cos(\psi - \varphi) \right] \exp(k_2 t) \right\} \tag{10.35}$$

where

$$k_1, k_2 = -\frac{1}{\tau_L} \pm \sqrt{\frac{R^2}{(4L)^2} - \frac{1}{LC}}$$

and

$$\varphi = \arctan \frac{\omega L - 1 / \omega C}{\sqrt{R^2 + (\omega L - 1 / \omega C)^2}}$$

Recognizing that both L and φ are small, we have approximately

$$k_1 = 1 / \tau_C \text{ and } k_2 = 2 / \tau_L$$

Substituting these k_1 and k_2 into Eq. (10.35) yields

$$u_C = \frac{M}{\tau_C} \hat{I} \cos\varphi \sin(\omega t + \psi - \varphi) - \sin(\psi - \varphi) \, e^{-t/\tau_C} - \frac{\omega L}{R} \cos(\psi - \varphi) \left(e^{-t/\tau_L} - e^{-t/\tau_C} \right) \tag{10.36}$$

Comparison of Eq. (10.36) and Eq. (10.34) reveals the error that occurs in transformation. The amplitude per unit error in the steady state is

$$\beta_{ss} = 1 - \cos\varphi$$

and the phase-angle steady state error is

$$\varphi_{ss} = \omega \tau_L / 2 - 1 / \omega \tau_C$$

In the transient mode

$$\beta_{tr} = \mp \cos\varphi (\omega \tau_L - 1 / \omega \tau_C)$$

and

$$\varphi_{tr} = -\varphi_{ss} \mp \beta_{tr}$$

or

$$\varphi_1 = -3/2 \, \omega \tau_L + 2 / \omega \tau_C \text{ and } \varphi_2 = -\omega \tau_L / 2$$

Here, minus signs and subscript 1 relate to odd half-periods and plus signs and subscript 2 to even half-periods. Thus, the error depends on frequency ω, self-inductance of the secondary winding L, and time constant τ_C.

A similar analysis can be carried out for the ratio and phase-angle errors in transfer of aperiodic component

$$i_a = \hat{I}_a \exp(-t / \tau_1) \tag{10.37}$$

where $\tau_1 = L_1 / R_1$ is the time constant of the short circuit.

As a rule $L / R \ll RC$, then Eq. (10.33) gives

$$u_{Ca} = \frac{M}{\tau_C} \hat{I}_a \frac{\tau_C}{\tau_C - \tau_1} \left(e^{-t/\tau_1} - \frac{\tau_1}{\tau_C} e^{-t/\tau_C} \right) \tag{10.38}$$

Comparison of (10.38) and (10.37) reveals that the aperiodic component is also transferred with an error. This error depends on the ratio $\delta = \tau_C / \tau_1$ and is smaller the higher the ratio. Because $\tau_C > \tau_1$, at some time instant $t > t_0$ the voltage u_{Ca} will change sign and become negative. The time t_0 can be determined by Eq. (10.38) when u_{Ca} crosses zero

$$t_0 = \tau_1 \frac{\delta}{\delta - 1} \ln \delta \tag{10.39}$$

The error in transfer of aperiodic component is largest at $t = t_0$ and is given by the expression

$$\gamma = \delta^{-\delta/(\delta - 1)} \tag{10.40}$$

For the aperiodic component, the ratio error of transfer can be decreased by increasing τ_C, whereas for the periodic component (especially high-frequency currents) a reduction in τ_L is necessary. An analysis of errors in measurements of current and its derivative allowing for the connecting cable parameters and input impedance of the amplifier is carried out in Ref. [10.10].

The total ratio error of the setup in a transient mode does not exceed 5%.

10.6 Optoelectronic Current Transformers

The development of electromagnetic c.t.s for extra high-voltage ratings, having reached a level of 1150 kV, faces with great difficulties. This relates to both ordinary and cascade-connected designs. The capacitor paper-oil insulation of high-voltage c.t. becomes unwieldy and results in heavy and large constructions. The cascade units suffer from reducing accuracy. The U-type construction [10.1] is also penalised by large size and weight. It has become obvious therefore that the method of electric insulation for c.t.s for high and extra-high voltage should be altered. One of the feasible ways is the development of a c.t. in which the signals of a current source at a high potential are transmitted optoelectronically to a receiver at earth's potential, which is intended to feed measuring instruments and relay protection devices.

Two principal modulation systems are in current use, with external and internal modulation of the light beam.

External modulation system. The functional details of this system are shown in Fig. 10.28*a*. A light source (1) and an optical system (2) form a light flux Φ_1 that is launched in a lightguide (3) towards the high potential modulation unit. The lightguide may be a lens system, a mirror-wall pipe, or optical fibre guide. The latter is free from many disadvantages pertinent to the two traditional systems. An optical fibre 10-mm diameter lightguide is a bunch of optical fibres of 10 μm diameter. Each fibre has a core made of transparent glass or plastic surrounded by and in intimate contact with a cylindrical cladding having a refractive index some one percent lower than that of the core so that total internal reflection takes place at their interface. The ends of all fibres are polished to a high-quality finish.

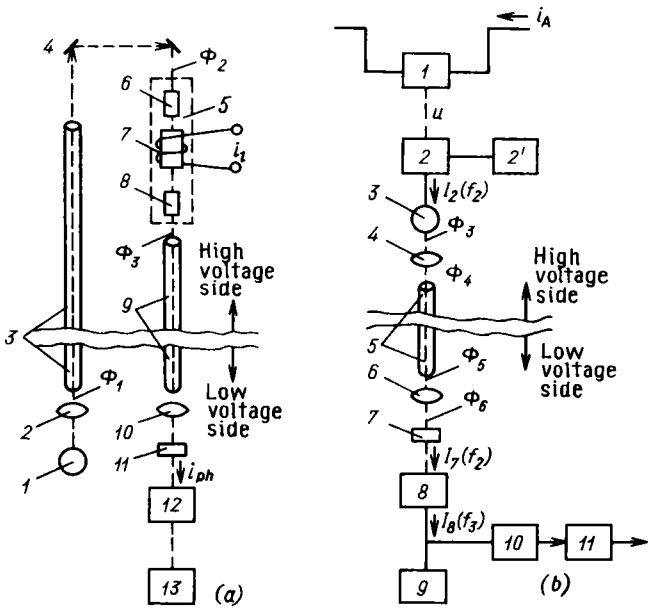

Fig. 10.28. Block diagram of optoelectronic c.t.s: (*a*) with external modulation of light flux, (*b*) with internal modulation

High-voltage optical fibre lightguides have been developed that are operable at rated voltage up to 1200 kV. The dielectric strength of such a lightguide attains 100 kV/m. The light propagation efficiency of 10-m strand is about 15%. To achieve the necessary dielectric strength the lightguide is placed inside a porcelain insulator kept at an air pressure of 0.2 MN / m^2 (gauge). New developments include lightguides in the form of solid glass rods which are simple to manufacture, and maintain and offer a longer service life.

The light beam conveyed by the lightguide (3) is diverted by a prism system (4) to the input of the modulating unit (5) constituted by a polariser (6), modulator cell (7) and analyser (8). This unit changes a light flux Φ_2 to a flux Φ_3 whose intensity depends on the magnitude of line current i_l. The physical principles underlying the modulator operation will be explained in the following paragraph. The following strand of lightguide (9) leads Φ_3 to the low voltage side. The lens (10) focuses the flux onto a light-electric transducer (11) which converts variations of light intensity into alterations of photocurrent i_{ph}. This current drives an amplifier (12) and feeds the burden (13).

The modulation process occurs as follows. A light beam arriving at the modulation unit is plane-polarised by a polariser (6). The plane-polarised light strikes the modulator (7) which is a Faraday cell. The cell is made of optically transparent materials such as heavy flint glass or quartz that rotate the plane of polarisation

of a plane-polarised light when it passes in the direction of the magnetic lines of force of a surrounding strong magnetic field. This is the Faraday effect. The angle of rotation θ is directly proportional to the strength H of the magnetic field [A / m] and to the length l of path [m] in the substance:

$$\theta = V l H$$

where V is Verdet's constant dependent on the properties of cell substance, temperatures, and some other factors.

Denoting the length of a magnetic line of force by l_m and the maximum angle of rotation of the plane of polarisation by θ_m, we get

$$\theta = V l H = V l i_1 w_1 / l_m = k_{ph} i_1 = k_{ph} \hat{I} \sin \omega t = \theta_m \sin \omega t$$

An obvious advantage of the optoelectronic c.t. with external modulation of light beam is the absence of complicated and numerous transducers at the high voltage side, that require a regulated current supply. However the variation of Verdet's constant with temperature is a clear disadvantage. The modulator and receiver elements are as a rule at different temperature conditions (one is up on the HV pole, the other is down at LV side) and compensation is a problem. Another setback of the Faradaic modulator is its sensitivity to the effects of stray magnetic fields produced by other currents.

Internal modulation system. The block diagram of the internal modulation system is shown in Fig. 10.28*b*. The primary transducer (1) usually delivers voltage proportional to the measured current. The intermediate transducer (2) performs signal modulation. In amplitude modulation this unit may be an amplifier, in frequency modulation the current is transformed in a signal of variable-frequency proportional to the current. In pulse-width modulation the relation between the pulse period and the pulse duration is made a function of the current, i. e., the current is transduced into a coded waveform.

Amplitude modulation is sensitive to external noise and imposes strict requirements on all transformation units and supplies. Thus the amplitude modulation solution is objectionable to developing a high accuracy optoelectronic c.t. The aforementioned disadvantages do no longer penalise the internal modulation technique based on discrete signal (frequency, pulse-width, and code modulation).

The intermediate modulator (2) fed by a regulated power supply (2′) delivers the signal to a light-electric transducer (3). In amplitude modulation this transducer operates within the linear portion of the lumen-ampere characteristic of the light-emitting diode. In frequency modulation the frequency of LED flushes is proportional to the line current i_l.

The optical system (4-5-6) of lenses and a lightguide conveys the modulated light beam to light-receiver photodiodes (7) which drive an amplifier (8). The load (9) consuming the discrete signal is hooked directly to the amplifier. An analog load receives this signal after a circuit of a frequency-analogue of code-analogue converter (10) and an analogue amplifier (11).

An optoelectronic c.t. with frequency modulation for 750 kV and a rated primary current of 2 kA developed in the USSR has the performance characteristics as fol-

lows: measurement channel limits, (0.2-1.2) $I_{1,r}$; accuracy class: discrete channel, 0.5, and analog channel, 1.0; measurement limits of protection channel, 0.5 $I_{1,r}$-20 $I_{1,r}$; accuracy class 3; phase-angle error of protection channel, $\pm$ 2 °.

10.7 Instrument Transformers for D.C. Transmission Systems

Extra-high voltage d.c. transmission systems become ever more important for transmission of high power. Pertinent control functions and protective service require measurement of system current. The d.c. transformer used for this purpose is essentially a choke capacitance-coupled amplifier operating in a forced magnetisation mode [10.12]. This regime is characteristic in that the control circuit carries a current which is governed by the control circuit parameters only.

The schematic diagram of such a device, referred to as a d.c. transformer in this text, built around two magnetic circuits is shown in Fig. 10.29*a*. The primary current to be measured flows around the control winding w_c usually made in the form of bus. The service windings w_s are connected in opposition. The load R_L is connected through a valve bridge in series with the service windings. The load can be ampermeters, current windings of meters of power, energy, and relaying protective devices. The service windings are excited by a voltage source U_e of power frequency 50 Hz.

The primary current $i_1 = i_c$ flowing through the control windings w_c magnetises both cores to saturation. Assume that core *I* is linked by a magnetic flux density B_c, produced by a control winding w_c, which adds with a magnetic flux density B_s produced by the service winding w_s. Then similar magnetic inductions B_c and B_s in core II act in opposition. Since core I is saturated, the a.c. resistance of w_{s1} is virtually zero. The current in service windings i_s is controlled by the reversal of

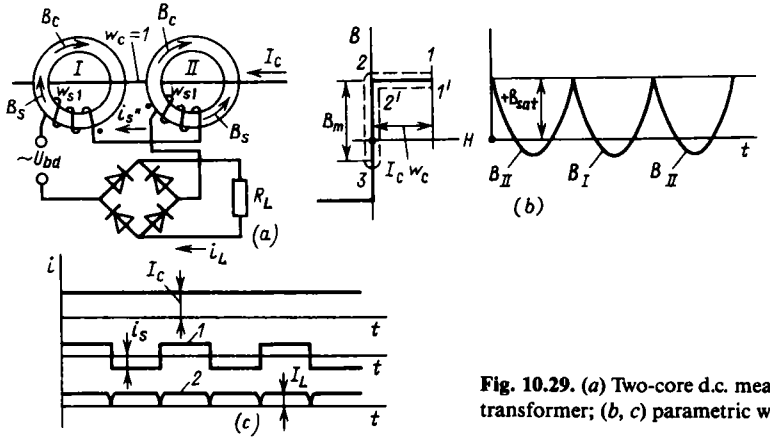

Fig. 10.29. (*a*) Two-core d.c. measurement transformer; (*b*, *c*) parametric waveforms

magnetisation in core II. For a material with an ideal magnetisation curve this process is shown in Fig. 10.29*b*. At low burden resistance B_L the e.m.f. of choke II balances the excitation voltage U_e. The respective variable flux density B_{II} obeys a sine law (Fig. 10.29*b*). In *B-H* coordinates the state of core is described by successive points 1, 2, 3, 2′, and 1′. Over the segment 1-2 the current i_s rapidly grows from zero to $i_s = i_c w_c / w_s$. Within segments 2-3 and 3-2′ the core is unsaturated and $Hl = 0$. Then

$$i_c w_c + (- i_s w_s) = Hl = 0$$

or

$$i_c w_c = i_s w_s$$

Because i_c = const, the excitation circuit carries the constant current

$$i_s = i_c w_c / w_s$$

This equation holds for mean current values as well [10.12]

$$I_s = I_c w_c / w_s$$

The currents I_s and I_c remain proportional to each other for I_s varying from 0 to 0.84 $I_{s,max}$ [10.12], here $I_{s,max} = U_e / R_s$, where U_e is the mean excitation voltage and $R_s = R_L + R_w$ is the total ohmic resistance of the secondary winding circuit. The process recurs in the following half-period, but the current i_s changes sign and will be governed by the reversal of magnetisation of core *I* because in this core B_c and B_s are of opposite sense.

Figure 10.29*c* shows the profiles of load current in the service winding (1) and in the load (2) for the transformer with an ideal magnetisation curve. The actual magnetisation curve differs from the ideal profile by a hysteresis, $\mu \neq \infty$ in the unsaturated zone and $\mu \neq 0$ in the saturation range. This causes distortions in the burden current (Fig. 10.30). The ideal rectangle *ABCD* gives way to a complicated curve *AEFD*, the error accumulating as the areas S_1 through S_4. Evaluation of these areas yields the resultant error of the d.c. transformer [10.13]. Clearly, the error will be reduced for core materials having a magnetisation characteristic close to the ideal curve.

It is important to note that variation of magnetic flux density in unsaturated magnetic circuits produces an additional even-harmonic current I_{2add}. Figure 10.31 illustrates how the e.m.f. of this harmonic occurs. In contrast with the process

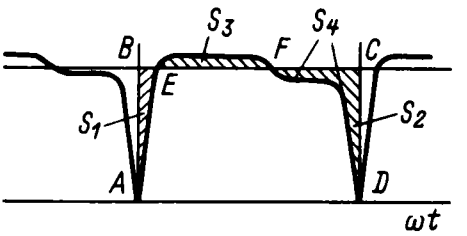

Fig. 10.30. Load current of an actual d.c. transformer

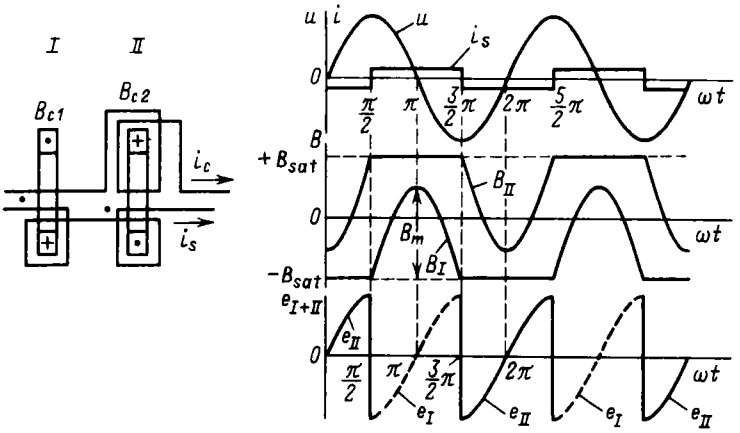

Fig. 10.31. Illustrating the appearance of even harmonics of the e.m.f. in the primary circuit

shown in Fig. 10.29, here the current I_c induces in the cores magnetic fluxes of opposite sense, $-B_{sat}$ in core *I* and $+B_{sat}$ in core II. The e.m.f. e_{II} is induced by B_{II}, and e.m.f. e_I by B_I. The resultant e.m.f. e_{I+II} produces the current I_{2add}. If Z_1 is the impedance of the primary circuit for even-harmonic currents, then $I_{2add} = E_{I+II} / Z_1$. This current produces an additional magnetisation (positive) as μ of the core material decreases [10.13].

The e.m.f. E_{I+II} is proportional to the ratio w_c / w_s and Z_1 is defined by the primary circuit configuration. At high I_c the ratio w_c / w_s is small and the current I_{2add} may be neglected. In testing when I_c is low the primary circuit is augmented by an additional inductive reactance to increase Z_1.

A number of schemes have been developed to compensate for valleys in the current curve [10.13]. One of them is shown in Fig. 10.32*a*. The secondary circuit is fed by two voltages shifted 90 ° with respect to each other. The scheme essentially contains two d.c. transformers operating onto a common load, R_L. The load currents in the individual d.c. transformers and the resultant load current i_L are plotted in the diagram at (*b*). The first unit delivers a load current i_{2A} and the second i_{2B}.

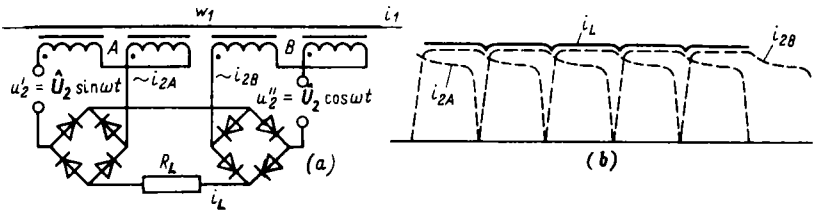

Fig. 10.32. (*a*) Duplex arrangement to smooth load current; (*b*) current oscillograms

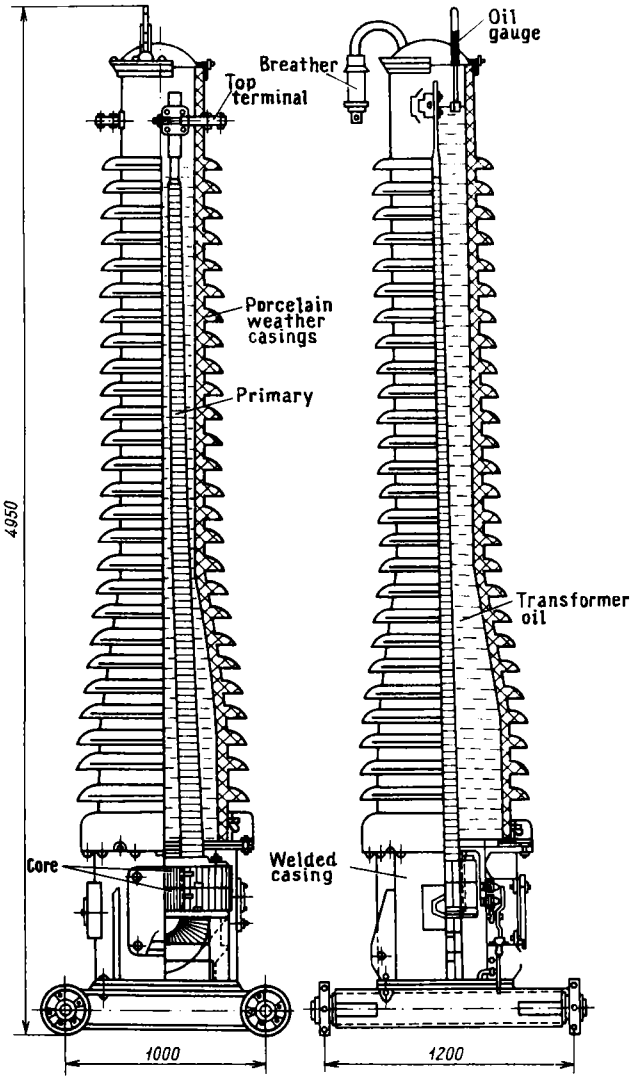

Fig. 10.33. Construction of a d.c. transformer for 400 kV

The resultant load current is well smoothed and small valleys in the waveform mean sharply reduced errors. Error calculation for these devices can be found in Ref. [10.13].

By way of example Fig. 10.33 shows the sectional view of the type TPTN-400 d.c. transformer for a rated voltage of 400 kV, primary current of 1000 A and secon-

dary current of 25 A. The rated power in the burden is 60 VA at unit rated power factor. It allows 5 times normal pirmary current without exceeding 3% error. The primary winding is made of a U-shaped copper tube. The secondary is separated from the primary by capacitor paper-oil insulation. The primary is threaded through two torus cores carrying the secondaries. The upper part of the primary is in a porcelain weather casing and its lower part and the cores in a welded housing. The housing and porcelain casing are filled with transformer oil. The primary taps are made as buses passed through the walls of the porcelain insulator. The cap carries a silica gel breather and oil gauge.

10.8 Choice of Current Transformers

The rated voltage of a c.t. should be consistent with the system voltage. The maximum admissible continuous current should be as close to the c.t. rating as possible to reduce ratio error. The class of accuracy is selected in agreement with the particular c.t. application: more accurate units (classes 0.5 and 1) are used as instrumental transformers, less accurate for relaying service.

The short-time current at the c.t. application site and the r.m.s. value of continuous short-circuit current must be below the mechanical and thermal short-time ratings of the selected unit. Manufacturers indicate mechanical and thermal time ratings of the select unit. Manufacturers indicate mechanical and thermal short time ratings of c.t.s as the respective per unit values in terms of rated primary current. Thus, the mechanical short-time rating is the current stated in terms of times normal which the c.t. can withstand even if the current is initially fully offset; the thermal short-time rating in per unit is the ratio of the r.m.s. value of current admissible (in heating terms) for a short time period (1 to 4 seconds) to the rated primary current.

Low current transformers possess sufficient mechanical and thermal short-time ratings, but in some applications these ratings are inadequate and one has to select a unit for a greater normal primary current in order to secure the necessary short time ratings. As a rule such a choice operates with a higher error because the rated current of the system finds itself appreciably below the transformer rating.

For c.t.s used in relaying service, the maximum admissible primary current rating must be above the anticipated short circuit value in the primary circuit.

Current transformers for differential protection systems must have identical maximum primary current ratings.

Selection of c.t.s should be made subject to the fact that the actual c.t. load includes connection leads in addition to the windings of instruments and relays.

10.9 Calculation of an Electromagnetic C.T. Illustrative Example

Given: Rated voltage $U_r = 10$ kV, rated primary current $I_{1,r} = 600$ A, frequency $f = 50$ Hz, rated secondary current $I_{2,r} = 5$ A, rated secondary burden $Z_{2L} = 0.4\ \Omega$, $\cos\varphi_{2L} = 0.8$, accuracy class 0.5, two cores, 1-s thermal rating $n_{th1} = 65$, and mechanical short time rating $k_m = 160$.

It is required to calculate the principal parameters and select the appropriate unit.

For the primary rated current 600 A, the required accuracy can be achieved with bar-type c.t.s. We select as a construction of departure the type TPOL-10 c.t. shown in Fig. 10.22. The appropriate analytical procedure could be as follows.

1. *Selection of winding wire.* The cross section of the primary is selected by the formula

$$s_1 = I_{1,r} / J$$

where the current density for copper is $J = 1.5\text{-}1.8$ A / mm^2; thus, the cross section

$$s_1 = I_{1,r} / J = 600 / 1.6 = 375 \text{ mm}^2$$

and the primary winding diameter

$$d_1 = \sqrt{4 s_1 / \pi} = \sqrt{4 \times 375 / 3.14} = 21.86 \text{ mm}$$

From the available copper profiles we choose a round bus of $d_1 = 22$ mm.

The cross section of the secondary winding

$$s_2 = I_{2,r} / J = 5 / 1.6 = 3.125 \text{ mm}^2$$

hence, the wire diameter

$$d_2 = \sqrt{4 s_2 / \pi} = \sqrt{4 \times 3.125 / 3.14} = 1.99 \text{ mm}$$

From the list of available wire types we select type PETV-939 wire (high-resistant enamel with polyether insulation, class B of heat resistance) with $d_2 = 2.00$ mm and $d_{ins2} = 2.12$ mm.

2. *Number of turns in the secondary*

$$w_2 = w_{2,r} = I_{1,r} w_{1,r} / I_{2,r} = 600 / 5 = 120$$

3. *Preliminary selection of core cross section.* Because the secondary resistance insulation thickness δ_1 is defined by the thicknesses of perforated and glass bands, flux density is taken within the range 0.06-0.1 T.

$$S_{core} = I_{2,r} Z_{2,r} / 4.44 f w_{2,r} B_m$$
$$= 5 \times 0.4 / 4.44 \times 50 \times 120 \times 0.06 = 0.00125 \text{ m}^2$$

4. *Evaluation of core size.* We take transformer steel (electrotechnical grade 1512) of 0.35 mm thickness. The sectional view of the core and windings is shown in Fig. 10.34.

The inner diameter of the core D_1 is governed by the thickness of buffer insulation δ_1, thickness of prime insulation δ_3, thickness of secondary winding δ_2, and wire diameter d_1 of the primary:

$$D_1 = d_1 + 2\delta_1 + 2\delta_2 + 2\delta_3$$

The prime insulation is epoxy compound with mean admissible dielectric strength $E_{mean} = 1.8$ kV / mm. Then

$$\delta_3 = U_r / E_{mean} = 10 / 1.8 = 5.6 \text{ mm} \approx 6 \text{ mm}$$

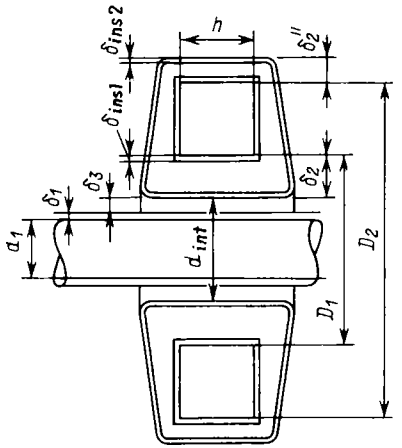

Fig. 10.34. Sectional view of the core and secondary winding

It is worth noting that the dielectric strength of epoxy compound used for moulded insulation of c.t.s rated up to 10 kV is E_{bd} = 20-30 kV / mm. The buffer insulation thickness δ_1 is defined by the thicknesses of perforated and glass bands. Assume δ_1 = 2 mm. Determine the thickness of the secondary winding. The internal diameter of c.t. window after the secondary has been wound

$$d_{int} = d_1 + 2\delta_1 + 2\,\delta_3$$
$$= 22 + 2 \times 2 + 2 \times 6 = 22 + 4 + 12 = 38 \text{ mm}$$

To determine the secondary thickness δ_2 we find the internal diameter of the core by the formula [10.12]

$$D_1 = \sqrt{(d_{int} + 2\delta_{ins1})^2 + 4A / \pi} + 2\,\delta_{ins2}$$

where A is the cross-sectional area of the ring-shaped secondary in the c.t. window

$$A = s_2\, w_2\, 4d^2_{ins2} / k_w\, \pi\, d_2^2$$

for the type PETV wire selected for this purpose, d_2 = 2.0 mm, d_{ins2} = 2.12 mm, and the proportion of wire in the winding cross section is k_w = 0.75, so that

$$A = 3.14 \times 120 \times 4 \times 2.12^2 / 0.75 \times 3.14 \times 2$$
$$= 120 \times 2.12^2 / 0.75 = 718.4 \text{ mm}^2$$

For the insulation placed atop the secondary we choose electric-grade cardboard with δ_{ins2} = 0.5 mm, and fit electric-grade cardboard between the core and the secondary for a thickness of δ_{ins1} = 1 mm. Now

$$D_1 = \sqrt{(38 + 2 \times 1)^2 + 4 \times 718.4 / 3.14} + 2 \times 0.5 = 51.15 \text{ mm}$$

with the allowance D_1 = 55 mm.

The thickness of the secondary is $\delta_2 = (D_1 - d_{int}) / 2 = (55 - 38) / 2 =$ 8.5 mm.

Let us verify the dielectric strength of the primary insulation at rated and test voltage, U_r = 10 kV and U_{test} = 42 kV (in compliance with GOST 1516.1-78). The maximum strength of the electric field at the surface of the primary at rated voltage

$$E = 2U_r / d_1 \ln \frac{D_1 - 2\delta_2}{d_1} = 1.67 \text{ kV / mm}$$

This strength is less than the allowable figure of 8 kV / mm.

The field strength at test voltage

$$E_{test} = \frac{2U_{test}}{d_1 \ln (D_1 - 2\delta_2) / d_1} = \frac{42}{11 \ln (55 - 17) / 22}$$
$$= 7 \text{ kV / mm}$$

is well below the allowable level for this compound E_{bd} = 20 kV / mm.

The axial length of the core is determined as

$$h = 2S_{core} / k_s (D_2 - D_1)$$

where D_2 is the external diameter of the core, k_s is the proportion of solid steel in the core length, and D_2 is selected such that $h \geqslant (D_2 - D_1) / 2$.

Assume D_2 = 115 mm, k_s = 0.95, then

$$h = 2 \times 0.00125 / 0.95 \times (0.115 - 0.055) = 0.044 \text{ m} = 44 \text{ mm}$$

Now we check h for consistency: the radial size of the section $(D_2 - D_1) / 2 = (115 - 55) / 2 = 30$ mm does not exceed the computed value 44 mm.

We select a type OL 55 / 115-45 core with D_1 = 55 mm, D_2 = 115 mm, and h = 45 mm. The middle magnetic force line of the core is

$$l_{mid} = \pi (D_1 + D_2) / 2 = 267 \text{ mm}$$

5. *Resistance of the secondary* is

$$r_2 = \varrho \, l_{av} \, w_2 / s_2$$

where $\varrho = \varrho_0 (1 + \alpha_R \theta_{2m})$; ϱ_0 is the copper resistivity at 0 °C; $\varrho = 1.58 \times 10^{-6} (1 + 0.004 \times 130) = 2.4 \times 10^{-6}$ Ω cm; θ_{2m} = 130 °C is the highest admissible temperature for class B insulation; α_R = 0.004 °C^{-1} is the temperature coefficient of resistance; and l_{av} is the average turn length [10.12]

$$l_{av} = 2h + D_0 - d_0$$

where $D_0 = D_2 + 2\delta_2''$; δ_2'' is the external thickness of the secondary winding, δ_2'' is the thickness of the secondary inside the c.t. window, $2\delta_2$ = 17 mm,

$$\delta_2'' = \delta_{ins1} + d_{ins2} + \delta_{ins2} = 0.5 + 2.12 + 1 = 3.62 \text{ mm}$$
$$D_0 = 115 + 2 \times 3.62 = 122.24 \text{ mm}$$
$$d_0 = D_1 - 2\delta_2 = 55 - 17 = 38 \text{ mm}$$
$$l_{av} = 2 \times 45 + 122.24 - 38 = 171.2 \text{ mm}$$

$$r_2 = 2.4 \times 10^{-6} \times 17.12 \times 120 / 3.14 \times 10^2 = 1598 \times 10^{-4} = 0.16 \text{ Ω}$$

In order to reduce the inductive reactance x_2 of the secondary in the equivalent circuit the turns are uniformly distributed over the core; if this condition is satisfied, $x_2 = 0$.

6. *Impedance of the secondary circuit* is

$$z_{02} = \sqrt{(R_2 + r_2)^2 + X_2^2} = \sqrt{(0.32 + 0.16)^2 + 0.24^2} = 0.54\,\Omega$$

where $R_2 = Z_{2,r} \cos \varphi_r = 0.4 \times 0.8 = 0.32\ \Omega$ is the resistance of load; $X_2 = Z_{2,r} \sin \varphi_r = 0.4 \times 0.6 = 0.24\ \Omega$ is the load reactance; and $r_2 = 0.16\ \Omega$ is the resistance of the secondary winding.

7. *Phase angle between* E_2 and I_2

$$\alpha = \arctan \frac{X_2}{R_2 + r_2} = \arctan 0.5 = 26\,^\circ 56'$$

8. *Ratio and phase-angle errors* will be calculated for a few fractions of the rated current, namely, 0.1, 0.2, 1.0, and 1.2 $I_{1,r}$ at $Z_{2,r}$.

The ratio error is determined as

$$\Delta I_{\%} = 100\,(I_0\, w_1 / I_1\, w_1) \sin(\alpha + \psi)$$

where $I_0\, w_1 = H_0\, l_{av}$ is the full m.m.f. and $H_0 = f(B_m)$ is the specific magnetising m.m.f. The magnetic flux density

$$B_m = E_2 / 4.44 f S_{core}\, w_{2,r}$$

where $E_2 = I_2\, z_{02}$ is the secondary e.m.f.

The phase-angle error will be found as

$$\delta = 3440 \frac{I_0\, w_1}{I_1\, w_1} \cos(\alpha + \psi)$$

Table 10.2

	Times 600 A rated current			
	0.1	0.2	1	1.2
I_2, A	0.5	1	5	6
E_2, V	0.27	0.54	2.7	3.24
B_m, T	0.008	0.016	0.08	0.097
$H_0 = f(B_m)$, A/m	3.0	4.12	11.16	11.2
$H_0 l_{av} = I_0 w_1$, A	0.8	1.1	3.09	3.36
ψ, °	14.4	15	22.5	23.7
$\sin(\alpha + \psi)$	0.65	0.66	0.76	0.77
$\cos(\alpha + \psi)$	0.76	0.75	0.66	0.64
$\Delta I_{\%}$	−0.866	−0.6	−0.39	−0.36
δ	34.85′	23.65′	11.69′	10.27′

The loss angle in the core steel ψ is evaluated with the specific m.m.f. as defined above. The results of this calculation are summarised in Table 10.2. The errors are seen to be well within the accuracy class 0.5 and no turn compensation is required.

A similar calculation will be carried out for a quarter of the rated load $Z_2 = 0.25\, Z_{2,r}$, namely,

$$R_2 = 0.25\, Z_{2,r} \cos\varphi = 0.08\ \Omega$$
$$X_2 = 0.25\, Z_{2,r} \sin\varphi = 0.06\ \Omega$$
$$z_{02} = \sqrt{(0.08 + 0.16)^2 + 0.06^2} = 0.25\ \Omega$$

9. *Evaluation of the maximum admissible primary current.*

(a) Calculation of the no-load characteristic $E_2 = f(I_{01})$, where $I_{01} = H_0\, l_s / w_1$.

Assume $B_m = 0.5$-1.75 T and derive from the magnetisation curve the values of H_0 and $E_2 = 4.44 f w_{2,r} B_m S_{\text{core}}$. The results are summarised in Table 10.3. The data of the table will be used to construct the curve $E_2 = f(I_{01})$.

(b) Calculation of $I_{01} = f(I_1)$ at $Z_2 = 0.4$, 0.6 and 0.8 Ω with $\cos\varphi = 0.8$. Taking various values of I_1 determine $I_2 = I_1 / k_r$ with $k_r = 120$, and find $E_2 = I_2 z_{02}$. Enter with this value of E_2 into the curve $E_2 = f(I_{01})$ to determine I_{01}. The results of this calculation are summarised in Table 10.4. The calculation was performed for three values of Z_2, namely,

at $Z_2 = 0.4\ \Omega$ (see item 6) $z_{02} = 0.54\ \Omega$

at $Z_2 = 0.6\ \Omega$

$$z_{02} = \sqrt{(0.16 + 0.6 \times 0.8)^2 + (0.6 \times 0.6)^2} = 0.73\ \Omega$$

at $Z_2 = 0.8\ \Omega$

$$z_{02} = \sqrt{(0.16 + 0.8 \times 0.8)^2 + (0.6 \times 0.8)^2} = 0.93\ \Omega$$

The results of this calculation are plotted in the form of curves $I_{01} = f(I_1)$ shown in Fig. 10.35.

(c) For k_{10} the magnetising current referred to the primary side is $I_{01} = 0.1\, I_1$. The straight line $I_{01} = 0.1\, I_1$ crosses the curves $I_{01} = f(I_1)$ at points defining the current I_1 at which the ratio error is 10%. The per unit factor of the maximum

Table 10.3

B_m, T	0.5	0.7	1	1.2	1.3	1.4	1.5	1.6	1.7	1.75
H_0, A/m	25.2	34.2	53	65	100	194	230	400	1000	1250
$I_{02} = \frac{H_0 l_{av}}{w_2}$, A	0.056	0.069	0.118	0.145	0.222	0.332	0.512	0.89	2.225	2.78
E_2, A	16.65	23.31	33.3	39.96	43.29	46.62	49.95	53.28	56.61	58.27
$I_{01} = k_r I_{02}$, A	6.7	8.27	14.13	17.4	26.6	39.8	61.4	107	267	334

Table 10.4

I_1, kA	5	6	7	7.5	8	9	9.5	10	11	12	15	
I_2, A	41.66	50	58.3	62.5	66.6	75	79.16	83.3	91.6	100	125	
E_2, V	22.5	28	31.5	33.75	36	40.5	42.7	45	49.5	54	67.5	$z_{02} = 0.54\Omega$
I_{01}, A	7.2	9.6	12	13.2	15	20.4	25.2	32.4	60	156	—	
E_2, V	30.4	36.5	42.6	45.6	48.6	54.75	57.8	60.8	—	—	—	$z_{02} = 0.73\Omega$
I_{01}, A	10.8	15.6	22.8	33.6	50.4	180	2.88	—	—	—	—	
E_2, V	38.7	46.5	54.2	58.1	61.9	—	—	—	—	—	—	$z_{02} = 0.93\Omega$
I_{01}, A	18	38.6	168	318	—	—	—	—	—	—	—	

primary overload is $k_{10} = I_1 / I_{1,r} = 14\ 500 / 600 = 24.17$ at $Z_2 = 0.4\ \Omega$, $k_{10} = 10\ 400 / 600 = 17.33$ at $Z_2 = 0.6\ \Omega$, and $k_{10} = 7600 / 600 = 12.67$ at $Z_2 = 0.8\ \Omega$.

Bachurin [10.1] recommends that the magnetic flux density $B_m \leqslant 1.75$ T be allowed (for steel 1512) at $k_{10} = I_1 / I_{1,r}$. Then $k_{10} = B_m / B_{m,r} \times 0.95 = 1.75 / 0.06 \times 0.95 = 30.7$. At $Z_{2,r} = 0.4\ \Omega$, $B_{m,r} = 0.06$ T. Under the circumstances k_{10} has a greater value than if obtained with the procedure outlined in Ref. [10.3].

10. *Heating with continuous current.* Because 10% overloads with respect to the primary current are allowable, the calculation will be carried out for $I = 1.1\ I_{1,r}$. The thermal field pattern is rather involved, therefore we assume a number of idealisations.

(1) The heat released by the secondary traverses through the epoxy layer of the insulation and is transferred to the surroundings through about one half of the cooling surface of the insulation.

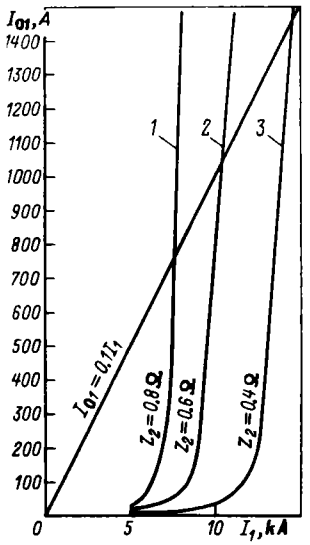

Fig. 10.35. To determining the maximum primary current

(2) The heat released in the primary winding is given out only through the bus connected to the end of the primary winding. The respective geometry is sketched in Fig. 10.36.

(a) Consider heating of the secondary winding. The winding temperature is estimated as

$$\Theta_2 = \Theta_0 + \tau_{sur} + \Delta\,\tau_{ins}$$

where $\Theta_0 = 40$ °C is the ambient temperature, τ_{sur} is the insulation surface superheat, and $\Delta\,\tau_{ins}$ is the temperature drop over the insulation thickness derived as follows

$$\Delta\,\tau_{ins} = I_2^2\, r_{02}\, R_{T1}\, R_{T2}\,(1 + \alpha_R\,\Theta_2)\,/\,(R_{T1} + R_{T2})$$
$$= I_2^2\, r_{02}\,(1 + \alpha_R\,\Theta_2)\, R_T$$

where r_0 is the winding resistance at 0 °C; and R_T, R_{T1}, and R_{T2} are the resultant, cylindrical, and butt-end thermal resistances of the insulation, respectively.

The quantity τ_{sur} can be evaluated by calculating the cooling surface with reference to Fig. 10.36. As a rule the c.t. has two cores, therefore the cooling surface per core is

$$S_{cool} = (S_1 + 2S_2)\,/\,2$$

where $S_1 = \pi\, D_{en}\, h_{en} = 3.14 \times 16 \times 22 = 1105$ cm^2 is the cylinder side surface; $S_2 = \pi\, D_{en}^2\,/\,4 - \pi\, d_1^2\,/\,4 = 197$ cm^2 is the butt-end surface; $D_{en} = 16$ cm is the diameter of the epoxy envelope; $h_{en} = 22$ cm;

$$S_{cool} = \frac{1105 + 2 \times 197}{2} = 749.5 \text{ cm}^2;$$

$$R_{T1} = (2\pi\,\lambda_{ins}\, l)^{-1} \ln\,(D_{en}\,/\,D_2) = 3.18 \text{ °C / W};$$

$\lambda_{ins} = 15$ W / (cm °C) is the thermal conductivity;

$$l = h_{en}\,/\,2 = 11 \text{ cm};$$

$R_{T2} = 4l_2\,/\,\lambda_{ins}\,\pi\,(D_2^2 - d_1^2) = 15.4$, where $l_2 = 2.5$ cm is the thickness of the butt-

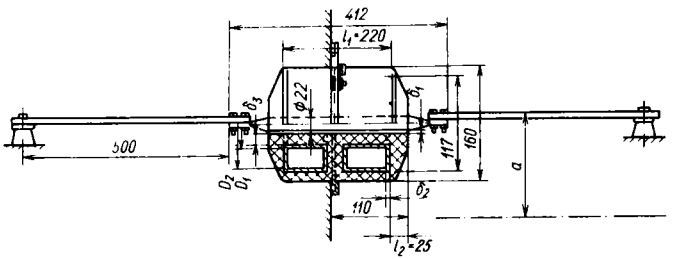

Fig. 10.36. Construction to calculate the mechanical capability of a c.t.

end insulation. Now,

$$\Theta_2 = \Theta_0 + \frac{I_2^2 r_{02}(1 + \alpha_R \Theta_2)}{\alpha S_{cool}} + \frac{I_2^2 r_{02} R_{T1} R_{T2}(1 + \alpha_R \Theta_2)}{R_{T1} + R_{T2}}$$

where $\alpha = 7$ W / m^2 °C is the heat transfer coefficient. Solving this equation for Θ_2 with $R_T^* = R_{T1} + R_{T2}$, we get

$$\Theta_2 = \frac{\Theta_0 \alpha S_{cool} R_T^* + I_2^2 r_{02} R_T^* + I_2^2 r_{02} \alpha S_{cool} \alpha_R R_{T1} R_{T2}}{\alpha S_{cool} R_T^* - \alpha_R I_2^2 r_{02} R_T^* - I_2^2 r_{02} \alpha S_{cool} \alpha_R}$$

which upon substitution yields $\Theta_2 = 64.35$ °C. This temperature is below the admissible level for class B.

Refine the calculation of the secondary resistance

$$r_2 = 1.58 \times 10^{-6}(1 + 0.004 \times 64.35)\, 17.12 \times 120 / 3.14 \times 10^{-2}$$
$$= 0.13\ \Omega$$

Because the resistance of the secondary winding has reduced, the error will be also lower.

(b) Consider heating of the primary winding. The temperature of the primary is

$$\Theta_1 = \Theta_0 + \tau_{exc} + \Delta \tau_1$$

where τ_{exc} is the excess temperature at the bus end,

$$\tau_{exc} = \tau_b + I_1^2 R_1 / 2p \lambda s_b$$

The excess temperature of the bus

$$\tau_b = I_1^2 \varrho / s_b \alpha S_0$$

where $s_b = 3.6$ cm^2 is the bus cross section; $\alpha = 10$ W / m^2 °C is the heat transfer coefficient for the bus; $S_0 = 13.2$ cm^2 / cm is the side surface of unit length (for 60 × 6 mm^2 bus); $\varrho = 0.022 \times 10^{-4}\ \Omega$ cm is the resistivity at $\Theta = 100$ °C, R_1 is the resistance of the primary winding at $\Theta = 100$ °C, and $I_1 = 660$ A.

In order to determine $\Delta \tau_1$ we need the thermal resistance of half length of the primary winding $R_{T1} = l_1 / 2 \lambda s_1 = 40 / 2 \times 4 \times 3.6 = 1.4$, the length of the primary winding $l_1 = 40$ cm, thermal conductivity for copper $\lambda = 4$ W / cm °C, the resistance of the primary winding $R_1 = \varrho l_1 / s_1 = 2.4 \times 10^{-6} \times 40 / 3.8 = 26.7 \times 10^{-6}\ \Omega$, and $p = (\alpha S_0 / \lambda s_b)^{1/2} = 0.032$.

The temperature difference in the primary bar over a length of $l_1 / 2$ is

$$\Delta \tau_1 = 0.5 I_1^2 R_1 R_{T1} = 8.8\ °C$$
$$0.5 I_1^2 R_1 p \lambda s_b = 13.3\ °C$$
$$\Theta_1 = 40 + (660^2 \times 0.022 \times 10^{-4}) / (3.6 \times 10^{-4} \times 10 \times 13.2)$$
$$+ (0.5 \times 660^2 \times 26.7 \times 10^{-6}) / (0.032 \times 4 \times 3.6)$$
$$+ 0.5 \times 660^2 \times 26.7 \times 10^{-6} \times 1.4$$
$$= 81.67\ °C$$

The actual temperature is lower as $R_1 < 26.7\ \mu\Omega$.

11. *Thermal short time current.* The thermal capability for the primary winding is

$$A_{sc} = (k_{1T} I_{1,r} / s_1)^2 \times 1 + A_r$$

where $k_{1T} = 65$ is the per unit value of the 1-s short time rating, $t = 1$ s, and A_{sc} and A_r are found by the curves for Θ_r and Θ_{sc} plotted for copper.

For the primary winding, $\Theta_r = 81.67$ °C and we find

$$A_r = 1.55 \times 10^4$$

$$A_{sc1} = (65 \times 600 / 375)^2 \times 1 + 1.55 \times 10^4 = 2.6 \times 10^4 \text{ A}^2 \text{ s / mm}^4$$

We find $\Theta_{sc1} = 150$ °C. For the secondary winding, $\Theta_2 = 64.35$ °C and we find $A_r = 1.4 \times 10^4$ A^2 s / mm^4

$$A_{sc2} = (65 \times 5 / 3.14)^2 \times 1 + 1.4 \times 10^4 = 2.47 \text{ A}^2 \text{ s / mm}^4$$

and $\Theta_{sc2} = 125$ °C.

12. *Mechanical short time rating.* For type TPOL c.t.s the calculation of mechanical rating is confined to the external mechanical rating defined by the interaction with the neighbouring phases. From the insulation standpoint, the least interphase distance is 12 cm [2.1]. With account of the size of the flange we take the interaxial distance equal to 35 cm. The bus is about 0.5 m long from the end of the primary to the first support insulator (Fig. 10.36). The relevant strength problem is statically indeterminate. The idealisations are as follows: the end of the bus connected with the c.t. is freely supported by the end of the c.t. primary, then the moment about the attachment is equal to the moment of the force $F_b / 2$ and the moment of the distributed force acting upon half the length of the primary winding $l = 41.2$ cm.

For the middle phase we have $F_{b,max} = \sqrt{3}\, k\, 10^{-7} I_{pk}^2$, where $k = 2l_b / a = 2 \times 50 / 35 = 2.86$ (we assume that the bus is infinitely long), $I_{pk} = I_{1,r} \sqrt{2}\ k_m = 600\sqrt{2} \times 160 = 1.36 \times 10^5$ A is the short-time current.

The force acting on the primary

$$F_{b,max} = \sqrt{3} \times 10^{-7} \times 2l I_{pk}^2 / a = 7542 \text{ N}$$

The specific force per unit length is $F_{sp} = F_{max} / l = 7542 / 41.2 = 183$ N / cm.

The bending moment about the attachment

$$M_{bend} = \frac{F_{b,max}}{2} \frac{l}{2} + \frac{F_{sp}}{2} \frac{l^2}{4} = 13.3 \times 10^4 \text{ N cm}$$

At the fixation, the epoxy insulator has the annular cross section with $D_{ext} = 16$ cm and $D_{int} = 2.2$ cm. The moment of resistance to bending

$$W_{bend} = \pi (D_{ext}^3 - D_{int}^3) / 32 = 402.96 \text{ cm}^3$$

The stress at the fixture $\sigma = M_{bend} / W_{bend} = 330$ N / cm^2 $< \sigma_{adm} = 6000$ N/cm^2, where σ_{adm} is the admissible bending stress.

Because the conductors are of finite length, the stress will be somewhat lower. The distance between the phases may be reduced.

13. *Calculation of e.m.f. across the open secondary.* We construct the curve $i = f(t) = \sqrt{2}\, I_{1,r} \sin \omega t$ in the time interval $t = 0.05$-5 ms. The field strength

Table 10.5

t, ms	0.05	0.1	0.2	0.5	1	2	3	4	5
i_1, A	13.32	26.64	53.25	132.7	262	498.5	686	806.8	848.5
$H_0 = \frac{i_1}{l_{av}}$, A/m	49.8	100	199	497	981	1867	2569	3022	3178
H_0, A/m	35.3	71	141	352.5	686	1324	1822	2143	2254
B_m, T	0.72	1.22	1.45	1.57	1.645	—	—	—	—
$\Phi \times 10^{-4}$, Wb	9	15.25	18.12	19.62	20.6	—	—	—	—

$H = iw / l$ is determined and the magnetic flux density B and flux $\Phi = BS$ are found from the magnetisation curve [10.14].

The results of the calculation are summarised in Table 10.5. The plot Φ versus time is constructed and the graphic differentiation technique is employed to determine

$$|e_{20}| = w_2 \, \mathrm{d}\Phi / \mathrm{d}t \approx w_2 \, \Delta\Phi / \Delta t$$
$$= 120 \times 9 \times 10^{-4} / 0.05 \times 10^{-3} = 2160 \text{ V}$$

This e.m.f. can also be calculated by means of E_{sp} (see Sect. 10.3).

REFERENCES

10.1 N. I. Bachurin: *Transformatory toka* (Current transformers). Energiya, Leningrad 1964.

10.2 I. M. Sirota: *Perekhodnye rezhimy raboty transformatorov toka* (Transients in current transformers). Izd. AN UkrSSR, Kiev 1961.

10.3 V. E. Kazanskii: *Transformatory toka v ustroistvakh releinoi zashchity i avtomatiki* (Current transformers for protective service). Energiya, Moscow 1978.

10.4 A. A. Chunikhin: *Elektrichestvo* No. 2, 26-30 (1973).

10.5 A. A. Chunikhin: *Elektrotekhnika* No. 9, 55-58 (1980).

10.6 A. A. Chunikhin *et al: Prospect VDNKh,* Moscow 1976.

10.7 A. A. Chunikhin and I. P. Shcheglov: *Elektrotekhnicheskaya promyshlennost. AVN* No. 10 (99), 7-10 (1976).

10.8 B. G. Stroganov and A. A. Chunikhin: *Elektrichestvo* No. 67-69 (1980).

10.9 A. A. Chunikhin and B. G. Stroganov: *Elektrotekhnicheskaya promyshlennost. AVN* No. 8 (112), 3-5 (1980).

10.10 I. B. Bolotin and L. Z. Eidel: *Izmereniya v perekhodnykh rezhimakh korotkogo zamykaniya* (Transient measurements on short circuit). Energiya, Leningrad 1981.

10.11 A. A. Chunikhin: *Elektricheskiye apparaty* (Switchgear). Energiya, Moscow 1975.

10.12 L. V. Shopen: *Beskontaktnye elektricheskiye apparaty avtomatiki* (Contactless apparatus of relaying service). Energiya, Moscow 1976.
10.13 I. S. Beletskaya and E. A. Limanov: *Transformatory postoyannogo toka i napryazheniya* (Measurement current and voltage transformers for d.c. transmission lines). Energiya, Moscow 1964.
10.14 V. V. Afanasyev (ed.): *Transformatory toka* (Current transformers). Energiya, Leningrad 1980.
10.15 V. V. Karasev and A. E. Filippov: *Elektrotekhnika* No. 7, 16-19 (1980).

11
VOLTAGE TRANSFORMERS

11.1 General

Voltage transformers (v.t.s) are used to transform the high primary voltage to low values suitable for standard ratings of instruments, meters, relays, and other measuring and control devices. The normal secondary ratings are 100 V or $100/\sqrt{3}$ V, which implies that standard instruments may be used to measure any voltage however high and voltage sensitive relays can be manufactured for a standard voltage independent of installation. Thus, a v.t. insulates measuring and control devices connected across the secondary circuit from the primary circuit operating voltages.

The primary winding of a v.t. is insulated from the secondary in agreement with the voltage class of the installation. To provide complete protection the secondary circuit should be earthed at one point.

The connection diagram of a single-phase v.t. is shown in Fig. 11.1. The primary winding w_1 is connected in the primary circuit through fuses *F1*. The secondary winding w_2 feeds the load, such as windings of measuring instruments or relays, connected to it through fuses *F2*. In addition to the earthed secondary winding, core *M* of the ordinary-design v.t.s should be also earthed.

Fuses *F2* protect the v.t. from a short circuit in the secondary circuit. Fuses *F1* protect the high-voltage system from short-circuits in the v.t. Incorporation of current-limiting fuses or expulsion-principle fuses with a limiting resistor is desirable. The resistance of the v.t. is high and in the event of a short circuit in the secondary circuit the current in the primary will be fairly low (about a few amperes) and might be insufficient to cause other types of fuse to operate.

The principal parameters of a v.t. are as follows:

Rated voltage of the primary and secondary windings are indicated on the

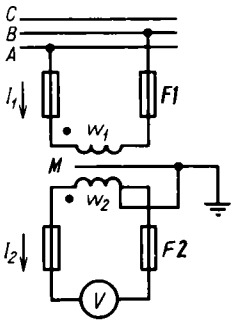

Fig. 11.1. Connection scheme of the 1-ph voltage transformer

nameplate. The normal voltage of the transformer is the one for the primary indicated on the nameplate.

Nameplate ratio is the rated primary to rated secondary voltage ratio of the transformer:

$$k_r = U_{1,r}/U_{2,r}$$

Voltage ratio error is defined as

$$\Delta u = \frac{U_2 k_r - U_1}{U_1} \tag{11.1}$$

where U_1 is the voltage applied to the primary winding and U_2 is the voltage applied to the secondary burden. If $U_1/U_2 = k_r$, then the ratio error is zero.

The convention for the positive direction of currents in a v.t. (Fig. 11.2) is the same as in current transformers (see Fig. 10.2). Here $U_2' = U_2 w_1/w_2$. The flux Φ leads by 90° the e.m.f. E_2 induced in the secondary (Fig. 11.3).

Phase angle error is expressed in minutes and is the difference in the phase position of the voltage applied to the secondary burden and the voltage applied to the primary winding. By convention, a phase error is positive when the secondary voltage phasor leads the primary voltage phasor.

The ratio error limit of a v.t. expressed in per cent is numerically equal to the transformer accuracy class [11.1]. Voltage transformer errors must not exceed the tabulated error limits when the primary voltage varies between 0.8 and 1.2 times normal value and output VA varies from a quarter to the full standard value.

The connection scheme of a v.t. (see Fig. 11.1) is the same as for a power transformer. Current in the secondary winding is defined by the load impedance

$$I_2 = U_2/Z_2$$

and the secondary power

$$P_2 = U_2 I_2 = U_2^2/Z_2$$

increases for lower Z_2.

Rated output power is the maximum power, taken at the rated power factor 0.8, for which the stated accuracy limits apply.

11.2 Phasor Diagram and Errors

The voltage ratio error occurs as a result of ohmic and reactive losses in the v.t. The equivalent circuit of a v.t. where all the quantities are referred to the primary side is shown in Fig. 11.2, and the respective phasor diagram in Fig. 11.3. The magnetic flux Φ induces a secondary e.m.f. E_2' that lags behind the flux by 90°. This e.m.f. produces a secondary current $I_2' = I_2 w_2/w_1$ which produces in the burden resistance R_2' and reactance X_2' a voltage drop U_2' measured at the secondary terminals. The same current produces a voltage drop across r_2 and x_2' of the secondary winding proper. The sum of these voltages makes the e.m.f. E_2'. The magnetising current I_0 leads the flux by a loss angle ψ. The voltage drop in the primary winding is $I_1(r_1 + jx_1)$.

By the Ampere circuital law (phasor) $I_0 w_1 = I_1 w_1 - I_2 w_2$ or

$$I_1 = I_0 + I_2' \quad \text{and} \quad I_2' = I_2 w_2 / w_1 \tag{11.2}$$

Then

$$I_1(r_1 + jx_1) = I_0(r_1 + jx_1) + I_2'(r_1 + jx_1)$$

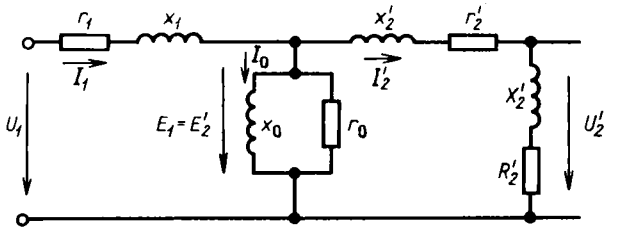

Fig. 11.2. Equivalent circuit of a voltage transformer

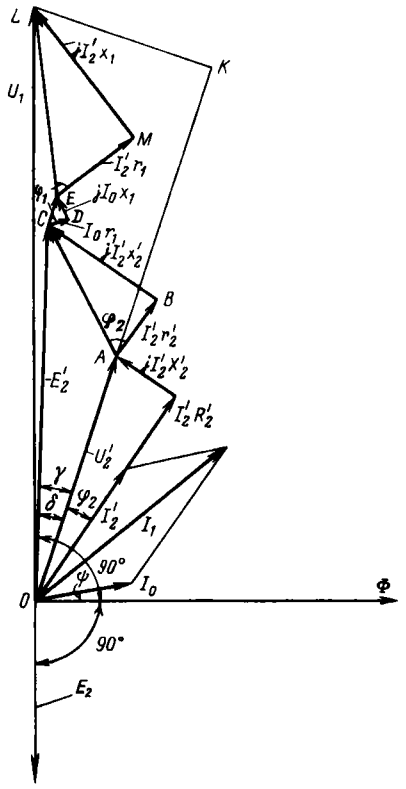

Fig. 11.3. Phasor diagram

With reference to Fig. 11.2

$$U_1 = I_0(r_1 + jx_1) + I_2'(r_1 + r_2') + I_2'j(x_1 + x_2') + U_2'$$

The triangle ABC in Fig. 11.3 represents the voltage drop produced in the secondary winding by I_2'. The sides of the triangle CDE represent the voltage drops produced across r_1 and x_1 of the primary by the current I_0. The triangle EML represents the voltage drops in the primary due to I_2'. If the errors in the actual transformer were absent, then $U_1/U_2 = w_1/w_2$ or $U_1 = U_2'$ and points A and L would be coincident. The errors occur because of the resistances and reactances of the v.t. and the presence of a no-load current.

Consider the voltage ratio error. Because the angle δ is small the difference of U_1 and U_2' may be replaced by the projection of $ACEL$ onto the U_2' axis. Therefore the error is defined by the segment AK. In an actual v.t. the angle γ is small and the angle $\varphi_{sc1} \approx \varphi_{sc2}$, so that some simplifications can be done in error evaluation.

The ratio error is found by projecting the phasors I_0r_1, I_0x_1, $I_2'r_1$, $I_2'r_2$, $I_2'x_1$, and $I_2'x_2'$ on the direction of U_2'. Then

$$\begin{aligned}\Delta u &= -AK/OK \\ &= -\frac{1}{U_1}\{I_0(r_1 \sin \psi + x_1 \cos \psi) \\ &\quad + I_2'[(r_1 + r_2') \cos \varphi_2 + (x_1 + x_2') \sin\varphi_2]\}\end{aligned} \tag{11.3}$$

The voltage ratio error is seen to consist of two parts. The first is defined by the no-load current, and the second by the load current. The error can be decreased by reducing both load resistance and reactance. Low resistance with large wire section can be achieved when current densities in the windings are low (about 0.3 A/mm^2). At such current densities the thermal load of the windings is rather low. The inductive reactance of the windings x_1 and x_2' can be reduced by placing the windings closer to one another.

For a given primary voltage U_1 the magnetising current is practically constant. In agreement with Eq. (11.3) the ratio error increases linearly with the load current I_2'. Because in the normal operating mode the voltage U_2' varies with I_2' only insignificantly, the output power P_2 is proportional to this current. The variation of voltage ratio error with output power is shown in Fig. 11.4*a*.

The voltage ratio error is also a function of the power factor: it increases as $\cos \varphi_2$ decreases. Dependence on the operating voltage can be revealed by looking at the open-secondary condition ($I_2' = 0$). If we assume that the angle of loss does not vary with the magnetising current I_0, then Eq. (11.3) suggests that Δu will be defined by the ratio of the magnetising current I_0 to the operating voltage U_1. The magnetic flux density B is proportional to U_1, and I_0 is proportional to H because $I_0w_1 = Hl$, hence the ratio error becomes proportional to H/B_m or varies in inverse proportion to the core permeability μ. The normal density is selected within 1.0-1.1 T. When the primary voltage varies from 0.5 to 1.1 rated value the permeability increases and the ratio error decreases.

It is worth noting that the voltage ratio error due to the open circuit current is low compared with that due to the load current. Therefore when the operating

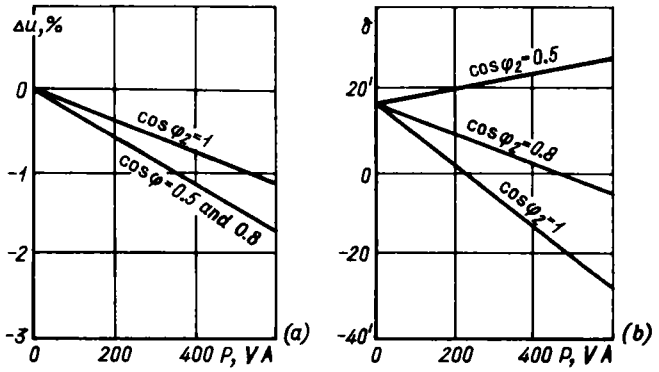

Fig. 11.4. Voltage-ratio and phase-angle errors as functions of secondary burden

voltage varies from 0.5 to 1.1 rated voltage, the ratio error changes primarily due to the load current I_2'.

The phase angle error is denoted by δ in Fig. 11.3. Because this angle is small we may take $OL \approx OK$, then $\tan \delta = KL/OL$ and (in minutes)

$$\delta = \frac{3440}{U_1} \{ I_0(r_1 \cos \psi - x_1 \sin \psi) + I_2'[(r_1 + r_2') \sin \varphi_2 - (x_1 + x_2') \cos \varphi_2] \} \tag{11.4}$$

A similar derivation can be found in Ref. [11.1]. The phase angle error also consists of two parts: one is defined by the no-load (open-circuit) current and the other by the load current.

Equation (11.4) indicates that the winding reactance introduces a negative error, whereas the resistance gives a positive phase error. Figure 11.4*b* shows the phase error as a function of output power P_2 at different power factors.

With the secondary winding open-circuited the phase error is positive. When the burden is purely ohmic (unity power factor), increasing power causes δ to change sign and become negative. At $\cos \varphi_2 = 0.5$ the phase error increases linearly with power and remains positive. It is instructive to note that the type of load affects the phase error to a greater extent than voltage ratio error, as can be gleaned from Fig. 11.4*a* and *b*.

For convenience of the following analysis we represent the voltage ratio error as the sum of the open-circuit error Δu_{oc} and load error Δu_L. Now from Eq. (11.3) we have

$$\Delta u_{oc} = (-I_0 r_1 \sin\psi - I_0 x_1 \cos \psi)/U_1$$
$$I_0 r_1 \sin \psi = I_1 r_1 (I_0/I_1) \sin\psi = U_{a1} I_a / I_1 = U_{a1} i_a$$
$$I_0 x_1 \cos\psi = I_1 x_1 (I_0/I_1) \cos \psi = U_{r1} I_r / I_1 = U_{r1} i_r$$

where U_{a1} and U_{r1} are the active and reactive voltage drops in the primary winding at the rated load, and i_a and i_r are the ratios of the active and reactive components

of o.c. current to the rated primary current. For $U_1 = U_{1,r}$ this yields the open circuit ratio error in the form

$$\Delta u_{oc} = -(u_{a1} i_a + u_{r1} i_r) \tag{11.5}$$

and the ratio error due to the load current

$$\Delta u_L = -(u_a \cos \varphi_2 + u_r \sin \varphi_2) \tag{11.6}$$

where $u_a = u_{a1} + u_{a2}$ and $u_r = u_{r1} + u_{r2}$ are the active and reactive voltage drops due to the load current taken as per unit values of the primary voltage.

Similarly for the phase angle error (in minutes) one can obtain

$$\delta_{oc} = 3440(u_{a1} i_r - u_{r1} i_a) \tag{11.7}$$

$$\delta_L = 3440(u_a \sin \varphi_2 - u_r \cos \varphi_2) \tag{11.8}$$

The limits of voltage ratio error and phase angle error should not be exceeded when the primary voltage varies from 0.8 to 1.2 $u_1/u_{1,r}$ and the output power varies from a quarter to the rated value. Denoting $u_1/u_{1,r} = \alpha$ and $I_2'/I_{2,r}' = P_2/P_{2,r} = \beta$ yields

$$\Delta u_{oc} = -(u_{a1} i_a + u_{r1} i_r)\frac{1}{\alpha} \tag{11.9}$$

$$\Delta u_L = -(u_a \cos \varphi_2 + u_r \sin \varphi_2)\frac{\beta}{\alpha} \tag{11.10}$$

and

$$\delta_{oc} = 3440(u_{a1} i_r - u_{r1} i_a)/\alpha \tag{11.11}$$

$$\delta_L = -3440\beta(u_a \sin \varphi_2 - u_r \cos \varphi_2)/\alpha \tag{11.12}$$

11.3 Error Compensation

The compensation of a voltage ratio error can be readily achieved by reducing the number of turns in the primary winding. The transformation ratio becomes lower than the rated ratio and the secondary voltage increases. This implies a positive ratio error which tends to compensate the negative error. Usually the compensating error is made such that on open circuit the v.t. may have the maximum positive error admissible for this class accuracy. The resultant voltage ratio error is given as

$$\Delta u = -\frac{1}{U_1}\{I_0(r_1 \sin \psi + x_1 \cos \psi) + I_2'[(r_1 + r_2') \cos \varphi_2 - (x_1 + x_2') \sin \varphi_2]\} + (w_{1,r} - w_1)/w_{1,r} \tag{11.13}$$

This turn correction does not affect the phase-angle error. The latter can be compensated for a three-phase voltage transformer only (Fig. 11.5*a*). The primary winding of this transformer consists of a basic part having a large number of turns (*AX*, *BY*, and *CZ*) and compensating turns put respectively on the limbs of phases *A*, *B*, and *C*. The phasor diagram in Fig. 11.5*c* shows the pre-correction phase vol-

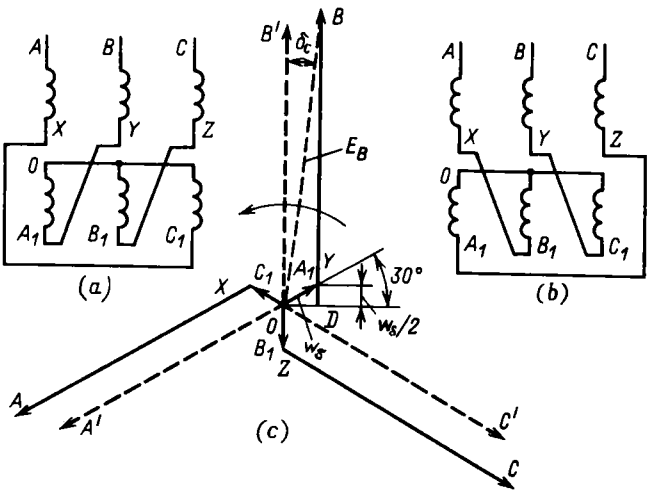

Fig. 11.5. Phase error compensation in a v.t.

tages OA', OB', and OC' and the phase B e.m.f. after correction

$$E_B = OB = OA_1 + OB'$$

As a result of the compensation the e.m.f. phasor of the primary E_B and, consequently, the phasor of the primary voltage, turns clockwise through an angle δ_c.

With an inductive burden the secondary voltage U_2' lags behind the primary U_1 by an angle δ. Causing the phasor U_1 to rotate clockwise reduces the actual angle between U_1 and U_2', thus reducing the phase angle error. If the ratio error is positive, the primary turn correction takes the form indicated in Fig. 11.5*b*.

Estimation of the compensating turns w_δ is carried out on the following grounds. Because δ_c is small, it can be written as

$$\delta_c = 3440 \frac{OD}{BD} = 3440(OA_1 \cos 30°)/BD$$
$$= 3440(w_\delta/w_{1,r}) \cos 30°$$

where $w_{1,r}$ is the full number of the primary turns per phase (AX), whence

$$w_\delta = \delta_c w_r/3440 \cos 30° = 0.336 \times 10^{-3} \delta_c w_r$$

Since the turns w_δ produce an e.m.f. in the primary winding, the turn correction should be carried out with allowance for this e.m.f.

Now, the turn compensation for the basic part of the primary winding is as follows:

$$\Delta w = w_{1,r} \Delta u_c + w_\delta \sin 30° = w_{1,r} \Delta u_c + w_\delta/2$$

where $\Delta u_c = (w_{1,r} - w_1)/w_1$.

11.4 Construction of Voltage Transformers

For voltage ratings up to 35 kV the v.t. construction is similar to that of power transformer. However, the magnetic flux density is considerably inferior to that in power transformers. This reduces ratio errors and in some cases allows for insulation testing by means of the induced voltage [11.1]. A source is connected to the secondary voltage while the open circuited primary is subjected to high voltage. Usually the secondary winding is fed by a twice rated voltage and the magnetic flux density should not exceed the saturation level.

In some situations the primary winding designed for a phase voltage operation appears at a line voltage. This should not lead to saturation of the magnetic circuit.

Single-phase v.t.s available for 35 kV have either both terminals of the high-voltage winding insulated or one terminal insulated the other being earthed.

Figure 11.6*a* shows the outline of a single-phase oil-insulated v.t. for 6 kV. Both leads of the primary winding are insulated from the casing.

A more promising approach in v.t. design and manufacture is associated with the use of plastic compounds (moulded insulation) in place of oil insulation. It offers an appreciable reduction of size and weight, and an easy maintenance no longer troubled by oil contamination. Voltage transformers with moulded insulation are free from fire hazard and convenient for installation in mobile substations and in modular-type switchgear installations. Figure 11.6*b* shows a type NOL 11-6 moulded-insulation v.t. for the same ratings as the oil-insulated unit shown nearby.

The overall dimensions of a v.t. are decided to a considerable degree by the amount of insulation. Therefore, whenever possible v.t.s are designed to measure phase-to-earth voltage, that is, the earthed terminal of the primary need not be insulated any longer. The linear voltage is obtained by star connecting the secondary windings of such transformers. This construction is advantageous in its lower size and cost. However, the measurement error increases since the errors of two transformers are added together.

Some connection schemes for single-phases v.t.s of ordinary construction are depicted in Fig. 11.7. The diagram at (*a*) shows two single-phase v.t.s with insulated

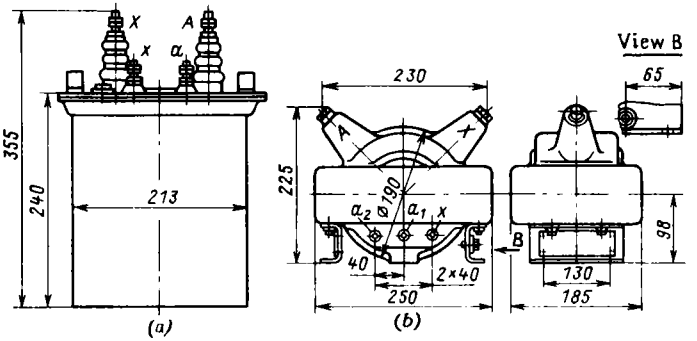

Fig. 11.6. Voltage transformers with (*a*) oil and (*b*) moulded insulation

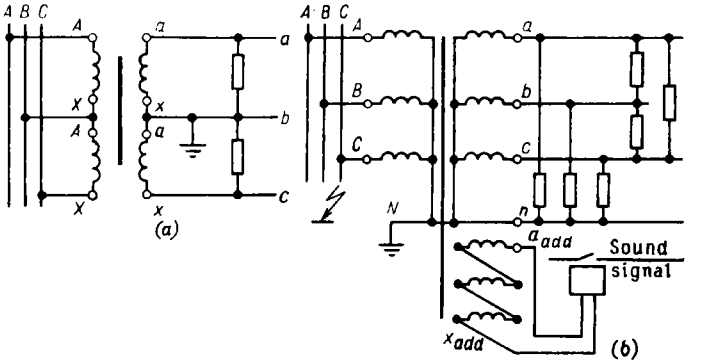

Fig. 11.7. Connection schemes of 3-ph voltage transformers

primary terminals. This "open-delta" scheme is a very convenient arrangement for power and energy measurements. Each of these v.t.s may be loaded into a burden up to a rated size. The output voltage is $U_{AC} = U_{AB} + U_{BC}$ (instruments are connected between points *a* and *c*). However, this connection is not recommended because of additional errors due to added errors of the two windings.

The connection shown in (*b*) allows for the use of v.t.s having one terminal of the primary earthed. Each winding is connected across the phase voltage, therefore the rated voltage of the transformer is $U_r/\sqrt{3}$. The secondary burden is connected into a star or delta arrangement. The rated voltage at the secondary terminals is $100/\sqrt{3}$ V.

For the purpose of insulation status monitoring and supply of the protective system that must operate in the event of a short circuit to earth, the v.t. is provided with additional windings a_{add}, x_{add}, connected into an open-delta arrangement. In symmetric operation, the sum of e.m.f.s induced in these windings is zero. If a connection to earth occurs for one of the lines, the e.m.f. equilibrium is disturbed and the voltage across the open-delta terminals is fed to a relay or conveyed to a signal system.

If the system neutral is earthed through an arc-suppression coil, an earth-phase fault of one phase, say *C*, does not lead to short circuit. The installation can continue its service for a long time. Under the circumstances the voltage of *C* (Fig. 11.7*b*) falls to zero, while the voltage of *A* and *B* increases to the line voltage. Accordingly the magnetic flux density in the cores of *A* and *B* also increases $\sqrt{3}$ times. In order to avoid undesirable heating and rise of error of such v.t.s, their magnetic circuits should not saturate under this rise of density.

In installations with the neutral earthed, an earth fault of one of the phases causes a short circuit. The relay protection rapidly disconnects the faulted segment. On a short circuit the sound phase voltage never rises above 1.2-1.3 times the phase voltage.

The size and cost of a v.t. can be cut down by joining three 1-phase instrument v.t.s into one three-phase unit. Three-limb and five-limb cores are common for such designs.

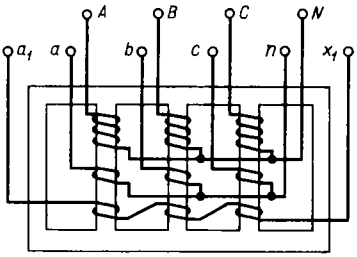

Fig. 11.8. Five-limb voltage transformer

Three-phase 3-limb v.t.s are made with the insulated zero point at the high-voltage side. This is explained by the short circuit hazard in networks with insulated neutral due to earthing of one phase if the v.t. used has its zero point earthed [11.1].

Assume that the windings of phases *A*, *B*, and *C* are placed on the three legs of a 3-limb core and the zero point is earthed. At a short circuit fault in phase *C* the windings of *A* and *B* appear at the line voltage while the winding of phase *C* is shorted. The magnetic fluxes of phases *A* and *B* will link the phase *C* leg and produce in the phase *C* winding an e.m.f. causing a short circuit current in this winding. This current can cause a fault of this winding.

For insulation state monitoring in systems with the zero point isolated, use is made of 5-limb three-phase v.t.s (Fig. 11.8). In this case, if one of the phases appears earthed, the fluxes of sound phases are linked through the exterior limbs with low magnetic resistance. The v.t. has an open-delta winding a_1x_1 that is used for signalling and relaying service. In symmetric operation, no output voltage appears at the terminals of this winding.

For voltages above 35 kV, the sharply increasing size and cost of v.t.s forces the designers to adopt a cascade arrangement. Two cascades are employed at 110 kV (Fig. 11.9*a*). Each of the cascades has its own magnetic circuit, denoted by M_1 and

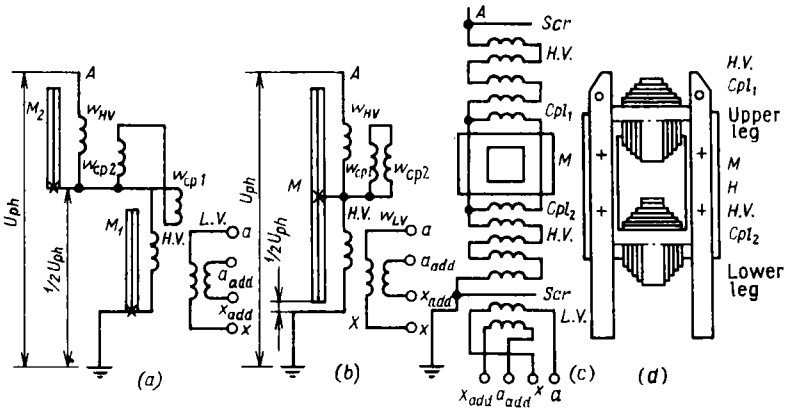

Fig. 11.9. Arrangement and scheme of v.t. windings

M_2, with a high-voltage winding w_{HV} designed for half the phase voltage. One end of this winding is connected with the core, the other is insulated from it for the half phase voltage. The lower stage has output windings ax and $a_{add}x_{add}$, one for feeding measuring instruments, the other for relaying service. The coupling winding w_{cp1} is placed on M_1, and w_{cp2} on M_2.

If no load is connected to the output windings, the voltage divides equally between w_{HV} because they have identical inductive reactances on no load. On load the secondary current demagnetises M_1 and reduces the flux linking this core. The reactance of M_1 also decreases so that in the absence of coupling windings the voltage would be divided unequally between the stages, the greater part being across the second stage.

The coupling windings serve the purpose of equalising the voltage between the windings on load. At open circuit the e.m.f.s are identical in these windings because of equal fluxes M_1 and M_2. The windings are connected in opposition, so that the equalising current is zero. On load the flux in M_1 falls, the e.m.f. in w_{cp2} becomes higher than in w_{cp1} and gives rise to an equalising current that demagnetises M_2 and magnetises M_1. This current is such that the upper element takes up half the load connected to the output windings.

A more advanced design of the Moscow Electric Works is that shown in Fig. 11.9*b*. This transformer has a single 2-limb core M, insulated from earth for a half phase voltage. The upper leg carries the coupling windings w_{cp} and high-voltage winding w_{HV} designed for $U_{ph}/2$. One end of these windings is connected to the core M, the other is insulated from the core for the voltage $U_{ph}/2$. The lower core leg carries the windings wound one over another in the following order: w_{cp}, w_{HV}, and output low-voltage windings w_{LV} atop.

To achieve a uniform distribution of voltage over the HV winding coils, screens, *Scr*, are placed atop and connected with the winding (Fig. 11.9*c*).

The assembled core with the windings is fixed to the transformer base through support insulators (Fig. 11.9*d*). This assembly is placed in a porcelain casing and filled with transformer oil.

A v.t. for 220 kV is assembled by staking two 110-kV units one above another. A similar arrangement is used for 500 kV v.t.s. Voltage equalisation is achieved with the aid of guard rings. The upper elements subjected to higher voltages are provided with stronger insulation. Figure 11.10 shows the outline of type NKF-500 voltage transformer for 500 kV.

It is important to note that the resultant resistance and inductive reactance exceed considerably that of the single unit therefore the accuracy class of the cascade v.t.s cannot be raised above that of the component units. General considerations concerning cascade v.t. design may be found in Ref. [11.1].

As has been noted above v.t.s are made for low current density. Where such a unit is used as a power source and the error is not critical, the load may be considerably raised. By way of example, the type NOM-10 v.t. of class 0.5 is rated for a secondary burden of only 80 VA, whereas the maximum output allowable is 720 VA.

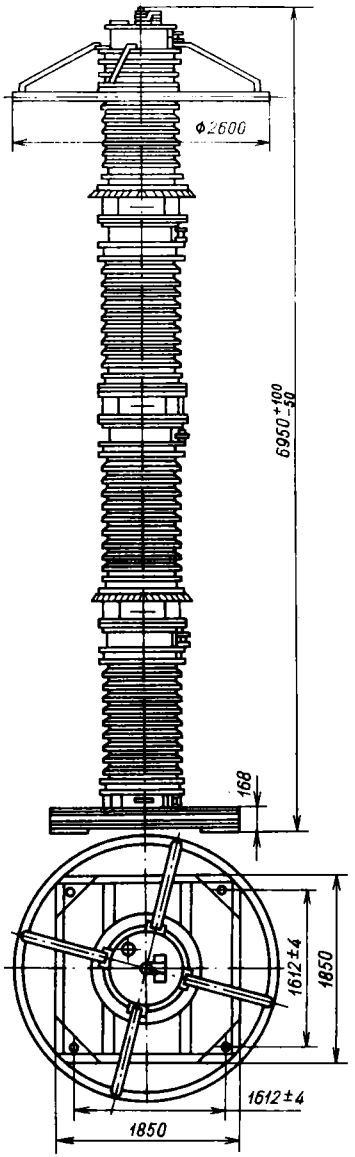

Fig. 11.10. Cascade v.t. for 500 kV

11.5 Components of Electromagnetic V.T.s

Cores. The core of low voltage v.t.s (up to 600 V) is assembled of stamped E-shaped laminations. Single phase v.t.s for operating voltage up to 35 kV are made shell-type Fig. 11.11*a*. The centre limb is with stepped cross-section perimeter for a better core-circle utilisation. The side limbs have a rectangular cross section. The yoke cross section is commonly taken by 20% larger than the limb cross section.

The core-type rather than shell type is used for 3-ph v.t.s (Fig. 11.11*c*). Each limb carries a set of coils of one phase. The 5-limb construction is common for systems with the neutral point isolated (Fig. 11.11*d*).

Table 11.1 summarises the dimensions of mass-produced Soviet magnetic circuits. The core material is predominantly 1512 (hot rolled) or 3412 steel strips 0.35-0.5 mm thick having small no-load losses, high permeability, and allowing a maximum values of magnetic flux density of 1.7 T in normal operation. This material is advantageous in that it offers size reduction of the core and of the entire transformer.

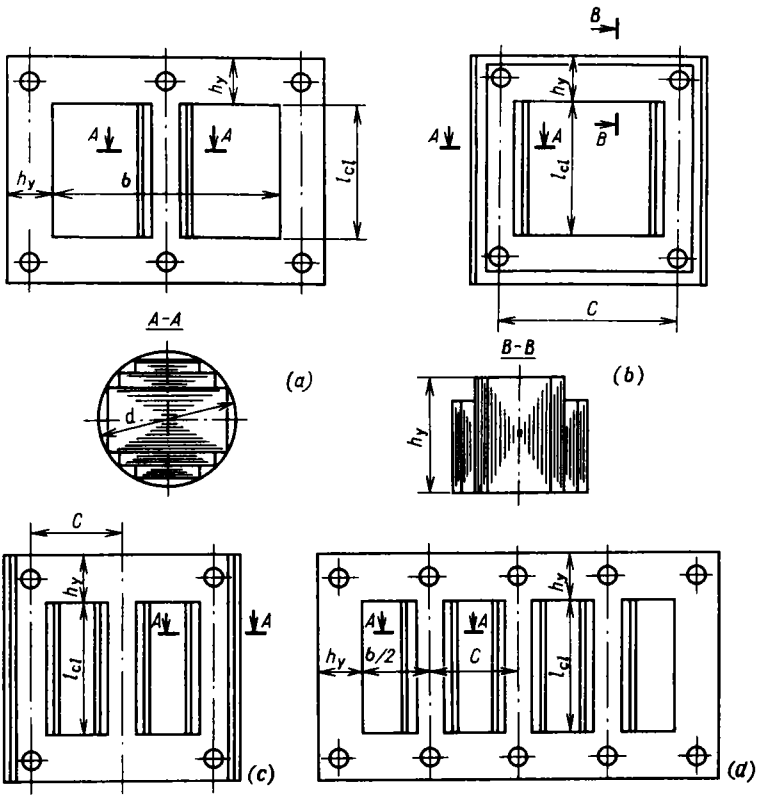

Fig. 11.11. Core forms of voltage transformers

Table 11.1

Type	Dimensions, mm					Net cross section,		Mass of steel, kg	Reference figure
	d	l_d	c	b	h_y	limb cm^2	yoke		
NOS-0.5	—	118	—	88	16	22.0	11.0	6.0	—
NOM-6									
NOSK-3	60	138		140	28	22.5	28.6	9.16	
NOSK-6-66	65	130	—	165	25	24.9	26.5	9.48	11.11*a*
NOM-10	70	170	—	180	28	30.6	33.3	14.32	
NOM-15	70	180	165	—	56	30.8	33.4	19.6	
NOM-35-66	70	256	—	235	26	30.6	30.5	18.67	
ZNOM-15-63	70	185	—	216	28	30.6	33.3	16.0	
ZNOM-20-63	70	215	—	216	28	30.6	33.3	17.42	11.11*a*
ZNOM-24	70	256	—	235	26	30.6	30.5	18.65	
NTS-0.5	55	85	100	—	45	17.6	18.8	6.96	
NTMK-6-48	55	140	120	—	45	18.4	19.2	8.3	
NTMK-10	70	180	160	—	56	30.6	33.3	31.5	
NTMI-6-55	65	70	—	158	25	26.3	26.5	3 × 7.05	
NTMI-10-66	65	130	—	158	25	26.3	26.5	3 × 9.47	11.11*d*
NTMI-18	70	275	195	228	52	31.1	30.9	66.7	11.11*a*
NTMI-20	70	135	—	190	26	30.6	30.5	3 × 14.3	
NKF-110-57	120	210	380	—	91	91.8	93.3	96.4	
NKF-220-58									11.11*b*
NKF-330	120	400	430	—	91	91.8	93.3	3 × 136	
NKF-500								4 × 130.2	

Windings. Dry and oil insulated v.t.s usually have windings wound with enameled varnished wire. For transformers rated on 110 kV and higher, enameled varnished wire with additional silk insulation is used. Moulded insulation transformers employ wire with resistant enamel unsolvable in epoxy resin, and double glass-insulated wire. The primary winding is wound with round wire.

In view of a low power of the v.t. and a high voltage of the primary winding the wire section is rather small. In order to achieve a better winding space utilisation the winding is wound with a high wire pretension. Wire rupture can be avoided by choosing a wire diameter above 0.2 mm. This wire size will also secure the desirable service strength of the primary winding. High-current secondary windings are wound by rectangular wire. It is important to stress that reliable operation of v.t.s depends to a considerable degree on the construction and quality of manufacture of the windings.

The construction of windings of a v.t. for a voltage up to 10 kV is shown in Fig. 11.12. The reactance of the windings is reduced by having both the primary and secondary windings of the same height. The secondary is insulated from the core by a cylinder of electric-grade cardboard. The secondary is insulated from the primary by a cylinder of electric-grade cardboard (4).

For easier operating conditions of the electric insulation, the primary coil is

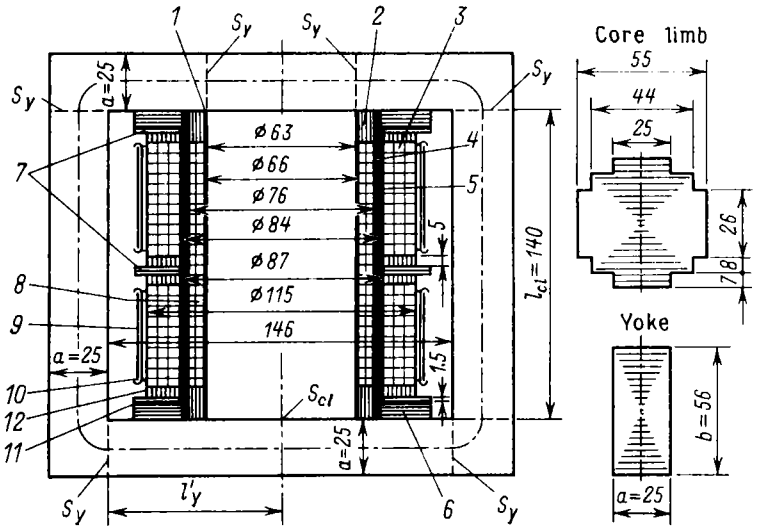

Fig. 11.12. Sectional view of a 3-kV voltage transformer: (1) 1.5-mm thick cylinder of electric grade, (2) edges, (3) HV winding (wire layers are wrapped with cable paper), (4) 4-mm thick cylinder of electric grade cardboard, (5) cable paper cylinder with edge collars, (6) end washers of electric grade cardboard, (7) intermediate and end spacer rings of electric grade cardboard, (8) LV winding (cable paper is interleaved with the layers), (9) electrostatic screen, (10) screen insulation, (11) edge collars of cylinder (5), (12) projections of HV interlayer insulation

made in two sections. Each section bears half of the voltage. Consequently, the voltage per layer reduces to half its normal value. The coils are connected to one another at the lower spacing ring (7). The winding taps are taken from the upper layers of the sections. All these constructional features contribute to the improvement of the coil electric strength. The coil proper is wound on a multi-layered cylinder with flanged edges (11). The insulation of coil butt ends from the core yoke is enhanced by means of end rings (6) made of electric-grade cardboard.

Voltage transformers for 10 kV and higher are made with stepped primary windings. As the voltage between the winding and the yoke increases, the spacing between these transformer elements also increases, i.e. the layers of the winding become shorter.

A steep voltage waveform striking the primary winding produces the greater nonuniformity of voltage distribution in the first layer of the coil. For the sake of voltage equalisation the transformer is provided with an electrostatic screen (9). This is a thin brass or aluminium sheet shaped into a closed loop around the winding. The screen provides an additional stray capacitance to the winding, which improves the uniform distribution of voltage over the first winding layer [11.2]. To avoid high gradients of electric field, the screen receives a cable paper or cardboard envelope (10).

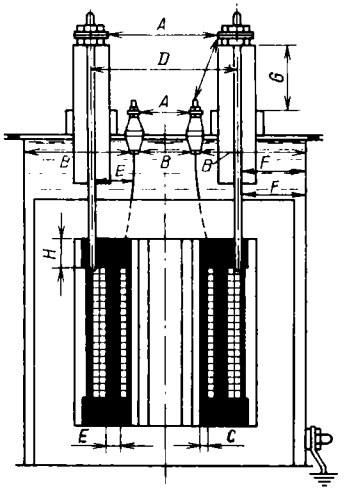

Fig. 11.13. Construction of v.t. insulation

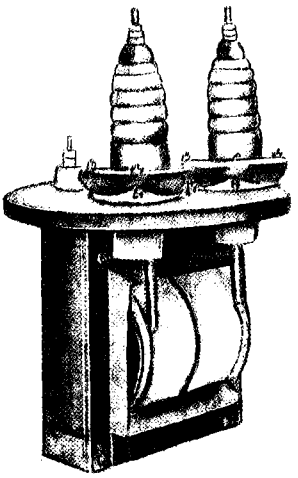

Fig. 11.14. 6-kV voltage transformer with housing removed

A 0.12-mm thick cable-paper band is interleaved between the layers of the primary winding. This band provides a reliable insulation between the layers. Tests indicated that the voltage of an incoming pulse was partitioned among the layers of the primary rather uniformly owing to a large interlayer capacitance of the winding.

Figure 11.13 shows in a schematic form the construction of electric insulation of a voltage transformer. The dielectric strength should be checked for the following spacings: (A) air gap; (B) oil gap; (C) uniform dielectric; (D) solid dielectric and air; (E) several layers of various solid dielectrics (electric-grade cardboard, cable paper layers, wire insulation); (F) several layers of solid dielectric and oil; (G) over the surface of solid dielectric in air; and (H) over the surface of solid dielectric in oil. The calculation of dielectric strength of these spacings is carried out in agreement with the recommendations of Chap. 2. The view of a 6-kV v.t. less the casing is pictured in Fig. 11.14.

11.6 Capacitor-Divider V.T.s

In high voltage systems, an economical and satisfactory voltage supply for measurement and protective purposes can be achieved by use of the capacitor-divider system shown in Fig. 11.15. The divider consists of two capacitive stages C_1 and C_2, where the capacitance of the upper stage is constituted by a number of series connected capacitors. The intermediate voltage reduced in inverse proportion to the stage capacitances appears across C_2. The capacitance of C_2 is an order of magnitude higher than that of C_1, therefore the through current in the capacitive circuit

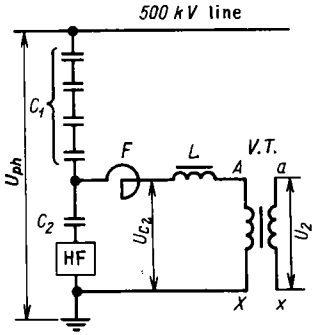

Fig. 11.15. Schematic diagram of a capacitor divider

is governed by the capacitance of C_1. The capacitance of C_2 is selected such that the voltage across this capacitor be within 4000-12 000 V. A further voltage reduction is achieved with an ordinary v.t. This transformer receives the voltage from C_2 through a reactor L. The secondary burden rated for 100 V is connected across the secondary winding labelled *ax*.

If the v.t. were connected to the capacitor C_2 without a series inductor (reactor), the voltage across C_2 would become sensitive to the burden and would fall for higher loads because of the lower input resistance of the v.t. The reactor is tuned in resonance with the cascade capacitor $C_1 + C_2$ at the power frequency, thus providing load independence for the output voltage.

Neglecting the open circuit current in the v.t., the system of Fig. 11.15 may be recasted into the scheme shown in Fig. 11.16*a*. To reveal the principal properties of the capacitor divider we assume that it is connected to an ideal, error-free v.t. Then this v.t. with the secondary burden may be replaced with the load impedance Z_2' referred to the primary side.

We invoke the method of superposition to treat this system. Disconnecting the circuit at point A yields

$$U_{C2}' = U_1 C_1/(C_1 + C_2)$$

Now we shunt the power source and apply the voltage U_{C2}' across the break (Fig. 11.16*b*)

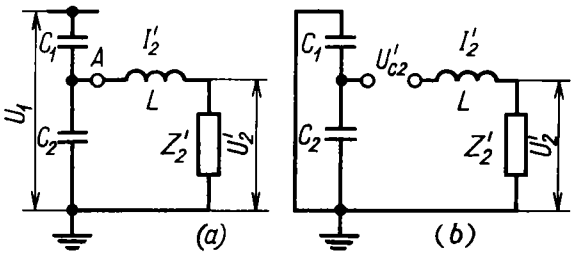

Fig. 11.16. Simplified analytical schemes for Fig. 11.15

$$U'_{c_2} = jI'_2X_L - j\frac{1}{\omega(C_1 + C_2)}I'_2 + U'_2$$

Because the reactor is tuned in resonance with the cascade capacitor $C_1 + C_2$, $X_L = \omega L = 1/\omega(C_1 + C_2)$ and

$$U'_{c_2} = U_1C_1/(C_1 + C_2) = U'_2$$

Thus, with a reactor tuned in resonance, the voltage across the load U'_2 is controlled solely by the ratio $C_1/(C_1 + C_2)$ and is independent of Z'_2. Under the assumptions made, the errors are controlled by the v.t. only.

It is worth noting that as the current I'_2 increases the voltage U'_2 remains virtually constant, whereas the voltage across the reactor I'_2X_L increases proportionally. Therefore a voltage can appear across the low stage capacitor that may be dangerous for its operation.

At a short circuit fault on the secondary side ($U'_2 = 0$), the tuned circuit will create a high voltage across C_2 that can break down this capacitor. This overvoltage is limited by a voltage arrester placed in parallel with C_2. To eliminate this dangerous regime, it is recommended to place a breaker in the secondary circuit to disconnect the s.c. current through the burden.

Until recently capacitor-dividers have been made with the capacitors formed by plates separated by capacitor paper-oil or carrier insulation of the through insulator. The low capacitance of the upper stage C_1 dictates low output power of the installation (15 VA at a 110-kV insulator). The voltage ratio error is within 5% and the phase angle error can be as high as 5°.

High-voltage overhead lines are widely used to convey high-frequency signals of communication and relaying service, therefore capacitor-dividers come in use built around capacitors of relatively large capacitance. This has led to an appreciably enhanced power levels taken from these dividers, attaining 1000 VA at high voltages. To prevent high frequency currents from entering the divider system, a h.f. rejection filter F is placed in series with the reactor. This filter prevents h.f. signals issued by the h.f. relay protective unit, *HF*, from entering the v.t. (Fig. 11.15).

The Soviet-made capacitor-dividers of accuracy class 1.0 allow output burdens up to 300 VA. Investigations indicate that capacitor-dividers of accuracy class 0.2 are feasible.

Coupling capacitors used in dividers usually have a capacitance within some tolerance zone, therefore in actual installations both reactor and v.t. have provisions for their parameter adjustment. The reactor inductance can be varied by means of the air gap in the butt-joints of the core and by the reactor winding. The voltage transformer ratio can also be varied with the aid of taps. Installations currently used to supply small power plants are underlaid by the same idea as in the considered capacitor-divider system.

A cost-effectiveness analysis for the capacitor-divider and cascade v.t.s indicates that divider systems are more advantageous at voltages above 110 kV.

The capacitor-divider provides a uniform distribution of voltage over the upper stage owing to the relatively large capacitance of constituting capacitors. In a v.t., the voltage distribution problem is more involved and aggravates at higher rated

voltages when the number of cascaded units has to be increased. At 400 kV and higher the cost of a capacitor-divider is about half as large as the cost of a v.t. At voltages below 110 kV the use of divider system fails to bring a remarkable advantage.

The advantages of capacitor-dividers are penalised by their tendency to overvoltages which takes place due to the ferroresonance phenomena. The point is that the capacitors and nonlinear inductance form a circuit that can resonate not only at the main frequency, but also at subharmonics. This can cause hazards for the insulation and give rise to disturbances that are capable of causing false operation of the protective systems. Breakdown of the connected instruments also should not be overlooked. It is worth noting, however, that many schemes have been developed to effectively limit these overvoltages.

One should not overlook also that the capacitor divider operation is sensitive to frequency variation of the measured voltage as this may offset the resonance condition of the tuned circuit.

11.7 Constant-Voltage Transformers

Like constant current transformers discussed in Sect. 10.7, the constant-voltage transformers depend for their operation on a choke-capacitance-coupled amplifier that operated in the forced magnetisation mode. The relevant schematic diagram is given in Fig. 11.17*a*. The control winding of the amplifier is connected to the high voltage line through a high-value resistance R_{add} (several ten MΩ). The current flowing in this winding is proportional to the operating (primary) voltage. Therefore, the high voltage is converted into a current that is measured by a constant current transformer (see Sect. 10.7).

The high value resistor in the control circuit complicates the operation of the system. The current flowing through the control winding is governed by the value of this resistor and at high voltages this resistance dissipates a large power. By way of example, at $U_r = 400$ kV and $I_c = 10$ mA, the power dissipated

$$P_{add} = U_{1,r} I_c = 400 \times 10^3 \times 10 \times 10^{-3} = 4 \text{ kW}$$

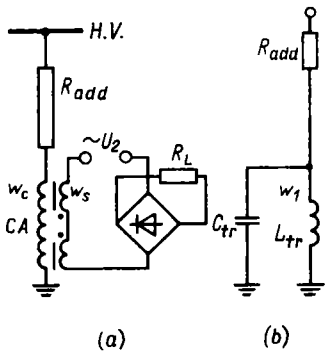

Fig. 11.17. Schematic diagram of a constant-voltage transformer

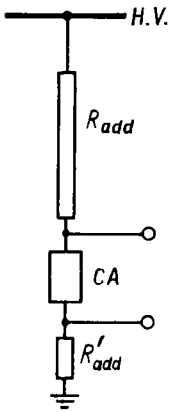

Fig. 11.18. Scheme of a constant-voltage transformer with a damping resistor

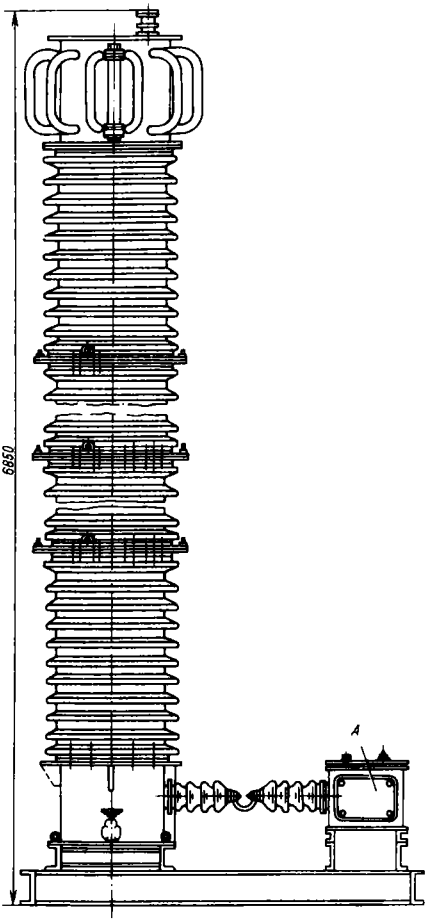

Fig. 11.19. Outline of a 400-kV constant-voltage transformer

The current I_c in the control winding w_c is to drive the amplifier core to saturation, that is $I_c w_c = H_s l$ where H_s is the strength of the saturation field, and l is the length of the magnetic circuit. Because I_c is small, the saturation has to be achieved with a large number of turns. For example, in a 400-kV constant-voltage transformer, $w_c = w_1 = 15\,000$. Such a multiturn primary (control winding) possesses a considerable stray capacitance C_{tr} that together with the inductance of this winding forms a resonance circuit (Fig. 11.17*b*). This circuit causes high frequency oscillations to appear in the primary and secondary circuits, thus contributing to the ratio error of the transformer.

This stray capacitance C_{tr} can be reduced by making the primary divided into individual sections. High frequency oscillations are damped with the aid of a damping resistor R'_{add} (Fig. 11.18). It raises the primary winding to the potential $I_c R'_{add}$

thus imposing a stronger insulation requirement. The wave profile of the secondary current can be smoothed with a duplex scheme described in Sect. 10.7. A relevant error analysis is given in Ref. [10.13].

The outline of a constant-voltage transformer is shown in Fig. 11.19. The choke-capacitance-coupled amplifier is placed in a separated steel casing (*A*) and filled with oil. The valley compensation in the waveform is achieved with the circuit represented in Fig. 10.35. The transformer is designed for 400 kV rated voltage, 10 mA rated primary (control) current, 0.5 A secondary burden current, 35 VA output power, and $\pm 1.5\%$ voltage ratio error at the rated load.

11.8 Optoelectronic Voltage Transformers

Traditional magnetic v.t.s are no longer suitable for the measurement of extremely high voltage and for tests of electric devices designed for this voltage because of large weight, size, and the errors associated with the use of cascade arrangements with large number of v.t. units. Optoelectronic voltage transformers are free from these disadvantages and offer a good choice under the circumstances.

Optoelectronic v.t.s employ external amplitude modulation of the light beam (Fig. 11.20). The relevant transducers are the Kerr cell (*a*) and Pockel's cell (*b*). The first is a transparent vessel filled with liquid dielectric (nitrobenzene) in which two electrodes are immersed to create an electric field due to the operating voltage. This field is at right angles to the light beam incoming on the cell (4) from a light source (1) through an optical system (2) and a polariser (3). The analyser (5) following the cell has its plane of polarisation at right angles to that of the polariser (3), so that in the absence of voltage U the intensity of light passing the analyser is zero.

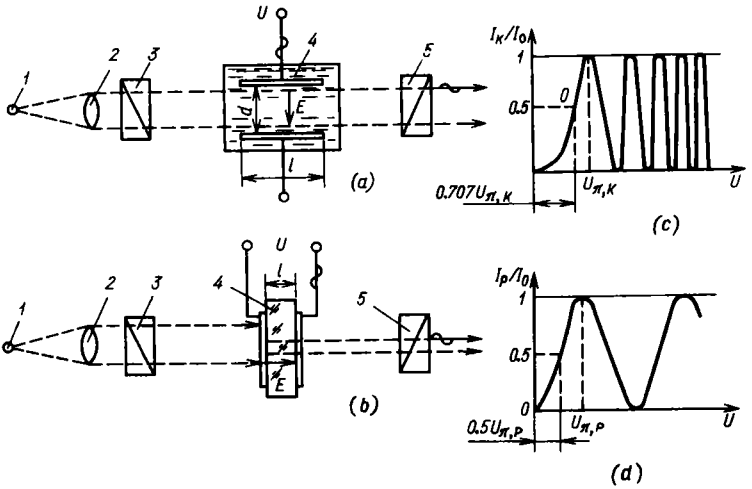

Fig. 11.20. Amplitude modulation of light in optoelectronic v.t.s.: (*a*) Kerr's cell, (*b*) Pockel's cell, (*c*) and (*d*) static characteristics of transducers

When a voltage U is applied to the cell, the relative light intensity passing the system is given as

$$\Phi_K/\Phi_0 = \sin^2(\pi klE^2) = \sin^2(\pi klU^2/d^2)$$

where k is the Kerr constant, l is the length of the light path in the liquid, E is the electric field strength, d is the distance between the plates, and Φ_0 is the intensity of light incoming on the cell. The intensity of the photoelectric signal from the Kerr cell is a square function of the applied voltage. This dependence is shown in Fig. 11.20*c*. It illustrates that a bias voltage of $0.707U_{\pi,K}$ is necessary to place the operating point at the mid point of the linear portion. This biasing condition is associated with considerable difficulties, therefore operation within a linear portion is attained by optical means: a plate of mica is inserted between the polariser and the cell to produce the effect of the required bias. In this setting the deenergised system is placed in point O.

In Pockel's cell (Fig. 11.20*b*), the electrodes confine a crystal of ammonium dihydrophosphate. Unlike Kerr's cell, in Pockel's cell the direction of electric field coincides with the direction of the light beam. The relative light intensity of the beam leaving the polariser (5) is given as

$$\Phi_P/\Phi_0 = \sin^2(\pi r_{63} n_0^3 U/\lambda)$$

where r_{63} is the electro-optic coefficient of the crystal, n_o is the ordinary refractive index, and λ is the wavelength of light.

The linear portion of the Pockel cell characteristic is seen to be wider than that of the Kerr cell characteristic. Like in Kerr's cell a bias of $0.5U_{\pi P}$ is necessary to place the quiescent point in the midpoint of the slope.

The measurement limits depend on the applied voltage only and are independent of the size of the crystal. The maximum admissible voltage is decided by the dielec-

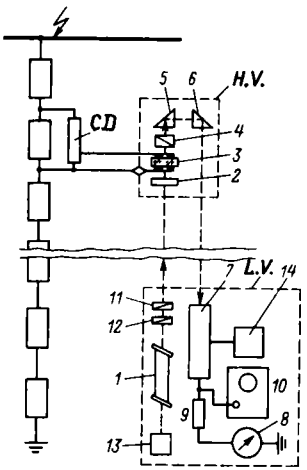

Fig. 11.21. Conceptual design of an optoelectronic voltage transformer

tric strength of the crystal. Therefore, a Pockel cell system is suitable for a few kilovolt range. A major advantage of Pockel's cell is its practically unlimited service life in a wide temperature range. Monochromatic light is not necessary. The maximum operating frequency is 10 MHz.

Figure 11.21 shows a schematic diagram of a setup built around an optoelectronic v.t. to measure the voltage across the break of a multi-break circuit breaker earthed with one of its terminals. The left-hand blocks in the figure represent the capacitors shunting the breaks, *CD* denotes the capacitor-divider of the optoelectronic v.t. cell, and H.V. and L.V. embrace the high-voltage and low-voltage units of the setup respectively.

The set up operation is as follows. The plane polarised laser beam (1) passes through polarisers (11, 12) adjusting the transformer sensitivity and a plate (2) which shifts the operating point in the middle of the linear portion. The beam passing through the Pockel cell (3) and a polariser (4) is returned down to earth by prisms (5, 6) to strike an electron multiplier phototube (7). The photocurrent is measured by a meter (8), and an oscilloscope (10) shows the voltage profile across a load resistor (9). Stabilised power sources (13, 14) feed the laser and photomultiplier. An optoelectronic v.t. developed in the USSR [11.3] has an operating range up to 2 kV.

11.9 Calculation of a Magnetic V.T. Illustrative Example

Given: The rated primary voltage, $U_{1,r} = 3$ kV; rated secondary voltage, $U_{2,r} = 100$ V; rated output power, $P_{2,r} = 50$ VA; and accuracy class 1. All the other parameters are as stated in Sects. 11.1 and 11.2.

It is required to design an appropriate v.t. and choose its basic parameters.

A feasible design procedure may be as follows.

1. *Cross section of core limb and yoke.*

$$S_{cl} = E_{1,r}/w_1 4.44 f B_m$$

Since the voltage drop in the winding is small, we may let $U_{1,r} \approx E_{1,r}$.

At operating voltage below 35 kV the ratio $U_{1,r}/w_1$ should be less than 1 volt per turn. The transformer power is small, therefore we may select (in view of low losses) low grade hot-rolled steel 0.5-mm thick with paper insulation between the laminations. For $U_{1,r} = 3$ kV we select $U_{1,r}/w_1 = 0.5$ volt per turn. Assume $B_m = 1.1$ T, then the core leg cross section

$$S_{cl} = U_{1,r}/4.44 f w_{1,r}/B_m$$
$$= 0.5/4.44 \times 50 \times 1.1 = 22.112 \times 10^{-4}\ \text{m}^2$$

The calculation will be carried out for a shell-type transformer (Fig. 11.11*a*). The cross section of yoke

$$S_y = 1.2 S_{cl}/2 = 13.267 \times 10^{-4}\ \text{m}^2$$

For steel laminations with paper insulation, a lamination stacking factor of $k_{ls} = 0.86$ is a good choice.

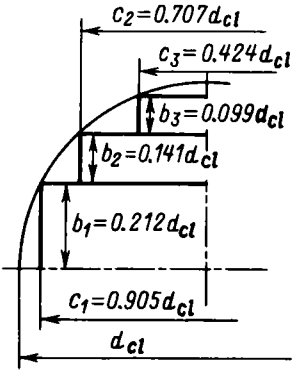

Fig. 11.22. Core limb cross-section geometry

The geometric cross sections of core limb and yoke are:

$$S'_{cl} = S_{cl}/k_{ls} = 22.112 \times 10^{-4}/0.86 = 25.71 \times 10^{-4}\,\text{m}^2$$

$$S'_{y} = S_{y}/k_{ls} = 13.267 \times 10^{-4}/0.86 = 15.427 \times 10^{-4}\,\text{m}^2$$

The step cross section of a core limb is shown in Fig. 11.22. Determine the dimensions of core steps assuming that there are five of them with three widths. For a five-step core, the core circle utilisation factor is $k_{cc} = 0.851$ [11.2], so that the circle area

$$S_{circle} = S'_{cl}/k_{cc} = 25.71 \times 10^{-4}/0.851 = 30.2 \times 10^{-4}\,\text{m}^2$$

The core limb diameter

$$d_{cl} = \sqrt{4S_{circle}/\pi} = 4 \times 30.2 \times 10^{-4}/3.14 = 6.2 \times 10^{-2}\,\text{m}$$

Now, with reference to Fig. 11.22, the optimal steep dimensions are

$$c_1 = 0.905d_{cl} = 5.6 \times 10^{-2}\,\text{m}; \qquad b_1 = 0.212d_{cl} = 1.315 \times 10^{-2}\,\text{m}$$
$$c_2 = 0.707d_{cl} = 4.385 \times 10^{-2}\,\text{m}; \qquad b_2 = 0.141d_{cl} = 0.8745 \times 10^{-2}\,\text{m}$$
$$c_3 = 0.424d_{cl} = 2.63 \times 10^{-2}\,\text{m}; \qquad b_3 = 0.099d_{cl} = 0.614 \times 10^{-2}\,\text{m}$$

The thickness of one lamination

$$\Delta = 0.5/k_{ls} = 0.5/0.86 = 0.5814\,\text{mm}$$

The geometric cross section of the core limb

$$S'_{cl} = 2c_1b_1 + 2c_2b_2 + 2c_3b_3 = 25.661 \times 10^{-4}\,\text{m}^2$$

The area of steel in the step cross section

$$S_{cl} = S'_{cl}k_{ls} = 25.661 \times 10^{-4} \times 0.86 = 22.0685 \times 10^{-4}\,\text{m}^2$$

The yoke has the rectangular cross section

$$S'_{y} = 15.427 \times 10^{-4}\,\text{m}^2$$

with the depth

$$b = 2(b_1 + b_2 + b_3) = 5.607 \times 10^{-2}\,\text{m}$$

and width

$$a = S_y'/b = 15.427 \times 10^{-4}/5.607 \times 10^{-2} = 2.75 \times 10^{-2}\,\text{m}$$

We choose $a = 2.5 \times 10^{-2}$ m, so

$$S_y' = ab = 14 \times 10^{-4}\,\text{m}^2, \quad 2S_y' = 28 \times 10^{-4}\,\text{m}^2$$
$$S_y = S_y'k_{ls} = 12 \times 10^{-4}\,\text{m}^2, \quad \text{and} \quad 2S_y = 24 \times 10^{-4}\,\text{m}^2$$

The number of laminations in one limb is the total of

$$n_1 = 2b_1/\Delta = 45, \quad n_2 = 2b_2/\Delta = 30, \quad \text{and} \quad n_3 = 2b_3/\Delta = 21$$

The number of laminations in a yoke

$$n = b/\Delta = 56.07/0.5814 = 96$$

Entering Table 11.1 with the figure for d_{cl}, one may find the NOM-6 a suitable core type.

2. *Winding turns and wire section.*

The rated primary current [11.1]

$$I_{1,r} \approx P_{2,r}/U_{1,r} = 16.7\,\text{mA}$$

Assume the current density $J_1 = 0.4\,\text{A/mm}^2$, then the primary wire cross section $s_1 = I_r/J_1 = 0.0416\,\text{mm}^2$ and the wire diameter is $d_1 = (4s/\pi)^{1/2} = 0.23$ mm. Standard enameled wire of this size has $d_1 = 0.29$ mm, $d_{1ins} = 0.33$ mm so that $s_1 = \pi d_1^2/4 = 0.066\,\text{mm}^2$.

The rated secondary current $I_{2,r} = P_{2,r}/U_{2,r} = 0.5$ A, therefore the wire cross section at the current density adopted above will be

$$s_2 = I_{2,r}/J_2 = 0.5/0.4 = 1.25\,\text{mm}^2$$

and the wire diameter

$$d_2 = \sqrt{4s_2/\pi} = 1.26\,\text{mm}^2$$

We choose a wire with $d_2 = 1.3$ mm, $d_{2ins} = 1.38$ mm, which gives $s_2 = \pi d_2^2/4 = 1.33\,\text{mm}^2$.

The number of turns in the high voltage winding

$$w_1 = U_{1,r}/4.44fB_mS_{cl} = 5567$$

The number of turns in the low voltage winding

$$w_2 = U_{2,r}/4.44fB_mS_{cl} = 186$$

Summarising the final data of the windings, on a core of $d_{cl} = 62$ mm,

$$w_1 = 5567 \quad w_2 = 186$$
$$d_1 = 0.29\,\text{mm} \quad d_2 = 1.3\,\text{mm}$$
$$d_{1ins} = 0.33\,\text{mm} \quad d_{2ins} = 1.38\,\text{mm}$$

The sectional view of the v.t. core and windings is shown in Fig. 11.12. The core is insulated from the secondary windings by a cylinder of electric grade cardboard with 63-mm inner diameter and 66-mm outer diameter. The distance from the winding to the yoke is 14-15 mm. It is filled by a collar (2) 14 mm thick.

Assume that the limb is 140 mm high. Then the low voltage winding is $H_{w2} = 140 - 28 = 112$ mm high. This winding is enveloped by a cylinder (4) of electric grade cardboard of 4-mm total thickness. This cylinder together with the flanged cylinder (5) form the major insulation between the low voltage and high voltage windings, (8) and (3) respectively. The high voltage winding also has a cable paper interlayer insulation. The projected portion of the interlayer insulation is assumed to be 5 mm wide.

End rings (6) of electric grade cardboard are installed between the flanged cylinder (5) and the yoke. In addition, a 1.5-mm thick cardboard spacer (7) is placed between the projected ends of the interlayer insulation (12) and the flanged cylinder. Similar rings are placed between the sections of the high voltage winding. The total space occupied by insulating materials, as measured along the axis of HV winding is

$$\Delta_{ins} = 2 \times 4\Delta_6 + 2\Delta_{11} + 4\Delta_7 + 4\Delta_{12}$$
$$= 2 \times 4 \times 1.5 + 2 \times 1.5 + 4 \times 1.5 + 4 \times 5 = 41 \text{ mm}$$

The height of one HV coil

$$H_{w1} = (140 - \Delta_{ins})/2 = (140 - 41)/2 = 49.5 \text{ mm}$$

Determine the number of turns per layer of LV winding

$$H_{w2}/d_{2ins} = 112/1.38 = 81$$

The LV winding has two complete layers and one layer with 24 turns. The interlayer insulation is made of two layers of 0.12-mm cable paper. The thickness of LV winding

$$\Delta_{w2} = 3 \times 1.38 + 2 \times 0.24 = 4.62 \text{ mm}$$

Assume $\Delta_w = 5$ mm. The collars prevent the extreme turns from slipping. A flexible wire of 1.5-mm^2 section is brazed to the end of winding and the place of brazing is insulated.

The low voltage winding is wrapped up in a 4-mm thick cylinder (4) of electric grade cardboard.

To improve the operating conditions for insulation, the high voltage winding is partitioned into two sections. The number of turns per layer

$$H_{w1}/d_{1ins} = 49.5/0.33 = 150$$

The number of layers in a coil

$$w_1/2 \times 150 = 5567 \div (2 \times 150) = 18.55$$

The 18 complete layers have 150 turns each and the 19-th layer consists of 84 turns wound over the screen with 0.74-mm diameter wire uniformly over the coil length. The screen is a copper or aluminium foil. The coil is wrapped up in a band of cable paper and strapped up with a surgical tape. The interlayer insulation is $2 \times 0.12 = 0.24$ mm thick.

The radial thickness of the HV winding

$$\Delta_{w1} = 19 \times 0.33 + 19 \times 0.24 + 1 \times 0.8 = 11.63 \text{ mm}$$

Assume that the HV winding is $\Delta_{w1} = 14$ mm thick. The inner diameter of this winding is

$$D_{in} = 66 + 2\Delta_{LV} + 2\Delta_{cyl} + 2\Delta_{cyl,fl}$$
$$= 66 + 2.5 + 2 \times 4 + 2 \times 1.5 = 87 \text{ mm}$$

The outer diameter of the HV winding

$$D_{out} = D_{in} + 2\Delta_{w1} = 87 + 2 \times 14 = 115 \text{ mm}$$

3. *Check of the electric strength of insulation spaces.*

(a) The electric strength of the longitudinal insulation between the HV and LV windings consists of the strength of a cardboard cylinder of thickness $\Delta_1 = 4$ mm with relative permittivity $\varepsilon_{1r} = 4$ and $r_2/r_1 = 84/76$ (see Fig. 11.12), and a flanged cylinder of cable paper with $\varepsilon_{2r} = 3$, $\Delta_2 = 3$ mm, and $r_3/r_2 = 87/84$.

The dielectric strength of the cylinder of electric grade cardboard can be determined as follows:

$$E_1 = \frac{U_{bd}}{r_1\varepsilon_1[\ln (r_2/r_1)/\varepsilon_1 + \ln (r_3/r_2)/\varepsilon_2]}$$

For the rated primary voltage 3 kV, the Soviet standard dictates that $U_{test} = 24$ kV and $U_{bd} = 1.2U_{test} = 28.8$ kV, therefore

$$E_1 = \frac{28.8}{\frac{76 \times 4}{2}\left[\frac{\ln (84/76)}{4} + \frac{\ln (87/84)}{3}\right]} = 5.163 \times 10^3 \text{ V/mm}$$

For the cylinder of cable paper

$$E_2 = \frac{28.8}{\frac{84 \times 3}{2}\left[\frac{\ln (84/76)}{4} + \frac{\ln (87/84)}{3}\right]} = 6.23 \times 10^3 \text{ V/mm}$$

These figures are fairly agreeable since the maximum strength of electric grade cardboard is 10 kV/mm and the maximum strength of cable paper is 16 kV/mm.

(b) Estimate the dielectric strength of a spacing between the HV winding and the vertical yoke. With reference to Fig. 11.12 this spacing filled with oil is 15 mm wide. The breakdown voltage for a point-to-earthed-plane electrode pair in oil is 28.8 kV.

(c) According to the Soviet standard the dielectric strength of the secondary winding insulation with respect to the limb is tested at 2 kV during 1-minute interval, therefore

$$U_{bd} = 1.2U_{test} = 1.2 \times 2 = 2.4 \text{ kV}$$

$$E = \frac{U_{bd}}{r_5 \ln (r_4/r_5)} = \frac{2.4}{(63/2) \ln (66/63)} = 1640 \text{ V/mm}$$

(d) Estimate the dielectric strength of the spacing between the HV winding and horizontal yoke. This spacing contains four rings of electric grade cardboard of 1.5-mm thickness and $\varepsilon_{r,cb} = 4$; a cylinder collar of cable paper with $\varepsilon_{r,p} = 3$ (1 ps × 1.5 mm); a cardboard spacer ring with $\varepsilon_{r,cb} = 4$ and $\Delta_{cb2} = 1.5$ mm. The flange between the HV winding and the spacer ring is made of cable paper with $\varepsilon_{r,p} = 3$ and $\Delta_p = 5$ mm. Because in this section flashover can occur over the surface of the paper, we omit this weakened section from our consideration and perform the calculation as for the case of a plane capacitor

$$E_p = \frac{U_{bd}}{\varepsilon_{r,p}(\Delta_p/\varepsilon_{r,p} + \Delta_{cb1}/\varepsilon_{r,cb} + \Delta_{cb2}/\varepsilon_{r,cb})}$$

$$= \frac{28.8}{3(1.5 \div 3 + 1.5 \div 4 + 6 \div 4)} = 4.042 \text{ V/mm}$$

$$E_{cb} = \frac{U_{bd}}{\varepsilon_{r,cb}(\Delta_p/\varepsilon_{r,p} + \Delta_{cb1}/\varepsilon_{r,cb} + \Delta_{cb2}/\varepsilon_{r,cb})}$$

$$= \frac{28.8}{4(1.5 \div 3 + 1.5 \div 4 + 6 \div 4)} = 3 \times 10^3 \text{ V/mm}$$

The electric strength of all the other insulation spacings shown in Fig. 11.13 is checked in a similar manner. This procedure is followed by the estimation of gap strength when subjected to impulse test voltage. The maximum test voltage is 42 kV for a full wave, and 52 kV for a chopped-wave impulse.

4. *Estimation of v.t. errors.* It will be carried out by the equations given in Sect. 11.2. The ohmic resistance of windings

$$r_1 = \varrho_{20} \frac{\pi D_{1,av} w_1}{s_1} = 0.0178 \times 3.14 \times 0.101 \times 5567 \div 0.066 = 476.4\,\Omega$$

$$r_2' = \varrho_{20} \frac{\pi D_{2,av} w_2}{s_2} \left(\frac{w_1}{w_2}\right)^2$$

$$= (0.0178 \times 3.14 \times 0.071 \times 186 \div 1.33)(5567 \div 186)^2 = 497.4\,\Omega$$

The reactance of windings will be calculated with reference to Fig. 11.23. The reactance of the v.t. in the equivalent circuit (see Fig. 11.2) referred to the

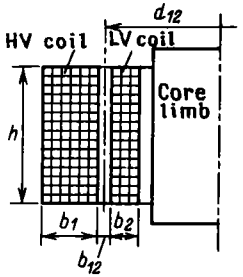

Fig. 11.23. Construction to calculate the reactance of windings

secondary side is

$$x_{sc} = w_2^2 d_{12} c k_{act}/80\,500h$$

where k_{act} allows for the deviation of the actual leakage flux from the ideal parallel flux because of the final axial size h of the windings in comparison with the radial dimension

$$k_{act} = 1 - (b_{12} + b_1 + b_2)/\pi h = 1 - (0.55 + 5 + 1.4) \div 11.2 = 0.93$$

$$c = b_{12} + (b_1 + b_2)/3 = 0.55 + 1.9 \div 3 = 1.18\text{ cm}$$

$$x_{sc} = 186^2 \times 8.15 \times 1.18 \times 0.93 \div (80\,500 \times 11.2) = 0.3432\,\Omega = x_1' + x_2$$

The reactance of the v.t. referred to the primary side

$$x_{sc}' = x_{sc}(w_1/w_2)^2 = 0.3432(5567 \div 186)^2 = 307.44\,\Omega$$

For the sake of estimation we may assume that the referred inductive reactances of the windings in the T-equivalent circuit are approximately equal. Then $x_1' = x_2$ and the reactance of the HV winding in the equivalent circuit is

$$x_1' = 0.5x_{sc}' = 0.5 \times 307.44 = 153.72\,\Omega$$

The calculation of active and reactive components i_a and i_r of magnetising current will be carried out as outlined in Refs. [11.1] and [11.2], namely

$$i_a = (p_{cl}G_{cl} + p_yG_y)/U_{1,r}I_{1,r}$$

where G_{cl} and G_y, kg, are respective masses of core limb and yoke (a calculation of mass is given in Ref. [11.2]), and $p_{cl} = f(B_{cl})$ and $p_y = f(B_y)$, W/kg are the actual specific losses in the core limb and yoke respectively. At the rated primary voltage,

$$B_{cl} = 1.1\text{ T}, \quad B_y = 1.01\text{ T}$$

$$p_{cl} = 1.67\text{ W/kg}, \quad p_y = 1.37\text{ W/kg}$$

$$G_{cl} = 4.66\text{ kg}, \quad G_y = 3.9\text{ kg}$$

and we get

$$i_a = 0.26$$

$$i_r = (q_{cl}G_{cl} + q_yG_y + n_{cl}q_{bj,cl}S_{cl} + n_yq_{bj,y}S_y)/U_{1,r}I_{1,r}$$

where q_{cl} and q_y are specific excitation (magnetisation) powers in the limb and yoke, A/kg; n_{cl} and n_y are the number of butt-joints in the limb of S_{cl} and yoke of S_y, and $q_{bj,cl}$ and $q_{bj,y}$ are specific excitation powers per unit area of butt joint of a core limb and yoke, respectively [11.2].

With reference to Fig. 11.12, $n_{cl} = 1$ and $n_y = 3$. Also at the rated primary voltage,

$$q_{cl} = 6.5\text{ VA/kg}, \quad q_y = 4.5\text{ VA/kg}$$

$$q_{bj,cl} = 0.76\text{ VA/cm}^2, \quad q_{bj,y} = 0.48\text{ VA/cm}^2$$

$$S_{cl} = 22.07\text{ cm}^2, \quad S_y = 24\text{ cm}^2$$

We get

$$i_r = 1.98$$

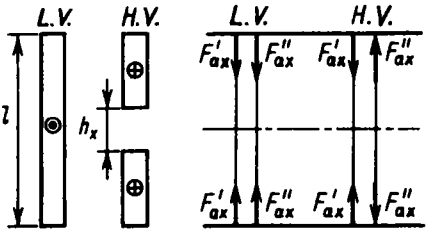

Fig. 11.24. Direction of the axial forces acting on the v.t. windings

The voltage-ratio error and phase-angle error will be calculated by Eqs. (11.10) and (11.12), where $\alpha = 1$, $\beta = 1$, $\cos \varphi_2 = 0.8$, $r_1 = 476.4\,\Omega$, $r_2' = 497.4\,\Omega$, $x_{sc}' = x_1 + x_2' = 307.44\,\Omega$.

$$\Delta u_{oc\%} = -(16.7 \times 10^{-3} \times 476.4 \times 0.26 \div 3000 + 16.7 \times 10^{-3} \times 153.72 \times 1.98 \div 3000) \times 100 = 0.238\%$$

$$\delta_{oc} = 34.4(16.7 \times 10^{-3} \times 476.4 \times 1.98 \div 3000 - 16.7 \times 10^{-3} \times 153.7 \times 0.26 \div 3000) \times 100 = 17.3'$$

$$\Delta u_{L\%} = -16.7 \times 10^{-3}(476.4 + 497.4) \div 3000 + 16.7 \times 10^{-3} \times 307.44 \times 0.6 \times 100 \div 3000 = 0.536\%$$

$$\delta_L = 34.4[16.7 \times 10^{-3}(476.4 + 497.4) \times 0.6 \div 3000 - 16.7 \times 10^{-3} \times 307.44 \times 0.8 \div 3000] \times 100 = 6.47'$$

The calculation for $\alpha = 0.8$ and 1.2 and for $\beta = 0.25$ and 0.75 is carried out in a similar manner. The errors, summarised in a table, should not exceed the values specified by the respective standard.

5. *Mechanical withstand capability of the v.t. (Fig. 11.24).*

The short-time current

$$I_{pk} = \sqrt{2} k_{mw} I_{sc}$$

where $k_{mw} = 1 - \exp(-0.01 U_a/U_r) \approx 1$, U_a and U_r being the active and reactive components of the voltage drop; $I_{sc} = U_{1,r}/Z_{sc} = 3000 \div 1077.459 = 2.784$ A with Z_{sc} being the impedance of the HV and LV windings:

$$Z_{sc} = \sqrt{(x_1 + x_2')^2 + (r_1 + r_2')^2}$$

$$= \sqrt{(307.44)^2 + (476.4 + 497.4)^2} = 1077.459\,\Omega$$

$$I_{pk} = \sqrt{2} k_{mw} I_{sc} = \sqrt{2} \times 1 \times 2.784 = 3.9376\,\text{A}$$

Determine the force acting on the winding in the radial direction. This force occurs as a result of the interaction of the longitudinal stray magnetic field with the winding current:

$$F_{rad} = B_{av} I_{pk} w_1 l_t \times 10^{-2} = 794.92\,\text{N}$$

where B_{av} is the mean magnetic flux density of the longitudinal field, T; w_1 is the number of turns in the HV winding; and $l_t = 0.3171$ m is the average turn length. The flux density is found as

$$\begin{aligned} B_{av} &= 0.4\pi I_{pk} w_1 k_R / 2l \\ &= 0.4 \times 3.14 \times 3.9376 \times 5567 \times 0.93 \div (2 \times 11.2) \\ &= 0.11436 \text{ T} \end{aligned}$$

where $l = 11.2$ cm is the winding height, and $k_R = 0.93$ is the Rogowsky coefficient.

The radial force F_{rad} tends to expand the HV winding and compress the LV winding. It is applied to the entire surface of the primary winding. The force bursting the turns of the HV winding is

$$F_\sigma = F_{rad}/2\pi = 794.92 \div (2 \times 3.14) = 126.515 \text{ N}$$

the relevant stress

$$\begin{aligned} \sigma_{rad} &= F_{rad}/w_1 s_1 = 120.515 \div (5567 \times 0.066 \times 10^{-2}) \\ &= 34.433 \text{ N/cm}^2 \end{aligned}$$

It lies well within the range of admissible stress $\sigma_{rad} = 30\text{-}50$ N/cm^2 for v.t.s of this rating.

The radial component of the flux density of the stray magnetic field produces an axial mechanical force. The winding compressive force is calculated as follows

$$F'_{ax} = F_{rad} c/2l = 41.875 \text{ N}$$

where $c = b_{12} + (b_1 + b_2)/3 = 0.55 + 1.9 \div 3 = 1.18$ cm.

The presence of a gap between the sections of the primary produces a force that tends to pull these sections apart:

$$F''_{ax} = F_{rad} h/k_R 4l'' = 794.92 \times 1.3 \div (0.93 \times 4 \times 4.2) = 66.14 \text{ N}$$

where $h = 1.3$ cm is the distance between sections of the primary winding (see Fig. 11.24), and $l'' = 4.2$ cm is the average length of the force line of the cross stray field, which is assumed equal to the distance from the core limb to the wall of the enclosure.

Now, the force compressing the insulating rings and applied to the yoke is

$$F_y = F''_{ax} - F'_{ax} = 66.14 - 41.875 = 24.265 \text{ N}$$

The force acting on the secondary is the sum of forces

$$F_{comp} = F'_{ax} + F''_{ax} = 41.875 + 66.14 = 108.015 \text{ N}$$

The compressive stress of the HV winding

$$\begin{aligned} \sigma_{comp1} &= F_y/\pi D_{av1} \Delta_{w1} = 24.265 \div (3.14 \times 10 \times 1.4) \\ &= 0.5517 \text{ N/cm}^2 \end{aligned}$$

The compressive force for LV winding

$$\begin{aligned} \sigma_{comp2} &= F_{comp}/\pi D_{av2} \Delta_{w2} \\ &= 108.015 \div (3.14 \times 7.1 \times 0.5) = 9.685 \text{ N/cm}^2 \end{aligned}$$

These stresses are well within the admissible range of σ_{comp} = 18-20 MN/m^2 for voltage transformers.

6. *Thermal withstand capability* [10.11].

$$\Theta_L = 20\ °C$$
$$A_L = 0.7 \times 10^4$$
$$I_{sc} = 2.784\ A$$
$$\Delta_{sc1} = I_{sc1}/S_1 = 2.784 \div 0.066 = 42.18\ A/mm^2$$
$$\Delta_{sc}^2 t = A_{sc} - A_L$$
$$\Theta_{sc} = 250\ °C$$
$$A_{sc} = 3.8 \times 10^4 A^2\ s/mm^4$$
$$t_1 = (3.8 \times 10^2 - 0.7 \times 10^4) \div 42.18^2 = 17.42\ s$$

7. *Evaluation of the ultimate v.t. load.*

Under ultimate load the wire temperature attains the maximum admissible value. The low voltage winding is under more severe cooling conditions. The heat released in this winding partially flows to the core through the insulating cylinder between the core and winding and partially to oil through the insulating cylinder between the windings and through the thickness of the entire primary winding. Recognising the complex conditions of cooling we assume simplifications in our analysis as follows.

(1) The heat is transported in radial direction only.

(2) No heat is transferred from the windings to the core.

(3) Core I^2R and eddy losses are transferred to the tank.

The maximum temperature will then occur in the secondary winding, being the sum of the ambient temperature Θ_0 = 40 °C taken as a datum and temperature differences in other points of the v.t. measured from this datum, namely

Θ_1 = temperature difference in the LV winding;
Θ_2 = temperature difference in the cylinder between the windings;
Θ_3 = temperature difference in the HV winding;
Θ_4 = temperature difference between a winding and oil;
Θ_5 = temperature difference from the bulk oil to the tank wall;
Θ_6 = temperature difference in the tank wall;
Θ_7 = temperature difference between the tank wall and the surroundings.

Tikhomirov [11.2] has found out that

$$\Theta_1 = 0.28 P_{sp2} a_2^2/\lambda_{av2}$$

where P_{sp2} is the specific loss power in the secondary winding ($P_{sp2} = P_2/V_2$, P_2 is in watts and the secondary volume V_2 is in cm^3); a_2 is the radial thickness of the secondary winding, cm; and λ_{av2} is the average thermal conductivity of the coil insulation found as [11.2]

$$\lambda_{av} = \lambda\lambda_{inl}(d' + \delta_{inl})/(\lambda\delta_{inl} + \lambda_{inl}d')$$

where λ_{inl} is the thermal conductivity of the interlayer insulation, W/°C m; d' is the insulated wire diameter, m; δ_{inl} is the thickness of the interlayer insulation, m; and λ is the thermal conductivity of the wire insulation, W/°C m.

In approximate calculations we may let

$$P_1 \approx P_2 \quad \text{and} \quad P_2 = P/2$$

here $P = I_1^2(r_1 + r_2')$ is the total loss in the two windings;

$$\Theta_2 = P_2 R_{th2}$$

where $R_{th2} \approx \delta/\lambda 2\pi Rl$ is the thermal resistivity of a cylinder of thickness δ, mean radius R, height l, and thermal conductivity of material λ;

$$\Theta_3 = P_2 R_{th1} + 0.28 P_{sp1} a_1^2/\lambda_{av1}$$

where R_{th1} is the thermal resistivity of the HV winding, $P_{sp1} = P_1/V_1$ is the specific power of the primary, and λ_{av1} is the average thermal conductivity of HV winding found in the same way as for the LV winding.

The thermal resistivity of HV winding R_{th1} is found with the equation for R_{th2} with λ_{av1} and the other relevant parameters such as radial thickness, average radius and length of this winding.

The temperature difference between the winding and oil is

$$\Theta_4 = k q_1^{0.6}$$

where $k = 0.285$; $q_1 = P/S_w$ is the heat flux density, W/m^2; S_w is the outer surface area of the HV winding.

The temperature difference between the bulk oil and the wall

$$\Theta_5 = k q_2^{0.6}$$

where q_2 is the heat flux density for oil-to-tank-wall heat transfer

$$q_2 = (P + P_{cl})/S_{tank}$$

where S_{tank} is the internal surface area of the tank to which the heat flux $P + P_{cl}$ is transported.

The temperature difference Θ_7 will be found by an equation from Ref. [11.2]. The temperature difference Θ_6 is small and can be neglected.

The temperature difference between the tank wall and the surroundings

$$\Theta_7 = [(P + P_c)1.05/(2.8S_{rad} + 2.5S_{conv})]^{0.8}$$

where P is the total loss in the copper of two windings, W; P_{cl} represents the losses in the core, W; S_{rad} is the radiating surface of the tank, m^2; S_{conv} is the surface of heat transfer by convection, m^2.

For the problem in hand we may approximately let $P_{cl} = 0.25P$ and $S_{conv} = S_{rad} = S$ so that

$$\Theta_7 = [1.05 \times 1.25P/5.3S]^{0.8}$$

For the enamel insulated wire used, the maximum admissible temperature is $\Theta_{max} = 105$ °C and the ambient temperature is $\Theta_0 = 40$ °C. The full temperature difference allowable is

$$\Delta\Theta_m = \Theta_{max} - \Theta_0 = 65 = \sum_{i=1}^{7} \Theta_i = f(P)$$

This equation is nonlinear, therefore it is commonly solved graphically: a number of P values are taken and the corresponding $\Delta\Theta_m$ is defined, then for $\Delta\Theta_m = 65$ °C one can find P. For the known power, the desired admissible primary current will be

$$I_1 = \sqrt{P/(r_1 + r_2')}$$

The admissible secondary current (approximately) is $I_2 = I_1 w_1/w_2$. The maximum output power therefore is $P_2 = U_2 I_2$.

REFERENCES

11.1 A. M. Dymkov, B. M. Kibel, and Yu. V. Tishenin: *Transformatory napryazheniya* (Voltage transformers). Energiya, Moscow 1975.

11.2 P. M. Tikhomirov: *Raschet transformatorov* (Transformer design). Energiya, Moscow 1976.

11.3 V. P. Zubkov and A. D. Krastina: *Optiko-elektronnye metody izmereniya toka i napryazheniya v ustanovkakh vysokogo napryazheniya* (Optoelectronic measurements of current and voltage in HV systems). Informelektro, Moscow 1975.

12
REACTORS

12.1 General

Principle of operation and construction. The reactor is essentially an inductance coil that serves to limit short circuit currents in the system or to compensate for system capacitance that otherwise might cause excessive voltage rises. To illustrate the principle of operation of a series inductor consider the scheme in Fig. 12.1. The a.c. generator feeds the busbar that supplies the lines to power consumers. We compare the behaviour of a line having a reactor installed after the circuit breaker with that which has not.

Under three-phase short circuit conditions the current behind the circuit breaker I_{sc1} is mainly governed by the inductive reactance of the generator

$$I_{sc1} = U_r/\sqrt{3}X_g \tag{12.1}$$

where U_r is the rated voltage of the system, V; and X_g is the transient follow inductive reactance of the generator, Ω.

If the nominal generator current is $I_{r,g}$ then the relative inductive reactance (with respect to resistance) of the generator will be defined as

$$x_g = I_{r,g}X_g\sqrt{3}/U_r \tag{12.2}$$

Now,

$$I_{sc1} = I_{r,g}/x_g \tag{12.3}$$

Note in passing that the circuit breaker is selected for the short circuit current I_{sc1}.

On a short circuit fault the busbar voltage will be zero. The short circuit current in the line with a reactor will be defined by the total reactance of the generator and reactor

$$I_{sc,L} = U_r/\sqrt{3}(X_g + X_L) \tag{12.4}$$

where X_L is the inductive reactance of the reactor, Ω.

The relative inductive reactance (in terms of resistance) of the reactor

$$x_L = I_{r,L}X_L\sqrt{3}/U_r \tag{12.5}$$

Usually one power source feeds a few dozens of plants, therefore the nominal line current is a small fraction of the rated current of the generator. The continuous current of the reactor is selected equal to the line current. Accordingly, $I_{r,L} \ll I_{r,g}$.

Assume that $x_g < x_L$, then from Eqs. (12.2) and (12.5) we obtain $X_L \gg X_g$ and

$$I_{sc,L} = U_r/\sqrt{3}X_L = I_{r,L}/x_r \ll I_{sc1}$$

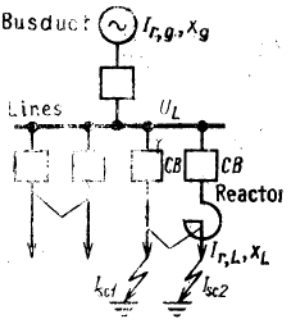

Fig. 12.1. Current-limiting reactor application

This implies that under the assumptions made above the short circuit current is controlled by the reactor parameters only.

The reactor is a rather reliable piece of equipment, therefore the other line apparatus are normally selected for the current $I_{sc,L} \ll I_{sc,1}$ allowing the distributing facilities of lower weight and cost.

Figure 12.2 pictures the distribution of voltage over the circuit on a short circuit fault behind the reactor and, for comparison, under normal operating conditions. Because $X_L \gg X_g$, on short circuit all the voltage is applied to the reactor and the busbar voltage U_b is close to the rated value. Under the normal operating conditions the load impedance is well above the reactor reactance, the voltage drop across the reactor is very small and almost the entire voltage is applied to the load.

Reactors may be placed between the sections of generator busbars (Fig. 12.3). On a generator short circuit these reactors are to limit fault current and diminish the damage to the generator. In the absence of reactors, short circuit current can rise to high values because the reactances of generators are low. Under normal condi-

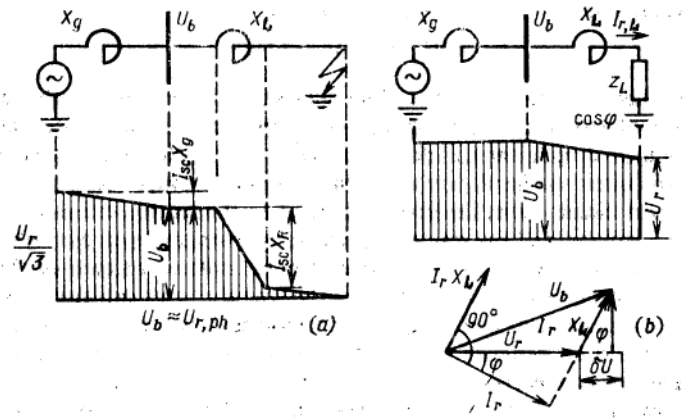

Fig. 12.2. Voltage distribution under (*a*) short circuit and (*b*) normal operating conditions

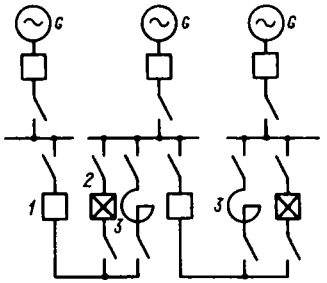

Fig. 12.3. Connection of reactors between generator busbars: (1) circuit breaker, (2) shunting switch, (3) reactor

tions such reactors carry only small equalising currents, therefore the reactance of these units may be taken rather high.

Principal parameters. By virtue of Eq. (12.2) the rated inductance of a reactor is given in H for U_r in kV as

$$L_L = 10^3 U_r x_L / I_{r,L} 2\pi f \sqrt{3} \tag{12.6}$$

Rated reactor voltage. The inductive reactance of a reactor is $\omega L_L \gg R_L$, therefore in estimations of voltage loss the reactor resistance may be neglected. The nominal voltage drop across the reactor, $I_{r,L} X_L$, leads the current by 90°.

The *percentage voltage drop* is the nominal voltage drop across the reactor taken as a percentage of the rated system voltage

$$\begin{aligned} \delta u_d &= 100 \delta u \sqrt{3} / U_r \\ &\approx 100 I_{r,L} X_L \sqrt{3} \sin \varphi / U_r = 100 x_L \sin \varphi \end{aligned}$$

For a power factor of 0.8 the relative voltage drop is $\delta u_d = 0.6 x_L$ and because usually $x_L \leqslant 0.1$ the voltage drop across the reactor in the normal operating mode is small. A further reduction of loss is achieved in duplex reactors discussed in Sect. 12.8 below.

The *reactive power* per phase, or *coil rating*, is

$$P_{ph} = I_{r,L}^2 X_L \times 10^{-3} \text{ kVA} \tag{12.7}$$

The *rated system voltage* is the line-to-line value stated in kV. From earth the reactor winding is insulated by porcelain support insulators. Under normal operating conditions the voltage drop in the coil does not exceed 10% of the phase system voltage, therefore the interturn insulation requirement is fairly moderate.

On a short circuit fault, the voltage applied to the reactor coil is close to the rated system voltage, and the reactor insulation appears under an overvoltage level that can occur in networks with the neutral point isolated or earthed through a reactor. The voltage across the reactors of the sound phases can rise to $3.2 U_r/\sqrt{3}$ and occurs in the form of high-frequency harmonics. The interturn insulation, accordingly, should be designed for this type and level of applied voltage.

The *rated reactor current* is the maximum continuous current for which the reactor is designed, i.e. the current that heats the winding to the maximum admissible temperature. The rated reactor current can be as high as 3000-4000 A producing

the active power loss in the winding up to a few tens of kilowatts. This loss is due to the high current flowing in the long conductor of the winding. In addition, there occur substantial losses on account of the strong magnetic field in which the reactor windings are immersed. This loss increases the total loss figure 1.3-1.5 times.

The *rated power of a three-phase reactor stack* (stated in kVA for U_r in kV)

$$\text{kVA} = U_r I_{r,L} \sqrt{3}$$

Mechanical and thermal short-circuit currents. If the relative inductive reactance of the reactor is above 0.03, then the maximum short circuit current that the reactor is to carry is

$$I_{sc} = I_{r,L}/x_L \tag{12.8}$$

This current is a point of departure in estimations of the thermal and mechanical strength of the structure. For $x_L < 0.03$, the calculation should take account of the source impedance. The thermal short circuit current heats the system without damage for a specified time interval t_{tw}. Sometimes, the thermal rating is specified as the product $I_{sc,L}\sqrt{t_{tw}}$.

The mechanical strength of the coil is defined in terms of the mechanical short-circuit current

$$I_{pk} = 1.8\sqrt{2} I_{sc,L} \tag{12.9}$$

Because the design of the current carrying parts and the choice of equipment for the distributing installation are carried out on the assumption that the short circuit current will be limited by the reactor, stringent requirements are imposed on the reactor reliability. The following discussion will be based on a fundamental study into the reactor reliability problem performed by G. V. Butkevich, V. V. Mikhailov, and I. I. Rotgauz.

12.2 Constructions of Reactors

Air-insulated concrete inductive reactors are a most popular type. Figure 12.4 shows a three-phase stacked arrangement of such a reactor. Multistrand wire (1) of an appropriate cross section is wound in the form of a coil on a mandrel. Concrete poured in special forms solidifies into vertical columns (2) that provide solid structural supporting frame for the individual turns of the moulded coils. The pins at the ends of the columns serve to secure the interphase insulators (3 and 4).

In order to attain a required strength of the electric insulation, after the concrete has been hardened the reactor is subjected to intense drying under vacuum, and impregnated two times with a moisture-resistant varnish.

Considerable spacing between turns and coils, 3.5-4.5 cm, facilitates cooling and improves insulation.

Reactors rated for high currents (above 400 A) use a parallel branch design and a transposition of turns for uniform distribution of current over the branches (see Fig. 12.6).

The coils are wound with a large cross section multistrand copper or aluminium cable wrapped up in a few layers of 0.12-mm cable paper with a cotton brading atop. The total thickness of the insulation becomes equal to about 1.5 mm.

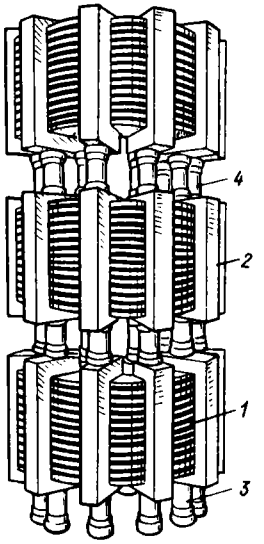

Fig. 12.4. Three-phase reactor stack assembly

It is common to use natural ventilation for reactor cooling. Large power released in the reactor necessitates that cooling ducts be provided especially for high current installations.

The resultant losses in the reactor vary from 0.1% to 0.55% of the reactor power rating, the higher losses relate to reactors with aluminium winding.

The clearance between the reactors in the stack is governed by the height of the support insulators. Since at 6-10 kV this height is small, large currents in the reactors may produce electrodynamic forces capable of demolishing the insulators working in compression and tension.

Air insulated concrete reactors have been used to advantage in indoor distribution installations up to 35 kV. Their advantages are offset by the bulky structure and heavy weight. Current designs with glass reinforced plastics and epoxy resin as insulating materials evolve in lighter and less bulky structures.

For outdoor installations operating at above 35 kV, inductive reactors are mostly of the oil-immersed type. The cross-sectional diagram of such a reactor is shown in Fig. 12.5. The winding (2) is wound on a form of insulating material like synthetic resin bonded paper laminate and immersed in a steel tank with transformer oil. Use of oil enables the designer to reduce the clearance between the winding and earthed parts and improves the cooling by means of convection. Oil-immersed reactors have lower weight and size than their air-insulated counterparts. The reactor taps are connected to the terminals of the through insulators (4). A major disadvantage of this arrangement is associated with inadmissible heating of the tank (1) by the magnetic flux of the reactor. It is necessary that negligible flux pass into the tank walls. Usually this is done by surrounding the coils with a screen in the

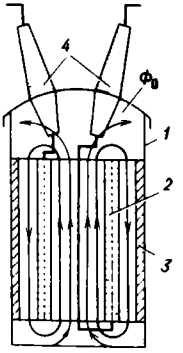

Fig. 12.5. Oil-immersed reactor

form of a copper ring (3). This ring increases the magnetic resistance and, consequently, decreases the magnetic flux through the tank walls.

An alternative solution to this problem is developed in the USSR in the form of coreless toroidal reactors where the leakage flux passes inside the torus and the external field is practically absent. This coil may be immersed in a steel tank with oil without any risk of wall heating. The reactors for 110 kV and above manufactured in this country have demonstrated better technical and economical performance than the construction shown in Fig. 12.5.

To conclude this topic a few words are in order on the use of ferromagnetic cores in inductive reactors. Such a construction would, of course, reduce the size of a unit, however, saturation under short-circuit current would reduce the current-limiting effect of the reactor. Therefore this design has not been accepted for current-limiting reactors.

12.3 Calculation of Reactor Inductance

In a preliminary estimation of the basic reactor dimensions the reactor inductance can conveniently be calculated by the Korndorfer formula

$$L = 10.5w^2D[D/2(b + h)]^{k_1} \times 10^{-6}\ [\text{mH}] \tag{12.10}$$

where $k_1 = 3/4$ for $0 < D/2(b + h) \leqslant 1$ and $k_1 = 1/2$ for $1 \leqslant D/2(b + h) \leqslant 3$; w is the number of turns in the winding; D is the average diameter (see Fig. 12.6*a*); b is the winding thickness, cm; and h is the winding height.

The inductance is a function of four variables, therefore a selection of reactor size and shape is a formidable problem. Using Eq. (12.10), V. V. Mikhailov [2.1] developed a nomograph for fast evaluation of the basic dimensions of a reactor.

For reactors of high voltage distribution systems, $0 < D/2(b + h) \leqslant 1$, therefore the calculation below will be carried out for this aspect ratio.

Equation (12.10) may be rewritten as

$$L = 10.5w^2D^{7/4} \times 10^{-6}/(2b + 2h)^{3/4} \tag{12.11}$$

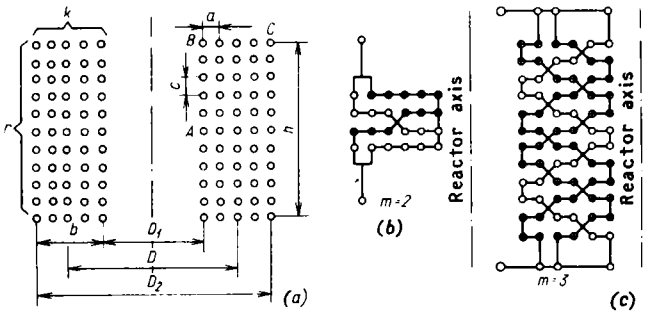

Fig. 12.6. Layout of winding turns

The number of turns is $w = kr$, where k is the number of turns in a row and r is the number of rows.

In Soviet-made air-insulated concrete reactors, the turns in a row are spaced at $a = 3.5$ cm, the distance between the adjacent rows being $c = 4.5$ cm. With reference to Fig. 12.6*a* we obtain

$$L = 10.5 \frac{(kr)^2 \times 10^{-6}}{2^{3/4}(rc - c + ka - a)^{3/4}} D^{7/4} = f(k, r)D^{7/4} \tag{12.12}$$

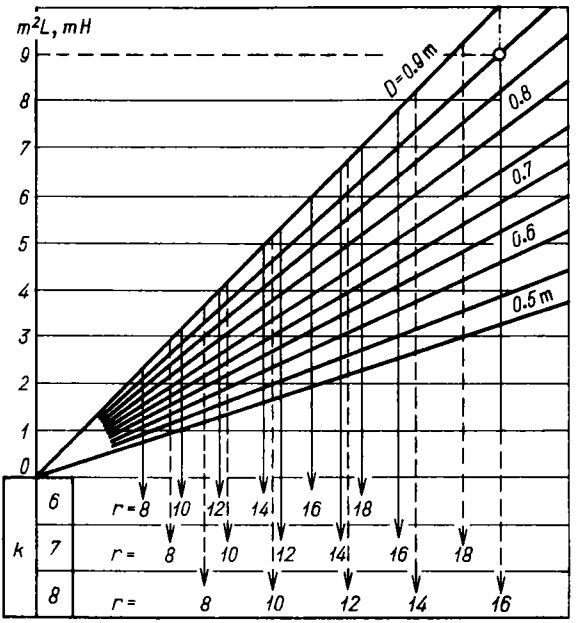

Fig. 12.7. Winding parameter nomograph

At a fixed D the inductance is thus a linear function of k and r. A number of such functions are plotted in Fig. 12.7. Entering the bottom table with a given k one ascends in an r-vertical to the appropriate D curve and projects the intersection onto the abscissa presenting the quantity m^2L in mH. The m^2 factor reflects the number of parallel circuits m in windings operated at heavy rated currents (above 300 A). The number of turns defining the coil inductance is $w = kr/m$, hence m^2L in the ordinate of Fig. 12.7.

When a required value of L or m^2L is specified, the average diameter D can be found as an intersection of this value with the r vertical for some selected k.

The reactor height is found as $h = c(r - 1)$ and thickness as $b = a(k - 1)$. For a and c other than those given above, the diameter for given k and r may be determined by the equations

$$\begin{aligned} D &= [Lm^2/f(k, r)]^{4/7} \quad \text{for } k_1 = 3/4 \\ D &= [Lm^2/f(k, r)]^{2/3} \quad \text{for } k_1 = 1/2 \end{aligned} \tag{12.13}$$

When the basic dimensions of the reactor are selected, it is recommended to check the inductance by the formula

$$L = w^2 D\Phi \times 10^{-6} \text{ [mH]} \tag{12.14}$$

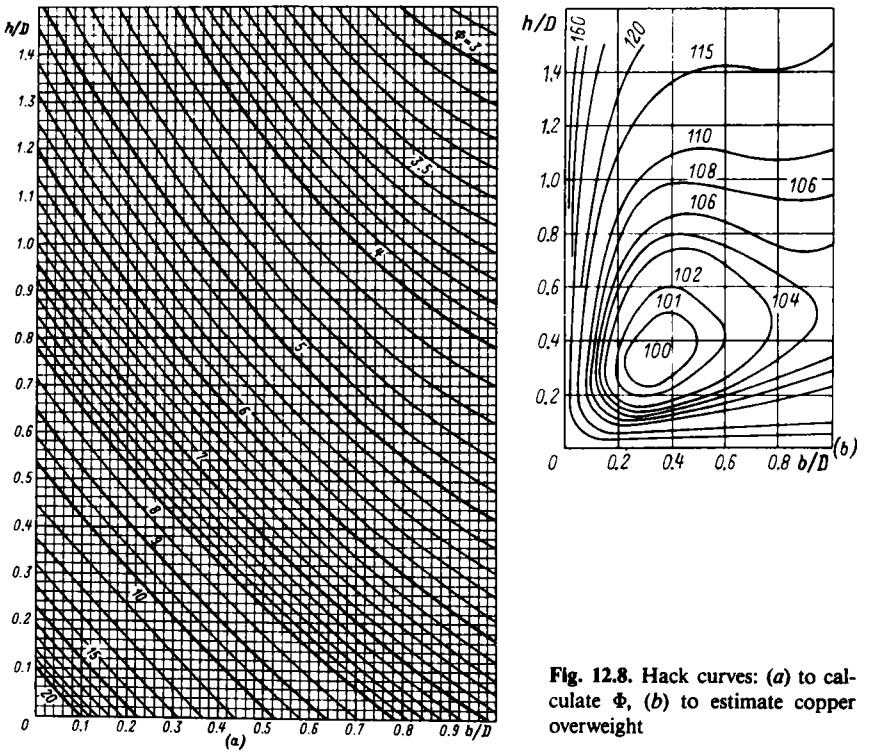

Fig. 12.8. Hack curves: (*a*) to calculate Φ, (*b*) to estimate copper overweight

where D is the average diameter in cm, and Φ is a parameter defined by the reactor dimensions as shown in Fig. 12.8. The calculated value should be within $\pm 5\%$ of the required value.

It must be noted that the vertical stacking of reactors into a three-phase arrangement alters the equivalent inductance of a phase reactor because of the mutual inductance of the phases. Therefore, an accurate evaluation of the equivalent phase inductance should allow for this phenomenon [12.1].

For a given inductance one may select a number of feasible versions with different dimensions of the reactor. It is desirable however, to choose the one with minimum winding mass. The Hack curves in Fig. 12.8*b* are the loci of winding mass (in relative units) plotted for various proportions of reactor dimensions. The minimum mass region is seen to be at $b/D = h/D = 1/3$. All other designs incur heavier windings because of greater length of wire. The selected dimensions of a reactor are verified for the winding mass against the optimum-mass design. The overweight should not be more than 5%. Designs with $h/D = b/D = 1/3$ are seldom used because with these proportions and the reactors arranged in the vertical stack the interphase insulators are subjected to crushing electrodynamic stresses. Normally reactors are elongated shapes, the optimal-mass proportions being adopted only when the units can be removed from each other or placed on special racks.

12.4 Thermal Design

Selection of conductor cross section. The guidelines in choosing a winding wire are as follows.

1. The selected cross section should ensure reliable operation of the reactor both at rated current and on a short-circuit fault.

2. The selected cross section should be economically feasible, in terms of annual revenue costs.

The larger cross section of those calculated for normal and short circuit conditions is usually adopted. The recommended current densities are given below.

Current density guidelines [A/mm²] in copper winding under continuous loading

Air-insulated disc winding rated up to 100 A	1.2-1.8
Air-cooled cable winding rated 150-3000 A	2-2.7
Oil-immersed winding for 200-1000 A	3-3.5

Copper-strand cable sections for concrete reactors

$I_{r,L}$, A	150	200	300	400	500	600	700	1000	1500
A, mm²	70	95	120	185	1 × 210	2 × 120	2 × 150	3 × 135	4 × 150
					2 × 120	2 × 135	3 × 185	3 × 150	4 × 175
						2 × 150			

If the calculation results in a cable section above 185 mm², several parallel branches of lower cross section should be used to match this load. For equalisation of the reactor current among the branches their resistance should be the same. Inductive reactances of branches are of decisive importance in the current distribution.

Figure 12.6*b* and *c* shows windings with two and three parallel branches. In

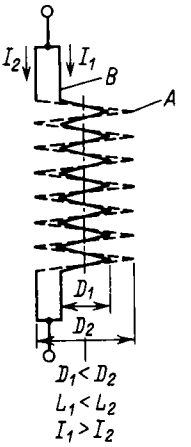

Fig. 12.9. Current distribution over parallel branches

laying out such a winding it is important that the branches be identically placed with respect to the magnetic field — to each turn of one branch there corresponds a turn of another branch being under the same conditions.

In a reactor shown schematically in Fig. 12.9 the diameter of branch *A* winding is larger than that of branch *B*. The currents in these branches are divided in inverse proportion to the branch inductance.

Nonuniform distribution of current among the branches increases the loss of active power and results in additional heating of some winding parts and reductions in reactor thermal and mechanical ratings. It is worth noting that the distribution of current among the branches is affected by the magnetic field of the neighbouring phases and the field of the second half of a duplex reactor (see Sect. 12.8).

Based on the nominal heating of air-insulated concrete reactors wound with copper wire the average current density may be taken equal to 2.3 A/mm^2, the optimal density being about 2.1 A/mm^2.

For aluminium wire, the optimal current density is 0.8-1.1 A/mm^2, the lower figure relating to a larger reactor.

Reactor heating and losses. The reactor losses are expressed as

$$\Delta P = k_{\text{add}} I_{r,L}^2 R k_{\text{par}}$$

where

$$k_{\text{add}} = 1 + k_0 k_s k_Q \frac{mw}{h} \left(\frac{f}{50}\right)^2 10^{-3} \tag{12.15}$$

is the coefficient of additional losses with k_0 taken from Table 12.1; k_s = (1.15-1.5) $\times 10^{-2} s$ (s in cm^2); k_Q = 1 for copper and 0.37 for aluminium; $I_{r,L}$ is the rated current of the reactor, A; $R = \varrho_{75}\, 1.03\pi Dw/ms$ [Ω] is the reactor a.c. resistance, the factor 1.03 allowing for the increase in wire length in coming from one layer to the next; and $k_{\text{par}} \approx 1.1$ accounts for losses due to nonuniform distribution of current over the parallel branches.

Table 12.1. Round Wire Coefficient k_0 as a Function of h/D and b/D

b/D	h/D									
	0.5	0.6	0.7	0.8	0.9	1.0	1.1	1.2	1.3	1.4
0.2	28.5	32.5	36.0	33.5	41	43.4	45.5	47.2	49.0	50.5
0.3	22.8	26.3	36.0	33.0	36.0	38.0	40.0	41.5	43.0	44.4
0.4	19.2	23.0	26.0	28.5	31.0	33.2	35.0	37.0	38.3	39.8
0.5	15.3	21.8	21.8	24.3	26.5	29.0	31.0	32.8	34.2	35.8

The magnetic flux of the reactor passes through the flanges of interphase insulators and results in additional losses [12.1]. On the average, each insulator incurs a loss about 15 W.

The electric field of the reactor produces active losses in the concrete structure. In estimating the total losses of active power per phase one may assume that the losses in concrete account for 10% of the losses in the winding.

The strong magnetic field of reactor causes heating of metal parts within its reach. Therefore the distance from the winding to the reinforced concrete wall of the reactor cubicle should be at least the external winding diameter.

Table 12.2. Coefficient C_h for Thermal Design of Air-Insulated Concrete Reactors

s, mm^2	Number of axial rows										
	10	12	14	16	18	20	22	24	26	28	30
					Copper wire						
70	270	264	258	253	248	243	239	235	231	228	225
95	337	329	322	315	309	303	298	295	289	285	282
120	400	390	381	373	365	358	252	346	341	337	333
135	438	426	415	406	398	391	384	378	373	368	364
150	475	463	452	442	433	424	416	409	403	398	393
185	555	541	528	516	505	496	486	478	471	464	458
210	608	591	576	563	551	540	530	521	512	506	505
					Aluminium wire						
120	297	290	284	278	272	267	263	259	—	—	—
135	324	316	309	303	297	291	287	283	—	—	—
150	350	341	334	327	320	314	309	305	—	—	—
173	388	378	370	362	354	347	341	336	—	—	—
185	408	397	388	380	372	365	358	352	346	340	335
210	450	438	427	418	410	402	396	390	384	379	374
240	498	486	474	464	454	444	436	429	422	416	410

Heating with rated current. Complicated cooling conditions of a reactor prevent a simple analytical procedure for the evaluation of winding temperature. For a single reactor wound with copper wire the excess of the winding temperature over the ambient temperature may be estimated by the formula due to E. S. Fried

$$\tau = 80K(I_{r,L}/mC_h)^2$$

where $K = 0.57D_1/(D_1 - 2.1N)$; $D_1 = D - b$ [cm] (see Fig. 12.6); N is the number of columns; and the coefficient C_h is taken from Table 12.2.

For the upper phase of a three-phase stack,

$$\tau = 100K(I_{r,L}/mC_h)^2 \tag{12.16}$$

This temperature is higher than that for the two lower phase reactors, as the upper unit is in the flow of air heated by the two lower reactors.

For horizontally spaced reactors, the formula due to A. K. Karpensky [12.1] provides a good approximation

$$\tau = \varrho_0 k_{add} J^2 s\beta(0.45 + 0.086r/\sqrt[3]{b_0/d - 1}) \tag{12.17}$$

where ϱ_0 is the resistivity of material at 20 °C, $\Omega\,\text{mm}^2/\text{m}$; s is the wire cross section, mm^2; J is the current density, A/mm^2; β is the ratio of the wire length to the length of its open portion; r is the number of horizontal layers; b_0 is the pitch of winding in the horizontal, mm; and d is the wire diameter, mm. This formula is valid for $10 \leqslant r \leqslant 24$, $1.35 \leqslant b_0/d \leqslant 1.8$, and $5 \leqslant k \leqslant 12$.

For the ambient temperature of 40 °C the winding temperature should not exceed 100-120 °C, the higher temperatures relate to the reactors with higher rated current.

The temperature profile within a reactor is rather complicated. The hottest area is at about two thirds of reactor height. The temperature difference between the hottest and cold (bottom) layer reaches 10-15 °C. In the radial direction, the hottest area is at a distance of $3b/8$ from the internal layer.

Thermal rating. The calculation of heating does not involve the heat released in the surroundings. The maximum allowable temperature levels are taken at 200 °C for copper windings, and at 180 °C for aluminium windings.

The time of thermal short-time current may be estimated by the equations

$$\begin{aligned} t_{tw} &= 11\,000/J_{sc}^2 \quad \text{for copper windings} \\ &= 4700/J_{sc}^2 \quad \text{for aluminium windings} \end{aligned}$$

where J_{sc} [A/mm^2] is the density of short-circuit current after the reactor.

12.5 Mechanical Rating

Internal electrodynamic strength. Distinction will be made between the electrodynamic forces, that occur inside the reactor due to the interaction of winding wire with the reactor magnetic field, and the mechanical forces due to the interaction of the adjacent phase reactors with one another. Accordingly, the mechanical rating of reactors will be treated in terms of the internal and external reactor strength under mechanical short-circuit current.

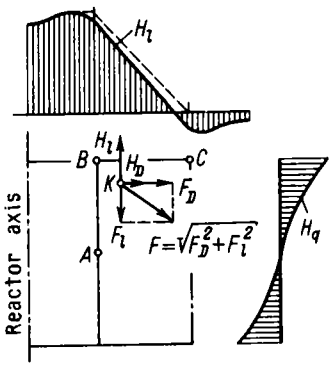

Fig. 12.10. Schematic diagram of the magnetic field profile in a reactor

The problem of internal mechanical rating may be solved in two ways. In one the force of interaction of one turn with other turns is sought. In the other, the resultant magnetic field of all the windings and the respective force is found with Ampere's rule. The first approach yields a more accurate solution, but it is extremely laborious. The second is more in error, but it is more tractable at each stage and far less laborious. We shall stick to the second approach that has been developed in depth by G. V. Butkevich and P. P. Chusov.

The simplified profile of the reactor field is depicted in Fig. 12.10. Consider the forces at point K. The axial component of the magnetic field H_l produces the radial force F_D that tends to tear the turn apart. The field strength H_l within the reactor varies in the radial direction insignificantly. Within the winding it falls off linearly to be practically zero for the external layer of the winding. In analysis the H_l is assumed to decay along the dashed line.

The radial component H_D remains invariable within a row, but varies with height as shown in the right-hand insert. This component creates an axial force F_l that compresses the reactor in the vertical. The resultant force is the geometric sum of F_D and F_l.

There are three characteristic points, A, B, and C, in every cylindrical reactor. At point A, $H_D = 0$ while the radial force is nonzero; at point C, $H_l = 0$ while the axial force is nonzero, and at point B both radial and axial components exist. The directional pattern of forces acting on the winding is represented in Fig. 12.11. These forces tend to compress the winding in height and thickness and extend its mean diameter.

The analytical procedure for the evaluation of these forces is as follows [2.1]. The force acting on the unit length of a turn [N/cm] at the respective points is

$$f_A = 5\frac{w}{mb}\left(\frac{I_r}{x_L}\right)^2 A_{h/2} \times 10^{-6} \tag{12.18}$$

$$f_B = 6\frac{w}{mb}\left(\frac{I_r}{x_L}\right)^2 A_h \times 10^{-6} \tag{12.19}$$

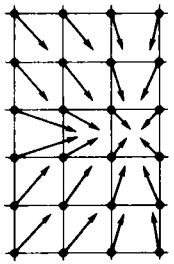

Fig. 12.11. Pattern of forces acting on reactor turns

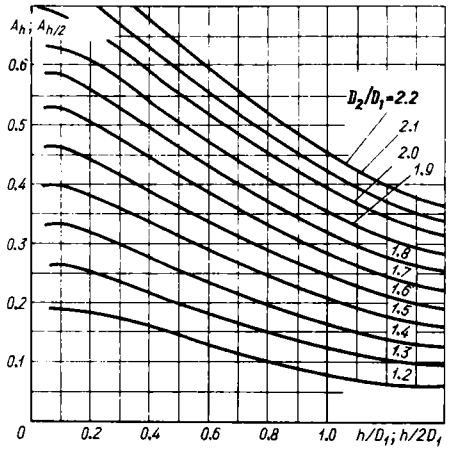

Fig. 12.12. Diagram for evaluation of forces acting on reactor turns

$$f_C = 2.8 \frac{w}{mb} \left(\frac{I_r}{x_L}\right)^2 A_h \times 10^{-6} \tag{12.20}$$

where $w = kr$ is the total number of turns in the reactor; m is the number of parallel circuits; b is the reactor thickness, cm; and $A_{h/2}$ and A_h are the parameters derived from the curves of Fig. 12.12. The curves are plotted for different diameter ratios D_2/D_1 shown in Fig. 12.6.

Equations (12.18-20) account for short-time short circuit current. If the values of f_A, f_B, and f_C are known, one can assess the strength characteristics of the conductors.

A turn segment between the adjacent columns may be treated as a flexible cable. Calculations indicate that the force is strongest at A and weakest at C (see Fig. 12.10). It will be noted, however, that the length of cable segment l at A and B is smaller than at C (Fig. 12.13). Therefore the strength characteristics should be checked at all three points A, B, and C.

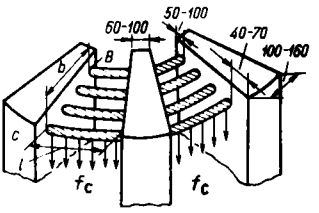

Fig. 12.13. Bending forces acting on the external turn. Column dimensions are in mm

The number of concrete columns in new installations is from 6 to 12 depending on, and growing with, the inductance and rated current of the reactor. The column height H exceeds the winding height h by 300-360 mm. The trapezoidal section of a column is approximately dimensioned in Fig. 12.13. The preliminary sketch of the reactor design is used to evaluate the length of cable segment between the columns involved in a strength analysis. The dimensions of column cross section are finalised following the mechanical strength analysis.

The tensile stress that occurs in a conductor is determined on the assumption that the turn segment is a flexible cable, namely,

$$\sigma = \sqrt[3]{f^2 l^2 E/6s^2} \tag{12.21}$$

where f is the specific force, N/cm; l is the length of a free cable segment, cm; E is the modulus of elasticity, N/cm^2; and s is the cable cross section, cm^2.

For copper, $\sigma \leqslant 150$ MN/m^2 and $E = 11.5$ GN/m^2, and for aluminium $\sigma \leqslant 65$ MN/m^2, and $E = 540$ GN/m^2.

If σ exceeds the ultimate values for the winding material, the length of free cable segment l should be diminished by increasing the number of columns N. In some situations a thicker wire can save the design.

Now we evaluate the mechanical strength of the columns. Assume first that the columns are absolutely rigid bodies and all radial forces applied to the winding are transmitted to the columns. Referring to Fig. 12.14 consider a segment of cable and a column. The force conveyed to the column by the cable segment is

$$f_t = 2\int_0^{\beta} f_{rad} \cos \varphi R d\varphi = f_{rad} D \sin \beta \tag{12.22}$$

where 2β is the segment angle per column equal to $2\pi/N$; N is the number of columns; f_{rad} is the specific radial force, N/cm; and D is the turn diameter, cm.

It is assumed that the axial field strength H_l varies linearly over the winding thickness (see Fig. 12.10). Then

$$f_{rad} = f_A \frac{D_2 - D}{D_2 - D_1}$$

Denoting $f_A = f_{max}$, the number of a turn in a row counting outward by M, and the increment of diameter on coming from one turn to the next by ΔD, we

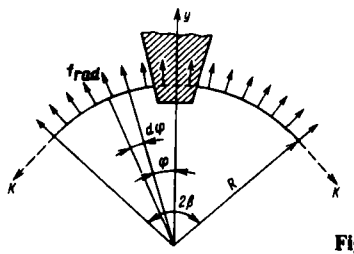

Fig. 12.14. Force exerted by a span of turn on the column

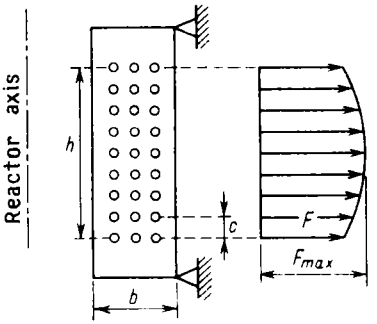

Fig. 12.15. Vertical distribution of the radial forces

have for the force transmitted by a turn to the column

$$f_t = f_{max} \sin \beta (D_2 - D)D/(D_2 - D_1)$$

where

$$D_2 = D_1 + (k - 1)\Delta D$$

and

$$D = D_1 + (M - 1)\Delta D$$

The force transmitted to a column from one turn is

$$f_M = \frac{f_{max} \sin \beta}{k - 1} (k - M)[D_1 + (M - 1)\Delta D]$$
$$= C(k - M)[D_1 + (M - 1)\Delta D] \qquad (12.23)$$

The force exerted by one row of turns per column is

$$F = \sum_{M=1}^{k} f_M$$

Figure 12.15 shows the distribution of this force over the height of the reactor. Some reduction at the reactor edges is associated with the lower axial field strength H_l.

The specific load on the column is

$$F_1 = F_{max}/c$$

Given the bending moment and section modulus one may determine the bending stress in the column. Calculations indicate that rigidly attached columns experience bending forces as high as 100-500 kN [12.1]. The columns have to deform to withstand this stress. In actual installations the columns are not fixed with absolute rigidity and a proportion of load is absorbed by the winding itself. If the reactor columns were put on rolls, i.e., allowed to move freely, the radial forces would be taken up by the winding. A proportion of the radial forces acting on the cable segment under consideration would be balanced by a force K representing the action of the rest of the winding (indicated by dashed lines in Fig. 12.14).

The force acting on a free column is

$$f_t' = f_t - 2K \sin \beta \tag{12.24}$$

By Hook's law

$$K = \lambda sE/l = \lambda sE/\pi D \tag{12.25}$$

where l is the elongation of the turn, s is the wire cross section, E is the modulus of elasticity, D is the turn diameter; and l is the turn length.

Because all the turns are moulded into the column they all have the same radial deformation ΔR, that is, identical elongation $\lambda = 2\pi\Delta R$.

Now, by virtue of Eq. (12.24)

$$f_t' = f - 2\lambda sE \sin \beta/\pi D = f - B/D$$

where B is a constant for the reactor concerned.

In view of Eq. (12.23)

$$f_t' = C(k - M)[D_1 + (M - 1)\Delta D] - B/[D_1 + (M - 1)\Delta D] \tag{12.26}$$

If we assume that H_l is invariable over the reactor height, then f_t' will be the same for all rows. Therefore, we may consider the equilibrium of forces for one row disregarding the effect of the other rows. Since the column is not attached, the sum of forces acting on the concrete column is zero, viz.,

$$\sum_{M=1}^{k} f_M' = 0$$

or

$$\sum_{M=1}^{k} c(k - M)[D_1 + (M - 1)\Delta D] = \sum_{M=1}^{k} \frac{B}{D_1 + (M - 1)\Delta D} \tag{12.27}$$

The left-hand side of this equation is the sum of forces transmitted to the concrete column from the winding

$$F = \sum_{M=1}^{k} f_M$$

Then

$$B = F \Big/ \sum_{M=1}^{k} [D_1 + (M - 1)\Delta D]^{-1}$$

Once the B value has been determined, we find the force applied to the concrete column by the first turn f_{t1}', second turn f_{t2}', and f_k'. Then the crushing stress is f_t'/S_{cr}.

The radial variation of f_t' is shown in Fig. 12.16. For $R < R_0$, f_t' is positive implying that the force is applied to column from the turns and moves the column. For $R > R_0$, f_t' is negative which implies that the column moves and extends the turns.

If the axial field strength H_l were invariable with reactor height, the columns would not experience a bending moment. In actual reactors the field is stronger in the mid-zone than at the ends and columns are subjected to bending stresses.

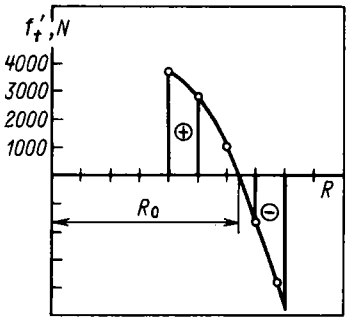

Fig. 12.16. Variation of f'_t with winding radius

The vertical variation of force F over the reactor is shown in Fig. 12.17. Replacing the curvilinear distribution at (*a*) with the linear at (*b*) yields for the bending moment about the midpoint of the column

$$M = (4\Delta F_{max}/h) \int_0^{h/2} (x - h/4)x \, dx = \Delta F_{max} h^2/24$$

Assuming that the minimum force F_{min} is $0.6F_{max}$ gives

$$\Delta F_{max} = 0.4F_{max}/2c = 0.2F_{max}/c$$

The bending moment about the middle of column

$$M = 0.2F_{max}h^2/24c \tag{12.28}$$

The bending stress

$$\sigma_b = M/W$$

where W is the section modulus that can be approximately determined by the formula

$$W = AB^2/6$$

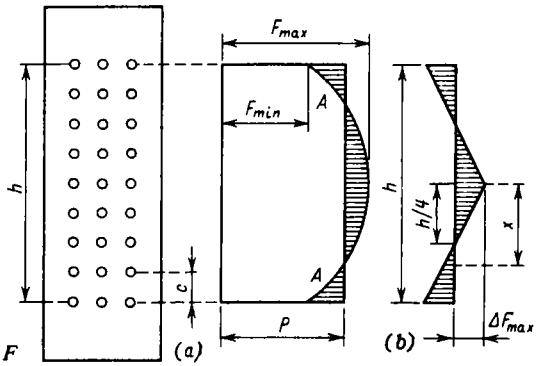

Fig. 12.17. Vertical profile of force F

with A being the average thickness of the column, and B the average width (radial dimension). It is worth noting that for unattached columns the bending stress in concrete is 1/15 the value for absolutely rigid units.

The column is subjected not only to bending deformation with tensile stresses in the external half of the section and compressing stresses in the internal half, but also to compression due to axial forces [12.1] produced by the transverse component of the flux density $\mu_0 H_D$ interacting with the turns. These forces cause compression stresses σ_{comp} over the entire cross section of the column. The axial stresses are maximum at the reactor ends and rapidly decay to the centre. Along a row of turns variation of axial stresses is insignificant.

The compressing stresses in a cross section are directly proportional to the sum of the axial forces produced by all turns at one side of the section. The resultant tensile stress at the most loaded area is

$$\sigma = \sigma_b - \sigma_{comp}$$

Sternin and Karpensky [12.1] have found that

$$\sigma_b = 1.33 \times 10^{-3} \frac{I_{pk}^2 w^2}{W} [3D - a(k + 1)]\xi \sin \beta$$

and

$$\sigma_{comp} = 0.0185 I_{pk}^2 w^2 \zeta / NS$$

where D is the mid-diameter of the reactor, cm; W is the section modulus of the column less the area occupied by wires, cm^2; a is the winding pitch; k is the number of turns in a layer; ξ and ζ are complicated functions of h/D; N is the number of columns; and S is the net section area of a column (less the area occupied by wires), cm^2.

Now, the condition of column stability $\sigma_b \leqslant \sigma_{comp}$ takes the form

$$1.33 \times 10^{-3} \frac{3D - a(k + 1)}{W} \xi \sin \beta \leqslant 0.0185 \zeta / NS$$

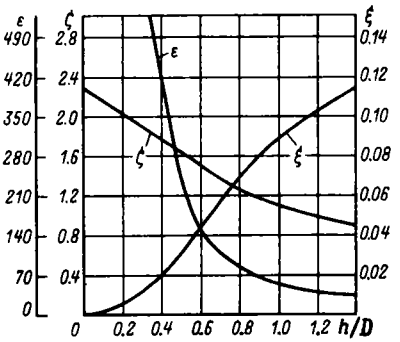

Fig. 12.18. Coefficients ξ, ζ and ε

For k = 6-14 the product $N \sin \beta$ varies insignificantly and equals 3.1, so that the stability condition rewrites as

$$\frac{S}{D[3D - a(k + 1)]} \leqslant 4.5 \frac{\zeta}{\xi} = \varepsilon$$

The functions ξ, ζ, and ε are plotted in Fig. 12.18.

External electrodynamic strength. Popular arrangements of a 3-phase reactor set are a vertical stack, horizontal in a row, in a triangle, and a stepped arrangement. The vertical stacking is more widely used being simplest and space saving. Therefore, in our consideration we touch first on the vertical arrangement of reactors.

For force analysis the energy approach is convenient, namely, for two reactors

$$F = i_1 i_2 \mathrm{d}M/\mathrm{d}x$$

where $M = w_1 w_2 G$ is the mutual inductance of these reactors, and G is the permeance for the coupling linkage. Then

$$F = i_1 w_1 i_2 w_2 \, \mathrm{d}G/\mathrm{d}x = i_1 w_1 i_2 w_2 \Psi$$

For analytical convenience Ψ is presented in graphical form as shown in Fig. 12.19. If we assume that the positive force is in the same sense as the distance between the reactors x, then for the same direction of currents and turns $\mathrm{d}M/\mathrm{d}x < 0$ and

$$F = i_1 i_2 \mathrm{d}M/\mathrm{d}x = -i_1 i_2 |\mathrm{d}M/\mathrm{d}x| = -i_1 w_1 i_2 w_2 |\Psi|$$

For $i_1 = i_2$ and $w_1 = w_2$

$$F = -(iw)^2 \Psi \tag{12.30}$$

For a three-phase system of currents,

$$\begin{aligned}
i_1 &= \hat{I} \sin(\omega t + \psi - \varphi) - \hat{I} \sin(\psi - \varphi) \exp(-t/\tau_a) \\
i_2 &= \hat{I} \sin(\omega t + \psi - \varphi - 120°) - \hat{I} \sin(\psi - \varphi - 120°) \exp(-t/\tau_a) \\
i_3 &= \hat{I} \sin(\omega t + \psi - \varphi - 240°) - \hat{I} \sin(\psi - \varphi - 240°) \exp(-t/\tau_a)
\end{aligned}$$

where ψ is the angle defining the instant of energising, φ is the angle characterising the circuit ($\tan \varphi = X/R$), and τ_a is the time constant of the aperiodic component.

To simplify our analysis we let $\varphi = 90°$ and assume that the aperiodic component is nondecaying, i.e. $\exp(-t/\tau_a) = 1$. Then

$$\begin{aligned}
i_1 &= 2\hat{I} \sin(\omega t/2) \sin(\omega t/2 + \psi) \\
i_2 &= 2\hat{I} \sin(\omega t/2) \sin(\omega t/2 + \psi - 120°) \\
i_3 &= 2\hat{I} \sin(\omega t/2) \sin(\omega t/2 + \psi - 240°)
\end{aligned}$$

The force acting on the upper reactor is

$$F = F_{12} + F_{13} = -i_1 i_2 w^2 \Psi_{12} + (-i_1 i_2 w^2 \Psi_{13}) \tag{12.31}$$
$$w_1 = w_2 = w_3 = w$$

Consider the case with all the reactors wound in the same direction and the current fed to the start of windings. Substituting the currents and rearranging yields

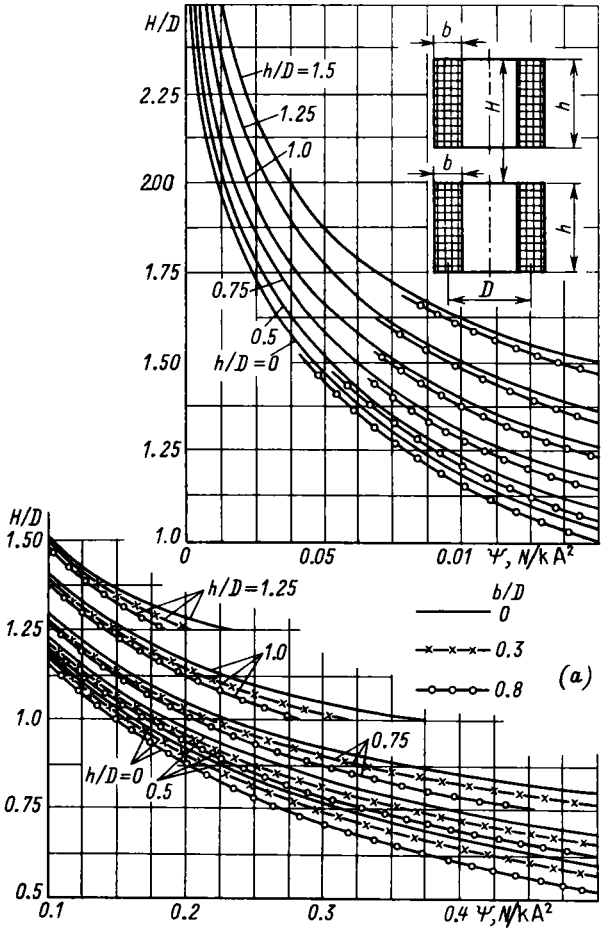

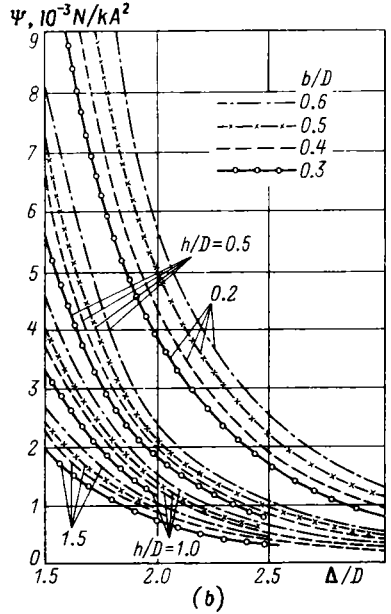

Fig. 12.19. Coefficient Ψ as a function of H/D, h/D, and s_c/D, where s_c is the distance between reactor axes: (*a*) vertical stack assembly, and (*b*) horizontal layout

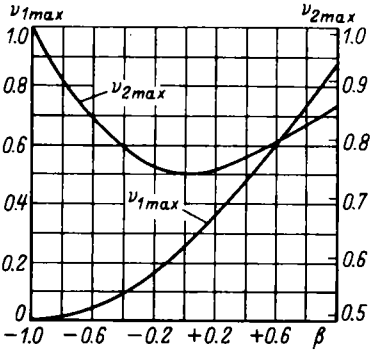

Fig. 12.20. Coefficients ν_{1max} and ν_{2max} as functions of β

for $\exp(-t/\tau_a) = 1$ and $I = 2\hat{I}$

$$F_1 = -I_{pk}^2 w^2 \psi_{12} \nu_1$$

with

$$\nu_1 = \sqrt{1 - \beta + \beta^2} \sin^2 \frac{\omega t}{2} \sin\left(\frac{\omega t}{2} + \psi\right) \sin\left(\frac{\omega t}{2} + \psi + \theta_1\right)$$

and

$$\beta = \Psi_{13}/\Psi_{12}$$

An analysis for maximum gives

$$\tan \theta_1 = \sqrt{3}(1 - \beta)/(1 + \beta)$$

$$\nu_1 = \nu_{1max} = \frac{1}{2}\sqrt{1 - \beta + \beta^2} - \frac{1}{4}(1 + \beta) \tag{12.32}$$

for $\omega t = 180°$ and $\psi = \psi_1 = -\theta_1/2$, and

$$\nu_1 = \nu_{2max} = -\frac{1}{2}\sqrt{1 - \beta + \beta^2} - \frac{1}{4}(1 + \beta) \tag{12.33}$$

for $\psi = \psi_2 = -\theta_1/2 + 90°$ and $\omega t = 180°$.

For ordinary makes, $\beta = 0.05$-0.15; for average analysis we let $\beta = 0.1$. The functions ν_{1max} and ν_{2max} are plotted in Fig. 12.20. If we neglect the effect of the third reactor by letting $\beta = 0$, then by virtue of Eqs. (12.32-33) we obtain $\nu_{1max} = 0.25$ and $\nu_{2max} = -0.75$. The maximum attracting and repulsing forces are then

$$\begin{aligned} F_{12,at} &= 0.25 I_{pk}^2 w^2 \Psi_{12} \\ F_{12,rep} &= -0.75 I_{pk}^2 w^2 \Psi_{12} \end{aligned} \tag{12.34}$$

Figure 12.21 shows variation of the force acting on the upper reactor in the stack plotted without account taken of the effect of the bottom reactor in the stack. The reactor of the third phase experiences the same forces if we neglect the effect of the upper reactor in the stack, namely,

$$\begin{aligned} F_{32,at,max} &= F_{12,at,max} = 0.25 I_{pk}^2 w^2 \Psi_{12} \\ F_{32,rep,max} &= F_{12,rep,max} = -0.75 I_{pk}^2 \Psi_{12} \end{aligned}$$

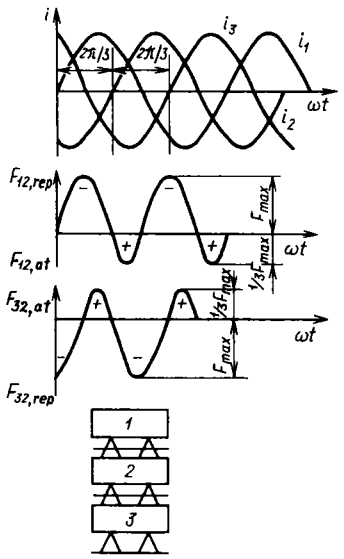

Fig. 12.21. Construction to evaluate the maximum forces in a vertical reactor stack

Because the interphase insulators possess only a weak tensile strength, the middle phase of the stack is reversed by changing the direction of the magnetic field for the opposite (the middle phase is wound in the reverse direction or is connected to the busbars with the winding end). Then at $\beta = 0$

$$\begin{aligned} F_{12,\text{at}} &= 0.75 I_{\text{pk}}^2 w^2 \Psi_{12} \\ F_{12,\text{rep}} &= -0.25 I_{\text{pk}}^2 w^2 \Psi_{12} \end{aligned} \tag{12.35}$$

The tension per insulator is then

$$f_1 = (F_1 - G)/N \tag{12.36}$$

where G is the reactor weight, N.

For the insulators supporting the upper reactor in the stack with allowance for the third (bottom) reactor, the admissible mechanical short circuit current is

$$I_{\text{pk}} = \frac{1}{w} \sqrt{\frac{f_1 N + G}{\nu_{1\max} \Psi_{12}}}$$

and for $\beta = 0.1$ and $\nu_{1\max} = 0.3$

$$I_{\text{pk}} = \frac{1.82}{w} \sqrt{\frac{f_1 N + G}{\Psi_{12}}}$$

The support insulators of the middle phase in the stack are less loaded in tension, for they have to bear the weight of the two upper reactors. Therefore, these insulators should be checked for compression

$$f_{\text{comp}} = (F_{\text{comp}} + 2G)/N$$

and

$$I_{pk} = \frac{1}{w}\sqrt{\frac{f_{comp}N - 2G}{\nu_{1max}\Psi_{12}}} \tag{12.37}$$

which for $\beta = 0.1$ becomes

$$I_{pk} = \frac{1.15}{w}\sqrt{\frac{f_{comp}N - 2G}{\Psi_{12}}} \tag{12.38}$$

To reduce the forces applied to the interphase insulators one can increase the distance between the centres of the windings. This is achieved by increasing the height of the column, however, this should not be made longer than the reactor winding by more than 300-350 mm as the strength of the column reduces at greater lengths [12.1].

Two-phase short circuit fault. With an inverted middle phase a two-phase short circuit current gives rise to the force compressing the interphase insulator that may be estimated as

$$f_{comp} = \frac{I^2_{pk,2ph}w^2\Psi_{12} + 2G}{N} \tag{12.39}$$

where $I_{pk,2ph}$ is the mechanical short time current of 2-phase fault

$$I_{pk,2ph} = \sqrt{3}I_{pk,3ph}/2$$

The compression force on a three-phase short circuit fault is

$$f_{comp} = (0.75I^2_{pk,3ph}w^2\Psi_{12} + 2G)/N \tag{12.40}$$

Comparing Eqs. (12.40) and (12.37) and allowing for current values, we can conclude that the compression force at a two-phase fault does not exceed the force at a three-phase fault. Therefore there is no need of an additional check of the interphase insulator for compressive load on a two-phase fault.

Under phase-phase short circuit conditions, between phases 1 and 3, the support insulators of the upper reactor work in tension (reactors are not inverted). Because the magnetic fields of the reactors are in opposition the reactance of the reactors will be decreased and the short circuit current will increase. The insulator checking should be carried out with the formula

$$f_{tens} = [I^2_{pk,2ph}w^2\Psi_{13} - G]/N \tag{12.41}$$

The horizontal arrangement of reactors is used as a rule at large rated currents (above 2000 A) or in low-ceiling rooms. Without reference to the effect of the third phase, the force acting on the first phase is

$$F_{1max1} = \nu_{max1}I^2_{pk}w^2\Psi_{12} = -0.25I^2_{pk}w^2\Psi_{12} \tag{12.42}$$

$$F_{1max2} = \nu_{max2}I^2_{pk}w^2\Psi_{12} = 0.75I^2_{pk}w^2\Psi_{12} \tag{12.43}$$

The value of Ψ_{12} is taken from the curves plotted in Fig. 12.22. Equations (12.42-43) have been derived in the same way as that for the vertical arrangement of phase reactors. In horizontal layouts the direction of forces with respect to the

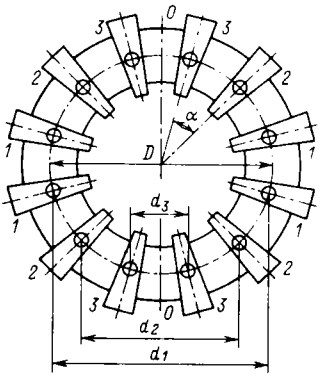

Fig. 12.22. Top view of a reactor to determine the mechanical rating of reactors in a vertical stack assembly

interphase insulators is of no significance. Therefore, the checking is performed by Eq. (12.43) only. The force acting on the middle reactor is

$$F_2 = F_{12} - F_{23} = I_{pk}^2 w^2 \Psi_{12} \nu_3 \tag{12.44}$$

where ν_3 may vary from $-\sqrt{3}/2$ to $\sqrt{3}/2$.

The calculated force for the middle phase is $F_2 = 0.867 I_{pk}^2 w^2 \Psi_{12}$. The horizontal layout does not require reversal of a winding any longer as it would increase the maximum value of force acting on the central reactor [12.1].

The interacting forces between reactors are applied to the middle portion of the winding. These forces tend to bend each insulator with a force F/N and extend it by the moment of this force

$$F/N = 0.867 I_{pk}^2 w^2 \Psi_{12}/N \tag{12.45}$$

The tilting moment causes extension of one and compression of other insulators. A moment tending to tilt the reactor produces tension forces in insulators *1*, *2*, and *3* (on the right of the *OO* axis in Fig. 12.22) and symmetrical compression forces (on the left of *OO*) so that the tilting moment is

$$M = FH_{conc}/2 = 2f_1 d_1 + 2f_2 d_2 + 2f_3 d_3 \tag{12.46}$$

where H_{conc} is the height of the concrete structure.

Within the Hookean region a force acting on an insulator is proportional to the insulator deformation. Therefore the farther from the reactor axis, the stronger is the force in the insulator, that is

$$f_3 = f_1 d_3/d_1 \quad \text{and} \quad f_2 = f_1 d_2/d_1 \tag{12.47}$$

which carries Eq. (12.46) to the form

$$M = 2f_1(d_1^2 + d_2^2 + d_3^2)/d_1^2$$

The interinsulator spacings are

$$d_1 = D \sin (5\alpha/2)$$
$$d_2 = D \sin (3\alpha/2)$$
$$d_3 = D \sin (\alpha/2)$$

The tension force

$$f_1 = \frac{M \sin^2 (5\alpha/2)}{2D[\sin^2 (5\alpha/2) + \sin^2 (3\alpha/2) + \sin^2 (\alpha/2)]} = (M/D)K_N \qquad (12.48)$$

The coefficient K_N is a function of the number of columns only. The extending force is partly opposed by the reactor weight

$$f_{\text{tens}} = f_1 - G/N$$

The spacing between reactors can be reduced by linking them with horizontal ties. These ties must possess the adequate mechanical strength and must be designed for the respective test voltage.

12.6 Insulation

As a rule reactors are connected to the network by cable lines, therefore they are not subjected to atmospheric overvoltage. Reactors are mostly affected by switching overvoltage that can raise the potential of the sound phases up to $3.2U_r$ and are rich in high-frequency harmonics [12.1].

The distribution of voltage in reactors is more uniform than in transformers. Available experimental evidence shows that the maximum voltage per winding layer in a 10-kV reactor never exceeds 1.5 kV. With insulated wire of $s = 120\,\text{mm}^2$ the dielectric strength of the spacing ($c = 4.5$ cm, see Fig. 12.6) is 70 kV and increases for larger cross sections. Practical experience with many thousand reactors has revealed no case of insulation breakdown at $a = 3.5$ cm and $c = 4.5$ cm even for contaminated insulation.

It would be a good practice to check the state of the concrete in service. If the resistance measured between the reinforcing elements of the insulator and the winding tap is less than 3 MΩ, then the reactor should be cleaned, dryed and tarnished.

12.7 Taps and Contacts

The reactor taps and its connections with the buswork of the distribution installation refer to the critical parts of the system. The leads of the reactor are brazed to the taps. Connection to the buswork may be either by brazing the taps to the buses of the switchyard or by bolted joints. Brazed joints are more reliable. Where bolted joints are preferred, it is desirable that the contact and the bus have the same temperature. For this purpose it is required that

$$R_c/R_{\text{bus}} = A_c/A_{\text{bus}}$$

where R are the resistances and A the cooling areas of the contact and bus.

To achieve a stable contact copper buses should receive a coat of tin, and aluminium parts to be connected should be dressed in petrolatum. The bolted contact is sealed by tarnishing.

A contact should not have residual deformations on a short circuit fault. Therefore the bolts should be equipped with spring washers that reduce mechanical stress in the bolted joint. To reduce the effect of buswork on the reactor the bus is taken to the reactor in a radius. The bus insulator should be within 350 mm of the reactor tap.

12.8 Duplex Reactors

The duplex reactor is essentially two strongly coupled half-coils connected aiding and placed one above another. This arrangement reduces voltage drop and saves space of the substation room. The reactors can be applied to any system with separate feeder circuits that will remain isolated under all circumstances.

Connection diagrams of duplex reactors are shown in Fig. 12.23. The total current of two feeders flows into point (3) of coil connection, and the loads are connected to feeders at points (1) and (2). The currents I_1 and I_2 through each half of the coil flow in opposite directions and the fields of the coils oppose each other. As a result the inductive reactance of each branch is reduced. Neglecting the resistance of the reactor winding, the voltage drop across one branch of the reactor

$$\Delta U_1 = I_1 X_d - I_2 X_M$$

where X_d is the reactance of the duplex reactor half coil, $X_M = \omega M$ is the reactance due to the mutual inductance M. The equivalent reactance of the first half coil

$$X_1 = \Delta U_1 / I_1 = X_d - I_2 X_M / I_1$$

For the second half coil,

$$X_2 = \Delta U_2 / I_2 = X_d - I_1 X_M / I_2$$

When the coil currents are identical, $I_1 = I_2$,

$$X_1 = X_2 = X_d - X_M = X_d(1 - X_M/X_d) = X_d(1 - K)$$

where K is the coupling coefficient of the half coils.

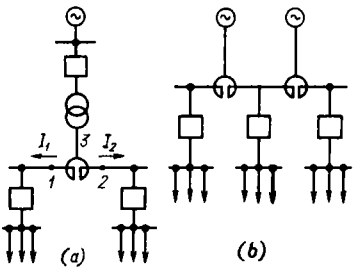

Fig. 12.23. Networks with duplex reactors

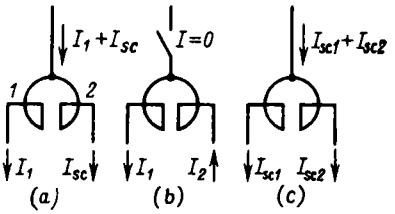

Fig. 12.24. Duplex reactor duties

The relative reactance of the reactor is conventionally taken as the reactance of one half coil in per unit of rated reactor resistance when the other half coil carries no current.

For U_r in kV it is given as

$$X_{d,rel} = I_r X_d \sqrt{3}/1000 U_r$$

The coupling coefficient is a principal parameter of a duplex reactor. It depends on the spacing between the half coils and increases as the coils are placed closer to each other. Ordinarily it varies between 0.4 and 0.6. A growth of K is paralleled by the growth of the electrodynamic forces tending to tear one half coil from the other. In the rated operating mode the reactance of one half coil decreases by 40-60% and the voltage drop across the reactor decreases.

Three commonly occurring modes of reactor operation are worth discussing.

(1) A fault occurs in one feeder and the fault current flows in feeder (2) in Fig. 12.24*a*. Feeder (1) carries rated current or has no current at all. The short circuit current in feeder (2) is solely controlled by the reactor reactance X_d

$$I_{sc} = I_r / X_{d,rel}$$

The current in feeder (1) does not practically affect the fault current being small compared with I_{sc}. This fault current induces in half coil (1) an emf $E_1 = I_{sc}\omega M$ which may exceed the rated reactor voltage almost twice [12.2]. Overvoltages occurring in this mode also limit the coupling coefficient K.

(2) Currents in the feeders flow to the same side as is the case with one of the generators disconnected, diagrams (*b*) in Figs 12.23 and 12.24. The inductive reactance of the branch increases

$$X_1 = X_2 = X_d(1 + K)$$

The total reactance of the reactor is then $X = X_1 + X_2 = 2X_d(1 + K)$. The magnetic fields of the half coils are not in opposition any longer and a force of attraction occurs between them.

(3) Both feeders carry short circuit currents (Fig. 12.24*c*). Under the circumstances the reactance of the branches reduces at $I_{sc1} = I_{sc2}$ to $X_1 = X_2 = X_d(1 - K)$ and they carry increased fault currents. In view of the closely spaced coils, fault currents produce large forces between them and can produce an adverse effect on the reactor stability.

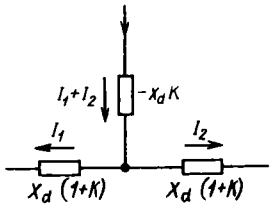

Fig. 12.25. Equivalent circuit of a duplex reactor

Figure 12.25 shows the equivalent circuit of the duplex reactor valid for all modes of reactor operation.

In mode 1 of a faulted feeder (2) the current I_1 may be neglected and the resultant reactance is

$$X = -X_dK + X_d + X_dK = X_d$$

For mode 2 with $I_1 = I_2$,

$$X = X_d(1 + K) + X_d(1 + K) = 2X_d + 2KX_d$$

For mode 3 we let

$$X_1 = [(I_1 + I_2)(-X_dK) + I_1X_d(1 + K)]/I_1 = X_d - KX_d$$

The internal electrodynamic strength of the reactor for mode 1 is evaluated in the same manner as for an ordinary current-limiting reactor. For mode 3 the mechanical short-circuit current reduces to more than a half value compared with mode 1 and is stated in the manufacturer's data sheet. This current is calculated as follows.

The force between the half coils is

$$F = I_{pk1}I_{pk2}w^2\Psi$$

where I_{pk1} and I_{pk2} are peak values of short circuit current in the branches, kA; w is the number of turns in the reactor and the coefficient Ψ is found by the curves plotted in Fig. 12.26.

The maximum admissible tensile stress for concrete columns of the reactor is 100 N/cm^2, hence

$$I_{pk1}I_{pk2}w^2\Psi \leqslant 100\,Ns_{col} \tag{12.49}$$

where N is the number of columns and s_{col} is the cross section of the column less the area occupied by the winding. Rewriting this inequality gives

$$\sqrt{I_{pk1}I_{pk2}} \leqslant \frac{10}{w}\sqrt{Ns_{col}/\Psi}$$

To increase the mechanical rating of the reactor in this duty the reactor design should be modified as follows [12.2]. The first 4-5 rows of the coil windings that experience the more severe mechanical loading must be tied up with a glass fibre band. The column concrete must be a high strength mix. In addition, the bolts securing the half coils together should be applied.

Because mode 3 is the most severe duty for a duplex reactor, it is recommended

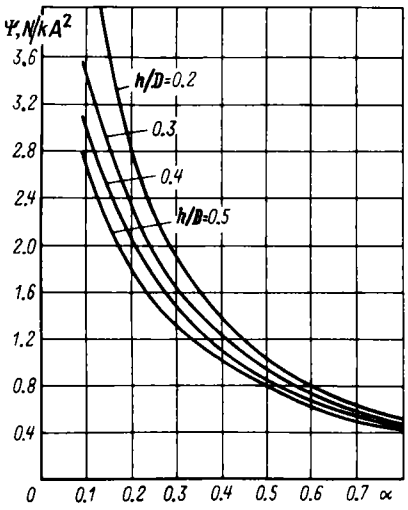

Fig. 12.26. Duplex reactor Ψ as a function of h/D and b/D, where h is the height of a half coil

to connect the half coils to different buses in order to avoid simultaneous short circuit faults on branches (1) and (2).

Three-phase duplex reactors may be erected in the form of a vertical stack, a vertical stack secured to the ceiling, and a horizontal layout more appropriate at heavy currents.

The methodology of evaluation of the external mechanical strength for duplex reactors does not differ from that for ordinary current-limiting reactors.

12.9 Calculation of a Reactor. Illustrative Example

Given: $U_r = 10$ kV, $I_r = 600$ A, $x_L = 0.03$, $f = 50$ Hz, $t_{tw} = 2$ s. The construction is a dry-type concrete structure wound with copper wire. It is required to calculate and select the principal parameters of the reactor. An appropriate calculation procedure may be as follows.

1. *Selection of cable cross section.* The current density J_r under normal conditions may be taken equal to 2.2 A/mm^2, so that the cross section of the cable

$$s = I_r/J_r = 600/2.2 = 273 \text{ mm}^2$$

Because this cross section exceeds 185 mm^2, the two-parallel-branch technique is recommended. We select 135-mm^2 cable.

Cable cross section may be selected for the optimal current density J_{opt}. If $J_{opt} > J_r$, then the choice must be checked for heating. The thermal rating of a copper winding is found with

$$I_{sc} = I_r/x_L = 20\,000 \text{ A}$$

therefore $J_{sc} = I_{sc}/s = 74.04\ \text{A/mm}^2$, and

$$t_{tw} = 11\,000/J_{sc}^2 = 11\,000(74.04)^2 = 2\ \text{s}$$

2. *Reactor inductance and size.* The inductance of the reactor is

$$\begin{aligned} L &= 10^3 U_r x_L / I_r 2\pi f\sqrt{3} \\ &= 10^3 \times 10 \times 0.03/(600 \times 2 \times 3.14 \times 50\sqrt{3}) \\ &= 0.92\ \text{mH} \end{aligned}$$

The reactor height is $h = (r - 1)c$, reactor thickness $b = (k - 1)a$, where $a = 3.5$ cm, k is the number of turns in a row, $c = 4.5$ cm, and r the number of rows.

Referring to Fig. 12.7, the number of parallel branches $m = 2$, so that $m^2L = 4 \times 0.92 = 3.68$. Assume $k = 6$ and $r = 12$, then $D = 86$ cm. The reactor height is $h = 49.5$ cm and thickness $b = 17.5$ cm.

Check the inductance by the Hack formula $L = w^2 D\Phi$ mH, where w is the number of turns, D the middle diameter, cm; and Φ the shape function (Fig. 12.8).

$$w = kr/m = 36$$
$$b/D = 0.203 = 17.5 \div 86$$
$$h/D = 49.5 \div 86 = 0.576$$
$$\Phi = 7.8$$
$$L = 36^2 \times 86 \times 7.8 \times 10^{-6} = 0.87\ \text{mH}$$

The actual inductance is seen to differ from the calculated value by about 5% which is within the admissible limits.

For $b/D = 0.203$ and $h/D = 0.576$ the curves of Fig. 12.8*b* indicate that the selected construction has a copper overweight of 102%, which is fairly acceptable as the overweight limit equals 105%.

For uniform distribution of current among the branches, these must have identical inductances. The arrangement of turns is similar to that shown in Fig. 12.6.

3. *Reactor heating and losses.* Recall that

$$R = \varrho_{75} l k_{add}/m^2 s$$

where $l = 1.03\pi Dmw \times 10^{-2}$ m is the length of wire and k_{add} is the coefficient of additional losses.

The d.c. resistance

$$R = \varrho_{75} l/m^2 s = 0.0216 \times 198.3 \div (2^2 \times 135) = 0.008\ \Omega$$

$$k_{add} = 1 + k_0 k_s k_\varrho (wm/h)^2 (f/50)^2 \times 10^{-3}$$

where $k_0 = 32$ is taken from Table 12.1 for $h/D = 0.58$ and $b/D = 0.2$. For copper $k_\varrho = 1$, and $k_s = 1.3s$ (s in cm^2).

Now,

$$k_{add} = 1 + 32 \times 1.75 \times 1(36 \times 2 \div 49.5)^2 \times 10^{-3} = 1.12$$

The loss of power in one phase of the reactor

$$P = I_r^2 R k_{add} = 1.12 \times 600^2 \times 0.008 = 3225.6\ \text{W}$$

The loss of power in insulator fixtures $P_{ins} = NP_0$, where N is the number of insulators equal to the number of columns and P_0 is a power loss per insulator equal to 15 W.

The power loss in concrete is taken to be 10% of the loss in copper, that is, 0.3 kW. Now,

$$P_{total} = 3.2 + 0.3 + 0.18 = 3.7 \text{ kW}$$

The heating of reactor windings will be calculated by Eq. (12.16) for a vertical stack of the three-phase assembly. For the upper reactor,

$$\Theta_r = \Theta_0 + 100k_r(I_r/mC_h)^2$$
$$k_r = 0.57D_1/(D_1 - 2.1N) = 0.9$$

where D_1 is the internal winding diameter equal to $D - b = 86 - 17.5 = 68.5$; $N = 12$ and $C_h = 426$ is found in Table 12.2. Substituting the numerical values yields

$$\Theta_r = 40 + 100 \times 0.9(600/2 \times 426)^2 = 85 \text{ °C}$$

4. *Internal electrodynamic strength.* Determine the specific (per cm length) forces at points A, B, and C shown in Fig. 12.12.

$$f_A = 5 \times 10^{-6}(w/mb)(I_r/x_L)^2 A_{h/2} \text{ [N/cm]}$$
$$f_B = 6 \times 10^{-4}(w/mb)(I_r/x_L)A_h \text{ [N/cm]}$$

In order to determine $A_{h/2}$ by the curves plotted in Fig. 12.12 we find

$$D_2/D_1 = (D_1 + 2b)/D_1 = 103.5 \div 68.5 = 1.51$$
$$h/2D_1 = 49.5 \div (2 \times 68.5) = 0.362$$

so $A_{h/2} = 0.352$ and

$$f_A = 5 \times 10^{-6} \times 36(600 \div 0.03)^2 \times 0.352 \div (2 \times 17.5) = 725 \text{ N/cm}$$

Having found the coefficient A_h by the curves of Fig. 12.12 for the ratio h/D_1, we determine

$$f_B = 6 \times 10^{-4} \times 36(600 \div 0.03)^2 \times 0.26 \div (2 \times 17.5) = 640 \text{ N/cm}$$

and

$$f_C = 2.8 \times 10^{-6}(w/mb)(I_r/x_L)^2 A_h$$
$$= 2.8 \times 10^{-6}(36 \div 2 \times 17.5)(600 \div 0.03)^2 \times 0.26$$
$$= 300 \text{ N/cm}$$

The stress in the wire material will be determined with Eq. (12.21). Having determined the values of b, h, and D, and specified the number of columns N, we are able to produce an approximate design of the reactor to estimate the lengths of free cable segments at points A, B, and C. At points A and B the free cable span

is about 100 mm and at C it is 150 mm (see Fig. 12.13). Recalling that

$$\sigma = \sqrt[3]{f^2 l^2 E/6s^2}$$

and substituting the numerical values, we have

$$\begin{aligned}\sigma_A &= \sqrt[3]{725^2 \times 10.3^2 \times 1.15 \times 10^6 \div (6 \times 1.35^2)} \\ &= 14\,000 \text{ N/cm}^2 \\ \sigma_B &= \sqrt[3]{640^2 \times 10^2 \times 1.15 \times 10^6 \div (6 \times 1.35^2)} \\ &= 13\,500 \text{ N/cm}^2 \\ \sigma_C &= \sqrt[3]{300^2 \times 15^2 \times 1.15 \times 10^6 \div (6 \times 1.35^2)} \\ &= 13\,600 \text{ N/cm}^2\end{aligned}$$

which are well below the maximum admissible stress for copper, 15 000 N/cm^2.

The strength analysis will be carried out for the case of unattached columns. The constant B for Eq. (12.27)

$$B = F \sum_{M=1}^{k} [D_1 + (M - 1)\Delta D]^{-1}$$

where ΔD is the increment of diameter in coming from one turn to the other.

$$\Delta D = (D_2 - D_1)/(k - 1) = (103.5 - 68.5)/5 = 7 \text{ cm}$$

where F is the sum of all forces acting in one row

$$F = f_{t1} + f_{t2} + f_{t3} + f_{t4} + f_{t5}$$

By virtue of Eq. (12.23)

$$f_{tM} = C(k - M)[D_1 + (M - 1)\Delta D]$$

where

$$\begin{aligned}C = f_A \sin \beta/(k - 1) &= 725 \times 0.259 \div (6 - 1) = 37.6 \text{ N} \\ f_{t1} &= 37.6(6 - 1) \times 68.5 \approx 12\,900 \text{ N} \\ f_{t2} &= 37.6(6 - 2)(68.5 + 7) \approx 11\,300 \text{ N} \\ f_{t3} &= 37.6(6 - 3)(68.5 + 2 \times 7) \approx 9300 \text{ N} \\ f_{t4} &= 37.6(6 - 4)(68.5 + 3 \times 7) \approx 6700 \text{ N} \\ f_{t5} &= 37.6(6 - 5)(68.5 + 4 \times 7) \approx 3640 \text{ N} \\ f_{t6} &= 0\end{aligned}$$

and the total force

$$F = 12\,900 + 11\,300 + 9300 + 6700 + 3640 = 43\,840 \text{ N}$$

The constant B may be determined now as

$$\begin{aligned}B &= 43\,840 \div [68.5^{-1} + (68.5 + 7)^{-1} + (68.5 + 14)^{-1} \\ &\quad + (68.5 + 21)^{-1} + (68.5 + 28)^{-1} + (68.5 + 36)^{-1}] \\ &= 605\,000 \text{ N cm}\end{aligned}$$

The forces exerted by the turn on the column

$$f'_{tM} = C(k - M)[D_1 + (M - 1)\Delta D] - B/[D_1 + (M - 1)\Delta D]$$

$$f'_{t1} = f_{t1} - B/D_1 = 4580\ \text{N}$$
$$f'_{t2} = f_{t2} - B/(D_1 - \Delta D) = 3300\ \text{N}$$
$$f'_{t3} = f_{t3} - B/(D_1 + 2\Delta D) = 1680\ \text{N}$$
$$f'_{t4} = f_{t4} - B/(D_1 - 3\Delta D) = -60\ \text{N}$$
$$f'_{t5} = f_{t5} - B/(D_1 + 4\Delta D) = -2620\ \text{N}$$
$$f'_{t6} = f_{t6} - B/(D_1 + 5\Delta D) = -5850\ \text{N}$$

The crushing stress at the turn contact areas

$$\sigma_{cr} = f'_t/Ad_{cable}$$

where A is the column thickness equal to 11 and 15.8 cm (taken by the draft design) and d_{cable} is the cable diameter equal to 1.3 cm approximately.

The crushing stress for the first and sixth turns

$$\sigma_{cr1} = 4580 \div (11 \times 1.3) = 32\ \text{N/cm}^2$$
$$\sigma_{cr6} = 5850 \div (15.8 \times 1.3) = 28.98\ \text{N/cm}^2$$

are within the admissible limits for the concrete columns.

The bending stress in a concrete column

$$\sigma_{bend} = 0.2\Delta F_{max}h^2/24cW$$

where $W = AB^2/6$, $A = 13.4$ cm is the average thickness of the column, and $B = 24.5$ cm is the column width; then,

$$W = 13.4 \times 24.5^2 \div 6 = 1340\ \text{cm}^3$$

and

$$\sigma_{bend} = 0.2 \times 43\,840 \times 49.5^2 \div (24 \times 4.5 \times 1340) = 49\ \text{N/cm}^2$$

As a rule the standardising documents stipulate the compression and tensile stresses. It is desirable to use concrete with a tensile strength of at least 200 N/cm^2 (this strength is always lower than the bending figure).

5. *External mechanical strength.* The outline of a three-phase reactor stack is shown in Fig. 12.27. The middle phase has an inverted winding. For simplicity of estimation we neglect the effect of the third (lowest) phase. The maximum attractive force imposed on the insulators of the upper reactor is

$$F_{at} = \frac{3}{4}(I_{pk}w)^2\Psi = 265\,458\ \text{N}$$

The coefficient Ψ is found with the curves in Fig. 12.19*a*; for $h/D = 49.5 \div 86 = 0.576$, $b/D = 17.5 \div 86 = 0.2$, and $H/D = 1.186$, $\Psi = 0.105$ N/kA.

The maximum repulsive force

$$F_{rep} = \frac{1}{4}(I_{pk}w)^2\Psi = 0.25(51 \times 36)^2 \times 0.105$$
$$= 88\,486\ \text{N}$$

In addition to electrodynamic forces the insulators are also subjected to reactor

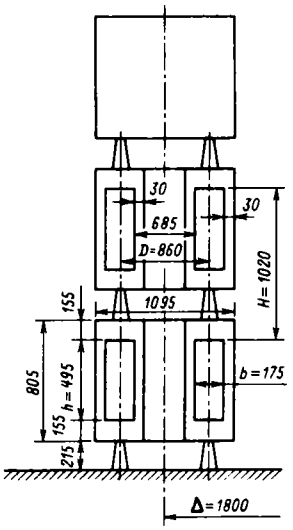

Fig. 12.27. Three-phase reactor stack assembly (dimensions in mm)

weight

$$G_L = G_{Cu} + G_{conc} + G_{ins}$$

where G_{Cu} is the weight of copper winding, G_{conc} the weight of concrete, and G_{ins} the weight of insulators.

$$G_{Cu} = V_{Cu}\gamma_{Cu} = sl\gamma_{Cu} = 1.35 \times 198.3 \times 9000 = 2400\ \text{N}$$

The column cross section (α is the column angle)

$$S_{col} = \frac{\alpha}{360}\pi(R^2 - r^2) = (16 \div 360) \times 3.14(2830 - 1070) = 246\ \text{cm}^2$$

The volume of the column

$$V_{col} = S_{col}H = 246 \times 81 = 2 \times 10^{-2}\ \text{m}^3$$

With γ_{conc} = 1800-2400 kg/m^3, the column weight

$$G_{conc} = \gamma_{conc}V_{col}N = 2200 \times 2 \times 10^{-3} \times 12 = 5280\ \text{N}$$

The type OF-10-750 insulators, well suiting the requirements, are characterised by f_{tens} = 5000-7500 N, f_{comp} = 30 000 N, f_{bend} = 7500 N, and G_{ins} = 50 N. Accordingly, the weight of 12 insulators is 600 N, and the total reactor weight will be G_L = 2400 + 5280 + 600 = 8280 N.

The forces applied to an insulator of the upper reactor

$$f_{tens} = F_{rep}/N - G_L/N = 88\,468 \div 12 - 8280 \div 12 = 6682\ \text{N}$$
$$f_{comp} = F_{at}/N + G_L/N = 265\,458 \div 12 - 8280 \div 12 = 21\,431\ \text{N}$$

These forces are within the admissible limits for the insulator in question.

On a short circuit fault after the upper and lower reactors an attractive force occurs between these reactors that tends to expand the support insulators

$$f_{tens} = I_{pk}^2 w^2 \Psi_{13}/N - G_L/N$$
$$= [(51 \times 36)^2 \times 0.008 - 8280]/12 = 1550\,\text{N}$$

where $H/D = 2.37$, $\Psi_{13} = 0.008\,\text{N/kA}^2$, and it has been assumed that $I_{pk,2ph} \approx I_{pk,3ph}$.

For the horizontal layout of the reactors, the tensile force imposed on the insulator is

$$f_{tens} = f_1 - G_L/N$$

where by Eq. (12.48) $f_1 = FH_{conc}k_N/2D$.

For the 12-column structural design, $k_N = 0.322$; $F = (I_{pk}w)^2\Psi \times 0.867$, and the coefficient Ψ is selected from Fig. 12.19*b* for $h/D = 0.58$ as $\Psi = 20 \times 10^{-3}\,\text{N/kA}^2$.

If we assume that the distance between reactor axes is $\Delta = 160\,\text{cm}$, then $\Delta/D = 160 \div 86 = 1.86$. Now,

$$F = (51 \times 36)^2 \times 20 \times 10^{-3} \times 0.87 = 58\,451.3\,\text{N}$$
$$f_1 = 5845 \times 13 \times 81 \times 0.322 \div (2 \times 86) = 8863.5\,\text{N}$$
$$f_{tens} = 8863.5 - 8280 \div 12 = 8173.5\,\text{N}$$

Since the maximum admissible tension force for the selected insulator type is 7500 N, we have to increase the interaxial distance to be 180 cm. Then $f_1 = 7533.9\,\text{N}$ and $f_{tens} = 6846.9\,\text{N}$ which are already within the admissible limits.

REFERENCES

12.1 V. G. Sternin and A. K. Karpenskii: *Tokoogranichivayushchie reaktory* (Current-limiting reactors), Energiya, Moscow 1965.

12.2 A. A. Vasilyev (ed.): *Elektricheskaya chast stantsii i podstantsii* (Switchgear of generating plants and substations). Energiya, Moscow 1980.

13
SURGE ARRESTERS

13.1 Application and Characteristics

Surge arresters are applied on electric systems to protect electric equipment and machinery against the effects of overvoltages that result from lightning strokes, switching surges, and other disturbances. Surge arresters are connected in shunt with equipment to be protected and perform their function by providing a relatively low-impedance path for surge currents so that the surge arrester protective level is lower than the insulation withstand strength of the equipment being protected. Arrester protective level is the voltage appearing across the terminals of the arrester at sparkover or during the flow of current through the arrester after sparkover. The simple and reliable overvoltage control by surge arrester protection relaxes the requirements imposed on the basic insulation level (BIL) of the protected equipment which results in smaller and cheaper installations.

13.2 Tube-Type Arresters

The construction of a tube type arrester is schematically shown in Fig. 13.1. The housing tube (1) is made of insulating material capable of releasing gas when heated or provided with an insert of a gas-generating material. One end of the tube is sealed by a metal cap that holds a central rod electrode (2). A ring electrode (3) is attached to the other end of the tube. The spacing between the two electrodes labelled S_1 is the internal discharge gap. The external discharge gap S_2 separates the tube from the phase lead in order to prevent the decomposition of gas-generating material by leakage currents.

The discharge gaps of this arrester are designed so that they spark over by a lightning stroke impulse and provide a path for the impulse current to earth. The power follow current supporting the high temperature discharge decomposes the

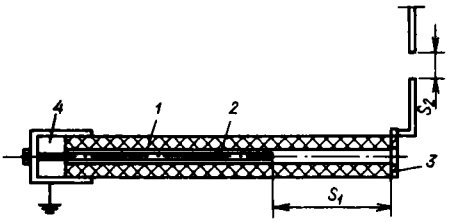

Fig. 13.1. Construction of open tube-type arrester

tube material with a spurious release of gas and pressure rise within the tube. The puff of gas toward the open end of the tube provides a blowing action that aids arc extinction at the next current zero.

The voltage/time protective characteristic of this surge arrester is controlled by the lengths of external and internal gaps and has a shape typical of arc spacing with extremely nonuniform electric field.

The low-current high-duration withstand and high-current withstand of this type of surge arrester depend on the tube channel dimensions. The high-current withstand is limited by the mechanical strength of the arrester body, and the low-current withstand is governed by the pressure at which reliable extinction of follow current is still possible.

Surge arresters with phenolic-resin-plastic casing use fibre as a gas generating material. A pocket at the closed end serves as a buffer space aiding in accumulation of gas and intensive blasting at a current zero. An alternative tube material is rigid vinyl plastic which offers higher insulating strength and gas generating activity, higher mechanical strength and, consequently, a higher high-current withstand.

An important requirement of these devices is a free space at the outlet end of the arrester where there should be no leads of other phases, earthed structures, and overlap with outlet zones of surge arresters protecting other phases. The dimensions of such zones can be substantial, say, 3 m length and 1.5 m width for a 35-kV arrester.

The principal disadvantages of tube-type arresters are the outlet zone requirement, unstable performance, and a steep protective characteristic. It is no more chance that in new installations these devices have been largely supplanted by upgraded valve-type surge arresters.

13.3 Valve-Type Surge Arresters

Valve-type surge arresters consist of single or multiple spark gaps in series with nonlinear valve resistors. Some of these devices have resistors and capacitors connected in shunt with the spark gaps to control the distribution of voltage of various surge length over the spark gaps. The shunt resistors equalise the distribution of slowly-varying power-frequency voltages and switching overvoltages over the spark gaps. The shunt capacitors are used for both voltage equalisation and adjustment of protective characteristic primarily in lightning overvoltage protection service.

A lightning surge exceeding the breakdown voltage of the spark gaps causes their discharge and the gaps and nonlinear resistor begin to carry impulse current and then a follow current. The overvoltage applied to the protected insulation will be controlled by the voltage drop due to these currents across the nonlinear resistor whose volt-ampere characteristic is presented in Fig. 13.2.

To discuss the principal characteristics of surge arresters we resort to the simplified diagram of current and voltage histories in a surge arrester sparked over by a lightning stroke (Fig. 13.3). When the voltage in the system increases to the breakdown level, the gaps spark over and carry an impulse current whose amplitude value is associated with the discharge voltage across the arrester U_d.

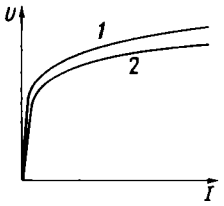

Fig. 13.2. Volt-ampere characteristic of nonlinear resistors ($\alpha_1 > \alpha_2$)

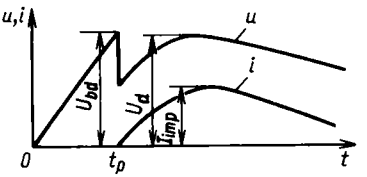

Fig. 13.3. Voltage across and discharge current in the arrester

Basic characteristics of a surge arrester include arrester protective level, measured as switching surge sparkover at power frequency discharge voltage; discharge voltage; rated discharge current; rated arrester voltage; arrester rating as the maximum admissible overvoltage or extinction voltage, that is, the r.m.s. value of maximum voltage across the arrester at which a reliable arc extinction can be achieved; and the last but not the least, the coefficient of protection for a given surge waveform (front rise × pulse width microseconds).

The extinction voltage is governed by the arrester duty. If a lightning stroke have caused earthing of one phase and arrester sparkover in the other phases, then the voltage in the sound phases will increase. Therefore, for valve-type arresters installed on the systems with the isolated neutral, the extinction voltage is assumed to be 1.1 times the rated voltage. The coefficient 1.1 allows for the rise of voltage due to voltage regulation of the plant.

For valve-type arresters operating on the systems with the neutral solidly earthed, the extinction voltage is 0.8 times the rated voltage.

The coefficient of protection characterises the arrester efficiency

$$k_{pr} = U_d/\sqrt{2}U_{ext}$$

A reduction of this coefficient is achieved in two ways, namely, by using nonlinear resistors with flatter volt-ampere characteristics (curve (2) in Fig. 13.2) and by improving the arc extinction properties of the spark gap. Let us consider how these principles are realised in the actual arrester constructions.

The nonlinear valve resistor must be able to restore its capability after the discharge current ceases. When the maximum current due to lightning overvoltage flows through the resistor its resistance should be a minimum in order that the discharge voltage, mainly controlled by the voltage drop in the resistor, should not exceed the specified level. The resistor should also reduce power follow currents to a level where the spark gaps ensure reliable extinction of the power follow current. These valve properties of sharp variation of resistance with voltage are characteristic of the materials based on silicon carbide.

Silicon carbide is produced from silicon oxide reduced by carbon at 2000-2500 °C. A barrier layer formed at the surface of silicon carbide grains owes its existence to a space charge appearing at this surface and, in some cases, to a film of silicon oxide. Grains of silicon carbide have a low resistivity controlled by

the production technology of silicon carbide powder. The resistivity of the barrier layer is a nonlinear function of the current density and voltage gradient. At low voltages it is 6-8 order of magnitude higher than the resistivity of grains proper. Under the circumstances all the voltage is applied to the barrier layer which controls the resistance of the valve resistor. At higher voltages the resistance of the barrier layer falls off and the momentary resistance of the valve resistor is already governed by the bulk silicon carbide.

Nonlinear resistors of valve-type arresters are produced as discs of various diameters (up to 130 mm) 10-60 mm high. The flat surface of discs is covered by aluminium, and the cylinder surface receives a coat protecting the discs from flashover.

Silicon carbide grains are bound by binders which do not require high annealing temperature, for example, by water glass or by those which require sintering at temperatures above 1000 °C. Materials of the first group are used for making series resistors while those of the second group are used for both series and shunt resistors.

High temperature annealing burns out a part of barrier films thus rising the current capability of the material but flattening the nonlinearity.

Shunting resistors are shaped into arcs of various thickness that embrace spark gaps. Shunt resistors have metallised ends with holes for joining with one another and connection with spark gaps.

In the 10-20 kA range of currents static volt-ampere characteristics plotted to the logarithmic scale may be approximated by two variously slanted straight lines with a narrow transition zone between them (Fig. 13.4). Each line segment is described by the equation $U = AI^{\alpha}$, where α is the resistor nonlinearity coefficient which is higher in the range of small currents than in the range of high currents. The values of A and α depend on the resistor material and resistivity.

Every current pulse leaves a trace of destruction in the series resistor as a result of a breakdown of the barrier layer in some grains of silicon carbide. Multiple application of current pulses leads to the total breakdown of the resistor which occurs sooner the higher the magnitude and duration of the current pulses. Therefore the current carrying capability of a valve-type arrester is limited and is usually charac-

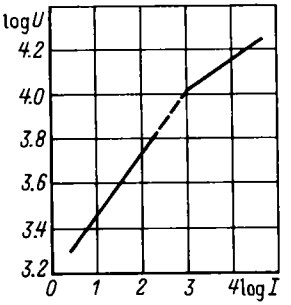

Fig. 13.4. Volt-ampere characteristic of a silicon carbide disc of 100 mm diameter and 60 mm height for the 1-10 000 A range

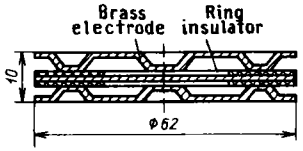

Fig. 13.5. Spark gap element of a valve-type arrester

terised in terms of the maximum 20 × 40 μs current wave or 2-μs rectangular current wave (in some cases the crest of a 3 × 8 μs current impulse), that the valve-type arrester must withstand 20 times without detrimental effects to its structure.

The arc extinction properties of spark gaps have been improved by enhanced design. The spark gap constructions may be loosely subdivided into two large groups. In constructions belonging to the first group the arc remains practically in the place where the discharge has occurred; in those belonging to the second the magnetic blowout is harnessed to elongate the arc in extinction. The second group is more numerous. The electromagnetic action is produced by the magnetic field due to special configuration of the electrodes, or by permanent magnets or coils carrying follow current.

Figure 13.5 shows a spark gap with the stationary arc. It is constituted by two stamped brass electrodes and a ring insulating spacer 0.5-0.6 mm thick. The material and thickness of the electrodes are selected so as to ensure the required stiffness. The gap between the electrodes must not alter either with the loading of the springs compressing the electrodes, or with the action of electromagnetic forces that are produced by heavy pulse currents and tend to separate the electrodes. Electrode thickness is selected at least 0.8 mm to preclude unnecessary effects of the heating by surge and follow currents and ensure a stable arrester protective level. Brass is a corrosion-free material offering a faster recovery of the dielectric strength than copper.

The insulating spacers are made of micanite or electric grade cardboard that possess rather high permittivity. Therefore, at the contact of the electrodes with the insulating spacer considerable strength of the electric field (tangential component) causes partial discharges that stabilise the breakdown characteristics of the spark gap and improve its protective characteristic. This type of spark gap interrupts follow currents as high as 80-100 A.

Figure 13.6 shows a spark gap construction harnessing the action of a magnetic field produced by permanent magnets. The gap is formed by two concentric electrodes (1) and (2) insulated by spacers of electric grade cardboard (3) and micanite (4). The spark gap is activated by ionisation due to intensifier electrodes (6) with a micanite gasket.

When the gap sparks over, an arc formed between the electrodes is set by a permanent magnet (5) into fast rotation around the annual gap and receives intense cooling. If the arc interrupts, the dielectric strength recovers much faster than in a stationary arc gap as the temperature of the moving arc electrodes at the current zero is markedly lower and the thermo-emission of electrons is slower than for the stationary arc gap.

A rotating-arc gap can extinguish follow currents up to 250-300 A allowing for

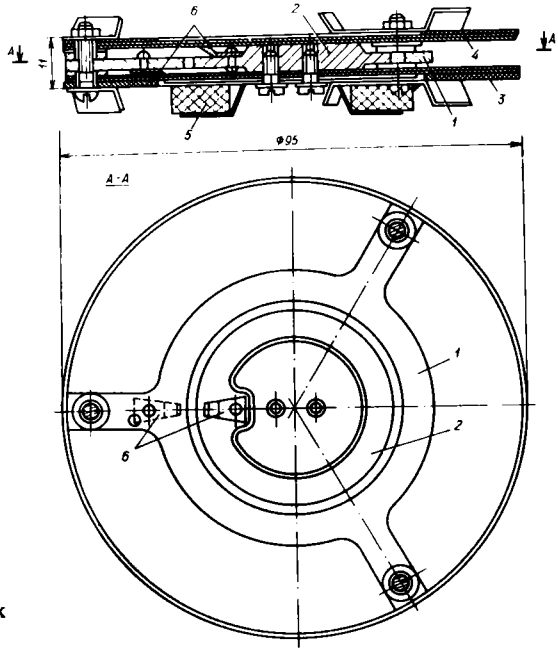

Fig. 13.6. Construction of a spark gap with revolving arc

fewer nonlinear resistor discs and depressing the discharge voltage. For surge arresters with simple arc horns subjected to 5000 A crest impulse, the coefficient of protection is 2.25-2.4 whereas for arresters with magnetic blowout of the arc it is 1.7-2.0.

A further reduction of coefficient of protection is achieved with current-limiting gaps shown in Fig. 13.7. This construction makes the arc to move inside a narrow

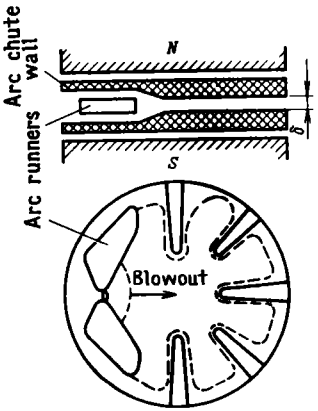

Fig. 13.7. Current-limiting arrester with elongated arc

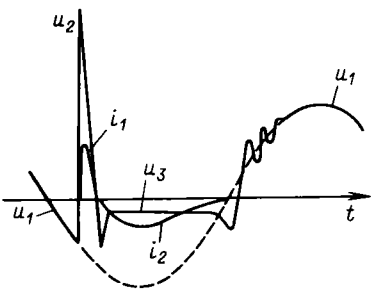

Fig. 13.8. Gap voltage and current versus time

main gap of the extinction chamber and elongate within this chamber. Two electrodes are between the walls of the extinction chamber in a magnetic field (N-S) produced by aiding connected blowout coils or by opposite poles of permanent magnets. The blowout force causes the arc to move over the electrodes and elongate within the narrow slit δ. Inside the slit the voltage across the arc reaches 800-1600 V, the resistance of the elongated arc rises considerably and limits the power follow current.

Possible variations of current and voltage with time in such a current-limiting gap are illustrated in Fig. 13.8. When an overvoltage surge u_2, in antiphase with the system e.m.f. u_1, breaks down the gap, the arc begins to carry an impulse current i_1. At the nearest current zero the arc restrikes and passes a follow current i_2 that produces a voltage drop u_3 across the gap. When the follow current crosses zero, the voltage recovery begins and if the gap electric strength curve lies above the recovery voltage curve, no restriking will occur any longer. The current limiting effect of arc resistance reduces the phase difference between the current and power-frequency voltage thus creating easier conditions for voltage recovery.

Station arresters are assembled of such current limiting gaps connected in series. Uniform distribution of voltage over these gaps in handling a follow current is achieved by means of high-value resistors connected in shunt.

New Soviet installations exploit mass produced valve-type arresters categorised in series as follows: series RVP substation arresters, series RVS station arresters, series RVM magnetic arresters, series RVMG magnetic lightning surge arresters, series RVMK magnetic combined arresters, series RVT current-limiting arresters, and series RVRD elongated-arc arresters. According to protective properties the arresters for all voltage classes are divided in four groups as follows: series RVT and RVRD make up group 1, series RVM makes up group 2, series RVC makes up group 3, and series RVP makes up group 4. The best performance is demonstrated by the valve-type arresters of group 1 which have the lower discharge voltage, whereas the group 4 arresters have the worst characteristics of all.

Substation valve-type arresters are rated for 3, 6, and 10 kV. Figure 13.9 is a sectional view of such an arrester with 6-kV rating. The assembly of spark gaps (4) and series resistors (6) are placed inside a porcelain housing (7) and compressed by a spring (9). The position of silicon carbide resistor inside the housing is fixed by a felt (10). The silicon carbide discs of currently produced discharges are 55 mm

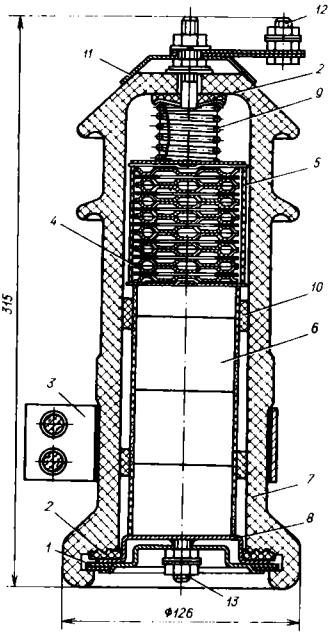

Fig. 13.9. Type RVP-6 valve-type arrester

in diameter and 20, 40, or 60 mm heigh, metallised over the contact areas and insulation-coated over the cylinder surface.

The spark gaps are assembled inside an insulating cylinder (5). The arrester is sealed by ozone resistant rubber gaskets (2). The upper sealing is covered by a metal cover (11), the lower sealing is covered by a diaphragm (8) and locked by metallic presssing elements (1). The arrester is secured by a clamp (3). Bus connections are effected by a bolt (12) for the current carrying bus, and by a stud (13) for the earthing bus.

Station arresters are manufactured as five standard elements rated 15, 20, 30, 33, and 35 kV. These elements are assembled in series connected stacks for a required protective level from 15 to 220 kV. For uniform distribution of voltage over the spark gaps, each group of four gaps is shunted by a resistor. A sectional view of such an arrester rated for 15 kV is presented in Fig. 13.10. The top and bottom of the porcelain housing (3) are occupied by assemblies of spark gaps (5) confining a stack of silicon carbide discs (4). This arrangement of spark gaps reduces the impulse coefficient of the arrester. The necessary contact loading is provided by springs (6) shunted with copper bands.

The upper and lower ends of the porcelain housing are reinforced by silumin flanges (2). A silumin or brass cover (1) seals the housing by means of an ozone-resistant rubber gasket. The assemblies of spark gaps are set in insulating cylinders and shunted by silicon carbide (Thyrite) resistors.

Magnetic valve-type arresters for 3-35 kV make up the RVM series, and for

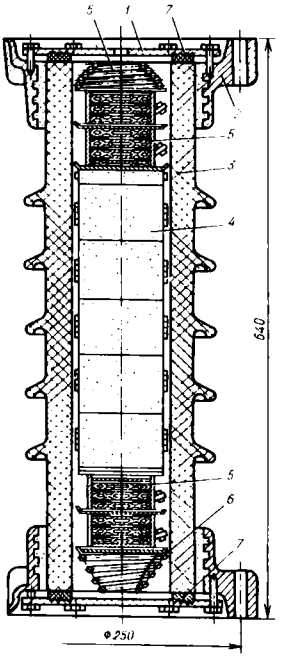

Fig. 13.10. Type RVS-15 valve-type arrester

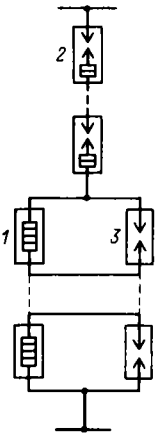

Fig. 13.11. Scheme of type RVMK arrester elements

110-750 kV the RVMG series. The arresters of the first series rated for 3-10 kV are designed for protection of rotating machinery having a lower impulse insulation withstand (BIL), therefore these arresters are designed to have a low impulse coefficient (0.6-0.65) for sparkover waveforms corresponding to lightning overvoltages. This requirement is met by providing a nonuniform distribution of impulse voltage over the spark gaps with shunt capacitors for the two lowest groups. The elements characteristic of this series are series resistors of silicon carbide discs 130 mm diameter and 50 and 60 mm height spark gaps with rotating arcs (see Fig. 13.6), and shunt resistors of a semiannual form.

Series RVMG arresters for high classes of lightning overvoltage are assembled of a standard unit rated for 33 kV. The nonlinear resistor material is silicon carbide.

Arresters of the combined series RVMK owe their name to the type of protection they offer, namely, a combined service on the systems with lightning and switching overvoltage hazards. They are designed for ratings up to 1150 kV. This series exploits spark gaps with magnetic arc extinction and silicon carbide nonlinear resistors.

Owing to high nonlinearity exhibited by the silicon carbide material used in these valve-type arresters in passing impulse currents of lightning overvoltages the discharge voltage attains high values inacceptable from the standpoint of insulation

withstand. The switching overvoltage duty, on the other hand, with its lower amplitudes of currents and longer duration of current surges is more compatible with the material of these nonlinear resistors. Limitation of the discharge voltage at lightning overvoltages is achieved by network design for this series of arresters. The connection scheme of the elements into an arrester is shown in Fig. 13.11. When the arrester operates at a switching overvoltage, the gaps of the main elements (2) spark over. The arc extinction of the follow current limited by the main (2) and valve-type (1) elements occurs at a voltage of up to $1.6U_{ph}$.

When this arrester operates at lightning overvoltages, the first to spark over are the gaps of the main elements (2) so that current flows through both types of elements (2) and (1). As soon as the amplitude of the rising current impulse attains about 2000 A, the voltage drop in the valve-type elements (1) causes breakdown of spark gaps (3), the resistors of the valve-type elements (1) become shunted and the voltage across the arrester falls off.

A modification of this series has been achieved in the form of arresters with increased extinction voltage. This increase has been achieved with a greater number of spark gaps. To prevent a simultaneous rise in discharge voltage, this arrester is equipped with special firing spark gaps.

Arresters of the RVT series have been developed for 3-10 kV and 110-500 kV. They employ current-limiting gaps with narrow arc chute (see Fig. 13.7) and nonlinear silicon carbide resistors. The scheme of a current-limiting arrester rated 3-10 kV is shown in Fig. 13.12. The spark gaps (SG) with elongated arcs are connected in series with blowout coils (BOC). When the gaps spark over, the rapidly rising current impulse may cause increased voltages across the coil terminals. To protect coil insulation from these voltages they are shunted by bypass spark gaps (BSG). The shunt resistors R_{sh} provide uniform distribution of power frequency voltage

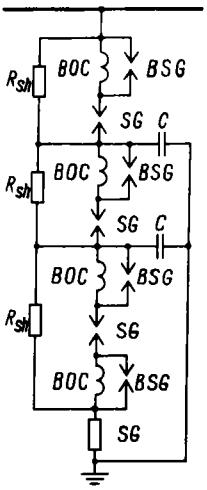

Fig. 13.12. Schematic diagram of type RVT arresters rated 3-10 kV

over the gaps. The capacitors C provide a sharply nonuniform distribution of the impulse discharge voltage over the gaps, thus reducing the impulse coefficient.

After the impulse current has been interrupted and the arc of the follow current extinguished in the bypass gap, the power-frequency follow current begins to flow through the blowout coils producing a magnetic field that extinguishes the follow current in the narrow chute of the arc extinction chamber.

In series RVRD arresters with elongated arc, permanent magnets based on barium ferrites are employed instead of blowout coils. This construction provides a more efficient arc extinction, therefore the discharge voltage in arresters of this series is 1.25 times the level of the RBT-series arresters.

Arresters for d.c. stations also incorporate nonlinear resistors. The arc burning without current zeroes has to be extinguished with the aid of magnetic action.

13.4 Overvoltage Limiters

Nonlinear overvoltage limiting devices have been developed in the Soviet Union on the base of a new zinc-oxide material. These devices are rated for 110-500 kV and provide switching overvoltage limitation to a level of $1.8U_{ph}$ and lightning overvoltage limitation to a level of $(2.0\text{-}2.4)U_{ph}$. The voltage-current characteristic of a nonlinear overvoltage limiter is presented in Fig. 13.13. As can be seen, a reduction in overvoltage from $2U_{ph}$ to U_{ph} is accompanied by a reduction of the current flowing through the resistors to one millionth of the former value. Therefore, the follow current in these devices is small (milliamperes) and the power released in such resistors is also small. This allows one to build overvoltage limiting devices doing without spark gaps and offering considerably higher reliability. Figure 13.14 presents the

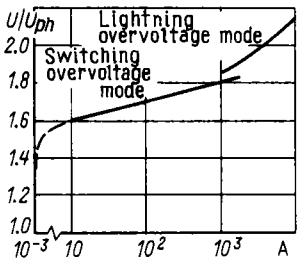

Fig. 13.13. Volt-ampere characteristic of a 500-kV current limiting resistor

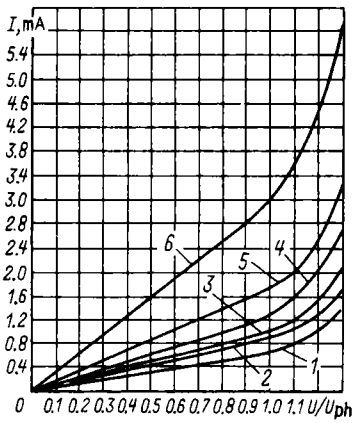

Fig. 13.14. Current versus voltage (in per unit of U_{ph}) curves for various types of current limiting resistors: (1) 110U1; (2) 150U1; (3) 220U1; (4) 1-110 HLCh; (5) 330U1; and (6) 500U

mean current for a few overvoltage limiting resistors rated 110-500 kV as a function of power frequency voltage in per unit of phase voltage.

The high nonlinearity of overvoltage limiting resistors (nonlinearity coefficient is about 0.04 for high currents) aids in a considerable reduction of current impulse width when the resistor handles switching overvoltages.

At low voltages across an overvoltage-limiting resistor, $(0.1\text{-}1.3)U_{ph}$, it carries small current so that spark gaps are no longer needed (Fig. 13.14).

For all voltage classes, overvoltage limiting resistors are assembled in single-unit porcelain housings of height and diameter close to that of support insulators for the same voltage class, but considerably smaller than these dimensions of the respective surge arresters. By way of example, a 220-kV resistor is half as tall and one third as light as the RVMG-220 lightning valve-type arrester.

14
MODULAR SWITCHGEAR INSTALLATIONS

14.1 General

The modular-designed switchgear installation is a type of assembly in which the substation switchgear is assembled (on site) of all the necessary mass-produced electric equipment and protective circuits. This approach to switchgear design offers faster phase-in of new capacities, higher reliability of the power system, enhanced maintenance safety, and automated production lines in the switchgear manufacture. This way of substation mounting has been recognised as more advantageous than the traditional assembly of miscellaneous compatible equipment [14.2].

14.2 Modular Installations for 10 kV

A typical modular-switchgear cubicle is shown in Fig. 14.1*a*. The scheme of the high-voltage circuit is shown in Fig. 14.1*b*. The equipment is mounted into a welded steel cubicle. For better safety the cubicle is separated into compartments.

Compartment *A* houses busbars fixed to support insulators.

Compartment *B* houses a circuit breaker (1) with a drive mechanism (2), and compartment *C* houses a measurement current transformer (4) and a line conductor pot head (5).

The circuit breaker (1) is connected to the buswork and the current transformer by plug-in contacts (3) with a cluster or finger-type contact.

Compartment *E* houses control cables, and compartment *D* the relaying and measurement equipment.

The sectionalised cubicle aids in separation and confinement of a fault preventing its spread over the entire installation.

A bus-to-bus fault gives rise to an electromagnetic force moving the arc at a speed of hundreds of metres per second and the arc can cause severe mutilative effects. In order to prevent arc propagation new installations are equipped with buswork having solid insulation of glass cloth impregnated by epoxy resin.

The circuit breaker is a key element of the cubicle. Because the separating walls of the cubicle are sheet steel of comparatively moderate strength, a breaker explosion may lead to the propagation of the failure over the entire installation. Therefore, modular cubicle-type installations are equipped with flame-proof vacuum, magnetic, or air circuit breakers. Low-oil-content circuit breakers are far less liable to fire than bulk-oil units and may be used in cubicle type substations too. By way of example Fig. 14.1 represents an installation built around a low-oil type VMP-10 circuit breaker.

Gases generated in circuit breaker operation should be free to leave the cubicle

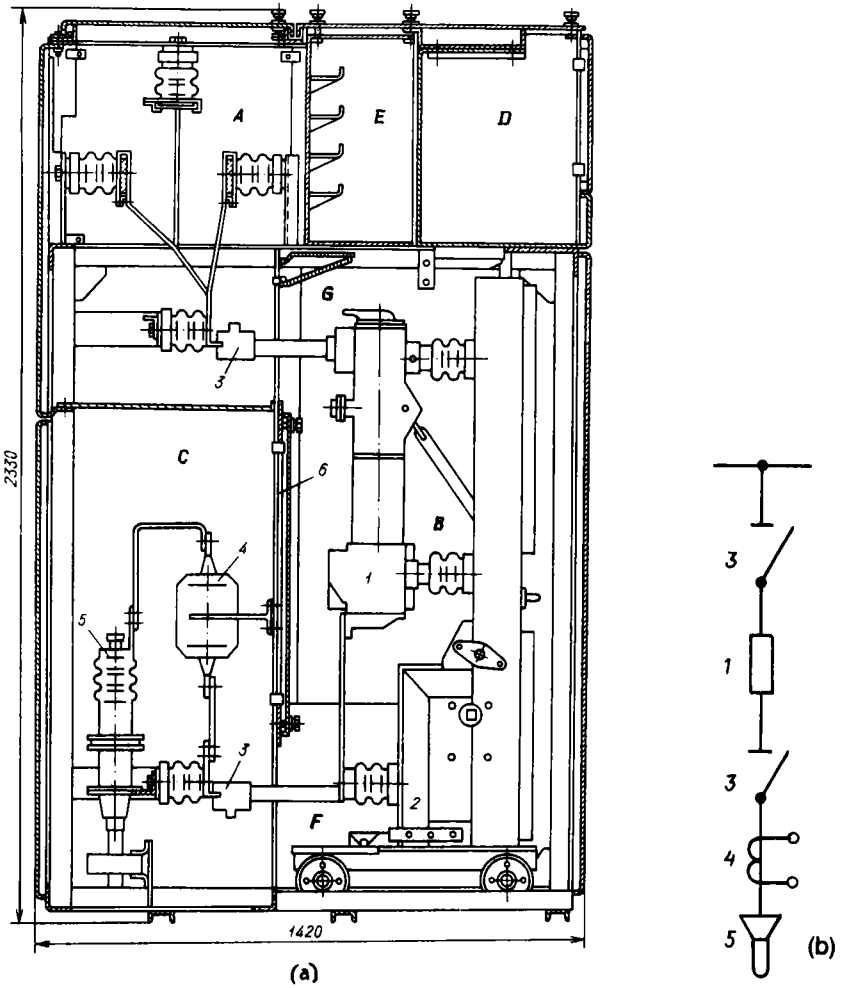

Fig. 14.1. Metal-enclosed switchgear cubicle for 10 kV

through a gas vent, otherwise their accumulation may lead to an explosion fired, say, by a poor contact in the buswork.

In high-power interruptions, exhaust gases should be vented in the atmosphere through pressure-relief ducts (see, e.g., Fig. 5.9). Explosion hazard can be depressed by placing the auxiliary contacts of the control circuit into a separate compartment, for the interruption gas may explode due to a spark that occurs in the circuit of a tripping or reset coils of the drive mechanism.

The cubicle walls are thin but large in area, therefore they may be deformed even by small excess pressures inside the cubicle. To prevent this situation cubicles are equipped with spring loaded pressure relief valves.

At interrupting capacities up to 350 MVA, a good practice for installations concerned would be to use a spring-actuated drive built in the mechanism of the circuit breaker. In view of a low power requirement (100 W) of the motor charging the spring an independent power supply (battery) is no longer needed.

New cubicle-type installations have a drawout circuit breaker mounted on a trolley along with the drive. This assembly may be easily disconnected and withdrawn from the cubicle for maintenance and repair. The plug-in contact arrangement is readily adaptable for interlocking to warrant safe maintenance conditions. The mechanism of withdrawal is interlocked with the mechanism of the breaker. The latter can be removed only when de-energised.

The breaker trolley has three fixed positions: the service position when the attendant isolator is closed, the test (intermediate) position when the isolator is open but the relay, measurement, and drive control circuits remain energised, and the disconnected position when all the circuits are de-energised, the breaker is disconnected and can be drawn out of the cubicle. If a repair of the breaker is required, another module of the same capacity can be retrofitted in its place.

When the trolley is withdrawn from the service position to the test position, the metal shutters (6) close the openings *G* and *F* in the wall and separate compartment *B* from compartments *A* and *C* that may be at a high voltage. The barriers move open when the breaker is fitted back into the service position. The energised control circuits in the intermediate position allow for breaker testing. The most reliable connections for these circuits are by means of plug-in connectors fitted at the ends of flexible cables.

Instead of more common vertical-break disconnecting switches, the modular design gives preference to plug-in disconnectors. The movable finger contacts (3) are fixed to the stiff buses connected with the break bushings. The stationary contacts in the form of solid buses are supported by support insulators. When the breaker trolley is moved in the service position, the fingers of the movable contacts embrace the stationary pins and ensure a reliable electric contact. This construction is a reliable option up to ratings of 3000 A.

The current transformers (4) for these installations are mostly of moulded insulation type. Oil-immersed voltage transformers are ousted by moulded insulation units. These transformers are flame-proof, have smaller size, and are free from troubles associated with oil contamination and level monitoring.

Relay protective devices and measuring instruments are mounted on the hinged front cover of compartment *D*. For inspection and maintenance, this cover is swung open and all the instruments become readily accessible. The devices are connected with the rest of the control circuit by a multicore flexible cable.

Figure 14.2 shows a new small-sized type KM-1 modular installation developed around an upgraded low-oil-content circuit breaker for 10 kV, continuous current of 1600 A, and interrupting capability up to 31.5 kA. The breaker (1) has a spring assisted drive (2) and is connected to the circuit with the aid of plug-in connectors with cluster contacts (3). The insulating sleeves (4) protect the contacts from the

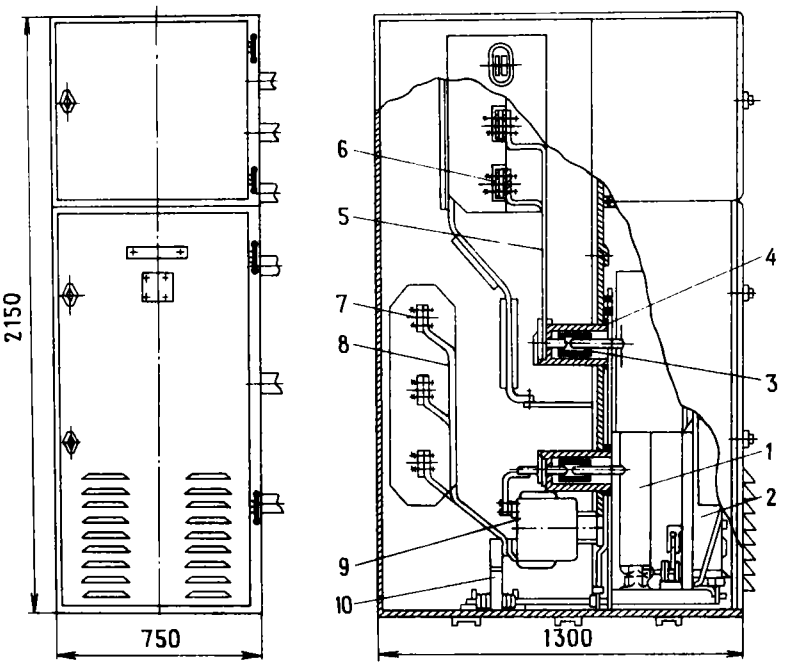

Fig. 14.2. Metal-enclosed switchgear cubicle rated 10 kV

dust and aid in improving the dielectric strength. Buses (5) connect the upper contact of the breaker with buswork (6). Buses (8) connect the lower contact with the main bus (7). Current measurements are effected with a current transformer (9) with mould insulation. Measuring voltage transformers are also of moulded insulation type. The earthing switch (10) provides earthing of the line buses during maintenance operations.

Figure 14.3 shows the outline of a small-sized modular substation whose cubicle houses two vacuum circuit breakers (1) placed one above another for space economy. The voltage ratings are 12, 15, and 40 kV; the continuous current is up to 3000 A, and interrupting capacity up to 31.5 kA. Vacuum circuit breakers are very attractive for modular switchgear installations because of their small size and long maintenance-free service life (25 years), and accordingly low maintenance costs for such installations.

Designers of modular switchgear installations take pains to prevent occurrence of arc. However, if arc occurs, for instance in insulation flashover, the design should somehow cope with the pressure buildup inside the cubicle. Estimations of this pressure with the analogue circuits substituted for the actual installation have indicated that for an r.m.s. current of 20 kA at 20 kV with all pressure relief valves open the gauge pressure may rise to 0.12 MN/m^2. The pressure rise peaks at the peak short circuit current.

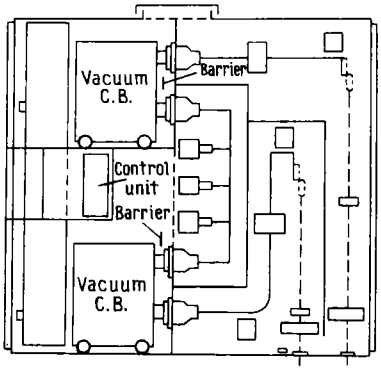

Fig. 14.3. Horizontal drawout metal-clad switchgear rated 40 kV

Size reduction of metal-clad switchgear and considerable improvement of system reliability can be achieved by using solid insulation for the buswork and for all current carrying parts of the installation. This way, however, presents formidable difficulties, especially at large nominal currents.

14.3 SF_6-Insulated Substations

At voltages above 35 kV the switchgear using solid insulating materials is no longer at technological and economical advantage. Owing to a large thickness of the material its inhomogeneity becomes a significant factor. In addition, a nonuniform distribution of voltage gives rise to areas with considerable strength of electric field. It is rather difficult therefore to design switchgear components on a modular basis because of the complicated technology of solid-insulation switchgear. These complications explain why transformer oil was used in metal enclosed substations for 110 kV and above in the 1930s. Oil easily fills all voids and provides uniform insulation between the current carrying parts. Such modular stations were developed in a number of countries for underground and indoor applications.

Use of transformer oil would appreciably reduce the space occupied by the modular station. However, oil possesses a number of setbacks limiting the development of oil-insulated switchgear. A large volume of oil in the enclosure, for example, would call for large expansion spaces. The properties of oil alter in service. Such contamination as water, for example, markedly reduces its dielectric strength, so the oil should be dried in regular intervals. Oil cleaning required special facilities to say nothing of fire hazard that bars the use of oil-insulated stations near large factories and in urban areas. An arc burning in oil contaminates it with carbon and reduces its dielectric strength. Attempts aimed at developing insulating liquids free from these disadvantages have failed [2.4]. Although oil-type circuit breakers are rather popular, oil insulated modular stations have not become common.

Fluorogas insulation was found to have a decisive edge over transformer oil.

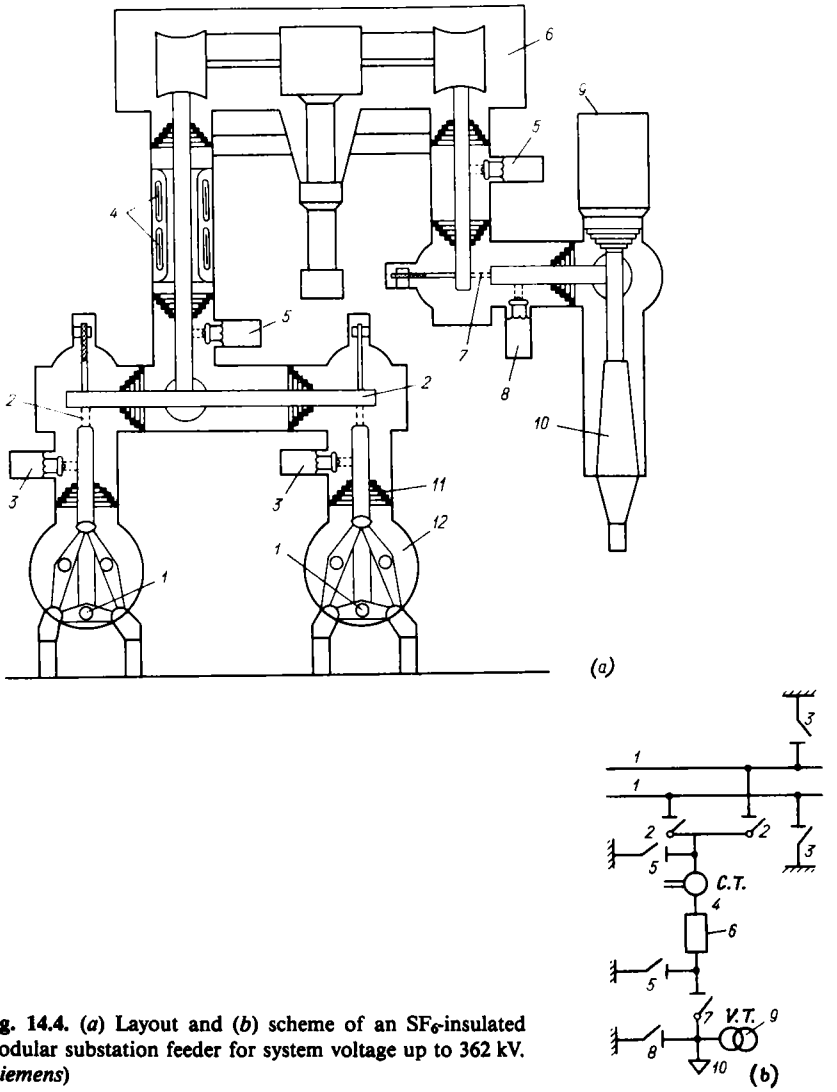

Fig. 14.4. (*a*) Layout and (*b*) scheme of an SF_6-insulated modular substation feeder for system voltage up to 362 kV. (*Siemens*)

It is not penalised by ageing phenomena, is uniform in properties, and flame-proof. Air may be also used for insulating modular substations, however its dielectric strength is only one third of that for SF_6 at the same pressure, therefore an air-insulated station should be pressurised three times as high as an SF_6-insulated unit. Accordingly, the metal enclosure of an air-insulated unit should have higher strength, which would mean thicker walls and greater weight of the cubicle.

The arc extinction capacity of SF_6 gas is four times as strong as that of air which makes SF_6 insulated switchgear a far more attractive proposition for modular substations.

For many installations the area occupied by the substation is a critical factor. This relates to urban areas, industrial territories, zones of power station dambs, and mountain areas.

Siemens reported that an SF_6-insulated outdoor substation for 500 kV reduced the area requirement from 30 000 m^2 for an ordinary installation to 920 m^2. Small size of SF_6 insulated switchgear is advantageous for indoor applications, where climatic considerations are no longer significant. The metal-enclosed design renders SF_6 insulated units insensitive to saline deposits in marine applications, to industrial sediments and acid rains, and to sand storms. The last but not the least, small area requirements and space requirements reduce the cost of construction — an important consideration in rock terrains.

Figure 14.4 shows a Siemens SF_6-insulated switchgear station for system voltage up to 362 kV. The round busbars (1) of all 3 phases are confined by a cylindrical bus duct (12). This assembly reduces the widths of a 170-kV installation to almost one half and cuts down the space occupied by the station compared with the segregated busbar arrangement. This design allows for lower losses in the duct and admits steel as material for the enclosure. Owing to lower cost, higher strength and melting point than that of aluminium alloys steel allows higher pressures of SF_6 gas (up to 0.48 MN/m^2) at higher voltage ratings. Steel ducts resist the burning action of occasional arc and a pressure rise owing to this heating. Confining three phase bars in one duct reduces gas leaks by 30% as compared with phase-segregated busbars.

The busbar (1) can be discriminated (in the de-energised state) by an isolator (2) and earthed by an earthing switch (3). Both the isolator and earthing switch are provided with motor drives. From the left or right busbar (1) the voltage is supplied to a two-break piston-type circuit breaker (6). Operation of such a breaker was discussed in Sect. 4.11. The breaker is operated by a pneumohydraulic drive. Safety conditions for the period of maintenance or overhaul are ensured by earthing the breaker terminals with the aid of the earthing switch (5). The current transformers (4) feed the instrumental and protective circuits. High voltage is measured with the SF_6-insulated voltage transformer (9). The isolator (7) is connected to the feeder cable sealing end (10).

During repair operations the line isolator (7) is locked open and the line is earthed by the earthing switch (8). The individual modules of the installation are separated by ribbed epoxy insulators (11). The ribbed surface enhances their strength against flashover. Segregation of the modules allows for better control of pressure in each module. Module envelopes are made rather strong and when an arc occurs inside the duct the pressure rise breaks down a pressure relief membrane in a matter of milliseconds thus preventing the duct explosion. All the other modules remain pressurised. This gastight construction warrants a gas leak rate of only 0.5% a year. Liquid vapours are absorbed by breather filters which are usually replaced once a decade.

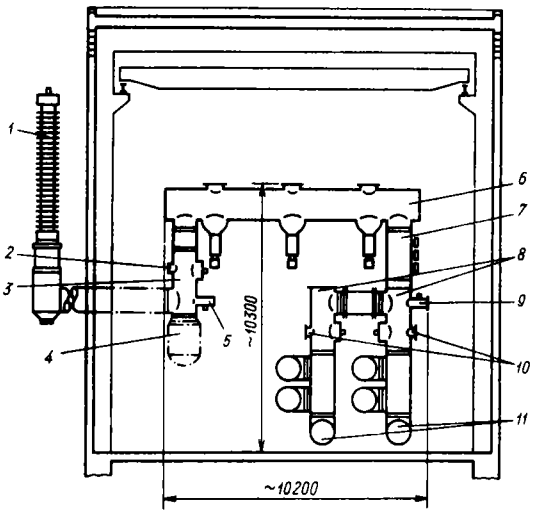

Fig. 14.5. Layout of an SF_6-insulated switchgear cubicle for system voltage up to 800 kV. (*Siemens*). (1) Through insulator for outdoor application, (2) connection of maintenance earthing switch, (3) feeder isolator, (4) voltage transformer, (5) feeder earthing switch, (6) power circuit breaker, (7) current transformer, (8) bus isolator, (9) maintenance earthing switch, (10) bus earthing switch connection, (11) busbars

SF_6-insulated modular substations are equipped with a well-phanned system of interlocks that preclude misoperations and ensure safety conditions during maintenance and repair. The single line scheme of an SF_6-insulated modular substation is shown in Fig. 14.4*b*.

Figure 14.5 shows the layout of a Siemens SF_6-insulated substation for operating voltage up to 800 kV. Each phase of this improved installation is isolated into a segregated busbar. The key module is a six-break piston-type circuit breaker.

When the ambient temperature drops below -40 °C a proportion of the insulating gas turns into the liquid phase impairing the gas insulation properties and arc-extinction capability. The liquefaction temperature of the gas can be decreased by admixture of other gases. Satisfactory performance has been obtained for equal volumes of SF_6 and He when operating temperature can be reduced down to -50 °C.

If ambient temperatures as low as -30 to -40 °C are anticipated, indoor installation is recommended for SF_6 insulated switchgear. The cubicle may not be provided with heating appliances — the necessary temperature will be provided at the expense of losses in the switchgear proper. Clearly outdoor application of such switchgear requires protective measures against icing, freezing temperatures, and overheating by the sun. Enclosing SF_6-insulated switchgear is therefore more desirable — easier maintenance and overhaul and independence of switchgear operation of climatic conditions are worthy of note. After 10 years of service the wear

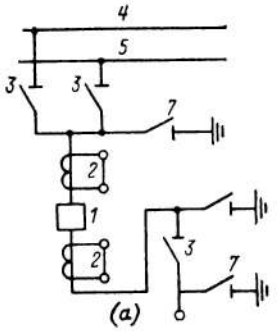

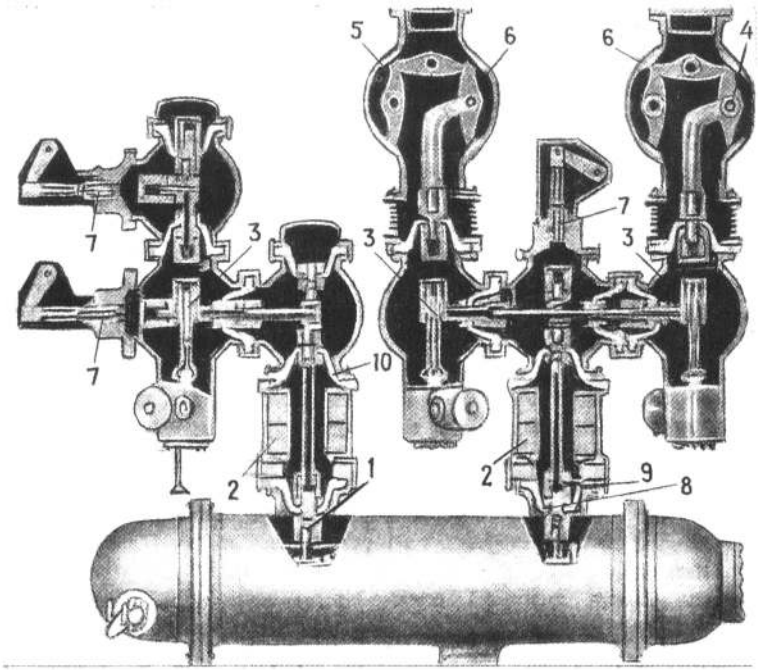

Fig. 14.6. Soviet-made 110-kV modular switchgear installation

of contacts in an SF_6-gas circuit breaker is barely noticeable. Therefore, a 10-year maintenance period is common.

Soviet developments in this area include 110-kV and 220-kV designs. The major technical data for the 110-kV SF_6-insulated modular switchgear are displayed below.

Rated voltage	110 kV
Nominal busbar current	1.6 kA
Nominal feeder current	1.25 kA
Interrupting capacity	40 kA
Maximum making current (peak)	102 kA
Total break time	40 ± 5 ms
Interrupting speed of c.b. contacts	5.5 m/s
Total make time	80 ± 20 ms
Arcing time in circuit breaker	20 ms
Rated SF_6 gas pressure (gauge)	
in circuit breaker	0.6 MN/m^2
in voltage transformer	0.4 MN/m^2
in other components	0.25 MN/m^2

The installations for 110 kV are manufactured with one or two systems of busbars. Figure 14.6*a* shows the scheme of a pole with two busbars and the diagram at (*b*) illustrates the layout of a line substation switchgear. The SF_6-insulated circuit breaker (1) has one break per pole and an interrupter design shown in Fig. 4.58. The pneumatic drive of the movable contact operates at a pressure of 2.0 MN/m^2. The current transformer (2) is also of SF_6-gas type. The secondary winding taps allow for ratio alteration (600/1, 800/1, and 1200/1). The busbars (4) and (5) are connected and disconnected by the isolators (3). The three phase set of busbars is sealed in a single tank (6). Earthing switches (7) ensure earthing of de-energized system parts. The earthing switches and isolators are operated by a pneumatic drive developing a pressure of 0.6 MN/m^2. Individual modules of the installation are separated from one another by insulator baffles (10). Electrical connection of the system modules is effected with the aid of multiple-finger cluster contact assemblies (9) and current carrying rods (8).

Other Soviet developments in this field include 1150-kV a.c. and 1500-kV d.c. designs.

14.4 Constructional Designs of SF_6-Substation Modules

For safe and convenient maintenance, modular substations are equipped with disconnecting and earthing switches. Isolators disconnect the de-energised module to be maintained or overhauled. Clearly, the reliable operation of these components affects the operation of the entire substation.

The necessary margin of electric strength between the contacts of an open isolator is achieved by inserting screens making the intercontact field more uniform. Auxiliary contacts are provided to signal the position of the main contacts. In addition the driving mechanism of isolator is equipped with a mechanical indication of isolator-contact position. Some designs meet the requirement by providing a window (Fig. 14.7).

Earthing switches may be divided into three types. One type covers service switches that provide earthing for de-energised parts. This is a low-speed switch actuated manually or mechanically. The second type is a high-speed earthing switch that may close on a short circuit current. This type of earthing switch is installed on busbars and cable bushings. The third type of switch serves protective purposes. It closes the earthing path in less than 100 ms. This switch protects the modular switchgear from the mutilative effect of arcing inside the enclosure. Use of a photocell as an arc signalling probe connected with the switch drive aids in reducing the time of arcing. The drives may be pneumatic, or spring assisted — the spring being motor or manually charged.

Dimensions of SF_6-insulated substations are reduced by integrating the isolator and earthing switch in a single module. Figure 14.7 shows the sectional view of such a module for the 110-kV design. The movable contact (1) of the isolator is connected with the drive (3) by an insulating rod (2). The stationary contacts of isolator (4) and earthing switch (5) are secured to cone insulators (6). The movable contact of earthing switch (7) is in the drive housing (8). The membrane (9) is broken down by a pressure surge due to arcing inside the enclosure.

The module is integrated into the switchgear system with the help of flanges (10). The current-carrying rods of the adjacent modules enter the stationary contacts (11). The screens (12) and (13) are installed to equalise the electric field strength.

The isolator drive is equipped with an indicator of contact position and the auxiliary contacts of the indication and signalling systems. The isolator enclosure has a window (14) to monitor the contact position.

The double O-ring seal (15) provides a gastight joint of insulators (6) and metal flanges (10). The ring material is a variety of synthetic rubber.

Current transformers. Ferromagnetic c.t.s are common for these designs. The

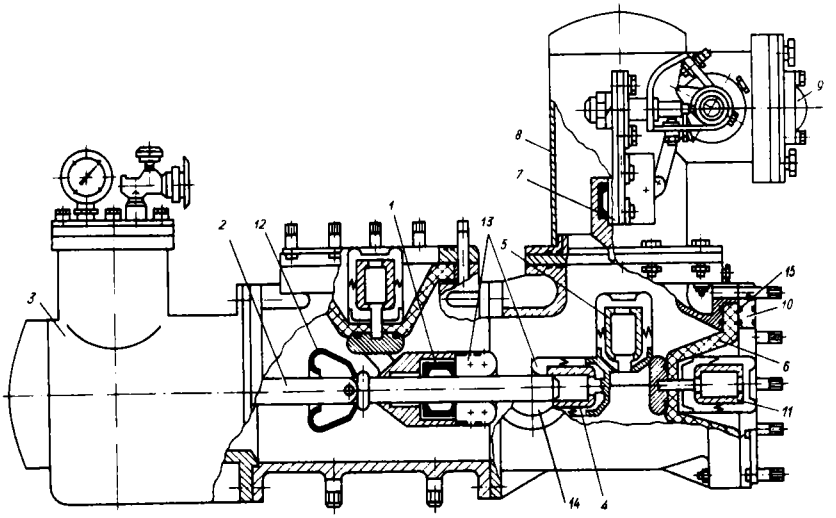

Fig. 14.7. Isolator and switch for integration with an SF_6-insulated substation rated 110 kV

primary winding is a current bus usually in the form of a pipe. The secondary winding is uniformly spread over a toroidal core. The core and secondary assembly is encapsulated with epoxy resin. The insulating medium is SF_6 of the switchgear insulation. For the electric field that occurs between the bus of radius r and the earthed screen of radius R between the bus and transformer the optimal ratio of radii is $R/r = e$. For designs with aluminium enclosure the latter takes up the role of the screen. The maximum field strength at the bus conductor is $E = U_{test}/r$. Whenever the transition mode is anticipated, a nonmagnetic gap is provided in the magnetic circuit. The gap is made rather large to limit the aperiodic component of magnetic flux density where measurement of only periodic component is necessary.

Voltage transformers. At system voltage up to 220 kV magnetic v.t.s with epoxy or film-SF_6 insulation are the best choice for modular designs. At higher ratings the dimensions of v.t.s influence the overall dimensions of the installation. Therefore instrument transformers based on capacitor-dividers should be used at voltages upward of 220 kV. A classic scheme with a step-down v.t. (see Fig. 11.15) or solid-state amplifier will also suit the purpose. In the last case, capacitor C_1 is formed by the bus and a cylindrical electrode separated by a safe layer of SF_6 gas. Capacitor C_2 gives the input signal to the amplifier. The error of this arrangement consists of the error due to the divider and the error of the amplifier due to variation of the input resistance and gain (effects of power supply instability, ambient temperature, type and amount of load, and ageing of circuit components). Present developments include capacitor-dividers with solid-state amplifier of 500 VA rated power.

Surge arresters. Surge arresters incorporated in SF_6-insulated modular substations are the valve-type arresters with sufficient protective margin for both switching and atmospheric overvoltages. The spark gaps and nonlinear resistors are housed in an insulator tube filled with dry nitrogen. Uniform distribution of voltage over spark gaps is achieved with special cylindrical covers. The earthed cylindrical enclosure is insulated from the cylindrical covers by SF_6 gas at a pressure of 0.25 MN/m^2.

Enclosures. New installations use aluminium alloys and constructional steel for enclosures. The magnetic field due to the bus current induces in the enclosure currents that can attain values equal to the primary current. Aluminium alloys have a decisive edge over steel enclosure from the eddy load standpoint because of lower resistivity. However, it has a higher permeability to SF_6 gas and may allow moisture of atmospheric air inside the enclosure. Besides these alloys are not so strong as steel and can be burnt through by an arc.

Steel enclosures offer high mechanical strength, arc resistance, and impermeability to gases. However steel incurs large losses in phase-segregated busbar designs. A way out is the use of three-phase busbars when all the phases are confined in one enclosure. This design offers smaller dimensions of the installations and gas leak rates as low as 0.5% a year.

Recognising that a large proportion of power system personnel is involved in maintenance of networks and switchgear, wide acceptance of SF_6-insulated modular switchgear would sharply reduce labour requirements and cut down maintenance costs.

INDEX

Air circuit breakers, 51
  air tank of, 98
  contact operating mechanism, 89
  continuously pressurised, 103
  control system of, 91
  design, 100
  equivalent circuit of, 75
  gas dynamics of, 79
  illustrative analysis of, 126
  interrupter, 85
  layout of, 53
  suspended, 110
Arc behaviour in air flow, 54
Arc chute design, 176, 179
Arc extinction with shunt resistors and capacitors, 71
Arresters, 336
Axial blast extinction chambers, 51
Axial blast interrupters, 64

Blast nozzle, 57, 62
Bushing insulation, 27

Chernyshov synchronisation circuit, 49
Circuit breakers, 11
  a.c., 38
  air, 51
  development trends for oilless c.b.s, 124
  duty cycles, 39
  interrupting capacity, 39
  interrupting rating, 38
  magnetic air-break, 169
  mechanical withstand capability, 41
  oil immersed, 137
  rate of rise of recovery voltage, 40
  reliability, 42
  SF_6, 116
  stability at s.c. current, 41
  vacuum, 183
Condenser bushing, 29
Coordination between inner and outside insulation, 18
Creepage distance, 18, 20
Current limiting reactor, 12
Current transformers, 220
  calculation of, 254
  choice of, 254
  construction, 241
  coreless, 245
  effect of burden impedance, 225
  equivalent circuit, 220
  error compensation, 228
  operating modes, 230
  optoelectronic, 247
  phasor diagram, 221
  ratio error, 224
  reclosing duty, 238

Dielectric strength of transformer oil, 26
Differential valve, 91
Direct action valve, 96
Disconnecting switch, 11, 200
Discriminators, 200

Earthing switches, 27
Expulsion-fuse cutout, 218

Fusegear, 212
  construction, 138
  protective characteristics, 212

Instrument transformers for d.c. systems, 250
Insulation
  bushing, 27
  distance, 18
  level for SF_6 installations, 24
  mechanical strength, 34
  reactor, 325
  SF_6, 111
  solid materials, 30
  switchgear, 18
  voltage transformer, 281
Interrupter geometry, 67
Interrupting current ratings, 9
Interrupting chamber parameters, 85

Lightning arresters, 12
Limiting arresters, 12
Load switches, 208
  magnetic air, 210
  puffer, 209
  vacuum, 211

Magnetic air-break circuit breakers, 168
  arc speed, 176
  current-voltage behaviour, 171
  design, 182
  heating of chute walls, 174
  residual conductivity, 179
Mechanical withstand capability, 41
Metal enclosed switchgear cubicle, 349

Oil-barrier bushings, 28
Oil circuit breakers, 137
  auto-reclosing duty, 154
  bulk, 137
  design, 168
  driving mechanism, 156
  interrupters of, 146
  low-oil content, 137
  oil buffers, 163
  operating mechanism, 156
  pressure analysis, 149, 152, 150
  tripping mechanisms, 167
Overvoltage limiters, 346

Paschen's curve, 23
Peak momentary current, 16
Per unit concept, 16
Porcelain insulators, 34
  bending strength, 36
Protective systems, 13

Rated continuous current, 15
Rated making current, 41
Rated maximum voltage, 15
Rated system voltage, 15
Reactors, 300
  calculation of, 305, 329
  construction of, 303
  duplex, 326
  insulation, 325
  mechanical rating, 311
  parameters of, 302
  thermal design, 308
Recovery of dielectric strength in blast interrupters, 64

SF_6 circuit breakers, 116
  analysis of, 117
  construction of, 122
  tube-type, 336
  valve-type, 337
Switches, 198
  discriminators, 200
  earthing, 207
  isolating, 204, 207
  load, 208
Switchgear, 11
  characteristics, 15
  current ratings, 10
  development trends of, 124
SF_6-insulated substations, 352
Short-circuit current, 9, 10
Short-circuiting switch, 12
Short-time current ratings, 16
Surge arresters, 336
  magnetic valve-type, 344
  spark gap elements, 340
  station, 343
  installations, 15
  insulation, 18
  modular installations, 348
  rated voltage, 19
  ratings, 15
  requirements of, 16
  service voltage, 19
  voltage ratings, 10

Thermal withstand capability, 15
Transformers, 2
  current, 220
  instrument, for d.c. systems, 250
  voltage, 266
Transient recovery voltage, 40

Vacuum circuit breakers, 183
  construction of, 193
  electric strength, 191
  interrupting capacity, 186
  mechanical withstand, 189
  status and trends, 185
  thermophysical characteristics, 187
Voltage rating, 9
Voltage transformers, 266
  calculation of, 288
  capacitor-divider, 281
  components of, 278
  constant, 284
  construction of, 273
  errors, 269
  error compensation, 271
  nameplate ratio, 267
  optoelectronic, 286
  phasor diagram, 268
  voltage ratio error, 268